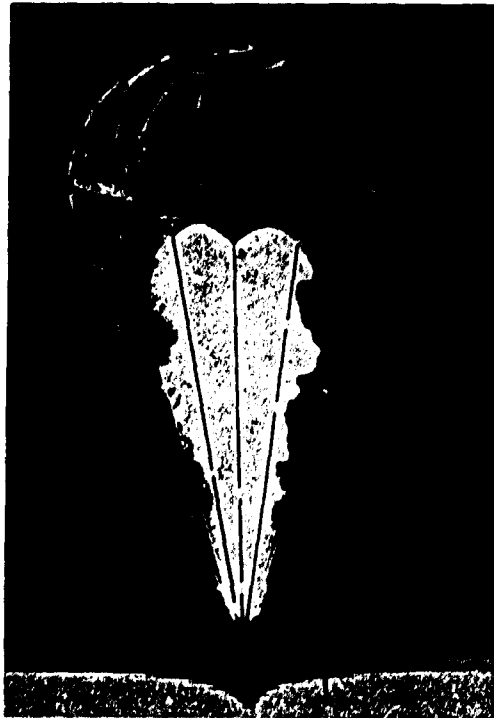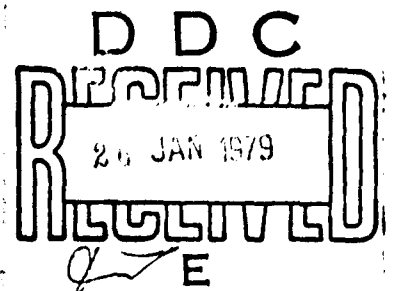LEVEL III ①

SIXTH INTERNATIONAL PYROTECHNICS SEMINAR

July 17-21,1978
Stanley Hotel
Estes Park, Colorado

HOSTED BY
University of Denver
Colorado Seminary
Laboratories for Applied Mechanics
Denver Research Institute

D D C

RECEIVED

2 6 JAN 1979

E

79 01 22 093

PROCEEDINGS
OF THE
SIXTH INTERNATIONAL PYROTECHNICS SEMINAR

17-21 JULY 1978

Chairman
R.M. Blunt, Laboratories for Applied Mechanics

Denver Research Institute
University of Denver
Colorado Seminary
Denver, Colorado
80208

The Proceedings of four earlier seminars in
this series can be obtained from:
NATIONAL TECHNICAL INFORMATION SERVICE
U.S. DEPARTMENT OF COMMERCE
5285 PORT ROYAL ROAD
SPRINGFIELD, VA 22161

Their Ordering Identification is:
First   -- AD 679911
Second -- AD 913407
Third   -- AD 913408
Fourth -- AD-A057599

AD-A063797

79 01 22 093

SIXTH SEMINAR PROCEEDINGS

INTRODUCTION

It was interesting and very pleasant to note that the number of papers that are to be presented at this Seminar is more than double the number presented at the First Seminar, and in fact they are almost double the number of pyrotechnists who participated in that Seminar. It was held at Harmony Lodge in Estes Park in 1968 and, although many of you thought we should return to Steamboat Springs for this meeting, it seemed more fitting to return to the Seminars' "birthplace." I sincerely hope that all of you who attend this Seminar will find it both informative in technical matters and refreshing as an experience.

As you know, these Seminars exist only to provide you, the practicing pyrotechnicists, with a forum. My thanks to all of the authors who provided the material for this Seminar, and to those whose attendance and participation have supported it. I would also like to recognize the support that was always given so freely by Gunther Cohn, who was the editor of "Explosives and Pyrotechnics" until his death on November 22, 1977.

It has been a very enjoyable "decade of seminars," thanks to which I have made many new friends. I hope these will continue to meet the needs of the pyrotechnic community and eventually lead to the creation of a "Pyrotechnic Society." It would be useful to have a centralized source, or focus, to speed the transfer of information, to answer questions, and to act as the "Sponsor" for these seminars.

R.M. Blunt
General Chairman

June 1, 1978
Denver, Colorado

TABLE OF CONTENTS

6th INTERNATIONAL PYROTECHNICS SEMINAR

M.R.L. SUBMISSION

GASLESS PYROTECHNIC CAPS

by

J. Bentley and P. Elischer

A gasless pyrotechnic percussion cap has been produced and tested. Its sensitivity has been shown to be comparable to M42 caps and preliminary tests indicate that the stability of the composition is satisfactory. The effect on sensitivity of height of fill, weight of fill and pressed density are investigated.

GASLESS PYROTECHNIC CAPS

Gasless delay compositions were developed primarily for use in hermetically sealed units. They can be ignited by all normal means of initiation including percussion caps and fuze heads; gasless fuze heads, which contain cerium/magnesium and lead oxide have been developed specifically for use with these gasless compositions.

Conventional percussion caps, which are currently being used with delays, contain "gassy" compositions and as a result, problems can arise when these are used in sealed systems. When ignited these caps produce a significant and variable amount of gas. This can cause variations in pressure and thus burning rate of the compositions. The pressures produced by these gases are sometimes sufficient to cause the cap to be ejected from the sealed unit; this premature venting will cause the burning rate of the composition to alter and can ultimately lead to operational defects. To overcome the problems of cap ejection and variable burning rate, sealed units containing conventional caps must have a free space between the cap and the delay composition sufficiently large to prevent high pressure from developing. This free space unduly increases the overall size of the sealed unit.

The use of a percussion cap containing a "gasless" priming composition could eliminate these problems without significantly affecting the burning characteristics and reliability of hermetically sealed units. On ignition, typical gasless caps produce 5-10 ml of gas per gram. A gasless cap containing 20 mg of composition would therefore produce 0.1 to 0.2 ml of gas and a unit based on such a priming cap would probably operate reliably if the free space was zero. The overall size of the unit could be significantly reduced, which is an important consideration in most applications.

Our aim was to develop a composition which, when filled into M42 cap assemblies, figure 1, would give a sensitivity comparable to the sensitivity of the M42 cap. The M42 cap was chosen as a control because it is a common service store and both empty and filled components were readily available.

A gasless priming composition SR57 is currently being used in the U.K. as a pyrotechnic stab-sensitive composition; SR57 is a mixture of boron (10%) and bismuth oxide (90%). During a previous investigation of stab sensitivity at MRL tetrazene was added to this composition in an attempt to improve its sensitivity. The resulting composition was moderately stab-sensitive but was very variable. A series of related compositions was investigated and it was found that a composition containing the following proportions :

Lead oxide	85.5 per cent
Boron	9.5 per cent
Tetrazene	5.0 per cent

did have good stab sensitivity, comparable to primary explosives.

SENSITIVITY

M42 caps were filled using the normal charge weight (20 mg) of the above gasless composition. This was pressed into the cap assemblies using a pressure of 19 MPa. The remaining assembly procedure was similar to that used for production of M42 caps. The sensitivities of these caps and of a selection of M42 caps were determined using a 56 g striker. The 50% functioning levels ($\bar{x}$) and standard deviations were determined using the Bruecton technique[1]. Sample sizes of 25 and drop height intervals of 5 mm were used. The results are shown as table I.

TABLE I

Cap	M42	Gasless pyrotechnic
Sensitivity (mJ) $\bar{x}$	119	117
σ	0.47	2.1

The results show that the sensitivities of the two caps are very similar and it would not be difficult to incorporate gasless caps into appropriate stores already using the M42 cap.

DETERMINATION OF PARAMETERS WHICH AFFECT CAP SENSITIVITY

The M42 cap assemblies previously tested were individually filled using a hand press. This procedure enabled the pressing load and the weight of compositions to be accurately controlled. This degree of control could not be expected in production where multiple filling is employed. A series of tests was carried out to assess the change in sensitivity with change in the major filling parameters.

PRESSING LOAD Vs SENSITIVITY

To investigate this relationship the filling procedure previously described was employed using a range of pressing loads. The weight of filling was kept constant at 20 mg. The composition was accurately weighed and pressed into the cap using a pressure of 2.8 MPa. After a batch consisting of fifteen caps, was completed the pressing load was increased by 2.8 MPa. This procedure was repeated until the pressing load reached 22.4 MPa. The sensitivities were determined as previously described except 25 g and 56 g strikers were used. The results are shown in table II.

TABLE II

Pressing load MPa	Ht of composition "mm"	Sensitivities (mJ) $\bar{x}$	
		25 g	56 g
2.80	1.30	–	138
5.61	1.27	111	130
8.41	1.14	112	124
11.22	1.14	109	121
14.02	1.17	107	120
16.83	1.14	101	115
19.6	1.14	103	103
22.4	1.09	106	107

The increase in sensitivity when the lighter striker was used is an expected trend[2] and the change in sensitivity with pressing load suggests that, above 10 MPa, pressing load has little effect on sensitivity. For later investigations a pressing load of 16-17 MPa was used.

WEIGHT OF COMPOSITION Vs SENSITIVITY

Composition weights ranging from 10 mg to 30 mg were pressed into M42 caps and the sensitivities were determined in the usual manner using a 56 g striker. These results are shown in table III.

4

TABLE III

Weight of composition "mg"	Average ht. of composition "mm"	Sensitivity (mJ) $\bar{x}$
10	0.86	108
15	0.99	111
20	1.14	117
25	1.27	121
30	1.42	126

The decrease in sensitivity with weight of filling, observed in the above results is consistent with sensitivity being related to the pressed density and is in line with the previous results. The variation in sensitivity with both pressure and weight of filling is small, so that production problems should be minimal.

THERMAL STABILITY OF CAPS

A number of caps were prepared using 20 mg of gasless pyrotechnic composition and a pressing load of 17 MPa. The thermal stability of caps was investigated by allowing them to condition in an oven held at 60°C. At monthly intervals, a number of caps were taken out of the oven and their sensitivities determined using a drop tower and a 56 g striker.

As control samples the sensitivities of caps stored at ambient were determined at both the beginning and end of the trials. The results, shown in table IV, indicate that the gasless caps have an acceptable thermal stability. More detailed long-term cyclic tests would have to be carried out before the caps could be incorporated in a service store.

TABLE IV

Storage Time months	Sensitivity	
	Stored at 60°C	Control
0	117	117
1	119	−
2	116	−
3	114	−
4	113	116

The gasless caps were tested in a hermetically sealed unit shown in figure 2. The delay was filled with the following composition :

boron	12 per cent
bismuth oxide	63 per cent
chromic oxide	25 per cent

This composition has a bench burning rate of 3.0 seconds per inch. To ensure that the composition was adequately ignited an accurately weighed increment of SR 92 was pressed onto the delay composition. The burning times obtained for the hermetically sealed units incorporating the gasless pyrotechnic caps were as follows :

Mean $\bar{x}$	1.405 s
σ	0.095 s
Range	1.28 to 1.58 s.

Comparative tests have been carried out to determine the amount of gas evolved by the gasless cap and the M42 caps. This was done by firing a number of caps into a fixed volume of 0.5 cm^3 and monitoring the pressure-time characteristics. Representative traces for both the M42 and gasless cap are shown in figure 3 and the peak pressures obtained from these results are as follows :

	Gasless Cap average six readings	M42 average seven readings
Pressure MPa	2.8	35

The bulk of the gas generated when the gasless cap is ignited can be attributed to the tetrazene present in the stab-sensitive composition. Bearing this in mind, further work is planned to investigate the change in sensitivity with tetrazene content.

BIBLIOGRAPHY

1. Dixon, W.J. and Mood, A.M. (1948). A Method for Obtaining and Analysing Sensitivity Data. J. Am. Statist., 43, 109.

2. Voreck, W. and Dalrymple, E.W. Development of an improved stab sensitivity test and factors affecting stab sensitivity of M55 detonators PATR 4570 June 1972.

Fig 1   M42 CAP ASSEMBLY
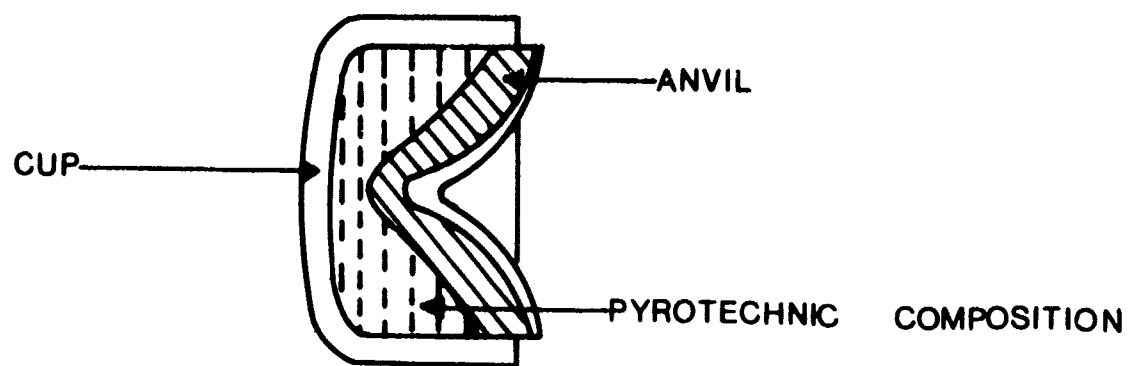
CUP⟶

ANVIL

PYROTECHNIC COMPOSITION

SCALE :-   1 cm = 0·114 cm

8

Fig. 2   GASLESS DELAY

WASHERS

GASLESS CAP

FREE SPACE

SR 92 (50 mg)

DELAY COMPOSITION

6 mm O.D. x 4 mm I.D. BRASS TUBE

B/PbO (60 mg)

GLASS – METAL SEAL

Fig 3   PRESSURE   TIME   CURVES

a   M42 Cap

PRESSURE (MPa)

TIME (ms)

b   Gasless Pyrotechnic Cap

PRESSURE (MPa)

TIME (ms)
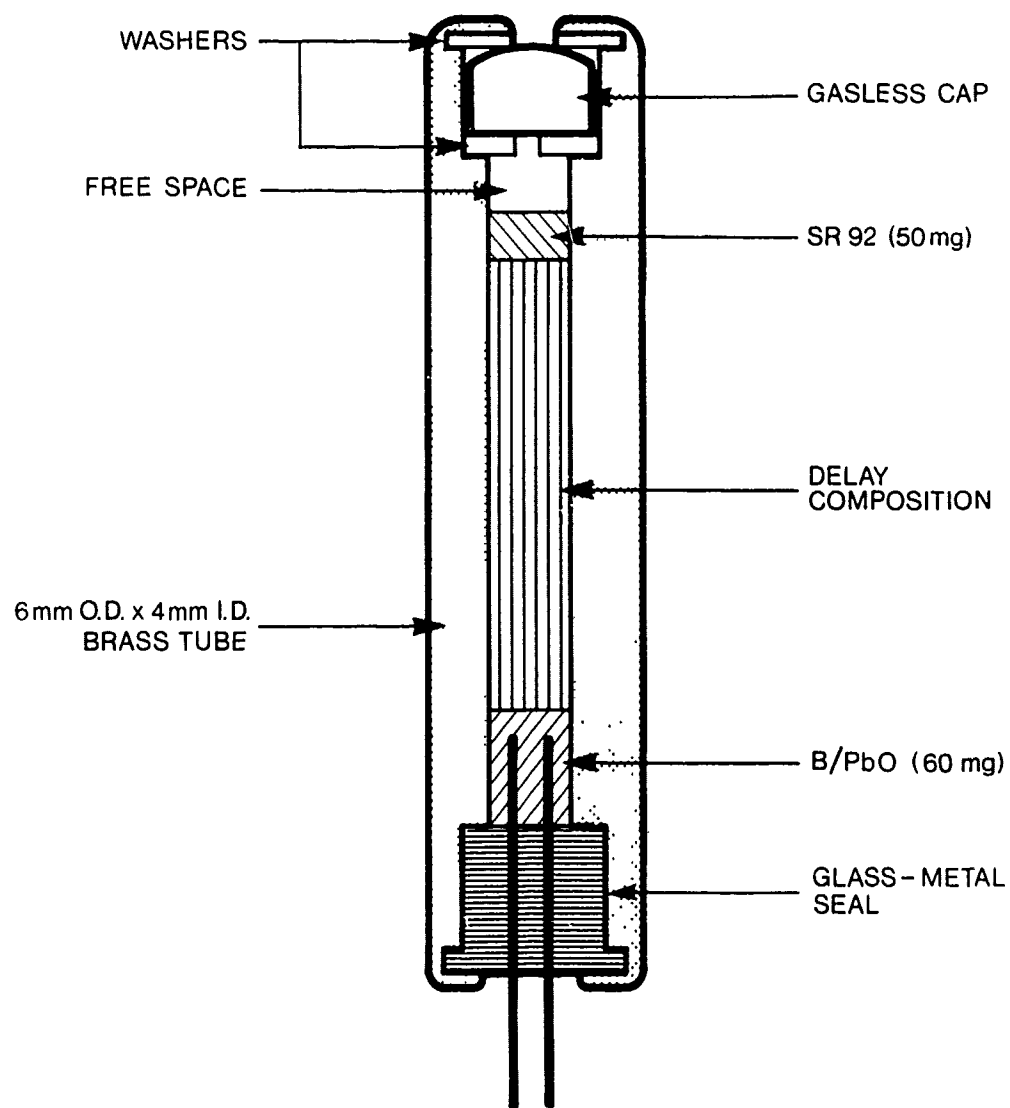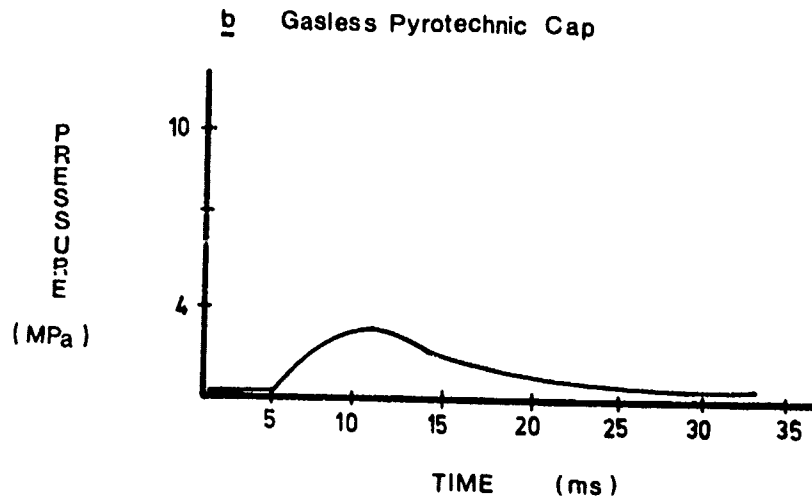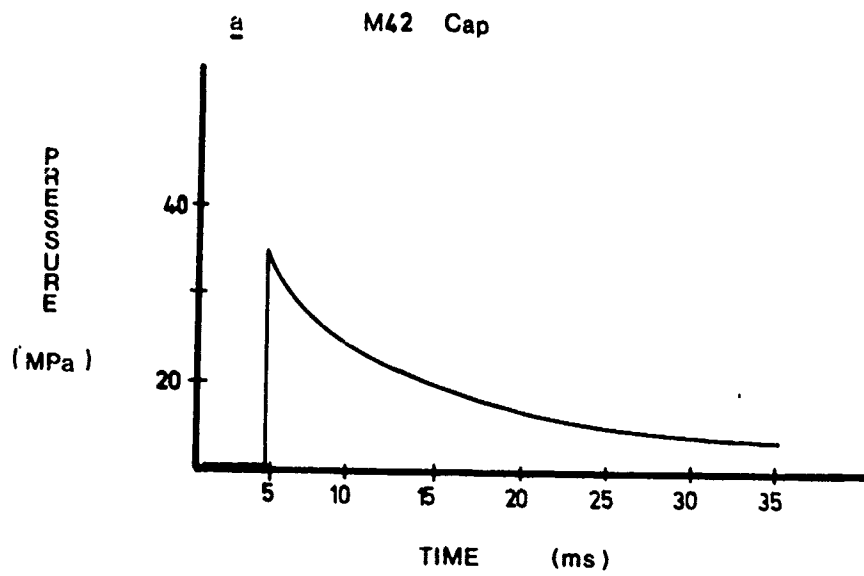
Compaction Studies of Palladium/Aluminum Powders

O. L. Burchett
Sandia Laboratories
Albuquerque, New Mexico

M. R. Birnbaum
Sandia Laboratories
Livermore, California

C. T. Oien
Sandia Laboratories
Livermore, California

A compaction study has been performed comparing pre-
dicted and experimentally determined density gradients in
palladium/aluminum mixtures of differing weight fractions. A
modified constitutive equation for porcus media was used to
predict the density gradients. The predicted density gra-
dients correlated well with radiographic data obtained from
radiographs of compacted pellets. The correlation has esta-
blished that the density gradients in compacted pyrotechnic
pellets can be analytically determined without restorting to
difficult and time consuming radiographic methods.

Compaction Studies of Palladium/Aluminum Powders*

O. L. Burchett
M. R. Birnbaum
C. T. Oien

I. Introduction

The results of an analytical-experimental study of the compaction behavior of palladium/aluminum (Pd/Al) powder mixtures has established that the density profile in Pd/Al powder compacts can be predicted from simple compaction test data. A modified mechanical equation of state for porous materials is fitted to the data obtained from a simple laterally constrained compaction test. The density gradients in the Pd/Al compacts that were predicted from the equation of state correlated well with the density gradients that were obtained from radiographs of the compacted pellets. Once the equation of state is determined for a particular powder, the density profile for a specific compact (i.e., compaction pressure, coefficient of friction and specimen geometry) can be calculated.

The procedure that is used to determine the compaction behavior of the powder first assumes a reasonable three parameter form of the equation of state and utilizes a fitting procedure to determine two of the equation of state's parameters. The third parameter must be assumed a priori. The powder compaction process is modeled as a one-dimensional, time independent, hydrostatic bulk process. ·Additional assumptions include: (1) a constant coefficient of friction between the constraint cylinder and the powder, and (2) an isotropic and homogenous powder. Application of the fitting procedure to the data from a compaction test results in the determination of a representative but non-unique equation of state which describes the powder's compaction behavior.

II. The Compaction Test

The laterally constrained compaction test utilizes a cylindrical constraint die to confine the power and two loading rams, the upper and lower loading rams, to compact the powder. Figure 1 presents a pictorial view of the test assemly. Friction between the constraint cylinder and the powder causes the force transmitted to the lower ram to be

less than the force applied to the upper loading ram. In
addition to the forces in the upper and lower loading rams,
the relative displacement between the loading rams is also
measured. A typical record from a compaction test is shown
in Figure 2. If there is little difference ($\leq 5\%$) between the
upper and lower loading ram forces, the compaction behavior
is easily determined since the compacted powder pellet is
subjected to essentially uniform axial stress and strain;
therefore the conventional engineering stress and strain mea-
sures can be used to convert the compaction test's force-
deflection data to a stress-strain path.

III. Mechanical Equation of State Determinations

The presence of axial stress and strain gradients in the
compacted powder prevents the direct conversion of the powder
compaction experimental force-deflection data to a stress
strain path. The force-deflection data from a laterally con-
strained compaction test consists of the applied and trans-
mitted forces and the relative axial displacement of the
loading rams at m different points along the force deflection
curves. Equilibrium and mass conservation permit the deter-
mination of the coefficient of friction between the constraint
cylinder and the powder and one parameter of the equation of
state at each of the m different data points (F_A, F_T, ΔL).
Consistency in the value of the previously determined para-
meter is used to establish the value of a second parameter.
Unfortunately, experience has shown that a three parameter
equation of state is required to represent the test data, and
since the fitting procedure will determine only two of the
equation of state's three parameters, one parameter must be
assumed a priori. Even though one parameter of the equation
is arbitrarily assumed, the fitting procedure produces a non-
unique but representative equation of state that will repro-
duce the test data.

Initially an equation of state which had been success-
fully used to describe the behavior of porous materials was
assumed[1] but early attempts to fit the equation to some pow-
der compaction test data resulted in the following modifica-
tion of the equation of state

$$\sigma = \sigma_o \left[1 - \left(\frac{\alpha - 1}{\alpha_o - 1} \right)^a \right]^b \tag{1}$$

where a, b, and σ_o are the unknown parameters. The initial
porosity and the porosity at particular normal pressure of σ
are α_o and α respectively. Porosity is defined as the ratio

of void free reference density, ρ_r, of the powder to the powder density, ρ; therefore in terms of the initial density, ρ_0, and the density, ρ,

$$\alpha_0 = \frac{\rho_r}{\rho_0} \tag{2}$$

and

$$\alpha = \frac{\rho_r}{\rho} \tag{3}$$

The strain, ε, is related to the porosity, α, such that

$$\alpha = \alpha_0 (1-\varepsilon) \quad . \tag{4}$$

Alternate forms of the equation of state with density, ρ, and strain, ε, as the independent variables are

$$\sigma = \sigma_0 \left[1 - \left(\frac{\rho_0 \rho_r - \rho_0 \rho}{\rho \rho_r - \rho_0 \rho} \right) a \right]^b \tag{5}$$

and

$$\sigma = \sigma_0 \left[1 - \left(\frac{\alpha_0 - \alpha_0 \varepsilon - 1}{\alpha_0 - 1} \right) a \right]^b \tag{6}$$

The powder compact is assumed to be in the form of a right circular cylinder of length, L, and diameter, D, so that equilibrium of the applied, transmitted and frictional forces requires

$$\frac{\pi}{4} D^2 \sigma_A = \frac{\pi}{4} D^2 \sigma_T + \int_0^L \pi D f \sigma(Z) \, dZ \tag{7}$$

where f is the coefficient of friction between the constraint cylinder and the powder and the other quantities are defined in Figure 3. Lack of knowledge of the variation of the stress, σ, with the axial position, Z, prevents the direct evaluation of the integral in Equation (7). If the cylindrically shaped compact is divided into n equal axial increments

14

of void free reference density, ρ_r, of the powder to the powder density, ρ; therefore in terms of the initial density, ρ_o, and the density, ρ,

$$\alpha_o = \frac{\rho_r}{\rho_o} \tag{2}$$

and

$$\alpha = \frac{\rho_r}{\rho} \tag{3}$$

The strain, ε, is related to the porosity, α, such that

$$\alpha = \alpha_o(1-\varepsilon) \tag{4}$$

alternate forms of the equation of state with density, ρ, and strain, ε, as the independent variables are

$$\sigma = \sigma_o\left[1 - \left(\frac{\rho_o\rho_r - \rho_o\rho}{\rho\rho_r \quad \rho_o\rho}\right)a\right]b \tag{5}$$

and

$$\sigma = \sigma_o\left[1 - \left(\frac{\alpha_o - \alpha_o\varepsilon - 1}{\alpha_o - 1}\right)a\right]b \tag{6}$$

The powder compact is assumed to be in the form of a right circular cylinder of length, L, and diameter, D, so that equilibrium of the applied, transmitted and frictional forces requires

$$\frac{\pi}{4}D^2\sigma_A = \frac{\pi}{4}D^2\sigma_T + \int_0^L \pi D f \sigma(Z)\, dZ \tag{7}$$

where f is the coefficient of friction between the constraint cylinder and the powder and the other quantities are defined in Figure 3. Lack of knowledge of the variation of the stress, σ, with the axial position, Z, prevents the direct evaluation of the integral in Equation (7). If the cylindrically shaped compact is divided into n equal axial increments

15

and a linear variation of the stress, σ, through the axial increment is assumed, equilibrium of the jth increment requires

$$\frac{\pi}{4}D^2 \sigma_j = \frac{\pi}{4}D^2 \sigma_{j+1} + \frac{\pi DfL}{n} \left(\frac{\sigma_j + \sigma_{j+1}}{2}\right) \qquad (8)$$

Therefore the stress, σ_{j+1}, can be expressed in terms of the stress, σ_A, as

$$\sigma_{j+1} = \sigma_j \left(\frac{nD - 2Lf}{nD + 2Lf}\right) \qquad (9)$$

and the transmitted stress, σ_T, in terms of the applied stress, σ_A, as

$$\sigma_T = \sigma_A \left(\frac{nD - 2Lf}{nD + 2Lf}\right)^n \qquad (10)$$

Solving Equation (10) for the unknown coefficient of friction, f, yields

$$f = \frac{nD}{2L} \frac{\left[1 - \left(\frac{\sigma_T}{\sigma_A}\right)^{1/n}\right]}{\left[1 + \left(\frac{\sigma_T}{\sigma_A}\right)^{1/n}\right]} \qquad (11)$$

Conservation of mass requires that

$$\frac{\pi}{4}D^2 L_0 \rho_0 = \frac{\pi D^2 L}{8n} \sum_{j=1}^{n} (\rho_j + \rho_{j+1}) \qquad (12)$$

Equation (1) can be inverted and expressed as

$$\rho_j = \frac{\rho_r}{1 + (\alpha_0 - 1)\left[1 - \left(\frac{\sigma_j}{\sigma_0}\right)^{1/b}\right]^{1/a}} \qquad (13)$$

where

$$\sigma_j = \sigma_A \left(\frac{nD-2Lf}{nD+2Lf} \right)^j \tag{14}$$

after assuming initial values for the parameters, a, b, and σ_o, the correct value of the parameter, b, can be determined by changing the value of b until Equation (12) is satisfied. If Newton's method is used, the value of b should be changed by

$$\Delta b = \frac{\dfrac{2L_o \rho_o n}{L} - \displaystyle\sum_{j=1}^{n} (\rho_j + \rho_{j+1})}{\dfrac{\partial \rho_1}{\partial b} + 2 \displaystyle\sum_{j=2}^{n} \dfrac{\partial \rho_j}{\partial b} + \dfrac{\partial \rho_{n+1}}{\partial b}} \tag{15}$$

with

$$\frac{\partial \rho_j}{\partial b} = \frac{-\dfrac{\rho_r}{\alpha_j^2} \left\{ \ln\left[1 - \left(\dfrac{\alpha_j-1}{\alpha-1}\right)^a \right] \right\}^2 \left(\dfrac{\alpha_o-1}{a}\right) \left(\dfrac{\alpha_o-1}{\alpha_j-1}\right)^{1-a}}{\ln\left(\dfrac{\sigma_j}{\sigma_o}\right)} \tag{16}$$

Ideally the value of the parameter, b, should be material dependent and should not change with each different point along the force deflection curves. If the parameter, b, varies significantly from point to point, the variation can be reduced by changing the parameter, σ_o. The variation $\bar{b}$ of the parameter, b, is defined as

$$\bar{b} = \frac{1}{m} \sum_{i=1}^{n} \text{abs}\left[b_i - \frac{1}{m} \sum_{i=1}^{n} b_i \right]. \tag{17}$$

Each time the parameter, σ_o, is changed, the paramter, b, must be re-evaluated at each of the m points along the force deflection curve. If a change of $\Delta\sigma_o$ in the parameter, σ_o, produces a change in the variation, $\bar{b}$, of $\Delta\bar{b}$, then using Newton's method the new increment of the parameter, σ_o, is

$$\Delta\sigma_{o_{new}} = - \frac{(\bar{b}-\bar{b}_{min})}{\left(\dfrac{\Delta\bar{b}}{\Delta\sigma_o}\right)} \tag{18}$$

17

where the minimum variations in the parameter, $\bar{b}$, is $\bar{b}_{min}$. Experience has shown that the minimum value $\bar{b}_{min}$ of the variation of the parameter, b, is small and is somewhat dependent on the assumed value of the parameter, a.

The powder has been assumed to compact hydrostatically so that the equation of state defines the relationship between the normal stress, σ, and the bulk strain, ε. Unloading is assumed to occur elastically, if after unloading the compacted powder pellet displays shear strength. The elastic modulus (Young's Modulus, E) cannot be determined from the compaction test data without (1) additional information (usually acoustical velocity measurements) or (2) assuming a value for Poisson's ratio, ν. Differentiating the mechanical equation of state with respect to the strain, ε, gives the bulk modulus, K, as

$$K = ab\sigma_o \left(\frac{\alpha_o}{\alpha_o - 1}\right) \left(\frac{\alpha - 1}{\alpha_o - 1}\right)^{a-1} \left[1 - \left(\frac{\alpha-1}{\alpha_o-1}\right)^a\right]^{b-1} \qquad (19)$$

and permits Young's modulus, E, to be written as

$$E = 3(1-2\nu) \; ab\sigma_o \left(\frac{\alpha_o}{\alpha_o-1}\right) \left(\frac{\alpha-1}{\alpha_o-1}\right)^{a-1} \left[1 - \left(\frac{\alpha-1}{\alpha_o-1}\right)^a\right]^{b-1} . \qquad (20)$$

Ten compaction tests were run on three different Pd/Al power formulations. The different powder formulations with respect to weight fractions of the constituents were: 94% Pd - 6% Al, 90% Pd - 10% Al and 80% Pd - 20% Al. Three specimens with the same nominal length-to-diameter ratio were compacted for each of the Pd/Al powder formulations. One additional compaction test was performed on a 94/6 Pd/Al specimen with a different length-to-diameter ratio. A summary of the test results is presented in Table I. Plots of the porosity ratio, α, versus the compaction pressure, σ, are presented in Figures 4 through 6 for each of the three different Pd/Al powder formulations. The results show that the porosity ratio versus the compaction pressure curves for each Pd/Al formulation have a scatter of less than 5%. Apparently the procedure that is used to determine the equation of state is relatively insensitive to the specimen geometry since a change in the length-to-diameter (L/D) ratio (see the results of 94/6 - 4, Table I) did not appreciably

affect the equation of state parameters. The coefficient of friction typically had a linear increase of 20% over the range of compaction pressures.

IV. Radiographic Procedure

Density variations as a function of Z are determined for the various Pd/Al compacts by radiographic techniques in conjunction with a scanning microdensitometer. The compacts are radiographed in the Macor* holder along with an empty Macor holder and a Pd step wedge with an Ir-192 gamma ray source to a background film density of 3.5. The imaging medium is Kodak R film with 5 mil Pb intensifying screens. Considerable effort was taken to reduce the noise level on the radiographs in order to minimize the error in the density calculations. Figure 7 shows a radiograph of a Pd/Al powder compact in its Macor holder, an empty Macor holder, and the Pd step wedge. The microdensitometer scans the radiograph on the lines indicated in Figure 7. Scans A and C are background readings which are averaged and then subtracted from scan B which is the powder compact in the Macor holder. The empty Macor and the step wedge are then scanned and corrected for local background variations. The corrected empty Macor scan is then subtracted from scan B to give the optical transmission as a function of Z for the powder compact alone. From the corrected step wedge scan a plot of optical transmission versus Pd thickness is obtained. Comparing the optical transmission of the powder compact to that of the step wedge an equivalent thickness, t_e, of Pd can be determined for the compact. Knowing the thickness, D, of the compact and the density, ρ_{Pd}, of the palladium, the density, ρ_c, of the compact versus Z can be expressed as

$$\rho_c(Z) = \frac{\rho_{Pd}\, t_e(Z)}{D} \tag{21}$$

V. Calculations and Experimental Results

Three Pd/Al weight ratios were investigated using the previously derived mechanical equations of state - 94/6,

---

*Macor is a Corning Glass Works Trademark for machinable glass ceramic code 9658

19

90/10, and 80/20. For a powder compact diameter of 6.35 mm
density calculations for the 94/6 mixture were performed for
three L/D ratios - 0.5, 1.0, and 5.0, corresponding to differ-
ent numbers of pressing increments needed to produce a powder
compact 31.8 mm in length. The coefficient of friction, f,
between the Macor holder and the particular Pd/Al powder
formulation was determined by substituting the relationship*

$$\sigma_j = \sigma_A e^{-4jfL/nD} \tag{22}$$

into equation (13) and requiring the coefficient of friction
to take a value which conserved the compact's mass. The
density profiles are given in Figure 8. To produce powder
compacts with a shallow gradient the ten increment compact
(L/D = 0.5) was selected and employed for all ratios. The
axial density variations were also computed for the 90/10 and
80/20 mixtures for (L/D) = 0.5 and the density profile vari-
ation from composition to composition was determined to be
small (Figure 9). The next three figures (Figures 10-12)
compare the measured and calculated densities for the three
L/D ratios for 94/6 and the agreement is quite good. For
L/D = 5.0 (Figure 10) the measured values go to zero at the
latter end of the powder compact since the powder was not
compacted during the pressing operation and fell out upon
removal from the pressing fixture. For the other two cases,
where multiple pressings were required to produce a complete
powder compact, both the first and last pressing measurements
are included since these tended to be different due to fix-
uring constraints. The agreement between the measured and
calculated density profiles for the 90/10 and 80/20 mixtures
were very similar to those shown in Figure 12 for the 94/6
ratio.

Using the same mechanical equation of state, density
profiles for 94/6 were also calculated for a smaller (2.54 mm)
diameter powder compact. A comparison between it and the
larger diameter results are given in Figure 13. These results
are very comparable to the L/D = 1.0 and 0.5 computations
already shown in Figure 8, and this is to be expected since

---

*Equation (22) was obtained by integrating the differential
equation which defines equilibrium of an axial slice of
cylindrical shaped powder compact, i.e.,

$$\frac{d\sigma}{\sigma} = -\frac{4f}{D} dL \tag{23}$$

the calculations depend only upon L/D and not upon the powder
compact diameter explicitly. In comparing the measured and
computer results for the small diameter powder compact for
the three powder ratios (Figures 14-16), it is seen that
assuming the mechanical equation of state to be invariant
with respect to powder compact diameter is an excellent
assumption.

VI. Closure

Excellent agreement was obtained between the calculated
and measured density profiles of a series of Pd/Al powder
compacts. The density profiles were calculated from mechani-
cal equations of state that were obtained from compaction
tests, while a radiographic technique was used to determine
the actual density profiles. The mechanical equations of
state were nonunique but realistic representations of the
Pd/Al powder's compaction behavior. A number of assumptions
were made in developing the procedure to determine the equa-
tion of state that represent approximations of the real com-
paction process. The principal assumptions were: (1) the
compaction process is a hydrostatic, one-dimensional process,
(2) the coefficient of friction between the constraint cylin-
der and the powder is independent of pressure, (3) the powder
does not have any significant time dependent behavior, and (4)
unloading does not produce any significant density changes.
Two-dimensional effects resulting from friction between the
constraint die and the powder and between the powder particles
were neglected. Studies[2] have shown that the radial vari-
ation in the density of other powder compacts is 10 to 15%.
The effect of friction between the constrain die and the pow-
der is considered to be much greater than the effect of
interparticle friction[3].

References

1. W. Hermann, J. Appl. Phys., 2490, <u>40</u> (1969).

2. H. Unckel, Arch. Eisenhutteniw, 18, <u>161</u> (1945).

3. R. P. Seelig and J. Wulff, Trans., Am. Inst. Mining Met.
   Engrs., 166, <u>492</u> (1946).

Table I

SUMMARY OF PALLADIUM-ALUMINUM POWDER COMPACTION TESTS

Palladium-Aluminum Powder Formulation	Parameter a	Parameter b	Parameter σ_o in Mpa	Initial L/D Ratio	Final L/D Ratio	Initial Porosity Ratio, α_o	Initial Density, ρ_o	Reference Density, ρ_o' in G/CC	Average Coefficient of Friction, f*
94/6-1	.125	1.813	3035	.553	.325	2.860	3.476	9.944	.1983
94/6-2	.125	1.807	2790	.554	.321	2.868	3.467	9.944	.2427
94/6-3	.125	1.767	2840	.546	.327	2.828	3.516	9.944	.2518
94/6-4	.125	1.811	2474	1.124	.644	2.909	3.419	9.944	.2181
90/10-1	.125	1.608	1847	.639	.366	2.970	3.005	8.925	.2129
90/10-2	.125	1.619	1843	.641	.368	2.977	2.998	8.925	.2432
90/10-3	.125	1.627	1971	.668	.383	3.103	2.876	8.925	.2480
80/20-1	.125	1.566	1579	.739	.437	2.734	2.599	7.104	.2601
80/20-2	.125	1.558	1526	.732	.431	2.705	2.626	7.104	.2546
80/20-3	.125	1.519	1438	.726	.433	2.685	2.645	7.104	.2538

*For a steel die with a diameter of 6.424 cm.

**Figure 1 - Cutaway of a Typical Laterally Constrained
Compaction Test Assembly for Powder Compacts**

Upper
Loading
Ram

Constraint
Cylinder

Powder
Compact

Lower
Loading
Ram

23
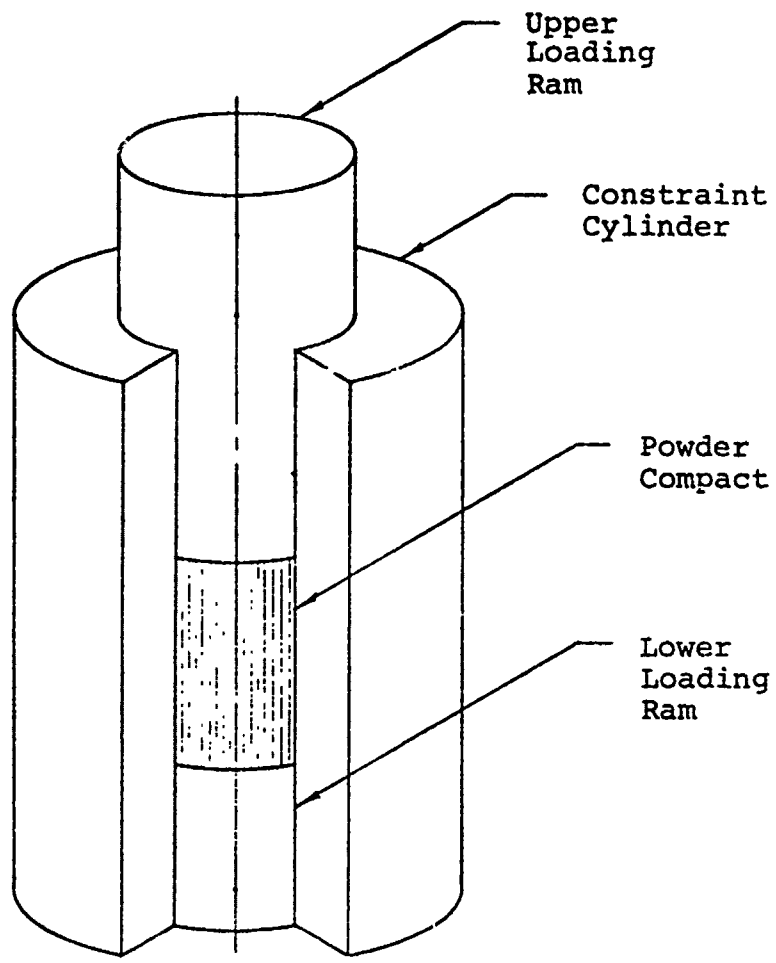
Figure 2 - Typical Data from a Laterally Constrained Compaction Test

Applied Force or Stress Upper Loading Ram

Force or Stress

Transmitted Force or Stress Lower Loading Ram

Relative Loading Ram Deflection or Engineering Strain
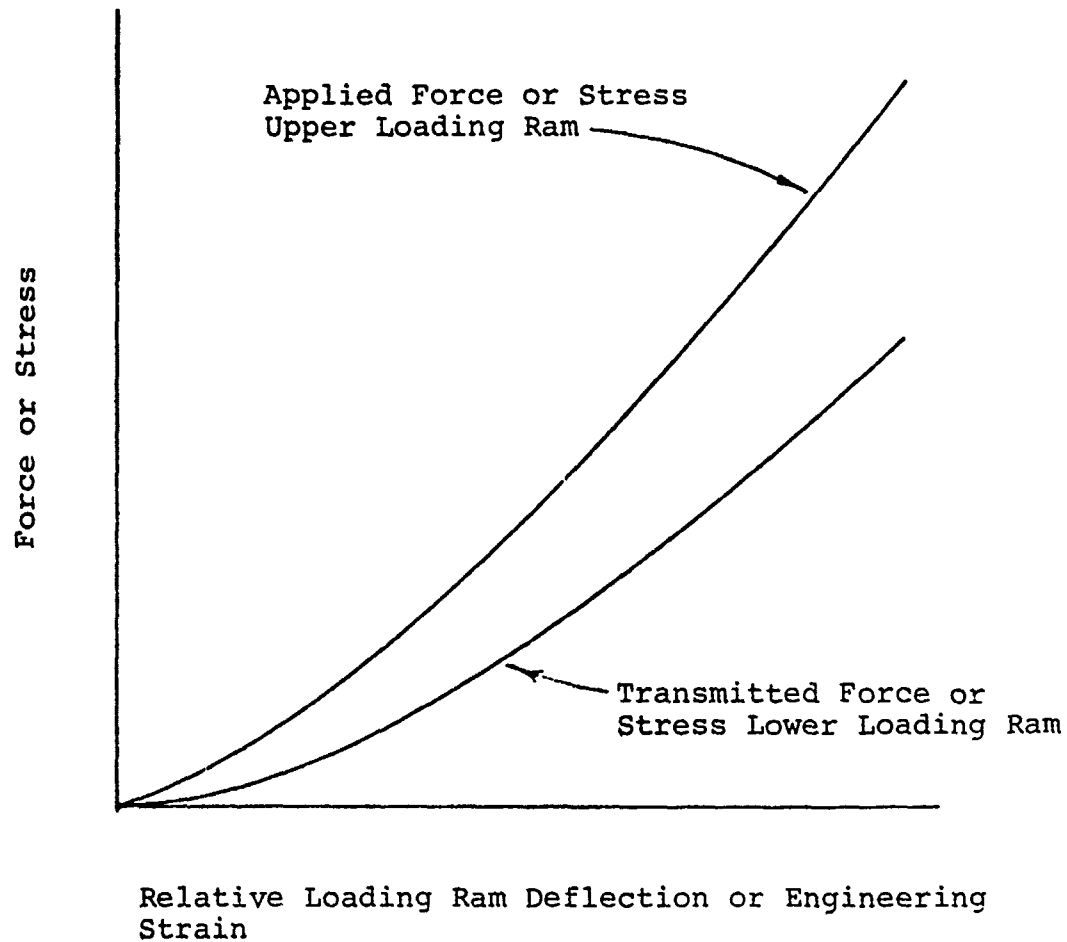
Figure 3 - Normal and Shear Stresses That Act on a Powder Compact
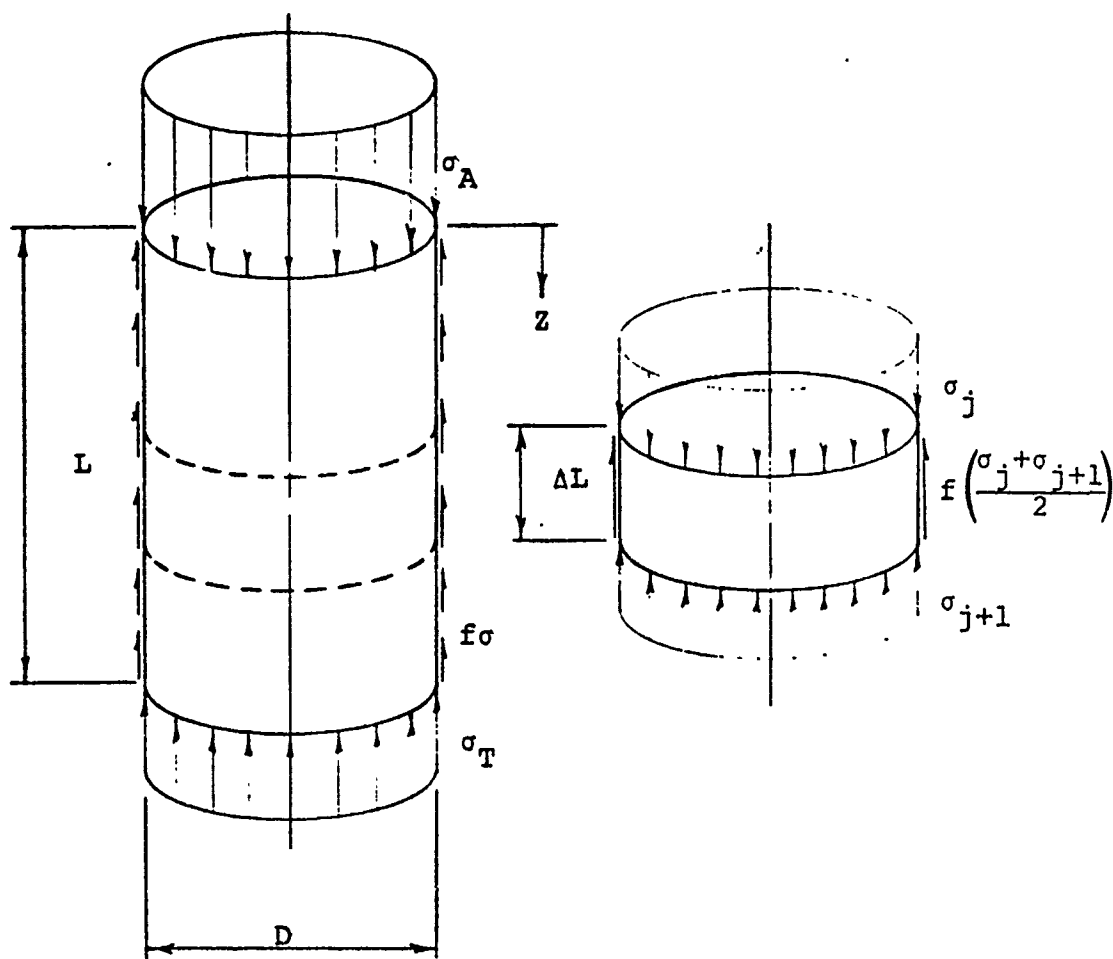
Figure 4 — Porosity Ratio Versus Compaction Pressure for the 94/6 Pd/Al Powder Compacts
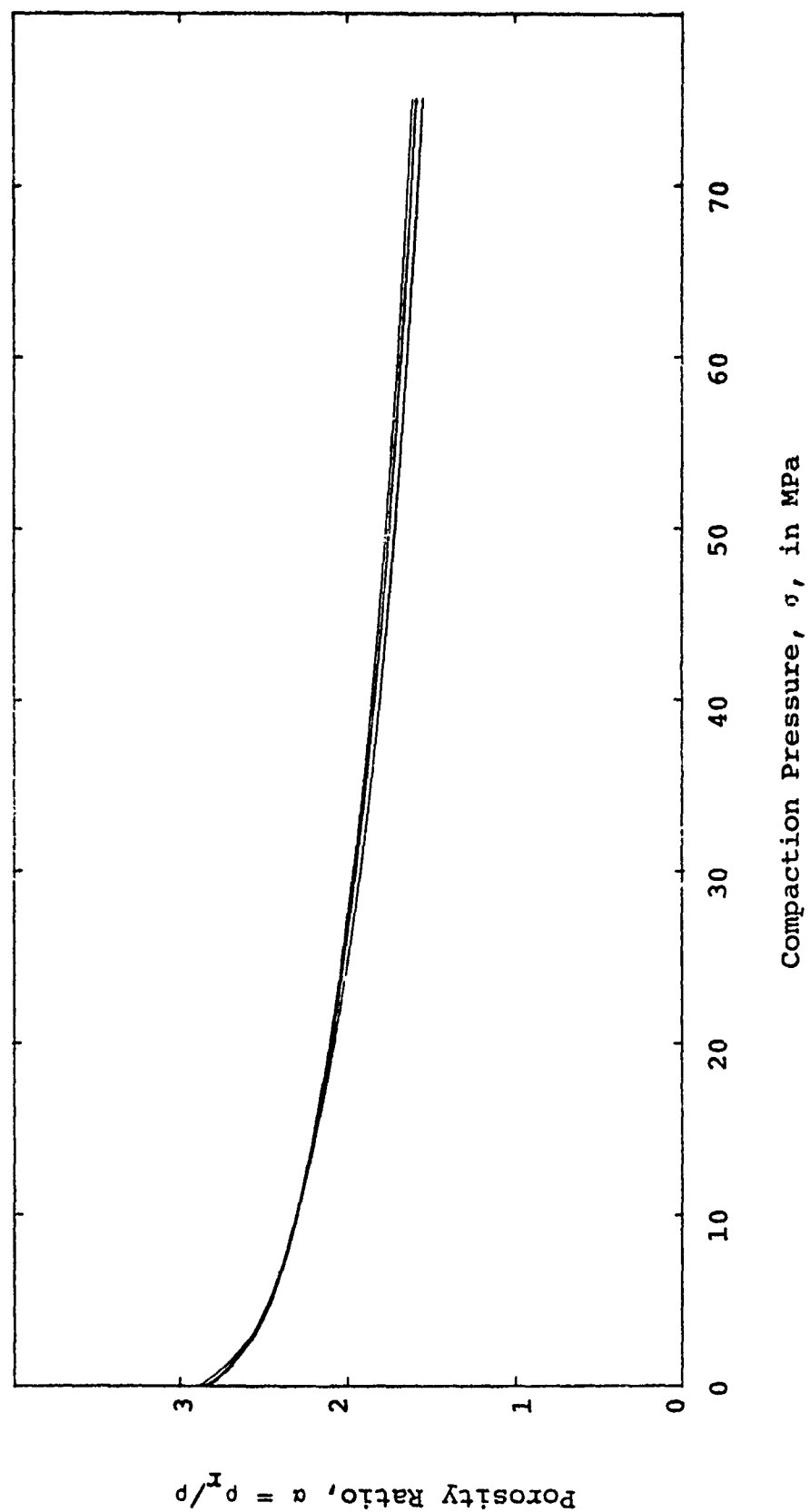
Figure 5 – Porosity Ratio Versus Compaction Pressure for the 90/10 Pd/Al Powder Compacts
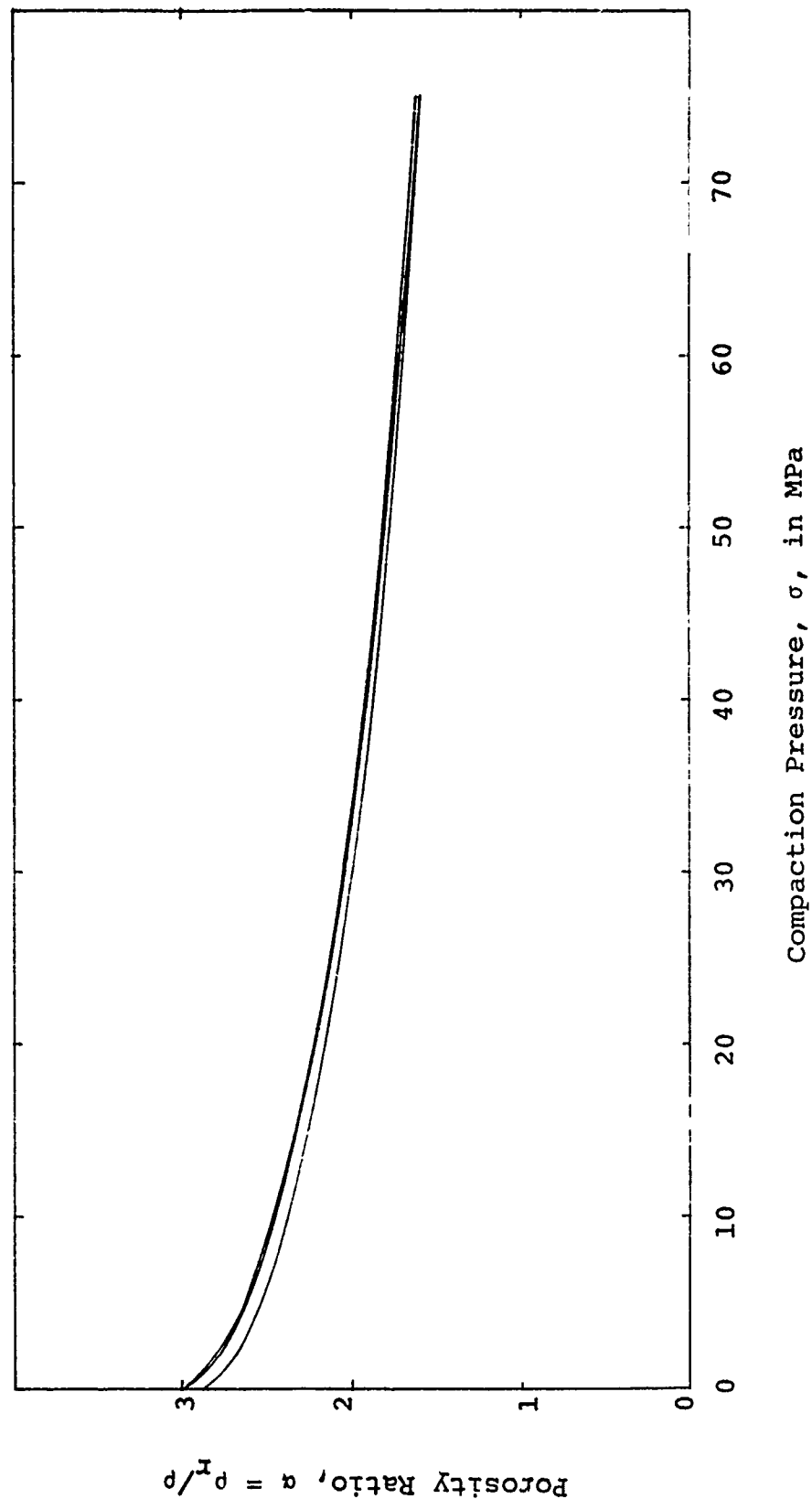
Figure 6 — Porosity Ratio Versus Compaction Pressure for the 80/20 Pd/Al Powder Compacts

28
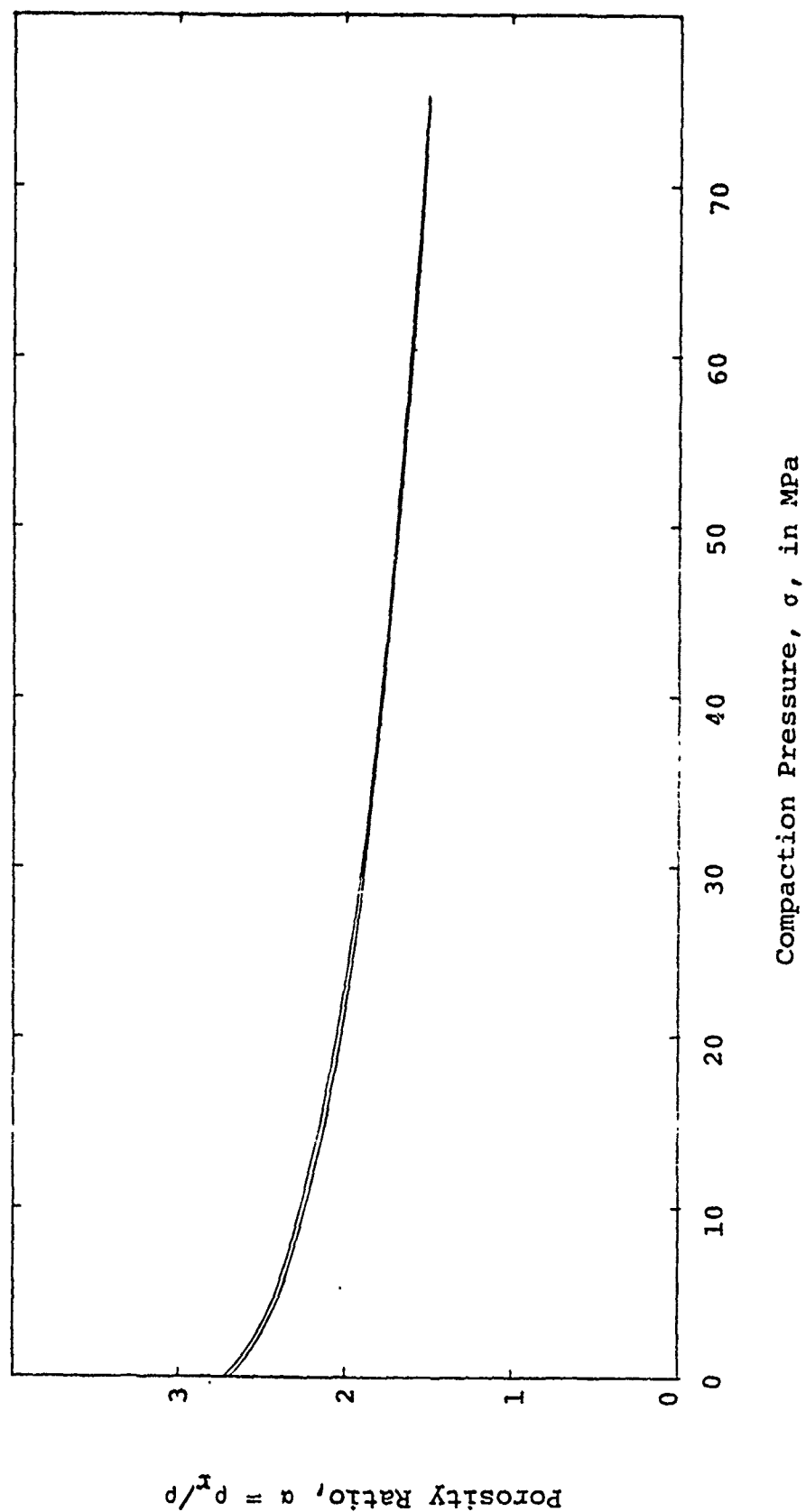
Figure 7 - Radiographic Setup to Determine The Density of a Pd/Al Compact

Pd Step Wedge

G   H   I

Powder Compact in Macor   Empty Macor

A   B   C   D   E   F

last pressing

L

Z

L

first pressing

D
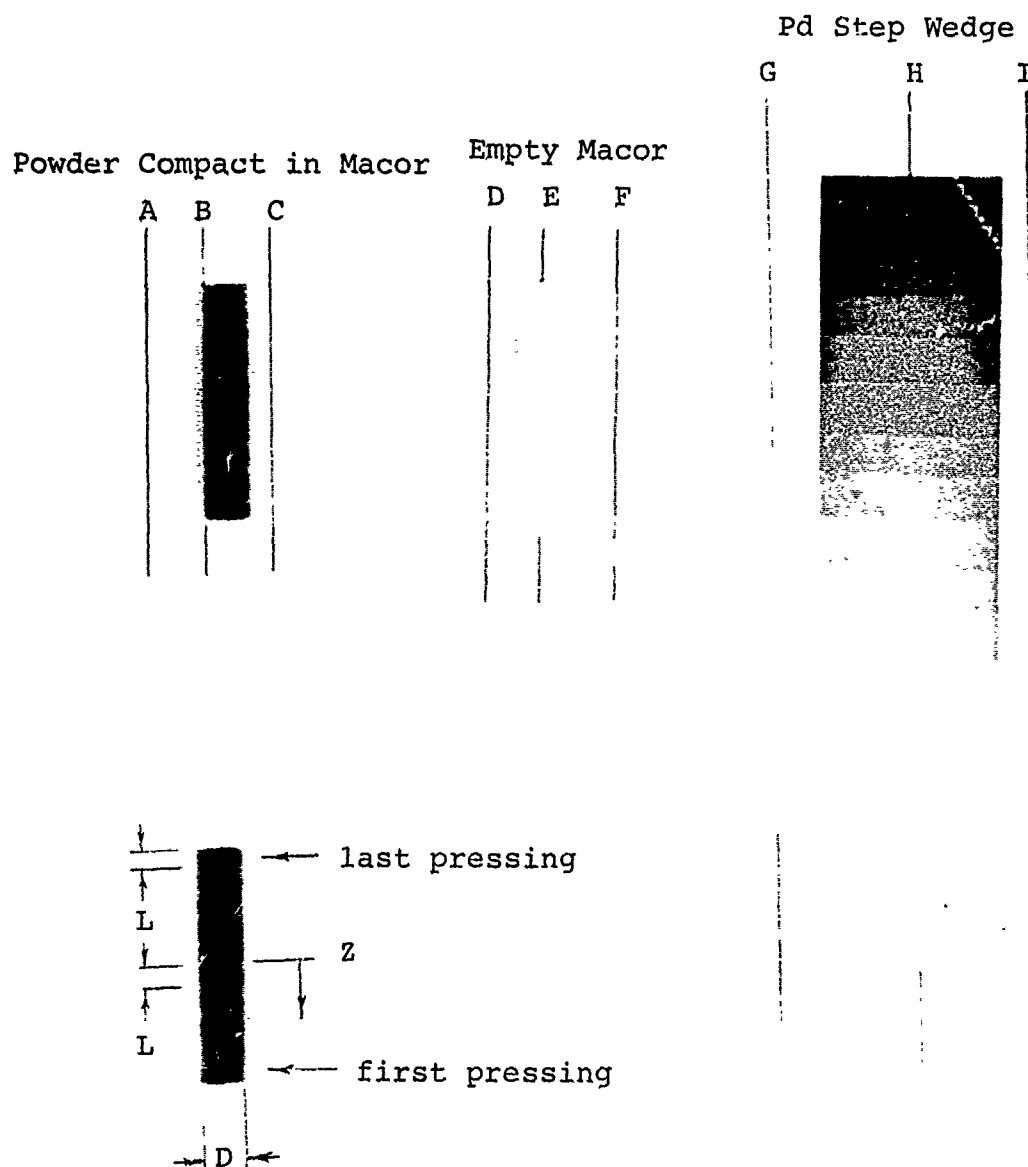
Figure 8 - 94/6 - Pd/Al, Calculated Density
Variation Versus the Number of Pressing
Increments (Diameter = 6.35 mm)
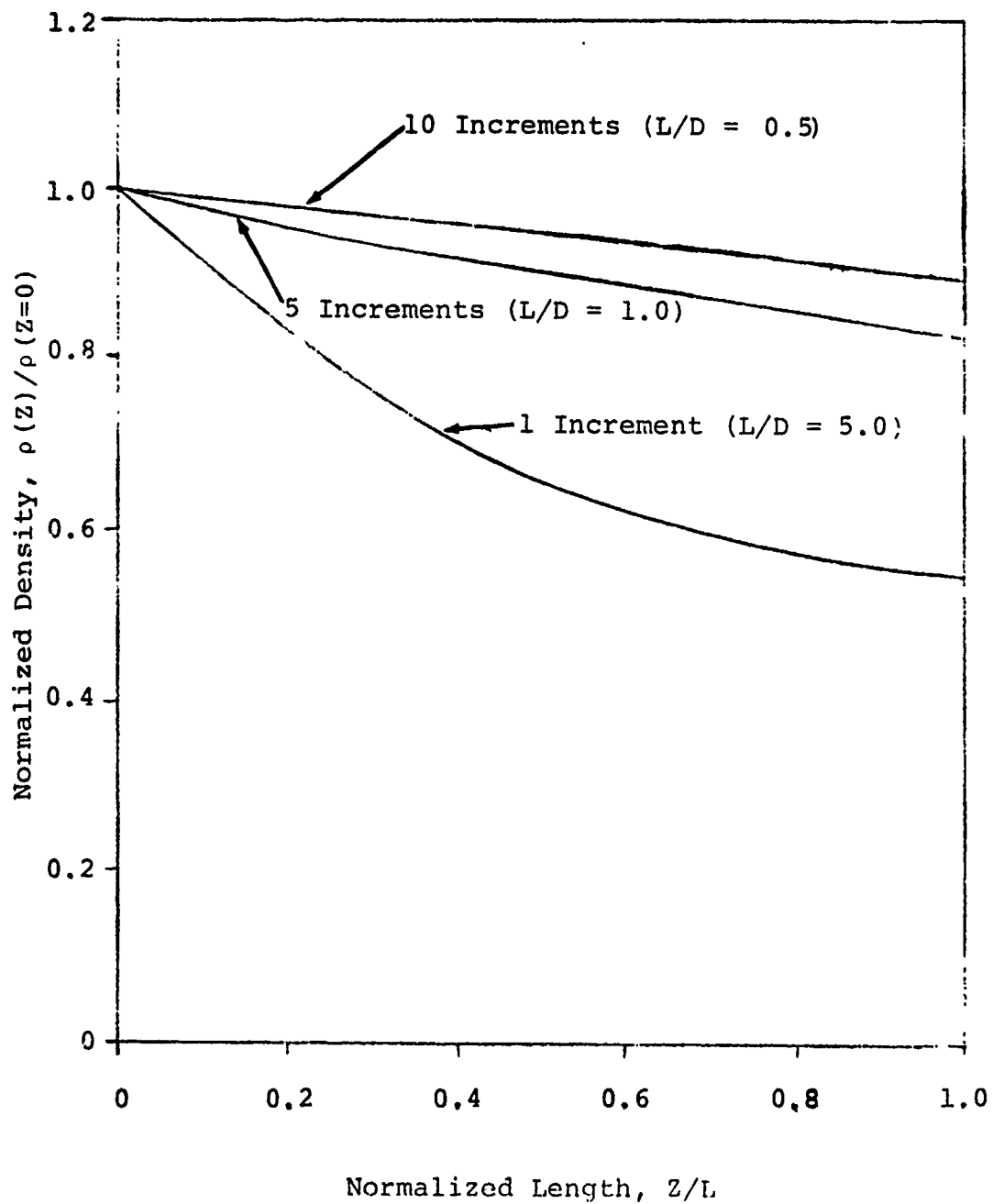
Figure 9 – Calculated Pd/Al Density Variation
Versus the Powder Material (10 Pressing
Increments, (L/D = 0.5) Diameter = 6.35
mm)
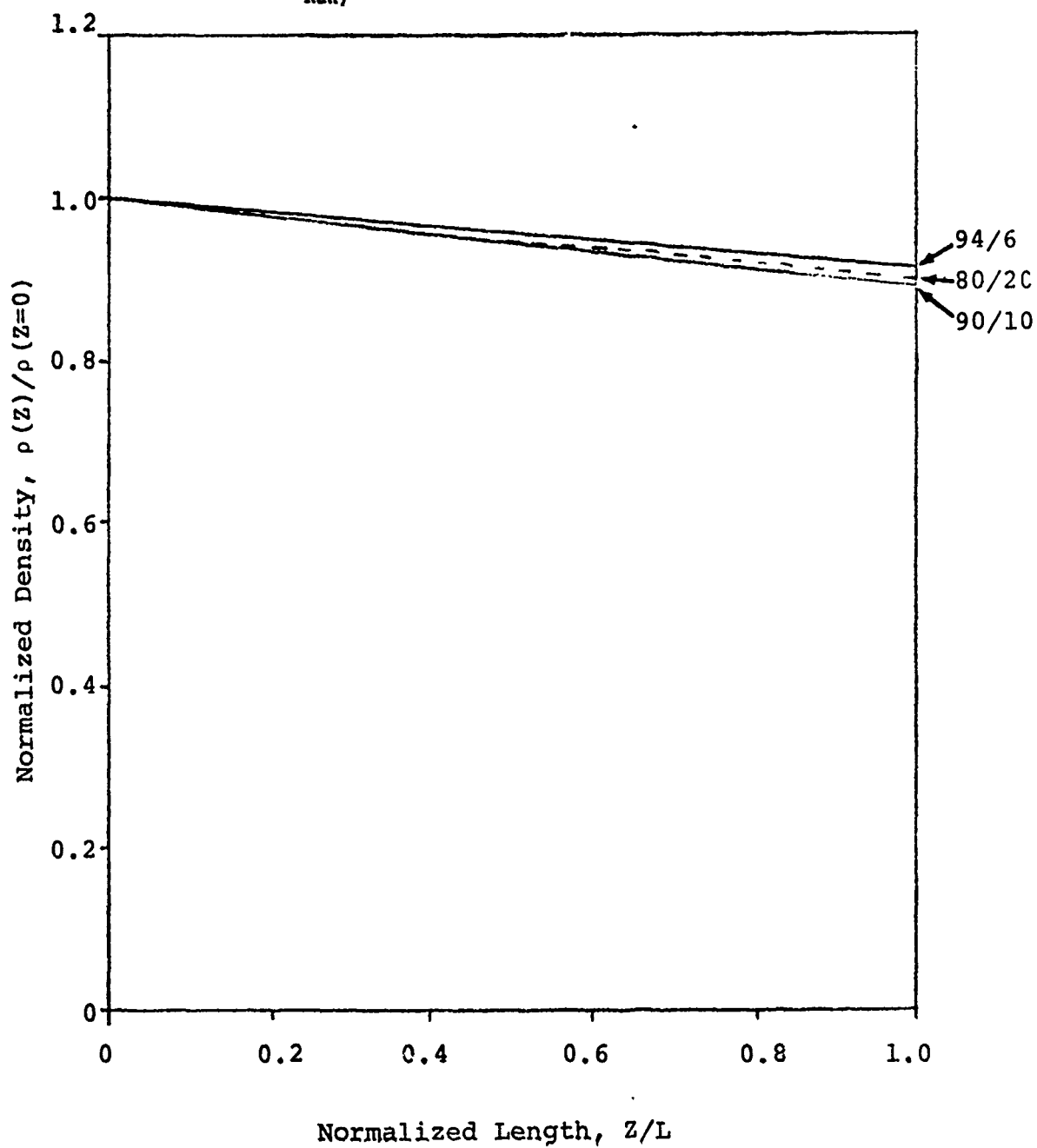
Figure 10 - 94/6 - Pd/Al, Comparison of Calculated and Measured Density Gradient (1 Pressing Increment, L/D = 5.0, Diameter = 6.35 mm)

Calculations

Measurements of Powder Compact 3

Normalized Length, Z/L
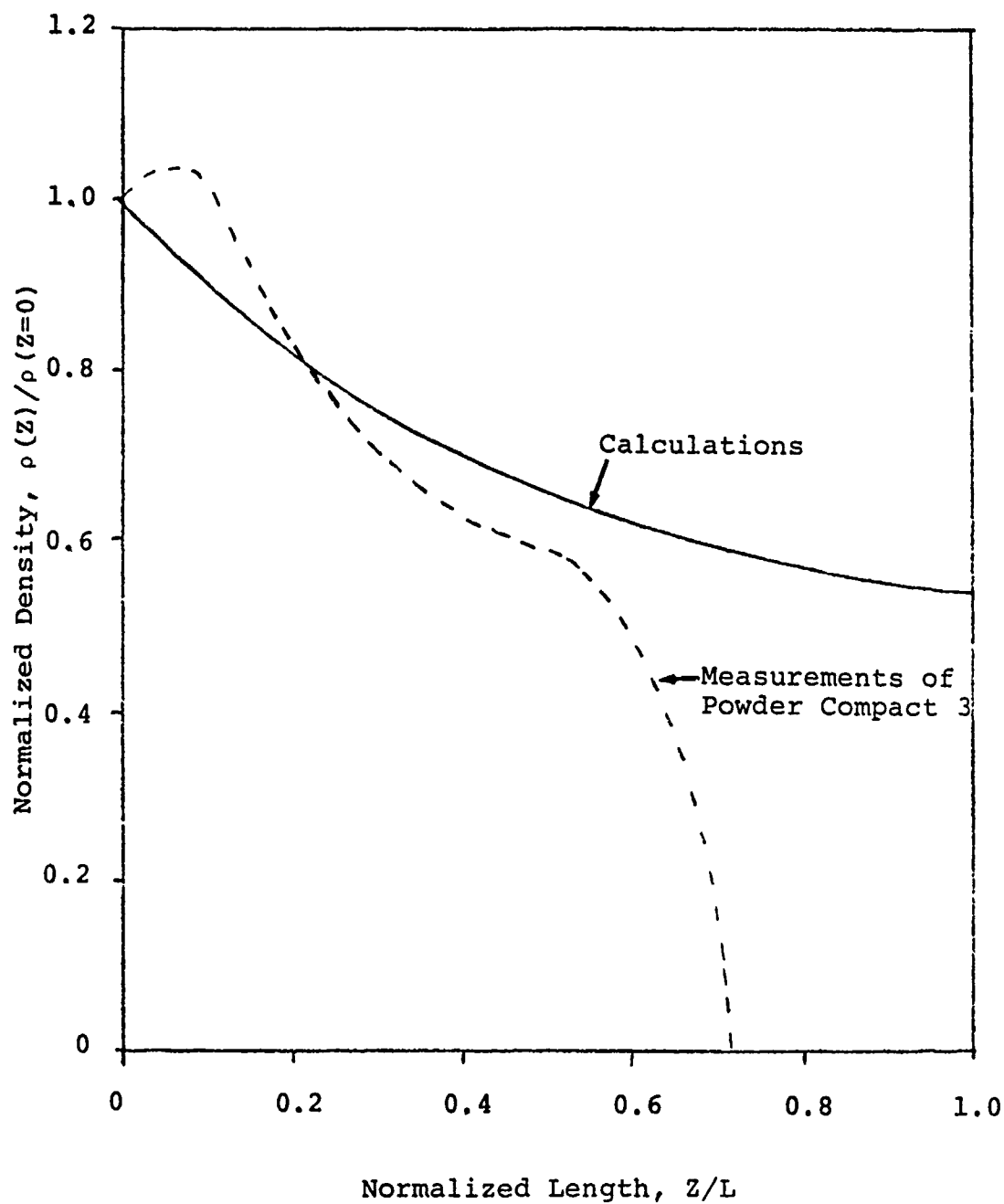
Figure 11 - 94/6 - Pd/Al, Comparison of Calculated and
Measured Density Gradients (5 Pressing Incre-
ments, L/D = 1.0, Diameter = 6.35 mm)
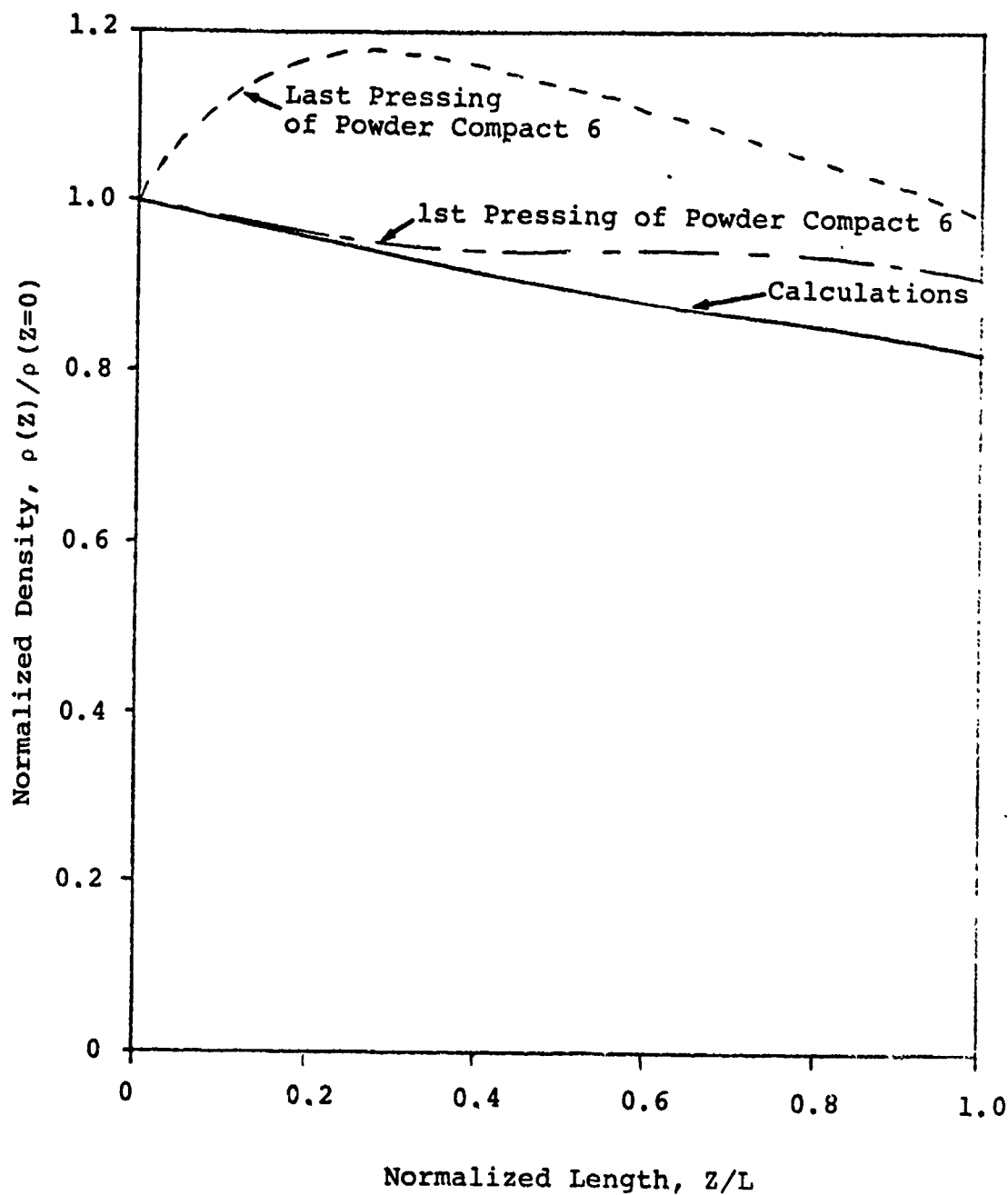
Figure 12 - 94/6 - Pd/Al, Comparison of Calculated and Measured Density Gradients (10 Pressing Increments, Diameter = 6.35 mm)
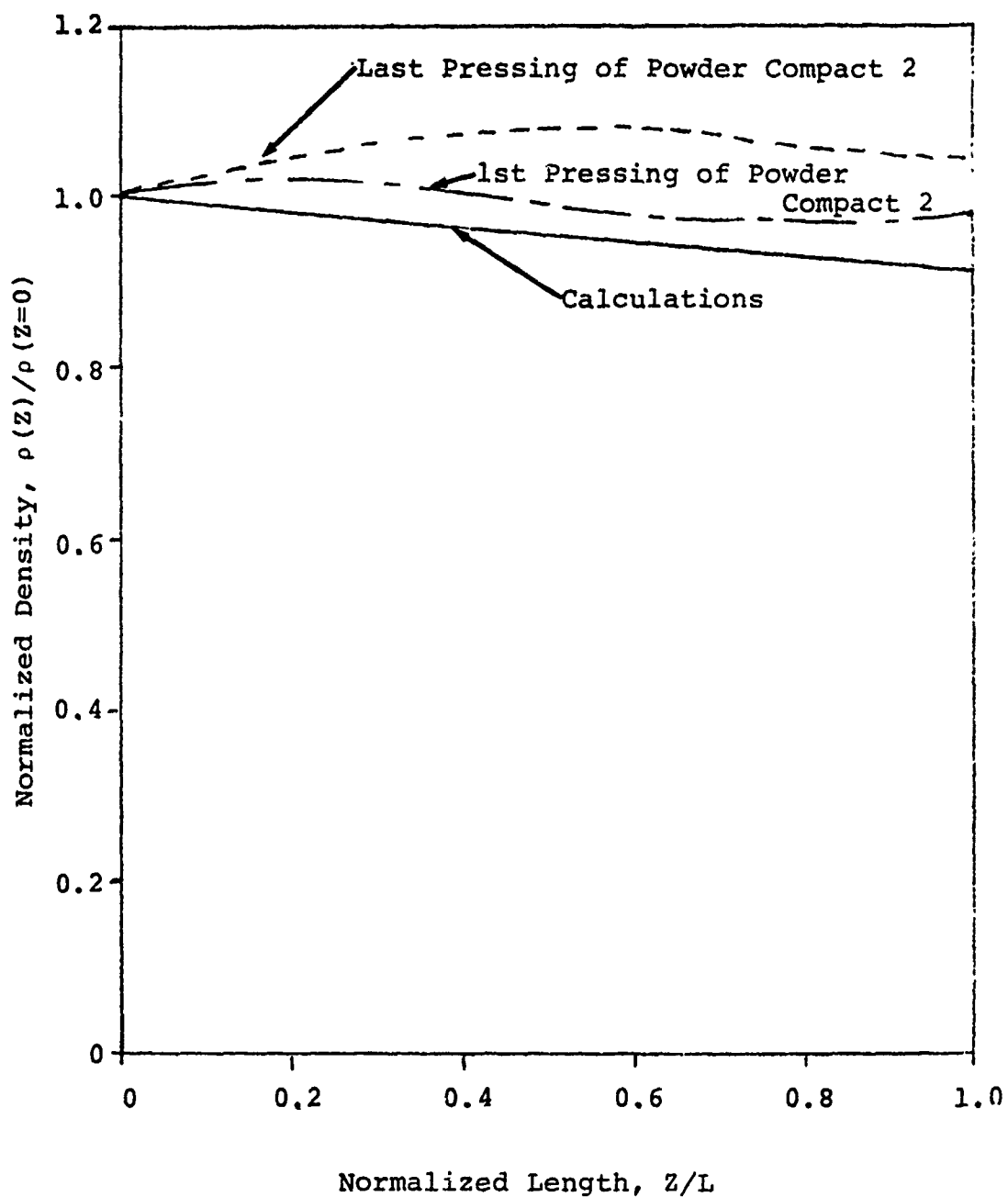
Figure 13 - 94/6 - Pd/Al Calculated Density Variation Versus the Powder Compact Diameter (10 Pressing Increments)
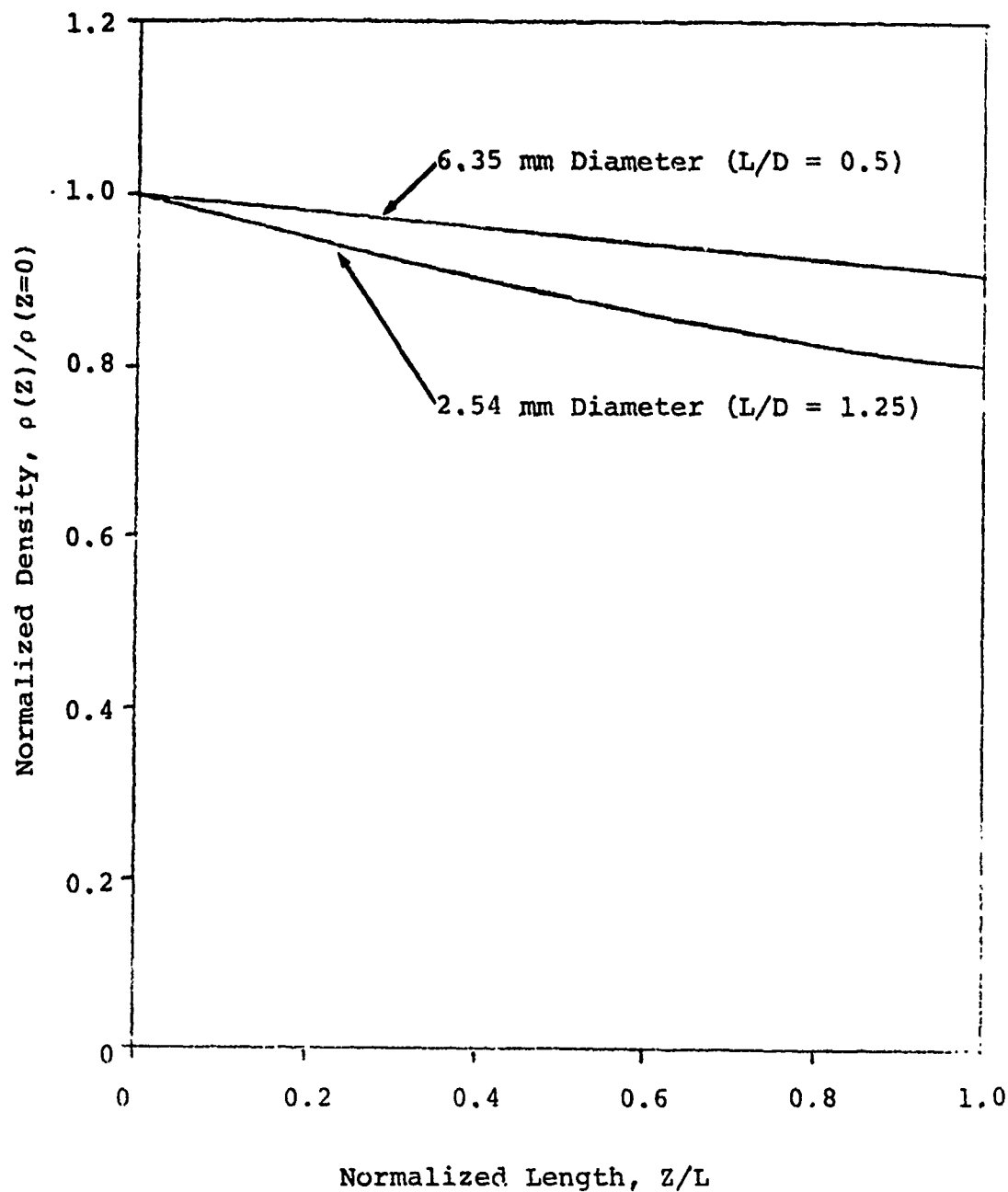
Figure 14 - 94/6 - Pd/Al, Comparison of Calculated and Measured Density Gradients (10 Pressing Increments, L/D = 1.25, Diameter = 2.54 mm)
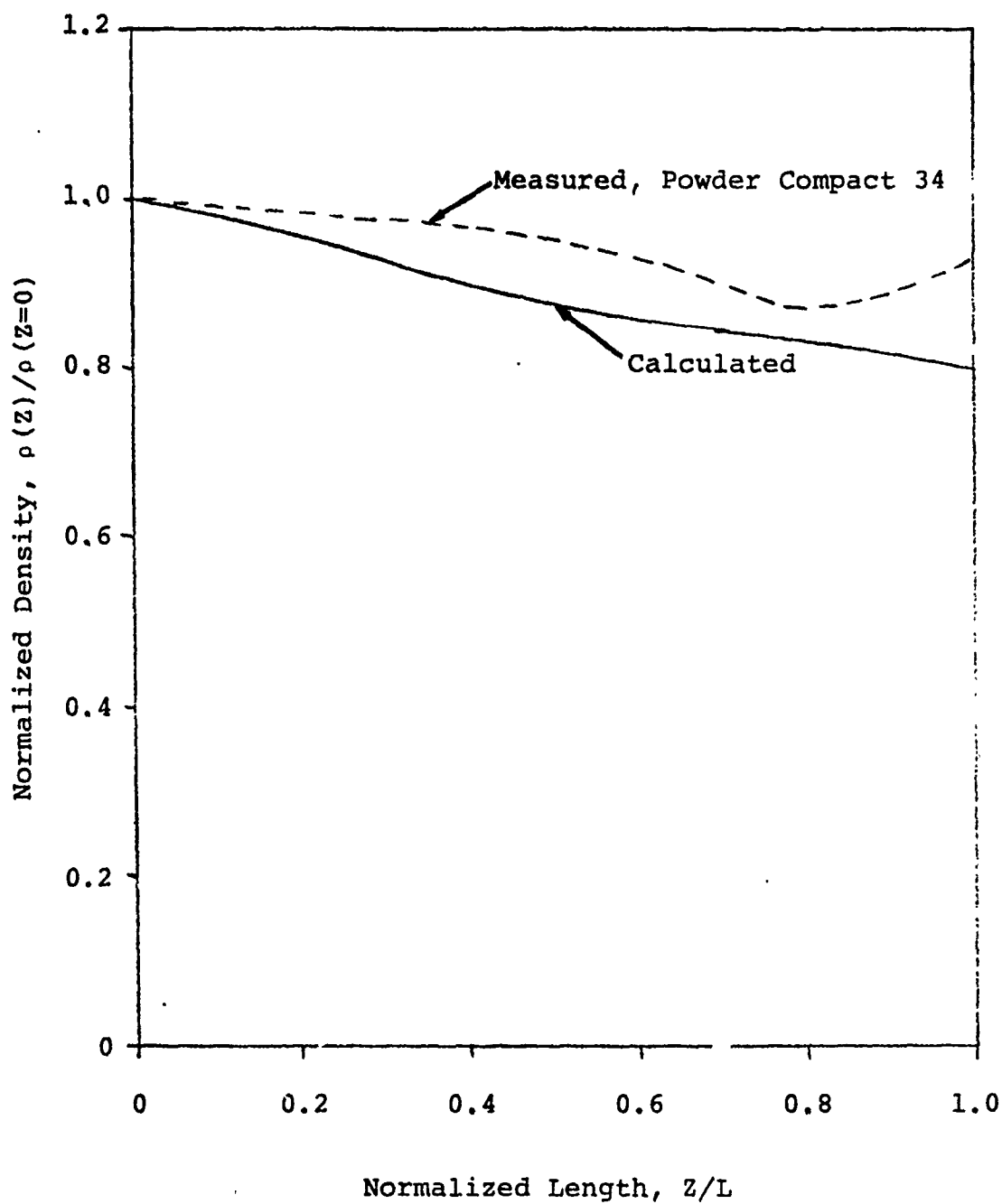
Figure 15 - 90/10 - Pd/Al, Comparison of Calculated and Measured Density Gradients (10 Pressing Increments, L/D = 1.25, Diameter = 2.54 mm)
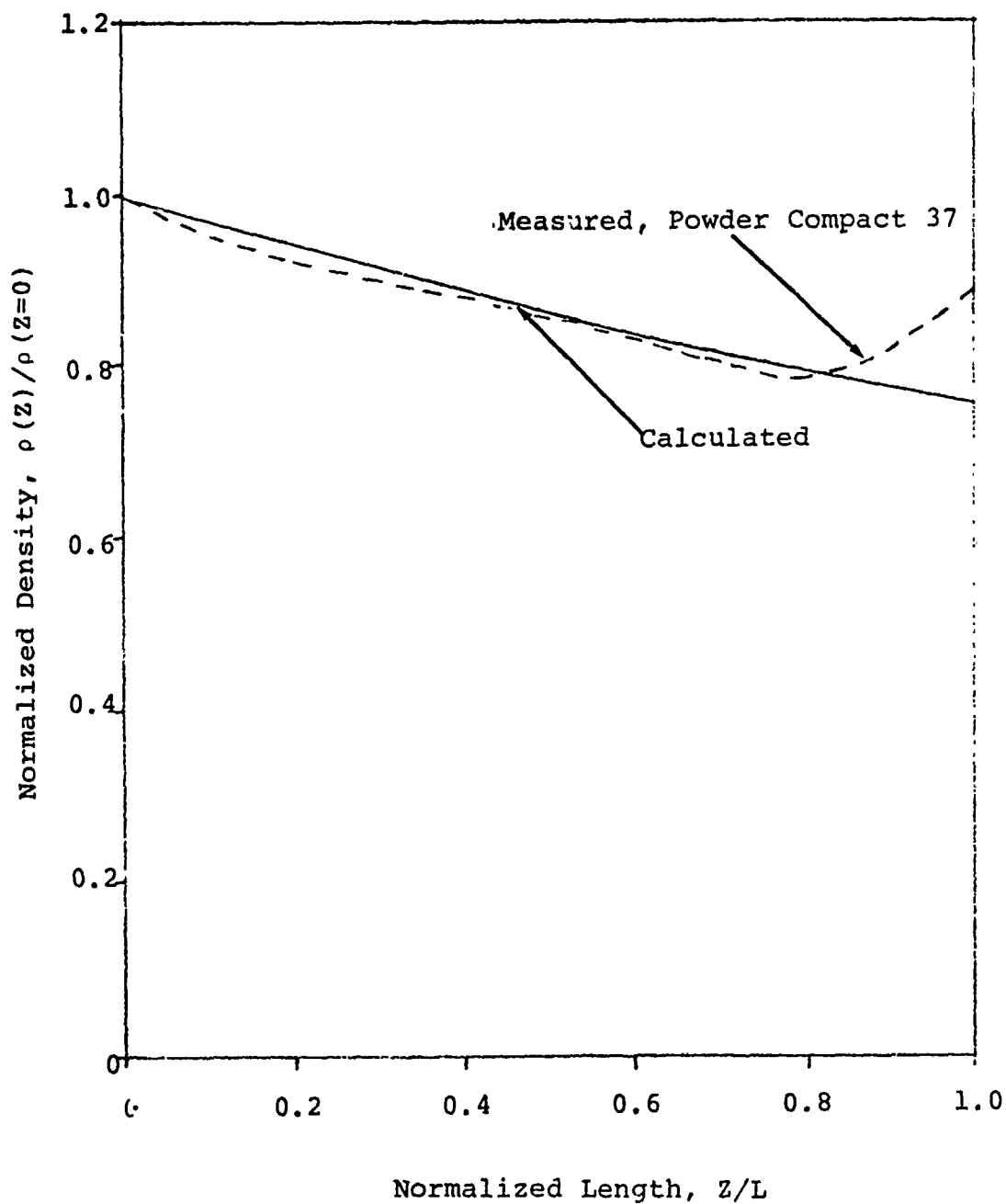
Figure 16 - 80/20 - Pd/Al, Comparison of Calculated and Measured Density Gradients (10 Pressing Increments, L/D = 1.25, Diameter = 2.54 mm)
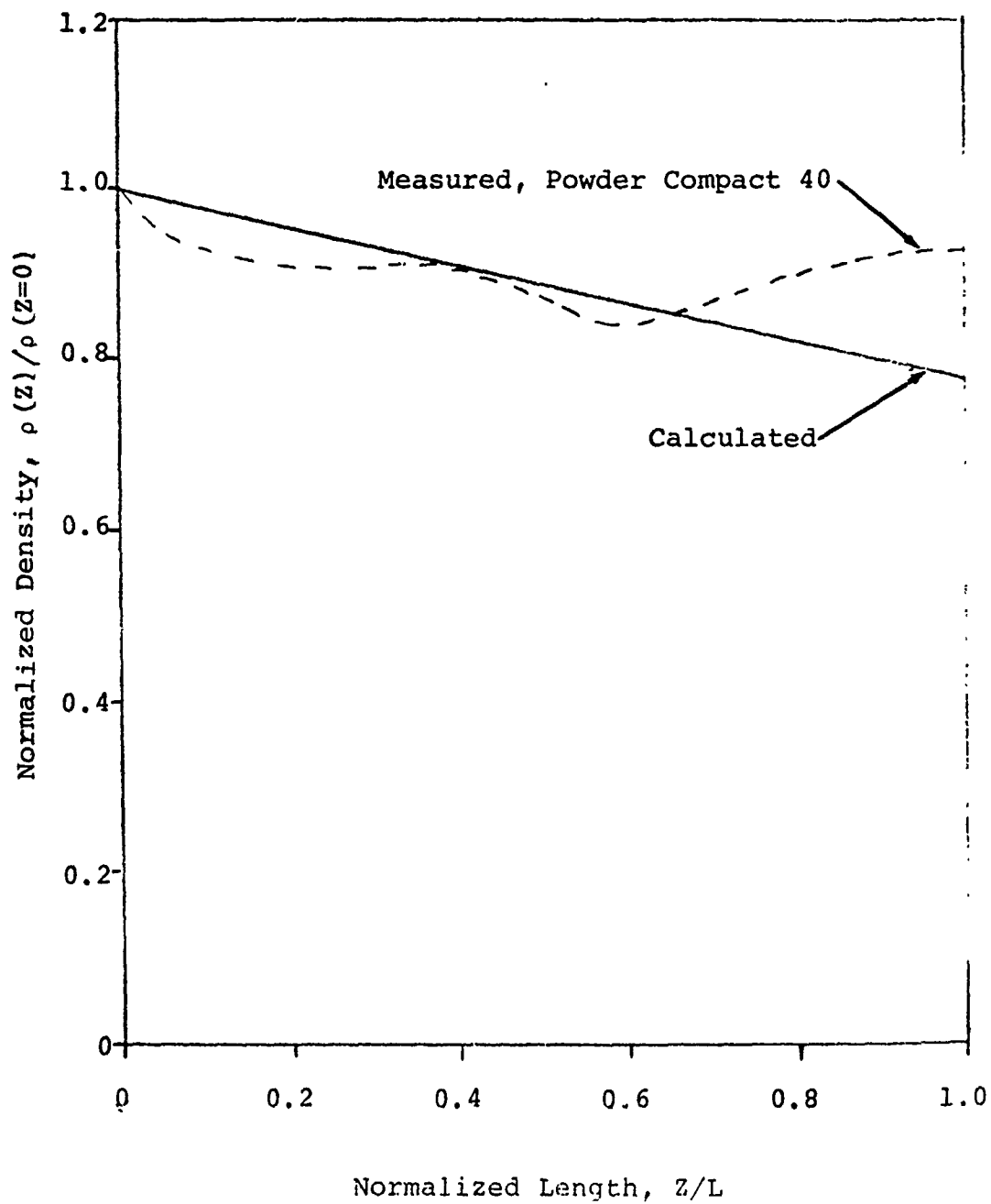
DETERMINATION OF PALLADIUM/ALUMINUM REACTION PROPAGATION RATES AND TEMPERATURES*

Michael R. Birnbaum
Sandia Laboratories
Livermore, CA 94550

ABSTRACT

Three experimental techniques--thermometry, framing and streaking photography, and dynamic radiography--were employed to determine the reaction propagation rates and temperatures of various mixtures of palladium and aluminum. Pellets of 94/6, 90/10, and 80/20 Pd/Al mixtures with an average density of 5×10^3 kg/m^3 were prepared and tested in an insulating sleeve. Pretest radiography was used to determine the density in the Pd/Al pellet as well as to observe any anomalies in the pressing of the pellet that might affect the performance of the pyrotechnic. Propagation rates were found to be ~40 mm/sec for 94/6 and ~500 mm/sec for 90/10 and 80/20. The burn temperatures were found to be ~1400°C for 94/6 and ~2400°C for 90/10 and 80/20. One-dimensional model calculations qualitatively compare well with experimental results.

Introduction

The gasless exothermic reaction of a palladium/aluminum (Pd/Al) mixture commences when the aluminum begins to melt, at 660°C. Since a eutectic forms at 615°C, it is possible for the reaction to occur below 660°C. However, the mixture still possesses a high autoignition temperature (>615°C). The congruent melting temperatures for the two stoichiometric ratios of interest, 88.7/11.3 and 80/20, occur at 1645 and 1430°C, respectively, with enthalpies of formation (heats of reaction) of 249 and 315 cal/g.

As part of our efforts to develop a better understanding of pyrotechnics, we have been investigating this reaction for Pd/Al mass ratios of 94/6, 90/10, and 80/20 in two different geometries. The propagation rates and temperatures of the pyrotechnics were measured and also calculated using a diffusion-controlled one-dimensional analysis developed by Hardt and Phung[1] and extended by Green[2]. To our knowledge, the only other experimental study for comparison is that of Kjeldgaard, Larson, and Gould,[3] who used somewhat different experimental conditions.

The experimental results were reproducible, both from test to test and with the three different measurement techniques. One of these in particular, an optical technique, gave excellent quantitative measurements for both propagation rate and temperature measurements while not disturbing the experimental environment. The model calculations gave the correct qualitative performance of the material. Quantitatively accurate calculations were not possible, however, because the walls of the pellet cannot be properly modeled (since it is only a one-dimensional computation) and the two-dimensional boundary conditions are quite important for the lowest-propagation-rate mixture.

Pd/Al Mixtures and Confinement Geometries

Three Pd/Al mixtures (by weight) were investigated: 94/6, 90/10, and 80/20. All were compressed to an average density of 5×10^3 kg/m^3. Theoretical densities are 9.9×10^3, 8.9×10^3, and 7.1×10^3 kg/m^3 for 94/6, 90/10, and 80/20, respectively. In order to obtain a uniform compaction, the pellets were made in a series of ten pressings. The powder was pressed and tested in a Macor* holder. The Macor served as an insulating sleeve to reduce heat sinking to boundary walls. For the two geometries chosen (Figure 1) the length-to-diameter ratios (L/D) were 0.5 and 1.25 for the large (6.35 mm) and small (2.54 mm) diameter pellets, respec-

---

*Macor is a Corning Glass Works trade mark for Machinable Glass Ceramic Code 9658.
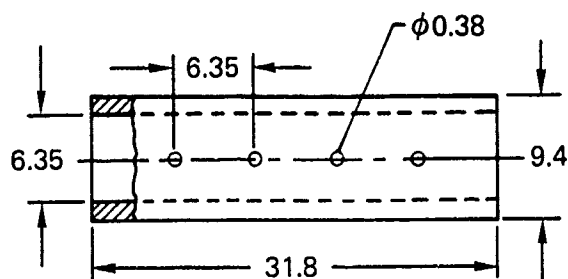
(a) THIN MACOR, PELLET DIAMETER = 6.35 mm.
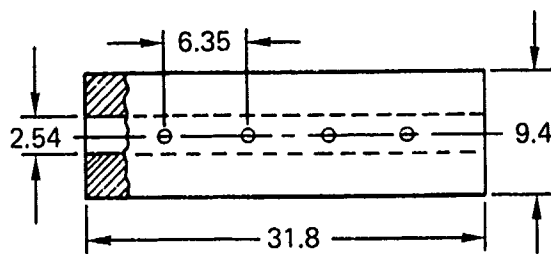
(b) THICK MACOR, PELLET DIAMETER = 2.54 mm.

Fig. 1. Geometries of the two sizes of Macor tubes.

tively. The density gradients were calculated using a porous-media compaction model[4] and measured using a standard microdensitometer; results are given in Figures 2 and 3 for the two pellet geometries and three mixtures used: the larger the L/D, the greater the axial density gradient due to the presence of wall friction. Our method of pressing generally caused the first pressing increment to be less dense than the last one.

All reactions were initiated by a squib simulator (bridgewire). The reaction product was Pd_2Al, for both 94/6 and 90/10, plus unreacted Pd, 47% and 11% of the total mass for 94/6 and 90/10, respectively. The stoichiometric ratio for Pd_2Al is 88.7/11.3. The 80/20 mixture is already stoichiometric (actual[1] 79.81/20.19) with the product of reaction being PdAl.

Measurement Techniques

Three different types of experimental systems were used to determine the propagation rate and temperature of the reacting Pd/Al pellets: (1) a thermocouple system, (2) a camera system, and (3) an
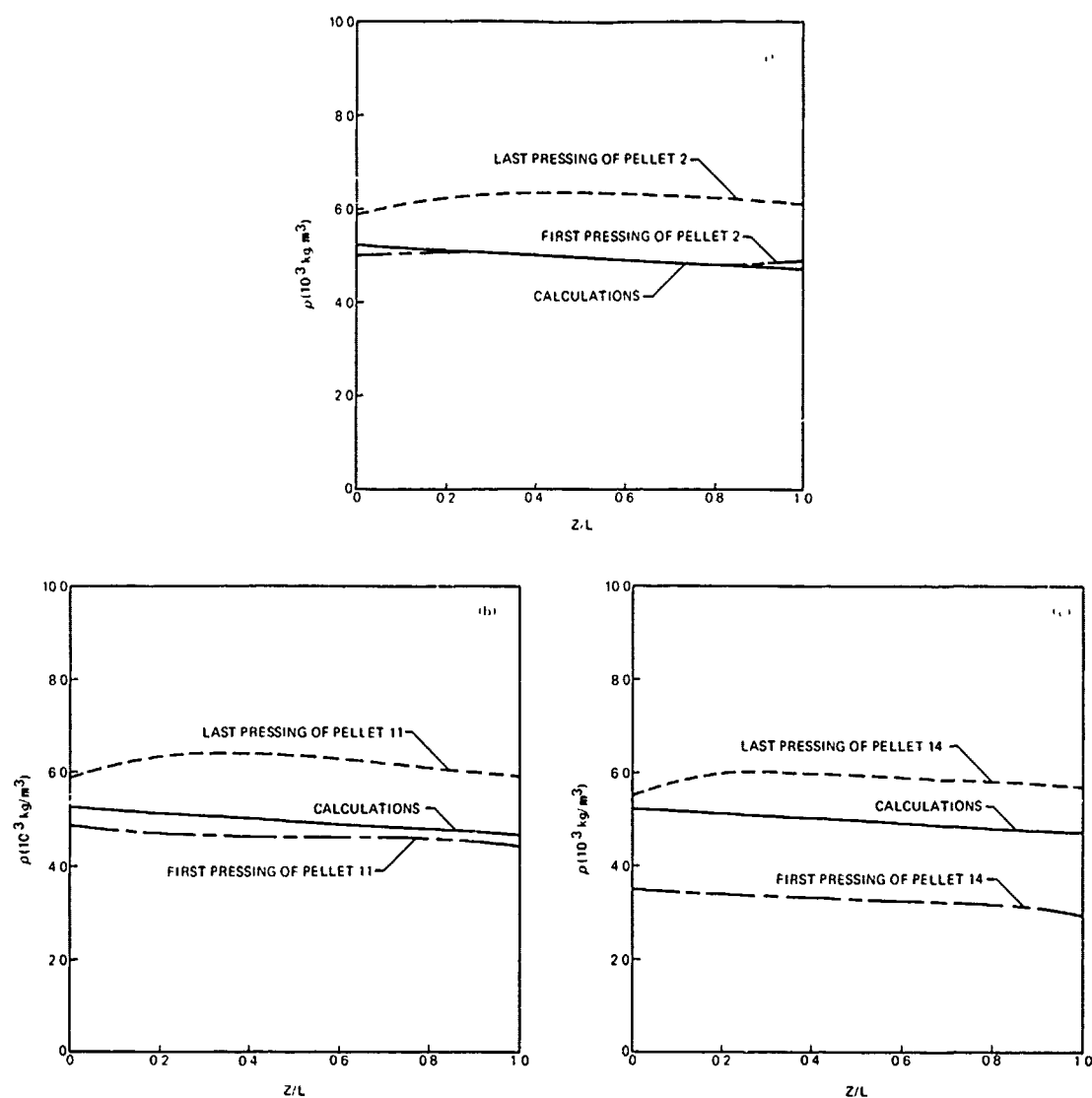
Fig. 2. Calculated and measured densities (10 pressing increments, 6.35-mm-diam pellet). Z is measured from the top of the pellet. (a) 94/6, (b) 90/10, and (c) 80/20 Pd/Al.

42
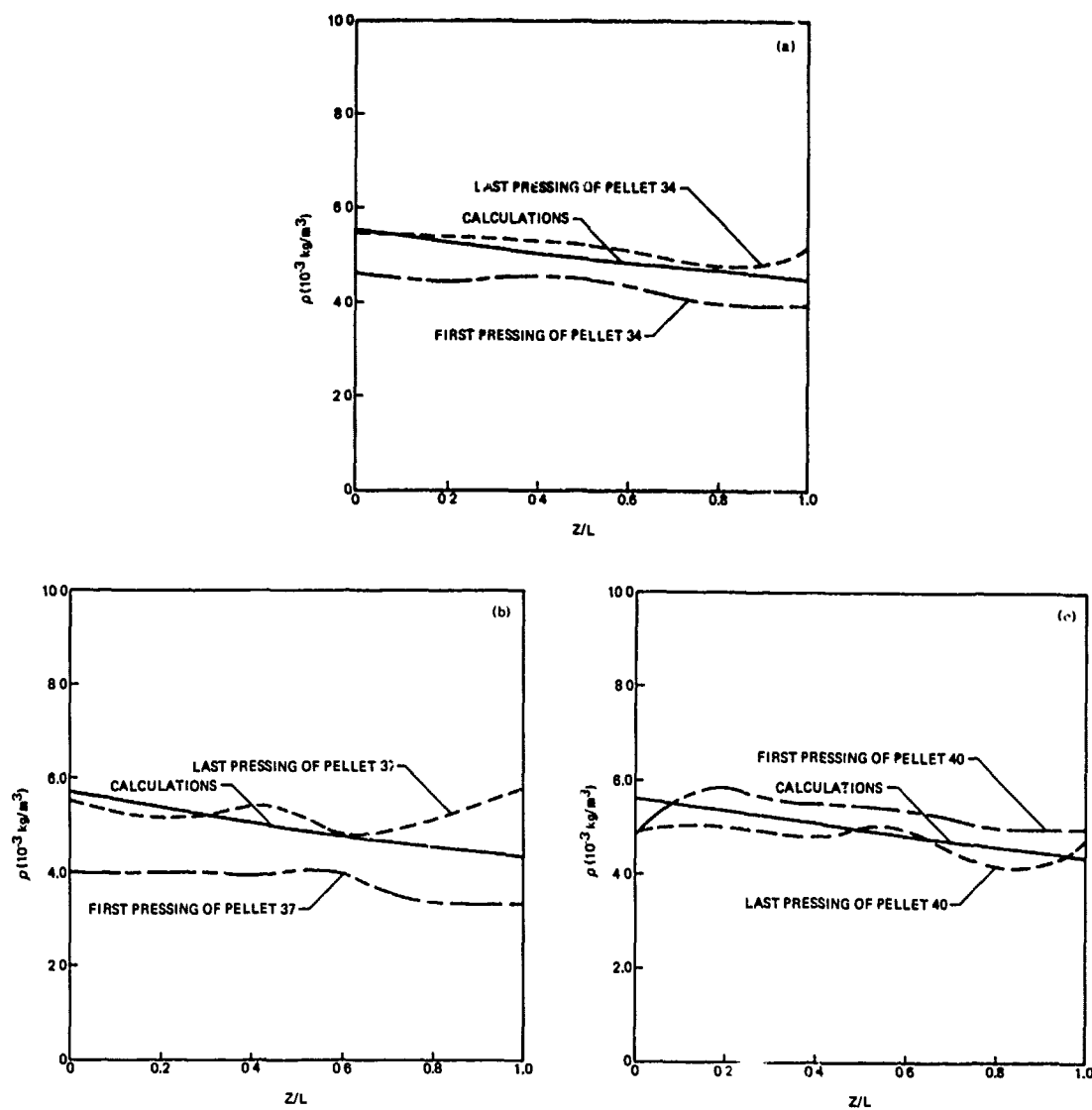
Fig. 3. Calculated and measured densities (10 pressing increments, 2.54-mm-diam pellet). Z is measured from the top of the pellet. (a) 94/6, (b) 90/10, and (c) 80/20 Pd/Al.

electro-optical radiation imaging system (Delcalix* equipment). Although the use of thermocouples is commonly accepted, we were concerned with their influence on the phenomenon being measured. Thus the two additional techniques, which do not perturb the pyrotechnic, were employed as separate checks.

(1) Thermocouple Measurements--Four thermocouples, spaced 6.35 mm apart, were used per test, with the results recorded on an oscil- loscope. These were inserted through 0.38-mm-diameter holes drilled through the Macor and halfway through the pellet. The thermocouples measured the time of arrival of the burn front as well as the tempera- ture. Two types were used (depending upon the temperature range of interest): chromel/alumel and tungsten/tungsten - 26 wt.% rhenium, both of which were of the open-sheathed variety with a response time of less than 2 ms.

Figure 4 is a photograph of the test setup, showing thermocouples, squib simulator, and holding frame. The squib simulator was activated by a capacitative discharge fireset in order to exclude 60-cycle ac noise from producing interference on the oscilloscope trace.

(2) Camera Measurements--From initial thermocouple measurements, it was determined that 94/6 was burning at approximately 40 mm/s and the 90/10 and 80/20 mixtures at 500 mm/s. Based on the propagation rate of the burning pellets, one of two cameras was used: a framing camera (Bolex) recording at 32 frames/s for 94/6 and a streaking camera (HyCam) recording at 1219 mm/s using Plus X black and white film for 90/10 and 80/20. To obtain an optical measurement of the temperature, a known temperature source was calibrated versus the optical transparency of the film. This was done using both thick- nesses of Macor as attenuators. From the test-film data, both propagation rate and temperature could be determined.

A view of the experiment when the framing camera was employed is given in Figure 5. The distance from the camera to the Macor is held fixed from test to test in order to be able to use the precalibrated temperature-source information. The framing and streaking cameras can be quickly interchanged.

(3) Radiographic Measurements--For the electro-optical dynamic radiation imaging system the experimental configuration was very similar to that shown in Figure 5 for the camera system. Figure 6 shows a schematic of the Delcalix system. A continuous 400-kV x-ray source (1) formed the pellet image, which was converted into an optical signal by a gadelinium-oxide scintillator (3) and then recorded on a video tape recorder (8) at 30 frames/s. The Isocon TV camera tube (6) has improved capability at low light over the previously standard Orthicon.

*Delcalix is a registered trademark of Old Delft Corporation of America, based in Holland.

THERMOCOUPLE LEADS

STEEL HOLDING
FIXTURE

MACOR HOLDER
(with Pd/Al inside)

LEADS TO
FIRESET

SQUIB
SIMULATOR
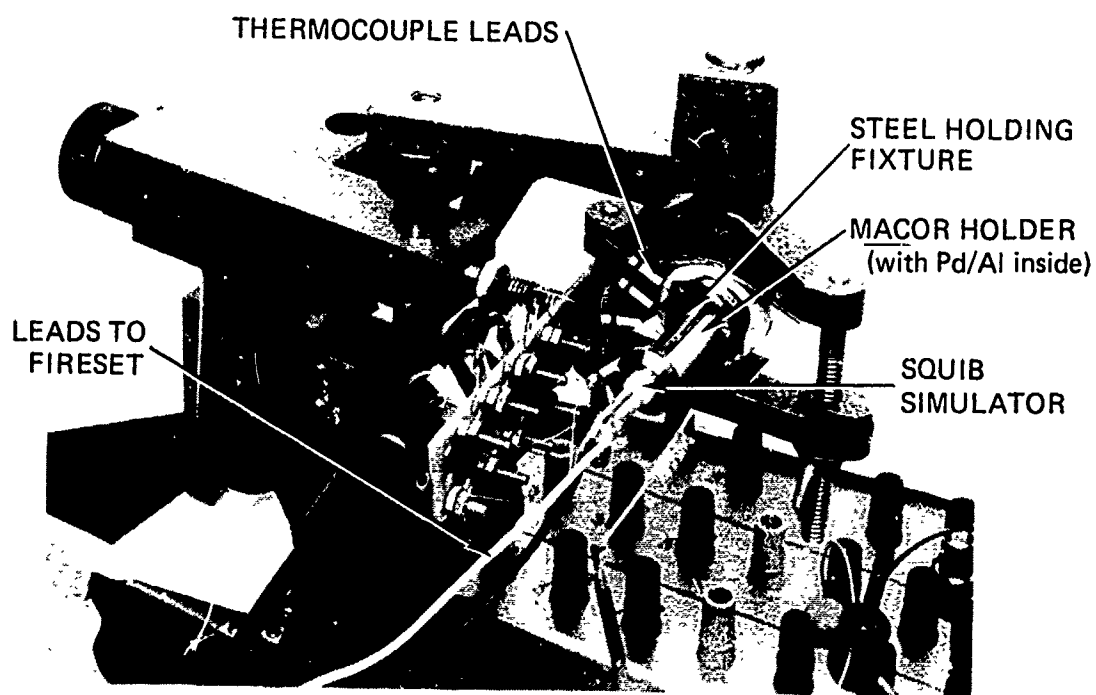
Fig. 4. Thermocouple measurement setup
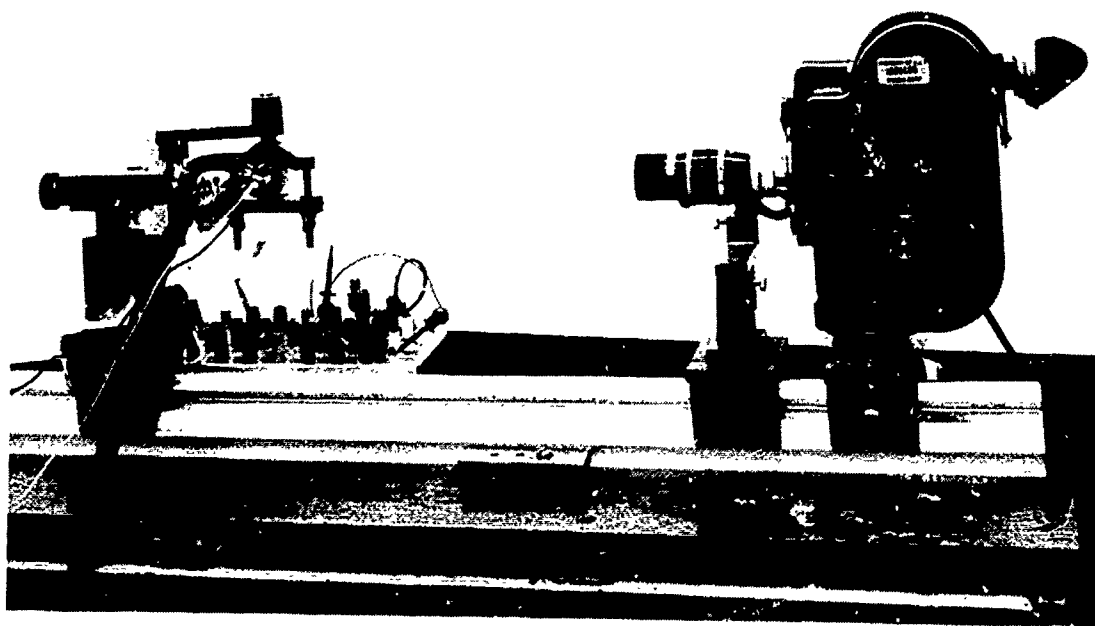
Fig. 5. Framing-camera measurement setup
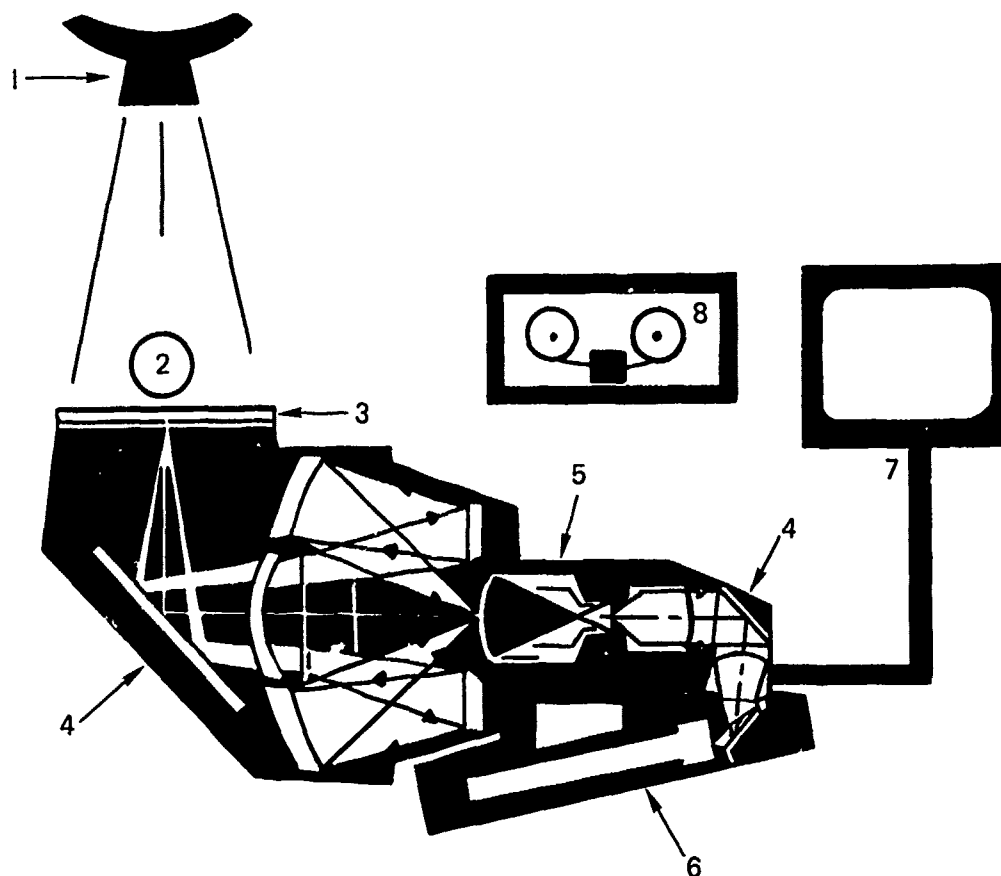
1 RADIOGRAPHIC SOURCE

2 RADIOGRAPHIC OBJECT

3 SCINTILLATOR (32 cm DIAMETER)

4 LIGHT FOCUSING OPTICS

5 IMAGE INTENSIFIER TUBE

6 ISOCON TV CAMERA TUBE

7 TV MONITOR

8 VIDEO TAPE RECORDER

Fig. 6. Schematic of the Delcalix electro-optical imaging system.

In reducing the data, the tape was examined frame by frame, and the leading edge of the density change was thereby located. Then, from the framing rate, the axial speed of material movement was determined.

Experimental Results

Figures 7 and 8 show typical oscilloscope records using the chromel/alumel (94/6 test) and tungsten/tungsten-26% rhenium (80/20 test) thermocouples respectively. When the propagation front reaches the first thermocouple, the other thermocouples show a spurious signal response due to electrical noise in the system. The chromel/alumel traces recover quickly while the W/W-26% Re ones have a long recovery time (and thus exhibit a shift in base line). The magnitude of the thermal response must be measured from the new baseline. Knowing the spacing between the thermocouples and the time of arrival of the propagation front allows one to determine the propagation rate. The magnitude of the scope trace is proportional to the temperature of the pellet.

A series of framing-camera photographs (Figure 9) clearly show the location of the propagation front as a function of time for a 94/6 pellet. A streaking-camera photograph of one of the 90/10 mixtures is given in Figure 10. This record shows that the propagation front does not proceed at a constant rate, but rather oscillates. These oscillations are caused by the changes of density that occur across each pressing increment.

A comparison of thermocouple and optical camera propagation rates measurements is given in Figure 11 for the 6.35-mm-diameter pellets. There is excellent reproducibility from test to test and between experimental techniques. The oscillation in the propagation rate is very evident for the 94/6 mixture (Figure 11a) where the data were taken with a framing camera. The photographic record, giving over 25 frames per test, gives sufficient detail of the propagation rate to permit this determination. The thermocouples produce only four data points per record, thus allowing only a generalized pattern of the propagation rate to emerge. An increase in the propagation rate occurs near the pressing interfaces where the pellet changes from a lower-density (end of one pressing) to a higher-density (top of next pressing) material. The 94/6 material, because of its low propagation velocity, is more sensitive to density changes than the 90/10 or 80/20 mixtures, which also exhibit this oscillation behavior (Figure 11, b and c). There is more oscillation at the beginning of the pellet than at the end since the pressing interfaces are more distinct at the beginning of the pellet. The latter part of the pellet generally has a more uniform appearance with less distinct pressing interfaces.

The 94/6 mixture has a propagation rate between 32 and 47 mm/s. The corresponding values for the 90/10 and 80/20 ratios were

47
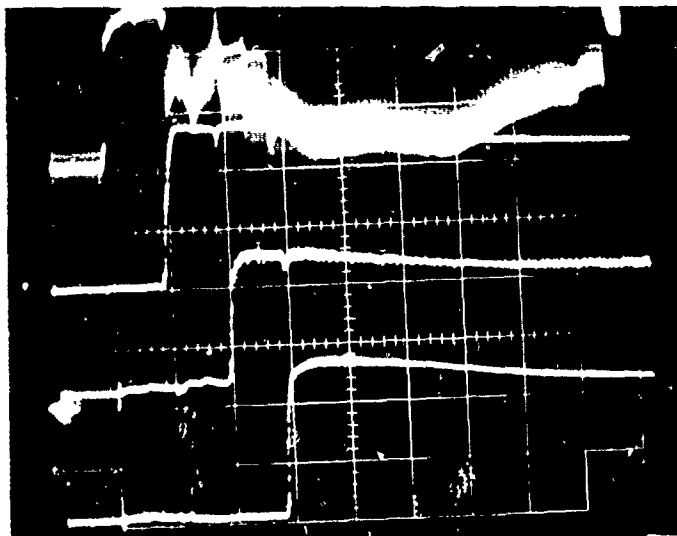
Fig. 7. Traces of the four chromel/alumel thermocouples on a 94/6 pellet (sweep rate is 200 ms/division).
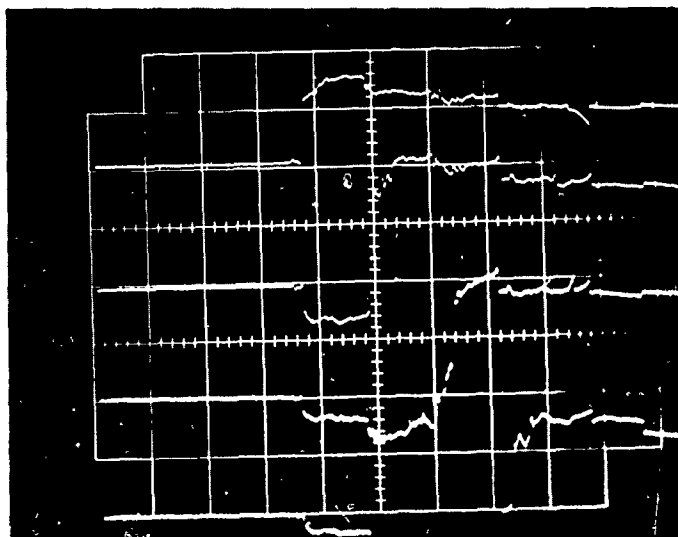
Fig. 8. Traces of the four W/W-26% Re thermocouples on a 80/20 pellet (sweep rate is 10 ms/division). Note the base-line shifts.
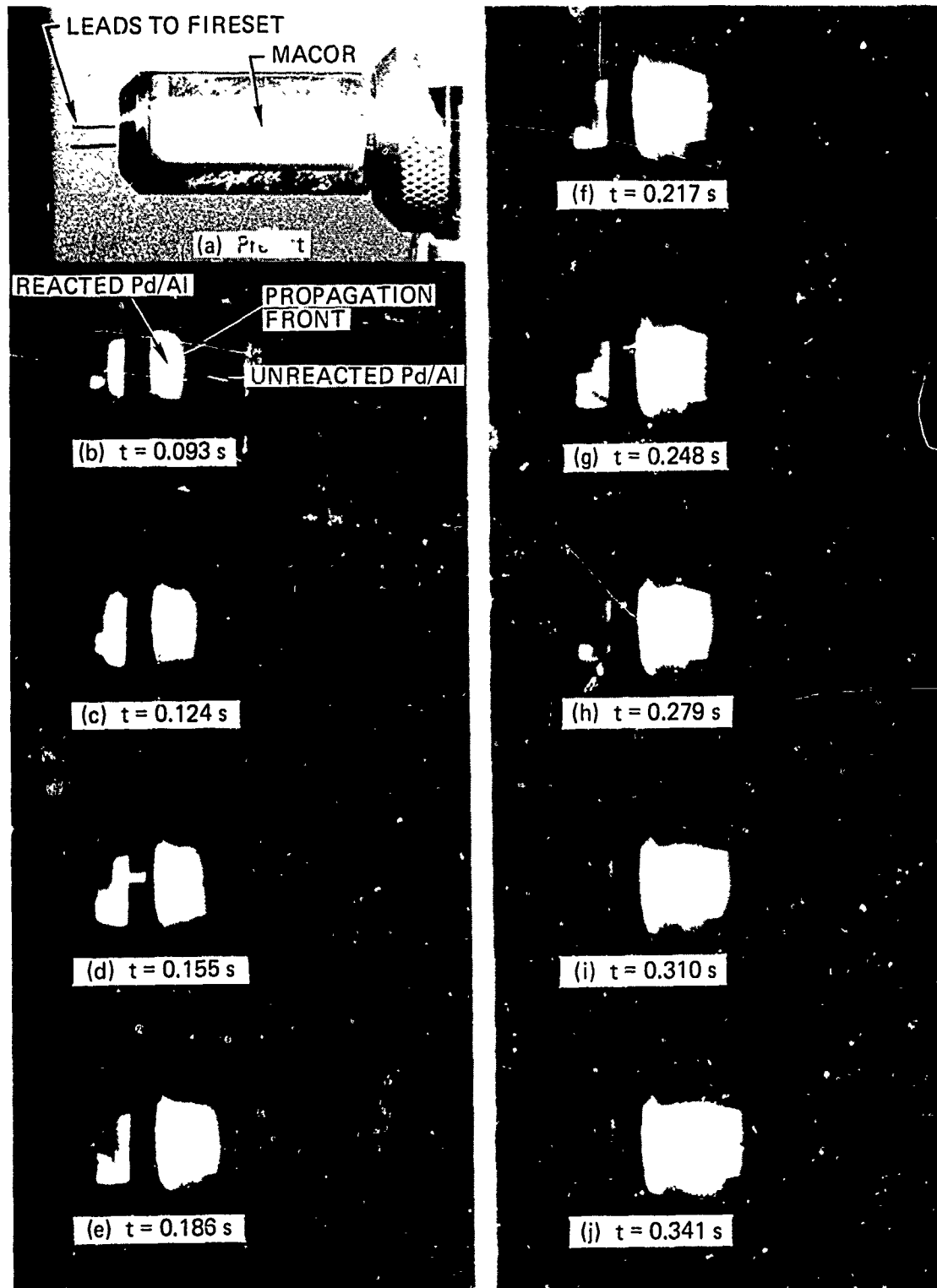
Fig. 9. Framing-camera photographs of a 94/6 pellet.

(k) t = 0.372 s

(l) t = 0.403 s

(m) t = 0.434 s

(n) t = 0.465 s

(o) t = 0.496 s

(p) t = 0.527 s

(q) t = 0.558 s

(r) t = 0.589 s

(s) t = 0.620 s

(t) t = 0.651 s

Fig. 9. (continued)

(u) t = 0.682 s

(v) t = 0.713 s

(w) t = 0.744 s

(x) t = 0.775 s

(y) t = 0.806 s

Fig. 9. (continued)

FRONT EDGE OF PELLET

THERMOCOUPLE WIRES

PROPAGATION FRONT

END OF PELLET
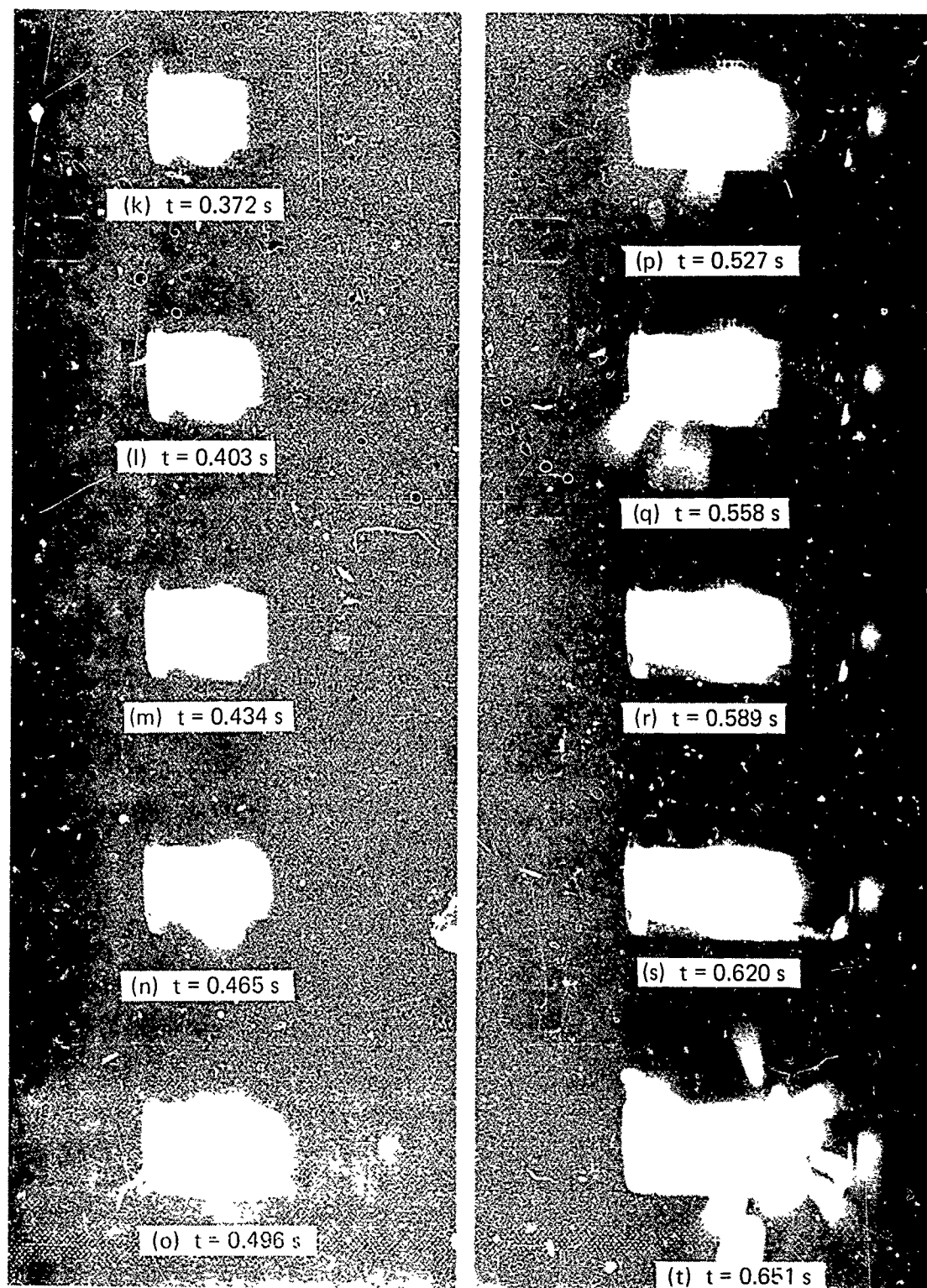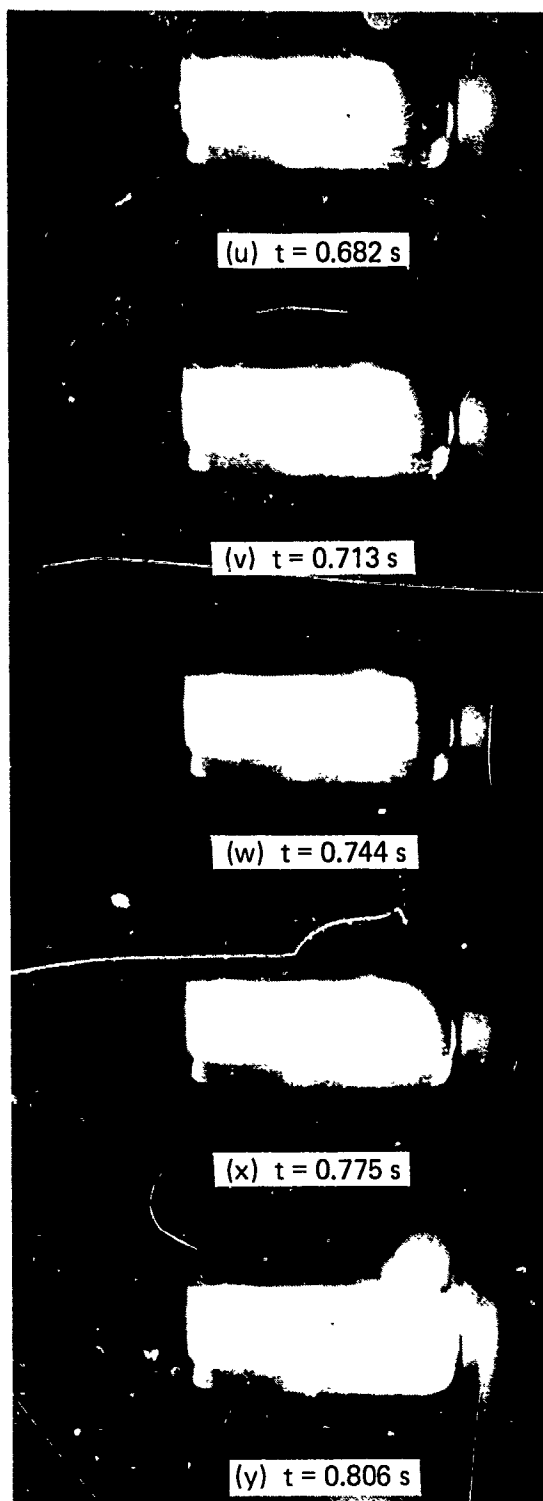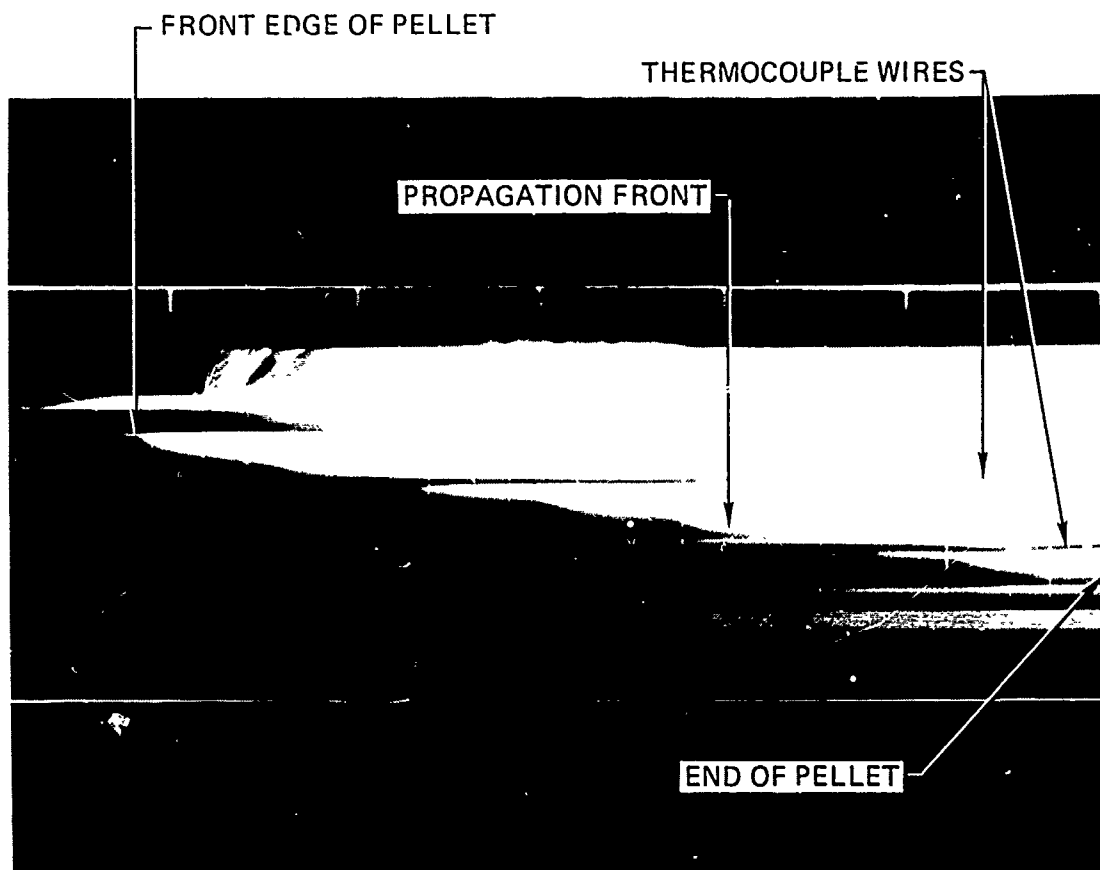
Fig. 10. Streaking-camera photograph of a 90/10 pellet.

390-600 mm/s and 480 mm/s, respectively. The burn temperatures, as measured via thermocouples, were 1300-1500°C for 94/6 and 2200-2600°C for 90/10 and 80/20. Using the optical method, these temperatures were 1400-1600°C for 94/6 and 2200-2600°C for 90/10 and 80/20. The 94/6 ratio has also been examined by Kjeldgaard et al.[3] for different geometries. They recorded lower temperatures (<1000°C) and higher propagation rates (>193 mm/s).

For the 2.54-mm-diameter pellets, the 94/6 mixture would not propagate and quenched itself within a distance of a pressing increment. The propagation rates and temperatures of the 90/10 and 80/20 mixtures were unaffected by this size change (Figures 12). For these mixtures it will be necessary to use smaller-diameter pellets to observe the effects of wall quenching.
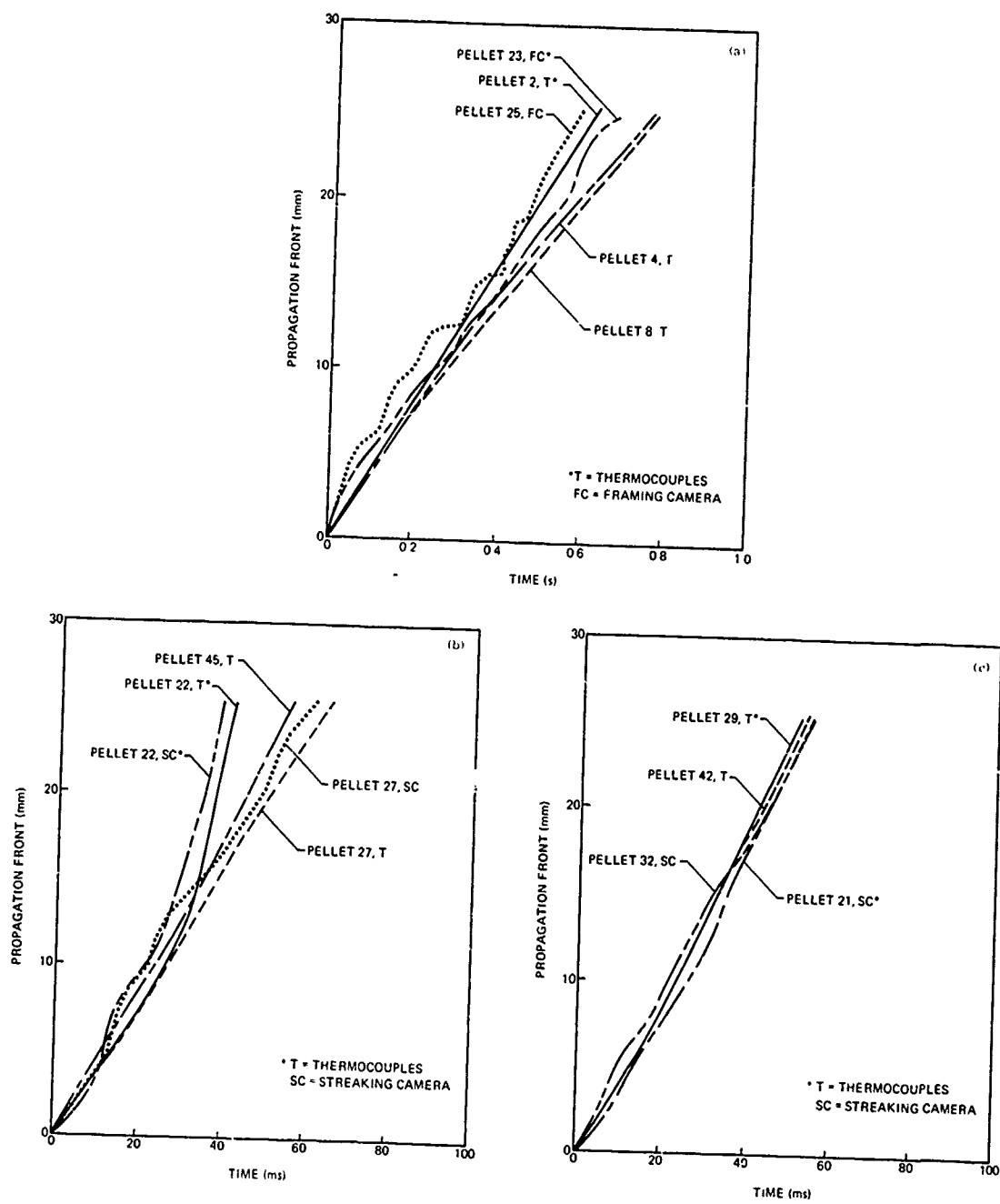
Fig. 11. Propagation rate measurements for (a) 94/6, (b) 90/10, and (c) 80/20 Pd/Al mixtures (10 pressing increments, 6.35 mm diam).
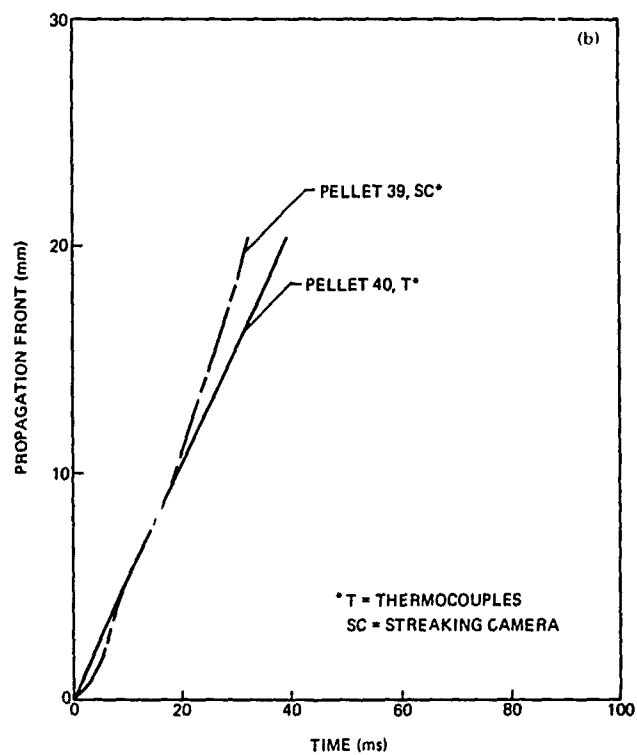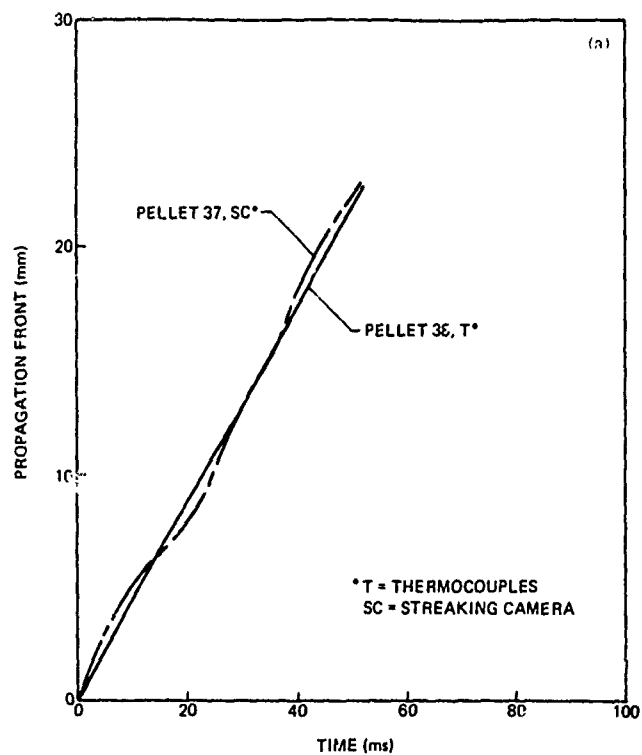
Fig. 12. Propagation rates and temperatures for (a) 90/10 and (b) 80/20 Pd/Al mixtures (10 pressing increments, 2.54 mm diam).

Delcalix records for 94/6 and 80/20 mixtures (6.35-mm-diameter) are given in Figures 13 and 14, respectively. For the 94/6 mixture, we are observing every seventh or eighth frame and for the 80/20 every frame. A marker has been established at the leading edge of the material movement for each frame. The density change first occurs at the pellet - Macor interface. The axial rate of this material movement is between 40-50% of the propagation rate for all three mixtures. The density change corresponds to the movement of molten material into the less dense region at the outside of the pellet.

Computational Results and Experimental Correlation

A one-dimensional diffusion-controlled model[1,2] was used to model the propagation process. The heat of reaction, activation energy, and pre-exponential factor for the 94/6 and 90/10 mixtures were the same since the product of reaction is identical, Pd_2Al. The heat of reaction used was 249 cal/g, the pre-exponential factor was set at 1.0 cm^2/s, and the activation energy at 16×10^3 cal/mole. The unreacted Pd, 47% and 11% of the total mass for 94/6 and 90/10, respectively, produces differing propagation rates and temperatures for the two mixtures. For the 80/20 material, the heat of reaction, pre-exponential factor, and the activation were set at 315 cal/g, 1.0 cm^2/s, and 21.9×10^3 cal/mole.

Table I lists the calculated propagation rate and burn temperature for each mixture. These values show good agreement (Table II) with previously found experimental values.

A major value of a simple numerical technique is the capability of employing it for parameter sensitivity studies. These allow one to determine the important physical variables in a phenomenon. Our optical experimental results showed the effect of density change on the propagation rate. This was examined numerically where the thermal conductivity, which is very sensitive to density variations, was varied concurrently with the pellet density. Density shifts of

Table I. Calculated Values for the Pd/Al Mixtures.

Mixture	Propagation Rate (mm/s)	Temperature (°C)
94/6	50	1200
90/10	420	2300
80/20	500	2700

Marker showing leading
edge of density change

Macor

Pd/Al

Macor
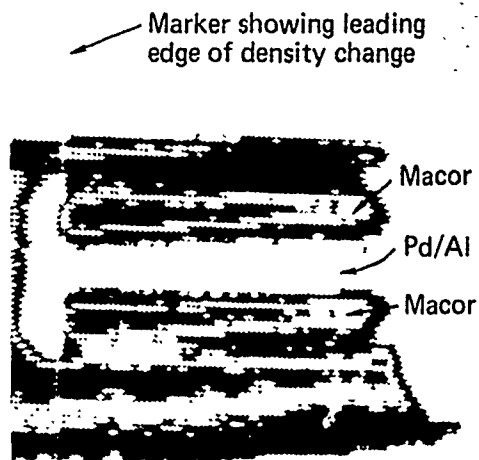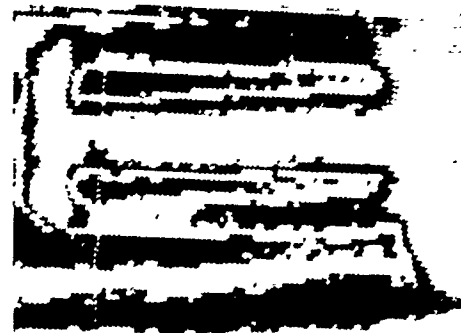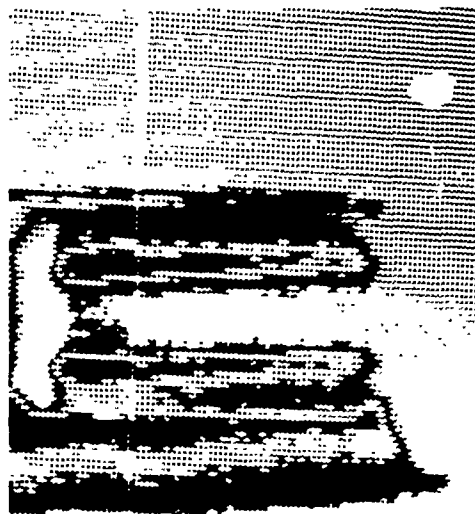
(a) Pretest

(b) t = 0 ms

(c) t = 231 ms
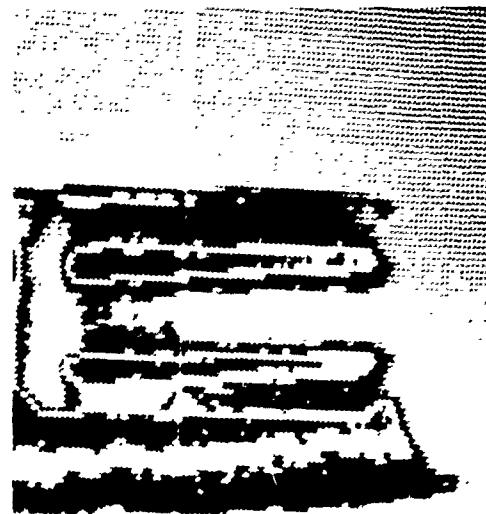
(d) t = 495 ms

Fig. 13. Selected frames of a 94/6 Pd/Al pellet using the Delcalix
system.
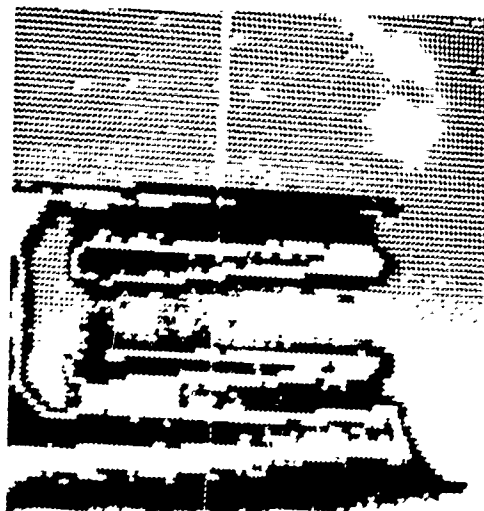
(e) t = 726 ms
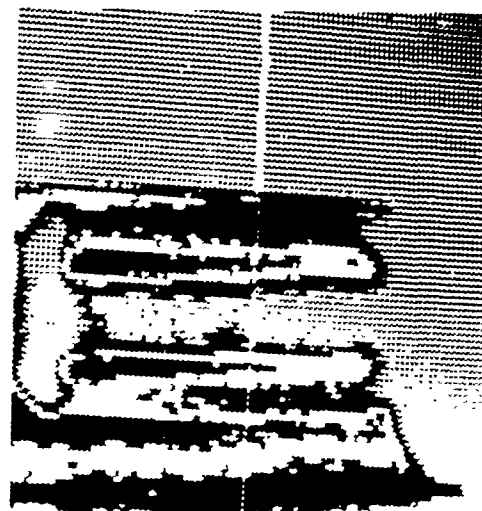
(f) t = 990 ms
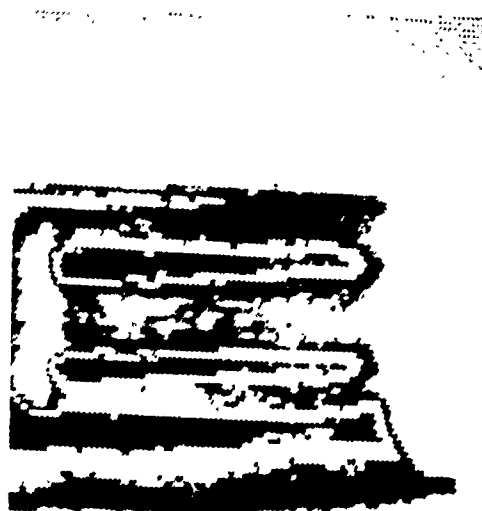
(g) t = 1254 ms
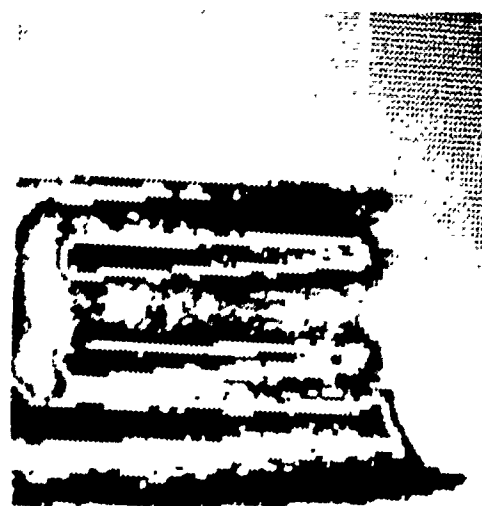
(h) t = 1518 ms

Fig. 13 (continued)

Marker showing leading edge of density change

Macor

Pd/Al

Macor
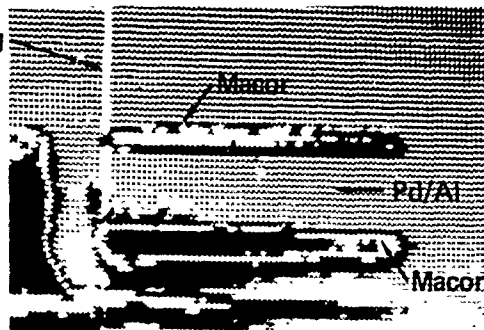
(a) Pretest

(b) t = 0 ms

(c) t = 33 ms

(d) t = 66 ms

(e) t = 100 ms

Fig. 14. Selected frames for a 80/20 pellet using the Delcalix system.
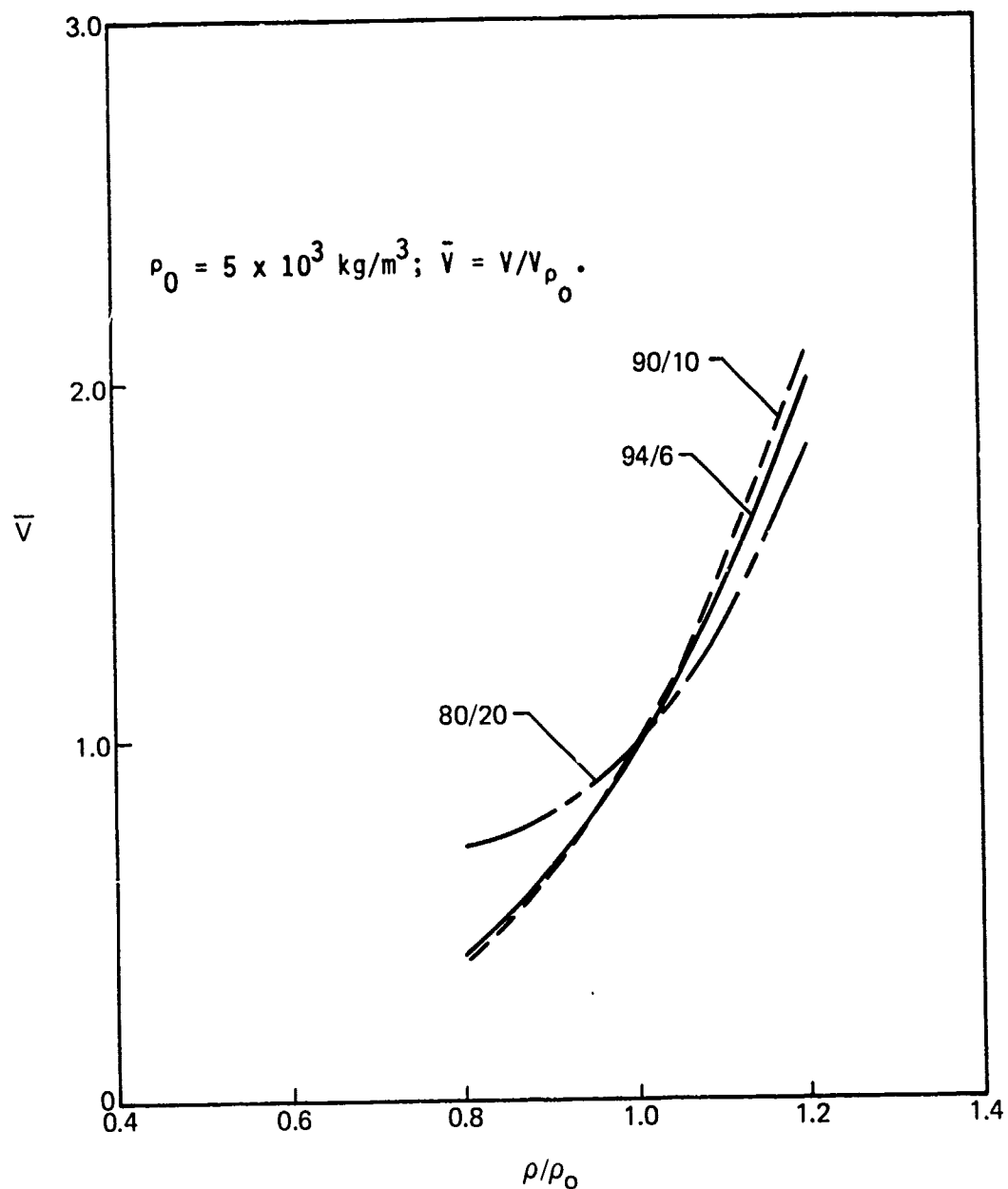
Fig. 15. Calculated propagation rates versus density, in dimensionless units, for the three Pd/Al mixture ratios.

Table II. Correlation Between Experimental
and Calculated Values.

Mixture	Propagation Rate (mm/s)		Temperature (°C)	
	Experimental	Calculated	Experimental	Calculated
94/6	32-47	50	1300 - 1500	1200
90/10	390-600	420	2200 - 2600	2300
80/20	480	500	2200 - 2600	2700

20% cause thermal conductivity changes upwards of a factor of
five. It is this thermal conductivity variation which then produces
large propagation rate shifts. Figure 15 shows, in a dimensionless
format, propagation rate versus density for all three mixture ratios.
This corroborates the oscillatory behavior observed in the optical
measurements.

It has already been noted that the 94/6 ratio does not propagate
in the 2.54-mm-diameter-size pellet. The calculations, discussed
above, noted the reduced propagation rate in the low-density region
of a pressing. For 94/6, it is reduced to approximately 15 mm/s.
With the boundary so close in this geometry, the propagation slows
and is quenched in the lower-density region of the first pressing.

Conclusions and Future Activities

In our present studies of three (94/6, 90/10, 80/20) Pd/Al
mixtures with two different diameters (6.35 and 2.54 mm), we measured
the propagation rates and temperature using thermocouples and optical
camera measurements. The thermocouples had no demonstrable effect on
the measurements for these diameters. Similarly, a one-dimensional
diffusion-controlled analysis correlated with the measurements for
the 90/10 and 80/20 mixtures, which did not exhibit wall quenching in
the present geometries. The analysis also explained the oscillatory
behavior of the propagation rate as a function of density and thermal
conductivity. The reaction for the 94/6 mixture was observed to be
very sensitive to geometry changes, and computations helped to show why.

In the future we will investigate smaller-diameter pellets of
the 90/10 and 80/20 mixtures to determine two-dimensional effects.
Similarly, a two-dimensional analysis will be performed to determine
the minimum diameter required to sustain propagation for each mixture
ratio.

The Delcalix data must be analyzed to determine its physical significance. We can, however, use the results to demonstrate that the pyrotechnic mixture is burning. Both the optical and Delcalix techniques provide a nonperturbing environment for observing pyrotechnic burning, although the optical method can only be employed with a transparent holder.

Acknowledgments

References

1. A. P. Hardt and P. V. Phung, "Propagation of Gasless Reactions in Solids. I. Analytical Study of Exothermic Intermetallic Reaction Rates," Combustion and Flame, Vol. 21, pages 77-89 (1973).

2. R. M. Green, "The Performance Prediction of a Thermochemically Driven Gas/Solid Dissociation Reaction," Sandia Laboratories Report No. SAND78-8011, March 1978.

3. E. A. Kjeldgaard, D. W. Larson, and D. J. Gould, "Thru Bulkhead Ignition of Pyrotechnics: An Analytical and Experimental Investigation," Sandia Laboratories, presented at the Fourth Pyrotechnic Seminar, Denver Research Institute, July 1974.

4. O. L. Burchett, M. R. Birnbaum, and C. T. Oien, "Compaction Studies of Palladium/Aluminum Powders" (appearing in these Proceedings).

DREV PROCESSING TECHNIQUES FOR CASTABLE PYROTECHNICS

by

G. Couture

Defence Research Establishment Valcartier
P.O. Box 880, Courcelette, P.Q.
GOA 1RO

ABSTRACT

The work done at DREV in the field of castable pyrotechnics, in recent years, was mainly based on the use of in-house granulated dyes formulated with the well known ARCO R45 Poly bd liquid Resin hydroxyl-terminated polybutadiene. Processes for compacting commercial fine dyes and grinding them into suitable granulated material will be discussed as well as the properties of the material and its advantages with respect to the manufacture of smoke compositions for signaling smoke grenades. In addition to the granulating, a coating process is sometimes used to increase the resistance of the dye to the shear action of the mixer blades. White smoke mix, equally castable and polymer based were produced under the form of large thin roll-formed sheets. Process and equipment used to produce these sheets will be discussed.

DREV PROCESSING TECHNIQUES FOR CASTABLE PYROTECHNICS

by

G. Couture

Defence Research Establishment Valcartier
P.O. Box 880, Courcelette, P.Q.
GOA 1RO

INTRODUCTION

This paper reviews the processing techniques used at DREV
in recent years in the field of composite pyrotechnic compositions.
Most of our work has been carried out with the use of the well known
R-45M hydroxyl-terminated polymer vulcanized with an isocyanate.
The colored smoke compositions dealt with herein consist primarily
of an organic dye, $KClO_3$, lactose (or sulfur) and sodium bicarbonate
dispersed in an elastomeric binder. However this binder alone was
not the magic solution to assure the castability of the compositions;
it was evident from the outset that the viscosities required for a
castable product (less than 5 kilopoises, kP) could not be met with
the available commercial powders, since their mean particle size was
always less than 20 μm.

The substitution of a commercial dye with a granulated material
having an average particle size of 650 μm made possible the preparation
of true-castable products. These low-viscosity compositions have an
end-of-mix, (EOM) viscosity generally lower than 3 kP for 80% solid
loads, and can be cast into the tubes by gravity alone.

The paper is divided in two sections. In the first part, we
discuss two processes used at DREV to granulate the commercial fine
dyes and to coat the granules to improve processing and mechanical
properties of the compositions. The second part presents a technique
used to prepare thin flexible sheets of composite compositions.

SECTION I

GRANULATION BY FUSION, CRYSTALLIZATION AND GRINDING

The first method used was designed for the granulation of
1-amino-anthraquinone (1-AAQ) and consists of melting, recrystallizing
and grinding the commercial product. The fraction required was re-
covered by sieving and the remnants re-melted.

Description of the Method

Orange dye (1-AAQ) is a relatively pure product, with a melting point of 252°C. It can thus be melted slowly without causing too much sublimation. However, occasional stirring is required in order to ensure permanent contact between the solid phase and the melting phase. Without such stirring, a cavity appears above the liquid, causing overheating of the already melted fraction and sublimation of a portion thereof. 2-litre stainless steel beakers are used, into which 1 kg dye may be poured in successive steps. A hotplate is sufficient to melt the dye within a reasonable amount of time, while leaving the cover cool enough to recover the small fraction of dye that is sublimated. The molten dye is then poured into disassemblable moulds where recrystallization at ambient temperature occurs. The 15 cm cubes thus obtained are subsequently ground to the desired size. Because of the fragility of the material, grinding must be gradual in order to prevent excessive friction that could cause an increase in the amount of fine particles.

The first operation consists of breaking the blocks into 3 to 4 cm pieces that can be fed into an ice-crusher-type blade crusher, where they are reduced to less than 1 cm. The dye is then processed through 4 pairs of 12 cm diameter differential rollers (20 and 40 rpm). Their spacing diminishes gradually (5, 3, 1.5 and 0.75 µm) so that the gap of each roller pair is half the size of the pieces admitted. Any attempt to reduce the number of passes leads to a rapid rise in the fine particle ratio.

Discussion of the Method

Acceptable grain size was obtained after removing the less-than-100 µm fraction by sieving. That fraction amounts to approximately 20% of the total dye quantity processed and is subsequently recirculated with the commercial dye. Average size after sieving ranged from 300 to 500 µm, but higher figures could have been obtained by increasing the roller gap. Difficulties were encountered when that method was applied to other dyes, such as red, blue, violet, yellow and green. Those dyes are usually a mix of materials having different melting points; the melting of that mix therefore causes overheating, degradation and excessive sublimation. Furthermore, the blocks obtained after recrystallization are not of homogeneous hardness. Even with 1-AAQ, grinding is a series of delicate and complex operations.

GRANULATION BY COMPACTION AND GRINDING

Due to the drawbacks of dye melting, another solution was found by developing a second method (Figure 1) comprising only mechanical operations effected with equipment already available at DREV. The
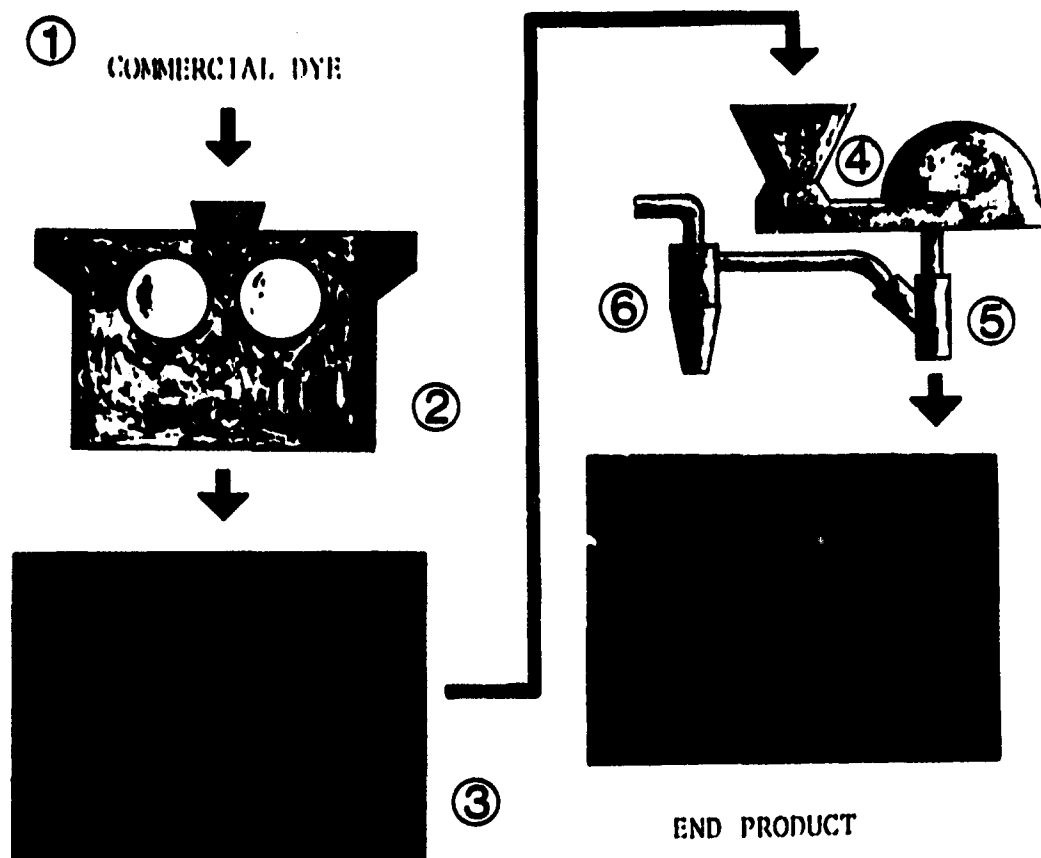
FIGURE 1 - Granulation by Compaction and Grinding

commercial dye (1) of an average size of 14 μm is first compacted by
a laminating roller mill (2), then granulated in an hammer crusher (4).
The separator (5) frees the granulated material from its fine particles
and directs them towards cyclone (6) where they are recovered. The
capacity of the installation is in the order of 20 kg/h.

Description of the Equipment

The rolling mill used for compacting (Figure 2) has 2 25 cm long,
15 cm diameter rollers turning at 8 rpm. In order to achieve higher
local pressure, material is fed only over a limited (15 cm) section of
the roller surface. The compacted dye has the shape of little plates
(item 3, (Figure 1), which are then granulated in a Bantam Model
"Mikro Pulverizer" hammer pulverizer (Figure 3).

The procedure is completed by a separator that removes particles
of less than 75 μm produced during the grinding. When leaving the
grinder, the dye falls through the separator shown in Figure 3, which
consists of a chamber equipped with baffles designed to slow down
the fall of the particles and to facilitate the elimination of fine

65
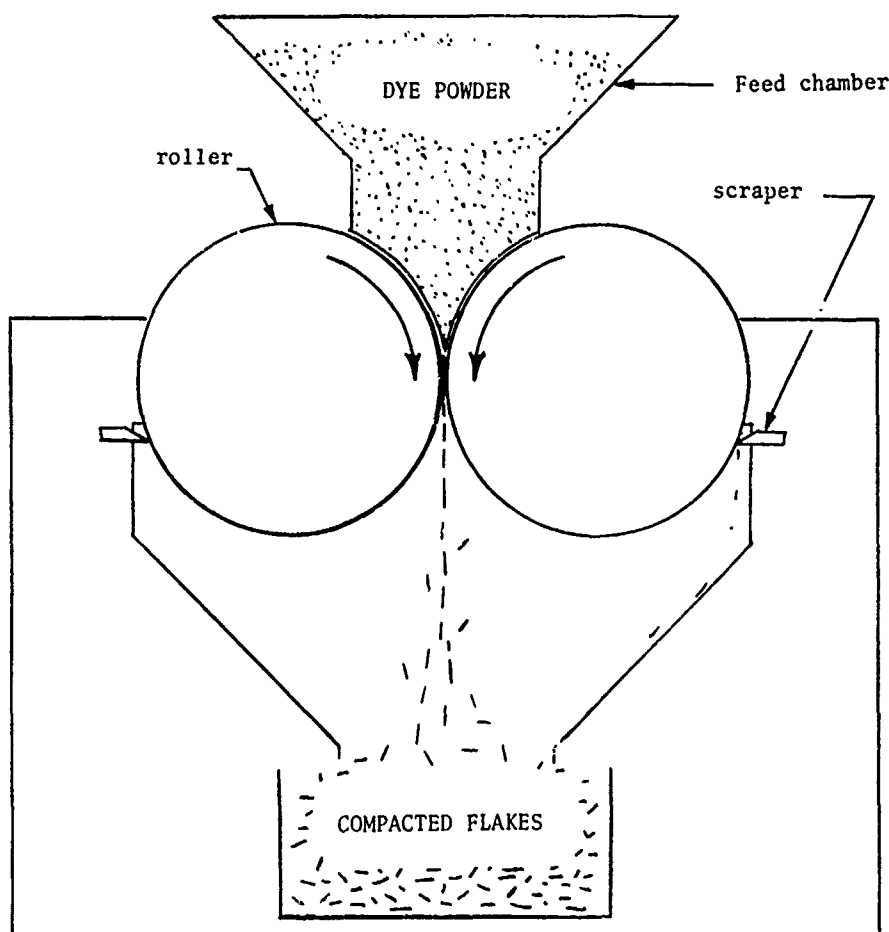
FIGURE 2 - Laminating Roller Mill

particles. An air current carries the latter towards a 15 cm cyclone where they are recovered and recirculated towards the compactor. Air circulation is provided by a (constant pressure) compressed air jet through a venturi located in the hose linking the separator to the cyclone. That syphon creates a negative pressure in the separator and eliminates dust leakages. Furthermore, higher efficiency is achieved due to the larger air flow in the cyclone.

Operating Conditions

The operating conditions of the rolling mill vary according to the dye processed, as specified in Table I. A first pass is made with the rollers fully closed (gap = 0) and 0.6 mm thick plates are obtained. This treatment is sufficient for orange (1-AAQ), but for other dyes (red, violet, yellow, green and blue) the plate surface is dull instead of shiny, a sign of insufficient compaction. A second processing is required and the setting of the rolls will vary with the color as shown on the table. However, these values are specific
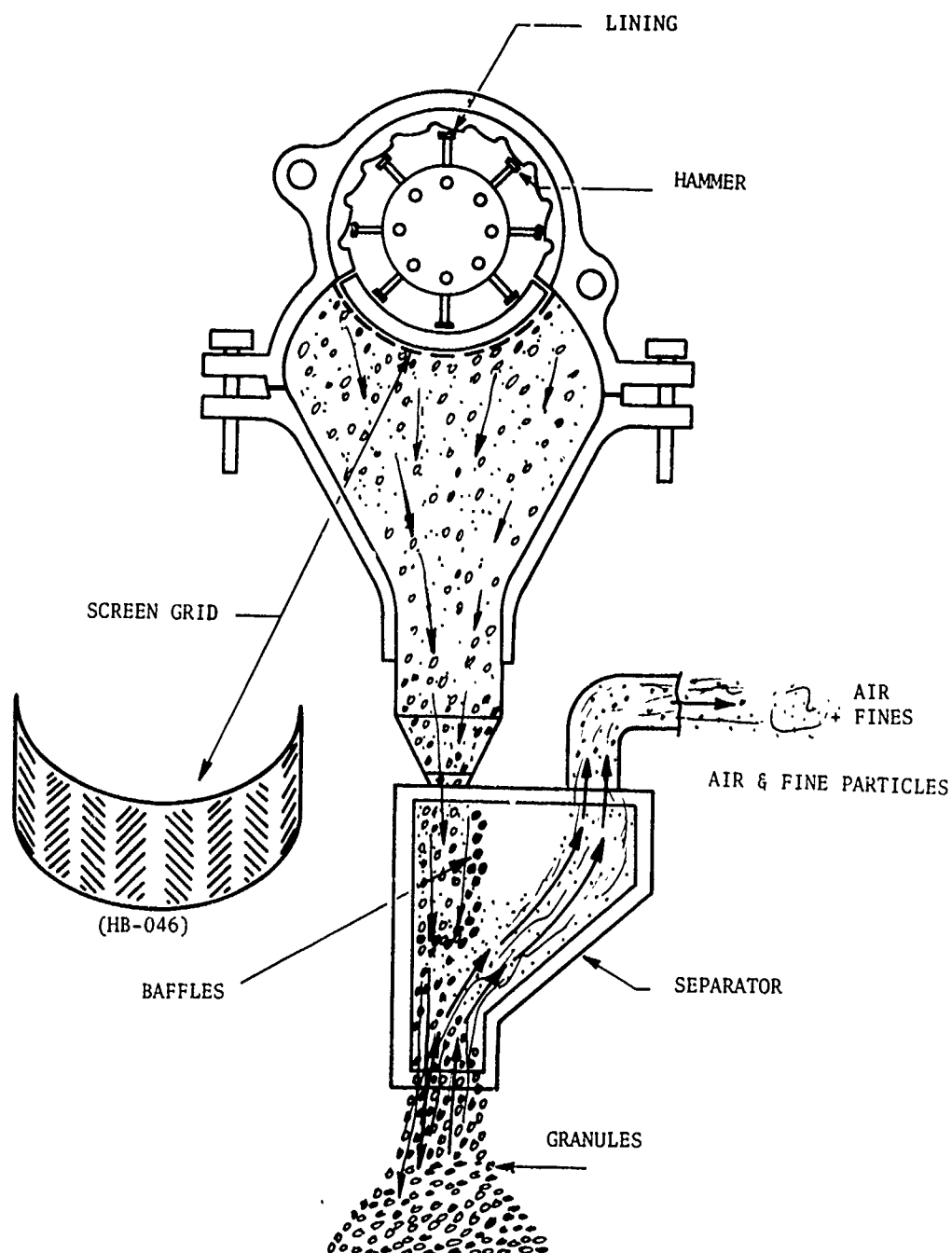
FIGURE 3 - Hammer Crusher and Separator

TABLE I

GAP BETWEEN THE LAMINATING ROLLERS

Product	Pass 1 Gap (mm)	Pass 2 Gap (mm)	Final Flake Thickness (mm)
Orange (1-AAQ)	0	-	0.63
Orange (α-AAQ)	0	-	0.56
Red (1-MAAQ)	0	0	0.58
Violet	0	0.5	1.1
Yellow	0	0.5	1.1
Green	0	0.6	1.2
Blue	0	0.6	1.2

to one particular lot and variations in the setting of the rolls for the second treatment can occur with lots. In all instances a difference of about 0.6 mm between the roller gap setting and the thickness of the plates is noted, and is due to the rollers being forced apart by the high pressure exerted.

The size of the ground particles may be changed either by varying the speed of the rotor, or by changing the grid that screens the exit the crusher chamber. In order to reduce the amount of fine particles, the rotor speed was set at 850 rpm, which is the minimum speed below which the crusher gets jammed. However, the average particle size by weight may be adjusted from approximately 500 to 1000 μm according to the grid used. Figure 4 shows the grain sizes obtained when processing 1-AAQ orange dye with various grids prior to separating the fine particles. The HB-046 herringbone slot grid was chosen for producing the granulated material because it yields the best distribution: less than 10% by weight fine particles (<100 μm) and very few particles above 1000 μm. The smaller (HB035 and 027) grids increase the amount of fine particles and reduce average size. whereas grids with a larger opening lead to a considerable increase of the fraction 1000 μm and up, without reducing significantly the amount of fine particles.
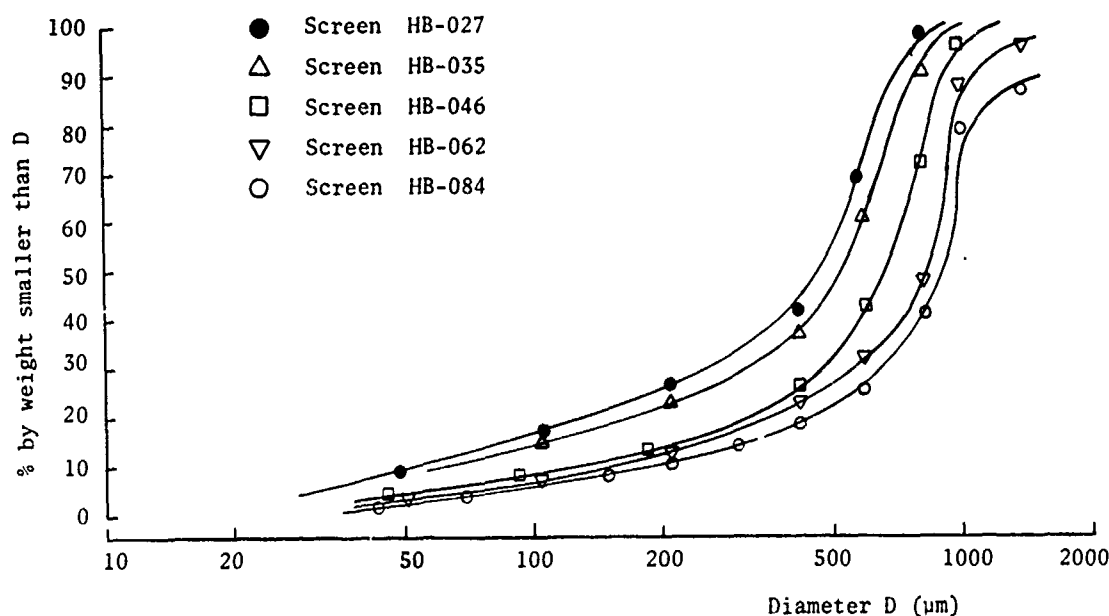
FIGURE 4 - Particle size distribution at the crusher exit
before separation of the fine particles, for
different screens.

The separator is used to eliminate the fine particles produced
by this method. Their presence in the end product is undesirable for
two reasons: they are a source of dust during handling and increase
viscosity during the manufacture of composite mixes, due to the
fact that the solids other than the dye, i.e. the $KClO_3$, the lactose
and others, saturate the suspension of fine particles (their size
is less than 20 µm). Most of the 8 to 16% by weight less than 100 µm
at the crusher exit must be eliminated by means of a separator.

Figure 5 shows the variation of the distributions obtained
for the various dyes, after fine particle separation. Air flow
was always 3.5 dm^3/s, except for violet dye, where 4.0 dm^3/s was
used. This method yeilds granulated material of average size 500 to
750 µm and completely free of fine particles 50 µm and less.

PROPERTIES AND ADVANTAGES OF THE GRANULATED MATERIAL

For the purpose of comparing and estimating the quality of
the granulated dyes, density measurements were made on the various
powders and granulates. Dye density was determined (Table II) by
measuring - by means of the mercury displacement method - the volume
of the 1/2 cm^3 tablets obtained by pressing (55.1 mPa) the powders
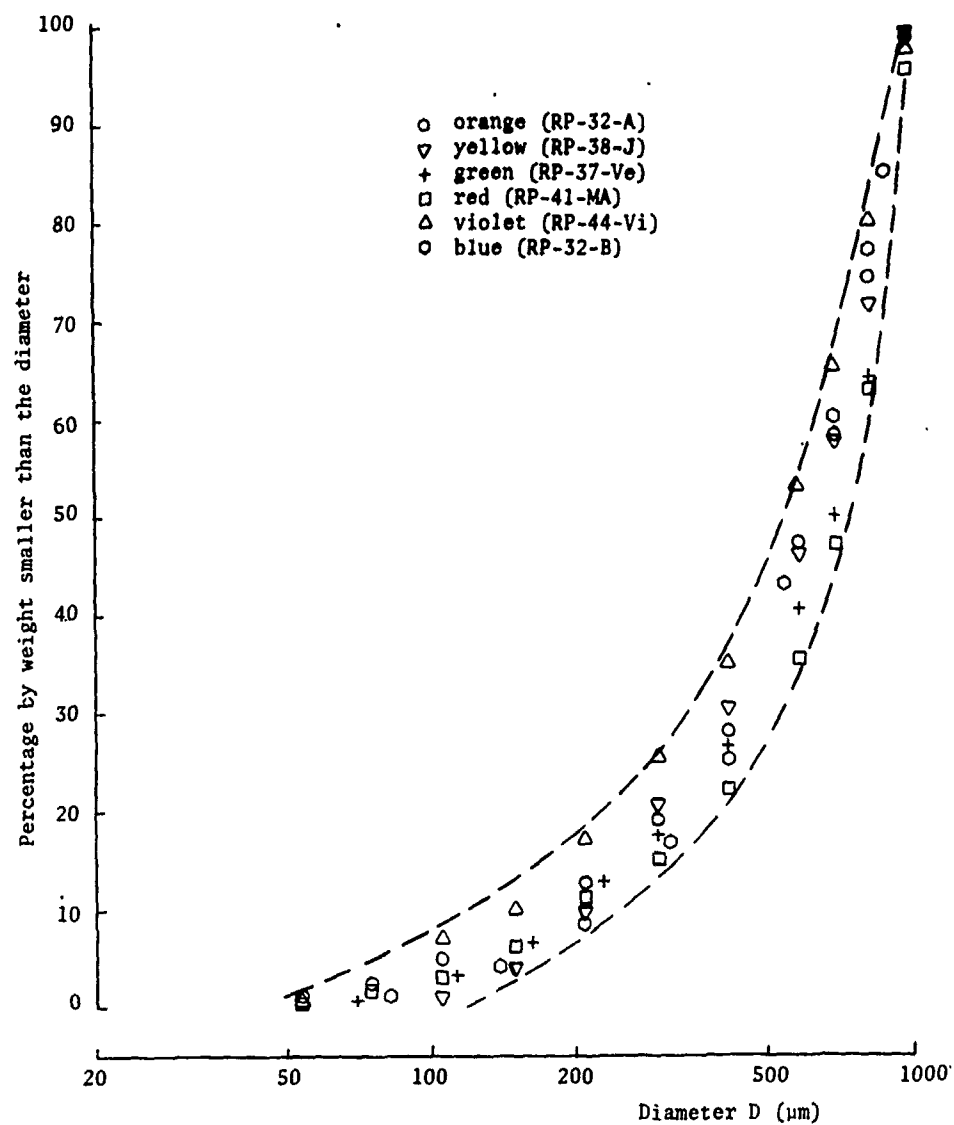
FIGURE 5 - End Product Particle Size Distributions

TABLE II

DENSITY OF THE VARIOUS DYES

Dye	Crystal Density (g/cm^3)	Flake Density (g/cm^3)
Orange (1-AAQ)	1.43	1.40
Red (lot R-300)	1.33	1.33
Red (lot R-302) (no dextrin)	-	1.21
Violet	1.30	1.28
Blue	1.40	1.40
Green	1.33	1.29
Yellow	1.38	1.37

available on the market. The accuracy of that procedure was checked by measuring in the same way substances of known density. These figures therefore represent the actual density of each dye.

Table II also shows the density of the plates obtained after compaction. Those figures were measured by mercury displacement as well. The similarity between plate density and the actual dye density shows the effectiveness of the roller compaction method.

The apparent density of commercial powders and of granulates was obtained by measuring - after 30 seconds' vibration - the volume taken up by a known weight of dye inserted into a 100 cm^3 graduated tube. The results are shown in Table III opposite the figures found in the literature. There is a considerable increase in apparent density when switching from fine material to type II granulated material. For instance, the respective figures are 0.45 and 0.83 g/cm^3 for yellow dye. That table also contains the corresponding compaction indices "ε", where "ε" is the ratio between apparent and real density and represents the share of volume taken up by the solid. The results show that granulation has almost doubled the value of "ε".

TABLE III

APPARENT DENSITY AND COMPACTION INDEX OF
GRANULATED MATERIAL VS. FINE POWDERS

| Dye | Apparent densities (g/cm^3) | | | Compaction index | |
| | Specified | Measured | | | |
	Fine (10-20 μm)	Fine	Granulated Type II	Fine	Granulated Mat Type II
Orange	-	0.55	0.94	0.38	0.66
Red	0.30 ± 0.15	0.20	0.74	0.15	0.56
Blue	0.35 ± 0.15	0.20	0.72	0.31	0.56
Green	0.40 ± 0.20	0.48	0.75	0.44	0.55
Yellow	0.36 ± 0.10	0.45	0.83	0.33	0.60
Violet	0.35 ± 0.10	0.43	0.83	0.33	0.61

Table IV gives the apparent densities and compaction indices achieved with the various 1-AAQ orange dye types. Thus "ε" is 0.66 for type II 660 μm granulated material obtained by compaction and grinding as opposed to 0.38 for 15 μm commercial dye. That is a 73% gain due to the large average size and to the broad range of particle sizes.

TABLE IV

COMPACTION INDEX "ε" FOR VARIOUS FORMS OF 1-AAQ

Type	Avge size by weight (μm)	Apparent density (g/cm^3)	ε
Commercial Powder	15	0.55	0.38
Granulated Mat. Method I	400	0.84	0.59
Granulated Mat. Method II	660	0.94	0.66

Effect of the Granulated Material on the Smoke Composition Manufacturing Characteristics

Figure 6 shows the end-of-mix viscosity variations for the various 1-AAQ grades. At 75% by weight solids, substitution of fine dye by type I (350 µm) granulated material reduced viscosity by a factor of 10. A mix containing 82% by weight solids could thus be obtained, even while staying below the 5 kP castability threshold. The type II (660 µm) granulated material was taken one step further, and mixes containing in excess of 85% by weight solids are now feasible.

Table V shows the end-of-mix viscosities recorded for various mixes comprising 20% R-45M, HTPB binder. One can classify these mixes into three classes: the orange composition which has the lowest viscosity, the red with the top value and the others averaging 2 kP. The variations can be ascribed to variations in compaction between dyes as well as to variations in dye concentration. The solid phase contains approximately 60% by volume granulated dye in all cases except for orange mixes (67%). Use of a dye other than orange thus means a departure from the optimum concentration of 65% by volume large particles, and an increase in mix viscosity due to the lower compaction rate of the solid phase. However, this does not
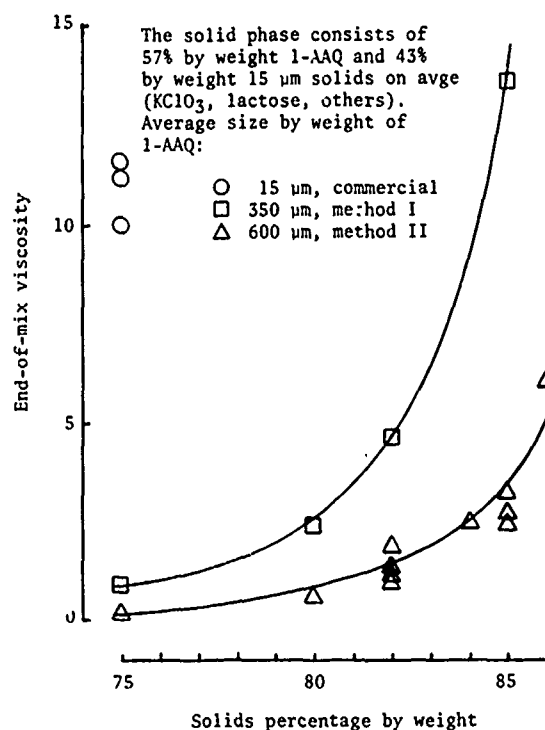
FIGURE 6 - Mix Viscosity Variation according to the Size of 1-AAQ Dye

TABLE V

END-OF-MIX VISCOSITIES (kP) FOR DIFFERENT DYES

Dye	Viscosity (end-of-mix)*
Orange (1-AAQ)	0.5 @ 1.0
Red (1-MAAQ)	5.0
Violet	2.5
Yellow	1.7
Green	2.1
Blue	2.5

* These viscosities are for mixes containing 20% by weight binder. Type II dye is 50% of the solid phase (57% for orange). Above figures at a temperature of 60°C.

explain the higher value (5 kP) for the red which has almost the same compaction as the green, the violet and the yellow. With the red, the paste is deeply colored suggesting some attack of the dye by the binder or a breaking of the granulated grains by the high shear action of the mixer itself. While this figure of 5 kP is still low, it is close to the castability limit; this means that the red composition has a loading capacity limited to about 80% by weight while the others can be loaded beyond 80% before reaching the castability limit.

COATING OF DYES

The dyes are know to reduce the curing potential of the curative. The red is much more active than the others; for example, formulations containing red dye show a Shore "A" hardness of 22 as compared to 30 for the others after 6 days at 60°C. This brought us to look for a means to protect the dye from the action of the mixer and the attack of the binder. This should reduce the EOM viscosity and increase the end-of-cure hardness. The solution was to treat the granules with an epoxy known to be compatible with the R-45M binder, thus preventing breakage and also providing an inert protective barrier at the surface of the dye.

Fabrication

The key was to apply a uniform coating on the surface of the granules while preventing them from sticking to each other and forming a hard cake. To achieve this the coated granules were dispersed in water, and the dispersion maintained by agitation until curing of the epoxy coat was complete. While soluble to some degree in most solvents and organic liquids, the dyes are practically insoluble in water. Another interesting point is that water has a catalytic effect on the reaction of an amine and an epoxy group. The coating agent used is a mixture of 85 parts by weight of epoxy resin "EPON 815", (DGEBA plus 11% butylglycidyl ether) and 15 parts of BDMA (benzyldimethylamine) as curing agent. The amount required is ten parts of epoxy for 90 parts by weight of granulated dye.

The installation used for coating consists of a 5-gallon Teflon lined vessel containing a baffle and a 5 inch (12 cm) marine-type mixing propeller. In operation the propeller is rotated at 150 rpm and the vessel is maintained at constant temperature by controlling the flow of steam through the jacket. The reactor is first filled with water and agitated while being heated to the reaction temperature ($60^{\circ}C$); the granulated dye is then poured into the reactor, followed by the required amount of premixed epoxy coating agent. Due to the agitation the coating agent readily forms an emulsion which fixes itself to the surface of the dye. The agitation as well as the temperature are maintained for two hours. The suspension is then filtered and rinsed with cold water, drained and placed in an oven at $100^{\circ}C$ for 2 days to dry. Success is assured if strong turbulent mixing is maintained to keep the dye well dispersed and prevent aglomeration; this agitation must be maintained until the reaction has proceeded to the point where the particles will not stick together.

Advantages of Coated Dye

Burning tests conducted with generators filled with compositions formulated with treated and untreated dyes showed equivalent results in terms of burning time and smoke performance (color and volume). However, processing, curing characteristics and mechanical properties are influenced differently depending on the color of the dye.

Most of the work was carried out with red dye as this technique was developed primarily to solve the processing problems encountered with this dye. Table VI contains EOM viscosities (measured at $60^{\circ}C$ with a Brookfield Model RVF 60 min after the addition of the curing agent) and Shore "A" hardness after 6 days of curing at $60^{\circ}C$ for coated and uncoated red dye compositions. Each composition has a solid distribution of 38, 32, 8 and 2 parts of dye, KCl_3, lactose and sodium bicarbonate. At 80% solids, the EOM viscosity is reduced from 5 to 2.2 when coated dye was used instead of granulated dye; however the drop in viscosity becomes greater when the solids load is increased.

TABLE VI

EFFECT OF COATED DYE IN RED COMPOSITIONS

Solids % by wt.	Dye	EOM Viscosity kP @ 60°C	Shore "A" Hardness (6 days @ 60°C)
80%	UNCOATED	5	22
	COATED	2.2	45
84%	UNCOATED	21.1	23
	COATED	2.8	45

NOTE: Solid Load: 38, 32, 8,2 parts by wt of Dye, $KClO_3$, lactose, $NaHCO_3$.
Binder (% by wt): R-45M-55, IDE-30, DDI-15.

At 84% the EOM viscosity is lowered from 21.1 to 2.8 kP. The use of coated dye influences the physical properties of the cured composition as well. With treated dye, hardness is double that obtained with untreated dye.

Table VII shows comparative results for green, violet, red and yellow compositions containing 80% solids. In all cases, the curing mechanism is influenced by the dye because the Shore "A" hardness and mechanical properties are improved by the use of coated dye. While the EOM viscosity is not really reduced with other than the red dye there is actually an increase with the yellow dye. The general improvement in hardness and mechanical properties shows that the coating stops the negative action of the dye on the R-45M based binder.

The technique developed at DREV for coating dye with an epoxy proved to be a solution to the high viscosities and the poor curing of the red compositions formulated with R-45M polybutadiene. At 80% solids the coated dye was required with red only; with other colors, the coating improves curing and mechanical properties but acceptable results can be obtained with uncoated dye. However we believe that it will be imperative in the future to use coated dyes if higher solid loadings are required in castable coloured smoke compositions.

TABLE VII

Color	Dye	EOM Viscosity kP @ 60°C	Hardness Shore "A" 6 days @ 60°C	Mechanical Properties at 22.8°C (aging 0 day)		
				σ_m kPa	ϵ_m cm/cm	Modulus kPa
Red	UNCOATED	5.0	42	350	30	1900
	COATED	2.2	45	420	26	3500
Violet	UNCOATED	2.5	30	370	40	1700
	COATED	2.6	45	600	31	3470
Yellow	UNCOATED	1.7	46	530	32	3400
	COATED	6.0	56	--	-	-
Green	UNCOATED	2.1	33	370	35	2150
	COATED	1.6	48	475	26	4640

NOTE: Red Comp.: 38, 32, 8, 2 parts by wt of Dye, $KClO_3$, Lactose, Sod. bic.
Others: 40, 30, 8, 2   "   " " " "   " "   "   "
Binder(% by wt): R-45M-55 ; IDP-30; DDI-15.

SECTION II

ROLL-FORMED SHEETS OF COMPOSITE SMOKE COMPOSITION

In this section we will discuss the production of white smoke compositions in the form of thin flexible self-adhesive sheets. These sheets were produced from castable-type compositions based on the R-45M/DDI system. In the particular case of the white smoke composition, however, major modifications were made to the binder formulation to ensure proper curing and properties suitable for roll-forming.

The white smoke compositions that was used in this study was made up from the following ingredients:

Dechlorane (11.5 μm, Hooker Chemical Co.) 10-30% by weight,
Zinc Oxide (.8 μm, JT Baker No. 4360) 36% by weight,
NH_4ClO_4 (200 μm, St-Lawrence Chem) 10-40% by weight,
Binder: R-45M (ARCO Chem),
         DDI-1410 (General Mills) } 16% by weight.
         (NCO/OH = 1.8)

The unusually high NCO/OH ratio of 1.8 is the result of the consumption of the isocyanate by the zinc-oxide; tests conducted with standard binder having a NCO/OH of 1.0 and solid ingredients (ZnO, dechlorane, NH_4ClO_4) resulted in improper curing.

The first step of the fabrication consists of mixing the ingredients in a cone vertical model 8CV mixer according to the standard procedure for preparing composite compositions. The compositions were cast into 20 x 30 cm polyethylene liner bags. These bags were sealed and the composition was allowed to cure. By placing about 1 kg in each bag we obtained 20 x 25 x 1 cm cakes. After 24 hours of curing at $50^{o}C$, they reached a Shore "A" hardness of 20 which was the required value for rolling. The bags were then cut and discarded and the cakes were fed into the rolling mill. This rolling mill, Figure 7, was identical to that used for the compaction of dye (SECTION I); the two 15 cm diameter by 25 cm long rolls rotate at 8 RPM. The gap of the rolls was adjusted to the desired sheet thickness. (The setting for the first pass should not be less than 3 to 4 mm, however. It is suggested to make one or two passes at this thickness and then to proceed to the final setting. In the case of the thinnest sheet a total of four to five passes are required.)

These white compositions will cure to a final Shore "A" hardness of 70; however they must be roll-formed when they are only partly cured i.e. when the hardness is less than 30. At that point, the paste will still contain unreacted groups which will give a self-adhesive sheet. If desirable, the sheet can be bond immediately to another material like a casing or a rigid support. The final curing period of 5 days at $60^{o}C$ will then strengthen this bonding. When such bonding properties are not wanted, the sheets can be spaced with a non-adherant material such as polyethylene sheets and allowed to cure. They then can be used as completely-cured flexible sheets without adhesive properties.

The thickness of the sheet that can be produced depends on the hardness of the composition at rolling time. Figure 8 illustrates the conditions that must prevail; the hardness must be between 10 and 30. Above this range the material is over-cured: it is too hard and tends to return to its original shape. Below 10, the opposite situation occurs, where it is too soft and sticky. The minimum thickness that can be obtained with this type of composition is 1.0 mm, and the thickness varies inversely with the hardness. For thicker sheets, it is preferable to use softer (less cured) compositions while thinner sheets will be prepared more easily from harder compositions. A hardness of 18 to 20 is suitable for all thicknesses.

These sheets can be used in many applications. Their adhesive properties make them applicable in special arrangements; they can be bonded against a support like cardboard, a casing or any other material. They can be rolled with some spacings to make multi-perforated-type high-burning surface grains. They can be stamped into wafers or
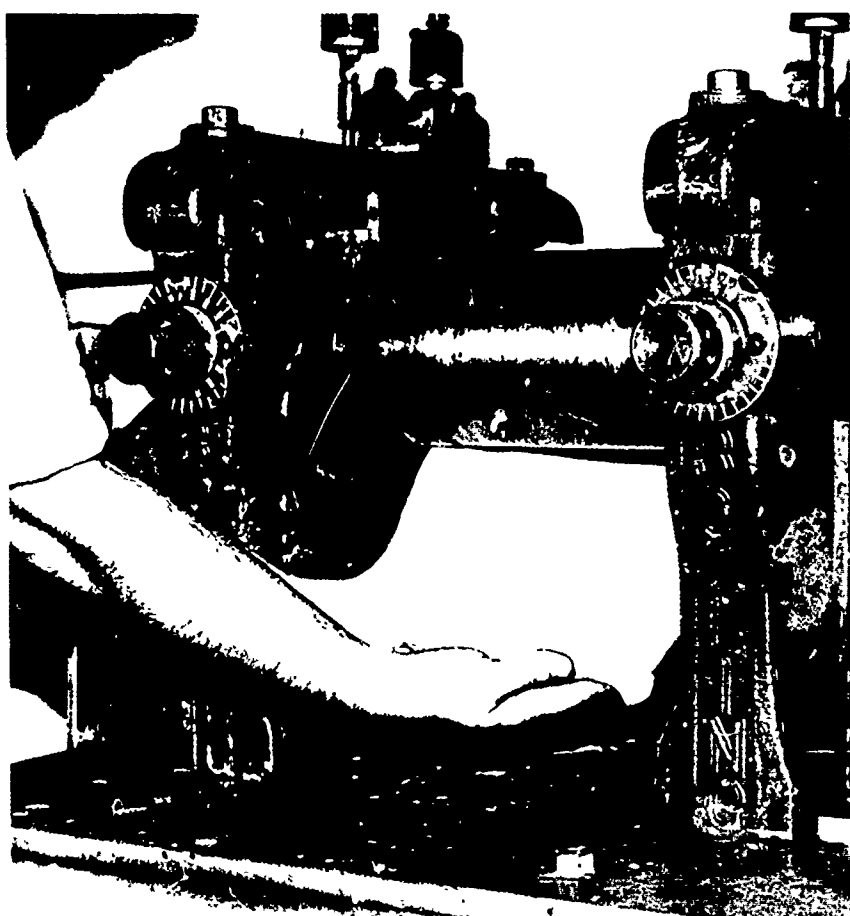
FIGURE 7 - Laminating Roller Mill

small pieces that can be assembled in various ways for special effects
of shape, burn surface and duration of burning. They can be worked
fully cured as well when adhesive properties are not required.

Tests conducted with other composite like coloured smoke described
in Section I, showed that they are suitable for rolling in about the
same conditions. However the presence of dye particles restrict the
minimum thickness of the sheets.
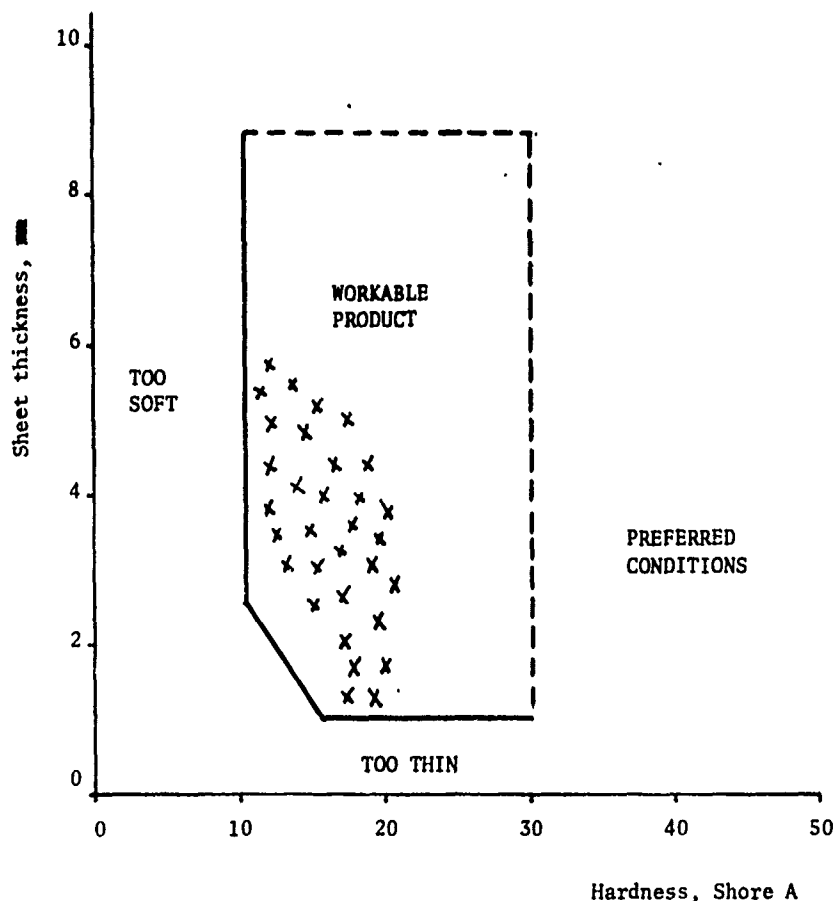
FIGURE 8 - Conditions Required for Rolling

CONCJLSION

The granulation of organic dyes used in smoke compositions
has provided a solution to the problem of high mix viscosity. Whereas
the maximum solids loading of orange compositions was in the order
or 75% by weight (10-12 kP) with the powder dye available on the
market, it is now possible to obtain mixes containing up to 85% by
weight solids and having an end-of-mix less than 3.5 kP, with granu-
lated material of an average size of 650 m.

Equivalent improvements were obtained with the other dyes,
but their end-of-mix viscosity remains higher than that of 1-AAQ.
At virtually identical grain sizes the castability thresholds are

all above 80% by weight except for the red which shows marginal castability and improper curing at 80% by weight solids loading. In the latter case, the application of a protective coating of epoxy on the surface of the granules provides a barrier against the erosive action of the mixer and the attack of the binder.

Used in the same proportions as the dye available on the market, the granulated material as well as the coated dye did not affect combustion or smoke quality (colour and volume). However, the improved smoke composition manufacturing properties made it possible to raise the smoke composition solids loading, thus providing a considerable improvement in overall generator efficiency.

The work on a white smoke composition resulted in the development of a technique to produce thin sheets of flexible material with adhesive properties. This technique is not limited to white smoke compositions; it can be applied to all composite colored smoke and propellant compositions provided that they possess properties suitable for rolling. We believe that this technique should widen the applications for composite compositions by increasing the shapes and special arrangements that can be realised.

ON THE DESIGN AND DEVELOPMENT OF INSTRUMENTATION FOR STUDYING TRANSIENT FLAME PROCESSES

M. Bonner Denton, John Algeo and Scott B. Tilden
Department of Chemistry
University of Arizona
Tucson, Arizona 85721

ABSTRACT

Studies into the implementation and use of computer automated high-speed mapping techniques are described. Considerations involved in the development of experimental hardware and software are discussed.

INTRODUCTION

Due to the complex interactive nature of the processes occurring within heterogeneous flame systems, conventional manual experimental approaches often impose severe limitations on the nature and depth of the studies which can be realistically implemented. Many of the experimental problems encountered are even more difficult to overcome when studies must be conducted on transient combustion processes. A promising solution to many of these limitations has resulted from the development of an interactive computer controlled experimental system capable of providing high speed two- and three-dimensional contour maps detailing user selected combustion processes.

This paper will present many of the considerations and design parameter trade-offs which must be resolved during the development of such an experimental system. Both data detailing the system's current performance, studying conventional analytical flames, and the modifications necessary to extend these techniques to actual pyrotechnic flares will be considered.

EXPERIMENTAL

A variety of possible approaches exist for implementing high speed flame mapping, each of which has a combination of advantages and disadvantages.

In general, most approaches for rapidly acquiring an emission profile at a designated wavelength can be broken up into electronically scanning detectors coupled with a large area wavelength isolation device and fixed detectors coupled with a small area wavelength isolation device and an opto-mechanical scanner.

In deciding the relative merits of each of the possibilities within these two categories, a variety of criteria must be considered. These include:

(1) Wavelength regions to be studied

(2) Ease with which a specific wavelength can be selected

(3) Required wavelength resolution

(4) Photometric accuracy

(5) Photometric dynamic range

(6) Scan Speed

(7) Number of data points required

(8) Error detection

(9) Experimental flexibility

(10) Capability for performance upgrading

(11) Complexity/cost/reliability

In general, the available electronically scanning detectors provide superior scanning speed but possess other limitations. Vidicons, solid state diode arrays etc., currently are limited by poor photometric dynamic range, image blooming, limited wavelength

response, and inherent dependence on optical filters for wavelength isolation when operated in an X-Y spatially scanning mode. While image disector tubes provide a very reasonable dynamic range, image blooming is still a problem along with the other limitations encountered with arrays and vidicons.

Opto-mechanical scanning techniques while inherently much slower, can still be easily operated at speeds sufficiently fast to study many of the processes of interest occurring in pyrotechnic flares.

The greatest asset of opto-mechanical scanning lies in the great flexibility regarding selection of both the wavelength isolation device and the optimum detector type for the study at hand.

A wide variety of detectors including many types of photomultipliers can be used for ultraviolet, visible and near infrared regions, while photoconductive and photovoltaic solid state devices can be employed in the infrared region. The ability to use conventional grating monochromators provides convenient wavelength selection and the choice of resolution versus throughput.

The current configuration of the computer controlled high speed flame mapping system which has evolved is diagrammed in Figure 1 and shown in Figures 2-4. While initial developmental studies have been conducted on conventional, carefully characterized analytical flames, great care has been taken whenever possible to ensure that the techniques developed can be transferred to pyrotechnic flare devices. The ten-facet scanning mirror employs 38 mm square mirrors. The first five facets are set at zero, one, two, three, and four
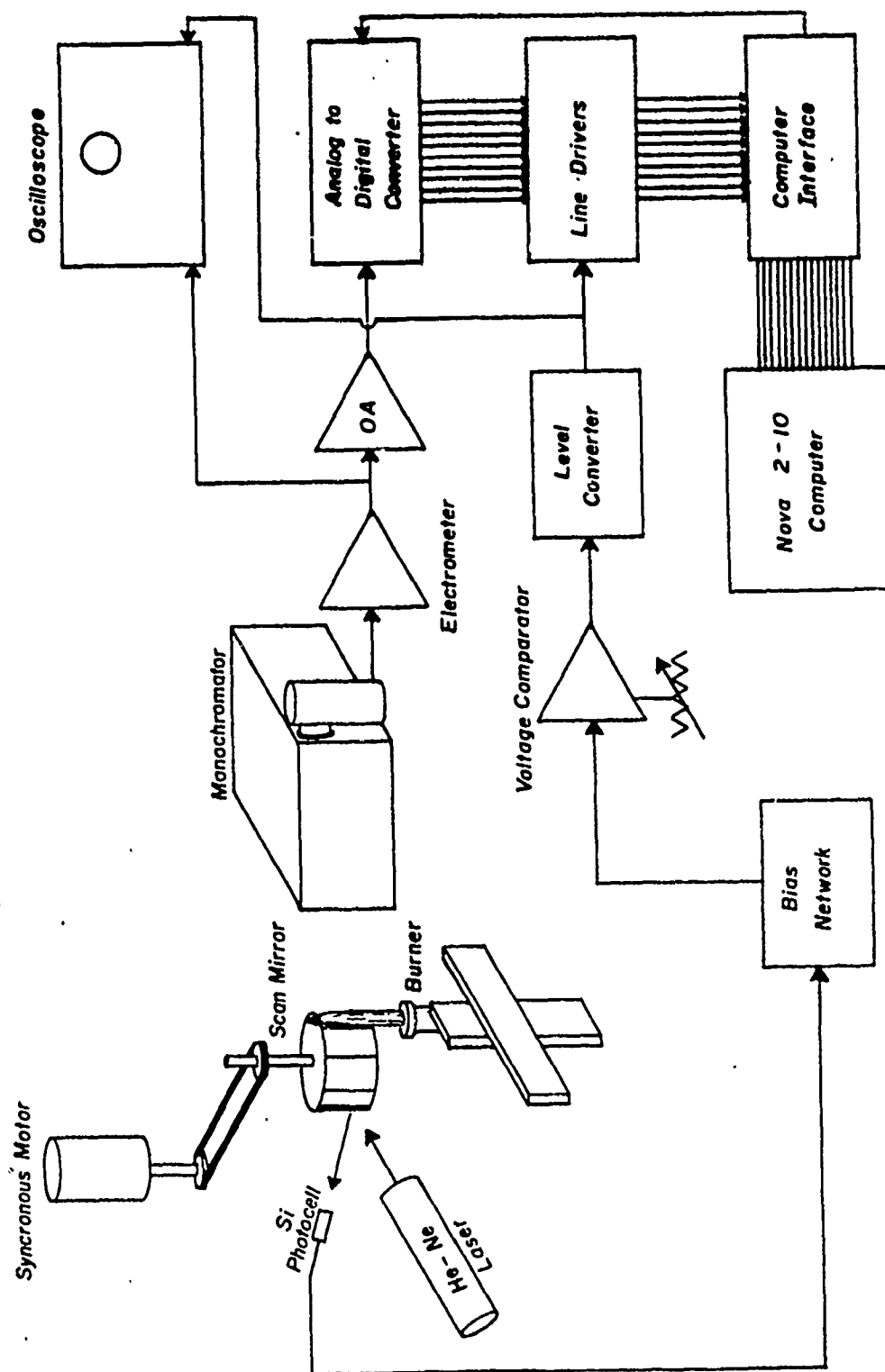
Figure 1: Diagram of the High Speed Flame Mapping System.

86
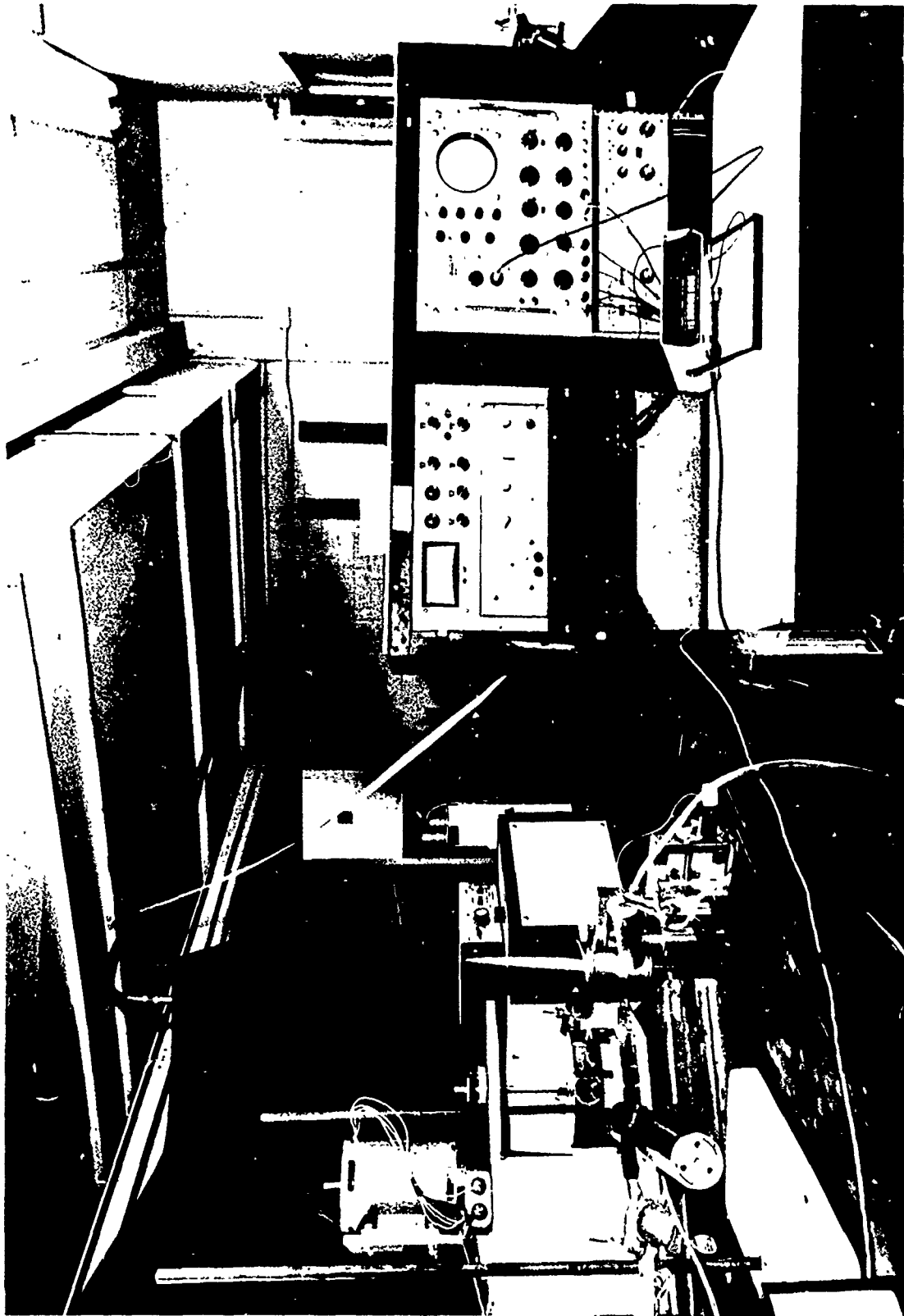
Figure 2: Overall Photograph of the High Speed Flame Mapping System.

87
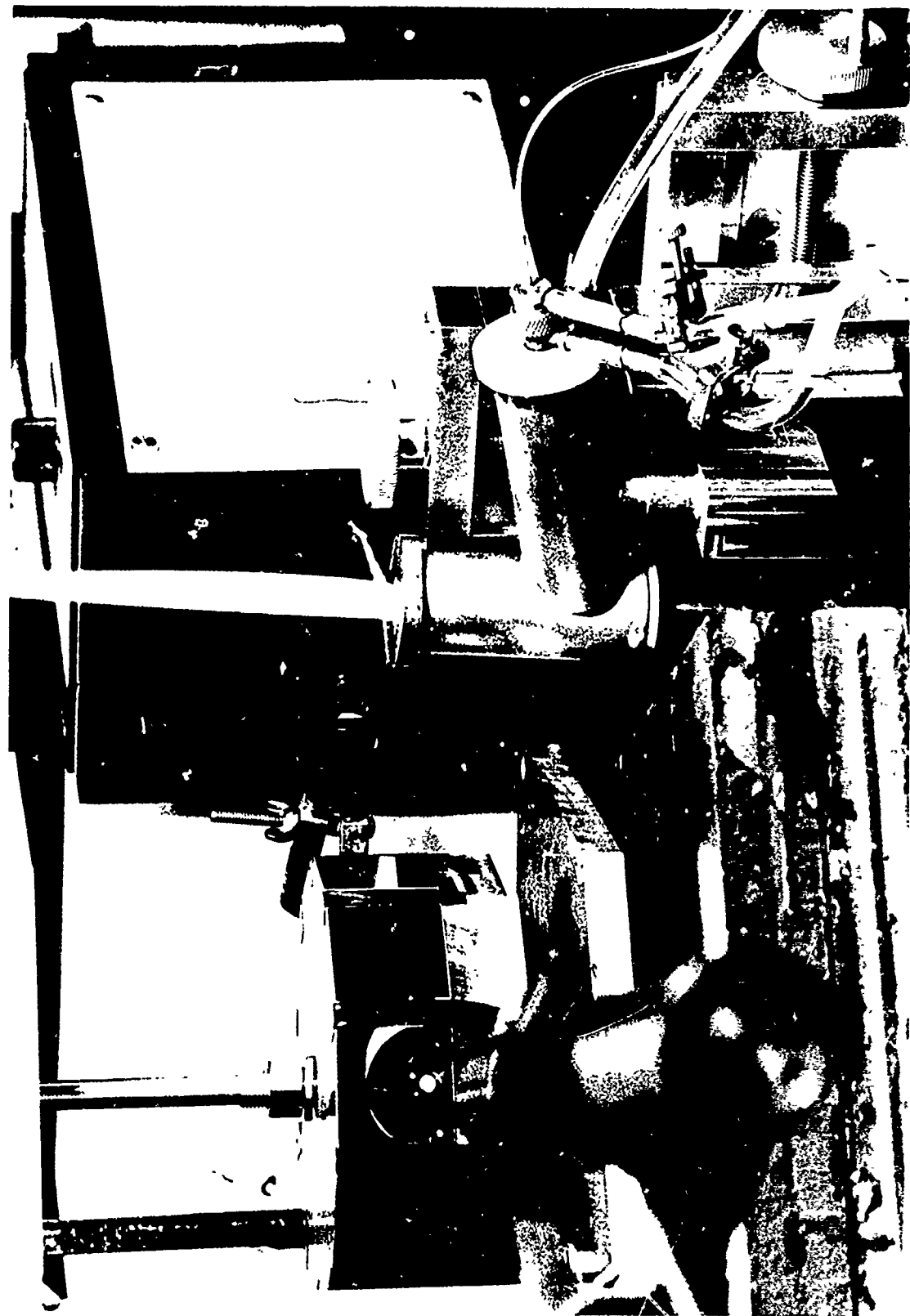
Figure 3: Close-up Photograph cf the Optical Table Showing Scan Mirror, Flame Monochromator, etc. (Note: helium neon laser used for synchronization can be seen as a reflection in one of the mirror facets.)
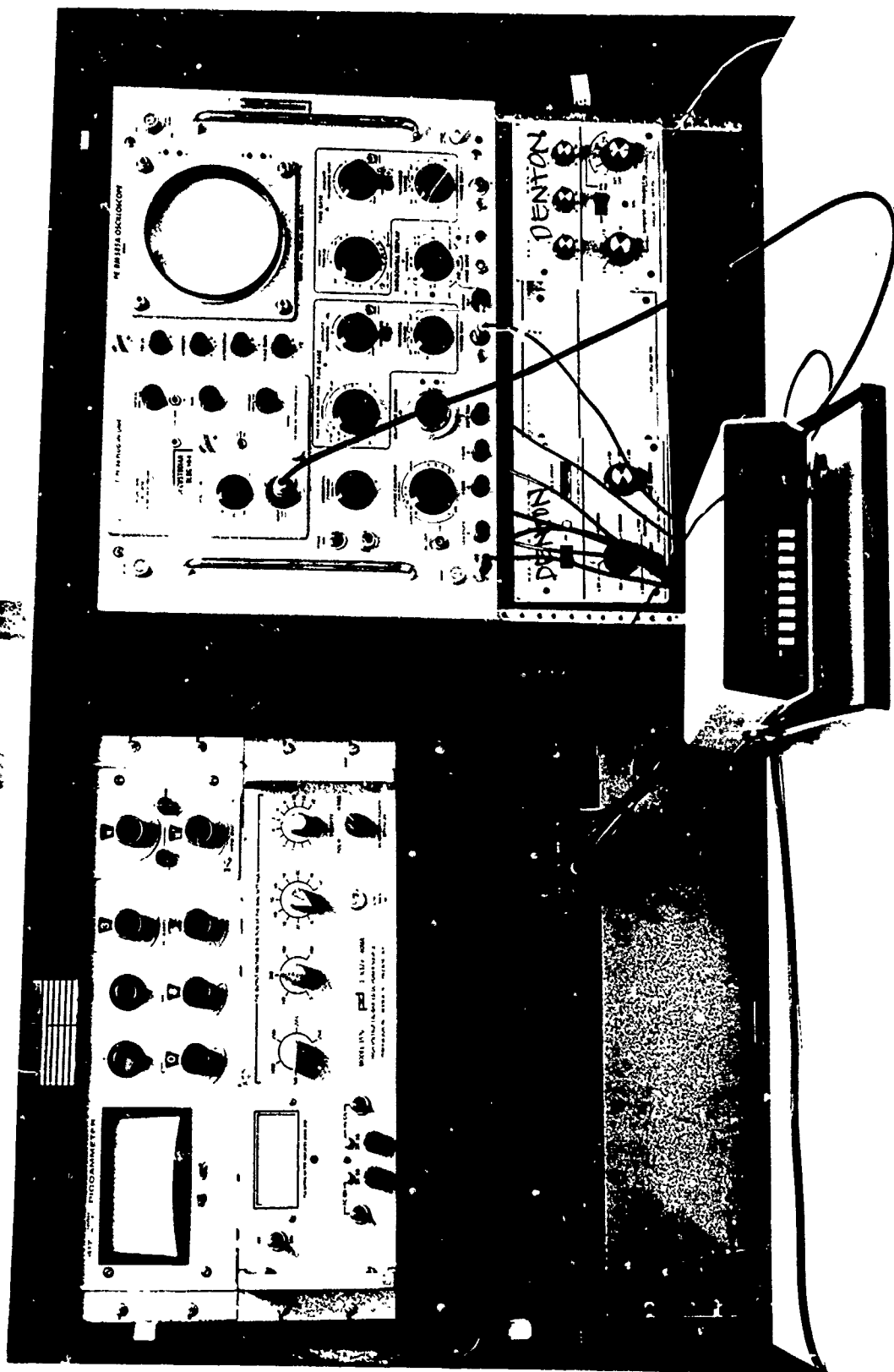
Figure 4: Close-up of the Electronics Console.

degrees. The next five facets are set at half degree offsets, creating an "interlaced" raster format which can be utilized for increasing the effective scanning speed when necessary. A synchronization pulse is derived by deflecting the beam from a 1.5 mW helium-neon laser onto a photoconductive detector which has been suitably positioned and masked to receive the laser beam only during exact alignment with a single mirror. The signal from the biased photo cell is conditioned with a voltage comparator, converted to TTL logic levels, and used for all subsequent timing during each individual flame scan. Photons emitted by the various areas of the flame under study are sequentially reflected from the scan mirror onto a pinhole iris, 1.0 mm in diameter, placed in front of the monochromator entrance slit. The 350 mm focal length f/6.8 GCA McPherson EU700 monochromator equipped with a 1180 1/mm 5000 $\overset{\circ}{\text{A}}$ blazed grating provides resolution of approximately 0.5 $\overset{\circ}{\text{A}}$. Presently, a R212UH photomultiplier tube is mounted in a Pacific Photometric Instrument housing containing an integral high-speed preamplifier which can be either employed or bypassed at the operator's desire.

The signal is subsequently fed to a modified Keithley Instruments Model 417 high-speed picoammeter whose output signal is degitized under computer command with a Burr Brown Research Model ADC-80 high-speed (20 usec/data point), ten bit resolution analog to digital converter. Analog display is provided by a Tektronix RM585A oscilloscope equipped with a type 86 high-speed plug-in.

The output of the analog to digital converter is subsequently
transferred through a set of parallel line drivers to a special
computer interface and, finally, a Data General NOVA 2-10
computer containing 16K words of memory. Mass data and software
storage is provided by an Xebec XFD-200 dual drive disc system,
while plotting is performed by either a Tektronix 4010 graphics
terminal or a Hewlett-Packard-Moseley Model 135 X-Y plotter.

Data Manipulation

Computerized data reduction can provide a variety of capa-
bilities which would not be possible utilizing less powerful
approaches.

Scan mirrors having the desired geometry are not available
commercially, dictating custom fabrication. While this might at
first appear to be an ambitious undertaking, problems associated
with holding precise optical tolerances, both on the offset angle
and radius for each mirror surface, can be easily sidestepped through
the use of the proper software correction techniques. In effect,
when an array of points is being translated into a map, the data
values are assigned locations offset by the required correction
factors.

In addition to reducing the mechanical tolerances required for
the rotating mirror assembly, problems associated with varying
mirror reflectivity can be eliminated through employing the proper
correction factors. The very serious problem of short term "flicker"
noise can be substantially reduced using weighted smoothing techniques

in both time and space. Consider that a single data grid is obtained containing randomly high and low values. A response surface can be smoothed considerably by employing a weighted average of each of the neighboring grid points. When the system is being scanned at a rate sufficiently faster than the rate of change of the phenomena under study, additional smoothing can be obtained by fitting a function to the response observed at a certain location as a weighted average based on time. This procedure is diagrammed in Figure 5. A smoothed time extrapolated series of maps could subsequently be generated on demand. Additionally, when it is valid to assume that the flame under study is symmetrical about its vertical axis, equivalent points on each side can either be simply averaged together or used in some more complex statistical treatment.

The presence of phenomena occurring on time scales faster than the total scan speed can be detected in two ways:

1. Comparing the signals observed from two adjacent mirrors (which are offset one degree) with that observed from the intermediate angle mirror on the opposite side of the scanner, can be useful for determining the presence of transients on time scales near the total scan speed. Figure 6A shows the absence of major changes as angles of 0 degrees and 1 degrees are compared with 0.5 degrees following a 100 millisecond delay, while 6B indicates short-term variation.

2. For vertically symmetrical systems, transients on time scales near a single horizontal scan can be detected by comparing the right-hand side with the left-hand side.

92
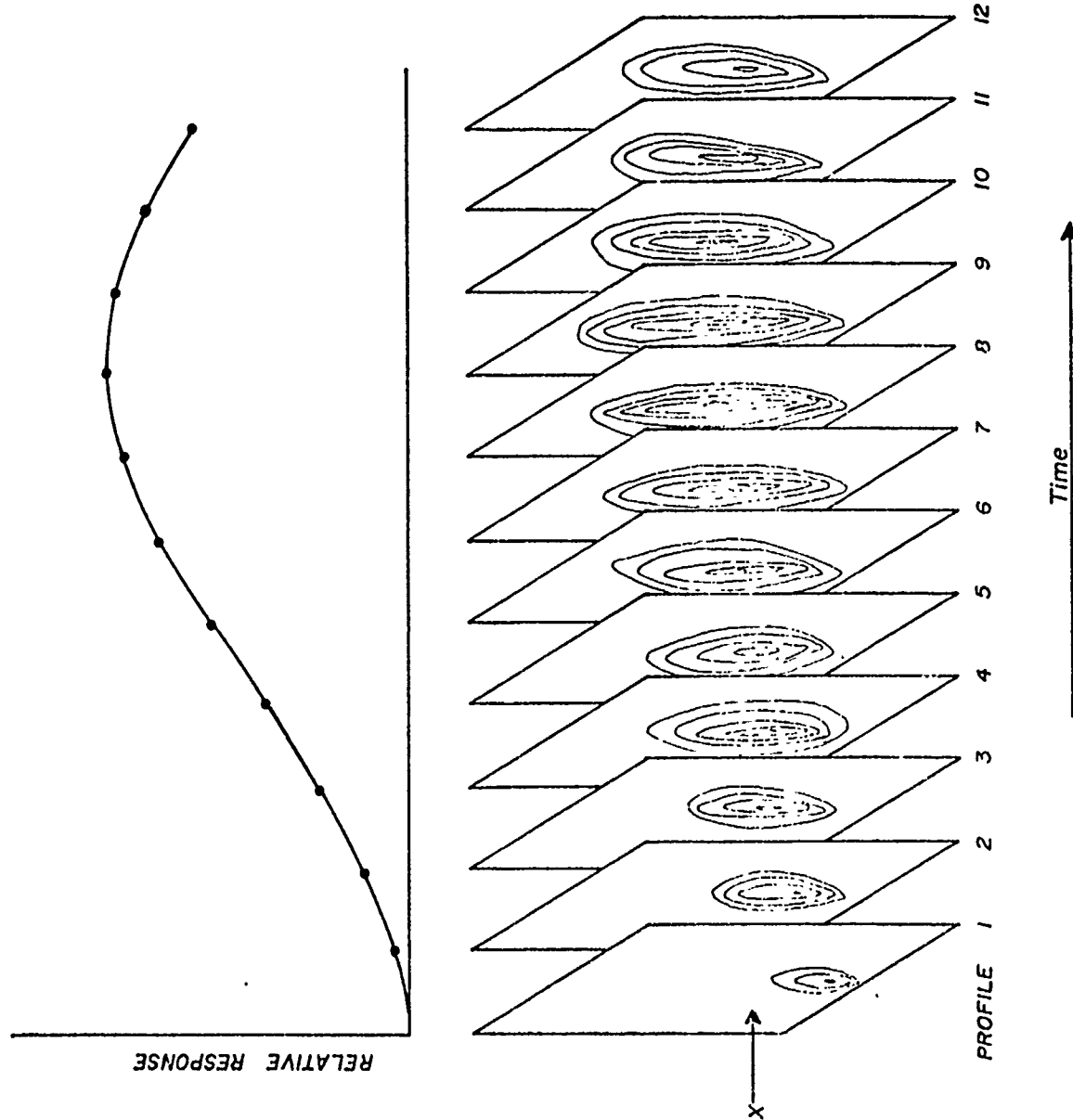
Figure 5: The Concept of Data Smoothing in Time by Curve Fitting to data obtained at a single location, X, to generate the smoothed curve above. (Curves of this type are then employed to generate each of the "smoothed maps".)

Figure 6A: Transient Phenomenon Occurring
Much Slower than Total Scan Speed.
(Note Signal at M_6 is between that
observed at mirrors M_1 and M_2.)
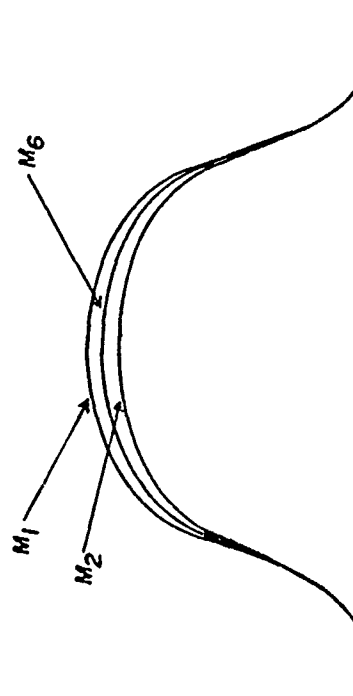
Figure 6B: Transient Phenomenon Occurring on Time Scale of
one Half Scan. (Note signal at M_6 much different
than M_1 or M_2.)

M_6

M_1

M_2

M_6

M_1

M_2

94
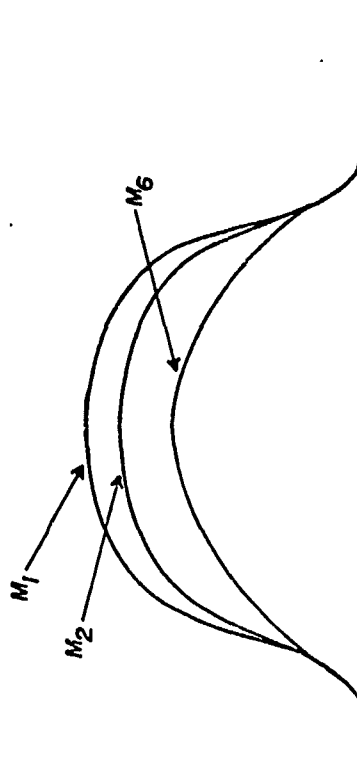
The experimental system has been used to generate two-dimensional 600 data point maps every 150 milliseconds or 300 data point maps every 75 milliseconds. Additionally, through the use of a specially derived approach based on Abel integral techniques, the system can generate three-dimensional profiles, horizontal "slices", and "thin film" verticle profiles.

Presently the system is being reconfigured to allow observation of pyrotechnic flare candles in a choice of ultra-violet, visible and infrared wavelength regions with the viewing zone to be in a special combustion chamber incorporating a high flow rate evacuation system.

ACKNOWLEGDMENTS

SIGNAL PROPELLANT EVALUATION

by

David R. Dillehay

Thiokol Corporation
Longhorn Division
Marshall, Texas

ABSTRACT

This paper deals with the analysis and solution of
a production problem on the M125 Series hand-held
signal. It is significant in that it points out the
subtle changes that may occur in pyrotechnic raw
materials that can have dramatic and confusing effects
on end item performance.

The specific example concerns catastrophic failure of
the signal rocket motor and the subsequent evaluation
and elimination of the problem. It was found that raw
material and processing changes resulted in loss of
physical strength of the propellant grain. Improve-
ment in materials and processing was not sufficient to
totally correct the change. A complete solution was
obtained by venting the head-end propellant spacer to
balance the internal pressure of the signal motor dur-
ing firing.

INTRODUCTION

The hand-held signal is a man-launched rocket that carries a pyrotechnic payload used for signaling or illumination. The propulsion system consists of a solid propellant grain burning in a stainless steel casing tube with a delay housing and nozzle plug closing the motor cavity and held in place by a stainless steel bolt. The propellant assembly is composed of three perforated increments glued together and inhibited on the ends and outside with Pettman Cement. The increments are consolidated from propellant composition made by incorporating calcium carbonate in black powder.

The signal is launched by striking a firing cap while holding the launcher barrel by hand. An initiating charge is ignited by a primer and provides the force to accelerate the signal to an exit velocity of approximately 50 ft/sec. The initiating charge also serves to ignite the propellant assembly. Normally, there is an ignition delay of 40 to 50 milliseconds between launch and propellant ignition. This allows time for the signal to clear the gunner's head and provides a margin of safety.

In 1976, Longhorn Army Ammunition Plant (LAAP) began manufacture of signals using propellant composition manufactured at the Belin Powder Works in Moosic, Pa. The Belin Powder Works was originally owned and operated by E. I. dupont deNemours & Co. In 1973, Gearhart-Owens, Inc. took

over operation of the plant and later operated under the name of Goex Corporation. This is currently the only commercial black powder plant in the western hemisphere.

In September of 1976, a Longhorn signal lot had a motor blow at Jefferson Proving Ground during acceptance testing. This motor failure prompted an immediate investigation to determine the cause of this unusual occurrence. The investigation included static tests from all propellant composition lots used from Goex Corporation. The tests showed a high level of propellant grain break-up and anomalous pressure-time traces from all lots. Based on these test data, a recommendation was made by Thiokol Corporation that the manufactured signal lots already tested and accepted be put in suspended status pending additional evaluation.

This paper will report on the evaluation and solution of this problem.

BACKGROUND

The nominal propellant composition formulation is as follows:

Potassium Nitrate	67.2%
Sulfur	9.4%
Charcoal	14.2% ·
Calcium Carbonate	9.2%

At the time of consolidation into propellant increments, the composition must contain 1.8 to 2.5% moisture.

The manufacture of propellant composition is exactly the same as black powder with the addition of calcium carbonate. The materials used are potassium nitrate, sulfur, charcoal, and calcium carbonate. The charcoal originally used for black powder was made by a retort process. Three and one-half years ago, at the time that Goex Corporation took over the operation of the Belin Works, the Environmental Protection Agency ruled that extensive anti-pollution measures be applied to the retort process. As a result, the vendor switched to a kiln process for the manufacture of charcoal. All charcoal purchased by Goex Corporation has been kiln charcoal.

The potassium nitrate is weighed into burlap bags in preparation for mixing. The required proportions of sulfur and charcoal are put in a ball mill with steel balls and milled to produce a "pulverize charge". The pulverized mixture is weighed into bags in preparation for mixing.

The materials required for approximately 450 lbs. of propellant composition are taken to the mix-muller. The muller consists of two 10-ton iron wheels with plows to give a mixing action similar to a Simpson Muller. The weight of the wheels provides a crushing action to reduce the particle size of the potassium nitrate and incorporate the materials in an intimate mix. During the mulling operation, water is added to keep the mix from dusting too much. The heat generated and the moisture present cause solution and re-crystallizing action of the potassium nitrate and leads to a highly mixed powder. The water is added, also, to adjust the final moisture content of the wheel cake to about 3 or 4%. Historically, the calcium carbonate content drops about 1% during the mixing operation and the potassium nitrate content increases approximately 1%. This seems to be due to an actual loss of calcium carbonate at the wheel mill (possibly due to dusting of the fine powder.) The operation of the wheel mill is an operator-judgment process. Experience with the look and feel of the powder plus adjustments based on local weather conditions are the main controls on the time of mixing. On completion of the mulling operation, the operator uses a wooden shovel to load the wheel cake into bags for transfer to the hydraulic press building.

The propellant composition is taken to the press mill and moved to a hopper. The powder is charged into a large box divided into compartments with aluminum plates spaced

100

approximately 2 inches apart. A hydraulic press is used to press the powder into blocks about 2 ft. x 2 ft. and 1-1/4 inches thick. The propellant composition blocks are removed from the press by hand and hand-fed into a chipper to reduce the blocks to small chunks.

The chunks of powder are taken to a corning mill where they are ground to size and screened to meet a finished product screen requirement. After the corning mill operation, the powder is taken to the glaze mill.

The glaze mill is only used to blend the powder from several wheel mills into a homogeneous product. No graphite is added to the propellant composition and the tumbling time is kept to a minimum. If it is necessary to reduce the moisture of the propellant composition, it is done in the glaze mill by blowing warm dry air through the glaze barrel. Each glaze barrel is identified as a powder lot and generally contains 2000 to 3000 lbs. of propellant composition.

After blending, each lot is run through a sifter to assure the final particle size distribution is within specification and the powder is packed into 25 lb. kegs.

Laboratory analyses on the propellant composition includes a compositional analysis, moisture, particle size distribution, burn time, and density. The burn time is run on a rolled lead tube segment and is reported in seconds/yard.

At LAAP, the propellant composition is pressed in a Stokes rotary press to make propellant increments 0.968 in.

in diameter and 0.686 in. long. A center perforation of 0.358 in. is formed with a core rod. Three propellant increments are joined with Pettman Cement and the outside and ends are inhibited with Pettman Cement. The assembly is placed in a steel casing tube as shown in Figure I. The propellant is held tightly in place by two cardboard spacers.

A modified closure for the head-end of the casing tube permits recording a pressure-time trace during burning. A typical normal pressure-time trace is shown in Figure II. Testing of the Goex propellant composition produced some normal traces and some highly irregular traces as shown in Figure III.

Another test procedure used for propellant evaluation is sound trace evaluation of flight tests. The signal is conditioned to a specific temperature (usually $-65^\circ F$, $70^\circ F$, of $160^\circ F$) and fired from a fixture. A recording oscillograph records the sound pickup from a microphone placed near the base of the fixture. A computer program is used to correct the sound timing for the travel of the signal resulting in very close agreement of static test burn times and flight test burn times. Using sound trace data and plotting histograms then gives a good picture of the performance of the signal propellant under dynamic flight conditions. Figure V shows a comparison of static test and flight test burn times for similar motors. Another parameter obtained from the sound trace is the ignition delay of the motor. If the delay

is too short, the signal motor comes up to pressure while at head level with the person firing the signal. Propellant failure at that point could be fatal. If the delay is too long, the signal will try to tumble due to the forward tail fin. On becoming propulsive, the signal may be pointed horizontally or even back towards the person firing the signal. Either case may result in serious or fatal injury.

TEST RESULTS

Static and flight tests on the propellants in production had shown that a serious problem existed. In discussions with Goex engineers, three possible changes in propellant composition were disclosed. First was the obvious change from retort charcoal to kiln charcoal. The kiln charcoal had been cited as an improvement in performance for black powder. No other system uses consolidated black powder in a free-standing propellant grain, however. Estes Industries uses pressed black powder in model rocket motors but supports the end burning grain by pressing in a cardboard tube. The effect of the change in charcoal on the physical properties of the propellant was not known. The second change was in the density of the propellant composition. There was no density requirement in the specification. The original propellant composition developed by duPont held the density in a range of 1.69 to 1.76 gm/cc. Goex found that they could increase the throughput of the plant by increasing the density. The last few lots tested

were in the density range of 1.79 to 1.83 gm/cc. Since the propellant composition is pressed to a density of 1.82 to 1.89 gm/cc., less particle deformation and mechanical interlocking would be expected with high density powders. The third possible change was in the calcium carbonate. There are two basic types of calcium carbonate - aragonite and calcite. The aragonite is generally orthorhombic and the calcite is generally hexagonal. X-ray diffraction patterns of calcium carbonate from old duPont propellant and from new Goex propellant showed both to be of the calcite type. The width of the diffraction pattern suggested, however, that the calcium carbonate used by duPont might have been finer than that used by Goex. Contact with Charles Pfizer & Co., supplier of calcium carbonate, revealed that the calcium carbonate being furnished to Goex was calcite with a scalenohedral crystalline structure. They did have a finer grade of calcium carbonate. All three grades of calcite that they manufacture would meet the specification requirements. The material Goex had been using was nominally 2.5 microns weight mean diameter. The finest calcium carbonate available was 0.8 microns weight mean diameter.

The first test tried was a reduction in the density of the powder. Goex made a powder lot and reduced the density of the propellant composition to 1.73 gm/cc. This material consolidated to a smoother, more uniform looking pellet but still exhibited evidence of break-up. The severity and fre-

quency of break-up was lessened over the high density powders, however,

A test plan was developed to evaluate the effect on propellant composition of 1) the type of calcium carbonate, 2) the quantity of calcium carbonate, and 3) the quantity of charcoal. The following formulations were manufactured by Goex for testing at LAAP:

Lot No.	% KNO_3	% C	% S	% $CaCO_3$	Sp. Gr. gm/cc	% H_2O
88-11	67.40	14.60	8.85	9.15	1.701	2.40*
88-12	66.10	14.15	8.65	11.10	1.756	2.60**
88-13	64.65	14.30	8.40	12.65	1.811	2.60*
88-14	67.25	12.10	11.10	9.45	1.773	2.70**
88-15	65.80	11.60	11.00	11.60	1.786	2.20**
88-16	67.45	10.60	12.55	9.40	1.791	2.35**

*Albagloss calcium carbonate (Charles Pfizer & Son, Inc.) - 0.8 micron, WMD

**Albacarr calcium carbonate (Charles Pfizer & Sons, Inc.) - 2.5 micron, WMD

Propellant composition from each lot was consolidated and assembled into signal motors for ballistic testing. Moters were tested both statically and in flight. Figure VI shows a comparison of flight burn times at 160°F. The flight tests showed break-up of propellants in all six lots at 160°F and at 70°F. Lot 88-16 had 5 motor blows in the first 15 signals tested at 160°F and testing was terminated on that lot at 160°F. None of the other lots used in signals blew

up at 70°F or at -65°F.

The motor blows with Lot 88-16 indicate that reduction in the amount of charcoal in the formula n reduces the tensile strength of the propellant composition. Since Lots 88-14 and 88-15 also reduced the charcoal content, these lots, as well as Lot 88-16, were eliminated from further testing.

The sound trace data were used to evaluate ignition delays in the signal motors. The analysis showed that Lot 88-13 had excessive ignition delays at all temperatures. Therefore, Lot 88-13 was eliminated from further testing. The ignition delay of Lot 88-12 was judged marginal at 70°F and unacceptable at -65°F. Ignition delay in Lot 88-11 was judged satisfactory at all temperatures. See Figure VII.

The remaining lot, 88-11, was similar in performance to the original propellant composition but with an improved ignition delay. The improvement in ignition delay could be attributed only to the reduction in calcium carbonate particle size. The improvement in ignition delay was a significant achievement, but the problem of propellant break-up in flight was still unacceptable.

Analysis of all the ballistic test data showed that the propellants were failing in tensile strength due to internal stress during motor firings. The signal rocket motor used a solid ring propellant spacer at each end of the propellant which seals the ends for the first 100 to 200 milliseconds of motor burning. See Figure I. During this time, the motor

106

assembly is subjected to an ignition pulse of 200-250 psi for 10-20 milliseconds, followed by a rise in chamber pressure to approximately 250 psi. See Figure II. At this time the aft propellant spacer usually burns through and allows pressurization of the volume behind the propellant grain, thereby equalizing the forces on the propellant assembly. This is seen on the trace as a momentary drop in pressure. No propellant break-ups have been observed in static tests after this equalization occurred.

It is standard practice in solid propellant rocket motors to provide a vent in the head end area (except on case bonded grains) to permit equalization of the pressure on the inside and outside of propellant grains. By maintaining a seal at the aft end of the grain, flow of propellant gases is prevented and satisfactory performance obtained. Since signal motors vent naturally approximately 150 milliseconds into the burn, it was decided to put a vented spacer in the head-end of the signal motor.

Various designs, from notched spacers to sections cut and glued to the grain, were tried and the final method chosen for ease of implementation in production was simply a 5/8 in. gap cut in a standard spacer. All of the vented spacer designs were successful in eliminating propellant break-up. To illustrate, propellant lot 88-8-6 was made into signal motors. This lot of powder was chosen because flight tests of 80 signals at 160°F using this powder re-

sulted in 9 motor blows and 46 short burn times indicative of propellant break-up. A total of 225 signals from this lot were then tested with various vented spacers. Not one single case of propellant break-up was recorded. See Figure VIII. Other propellant lots were similarly tested with the same results. See Figure IX. Static tests showed that normal pressures and burn times are recorded with vented spacers and examination of motor casing tubes showed no hot spots or other evidence of functional problems.

The vented spacer has been implemented in production along with the use of finer calcium carbonate in propellant composition manufacture. Thousands of signals have been loaded and fired without further propulsion problems.

This problem is not unique in production. Similar problems are frequently encountered in systems that have been successfully produced for years. Subtle changes in raw materials or even in component parts can creep into the system and result in rejects or hazardous items. Sometimes the tolerance on a parameter is at fault. Sometimes it is a change that is not even covered in the specification. Designers and users both should be alert to changes in materials or components that can result from improvements in technology, cost-saving short-cuts by a vendor, environmental requirements (causing process modifications), or even changes in raw material sources. Many examples can be cited where only one vendor's product can meet performance requirements

although no discernable difference exists from raw material acceptance tests. These instances retard advancement of pyrotechnics to a science and foster the "black magic" image we would like to shed.

Nozzle Plug

Bolt

Propellant Assembly

Head-end Propellant Spacer

Aft Propellant Spacer

Delay Housing

Casing Tube
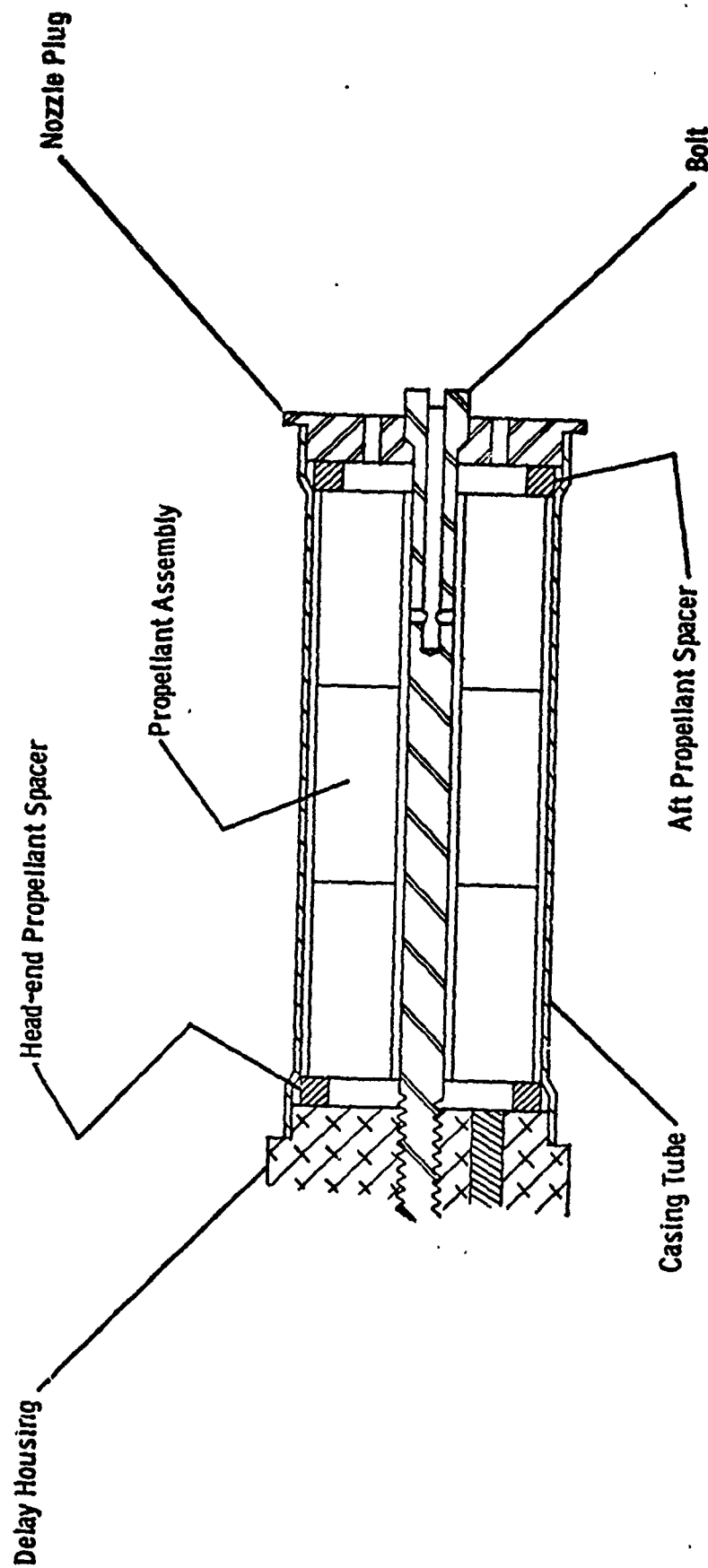
Note: Tail Fin omitted for clarity

SIGNAL ROCKET MOTOR

Figure 1.

110

PRESSURE – TIME TRACE

Figure 11.
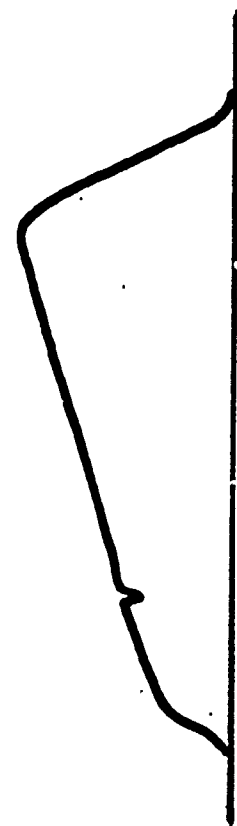
Normal Trace
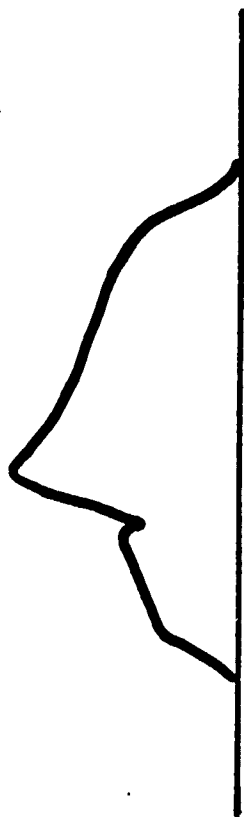
Moderate Break-up
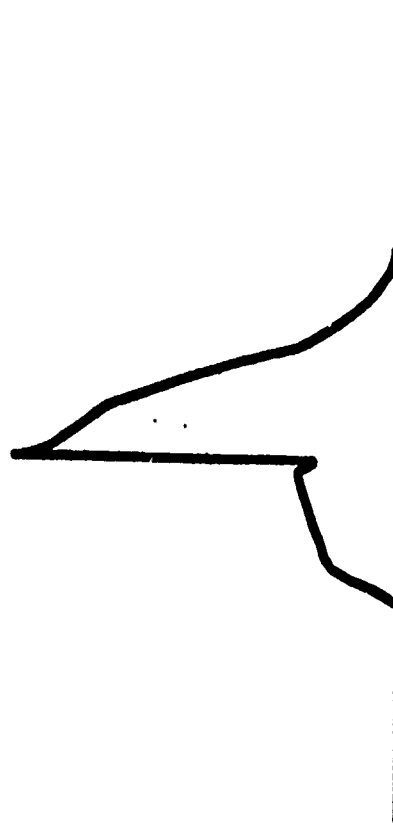
Severe Break-up
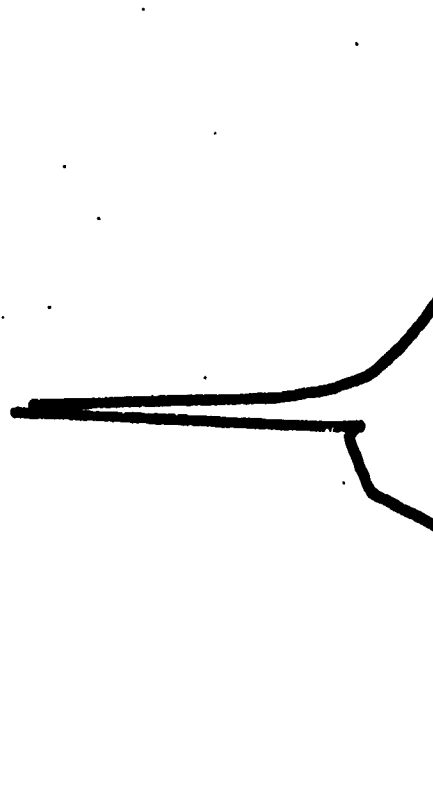
Catastrophic Break-up
(Motor Blow)

PRESSURE–TIME TRACES

Figure III.

112
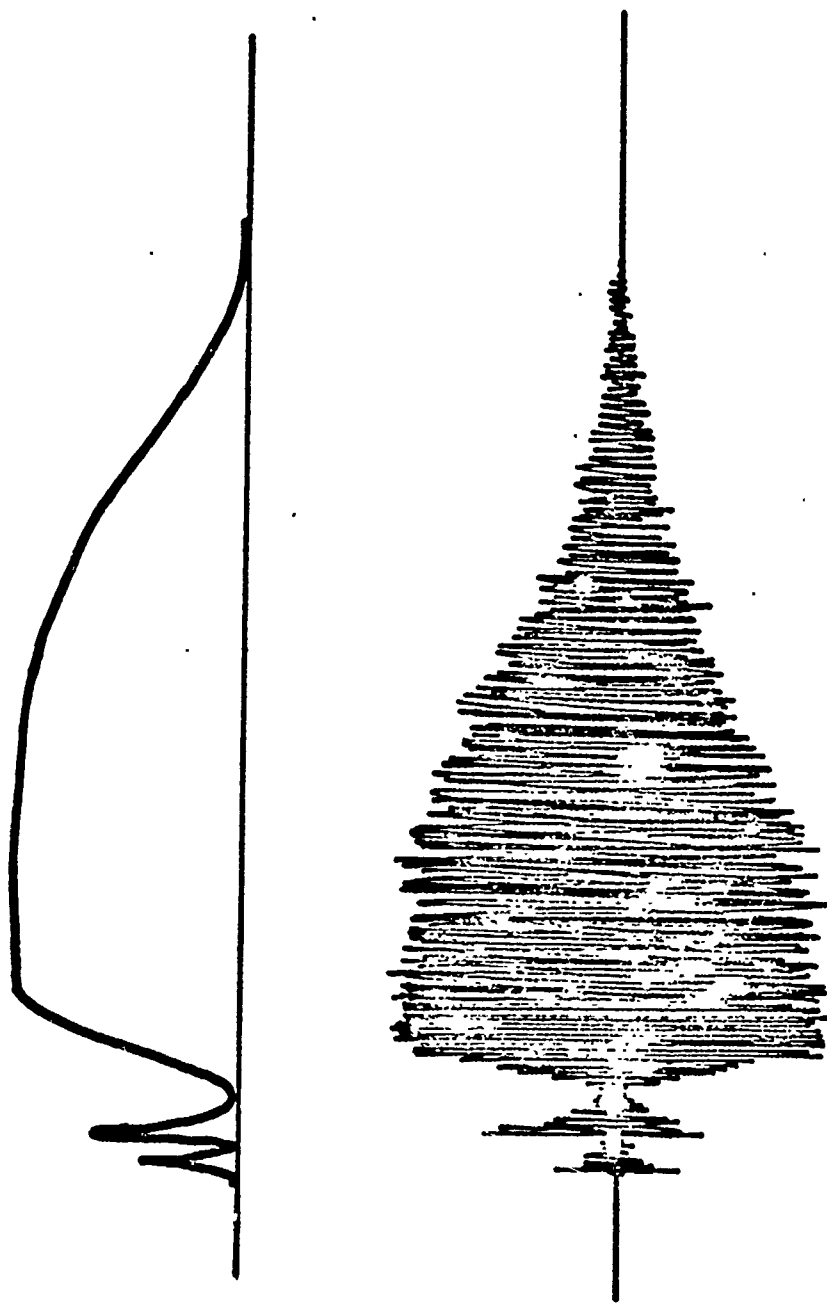
TYPICAL SOUND TRACE

Figure IV.
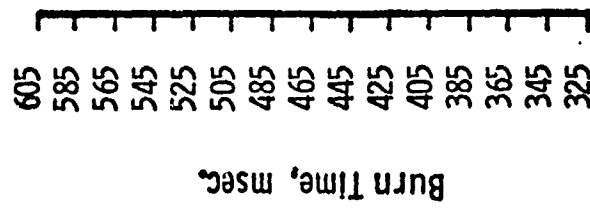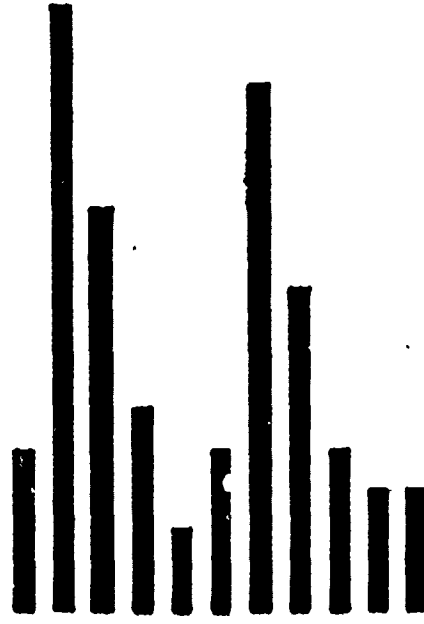
160°F MOTOR BURN TIMES

GOI-88-8-6
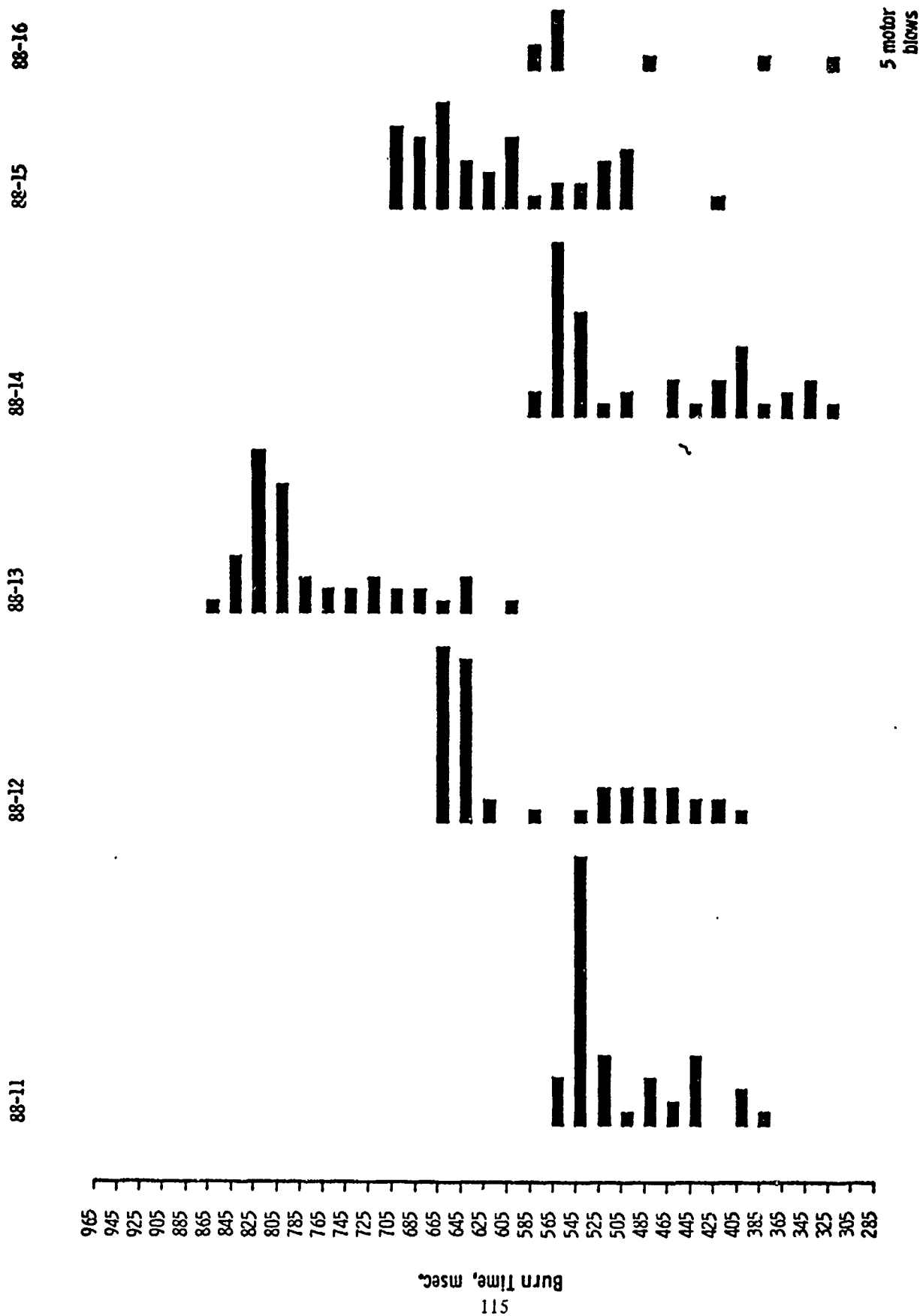
Figure V.

160°F FLIGHT MOTOR BURN TIME

Figure VI.

115

-65°F IGNITION DELAY

Figure VII.

116

GOI-88-8-6ʹ FLIGHT TESTS

160°F

Figure VIII.

585 565 545 525 505 485 465 445 425 405 385 365 345 325 305

Burn Time, msec.

117
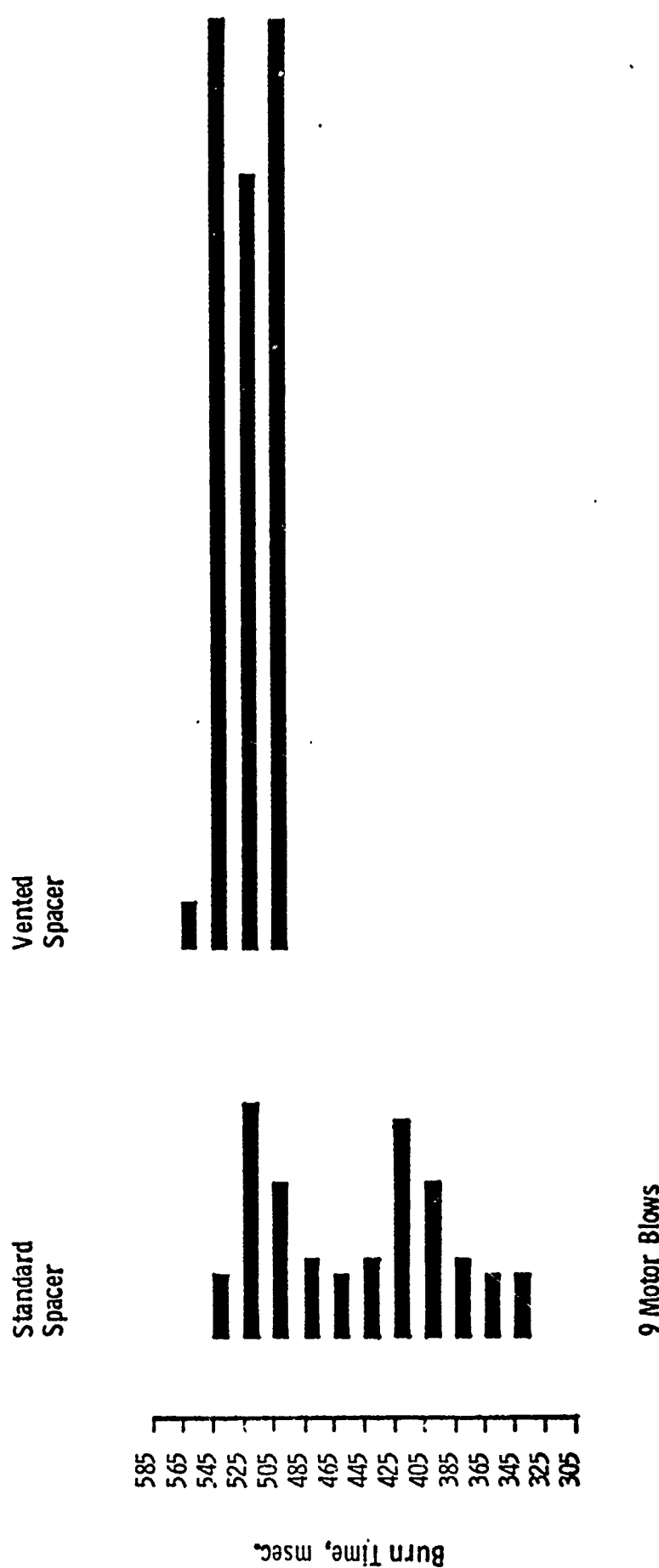
Vented
Spacer

Standard
Spacer

Burn Time, msec.

605
585
565
545
525
505
485
465
445
425
405
385
365
345
325
305
285
265
245
225
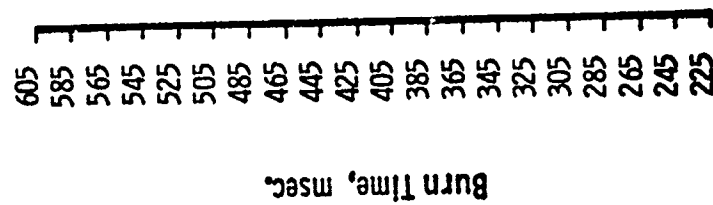
GOI-88-9-1 FLIGHT TESTS

160°F

Figure IX.

118

THE IGNITION AND DEFLAGRATION OF POTASSIUM PICRATE (KP) AND KP/EXPLOSIVES MIXTURES: LOW-VOLTAGE, NONPRIMARY DETONATORS

by

Robert H. Dinegar
University of California, Los Alamos Scientific Laboratory
Los Alamos, New Mexico

ABSTRACT

Potassium picrate (KP) has been examined as a material which can be easily ignited to deflagration by a hot wire for application in low-voltage detonators which contain no primary explosives. KP can be ignited by a 0.05-mm-diam Nichrome wire at the 1-A/1-W level.

KP mechanically blended with PETN or HMX in 10/90% by mass mixtures exhibit similar hot-wire ignition behavior to pure KP. These deflagrating mixtures generate higher pressures than pure KP and are therefore more useful as donor charges for accelerating an impact plate onto an acceptor charge or for driving a stress wave into a deflagration-to-detonation transition charge.

Ignition and deflagration of KP and KP/explosives mixtures have been studied in terms of their dependence on explosive, electrical, and configuration parameters. These results are applied to the development of detonators of two types, flying plate detonators and deflagration-to-detonation transition detonators.

I. INTRODUCTION

Potassium picrate (KP) is a high-temperature stable, crystalline substance that can be ignited to deflagration by a rapidly heated bridgewire. The voltages and currents necessary are in the area of several volts and amperes. KP mixed with secondary high explosives such as PETN and HMX also can be ignited at these same levels.

The development of the deflagration in ignited KP/ high explosive mixtures depends greatly upon density and degree of confinement. High-density (ca 1.6 g/cm³) mixtures confined in thick-walled steel or brass generated a maximum pressure of around 0.3 GPa in a volume of about 1 cm³, in several milliseconds.

We have not found pure KP useful in detonators. KP mixed with PETN or HMX, however, can be used as initiators of other explosive charges in low-voltage detonators containing no primary explosives.

II. KP MIXES AS DONOR CHARGES

KP mixed with PETN or HMX can be used as donor charges in hot-wire detonators in two ways. In the first, which is called "deflagration-to-detonation-transition" (DDT) initiation, the deflagrating donor charge is coupled directly to a confined secondary explosive charge. This transition charge must be of such type, density and size that the deflagration will change into a detonation. The second, which is called "flying-plate" (FP) initiation involves igniting the donor and using the pressure generated to shear a metal disk.[1] This flying plate moves across an air gap and impinges on an acceptor explosive. The acceptor explosive must be of such type, density and physical dimensions that it is shock initiated to detonation by the impacting flying plate.

A. Deflagration-to-Detonation-Transition Initiation

Figure 1 is a diagram of the assembly used in DDT initiation experiments. The igniter wire is Nichrome V, usually 0.05-mm diameter and 1-mm long. The donor charge normally is 7.6-mm diameter and 6.8-mm long. Coupled to the donor pressing is the transition charge. Its diameter is significantly smaller than that of the donor; it is 2.5 mm. In this charge the deflagration becomes a detonation. An acceptor pellet is placed against the face of the transition charge.

Table I shows the results of a rough survey of the KP/ PETN donor composition at two densities with a low-density PETN transition charge. It appears only KP/PETN donors of

120
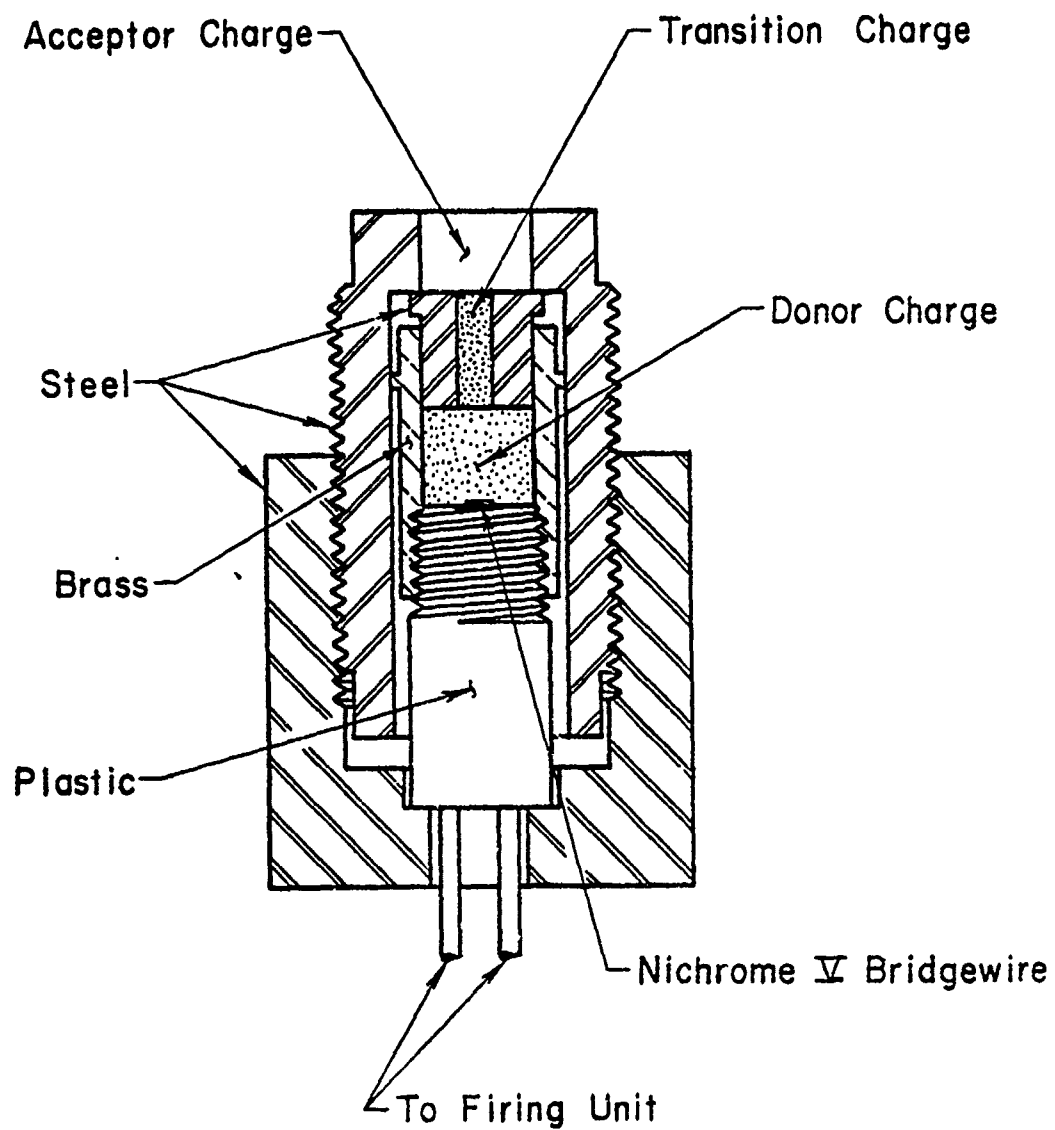
Figure 1   Deflagration-to-Detonation Transition (DDT) Assembly:
Reduced-Diameter Transition Charge

121

TABLE I

EFFECT OF DONOR CHARGE COMPOSITION AND LOADING DENSITY ON DDT REACTION

REDUCED-DIAMETER TRANSITION CHARGE

Transition Charge	Acceptor Charge
PETN S_o^P = 330 m²/kg	PETN S_o^P = 330 m²/kg
Density = 1.0 g/cm³	Density = 1.6 g/cm³
Diameter = 2.5 mm	
Length = 6.4 mm	
	Ignition Voltage = 2.5 V

Donor Charge			Result
Explosive	(% by mass)	Density (g/cm³)	D=Detonation ND=Ignition but no Detonation
KP	100	1.6	ND
"	100	1.2	ND
KP/PETN	90/10	1.6	ND
" "	50/50	1.6	ND
" "	25/75	1.6	D
" "	10/90	1.6	D
" "	90/10	1.2	ND
" "	50/50	1.2	D
" "	25/75	1.2	D
" "	10/90	1.2	D

less than 25% KP at high density, 1.6 g/cm^3, and below 50% KP at 1.2 g/cm^3, function satisfactorily.

KP/PETN 10/90 (% by mass) mix has been most extensively investigated as a donor. KP/PETN 10/90 mix, PETN, RDX, and HNAB at different densities have been used successfully as the transition charge. High-density PETN or 9407 PBX have been used as the acceptor charges. The criterion for achievement of detonation in the acceptor explosive was the production of a dent in a 20/24 Dural "witness" plate (18-mm thick), placed across the face of the acceptor charge. Table II shows these data.

KP mixed with HMX also has been investigated as a donor charge. Mixtures of composition 10/90% by mass KP/HMX, at a density of 1.6 g/cm^3, have been found to ignite satisfactorily. Table III shows the data with PETN of four different densities as the transition charge.

With both these donor charges there seems to be a maximum density of the transition charge that will build up to detonation in this configuration. This is consistant with the picture of the DDT mechanism drawn by Sulimov, where one aspect is the combustion products penetrating through pores into unreacted explosive, preheating the material and helping the initiation of a low-velocity detonation.[2]

The abrupt change in diameter between the donor and transition charges could cause the shearing effect shown by Campbell in 1976 to be necessary for the transition from burning to detonation in the propellant FKM at high-density.[3] Although in our system this may be helpful, it appears not to be necessary. DDT reactions have been generated without this discontinuity. Figure 2 shows the assembly used with KP/PETN 10/90 mix of density 1.2 g/cm^3. Here the donor and transition charges are the same diameter with the latter of slightly shorter length (5.0 mm vice 6.8 mm). Two detonations were obtained in four experiments. The two that failed appeared to be caused by incomplete burning of the donor. From these results we infer that the DDT that occurs with no change in donor/transition charge diameter is marginal. Since we have no difficulty in achieving DDT when the transition charge is smaller in diameter than the donor we conclude that here there is a margin over threshold conditions.

The effect of changing the length of the donor charge also has been investigated. KP/PETN 10/90 mix was the explosive as both the donor and small-diameter transition charge. With a density of 1.2 g/cm^3, the donor length could not be decreased significantly below 6.8 mm. With a donor density of 1.6 g/cm^3 its length could be shortened

TABLE II

EFFECT OF TRANSITION CHARGE EXPLOSIVE TYPE AND
DENSITY ON DDT REACTION

REDUCED-DIAMETER TRANSITION CHARGE

Donor Charge	Transition Charge	Acceptor Charge
KP/PETN = 10/90% by mass	Diameter = 2.5 mm	PETN[a]
KP S_o^P = 250 m^2/kg	Length = 6.4 mm	Density = 1.6 g/cm^3
PETN S_o^P = 330 m^2/kg		
		Ignition Voltage = 2.5 V

Donor Charge	Transition Charge		Result
Density (g/cm^3)	Explosive	Density (g/cm^3)	D=Detonation ND=No Detonation
1.6	PETN[a]	0.6	D
1.6	"	0.8	D
1.6	"	1.0	D
1.6	"	1.2	D and ND
1.6	"	1.4	ND
1.2	"	0.8	D
1.2	"	1.0	D
1.2	"	1.2	D
1.2	"	1.4	ND
1.6	KP/PETN 10/90	1.1	D
1.6	" "	1.2	ND
1.6	" "	1.4	ND
1.6	" "	1.6	ND
1.2	" "	1.2	D[b]
1.2	" "	1.2	D[b,c]
1.6	HNAB[d]	0.8	D
1.6	"	1.0	D
1.6	RDX	0.8	D
1.6	"	1.0	ND

---

[a]PETN: Reprecipitated from acetone with water; S_o^P = 330 m^2/kg
[b]Ignition Voltage: 40 V
[c]Dent observed in Al slug used in place of acceptor pellet
[d]HNAB: Reprecipitated from acetone with ethyl alcohol; S_o^P = 600 m^2/kg

TABLE III

EFFECT OF TRANSITION CHARGE DENSITY ON DDT REACTION

REDUCED-DIAMETER TRANSITION CHARGE

Donor Charge	Transition Charge	Acceptor Charge
KP/HMX = 10/90 % by mass	PETN[a]	PETN[a]
KP S_o^p = 200 m^2/kg	Diameter = 2.5 mm	Density = 1.6 g/cm^3
HMX S_o^p = 350 m^2/kg	Length = 6.4 mm	
Density = 1.6 g/cm^3		

Transition Charge Density (g/cm^3)	Result D=Detonation ND=No Detonation
0.6	D[b]
0.8	D[c]
1.0	D[c] and ND[b]
1.2	ND[b]

[a]PETN: Reprecipitated from acetone with water; S_o^p = 330 m^2/kg
[b]Ignition Voltage = 40 V
[c]Ignition Voltage = 3 V and 40 V
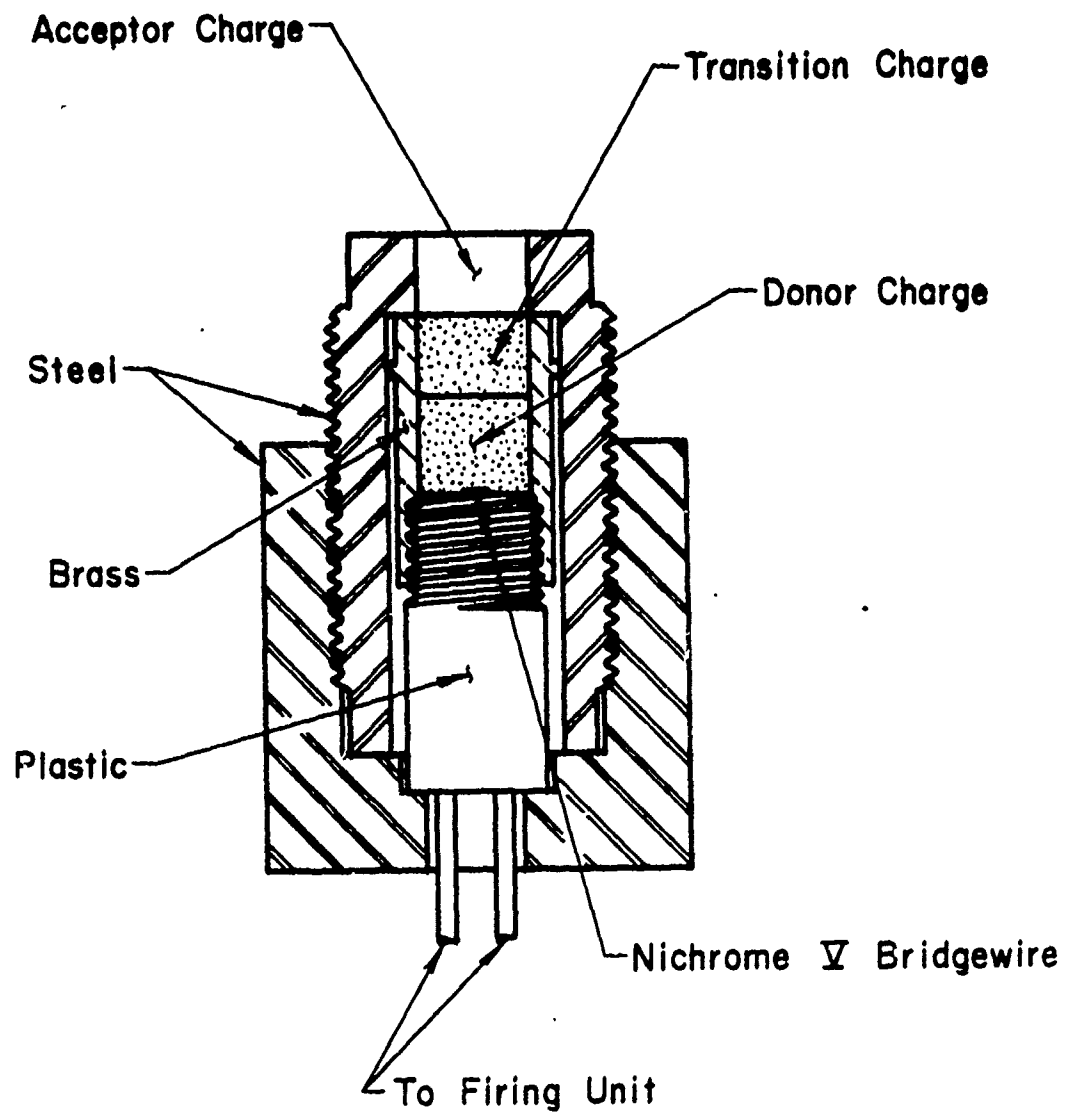
Figure 2   Deflagration-to-Detonation Transition (DDT)
            Assembly: Equal-Diameter Transition Charge

to slightly less than 4 mm. Failures were the result of no
ignition of the donor, thought to be due to inadequate con-
finement near the wire.

We have recently shown that DDT reactions will occur
in pure PETN and HMX if the conditions are correct. We
find these to be (1) high donor charge density with low
transition charge density, and (2) a large ratio of donor-
charge to transition-charge diameter. For PETN the particle
size is relatively unimportant; for HMX a high specific-
surface material is needed for adequate donor ignition.

B. Flying-Plate Initiation of Acceptor Charge

One assembly used in flying-plate initiation experiments
is shown in Figure 3. The igniter wire is again Nichrome V,
0.05-mm diameter and 1-mm long. The donor charge dimensions
are 7.6-mm diameter and 6.8-mm long.

As in the DDT reactions pure KP is deficient as a donor
charge. Only the thinnest of aluminum disks could be sheared
and these did not initiate acceptor pellets. KP/PETN mixtures
of 50/50 composition or more PETN, at loading densities
1.2 g/cm^3 or above, all drove flying plates that did initiate
high-density PETN, RDX and 9407 PBX pellets 7.6-mm diameter by
5.0-mm long. These results are shown in Table IV. Only
limited success was achieved with KP/HMX donors.

Experiments in which the aluminum flyer impacted on an
acceptor charge whose diameter was reduced to 2.5 mm - the
same as the flyer diameter - were successful with both types
of donors. Data obtained using KP/HMX 10/90 mix donors at
two densities are shown in Table V. It is evident that HMX
and HNAB acceptor pressings - at several loading densities -
can be used to initiate large high-density 9407 PBX booster
pellets.

Both KP/PETN and KP/HMX 10/90 mixes will initiate small-
diameter (ca 1 mm) high-density mild detonating fuse (MDF).
Lead-sheathed PETN and aluminum-sheathed HNS both have been
detonated by KP/PETN-driven flying plates. PETN MDF has been
set off by KP/HMX-driven flying plates. MDF, in turn, will
initiate high-density secondary explosives.

Another flying-plate device (Figure 4) also has been
used. This design has side-entering leads. Hopefully this
will allow additional rear confinement. The donor-charge
length is 6.2 mm in the second assembly instead of 6.8 mm.
The donor diameter is the standard 7.6 mm.
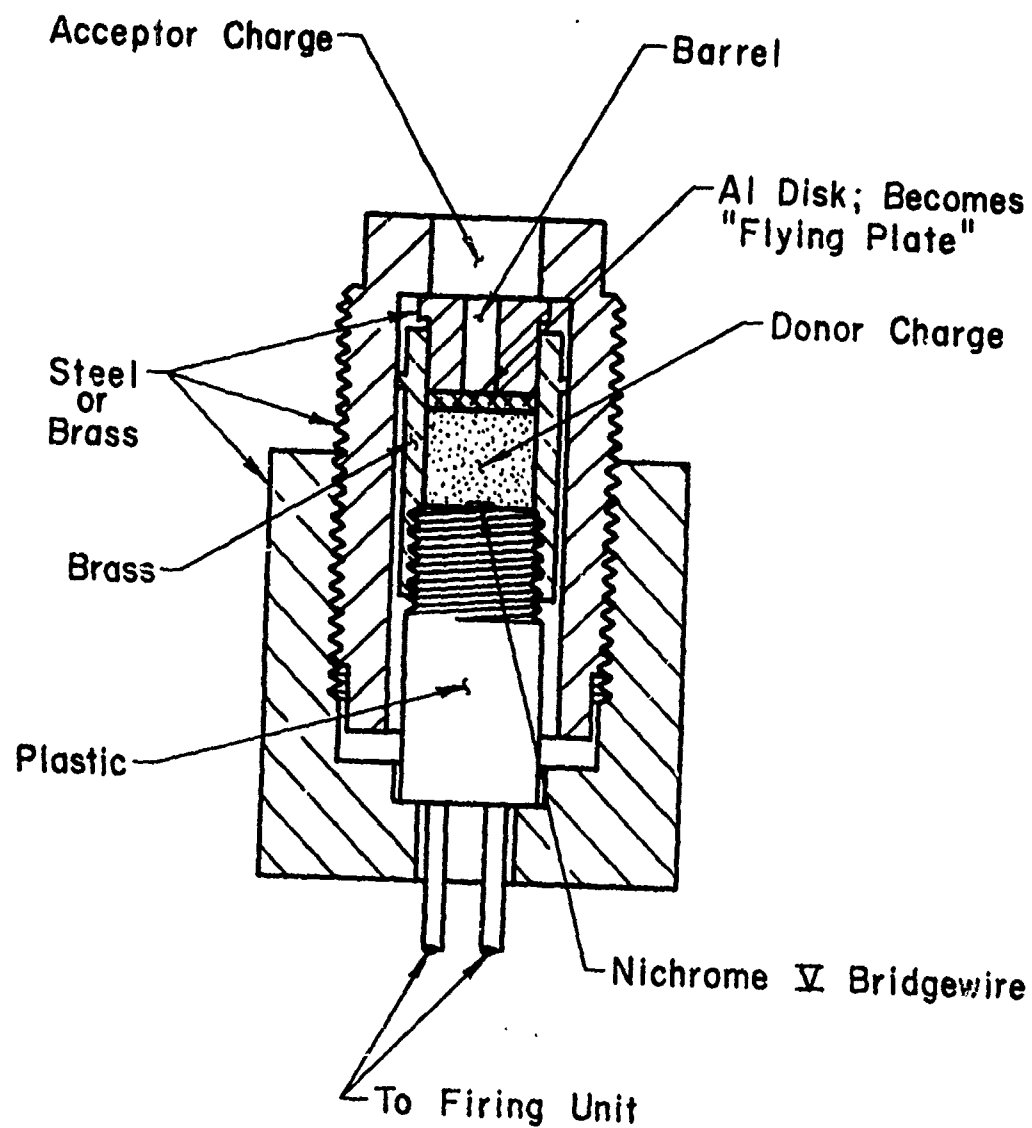
Figure 3   Flying-Plate Initiation Assembly

TABLE IV

FLYING-PLATE INITIATION OF ACCEPTOR EXPLOSIVES
LARGE-DIAMETER CHARGES

Donor Charge	Flying Plate
KP/PETN Mixes KP S_o^p = 250 m²/kg PETN S_o^p = 320 m²/kg	Flyer Material = 6061-T6 Al Flyer Barrel: Diameter = 2.5 mm Length = 6.4 mm

Donor Charge			Thickness	Acceptor Explosive	Ignition Voltage	Result
KP	PETN	Density	(mm)	Density	(V)	D=Detonation
(% by mass)		(g/cm³)		1.6 g/cm³		ND=No Detonation
90	10	1.6	1.27	PETN	40	ND[a]
90	10	1.2	1.27	"	40	ND
50	50	1.6	1.27	"	40	D
50	50	1.6	1.27	"	3	ND[a]
50	50	1.2	1.27	"	40	D
50	50	1.6	1.27	9407 PBX	3	ND[a]
25	75	1.6	1.27	PETN	40	D
25	75	1.2	1.27	"	40	D
25	75	1.6	1.27	9407 PBX	3	ND
10	90	1.6	1.27	PETN	3	D
10	90	1.6	1.27	"	3	D
10	90	1.6	1.27	"	40	D
10	90	1.6	1.27	"	40	D
10	90	1.6	1.27	"	40	D
10	90	1.2	1.27	"	3	D
10	90	1.2	1.27	"	3	D
10	90	1.6	1.27	9407 PBX	3	D
10	90	1.6	1.27	" "	40	D
10	90	1.6	1.27	" "	3	D
10	90	1.6	1.27	" "	3	ND
10	90	1.6	0.64	" "	3	D
10	90	1.6	0.64	" "	3	ND
10	90	1.2	1.27	" "	3	ND
10	90	1.2	0.64	" "	3	ND
10	90	1.6	1.27	RDX	40	D

---

[a]Disc not ruptured

TABLE V

FLYING-PLATE INITIATION OF ACCEPTOR EXPLOSIVES
REDUCED-DIAMETER CHARGES

Donor Charge	Acceptor Charge	Booster Charge
KP/HMX = 10/90% by mass	Diameter = 2.5 mm	9407 PBX
Densities = 1.4 and 1.6 g/cm^3	Length = 6.4 mm	Density = 1.6 g/cm^3

KP S_o^P = 220 m^2/kg

HMX S_o^P = 360 m^2/kg

Ignition Voltage = 2.5 V

Flying Plate
Flyer Material = 6061-T6 Al
Flyer Thickness = 0.64 mm
Flyer Barrel: Diameter = 2.5 mm
Length   = 6.4 mm

Acceptor Charge			Result
Type	S_o^P (m^2/kg)	Density (g/cm^3)	D=Detonation
HMX	360	0.8	D
"	360	1.0	D
"	360	1.2	D
"	360	1.4	D
HNAB	<100	0.8	D
"	<100	1.0	D
"	<100	1.2	D
"	<100	1.4	D

Al Disk; Becomes "Flying Plate"

Acceptor Charge

Steel

Barrel

Steel
or
Brass

To Firing Unit

Nichrome V Bridgewire

Donor Charge
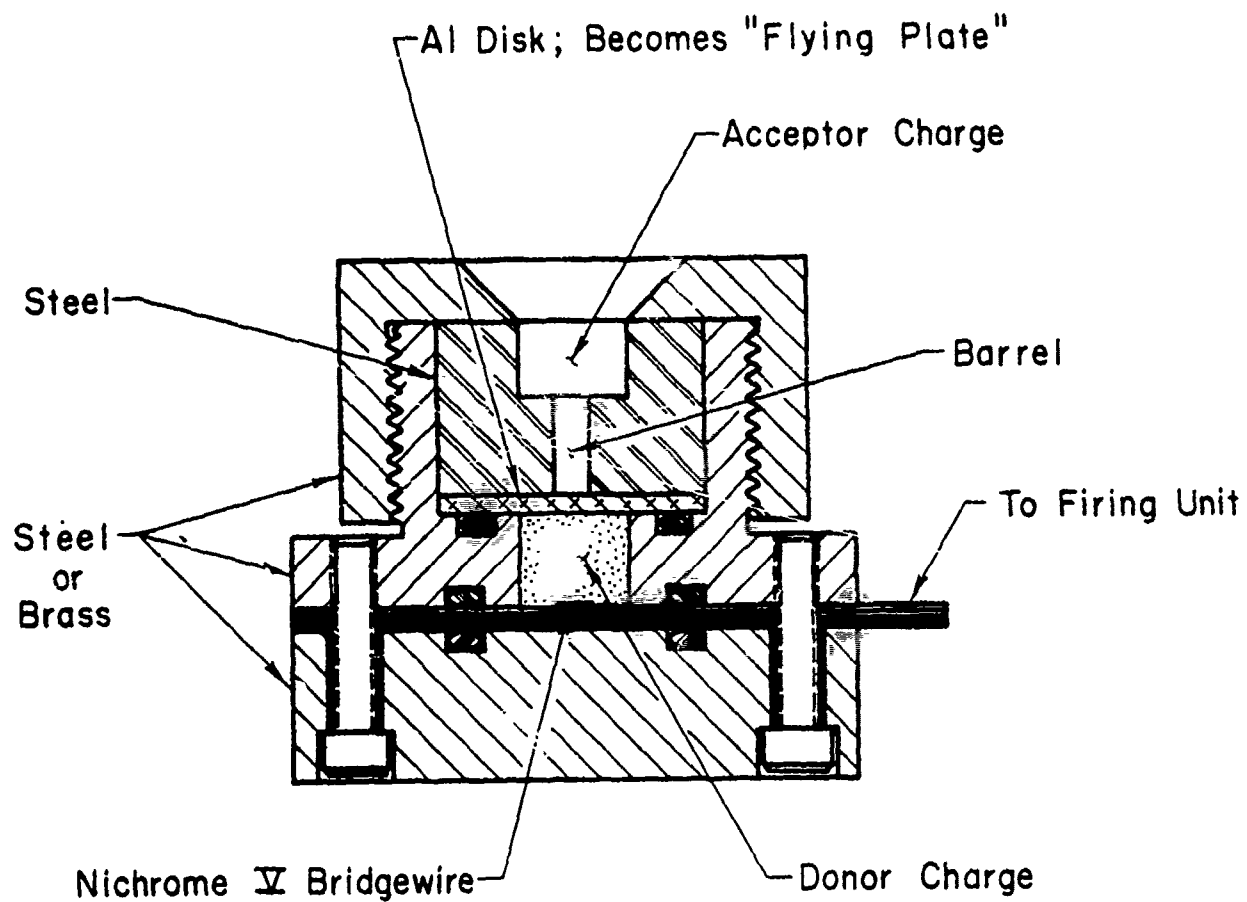
Figure 4   Flying-Plate Initiation Assembly:
            Reinforced Back Confinement

131

Experiments using both KP/PETN and KP/HMX 10/90 mix donors to drive flying plates to initiate 7.6-mm diameter by 5.0-mm long PETN booster pellets as well as MDF have been carried out successfully. These results are shown in Table VI.

TABLE VI

FLYING-PLATE INITIATION OF PETN AND
HNS MDF ACCEPTOR EXPLOSIVES

Donor Charge	Flying Plate
KP/PETN and KP/HMX Mixes Density = 1.6 g/cm^3	Flyer Material = 6061-T6 Al Flyer Thickness = 1 mm Flyer Barrel: Diameter = 2.5 mm Length = 5.2 mm

Acceptor[a] MDF Explosive	Booster[a] Pellet Type	Density (g/cm^3)	Ignition Voltage (V)	Result D=Detonation
Donor Explosive:	KP/PETN 10/90 Mix	$\overline{S}_o^p$ = 250 m^2/kg		
HNS	PETN	1.6	40	D
"	9407 PBX	1.6	3	D
PETN	PETN	1.6	40	D
Donor Explosive:	KP/HMX 10/90 Mix	$\overline{S}_o^p$ = 300 m^2/kg		
---	PETN 2 pellets long	1.3	40	D
HNS	9407 PBX	1.6	40	D
"	9407 PBX	1.6	40	D
"	9407 PBX	1.6	40	D

[a]MDF = Lead-sheathed PETN: ID   = 0.8 mm
    (5 grain/ft)   Length = 3.8 mm
                     Density >1.7 g/cm^3

MDF = Aluminum-sheathed HNS-II: ID   = 1.2 mm
                                 Length = 1.38 mm
                                 Density >1.7 g/cm^3

Booster = 9407 PBX: Diameter = 7.6 mm
                      Length   = 5.2 mm
                      Density=1.6 g/cm^3

REFERENCES

1. V. F. Lemley, et al, "Secondary Explosive Detonator Device," U.S. Patent No. 3,978,791 September 7, 1976.

2. A. A. Sulimov, et al, "On the Mechanism of Deflagration-to-Detonation Transition in Gas-Permeable High Explosive" in <u>Proceedings, 6th Symposium (International) on Detonation</u>, Coronado, CA, 24-26 August 1976 (ONR-Dept. Navy, Arlington, VA, 1977, ACR-221) p. 250.

3. W. Campbell, Los Alamos Scientific Laboratory, personal communication, 1977.

SPECTRAL ANALYSIS OF PYROTECHNIC HC1 EMISSIONS

CARL E. DINERMAN

NAVAL WEAPONS SUPPORT CENTER
APPLIED SCIENCES DEPARTMENT
CRANE, INDIANA 47522

INTRODUCTION

This is a report of a limited spectral analysis of HCl infrared emission produced by combustion of a solid pyrotechnic flare composition. In the present report the experimental rotational temperature is compared to the theoretically calculated temperature.

EXPERIMENTAL

Test flares about 1.6 cm inside diameter by 6 cm long and containing 10 g of composition pressed into phenolic tubes were made with the formulas shown in Table 1.

The flares were ignited in the NAVWPNSUPPCEN Crane test tunnel by a few grams of ignition composition pressed into the top surface, in conjunction with a length of quickmatch and an electric match.

During the more than 10 second burn time, spectra were taken with a rapid scanning spectrometer[1] focused on the flame about 2.5 cm above the burning surface with spectral scan duration of 50 ms. A 35 line/mm grating and 0.2 mm slits were used resulting in about 0.015 μm resolution (12 cm^{-1} at 3.46 μm).

Figure 1 shows a schematic of the experimental arrangement, while Figures 2 and 3 show the spectrometer. The signal averaged, system corrected, computer plotted spectrum of infrared emission from one of the compositions is shown in Figure 4.

Figure 4 shows, going from left to right (short to long wavelength) atmospheric water and carbon dioxide absorption near 1.8 μm, water emission near 2.8 μm, broken by atmospheric water and carbon dioxide absorptions in the same region, HCl emission from 3.2 to 4.2 μm, carbon dioxide emission from 4.2 to 4.7 μm, broken by atmospheric carbon dioxide absorption near 4.3 μm. There is underlying continuous emission throughout the whole region. The gap from 2.9 to 3.2 μm is due to very low spectrometer system response. Note that the intensity scale on the

---

[1] C. E. Dinerman, "Computerized Rapid-Scan Spectroscopy at NAVWPNSUPPCEN Crnae", NWSC/CR/RDTR-35, Naval Weapons Support Center, Crane, IN (July 1976). Available National Technical Information Service, 5285 Port Royal Road, Springfield, VA 22161, NTIS--ADA030269.

left is for the left half of the spectrum, and is 50% of the intensity scale on the right hand side. That is, the local intensity maximum near 2.8 μm is actually only 50% as high as the maximum near 4.4 μm.

Details of the 3.2-4.2 μm region of Figure 4 are shown in Figure 5.

The spectrum in this region consists of HCl rotation-vibration lines underlain by a graybody-like continuum and, near 3.2 μm, water vapor absorptions and emissions. The HCl emission lines are grouped into the P branch lines from 3.5 to 4.1 μm, and R branch lines, less well resolved, from 3.2 to near 3.4 μm. Spectroscopic notation is shown on the figure, indicating P branch lines from the 1-0 and 2-1 bands.

Spectra from separate flares of the same type are very similar, showing good reproducibility from flare to flare. The main difference between IR-9 and IR-12 spectra is that there is a larger underlying continuum in the latter group.

DATA ANALYSIS AND DISCUSSION

In order to learn more about the basic thermodynamic and kinetic processes occurring in the flame, the HCl peaks were analyzed to determine the rotational temperature using the following equation:[2]

$$I_{em} = \frac{C_{em}\nu^4}{Q_r} (J'+J''+1)e^{-B'J'(J'+1)hc/kT}$$

where I_{em} is the emission intensity, ν is the frequency (in wavenumbers) of a particular line, J' is the quantum number for the rotational levels in the upper vibrational state of the transition, J'' is the quantum number for the rotational levels in the lower vibrational state of the transition, B' is the rotational constant for the upper vibrational state, T is the absolute temperature, and h, c, and k are constants. C_{em} and Q_r can be considered constant for a particular vibrational transition.

A plot of

---

[2] G. Herzberg, Molecular Spectra and Molecular Structure. I. Spectra of Diatomic Molecules (D. Van Nostrand Co., Inc., Princeton, NJ, 1950), p. 205.

$$\ln \frac{I_{em}}{(J'+J''+1)\nu^4} \quad \text{vs} \quad J'(J'+1)$$

enables T to be obtained from

$$-\frac{B'hc}{kT},$$

the slope.

Since rotation-translation relaxation times are so short, it is expected that rotational temperatures would closely approach the translational temperature.

It was decided to use the P-branch data, rather than the R-branch, because of better resolution, less underlying continuum, and no interference from water vapor absorption/emission.

This technique has been applied to HCl flames in the past.[3-7] Figure 6 shows an example of a plot which is based on a spectrum of the emission from composition IR-12. This is for the P-Branch of the 1-0 transition. All such plots for either IR-9 or IR-12 had the same general shape, with a steep section near the left, leading to a small "knee", then to a linear portion. This is similar to the shape of the

[3] H. P. Broida, "Temperature of Flames", NBS Report No. 4418, National Bureau of Standards, Gaithersburg, MD. Available Defense Documentation Center, Cameron Station, Alexandria, VA 22314, DDC-AD080550.

[4] E. E. Bell, P. B. Burnside, and F. P. Dickey, "Spectral Radiance of Some Flames and Their Temperature Determination", J. Opt. Soc. Am. 50, 1286 (December 1960).

[5] F. D. Findlay and J. C. Polanyi, "The Hydrogen-Chlorine System in the MM Pressure Range. I. Energy Distribution Among Vibrationally Excited States", Canadian Journal of Chemistry 42, 2176 (1964).

[6] J. K. Cashion and J. C. Polanyi, "Infrared Chemiluminescence. I. Infrared Emission from Hydrogen Chloride Formed in the Systems Atomic Hydrogen Plus Chlorine, Atomic Hydrogen Plus Hydrogen Chloride, Atomic Hydrogen Plus Deuterium Chloride, and Atomic Deuterium Plus Hydrogen Chloride", Proc. Roy. Soc. A258, 529 (1960).

[7] J. T. Latimore, et. al., "H_2-Cl_2 Chemical Laser Program. Part 1--CHEMLUM Code for Spectroscopic Data Analysis", RK-CR-74-9, U.S. Army Missile Command, Redstone Arsenal, AL (January 1974). Available DDC--AD780178.

graph shown in reference 3. This shape remained the same whether peak heights or peak areas were used. A limited number of points from the P-Branch of the 2-1 transition were analyzed, but, due to the small peak size, scatter was present in the results between two flares of the same type.

Table 2 summarizes the results of the rotational analyses. Here, it can be seen that temperature from flares of identical composition are within 50K of each other, when examining the 1-0 data. These values experimentally derived are in agreement with those obtained experimentally in reference 4 for HCl flames.

In order to compare our experimental results with[8] computer predictions of adiabatic temperature, a NASA thermodynamic program was used. This program can predict temperatures and species resulting from the combustion of reactants under given conditions. By inputting the reactants (their relative amounts and heats of formation) and varying the amounts of air, the information derived in Table 3 is obtained. The temperatures and mole fractions so derived assume no radiation loss, which is certainly not the actual case. Nevertheless, those temperatures are within 200 K for IR-9 (compare with 1-0 results in Table 2). For IR-12 the computer predictions are from 200 to 600 K higher depending on the amount of air mixed in. Admittedly, it is difficult to decide which is the most reasonable percentage of air to be added.

Obviously, simple experiments and calculations like those described above cannot adequately serve to define the complex flame system under investigation. This flame is not expected to be homogeneous in either species type or concentration, or in temperature, as one progresses across or up the plume. Certainly there are non-equilibrium conditions. Furthermore, spectral resolution was insufficient to resolve any self-absorption that may have been present in the 1-0 bands, and the spectrometer field of view did not encompass the entire plume. However, given these handicaps it is interesting that there is gross correlation between theory and experiment at least for composition IR-9. One possible explanation for the larger discrepancy between theory and experiment for IR-12 is the following:

Composition IR-12 is more fuel-rich than IR-9 and therefore the effect of adding differing amounts of air should be more pronounced in raising the temperature. This is seen in Table 3, where the adiabatic temperature for IR-12 is lower than IR-9 at 0% air, but generally is higher than IR-9 after air is admitted. Above 10% air, the IR-12

---

[8] S. Gordon and B. J. McBride, "Computer Program for Calculation of Complex Chemical Equilibrium Compositions, Rocket Performance, Incident and Reflected Shocks, and Chapman-Jouguet Detonations", NASA SP-273, Lewis Research Center (1971). Available NTIS--N7137775.

adiabatic temperature is relatively constant. The spectrometer field of view, small compared to the plume size, is located relatively close to the burning surface, presumably in a region where air admixture is still low. The discrepancy between experiment and theory for IR-12, therefore, depends on how much air is assumed to enter the plume at the field of view position. If it is assumed that less than 10% air is added, the difference between theory and experiment for IR-12 is 200 K, as good as that for IR-9. Above 10%, the difference rapidly rises to about 600 K and remains there.

A further correlation between theory and experiment was attempted using the radiant source model developed by Dr. Goldman at Denver Research Institute. The goal here was to duplicate the experimental spectrum using temperature, HCl concentration, and spectral resolution as inputs into Goldman's model. However, there was only fair agreement since the radiant source model conditions were not optimized to match the experimental conditions. Therefore, the results are not shown here. More work needs to be done to establish correlation and to generate the correct HCl spectrum from Goldman's model.

[9] A. Goldman, et. al., "Distribution of Water Vapor in the Stratosphere as Determined from Balloon Measurements of Atmospheric Emission Spectra in the 24-29 μm Region", Applied Optics 12, 1045 (1973).

[10] A. Goldman, et. al., "Solar Absorption in the CO Fundamental Region", Astrophysical Journal 182, 581 (1973).

[11] A. Goldman, et. al., "Infrared Spectral Radiance of Hot HF and DF in The $\Delta v = 1$ Bands Region as Seen Through an Atmospheric Path", J. Quant. Spectrosc. Radiat. Transfer 14, 299 (1974).

[12] A. Goldman and S. C. Schmidt, "Infrared Spectral Line Parameters and Absorptance Calculations of NO at Atmospheric and Elevated Temperatures for the $\Delta v = 1$ Bands Region", J. Quant. Spectrosc. Radiat. Transfer 15, 127 (1975).

[13] R. N. Stocker and A. Goldman, "Infrared Spectral Line Parameters of HBr and DBr at Elevated Temperatures", J. Quant. Spectrosc. Radiat. Transfer 16, 335 (1976).

CONCLUSIONS

It is possible to obtain gross correlation between rotational temperatures derived from infrared vibration rotation spectra of pyrotechnically produced HCl emission, and theoretically calculated temperatures. In fuel-rich compositions, the amount of assumed air admixture can greatly change the theoretical results.

Table 1.   Flare Compositions (Wt. Percent)
to Produce HCl Emission

Ingredients	Formulas	
	IR-9	IR-12
Hydrazine Bisborane	30	27
Hexachloroethane	40	36
Ammonium Perchlorate	20	17
Boron	--	10
Sylgard 182 *	10	10

*This is used as a binder to hold the composition together. It is a product of Dow Corning Corporation, Midland, Michigan.

Table 2. Experimentally Determined Rotational Temperatures

| Flare | Temperature, K | |
	P Branch 1-0 Transition	P Branch** 2-1 Transition
IR-9 #1*	1799	--
IR-9 #2	1755	1553
IR-12 #1	1637	1910
IR-12 #2	1600	1536

---

*The rotations #1 and #2 refer to different flares with the same formula.

**2-1 data not as reliable as 1-0 data due to smaller intensities.

Table 3. Predicted Species and Plume Temperatures*

IR-9

Air**	Temp., K (Adiabatic)	HCl***	CO_2***	H_2O***
0	₁₅77	.195	.00002	.00035
10	1919	.189	.00004	.00079
20	1932	.177	.00006	.0011
30	1935	.164	.00008	.0014
40	1941	.148	.00008	.0015
50	1955	.131	.00008	.0015
60	2074	.117	.0011	.020
70	2277	.094	.0077	.092

IR-12

Air**	Temp., K (Adiabatic)	HCl	CO_2	H_2O
0	1807	.120	--	.00003
10	2252	.140	--	.00007
20	2247	.142	.00001	.00023
30	2207	.134	.00002	.0004
40	2167	.122	.00003	.0006
50	2125	.109	.00004	.0008
60	2080	.094	.00005	.0009
70	2196	.082	.00055	.010

---

*These were obtained from the NASA thermodynamic computer program (reference 9)

**Expressed as percentage of total reactants

***Expressed as mole fraction
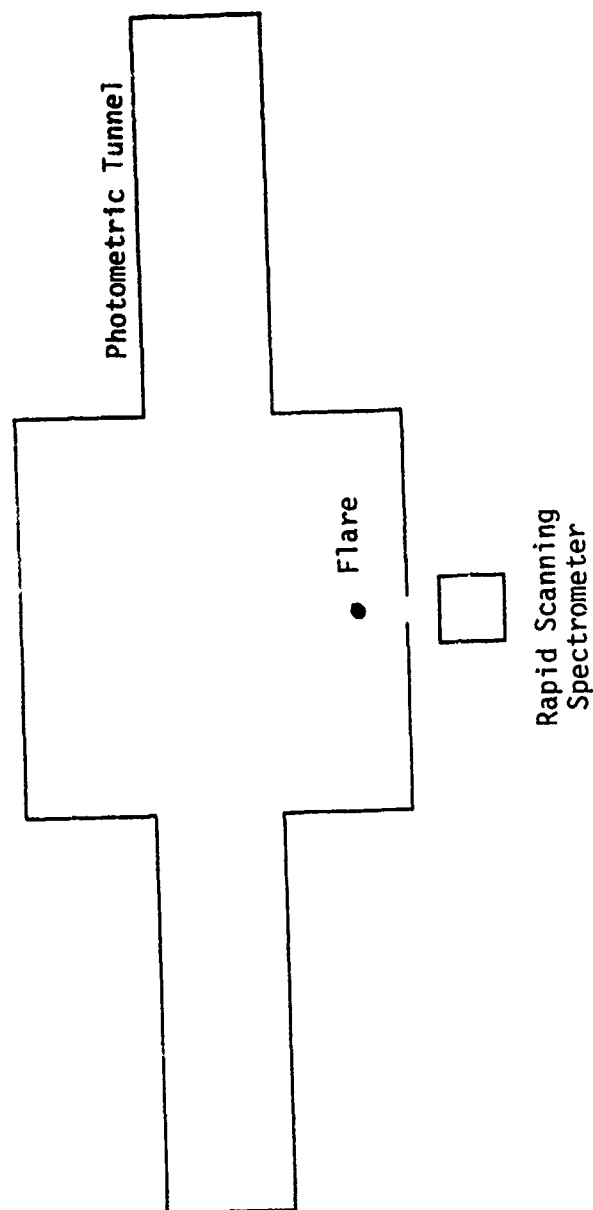
Figure 1. Typical Arrangement for Obtaining Flare Spectra. The flare is burned in the center of the NAVWPNSUPPCEN Crane photometric tunnel. The spectrometer views the radiation through a porthole.
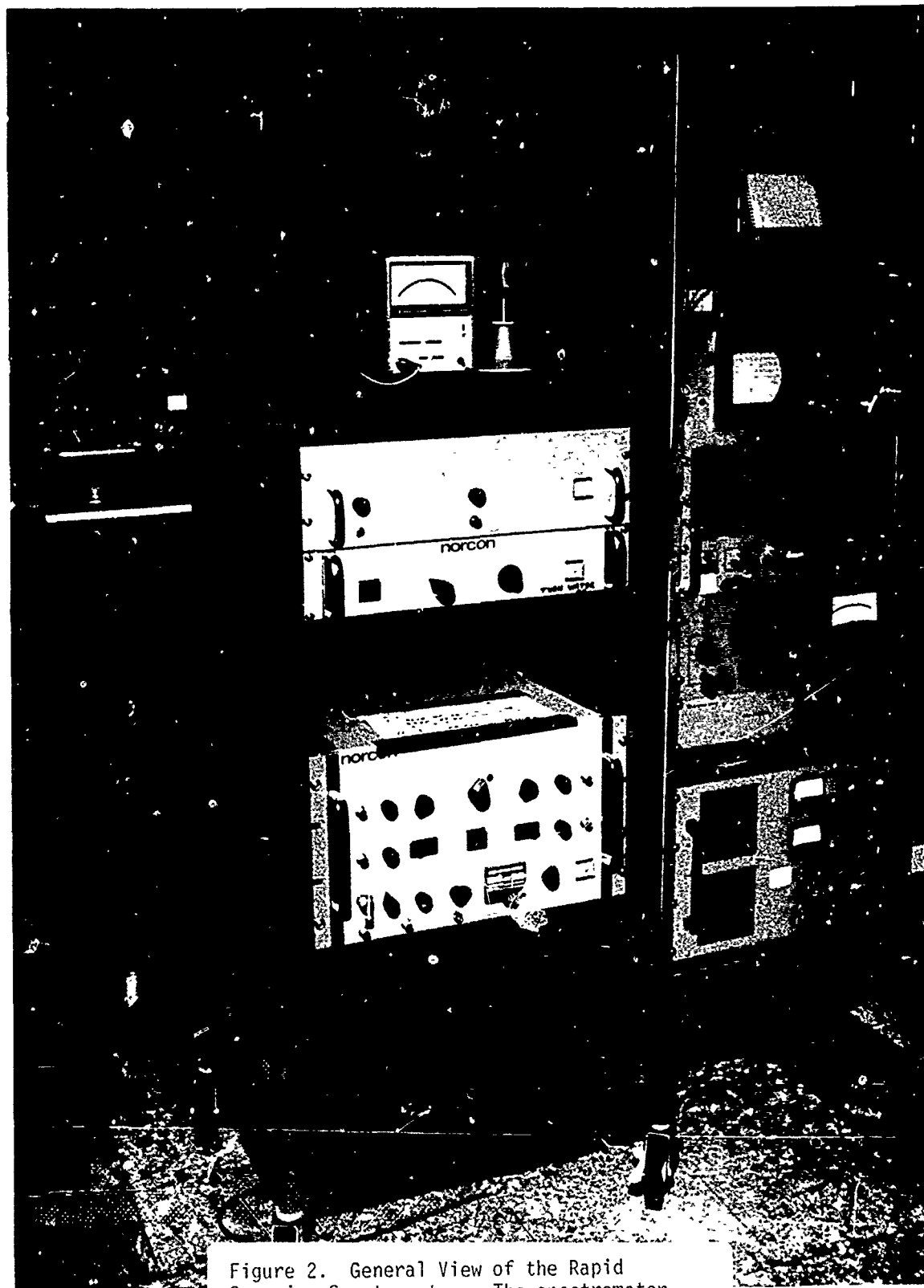
Figure 2. General View of the Rapid Scanning Spectrometer. The spectrometer is in the background and its associated electronics are enclosed in the electronics rack in the left foreground.
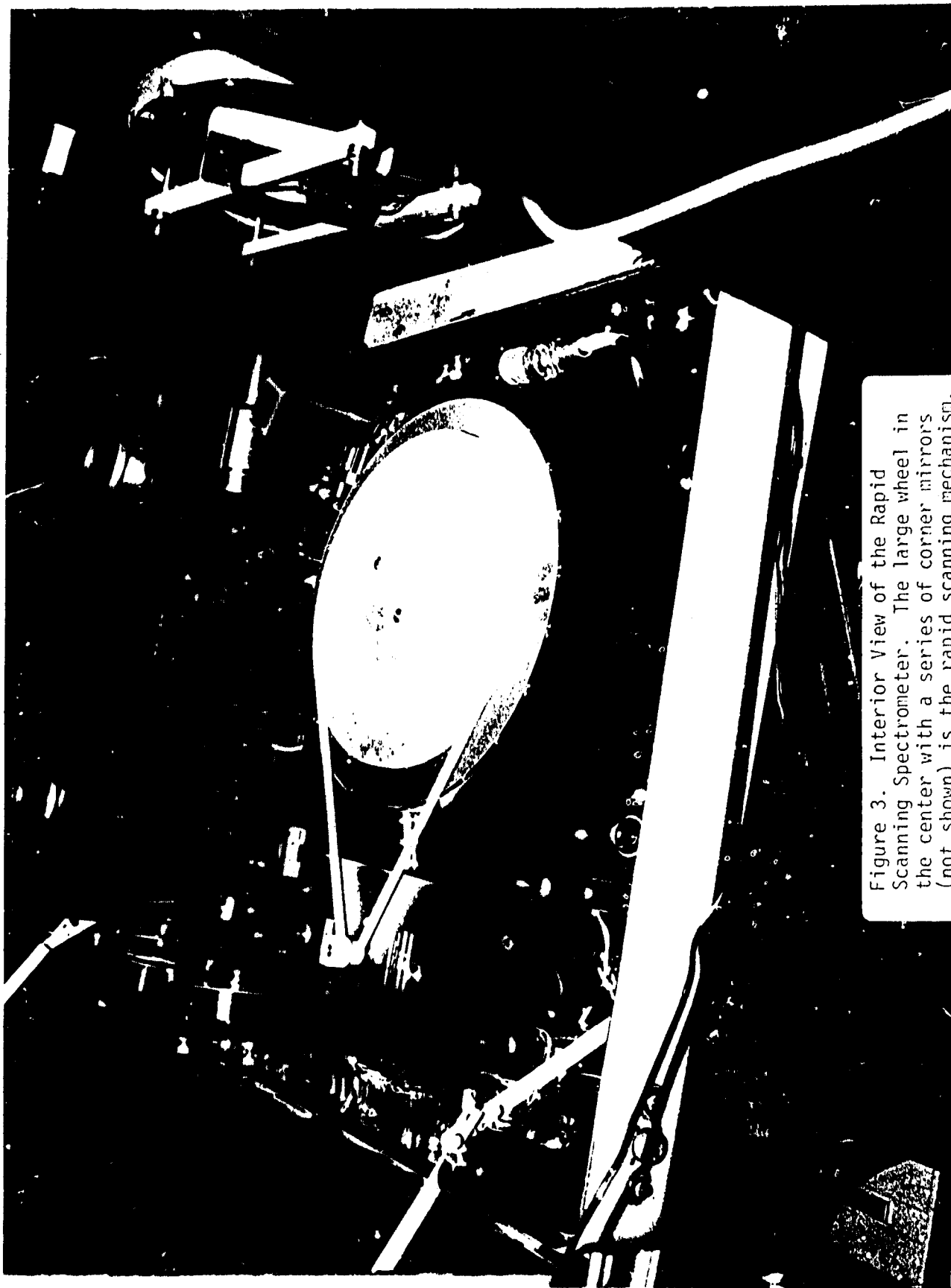
Figure 3. Interior View of the Rapid Scanning Spectrometer. The large wheel in the center with a series of corner mirrors (not shown) is the rapid scanning mechanism. The liquid nitrogen dewars for the two detectors can be seen in the extreme top, and the porthole is shown at the extreme right.
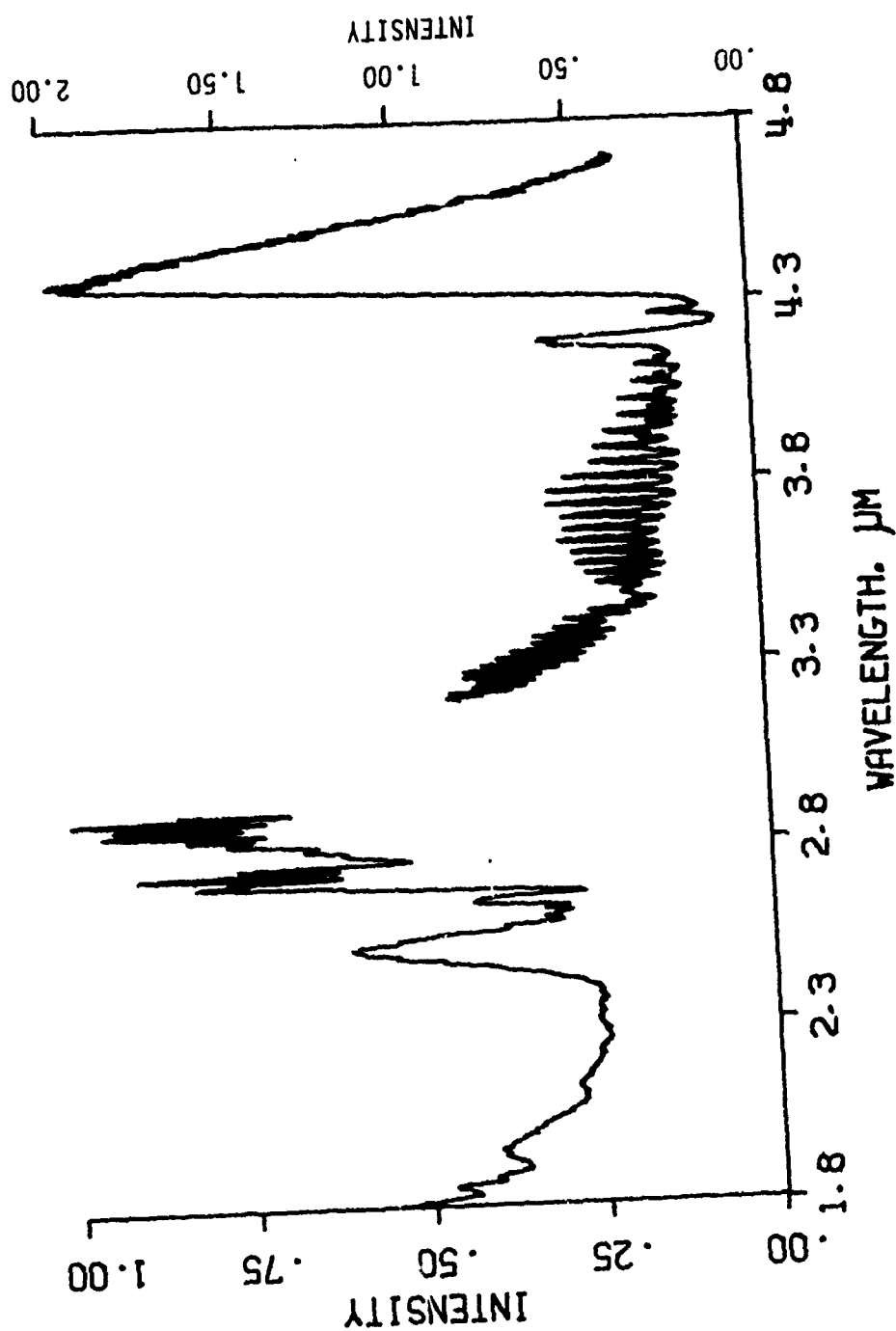
Figure 4. Relative Intensity Spectrum of Emissions From Pyrotechnic Composition IR-9. The left intensity scale is for the left half of the spectrum, and correspondingly for the right half.

148
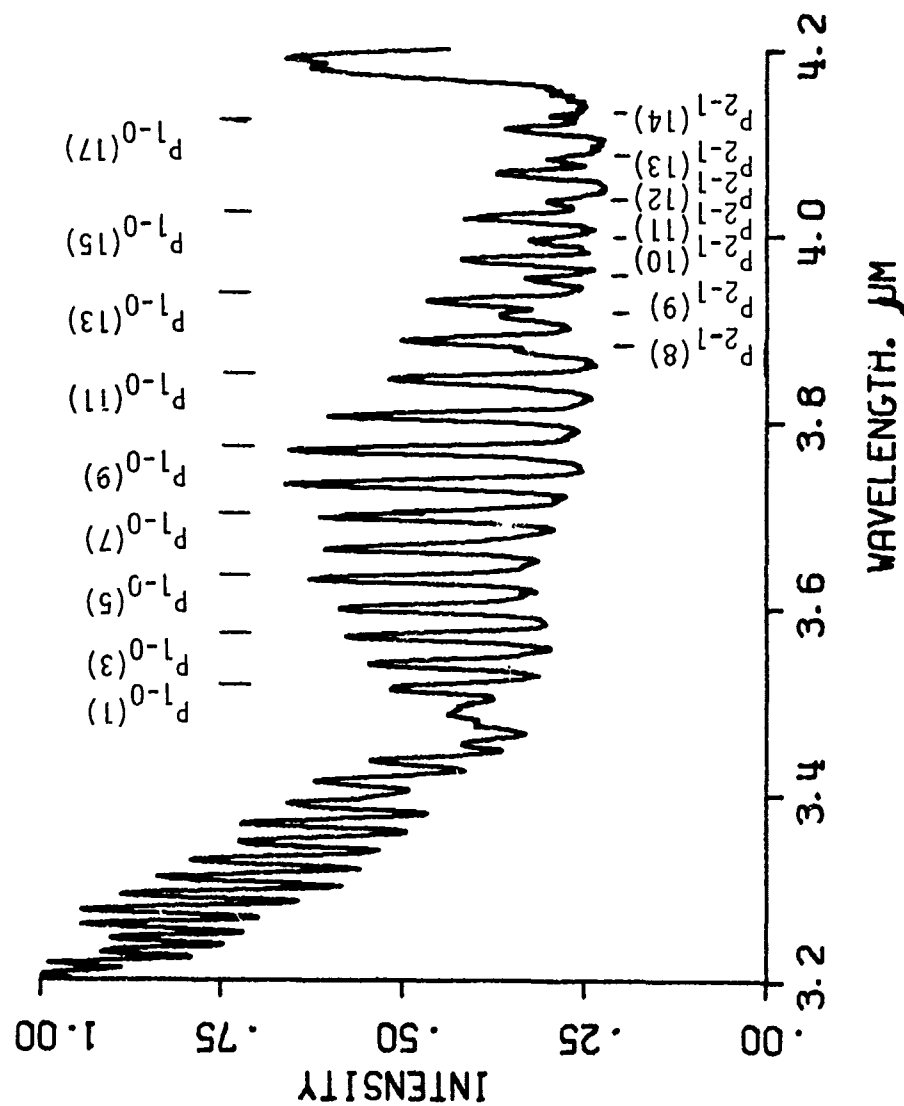
Figure 5. HCl Emission. This is an expanded portion of figure 4. Spectroscopic notation for the spectral lines is included.
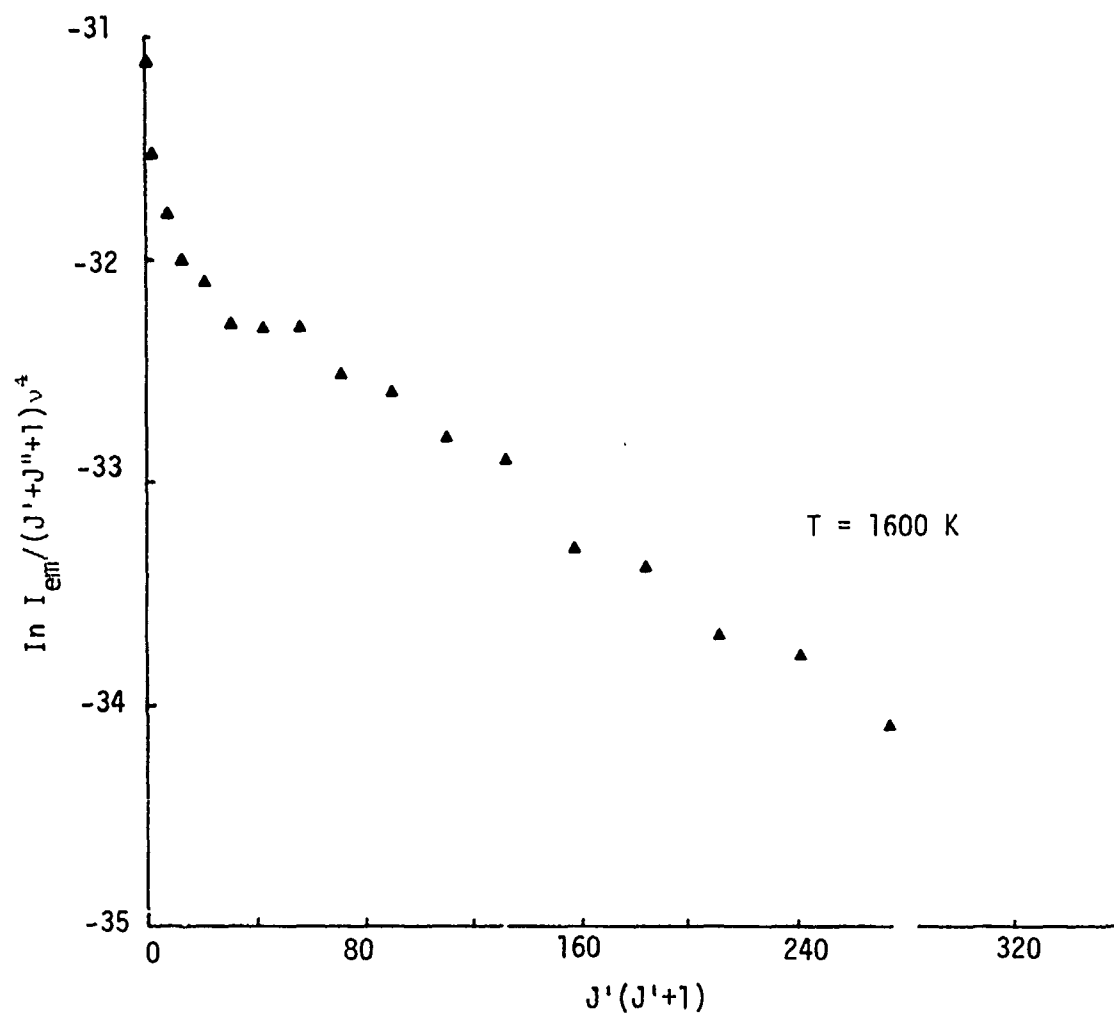
Figure 6. IR-12 #2. Plot of 1-0 P Branch Intensities. Temperature is determined from slope. See text and reference 2 for details of notation and method.

SAND78-0273

HEADER UTILIZATION IN NO-FIRE DESIGN*

A. B. Donaldson
Sandia Laboratories
Albuquerque, New Mexico   87185

ABSTRACT

In this presentation, a heat conduction problem which describes an
actuator no-fire condition is analyzed. The effect of header heat
sinking is specifically addressed. Additionally, the rise in the
actuator body temperature during a no-fire test and the time lapse
before header interaction during an all-fire test are briefly dis-
cussed. Finally, the analytic results are compared to experimental
results of no-fire conditions as a function of bridgewire-header
separation.

INTRODUCTION

In early design of hot wire ignitors, the bridgewire was placed well
into the pyrotechnic to provide good energy transfer to support the
ignition process. Later, the bridgewire was placed against the
header (which is normally a better conductor of heat than the pyro-
technic) in order to meet a no-fire goal, i.e., a maximum sustained
bridgewire current level for which the pyrotechnic will not ignite.
Still later, less sensitive pyrotechnics came into use to further
reduce risk of accidental ignition. In some cases, the resulting
high energy dissipation configurations coupled with low ignition
sensitivity has lead to poor ignition reliability. Therefore,
bridgewires may again be placed in the pyrotechnic. However, in-
stead of the random placement of the bridgewire in the pyrotechnic,

---

151

there should exist a dimension, δ, (the distance between the bridge-wire centerline and the header) for which all-fire conditions are sufficiently fast that the header does not affect the ignition process but for which no-fire conditions are sufficiently slow that the header can participate in the dissipation process. The analytical consideration of δ and its effect on all-fire/no-fire is the subject of this presentation.

<center>ANALYSIS</center>

Geometry

An end view of a typical bridgewire-pyrotechnic-header system is depicted in Figure 1. Because the geometry is not regular in the sense of Cartesian or cylindrical coordinate systems, it is convenient to map the problem into a regular geometry via conformal mapping. The mapping

$$iw = \frac{ia - z}{ia + z}$$

where $i = \sqrt{-1}$, a is an unspecified position on the y-axis, and w and z are complex numbers, maps the pyrotechnic-header surface into a circle that is concentric about the bridgewire, which itself has remained a circle. By using the decomposition $w = u + iv$ and $z = x + iy$, the mapping can be shown to satisfy the Cauchy-Reimann conditions

$$\frac{\partial u}{\partial x} = \frac{\partial v}{\partial y} \quad \text{and} \quad -\frac{\partial u}{\partial y} = \frac{\partial v}{\partial x}$$

which is a necessary condition for analytic mapping. If the radius about the origin in the w-plane is c, then

$$x^2 + \left[y - \left(\frac{1 + c^2}{1 - c^2} \right) a \right]^2 = \frac{4c^2 a^2}{(1 - c^2)^2}$$

represents circles of radius

$$r = \frac{2ac}{1 - c^2}$$

about the point $(0, y)$ where

$$y = \left(\frac{1 + c^2}{1 - c^2} \right) a$$

<center>152</center>

in the z-plane. In particular, the z-plane bridgewire surface is mapped into a w-plane circle of radius $c (\leq 1)$ and the z-plane pyrotechnic-header surface is mapped into the w-plane unit circle (both concentric about the origin). The constants a and c can then be expressed in terms of observable dimensions by

$$c = \frac{\delta}{r_o} - \sqrt{\left(\frac{\delta}{r_o}\right)^2 - 1}$$

and

$$a = \frac{1 - c^2}{2c} r_o$$

where r_o is the z-plane bridgewire radius and δ is the y-axis position which corresponds to the bridgewire centerline.

Bridgewire-Pyrotechnic-Header Conduction

Because the no-fire condition is sufficiently long that transients have disappeared, only the steady-state problem needs to be considered. Since the bridgewire is welded to massive conductive posts, an isothermal end condition will be used. (The spatial coordinate, z, was not modified by the previous mapping.) No dimensional bound will be considered for the external header surface since the isothermal end condition provides for communication with the surroundings. Other assumptions such as constant material properties, perfect interface conductances, constant current heating of the bridgewire, uniform radial bridgewire temperature, etc., will be used. In non-dimensional quantities, the w-plane problem can be written

$$\text{Bridgewire Conduction:} \quad \frac{\partial^2 \Theta_o}{\partial \xi^2} + 1 + \left(\frac{2\gamma_1}{\eta_o}\right)\frac{\partial \Theta_1}{\partial \eta}\bigg|_{\eta_o} = 0$$

$$\text{Pyrotechnic Conduction:} \quad \nabla^2 \Theta_1 (\xi, \eta) = 0$$

$$\text{Header Conduction:} \quad \nabla^2 \Theta_2 (\xi, \eta) = 0$$

Boundary Conditions:

1. $\Theta_1 \big|_{\eta_o} = \Theta_o$ 2. $\Theta_1 \big|_{\eta_1} = \Theta_2 \big|_{\eta_1}$

3. $(\gamma_1)\dfrac{\partial \Theta_1}{\partial \eta}\bigg|_{\eta_1} = (\gamma_2)\dfrac{\partial \Theta_1}{\partial \eta}\bigg|_{\eta_1}$

4. $\displaystyle\lim_{\eta \to \infty} \Theta_2 \to \text{finite}$

5. $\Theta_o\big|_\sigma = 0$

6. $\Theta_1\big|_\sigma = 0$

7. $\Theta_2\big|_\sigma = 0$

8. $\dfrac{\partial \Theta_o}{\partial \xi}\bigg|_o = 0$

9. $\dfrac{\partial \Theta_1}{\partial \xi}\bigg|_o = 0$

10. $\dfrac{\partial \Theta_2}{\partial \xi}\bigg|_o = 0$

The form of boundary conditions suggests utilizing a cosine transform, defined by

$$C_n\{F(\xi)\} = \int_0^\sigma F(\xi)\,\cos\,\beta_n\xi d\xi = f(n)$$

and inverse, defined by

$$C_n^{-1}\{f(n)\} = \frac{2}{\sigma}\sum_{n=1}^{\infty}\,f(n)\,\cos\,\beta_n\xi = F(\xi)$$

which reduces the problem to a system of three ordinary differential equations. This system is solved, subject to the remaining boundary conditions. This solution is then inverted, resulting in

$$\Theta_1(\eta_1\xi) = \frac{2}{\sigma}\sum_{n=1}^{\infty}\,A_n\left[I_o(\beta_n c) - G_n K_o(\beta_n c)\right]\cos\,\beta_n\xi$$

where

$$G_n = \frac{\left(\frac{\gamma_1}{\gamma_2}\right)\frac{I_1(\beta_n)}{K_1(\beta_n)} + \frac{I_o(\beta_n)}{K_o(\beta_n)}}{1 - \frac{\gamma_1}{\gamma_2}}$$

$$A_n = \frac{-(-1)^n}{\beta_n^2\left\{\beta_n\left[I_o(\beta_n c) - G_n K_o(\beta_n c)\right] - \frac{2\gamma_1}{\eta_o}\left[I_1(\beta_n c) + G_n K_1(\beta_n c)\right]\right\}}$$

and

$$\beta_n = \frac{(2n - 1)\Pi}{2\sigma} \quad .$$

This solution can be shown to approach the problem of a bridgewire in an infinite slab by letting $\gamma_2 \rightarrow \gamma_1$.

Since the highest temperature in the pyrotechnic will be at the coordinates ($\xi = 0$, $\eta = \eta_o$), this position will be used in future calculations. Although an ignition temperature is not necessarily a material property (constant), this concept can be utilized for very slow processes such as the no-fire test.

Actuator Heat-Up

The previous analysis can be used for estimating the excess temperature of the bridgewire center above that of the posts. However, depending on the actuator environment, the entire housing, including posts, can rise to a temperature much higher than the surroundings during a no-fire test. Therefore, t⁔ ⹁ magnitude of this rise adds to the absolute temperature of the bridgewire center and must be considered.

If the actuator is installed in a bulkhead which is constructed from a high thermal conductivity metal, then little actuator body temperature rise would be expected. However, if the actuator is suspended in a gaseous environment and can dissipate heat only by convection, then a different situation exists. Treatin⹁ the actuator as a "lumped mass", the differential energy equation can be written

155

$$mC_p\left(\frac{dT}{dt}\right) = i^2R - hA_s(T - T_\infty)$$

which has the solution

$$T - T_\infty = \frac{i^2R}{hA_s}\left[1 - e^{-\left(\frac{hA_s}{mC_p}\right)t}\right] \ .$$

The maximum temperature excursion (at steady state) is

$$T - T_\infty = \frac{i^2R}{hA_s} \ .$$

This quantity is then taken as the excess temperature of the post above that of the surroundings and the constants should be evaluated from experiments on the actuator under consideration.

Time Lapse Before Header Interaction

This topic is not part of the previous analysis but will be included here for completeness. Specifically, if the header is to be utilized for heat dissipation at long times, then how can this dissipation be eliminated for short time events, such as all-fire? This is accomplished by providing a sufficient space between the bridgewire and header so that no interaction results during normal time-to-ignition.

Although the heat transfer is governed by the diffusion rather than the wave equation, the concept of a propagating thermal boundary layer can be used. Until the thermal boundary layer reaches the header, the header cannot interact. Thus, the problem is to determine the position of the thermal boundary layer at the time when ignition normally occurs ($\sim$ 5 ms). The calculation will be based on the assumption of a geometry which is homogeneous, surrounding a bridgewire which is infinitely long.

Since interest is focused only on the propagation of the thermal boundary layer and not with the amplitude of the response, an exact matching of boundary conditions will not be required The analytic expression for the position-time of the thermal wave based on the heat balance integral approximation for a cylindrical hole subjected to a constant heat flux is [1].

$$-\frac{\alpha_1 t}{r_o} = \frac{+ (72\psi^2 - 96\psi + 36)\ln\psi - 13\psi^4 + 36\psi^2 - 32\psi + 9}{144(\psi - 1)(2\ln\psi + \psi - 1)}$$

where

$$\psi = 1 + \frac{\rho}{r_o}$$

and ρ is the position of the thermal front measured from the hole.

This estimate of time lapse before header interaction will be smaller than in the actual situation since a reflection of the "thermal wave" from the pyrotechnic-header interface to the bridge-wire should occur before any effect can be noted. However, since the velocity of the thermal front is not constant and the geometry becomes much more complicated, no attempt will be made to consider thermal wave reflections. The analysis, therefore, provides an estimate which is substantially shorter than what would be expected in the real situation.

DISCUSSION AND RESULTS

Although no detailed experimental data exists for direct comparison with the analytic model, no-fire data does exist for a design before and after a 0.0127 - 0.0254 mm (5 - 10 mil) deep spherical hole was machined in the header between the pins. Values for no-fire current (50% probability of firing during 300 sec exposure to constant current) were 1.4 amps and 1.2 amps respectively in an air environment at 333 K [2].

Other details of the design are:

1. Bridgewire: Tophet C*, 4.57×10^{-3} mm (1.80 mil) dia., 0.14 mm (55 mil) length, k_o = 21.0 W/m K

2. Pyrotechnic: $TiH_{0.65}/KClO_4$ (33/67), k_1 = 0.34 W/m K
    α_1 = 0.17 mm^2/sec, T_{ign} = 773 K

3. Header: TM-7 glass, k_2 = 1.0 W/m K

In a separate experiment with this actuator, a body temperature rise of 28 K was noted to result from a 0.313 amp current passing through the bridgewire. Hence,

$$hA_s = \frac{i^2 R}{\Delta T} = 136 \text{ W/K} \quad .$$

*Registered Trademark.

157

In order to account for the ambient temperature contribution, the actuator body heat-up contribution, and the excess temperature of the bridgewire above the posts, the following summation is used

$$T_{ign} = T_\infty + (T - T_\infty)_{actuator\ body} + \Delta T_{bridgewire\ excess}$$

The latter two contributions both depend on the current which is passing through the bridgewire.

Figure 2 shows the results of the calculation for this example. Also shown are the data values of no-fire current cited above. Because of uncertainty in the position of the bridgewire from the header, a δ variation is shown. In particular, no great care is taken to see that the bridgewire lays consistently against the header for that case, so an uncertainty in position of one bridgewire diameter is assigned. For the case of the hole under the bridgewire, a nominal value for δ of 1.016×10^{-2} mm (4 mils) $\pm$ 1 bridgewire diameter is assumed. This value is affected by two considerations: (1) a spherical hole is more effective than a flat bottom hole of the same depth in interaction with the bridgewire (hence, a reduction in "effective" depth), and (2) during pressing, the pyrotechnic compacts approximately 25% which would have the effect of shifting the bridgewire closer to the header. It can be observed from Figure 2 that there is qualitative agreement between the analytic curve and the two experimental values.

Figure 3 shows analytic results for the same configuration with the exception that different values of thermal conductivity were used for the header. This figure indicates the variation in no-fire current level with header materials of different thermal conductivity. In those calculations, the rise in the actuator body temperature is substantial. If the actuator is mounted in a bulkhead so that its temperature rise is negligible, then the curves of Figure 3 would be much more widely separated, i.e., a high conduction header would allow a much higher no-fire current than a poor conductor header.

Figure 4 shows the position-time plot of the thermal wave for the actuator under consideration. If the function time is to be on the order of 5 msec, then a $1.27 \times 10^{-2} - 1.52 \times 10^{-2}$ mm (5 - 6 mil) spacing (δ) should be more than sufficient to eliminate header interaction.

The response times for bridgewire and actuator body heat-up are quite different. Typically, the bridgewire reaches 99% of its excursion (above post temperature) in 50 - 100 ms, whereas the actuator body reaches 99% of its excursion (above ambient temperature) in 600 - 1200 s. Therefore, once the bridgewire temperature profile has been established, it is in quasi-steady state and it is possible that for marginal bridgewire current levels, ignition occurs as a result of the long time response of the actuator body heat-up, causing delayed ignition.

COMMENTS

As with any model, simplifying assumptions have been made to produce more tractable mathematics. To the extent that these assumptions describe the physical situation, agreement between the model and the experiment can be expected. Particular limitations of the analysis are: 1) parallel path electrical conduction in the pyrotechnic has not been considered, 2) the thermal contact conductance at the bridgewire-pyrotechnic and the pyrotechnic-header interface is assumed to be perfect (these considerations can be simply treated by extension of the analysis), 3) the bridgewire is homogeneous and the welds to posts are good so that hot-spots are not produced, and 4) the previously mentioned assumptions on geometry, material properties, and time independence must hold. In spite of these limitations, this analysis can be a useful tool for the component designer attempting to meet a no-fire specification.

REFERENCES

1. Lardner, T. J. and Pohle, F. B., "Application of the Heat Balance Integral to the Problems of Cylindrical Geometry", ASME Trans. J. Applied Mechanics (1961), pp. 310-312.

2. Private Communication, G. H. Bradley, Sandia Laboratories, February 15, 1977.
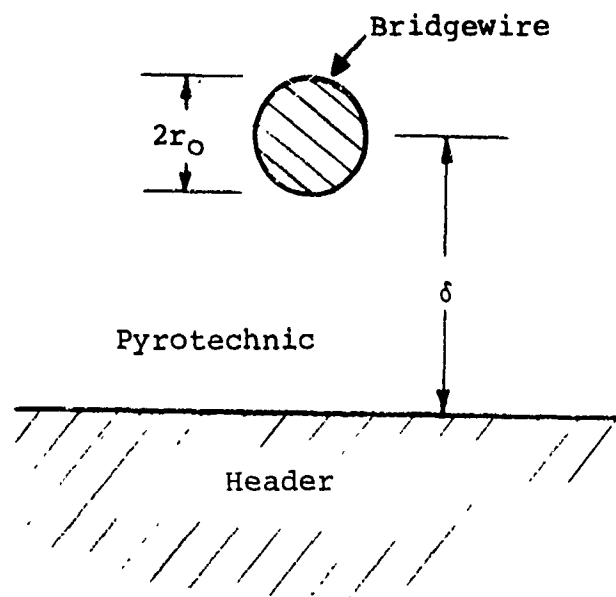
Figure 1

Schematic end view of bridgewire-
pyrotechnic-header system.
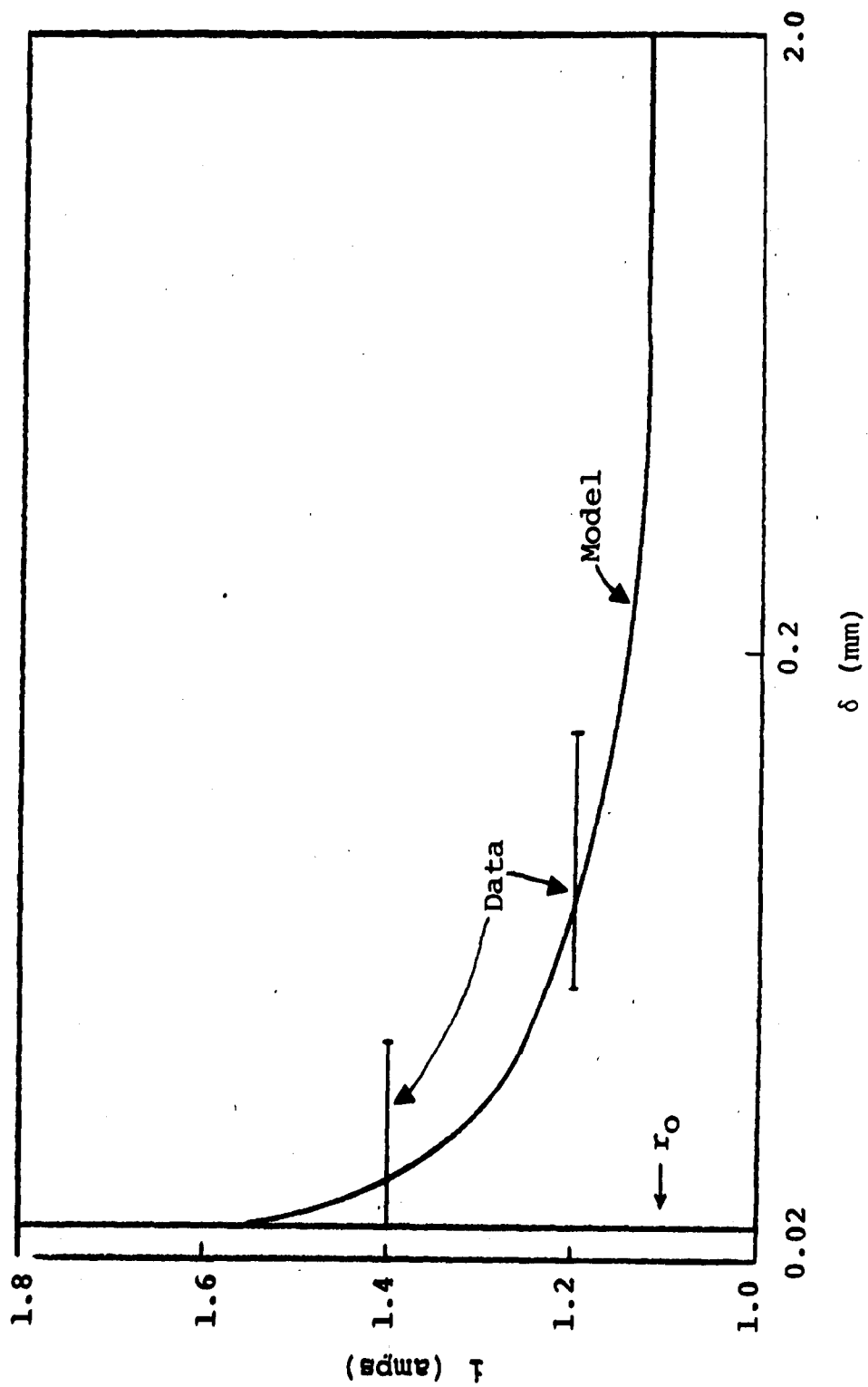
Figure 2

Comparison of no-fire current data
with model prediction.
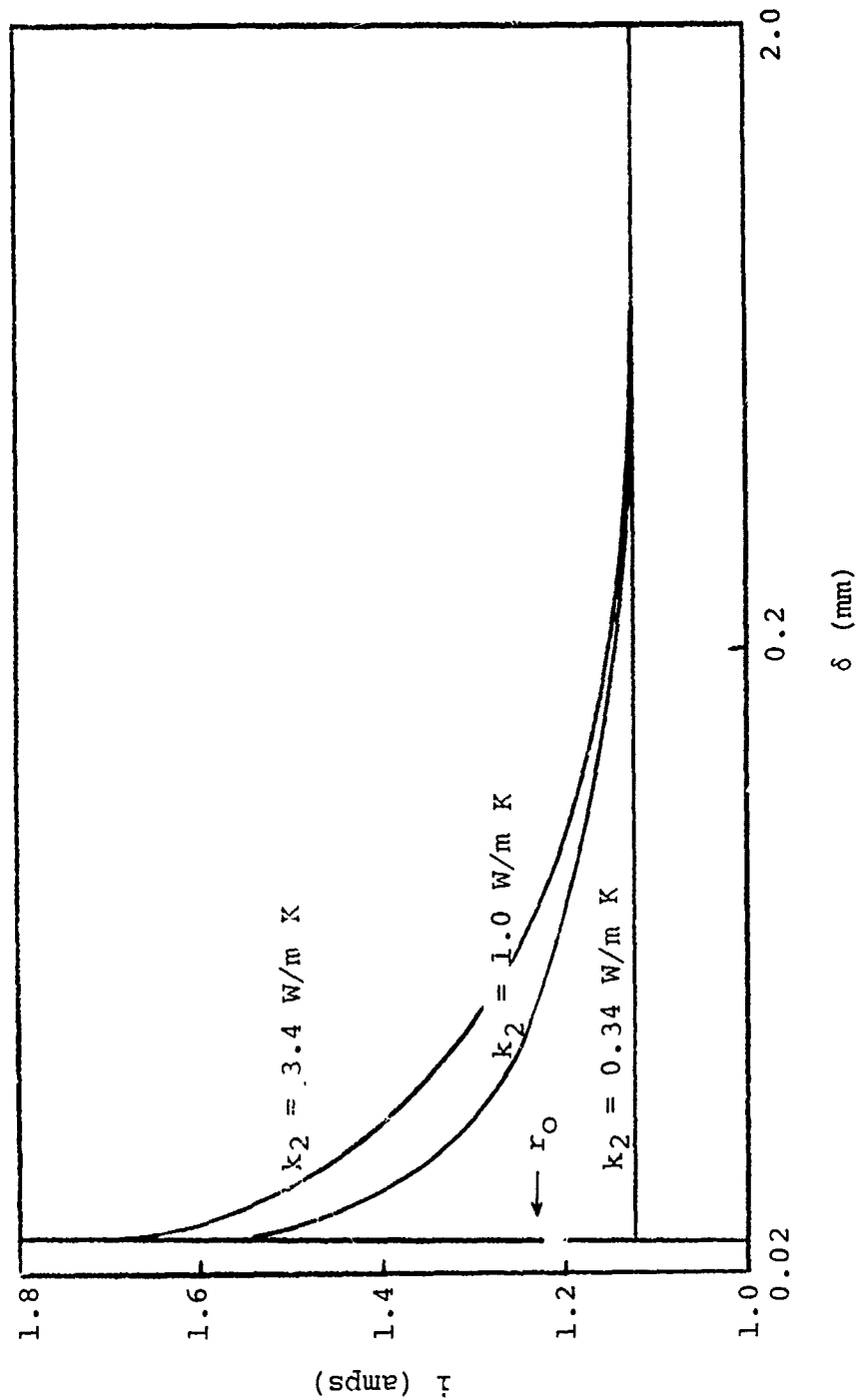
Figure 3

Model prediction of the effect of header thermal
conductivity on the no-fire current level, for
the example used in Figure 2.
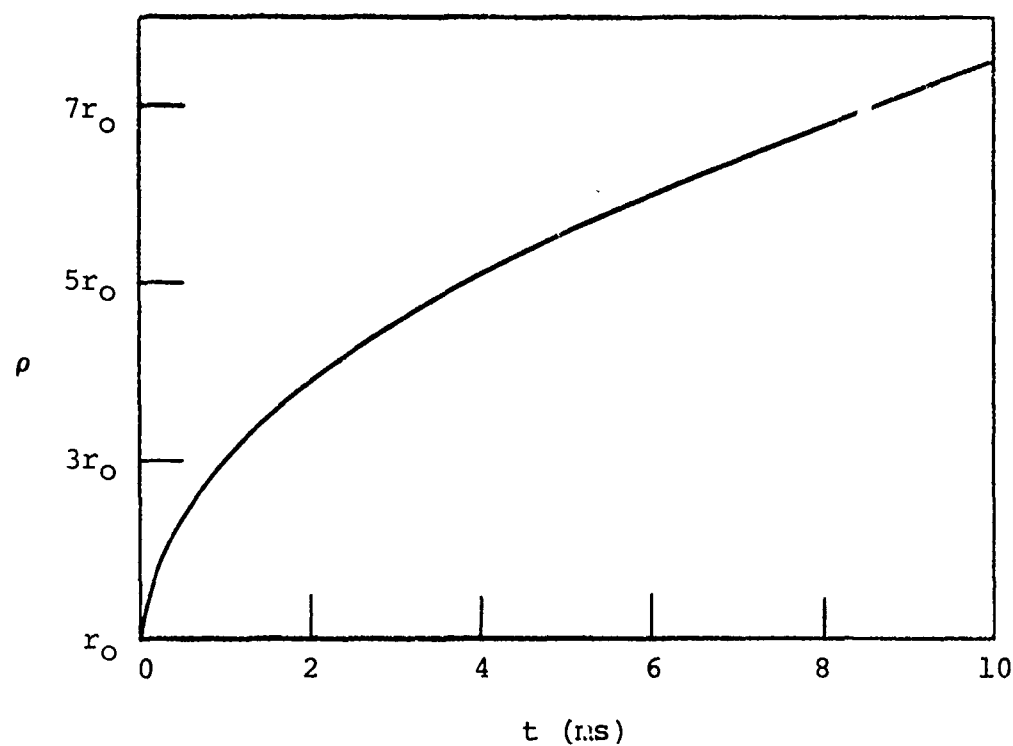
Figure 4

Position-time plot of thermal
wave propagating from bridge-
wire into pyrotechnic.

NOMENCLATURE

A_s — surface area of actuator

a — position on y-axis in z-plane

C_p — mean constant pressure specific heat of actuator

c — radius of circles in w-plane

h — convection heat transfer coefficient

$I_{0,1}/K_{0,1}$ — modified Bessel functions of the first and second kind, respectively, of order zero and one.

i — current

k — thermal conductivity

l — half-length of bridgewire

m — mass of actuator

R — resistance

$\mathcal{R}$ — resistivity

r — radius

$T, \Delta T$ — temperature and temperature excess, respectively

t — time

z — position variable

α — thermal diffusivity

$\gamma_{1,2}$ — ratio of thermal conductivity of pyrotechnic or header to that of bridgewire, respectively

δ — distance from header to bridgewire centerline (on y-axis)

η — r/a

Θ — $(T - T_{post})(\Pi r_o{}^2)^2 k_o/(i^2 \mathcal{R} a^2)$

ξ — z/a

ρ — distance of thermal wave from starting position

σ — l/a

Subscripts

$0,1,2$ $-$ designates bridgewire, pyrotechnic, header, respectively

∞ $-$ designates free stream, or surrounding value

DETERMINATION OF THE THERMAL DIFFUSIVITY OF PYROTECHNIC MATERIALS

Don E. Etter, David R. Kaser, and Layton J. Wittenberg

Mound Facility*
Miamisburg, Ohio

INTRODUCTION

Thermal diffusivity studies have been initiated to better characterize developmental pyrotechnic materials. Thermal diffusivity, along with density and specific heat, can be used to calculate another important thermophysical property, namely, thermal conductivity. A literature search revealed the relatively simple method commonly known as the flash-diffusivity method. This method, with appropriate modification to accent pyrotechnic materials at elevated temperatures, was selected for these studies.

METHOD AND APPARATUS

The flash-diffusivity method is based on the transient behavior of a specimen when one side is subjected to a short thermal pulse. As the heat pulse travels through the specimen, its back surface temperature rise is recorded as a function of time. This time-temperature history is directly related to the thermal diffusivity.

Parker et al [1] derived the simple relationship:

$$\alpha = 0.139L^2/t_{1/2},$$

where: α = thermal diffusivity
L = specimen thickness
$t_{1/2}$ = time required for back surface of specimen to reach half of the maximum temperature rise.

This relationship involves several simplifying assumptions:

1) The heat pulse is uniformly absorbed on the front face of an opaque specimen.

2) The heat pulse is of negligible time compared to the time required for heat propagation through the specimen.

3) The heat flow is one dimensional from the front face to the back face.

4) Heat losses of the faces are negligible.

5) The temperature rise within the specimen is small enough to consider the thermal properties as constant.

This method offers the advantage of not being necessary to quantitatively measure the heat flowing through the specimen. Additional advantages are that small specimen requirements permit rapid attainment of equilibrium conditions as well as offering desirable safety conditions for the study of pyrotechnic materials.

The method has an accuracy of $\approx \pm 5\%$ when values for standard materials are compared to accepted literature values. The largest error contribution is believed to be the reading of the Polaroid photograph of the time-temperature measurement.

A schematic of the thermal diffusivity apparatus is shown in Figure 1. The disc-shaped specimen is positioned inside the heater-thermocouple assembly, which allows the specimen to be supported primarily by the thermocouple, thus giving good contact. This technique works well with fragile specimens, such as pressed pyrotechnic materials. The specimen size is 6.35 mm (0.25 in.) diameter by varying thickness 0.76 to 3.17 mm (0.030 to 0.125 in.) depending on thermal diffusivity of the material under study.

Measurements are made by pulsing the front surface in ~1 msec with 1.5 J from an ir laser which is focused to a spot size slightly larger than the specimen. The transient temperature at the back face of the specimen is measured by a chromel-alumel thermocouple 0.10 mm (0.004 in. diam). The output voltage from the thermocouple is fed to a dc amplifier and subsequently to the Y-axis of an oscilloscope. Maximum amplification for this system is 30 μV full scale or 0.75°C.

A single-sweep, triggered simultaneously with the laser pulse, is presented on the oscilloscope and photographed with a Polaroid camera. Shown in Figure 2 is a typical temperature-time curve. The thermal diffusivity of the specimen can be calculated from this data.

The apparatus was designed to permit measurements to be made in any desired atmosphere. For measurements at elevated temperatures, it is necessary to null the thermocouple output at any constant temperature by using a bucking voltage. This allows the amplified ΔT signal-resulting from the laser pulse, to be measured.

Initial thermal diffusivity determinations were made at ambient temperatures on known materials; such as, SiO_2, Al_2O_3, 304 stainless steel, and ZrO_2 to demonstrate that the method was in agreement with accepted literature values [2].
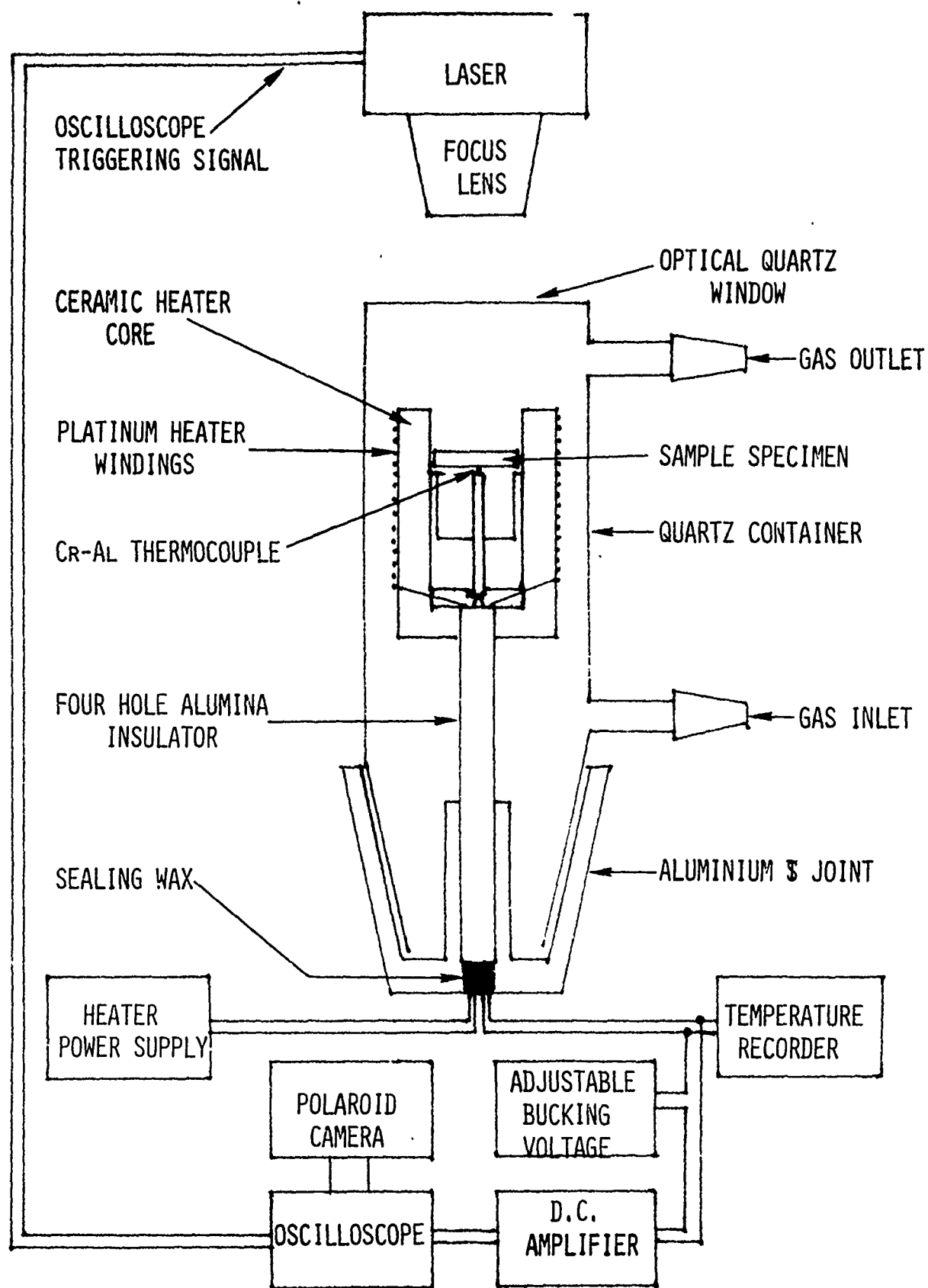
FIGURE 1 - A schematic of the thermal diffusivity apparatus.
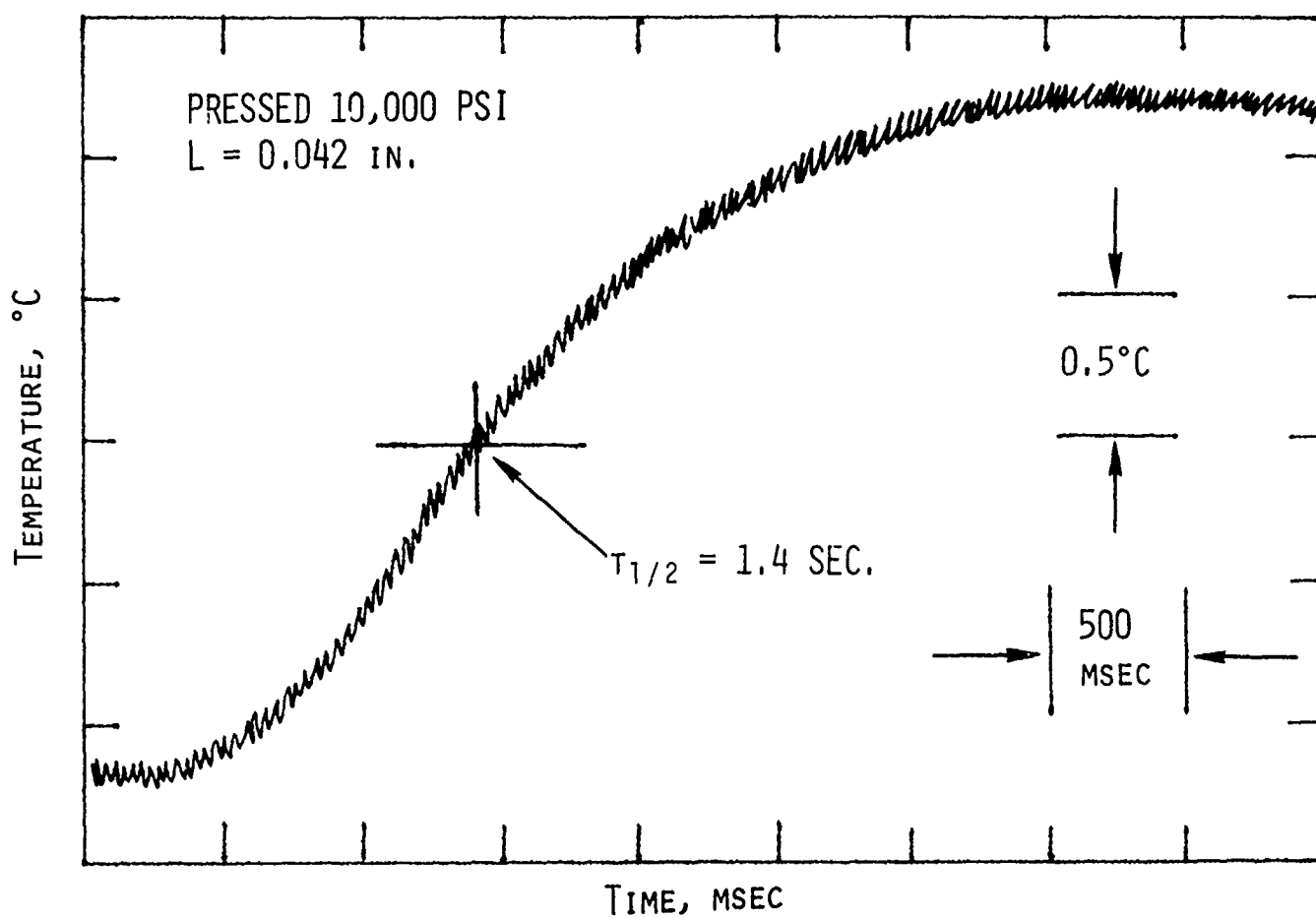
FIGURE 2 - Typical temperature-time curve for 33% $TiH_{0.65}$/67% $KClO_4$.

EXPERIMENTAL RESULTS

Several variables were investigated to determine which ones have a significant effect on the thermal diffusivity of associated pyrotechnic materials. The first study involved the thermal diffusivity measurement of $TiH_{0.675}$ as a function of temperature. This material was of particular interest since it is presently used in pyrotechnic blends, and the binary system between titanium and hydrogen exhibits a eutectoid near this composition at 319°C [3]. The initial determination was made in a 95% argon-5% hydrogen atmosphere. It is apparent from results shown in Figure 3A that a significant change occurred in the vicinity of the eutectoid temperature. Also, it is evident that a degradation of the material occurred since the thermal diffusivity value at ambient temperature was not the same before and after heating. Subsequent x-ray diffraction analysis showed an increase in hydrogen content to the degree that only single phase·substoichiometric gamma-titanium hydride was evident. The complex loss of the alpha-titanium phase explains the thermal diffusivity change. These data indicate that a 95% argon-5% hydrogen atmosphere is undesirable at elevated temperatures.

Because of the overwhelming quantity of $KClO_4$, this effect was virtually undetectable in the pyrotechnic blend ($TiH_{0.65}$/67% $KClO_4$), which is shown in Figure 3B.

These two determinations were repeated in an argon atmosphere, and the results are shown in Figures 4A and 4B. The contrast between Figures 3A and 4A is quite evident. It appears that the integrity of the $TiH_{0.675}$ was maintained in an argon atmosphere; however, the thermal diffusivity was found to decrease from ambient to 300°C, then stabilize between 300 and 400°C.

A comparison between the pyrotechnic blend in the two atmospheres, Figures 3B and 4B, exhibits very little difference--both decreasing in thermal diffusivity up to 300°C, then increasing slightly between 300 and 400°C.

Another variable investigated was the thermal diffusivity of $TiH_{0.675}$ as a function of density. The data are plotted in Figure 5, showing essentially a linear rise of thermal diffusivity as the density is increased. Over the density range of 2.18 to 2.37 g/cc, the thermal diffusivity increases from 39.3 to 46 x 10^{-4} cm^2sec^{-1}.

A linear relationship between thermal diffusivity and density was also found to exist for $KClO_4$ and $TiH_{0.65}$/67% $KClO_4$ blend materials. The $KClO_4$ thermal diffusivity increased from 12 to 16 x 10^{-4} cm^2sec^{-1} over a density range of 2.03 to 2.19 g/cc, whereas the blend exhibited only a very slight increase from 13.6 to 14 x 10^{-4} cm^2sec^{-1} when its density was increased from 2.09 to 2.28 g/cc. These data are shown in Figures 6 and 7, respectively.
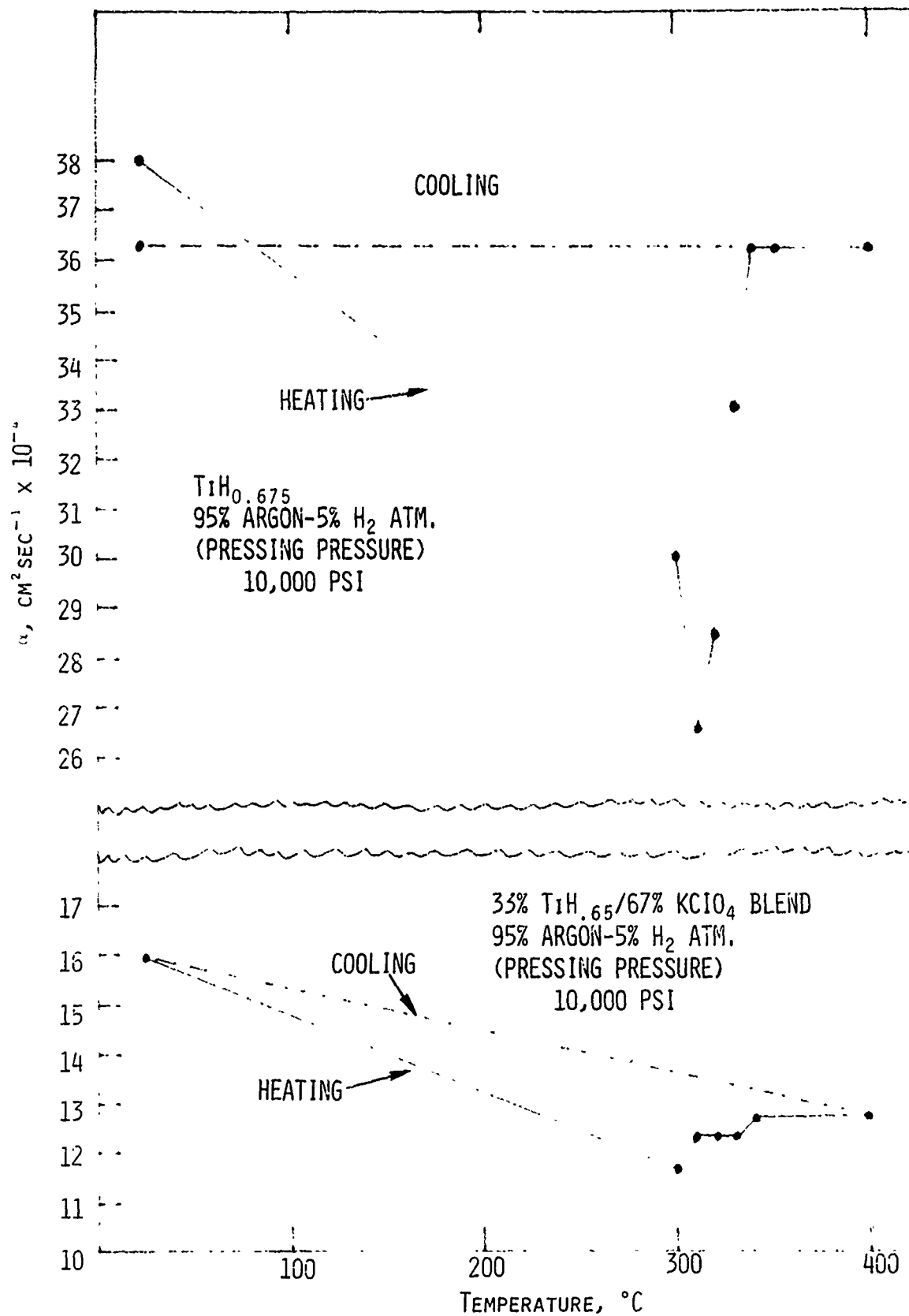
FIGURE 3A/3B - The thermal diffusivity of $TiH_{0.675}$ and 33% $TiH_{0.65}/67\%$ $KClO_4$ as a function of temperature in a 95% argon-5% hydrogen atmosphere.
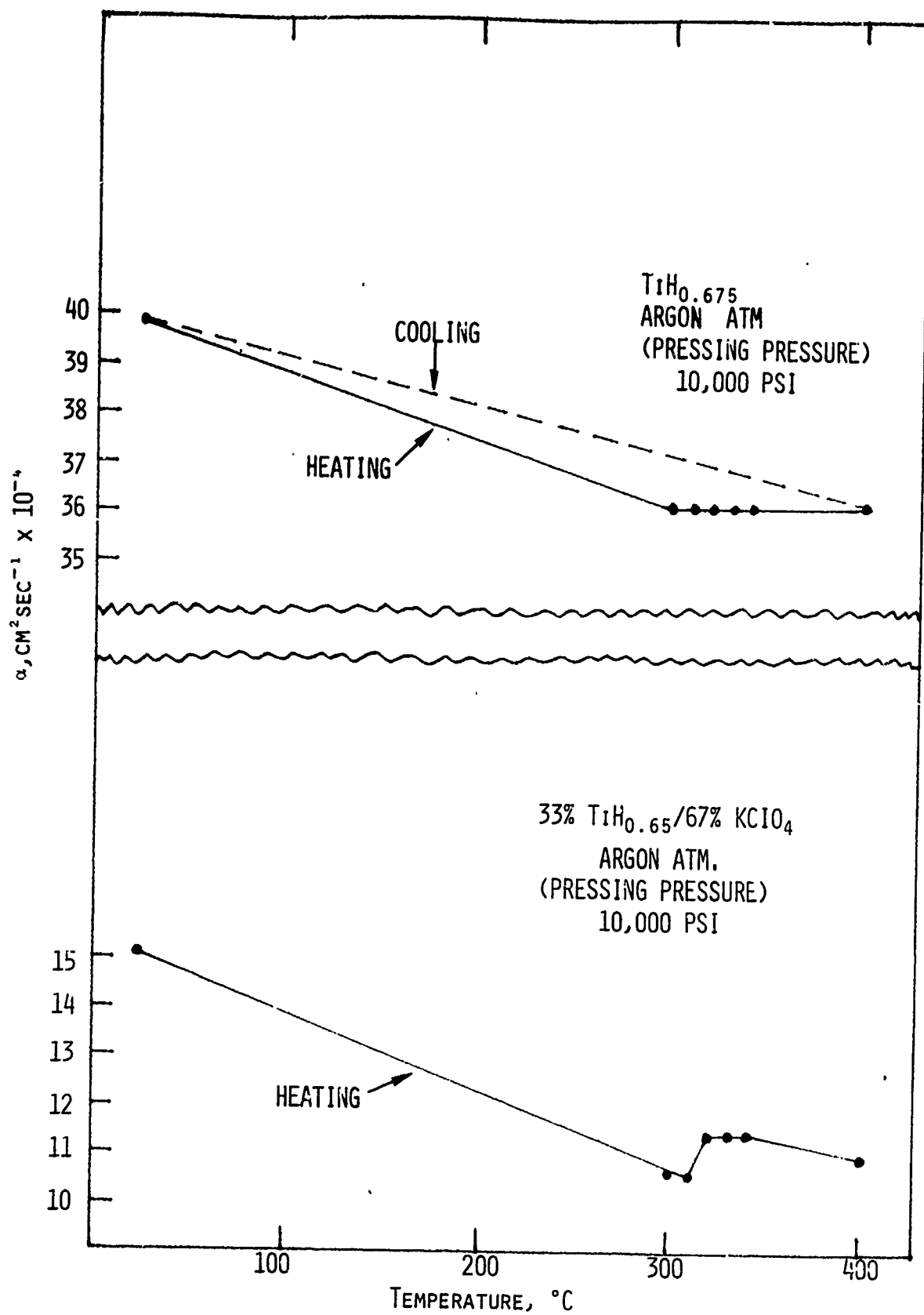
FIGURE 4A/4B - The thermal diffusivity of $TiH_{0.675}$ and 33% $TiH_{0.65}$/67% $KClO_4$ as a function of temperature in an argon atmosphere.
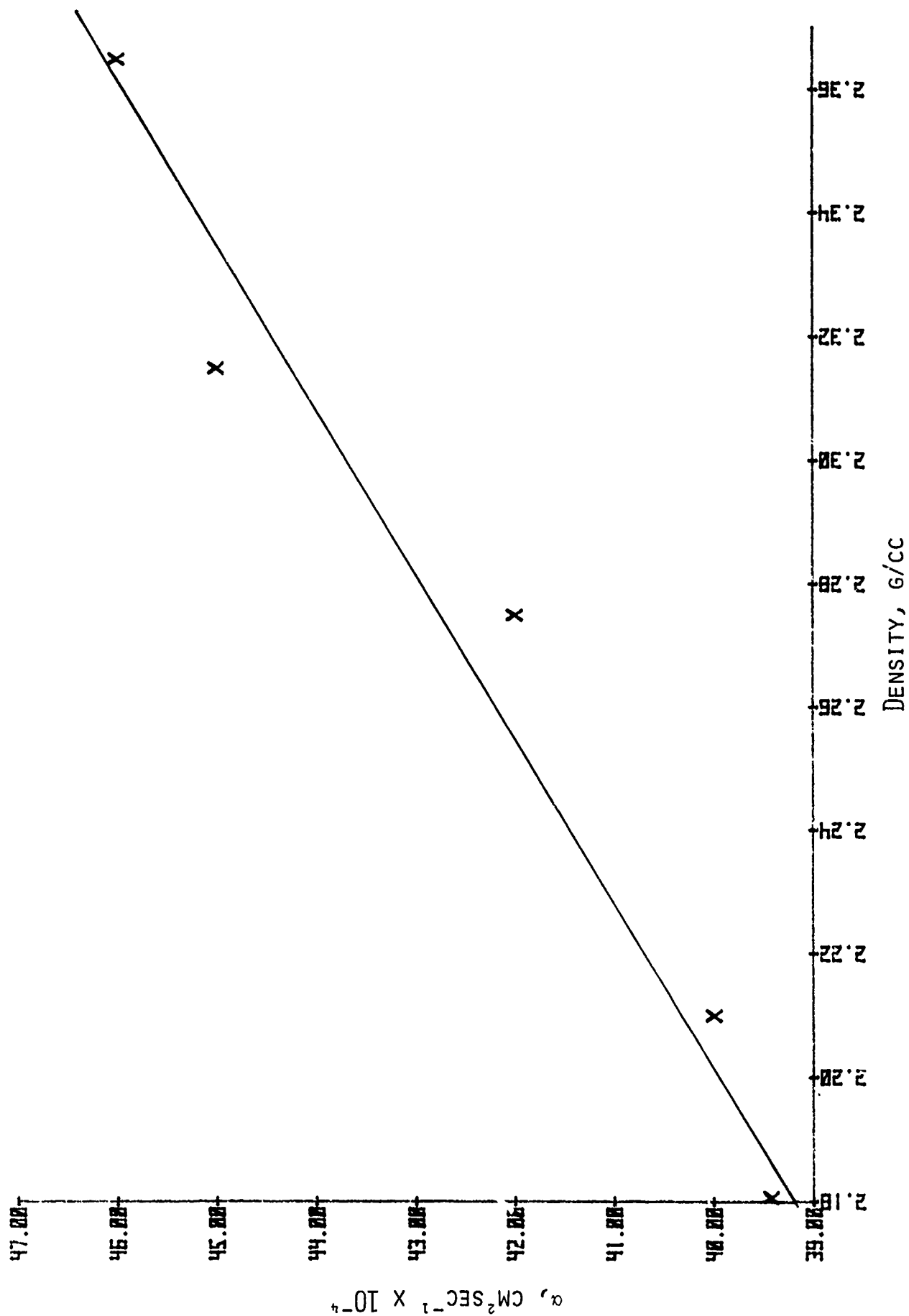
FIGURE 5 - Thermal diffusivity of $TiH_{0.67}$ as a function of density.

173
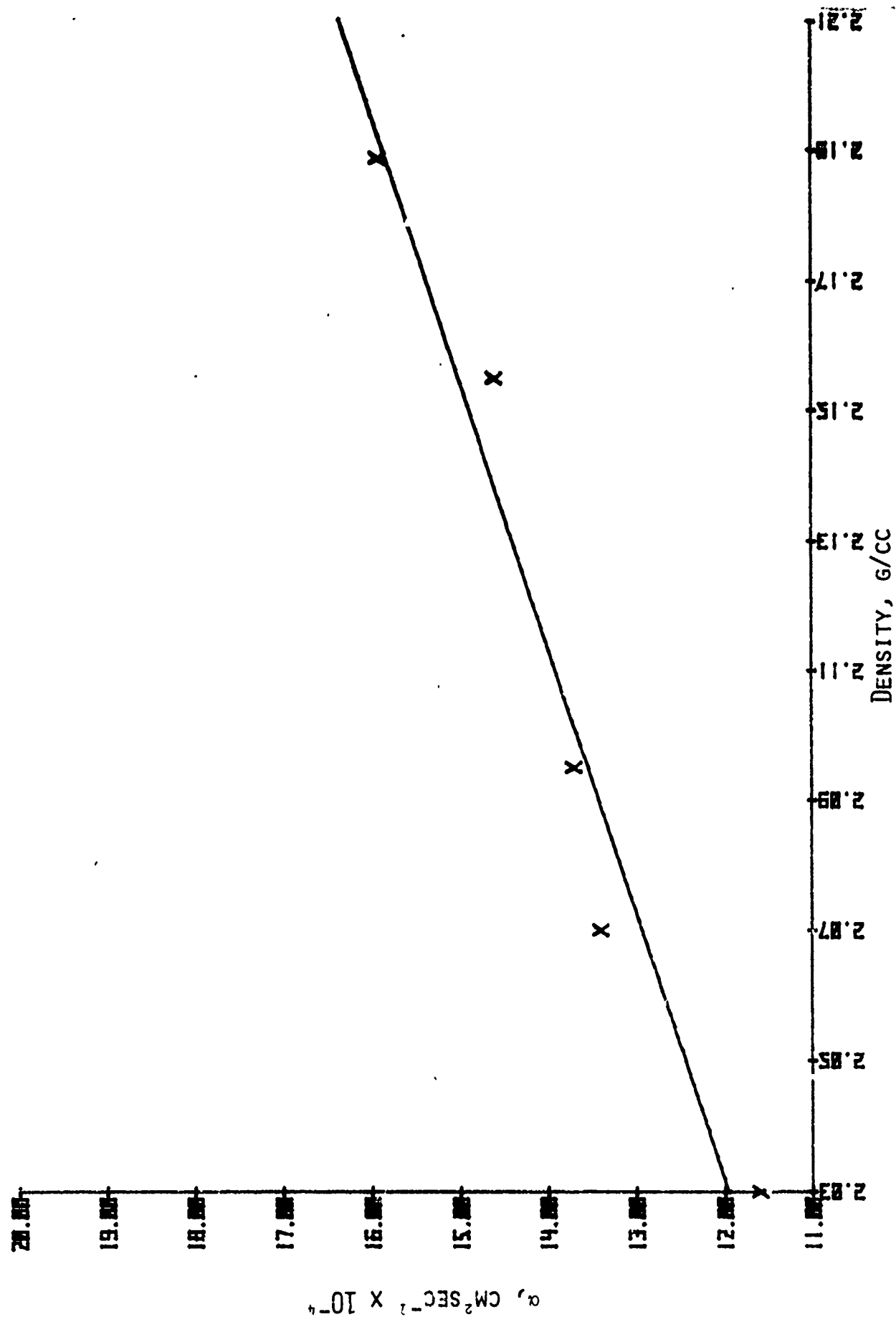
FIGURE 6 - Thermal diffusivity of $KClO_4$ as a function of density.
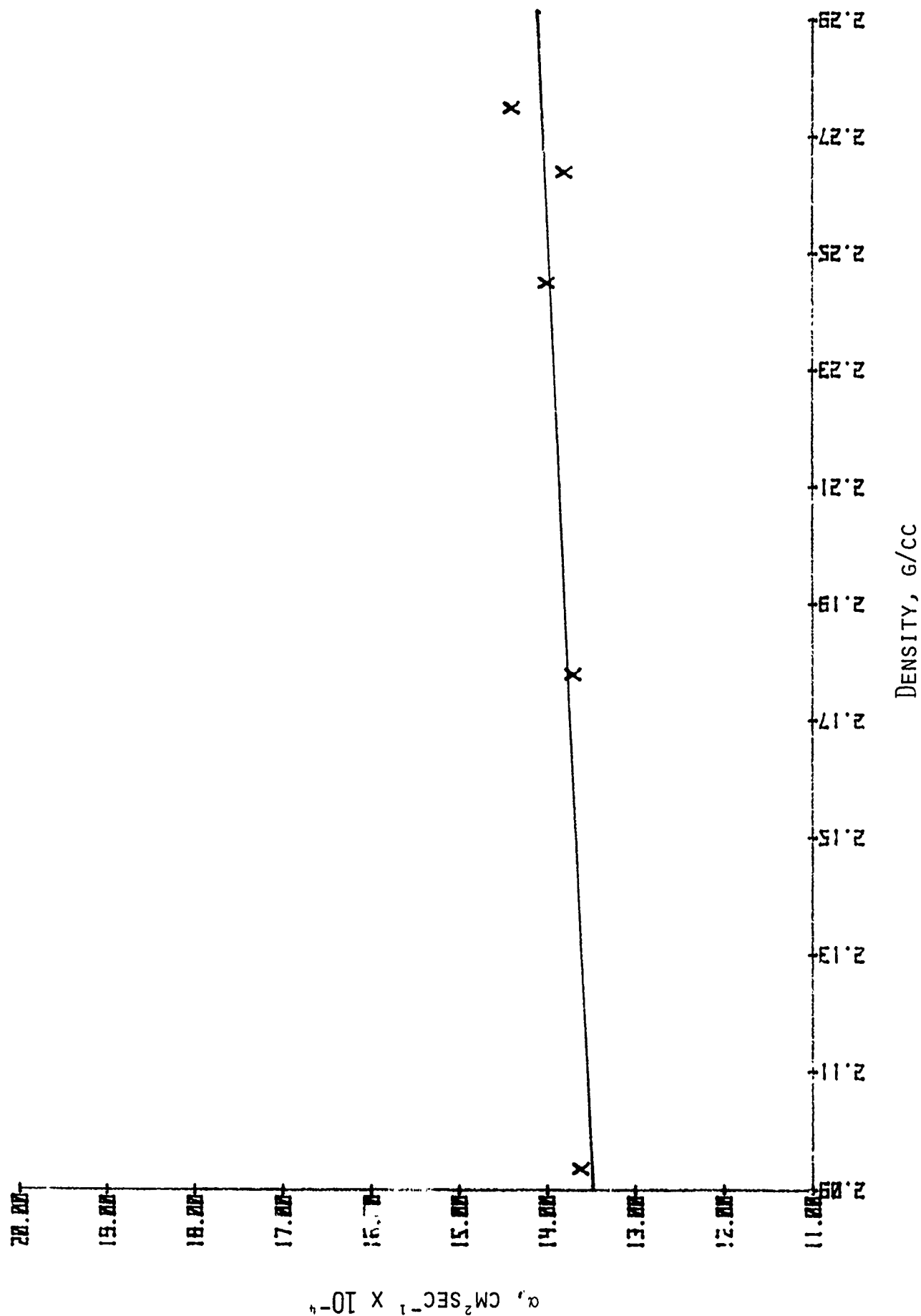
FIGURE 7 - Thermal diffusivity of 33% $TiH_{0.65}$/67% $KClO_4$ blend as a function of density.

The next experiment involved varying the $TiH_{0.65}$-$KClO_4$ blend ratio and measuring the thermal diffusivity. The results are that of a nonlinear curve, as shown in Figure 8. The data show the major effect of the $KClO_4$; the line just above the measured data is calculated using the mathematical model for one-dimensional composite membrane diffusion [3]. Although the calculated and the measured data do not match exactly, it is obvious that a good estimation can be obtained using this model.

The final variable investigated was the relationship between thermal diffusivity and the titanium-hydrogen ratio. Since a limited number of ratios were available, the study can only be considered cursory; however, the results indicated a linear decrease in thermal diffusivity of 40×10^{-4} to 26×10^{-4} cm^2sec^{-1} for samples ranging from $TiH_{0.38}$ to $TiH_{1.32}$, respectively.

SUMMARY AND CONCLUSIONS

The thermal diffusivity of $TiH_{0.675}$ was found to decrease from 40×10^{-4} to 36×10^{-4} cm^2sec^{-1} when heated in an argon atmosphere to 400°C. A decrease was also evident for the pyrotechnic blend of $TiH_{0.65}/67\% KClO_4$, under similar conditions, from 15×10^{-4} cm^2sec^{-1} to 11×10^{-4} cm^2sec^{-1}.

Substoichiometric titanium hydride compositions ranging from $TiH_{0.38}$ to $TiH_{1.32}$ show essentially a linear decrease in thermal diffusivity from 42×10^{-4} to 26×10^{-4} cm^2sec^{-1} as the hydrogen content is increased.

The effect of density on the thermal diffusivity of the hydride, $TiH_{0.65}$, which is most commonly used in pyrotechnic blends, shows a linear increase from 39.3×10^{-4} to 46×10^{-4} cm^2sec^{-1} for a density increase from 2.18 to 2.37 g/cc. In contrast, the blend ($TiH_{0.65}/67\% KClO_4$) exhibits a virtual independence of density over the range of 2.09 to 2.28 g/cc, yielding a thermal diffusivity of 14×10^{-4} cm^2sec^{-1}. These data indicate that the large quantity of $KClO_4$ in the blend is the controlling factor.

In addition, the study on varying the $TiH_{0.65}$-$KClO_4$ blend ratios showed that thermal diffusivity was affected nonlinearly, significantly favoring the influence of the $KClO_4$. This relationship was also found to closely resemble the mathematical model for one-dimensional composite membrane diffusion [3].

In closing, the flash diffusivity method has proven adaptable to such fragile specimens as pressed pyrotechnic materials. It also has the added feature of small specimen requirements--which is desirable when handling pyrotechnic materials.
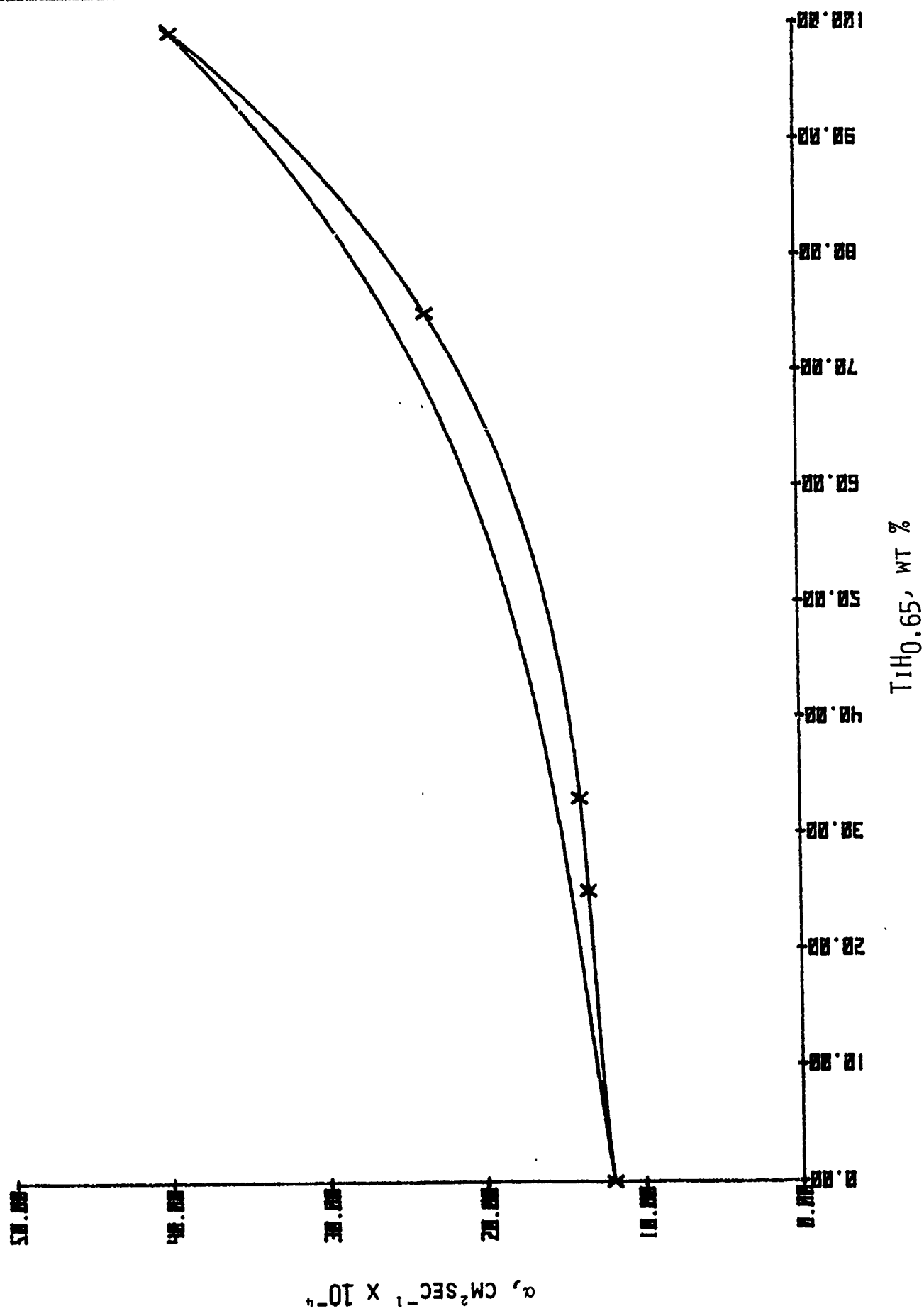
FIGURE 8 – TiH$_{0.65}$-KClO$_4$ blend ratio effect on thermal diffusivity.

177

ACKNOWLEDGEMENTS

REFERENCES

1. W. J. Parker, R. J. Jenkins, C. P. Butler, and G. L. Abbott, "Flash Method of Determining Thermal Diffusivity, Heat Capacity, and Thermal Conductivity," J. Appl. Phys., 32, 1679 (1961).

2. Y. S. Touloukian, Thermal Diffusivity, Thermophysical Properties of Matter, TPRC Data Series, Vol. 10, pp. 344, 378, 399 and 451.

3. M. Hansen, Constitution of Binary Alloys, McGraw-Hill Book Co., Inc., New York, 1958, p. 800.

4. J. Crank, The Mathematics of Diffusion, Oxford University Press, Oxford, 1970, p. 44.

BLACK POWDER EXPLOSIVES

F. L. FAHRINGER

PLANT MANAGER

Belin Plant, Moosic, Pennsylvania

ABSTRACT

The composition of black powder is potassium nitrate, sulphur and charcoal that is mixed, ground, kneaded, pressured and sheared to insure uniformity. Black powder is considered a low explosive,but transported and stored in magazines as a Class A explosive.

BLACK POWDER EXPLOSIVES

Between the Civil War and World War I scores of black powder plants grew into existence in Pennsylvania's upper anthracite region to supply the booming coal mining industries that became the backbone of the region's economy. In the year 1908 the Belin Plant was constructed by E. I. du Pont de nemours of Pennsylvania, a wholly-owned subsidiary of E. I. du Pont de Nemours and Company incorporated in Delaware. However, it was December 1911 before the first batch of black powder was made. With men and machines at work in small widely separated structures combining potassium nitrate, sulphur and charcoal to process the mixture into black powder, it became the second largest producer of black powder in a matter of 3 short years.

During World War I, World War II, the Korean and Viet Nam conflicts, millions of pounds of black powder were used and supplied by the Belin Plant.

Today, the sole producer of black powder in North America is located in Moosic, Pennsylvania. The Belin Plant, originally owned by E. I. du Pont, was acquired by Gearhart-Owen Industries, Inc. in April 1973. Because of the most recent spin-off between Gearhart and Owen the facility is presently owned and operated by GOEX, Incorporated, a wholly-owned subsidiary of Pengo Industries. Along with the Belin Plant they have the Cleburne, Texas plant where shaped charges and cast boosters are produced.

At the present time, a small quantity of black powder is sold to the government. Its uses are about 100% commercial, this includes sporting, fireworks, fuse,coal mining, specialty blasting, military ordnance devices and as a primer to initiate other types of propellants.

BLACK POWDER PROCESS DESCRIPTION

RAW MATERIALS

Granulated nitrate is fed into a crusher-feeder unit which breaks lumps and feeds through a conveyor and elevator to a vibrating screen where the coarser material is returned and foreign matter is stopped by magnets. Magnets are installed in other locations in the system to prevent foreign material from entering the batch weighing process.

Sulphur and charcoal are combined in proportion by formulation and pulverized to a very fine powder in a ball mill. The pulverizing is accomplished by two thousand pounds of stainless steel balls as the mill rotates slowly. The material is emptied through a fine screen and passed over magnets prior to being weighed and bagged.

GENERAL

The separate powder ingredients are inert, but any mixture of the three components is explosive at all stages of processing. Recognition of the attending hazards of manufacture requires the plant layout and methods to be designed for the maximum protection of personnel, equipment and property.

Black powder is a batch process and each step of the process is conducted in separate buildings. The distances of each building and the quantity of powder allowed is in accordance with the Table of Distances. The number of personnel allowed in or around each operation is posted and controlled to minimize exposure. Several of the operations are remotely controlled.

INCORPORATION OR MIXING

The preformulated ingredients of potassium nitrate and pulverized sulfur-charcoal mixture are spread evenly over the cast iron pan and a small amount of water is added at the wheel mill to produce the "wheel cake", a relatively loose, low density and formless moist mass. The wheel mills, which are edge runner type mills, consist of a massive cast iron pan and heavy cast iron rolls or wheels, aided by plows, which roll over the charge and grind, knead, press and shear the mixture to insure uniformity of composition.

PRESSING

The wheel cake is roughly broken through wooden rolls to reduce lumps. The powder is funneled and pressed between thin aluminum plates which are installed vertically and uniformly spaced,between which the charge is pressed by means of a horizontal hydraulic press. Here, the specific gravity of the black powder is determined by pressure and time of pressing. After pressing, the powder is removed in hard

cakes that measure 24 inches square and about one (1) inch
thick. The press cake is roughly broken between toothed
bronze rolls into "chip cakes" that measure about 1-1/2
inches.

GRANULATION

The "chip cake" is processed through a series of four
(4) pairs of crushing rolls, a shaker screen beneath the
rolls and a rotary screen or a bolter. The rate of feed,
spacing of the rolls and the mesh of the screens used will
vary to produce "green" grain in a range of sizes during
the same run.

The oversize is recirculated at the last station
until none remains while the undersize backdust is returned
to the Press Mill to be repressed.

GLAZING

The "green" grain is tumbled in the glaze barrel and
is subject to friction. The friction wears off the soft
and rough edges from the grain, smooths the grain surface
and creates heat to dry the grain. Additional hot or cool
air is applied to aid the process. Near the end of the
cycle graphite is added to apply a polish and luster to
the product. The material can be manufactured glazed or
unglazed.

PACKING

The material is then worked through a set of screens
for final sizing of the finished grain and eventually packed

into the desired containers.

Superfine Black Sporting Powder is available in
four (4) granulations - Military Specification in nine (9) -
Fuse in nine (9) speeds - "B" Blasting in six (6) and "A"
Blasting and Fireworks in seven (7) granulations.

To recapitulate, the powder is incorporated, pressed,
broken into pieces (or corned), glazed, dried, sifted,
packed and stored.

Improvements in Pyrotechnical Smoke

BY

Dr. H. Freiwald, Dr. G. Praehauser and A. Schießl

BUCK GmbH & Co, R & D Center

D - 8230 Bad Reichenhall
Federal Republic of Germany

Improvements in Pyrotechnical Smoke

Overview :

1. Smoke producing systems examined

    - Hexachlorethane (HC) - Smoke
    - Smoke resulting from red phosphorus as base (RP-Smoke)

2. Toxic characteristics of these smoke producing systems

3. Role of humidity in smoke generation

4. Investigations of these smoke producing systems
4. 1 Hexachlorethane Smoke

    - non-toxic (neutral) hexachlorethane smoke by addition of guanidine nitrate

    - description of the reaction mechanism of non-toxic HC - smoke

    - influence of reaction rate of HC smoke composition

4. 2 Phosphorus Smoke (RP-Smoke)

    - non-toxic (neutral) RP-smoke by addition of guanidine nitrate or urea nitrate
    - reaction mechanism of non-toxic RP-smoke composition
    - influence of reaction rate of RP-smoke composition

5. Manufacturing technology of such smoke mixtures

6. Examples of application

186

1. Smoke producing systems examined

The following pyrotechnical smoke systems were examined. The smoke producing components in these systems react with moisture in the air when smoke is developed :

- Hexachlorethane (HC) - Smoke :

$$3\ Zn\ +\ C_2Cl_6\ \longrightarrow\ 3\ ZnCl_2\ +\ 2\ C \qquad (1)$$

$$2\ ZnCl_2\ +\ H_2O\ \longrightarrow\ ZnO \cdot ZnCl_2\ +\ 2\ HCl \qquad (2)$$

The reaction of zinc chloride with atmospheric humidity resulting in the formation of chlorine water only takes place in the gaseous state. Solid zinc chloride with water gives off no smoke. The watery zinc chloride solution is only slightly acidic. And not dangerous from the acid content standpoint.

- Smoke resulting from red phosphorus as base (RP-Smoke) :

$$4\ P\ +\ 5\ O_2\ \longrightarrow\ 2\ P_2O_5 \qquad (1)$$

$$P_2O_5\ +\ H_2O\ \longrightarrow\ 2\ HPO_3 \qquad (2)$$

$$HPO_3\ +\ H_2O\ \longrightarrow\ H_3PO_4 \qquad (3)$$

Contrary to zinc chloride P_2O_5 in solid form also reacts with water to form phosphoric acid.

These smoke generation systems are known. They are used principally in military applications.

2. Toxic Characteristics of these Smoke Producing Systems

Poisonous properties that are contained in smoke clouds formed by fumes released from these smoke producing compositions are due principally to acids that have been developed.

As can be seen in the above reaction equation the resultant acid is always present in highly concentrated form. Only after exposure to moisture in the air is it diluted.

And so when such a smoke mass is used at a low rate of humidity, as in closed rooms for example, is the acid present in a high form of concentration, almost as an anhydrid or HCl gas. When such highly concentrated acids are inhaled, irreparable damages are caused. Under given circumstances, death can result. Accidents of that type have already occurred when smoke devices have been improperly applied.

The differences in the toxicity of phosphoric acid and hydrochloric acid are substantiated in the following manner :

Hydrochloric acid is a strong acid. Phosphoric acid is of average strength.

Dissociation Constant $\quad HCl \rightleftharpoons H^+ + Cl^- \qquad K = 10^7 \quad Mol/l$

Dissociation Constant $\quad H_3PO_4 \rightleftharpoons H^+ + H_2PO_4^- \qquad K = 7.10^{-3} Mol/l$
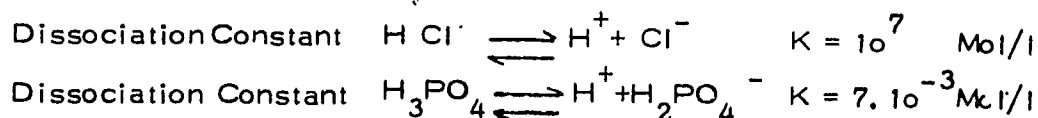
HCl is much more aggressive than phosphoric
acid.
This is only a gradual difference, however.
Naturally, phosphoric acid is also highly poi-
sonous in an ample concentration.

3. Role of Humidity in Smoke Generation

As is evident in the reaction equations of the two
smoke systems based on hexachlorethane and red
phosphorus mentioned earlier, the reaction of the
intermediate product of $ZnCl_2$ or P_2O_5 that is
formed with air is a sizeable factor in the deve-
lopment of smoke, and, at the same time, the smoke
performance.
Based on experience, that means that a weak smoke
production can be expected by extremely dry weather,
e. g. at relative humidity of 2o % and temperatures
over O° C.

In turn that means that in effective smoke producing
systems moisture from the air is always drawn on,
for example as with :

$Zn Cl_2$,

$Ti Cl_4$,

$Si Cl_4$,

$Sn Cl_4$,

P_2O_5,

$Cl SO_3H$.

189
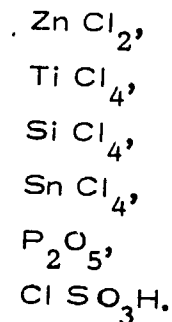
4. Investigations of these smoke producing
    systems

4.1 Hexachlorethane Smoke

The various ways there are to minimize toxity is
shown in the following :

As pointed out above, since a reaction with atmos-
pheric moisture cannot be dispensed with, so the
development of H Cl has to be reckoned with.
Non-toxicity, or a sizable reduction can only be
attained in a secondary reaction, namely in the
neutralization of the hydrogen chloride that has been
formed.

Thus, the following solutions to the problem are
conceivable :

- neutralization by simultaneously vaporizing the
  neutralizing agent as, for example, with ammonia
  or a derivative of ammonia.

  Neutralization can be achieved this way. However,
  the method has the following complicating disad-
  vantages :

  o   sizable increase in weight,
  o   considerable increase in volume,
  o   installation of two systems, separated
          from one another in one smoke device
  o   difficulties in controlling the vaporization
          rate of the neutralizing agent in order to
          obtain a neutrality in the smoke cloud
          that is built up.

- Neutralization by the addition of pyrolyzed base
  materials. These substances should be decomposed
  by the heat of the smoke mixture reaction, and

thereby neutralize the volatile bases of acidic
smoke producing components that result. For
example, this could be accomplished by guanidine
carbonate or ammonium carbonate.

This method, however, has the following disadvan-
tages :

- o sizable supplemental amounts and thereby
  an increase in volume required,

- o the smoke reaction mixture is cooled off
  considerably during the decomposition or
  vaporization of the base materials which
  result during the pyrolysis.
  That means the necessary reaction tempe-
  rature will no longer be attained. This is
  shown in weak smoke development. The
  reaction will shortly come to a standstill.

The reason is as follows :

As mentioned initially zinc chloride first reacts in
a gaseous state with atmospheric humidity, that
means the reacting smoke producing composition
must have a temperature higher than $730^{\circ}C$.
That is the boiling point of $Zn\ Cl_2$. A neutralizing
agent wich has a disintegration temperature or
vaporization temperature less than $730^{\circ}C$ thereby
delays attainment of reaction temperature. A pure
neutralizing agent would steadily require energy
to reach the vaporization point. This energy can
only be obtained from the reaction mixture.
Therefore, the reaction mixture would continually
be cooled. Add to this the fact that when the vapori-
zation temperature of the neutralizing agent lies
under the reaction temperature of the smoke pro-
ducing composition, wich is usually the case, the
reaction temperature is not achieved.

(In the case of HC composition the reaction temperature of zinc chloride lies higher than the vaporization point of $730^{\circ}C$).

    o   Chemical incompatibilities of most basic materials that could be considered, since the zinc in the HC composition easily reacts with acidic as well as basic substances.

        For that reason basic type substances as guanidine carbonate cannot be added without affecting storage capability. In most cases an immediate reaction results. That means that the proposed solution of separated neutralization systems has to be resorted to once again.

– Addition of a neutral agent that exothermally pyrolyzes in the formation of volatile basic matter.

  The substance to be added in this answer to the problem must have the following properties :

    o neutral (because of storage stability of the mixture)
    o it must pyrolyze to a vaporized base in an exothermal reaction.

A substance with these properties was found. It ist

$$\text{Guanidine Nitrate} \quad \left[H_2N - \overset{+}{C} \overset{\diagup NH_2}{\diagdown NH_2} \right] \cdot NO_3^-$$
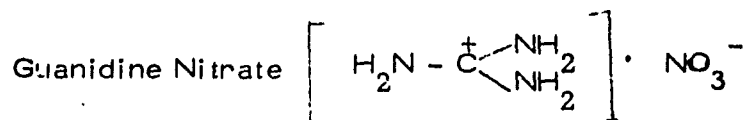
During the course of the reaction guanidine nitrate exothermally intervenes. NH_3 thereby results. This neutralizes the hydrochloric acid that is developed.

In order to understand the effect of guanidine nitrate
the reaction mechanism of the HC composition must
be examined somewhat closer.

The HC composition that was examined consists of
the following components :

> zinc
> zinc oxide
> hexachlorethane
> aluminium

Fundamental reaction mechanism:

$$C_2Cl_6 \longrightarrow C_2Cl_4 + Cl_2 \ldots\ldots\ldots 2\,C + 3\,Cl_2 \tag{1}$$

$$3\,Cl_2 + 3\,Zn \longrightarrow 3\,Zn\,Cl_2 \tag{2}$$

$$C_2Cl_6 + 3\,Zn \longrightarrow 3\,Zn\,Cl_2 + 2\,C \tag{3}$$

This reaction will only follow this way under ideal
conditions. Under normal conditions the reaction
chain is only possible with an Al additive in order
to increase the heat of reaction especially at the
beginning.

Equation (1) symbolizes the disintegration of hexa-
chlorethane by the removal of active chlorine.
2o1 KJ (=48K cal) are necessary to effect this
separation. (Source : D'Ans. Lax " Taschenbuch
für Chemiker und Physiker " Vol II, 1964, p. 1o59).

$$C_2Cl_6 + 2o1\ KJ \longrightarrow C_2Cl_4 + Cl_2 \ldots\ldots\ldots 2\,C + 3\,Cl_2 \tag{1}$$
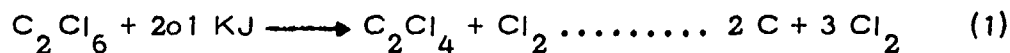
Aluminium is added because its chlorinating heat is considerably higher than of zinc. It is used as an energy transfer agent to bring the mixture up to the required reaction temperature and to hold it there.

Hence, the conventional HC compositions are composed of the previously mentioned components. Zinc oxide has a regulating effect on the intensity of the combustion and on the reaction time. The following reaction diagram is valid for such a reaction mixture :

$$2 \, C_2Cl_6 \longrightarrow 2 \, C_2Cl_4 + 2 \, Cl_2 \ldots\ldots 4 \, C + 6 \, Cl_2 \quad (1)$$

$$6 \, Cl_2 + 2 \, Al + 3 \, Zn \longrightarrow 2 \, Al \, Cl_3 + 3 \, Zn \, Cl_2 \quad (2)$$

$$2 \, Al \, Cl_3 + 3 \, ZnO \longrightarrow Al_2O_3 + 3 \, Zn \, Cl_2 \quad (3)$$

$$2 \, C_2Cl_6 + 2 \, Al + 3 \, Zn + 3 \, ZnO \longrightarrow 6 \, Zn \, Cl_2 + Al_2O_3 + 4 \, C \quad (4)$$
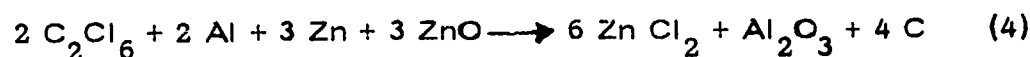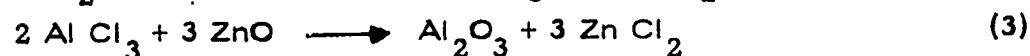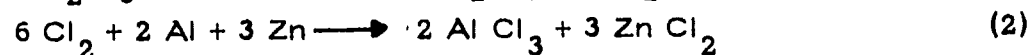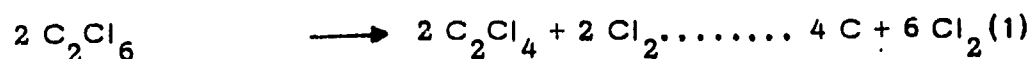
That aluminum plays a decisive role also is shown in the fact that a HC smoke can be made without metallic zinc and only with.

hexachlorethane
aluminum
zinc oxide

194

The reaction diagram for this smoke system looks like this :

I. Main reaction :

$$C_2Cl_6 \longrightarrow C_2Cl_4 + Cl_2 \ldots\ldots\ldots 2\,C + 3\,Cl_2 \qquad (1)$$

$$3\,Cl_2 + 2\,Al \longrightarrow 2\,Al\,Cl_3 \qquad (2)$$

$$2\,Al\,Cl_3 + 3\,ZnO \longrightarrow Al_2O_3 + 3\,Zn\,Cl_2 \qquad (3)$$

$$C_2\,Cl_6 + 2\,Al + 3\,ZnO \longrightarrow 3\,Zn\,Cl_2 + Al_2O_3 + 2\,C \qquad (4)$$
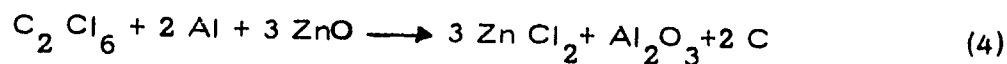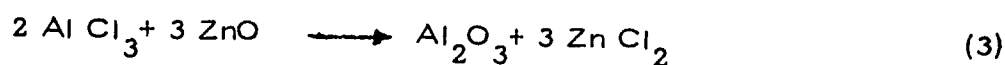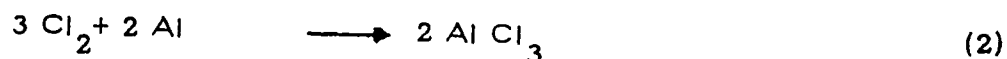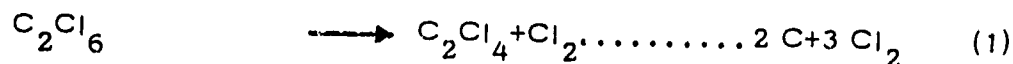
A second or side reaction also occurs alongside this reaction Zn O is reduced by C to Zn which is subsequently chlorinated.

II. Side reaction :

$$C_2Cl_6 \longrightarrow C_2Cl_4 + Cl \ldots\ldots\ldots 2C + 3\,Cl_2 \qquad (1)$$

$$3\,ZnO + 2\,C \longrightarrow 3\,Zn + CO + CO_2 \qquad (2)$$

$$3\,Zn + 3\,Cl_2 \longrightarrow 3\,Zn\,Cl_2 \qquad . \qquad (3)$$
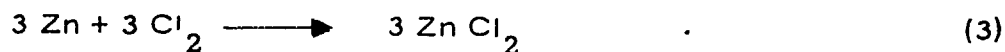
As can be seen in the respective diagrams, free carbon also results each time with the non-neutralized hexa smoke (without the addition of guanidine nitrate) . This can be detected by the gray color of the smoke.

However, should an oxygen carrier as guanidine nitrate, also be contained in the smoke producing composition, then the free carbon is oxidized by the free oxygen released by the guanidine nitrate to form carbon oxide or carbon dioxide. As a result of this additional oxidation reaction, the hot smoke neutralized by guanidine nitrate has a white color.

Reaction diagram of hot smoke neutralized by guanidine nitrate :

$$C_2Cl_6 \longrightarrow C_2Cl_4 + Cl_2 \ldots\ldots\ldots 2\,C + 3\,Cl_2 \quad (1)$$

$$\underbrace{3\,Zn + 2\,HNO_3}_{\text{from guanidine nitrate}} + 2\,C \longrightarrow 3\,ZnO + H_2O + N_2O + CO + C \quad (2)$$

$$3\,ZnO + CO + C \longrightarrow 3\,Zn + 2\,CO_2 \quad (3)$$

$$3\,Zn + 3\,Cl_2 \longrightarrow 3\,Zn\,Cl_2 \quad (4)$$

$$C_2Cl_6 + 3\,Zn + 2\,HNO_3 \longrightarrow 3\,Zn\,Cl_2 + 2\,CO_2 + N_2O + H_2O$$
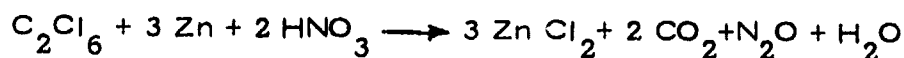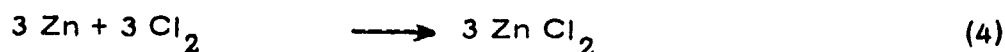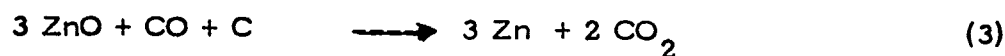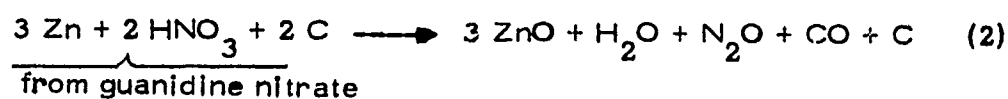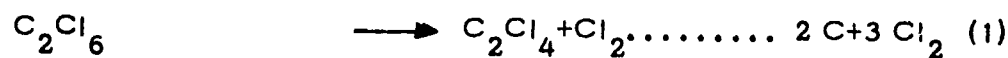
Neutralization Reaction :

$$3\,Zn\,Cl_2 + 3\,H_2O \longrightarrow 3\,ZnO + 6\,HCl \quad (1)$$

$$6\,HCl + 4\,H_2O + 2\,NHC(NH_2)_2 \longrightarrow 6\,NH_4Cl + 2\,CO_2 \quad (2)$$

$$3\,ZnCl_2 + 7\,H_2O + 2\,NHC(NH_2)_2 \longrightarrow 6\,NH_4Cl + 3\,ZnO + 2\,CO_2$$
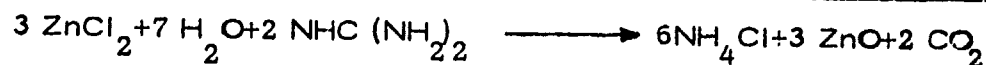
This becomes understandable when the energy balances are fashioned to these reaction mechanisms :

<u>HC Smoke with Zinc :</u>

$$C_2Cl_6 + 201 \text{ KJ} \longrightarrow C_2Cl_4 + Cl_2 \ldots\ldots\ldots 2 C + 3 Cl_2 \quad (1)$$

$$3 Cl_2 + 3 Zn \longrightarrow 3 Zn Cl_2 + 1.254 \text{ KJ} \quad (2)$$

_____

$$C_2Cl_6 + 3 Zn \longrightarrow 3 Zn Cl_2 + 2 C + 1053 \text{ KJ}$$

<u>HC Smoke with Al and ZnO</u>

$$C_2Cl_6 + 201 \text{ KJ} \longrightarrow C_2Cl_4 + Cl_2 \ldots\ldots\ldots 2 C + 3 Cl_2 \quad (1)$$

$$3 Cl_2 + 2 Al \longrightarrow 2 Al Cl_3 + 1.411 \text{ KJ} \quad (2)$$

$$2 Al Cl_3 + 3 ZnO \longrightarrow Al_2O_3 + 3 Zn Cl_2 + 484,5 \text{ KJ} \quad (3)$$

_____

$$C_2Cl_6 + 2 Al + 3 ZnO \longrightarrow 3 Zn Cl_2 + Al_2O_3 + 2 C + 1.695 \text{ KJ}$$
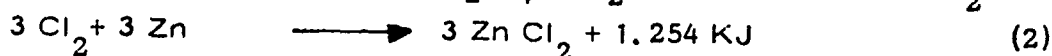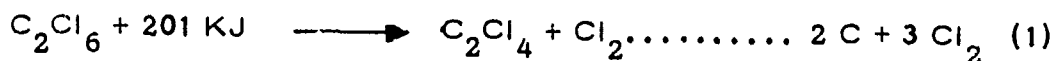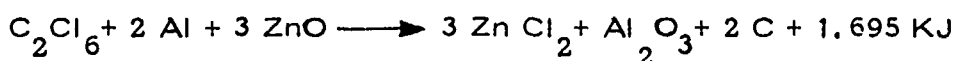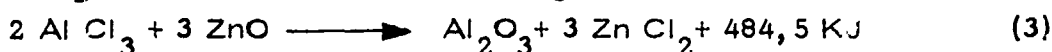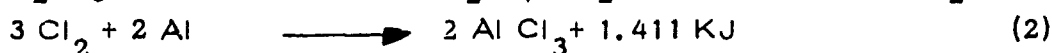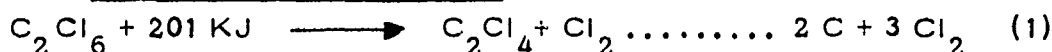
Naturally the energy balances lie higher in the case of HC smoke with Al and ZnO and Zn than for HC smoke with Al and ZnO.

Upon examination the aluminum was almost always quantatively reclaimed in the smoke residue.

<u>Neutralized (non-toxic) HC Smoke with Zn, ZnO and Guanidine Nitrate :</u>

The following reaction mechanism can be deduced :

I. $\quad C_2Cl_6 + 201 \text{ KJ} \longrightarrow C_2Cl_4 + Cl_2 \ldots\ldots\ldots 2 C + 3 Cl_2 \quad (1)$

$\quad 3 Zn + 2 HNO_3 + 2C \longrightarrow 3 ZnO + H_2O + N_2O + CO + C + 988 \text{ KJ} \quad (2)$
$\qquad$ (from guanidine nitrate)

$\quad 3 ZnO + CO + C \longrightarrow 3 Zn + 2 CO_2 - 370,5 \text{ KJ} \quad (3)$

$\quad 3 Zn + 3 Cl_2 \longrightarrow 3 Zn Cl_2 + 1247 \text{ KJ} \quad (4)$

_____

$\quad C_2Cl_6 + 3 Zn + 2 HNO_3 \longrightarrow 3 ZnCl_2 + 2 CO_2 + N_2O + H_2O + 1664 \text{ KJ}$

II. $\quad 3 Zn Cl_2 + 3 H_2O \longrightarrow 3 ZnO + 6 H Cl \quad (1)$

$\quad 6 H Cl + 4 H_2O + 2 NHC(NH_2)_2 \longrightarrow 6 NH_4Cl + 2 CO_2 \quad (2)$
$\qquad$ (from guanidine nitrate)

_____

$\quad 3 ZnCl_2 + 7H_2O + 2 NHC(NH_2)_2 \longrightarrow 6 NH_4Cl + 3 ZnO + 2 CO_2$
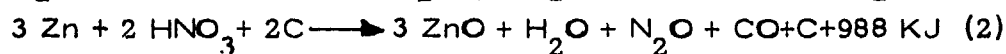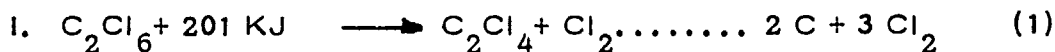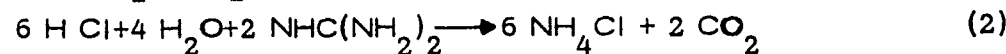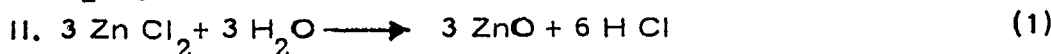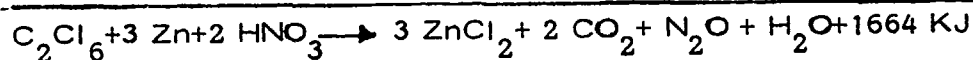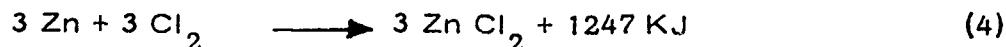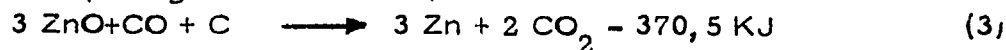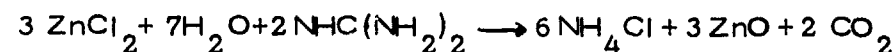
When the tree energy balances

1. HC Smoke with zinc : 1o53 KJ
2. HC Smoke with Al and ZnO : 1695 KJ
3. neutralized (non-toxic) HC smoke with Zn
   ZnO and guanidine nitrate : 1664 KJ

are compared with one another, it can be seen
that smoke systems 2 and 3 have almost the same
caloric values while reaction mixture 1 lies con-
siderable below.

Since the addition of aluminum to neutralized HC-
composition with guanidine nitrate is ineffective and
since aluminum remains in the residue (as sub-
sequently explained), it must be assumed that a
different reaction takes place in this case than
with a normal HC composition.

The following procedure was followed to clarify
the reaction mechanism :

In order to obtain an exact idea of the reaction
chain, the residue left by the hot smoke composition
after smoke production was analyzed. It was estab-
lished that the nitrate was fully converted. The entire
amount of aluminium that had been used was found
again in the residue. As further tests showed the
largest part of the residual aluminum was in metal
form, and not as an oxide, as with conventional HC
compositions.

That verified the fact that the aluminum did not take
part in the chemical reaction. To verify this fact,
a hot smoke neutralized with guanidine was prepared
in which no aluminum was present. All other components

however, were in identical relationships. This mixture could be ignited the same way as the neutralized hot smoke with aluminum, and emitted a similar thick white smoke in the identical reaction time.

This can be explained as follows :

In the case of conventional hot smoke the energy required to initiate the chlorinating reaction of zinc oxide, is drawn from the Al. This is chlorinated during a strong exothermic reaction, and then Chlorinates the zinc oxide in due course. What happens is the chlorination of the zinc or zinc oxide by the additional reaction heat of Al through $AlCl_3$ to Al_2O_3.

Since the aluminum is present in unchanged form with the addition of guanidine to conventional hot smoke composition, and after the reaction of the smoke producing charge, the additional energy required must result from a reaction of the guanidine. The temperature at which this reaction takes place must also lie lower than the chlorination temperature of aluminum.

As already mentioned the reaction of C to CO_2 is thereby involved. It can be assumed that the oxidation of C to CO_2 results not only in direct reaction with the nitrate, but also by means of an intermediate reaction with zinc. The second possibility is certainly favored.

And so, this reaction chain with guanidine is only possible with HC compositions which also contain metallic Zn in addition to ZnO. In no way is it valid for compositions with Al, Si or Ti.

The answer lies in the fact that the chlorination
heat of zinc is located considerably lower than
that of the other metals. This means that the conversion
of guanidine can take place in the desired direction,
namely in the development of basic types of decom-
position products. On the other hand a complete
decomposition takes place with the other metals.
The reaction is indeed completed, but a neutrali-
zation of the smoke does not take place.

Table 1 : Molar Heat of Formation of Metal Chlorides

	Fp [°C]	Kp °C	Source: Ch.D.Hodgman, R Weast und S. Selby: "Handbook of Chemistry and Physics"	Source: D'Ans. Lax: "Taschenbuch für Chemiker und Physiker"
$MgCl_2$	714	1418	$- 153,2$ Kcal Mol^{-1}	$- 641,4$ KJ Mol^{-1}
$ZnCl_2$	318	721	$- 99,5$ Kcal Mol^{-1}	$- 415,7$ KJ Mol^{-1}
$AlCl_3$	sublimed at 180		$- 166,8$ Kcal Mol^{-1}	$- 705,5$ KJ Mol^{-1}
$SiCl_4$	$-69,9$	56,7	$- 149,1$ Kcal Mol^{-1}	$- 577,4$ KJ Mol^{-1}
$SnCl_4$	$-33,3$	113,9	$- 127,4$ Kcal Mol^{-1}	$- 544,9$ KJ Mol^{-1}
$TiCl_4$	$-24,3$	136,5	$-183,5$ Kcal Mol^{-1}	$- 800,0$ KJ Mol^{-1}
PCl_3	-92	74,1	$- 76,9$ Kcal Mol^{-1}	$- 339$ KJ Mol^{-1}
PCl_5	Sublimed at 159		$- 106,6$ Kcal Mol^{-1}	$- 463,2$ KJ Mol^{-1}

Table 2: Molar Heat of Formation of Metal Oxides

Source: D'Ans. Lax: "Taschenbuch für Chemiker Physiker".

	Fp [°C]	Heat of Formation
Mg O	2802	$-601,2$ KJ Mol^{-1}
Zn O	1975	$-349,0$ KJ Mol^{-1}
Al$_2$O$_3$	2045	-1.675 KJ Mol^{-1}
Si O$_2$		$-859,3$ KJ Mol^{-1}
Sn O$_2$	1930	$-580,8$ KJ Mol^{-1}
Ti O$_2$	1855	$-943,9$ KJ Mol^{-1}
P$_4$O$_{10}$	569	-3096 KJ Mol^{-1}

Thus, if guanidine nitrate is added to a hexa-chlorethane / Zn/ZnO/Al mixture, the zinc combines with the guanidine to form ZnO before the aluminum begins to react. Thereby the quantity of heat set free is sufficient to set the chlorination in motion, or to break down the hexachlorethane. The reaction temperature is considerably lower than with pure HC smoke composition. Accordingly it can be assumed that the temperature required to transform the aluminum was not reached. In this case aluminum acts only in diluted form and does not enter into the reaction.

In summary, it can be said that an acceleration of the chlorination reaction occurs with the introduction of aluminum in a conventional HC composition. In the case of a neutralized HC composition, by a preliminary oxidation reaction.

Chlorination and oxidation quite consistently provide the same amount of energy that is needed for completion of the reaction in the time required.

HC-Composition with ZnO and Guanidine without Zn :

If zinc is replaced by zinc oxide in a neutralized HC composition, neutralization by guanidine cannot be accomplished for the following reasons :

Here the carbon from C_2Cl_6 is used both for reduction of the ZnO and for reduction of the nitrate. The necessary reaction heat therefore clearly lies below that of the HC composition with metallic zinc. The required reaction temperature is accordingly not reached.

Influence of the HC Composition Reaction Rate

The reaction between metals and hexachlorethane is a time reaction. The velocity results from the molar chlorination heat of the metals used and from the use of oxides instead of pure metals.

The addition of metals with high chlorination temperatures act to accelerate the reaction speed.
The effect of aluminium additives is known. Mg, Al-Mg-alloy metal powders, titanium are also possible for this purpose besides aluminium.

At constant weight proportions the effectivity of these additives increases as follows :

Ti – Al – Al/Mg – Mg

Besides the heat of chlorination, the reaction surface that is present also has an influence on the kinetic of the smoke reaction.

In this regard parameters such as the particle size, physical appearance, topochemical properties, lattice distortions of the powder, etc, and particularly the volatility of the chloride that has been formed are decisive.

In addition to the speed of the reaction, increase in the spontaneity of smoke development is also of tactical significance in military application Besides the chemical modifications previously mentioned this spontaneity is further influenced by the constructive design of the smoke producing device.

4.2 Phosphorus smoke (RP - smoke)

Phosphorus smoke compositions are made up of

> red phosphorus
> oxygen carrier
> binding agent

When phosphorus is ignited

$$4 P + 5 O_2 \longrightarrow P_4O_{10} + 3o96 \ KJ$$

phosphorus pentoxide is formed. This compound is an extremely hygroscopic substance with a relatively low evaporation point of $564^{\circ}C$ which guarantees a fine distribution of the phosphorus in the burning process.

As mentioned earlier phosphorus pentoxide changes to phosphoric acid in the atmosphere with the admission of water. The toxicity of phosphoric acid has already been explained. Therefore, the neutralization of phosphorus smoke composition is also of significant importance.

Reaction mechanism of phosphorus smoke :

Energy from burning red P with an oxygen carrier :

$$4 \text{ P rot} \xrightarrow{\hspace{6cm}} P_4 \qquad (1)$$

$$P_4 + 5 \text{ O}_2(\text{Luft}) \longrightarrow P_4O_{10} \qquad (2)$$

$$P_4O_{10} + 2 \text{ H}_2\text{O} \longrightarrow 4 \text{ HPO}_3 \qquad (3)$$

$$2 \text{ HPO}_3 + \text{H}_2\text{O} \longrightarrow H_4P_2O_7 \qquad (4)$$

$$H_4P_2O_7 + H_2\text{O} \longrightarrow 2 \text{ H}_3\text{PO}_4 \qquad (5)$$
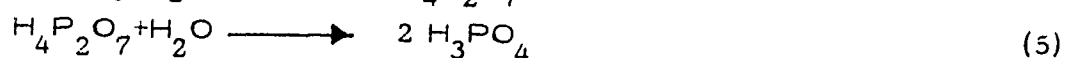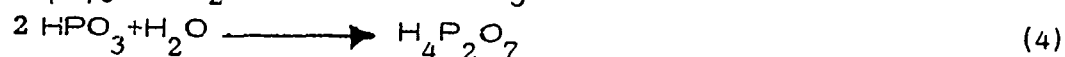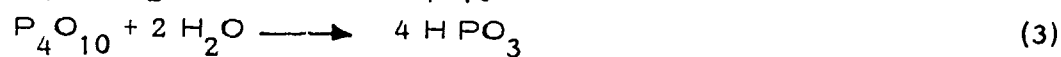
Heat released from burning phosphorus plus oxygen carrier is used to volatize excess phosphorus which had previously been added to the oxygen carrier. The excess red phosphorus is converted to white phosphorus, and with oxygen in the air burns off as P_4O_{10}.

This is further made possible because the ignition temperature of red phosphorus with air lies under its volatization temperature. Guanidine nitrate or carbamyl nitrate can also be used as oxygen carriers to burn off the red phosphorus. A transformation takes place similar to that which occurs with HC smoke where pyrolyzed basic products are formed. These neutralize the phosphoric acid produced.

Reaction mechanism of non toxic (neutral) phosphorous smoke :

$$2 \text{ P} + 2 \text{ NHC (NH}_2)_2 \cdot \text{HNO}_3 \longrightarrow P_2O_5 + 2 \text{ NHC(NH}_2)_2 + H_2O + N_2 \qquad (1)$$

$$P_2O_5 + 3 \text{ H}_2\text{O} \longrightarrow H_3\text{PO}_4 \qquad (2)$$

$$H_3\text{PO}_4 + \text{NHC (NH}_2)_2 \longrightarrow \text{NHC (NH}_2) \cdot H_3\text{PO}_4 \qquad (3)$$
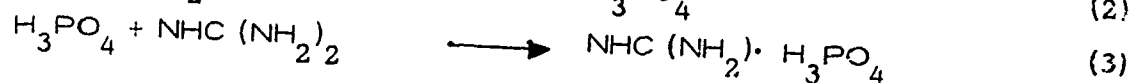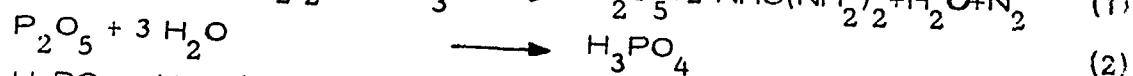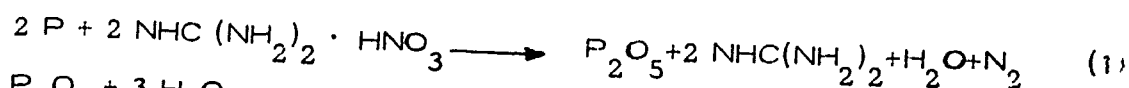
Influence of reaction velocity of RP smoke compositions

Based on the previous explanation, phosphorus can be brought to the reaction point not only by oxygen carrier admixtures (metal oxides, nitrates, amongst other) but also by halogenation agents (chlorapharaffin, hexachlorethane). The PCl_5 that builds up reacts with moisture in the air and forms P_2O_5 + HC l according to the formula.

$$2 PCl_5 + 5 H_2O \longrightarrow P_2O_5 + 1o\ HCl$$

Compared to the toxicity resulting from acids this smoke is considerable more toxic   than pure P_2O_5 smoke.

Combined oxidation and halogenatic reactions are also possible. In this situation phosphorus reacts into phosphorus pentaoxide or into phosphoric chloride. The surplus phosphorus admixture is volatilized by the energy that was released, and burned off with oxygen from the air.

The fastest reaction is obtained through stoichio-metricial mixtures (deflagration). The desired reaction speed is regulated by the addition of supplemental smoke producing substances (red phosphorus) to the stoichiometricial mixture thereby extending the reaction time and slowing it down. Beyond that, the speed of reaction is absorbable by means of organic binding agents which must be disintegrated by the heat of the reaction and thereby slow down the reaction.

5.   Manufacturing technology of such smoke mixtures

A few short statements regarding current manufacturing
processes of these type of smoke compositions yet
remain to be reviewed :

- HC smoke
  For HC smoke and neutralized HC smoke the
  components are mixed in the drying process, and
  are brought to use as a loose or shaken mixture.
  A payload pressed in block forms can also be
  inserted.

- RP smoke
  Here the components are mixed with a binder sus-
  pended in a non-inflammable solvent into a doughy
  mass. The smoke composition is then predried,
  granulated and secondarily dried. The granulation
  can be pressed into pellets or into formed shapes.

6.   Examples of application

These HC smoke compositions that have been improved
as to their toxicity and in their kinetic reaction
chain can be filled in all devices where a HC compo-
sition was used up to now.

An example is the Smoke Grenade, DM 1 HC :

      sectional picture
      picture of the smoke grenade
      smoke grenade launching system
      picture of smoke achievement

As an example of an application, a smoke grenade could be mentioned that contains pellets made of red phosphorus base. The smoke grenade is bursted in flight and the pellets dispersed after being ignited by an ignition dispersion charge. The reacting pellets already pull smoke trails while descending and cover the vehicle to be protected with smoke within a matter of seconds,

sectional picture Smoke Grenade - RP
performance pictures

FABRICATION AND UTILIZATION OF

CONSOLIDATED AL/CU$_2$O TH RMITES

PART II

Lowell D. Haws and Michael D. Kelly
Monsanto Research Corporation
Mound Facility
Miamisburg, Ohio 95342

Aaron Latkin
University of California
Lawrence Livermore Laboratory
Livermore, California   94550

INTRODUCTION

Thermite is the generic name for a class of metal/metal oxide materials that react exothermically. Thermites have been used for both a heat source and a molten metal source in many industrial applications. The most common is that of welding. Most thermites have been used in powder or granular form. The starting materials (metal and metal oxide) are pre-mixed and placed in a reaction vessel or hopper. The mixture is ignited by raising a localized portion to its ignition temperature. The reaction quickly proceeds linearly in all directions until the mixture has reacted. The reaction temperature is generally high enough to keep the reduced metal molten long enough to be useful for welding or casting.

We have been developing pressed thermite primarily as a compact and efficient heat source. The pressed material has many advantages over its granular counterpart. Some of these are:

- compactness
- machinability
- less surface area
- non-separable

These advantages make for a more useful material from the standpoint of packaging, efficiency, long life and reliability.

DEVELOPMENT AND TESTING

To be utilized as a compact heat source the pressed thermite is packaged in a metal container that also serves as (1) a heat sink, (2) a thermal conductor and (3) a reaction containment vessel. To fully utilize the pressed thermite we have expended considerable effort on a development program aimed at material characterization and practical utilization. Some of the problems and achievements will be described. The description and results of a typical test is described in Appendix A.

IGNITION

Several methods have been sucessfully used to ignite pressed thermite. The two methods that have worked most favorably are: 1) the ignition of a Pyrofuze* loop pressed into a small thermite pellet which is inserted into a cavity of the main thermite charge, and 2) the heat from the resistance and arc formation of a sharp metal electrode in contact with the thermite pellet. With these ignitors we were able to use a small portable 12 volt battery weighing under 2-pounds for reliable ignition. Two ignitor types are illustrated in Figure 1, Appendix A.

SEALING AND PRESSURE CONTAINMENT

One of the main difficulties encountered was the effect of pressure generation during the thermite reaction. As part of our material characterization effort we have obtained some pressure measurements of the thermite during and subsequent to the reaction. The limited data from a few tests indicate pressures generated in excess of 3.5 MPa (500 psi). The pressure rise was quite rapid, peaking out

* Trade name for Intermatallic Reactive Wire, Manufactured by Pyrofuze Corp.

in a few seconds, followed by a rapid decay (Figure 9). Pressure of this magnitude is certainly not difficult to contain. Sealing, however has proven to be quite a difficult problem. This was especially pronounced in assemblies having several instrumentation feed throughs. The burning thermite is quite reactive and apparently once an escape path is opened. however small, the pressurized reacting thermite vapors will often vent through the opening. Once a vent path is established the thermite will continue to erode and enlarge the opening allowing much of the thermite to escape. If, on the other hand, the escape path is long and narrow enough the escaping vapors will chill and seal the opening. Both of these events have been observed in our experiments. The escaping vapor appears to be mainly copper.

INSTURMENTATION OF TEST ASSEMBLIES

We have instrumented several thermite test assemblies to determine some of the reaction characteristics of the pressed thermite. The measurements of prime interest were temperature, pressure, and burn rate. Figure 2 shows a typical test configuration for pressure and temperature measurement.

TEMPERATURE MEASUREMENT

The temperature of major interest during a confined reaction is that of the reacting thermite or the reaction temperature. Realizing this would be quite difficult to measure without specialized instrumentation, we instead took temperature measurements in regions outside the reaction. From these measurements we were able to determine reaction temperatures by computational means. Much work was done in predicting and correlating temperatures using heat transfer computational techniques. The regions outside the reaction vessel were readily accessable for the placement of conventional thermocouples and good data was obtained.

PRESSURE MEASUREMENT

We have found pressure to be the most difficult property to measure during a thermite reaction. Two methods have been tried with some degree of success obtained for each. Our first attempt at pressure measurement was with commercial pressure transducers. Recognizing that reacting thermite would present many problems we tried several methods with varying degrees of success. In many cases the reacting thermite would either clog the tube or filter leading to the pressure transducer. At times the thermite would damage the sensing element before maximum pressure was reached. Diaphragm isolators and water cooled transducers were also tried.

The second approach was to use strain gages bonded to the external surface of the pressure container. With this indirect method we were able to correlate external strain with internal pressure. In some cases corrections would have to be made because of the effect of the heat upon the mechanical properties and of the thermal stresses induced upon the pressure container. We believe, however, that the peak pressure occurs so quickly that very little heat transfer has taken place.

BURN RATE MEASUREMENT

Two systems have been used to measure linear burn rate. The first was by direct observation of the burn using high speed photography, this method enables us to also observe the reaction process. We can see sputtering, gas evolution and obtain an objective and comparative view of the violence of the reaction. The second method employed is with fiber optics photography. With this method the reaction can be contained. We were thus able to determine whether containment affects the burn rate. In our tests with Al/Cu_2O thermite we found no significant difference in burn rates between confined and unconfined reactions. The burn for most formulations have been in the range of 4 cm/sec to 10 cm/sec.

213

UTILIZATION OF PRESSED THERMITE

The available energy of pressed thermite is quite respectable in comparison
with some other common substances considered to have a high energy content.

TNT	—	1000 cal/gm
Gasoline and Air	—	700 cal/gm Gasoline
Pressed Al/Cu$_2$O	—	530 cal/gm

Pressed thermite has many features that enhances its usefulness. It is compact,
insensitive, yet readily ignited. It is relatively inexpensive and can be
compacted to nearly full density in a number of ways and can be readily machined
by conventional methods to close tolerances.

Many useful applications can be envisioned for pressed thermite. One possible
product is that of a portable heat source, such as a cartridge heater for
emergency or remote use. One particular application might be as preheater for
diesel engines in cold weather. A cartridge containing the thermite could be
inserted into a recepticle in the engine block and ignited with the starter battery.
This could be designed to provide enough heat to enable startup in cold weather
in remote areas. Other similar applications may be possible. It is estimated
that 2 pounds of thermite will provide the energy equivalent of a 40 pound lead
storage battery.

REFERENCES

1. Chemical Heat Sources, Detonics Corporation - Final Report for Lawrence Livermore Laboratory, University of California, Livermore, California 94550 (UCRL 13601).

2. Alexander P. Hardt, Incendiary Potential of Exothermic Intermetallic Reactions AFATL - TR-71-87.

3. Thermit Welding - From AWS welding handbook, Chapter 57.

4. M. D. Jackson, Welding Methods and Metallurgy, Charles Griffin & Co. London, 1967 - Thermite Welding.

APPENDIX A

Thermite Burn Test

WHG-182 is a typical Thermite Burn Test conducted as part of our development program. Figure 2 shows a cross section of the test assembly. The part to be heated is the stainless steel cylinder forming the inner core. It is contained within a refractory metal can surrounded by pressed thermite in the form of right circular rings enclosed within a layer of rigid insulation. The outer pressure container is of 304 stainless steel. The thermocouple and ignitor leads are sealed with pressure fittings. Two identical pressure transducers were located on the bottom while all other leads came through at the top. The thermocouple locations are numerically identified.

Test Results

The thermite ignited, reacted completely and was fully contained. Data were obtained from all eight thermocouples. Of the two pressure transducers one failed to report any data. The other functioned normally. Upon disassembly it was observed that the thermite penetrated the insulation at several locations and condensed on the inner wall of the stainless steel outer pressure container. This undoubtedly accounted for some heat loss. The test parts before assembly are shown on Figure 3. Figure 4 shows the assembled unit. The pressure and temperature data is plotted in Figures 5 through 9.

BRAIDED PYROFUZE

PRESSED THERMITE PELLET

.5 CM

METAL ELECTRODE

PRESSED THERMITE PELLET

.5 CM

FIG. 1

THERMITE IGNITOR

IGNITORS

THERMOCOUPLE
LOCATIONS

STAINLESS
STEEL OUTER
CONTAINER

INSULATION
(HI TEMP)

THERMITE

REFRACTORY
METAL

STAINLESS
STEEL CORE
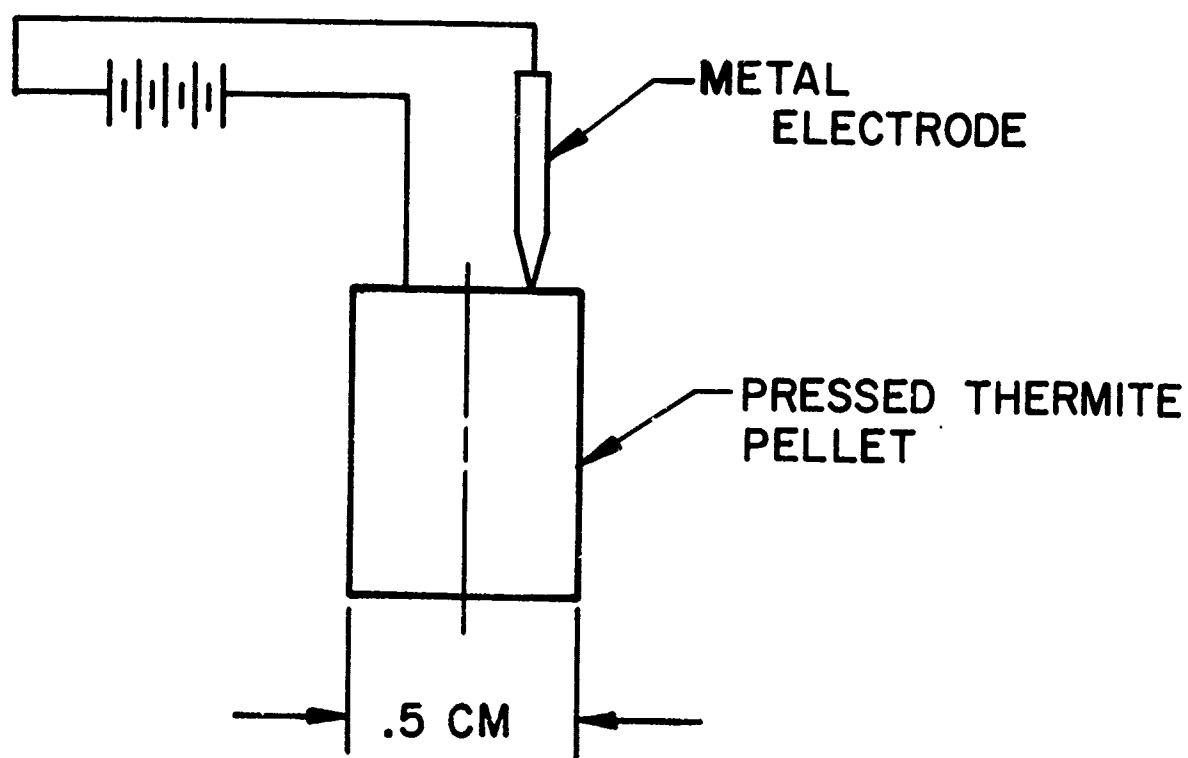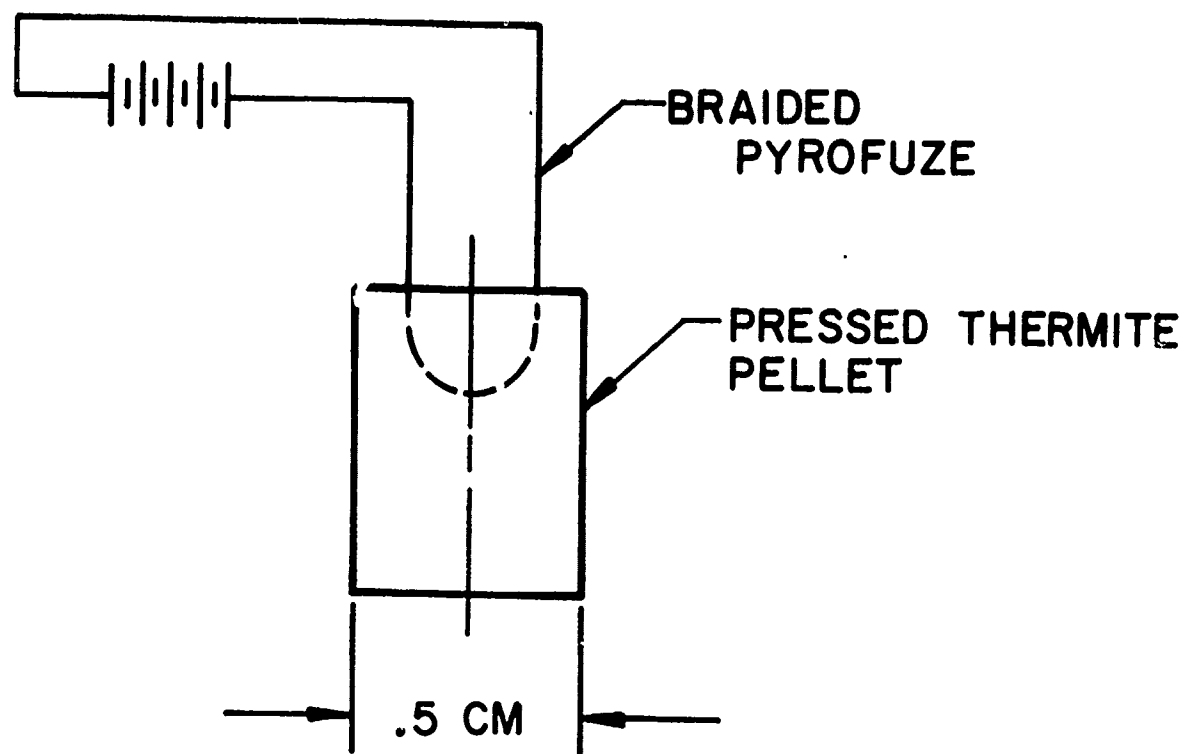
PRESSURE
TRANSDUCER
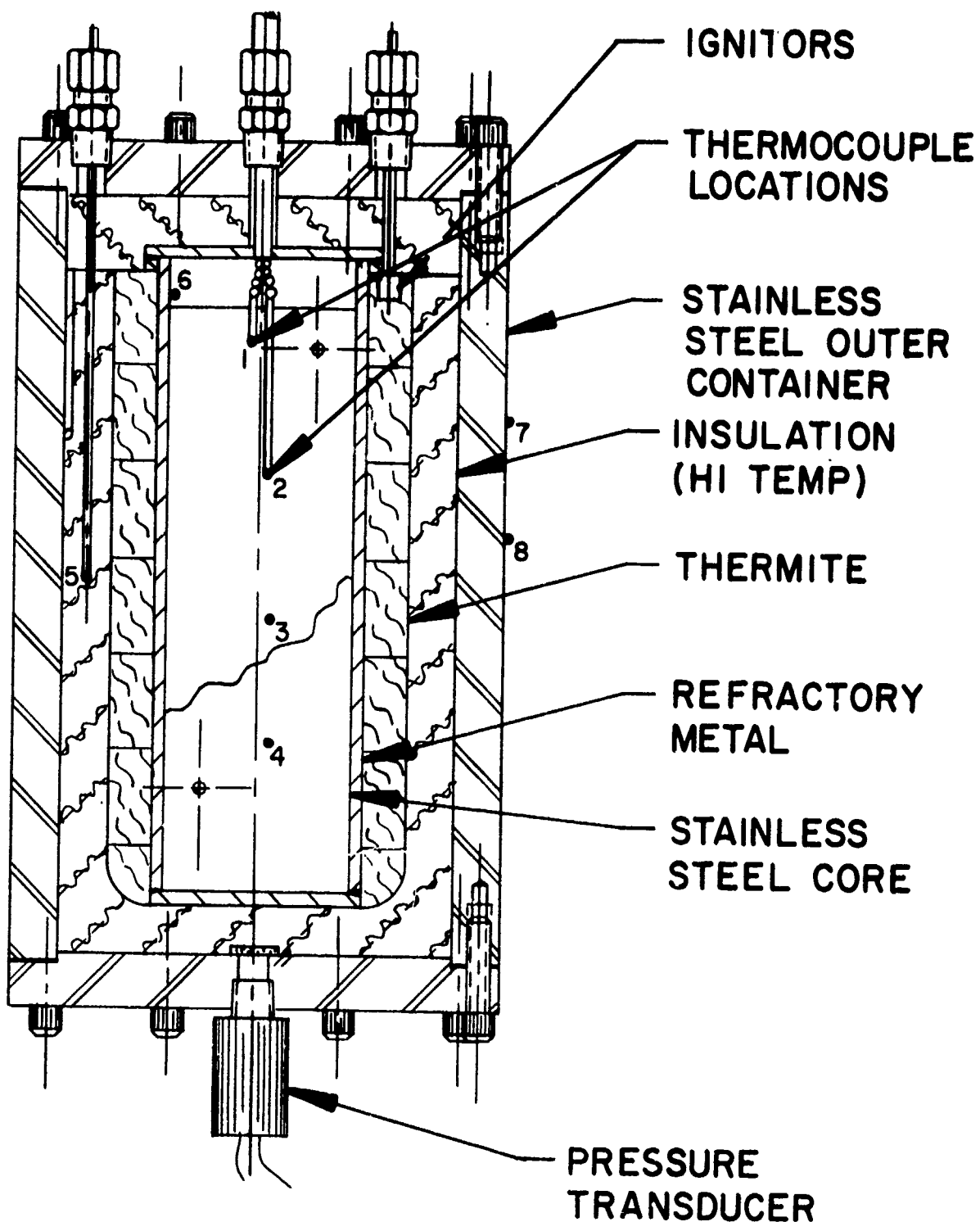
FIG. 2

THERMITE TEST ASSEMBLY
(NUMBERS INDICATE THERMOCOUPLE
LOCATIONS)
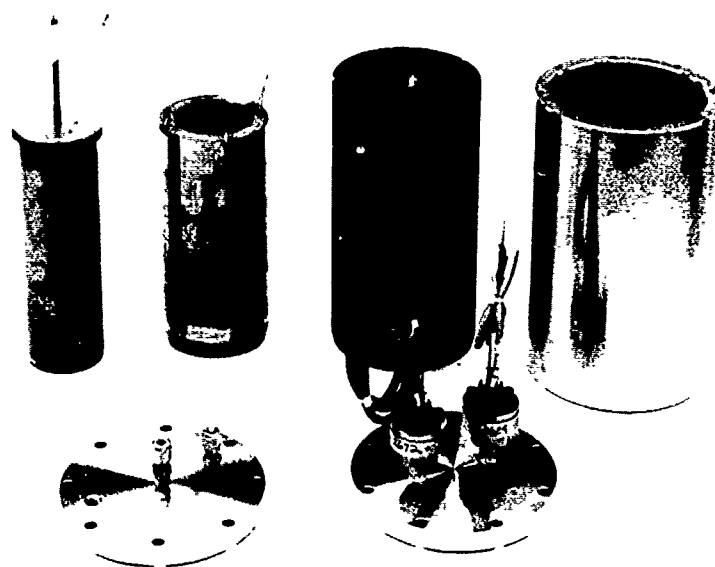
FIGURE 3 - WHG-182 BEFORE ASSEMBLY
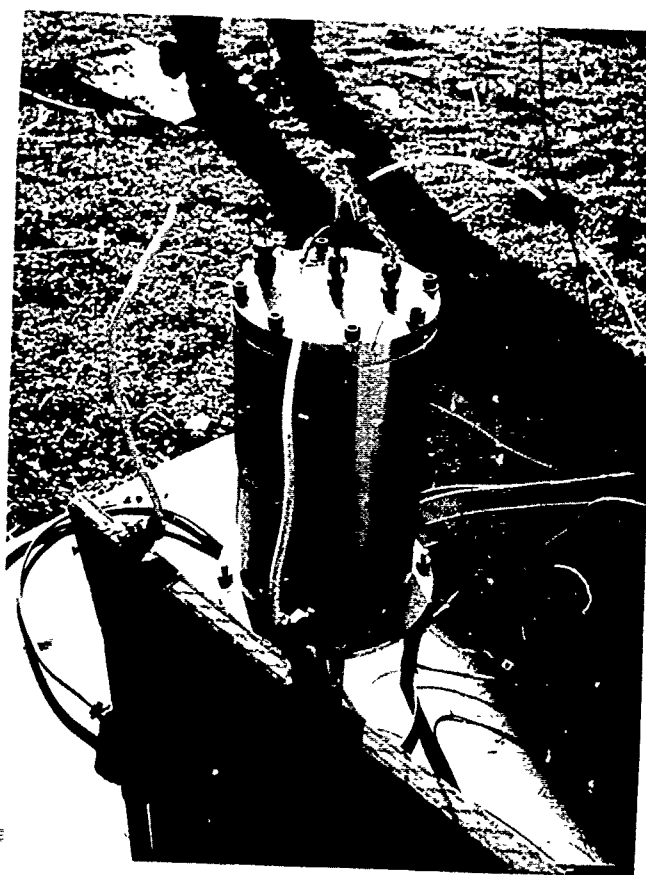
FIGURE 4 - WHG-182 TEST ASSEMBLY

FIGURE 5

FIGURE 6

220
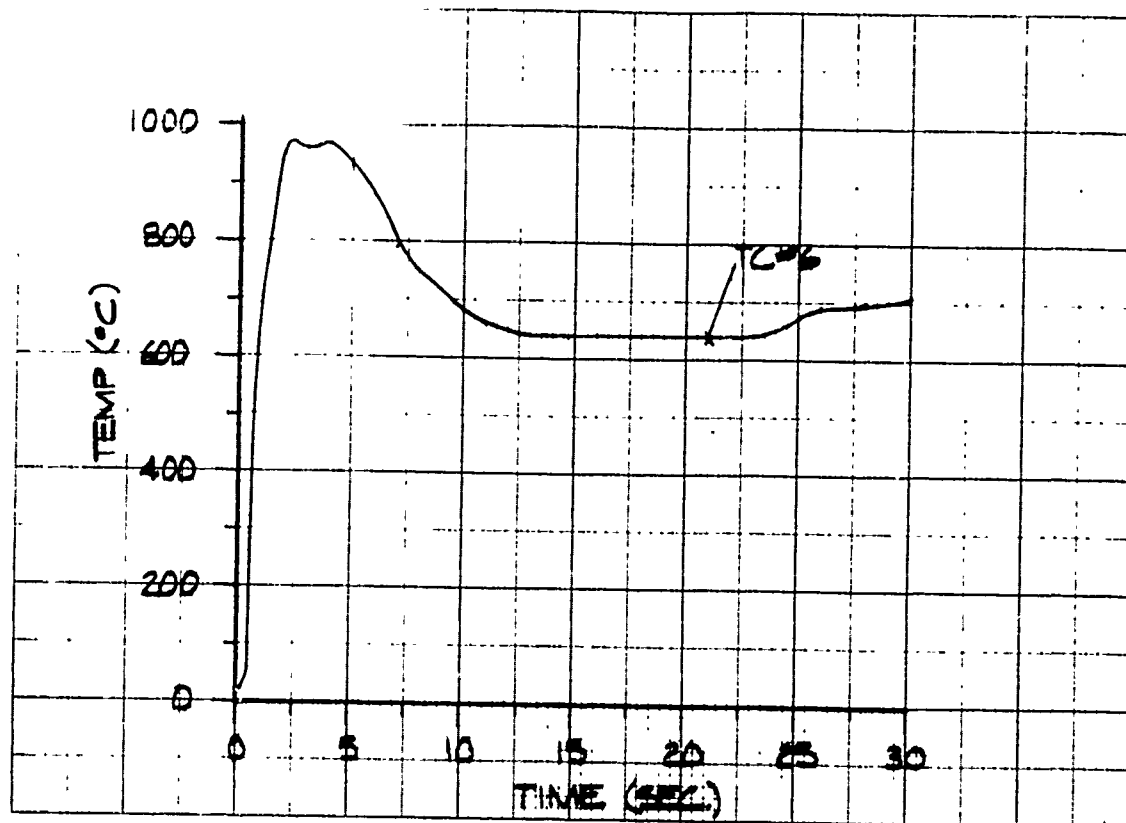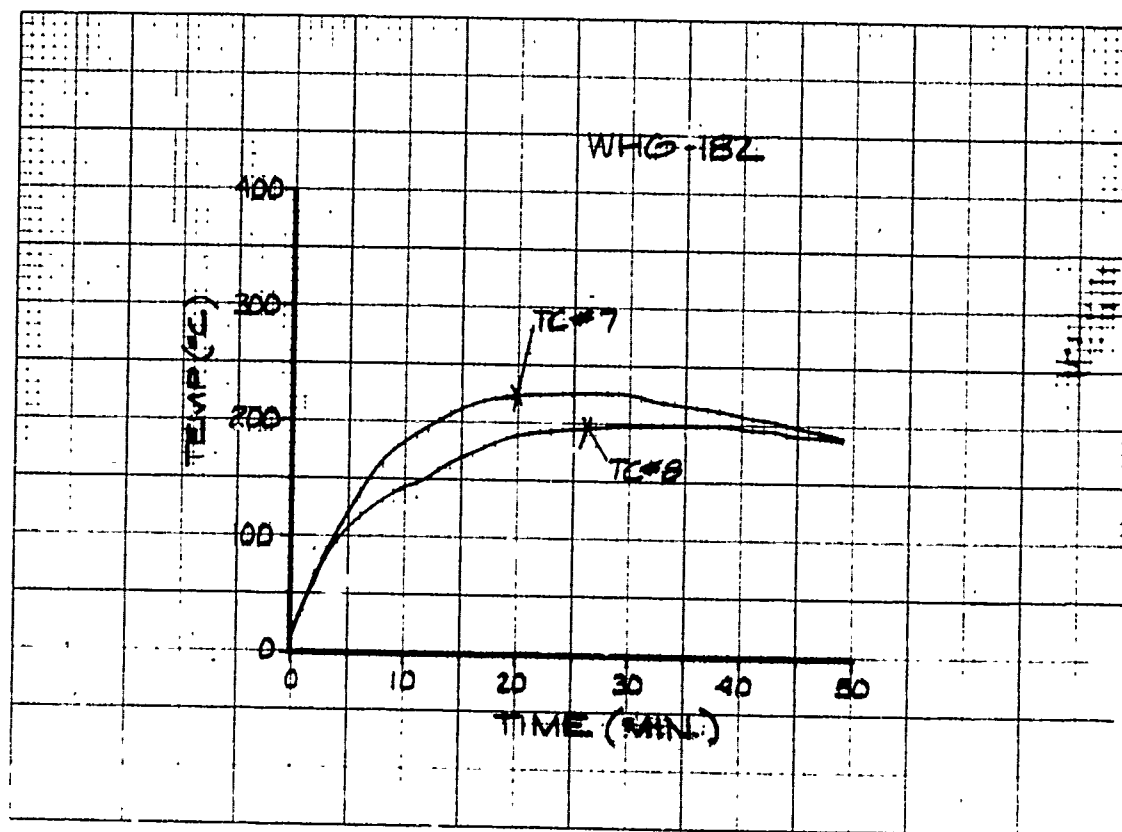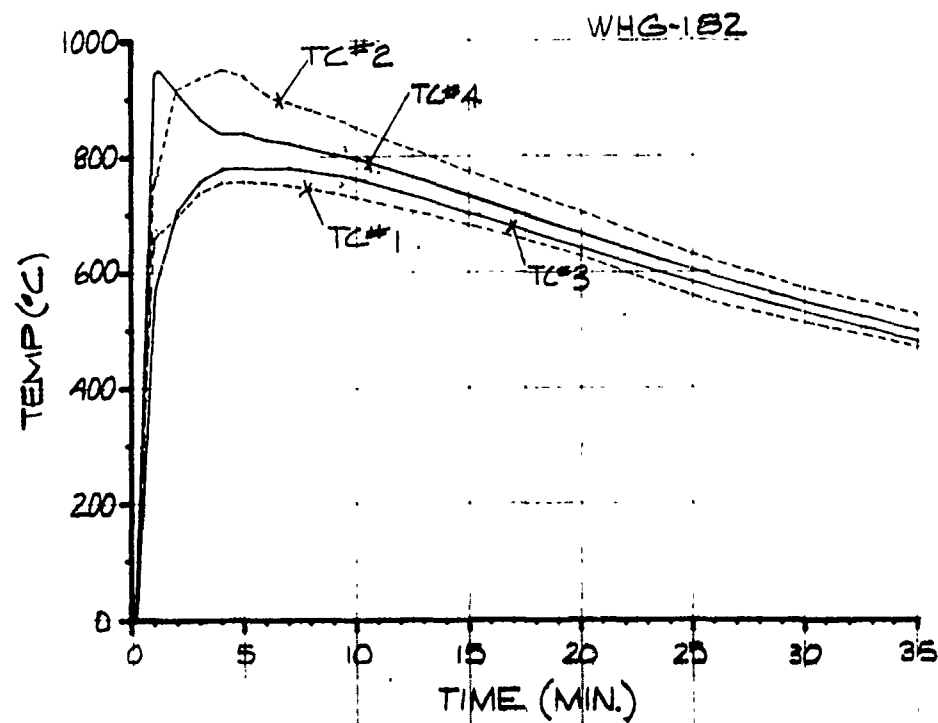
FIGURE 7

FIGURE 8

221
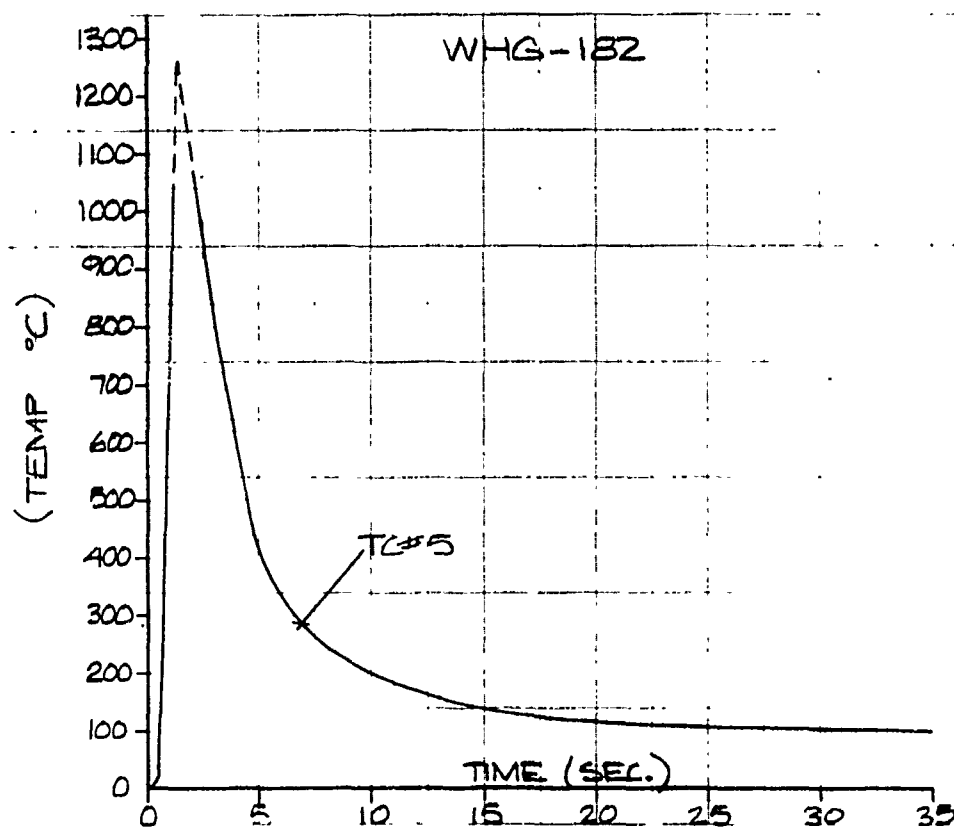
FIGURE 9

EFFECT OF FUEL STRUCTURE
ON SPARK SENSITIVITY OF 33/67 TiH_x/KClO$_4$ BLENDS*

John T. Healey and Morton L. Lieberman
Sandia Laboratories, Albuquerque, NM 87185

ABSTRACT

The development of safe pyrotechnic blends, possessing the characteristics of low electrostatic discharge sensitivity and ease of ignition by a hot wire, has prompted studies into the TiH_x/KClO$_4$ pyrotechnic system. Previous work has shown that a marked change in the spark sensitivity of the 33/67 TiH_x/KClO$_4$ pyrotechnic system occurs at a subhydride stoichiometry of approximately $TiH_{0.60}$.

This investigation was conducted to determine if any relationship exists between the microstructure of the TiH_x fuel particles and the spark sensitivity of the 33/67 blends. Nine subhydride compositions in the $TiH_{0.33}$ to $TiH_{1.32}$ range were investigated. The samples fell into three regions of the Ti-H phase diagram (three in each region). The hypoeutectoid samples displayed wide bands of α-Ti surrounding eutectoid regions. The samples in the vicinity of the eutectoid showed a characteristic fine lamellar structure, while the hypereutectoid samples showed etching of isolated eutectoid areas with the bulk of the material being the dihydride phase with islands of the lamellar structure present.

The results indicate that a relationship exists between the quantity and distribution of the α-Ti phase in the subhydride particles and spark sensitivity of the TiH_x/KClO$_4$ (33/67) pyrotechnic blends. In addition, the structure changes may also have provided an explanation of the phenomenon of dancing sparks observed by other investigators.

Introduction

Recent emphasis at Sandia Laboratories on increased safety of pyrotechnic components has led to a need to develop new safe pyrotechnic materials. Of primary interest is the production of electrostatic discharge insensitive pyrotechnic blends which possess a threshold spark ignition greater than 20 kV, which is a conservative estimate of a maximum human body electrostatic discharge. Simultaneously, this spark insensitive material must have acceptable sensitivity to ignition by a hot wire.

Fine titanium particles, blended with the potassium perchlorate oxidizing agent, are readily ignitable from a hot wire but are inherently dangerous due to the high sensitivity to electrostatic discharge. Conversely, fine titanium dihydride particles, similarly blended with potassium perchlorate, are very insensitive to electrostatic discharge and are also difficult to ignite from a hot wire. Efforts have been made to develop titanium subhydride compositions such that the resultant blends will possess acceptable values of both properties. Previous work[1] has shown that the electrostatic discharge susceptibility decreases markedly for subhydride stoichiometries greater than approximately $TiH_{0.60}$. These findings are shown in Fig. 1. The phase diagram for the titanium hydrogen system[2] shows that the entire composition range investigated falls within the α-Ti + γ-TiH_{2-y} two phase field as can be seen in Fig. 2. Therefore, the marked decrease in electrostatic discharge susceptibility does not correlate with any phase change in the subhydride. In addition, if the electrostatic discharge susceptibility were merely determined by the relative proportions of the two condensed phases, one would expect the properties to vary linearly throughout the two phase composition field, rather than sharply as has been observed. The purpose of the present study was to determine if the observed electrostatic discharge sensitivity could be explained as a function of the TiH_x particle structure.

224

Experimental Procedures

The TiH$_x$ powders were produced at Mound Laboratories using procedures developed by R. S. Carlson.[3] Each of the subhydride stoichiometries was prepared by heating a batch of the titanium dihydride powder to a preselected temperature (typically from 400° to 470°C), pumping away the evolving hydrogen to a pressure predetermined by prior calibration, then slow cooling to room temperature. To avoid spontaneous combustion of the oxide-free surfaces, the powders received a controlled, limited surface oxidation by exposure to small quantities of air prior to exposure to the atmosphere.

In all cases, the titanium dihydride powders were dehydrided at temperatures above that of the eutectoid temperature (see Fig. 2). This means that the production of the subhydride powders was accomplished by heating the γ phase into either the $\gamma+\beta$, β, or $\alpha+\beta$ phase fields, by pumping off hydrogen then cooling. The compositions of the resulting powders, given in Table I, fall into three general categories: (1) hypoeutectoid (atom ratio H/Ti = 0.33, 0.38, and 0.54); (2) in the vicinity of the eutectoid (H/Ti = 0.63, 0.65, and 0.68); and (3) hypereutectoid (H/Ti = 0.75, 1.10, and 1.32).

For the structural examination each of the subhydride powders was mounted in epoxy, ground with SiC papers, initially polished with 6.0 µm diamond, and finally polished on a vibratory polisher with 1.0 µm, 0.30 µm and 0.05 µm alumina.

Table I. Composition of the Titanium Subhydride Powders

Sample	H/Ti Ratio (atom ratio)
1	0.33
2	0.38
3	0.54
4	0.63
5	0.65
6	0.68
7	0.75
8	1.10
9	1.32

The polished samples were all etched, at room temperature for varying times, in a modification of Krolls etch given in Table II. This modified etch was developed to preferentially attack the α-Ti phase while producing little effect on the dihydride phase. The polished samples were coated with approximately 10.0 nm of Au-Pd in an argon sputtering unit to provide electrical conductivity. Examination of the polished and etched samples

Table II. Composition of Etchant Used

Component	Volume %
HF	2.0
HNO_3	3.5
H_2O_2	1.0
H_2O	93.5

was conducted with a Hitachi S-500 scanning electron microscope, as the resolution of optical microscopy was inadequate to distinguish the fine structure encountered.

Results

Figures 3 through 11 show typical structures obtained for each of the subhydrides. The lower subhydrides, $TiH_{0.33}$, $TiH_{0.38}$ and $TiH_{0.54}$, showed extensive etching in short times ($\sim$ 3 sec). These subhydrides, all of the hypoeutectoid group, show large bands or areas of etched material as well as some etching of fine lamellae in the regions between the bands. The quantity of the large etched regions decreases as the hydrogen content increases. The large etched bands are apparently regions of α-Ti, as the etch was developed to preferentially attack that phase.

The three samples in the region of the eutectoid; $TiH_{0.63}$, $TiH_{0.65}$, and $TiH_{0.68}$, all show a very fine lamellar structure. This would be a typical structure that one would expect to find occurring in the vicinity of a

eutectoid. The $TiH_{0.63}$ sample showed some etching of acicular bands as well. The orientation of the lamellae should correspond to the original Ti grain orientation present before initial hydriding.

The $TiH_{0.75}$ sample showed wide bands of unetched material surrounded by narrow etched bands. In addition, areas of the fine lamellar structure were also present. Both of the higher hydrides, $TiH_{1.10}$ and $TiH_{1.32}$, showed regions of very little etching and some areas of a spheroidal etching, possibly the result of etching small areas of the eutectoid structure out. The higher hydrides were etched for much longer time periods (~ 30 sec), as is evidenced by the etching of the epoxy mounting material surrounding the particles. Some areas showed etching of a fine lamellar structure.

Discussion

The structural changes observed in the TiH_x powders appear to correspond directly to changes in the electrostatic discharge susceptibility measured for the corresponding pyrotechnic blends. This would indicate that the TiH_x structure was the controlling factor in determining the response to an applied spark. The hypoeutectoid powders all showed large regions of the primary α-Ti phase; these are the heavily etched bands as seen in Figs. 3 through 5. In the vicinity of the eutectoid, these large bands of α-Ti disappear (see Figs. 6 through 8), which corresponds to the sharp decrease in the electrostatic discharge susceptibility. The hypereutectoid samples, as seen in Figs. 9 through 11, contained none of the regions of primary α-Ti and were correspondingly spark insensitive. The structural analysis combined with the previous electrostatic discharge studies indicates that the discharge susceptibility of the pyrotechnic blends is a function of the quantity and

distribution of the α-Ti phase present at the surface of the TiH_x fuel powders. In particular, the sharp decrease in discharge susceptibility is observed to correlate directly with the disappearance of the bands of the primary α-Ti structure and the appearance of the finer lamellar structure at the eutectoid even though the H/Ti ratio varies only slightly.

The structures observed appear to be consistent with typical equilibrium structures, indicating that the performance of the pyrotechnic blends will not vary with time due to microstructural changes in the TiH_x powders, but that these structures should remain thermodynamically stable.

Another phenomenon that is consistent with the structures observed is that of the "dancing sparks" first described by Leslie and Deitzel.[4] The dancing sparks condition was observed on certain of the subhydride composition pyrotechnic blends during electrostatic discharge sensitivity testing. This condition consisted of a series of sparks spreading over the surface of the material after the initial spark discharge. The condition lasted for several seconds usually without ignition of the blend. The compositions at which this phenomenon occurred were always close to the TiH_x eutectoid composition. The explanation of this occurrence appears to lie in the structure also. The compositions in the eutectoid region have bands of a fine lamellar structure which effectively isolates the alternating α-Ti lamellae from each other. When the initial spark is discharged, the isolated α-Ti lamellae coming to the surface burn, but the interior lamellae are separated and, with no large α-Ti regions, the reaction does not propagate throughout the particles. This creates the condition of dancing sparks as the sparks jump between the different particles with only the surface lamellae burning.

In view of the structures observed and the phenomenon of dancing sparks, two factors appear to contribute to the spark sensitivity of the pyrotechnic blends. The quantity and distribution, especially the connectivity of the α-Ti phase in the TiH_x powders, appear to be the controlling factors in determining the spark sensitivity of the pyrotechnic blends. The low hydride samples with the large primary α-Ti regions display high spark sensitivity. The hydrides in the eutectoid region do not contain these large regions, but display the characteristic of dancing sparks which may be the result of the distribution of the α-Ti phase, in particular a lack of connectivity of the α-Ti platelets. The higher hydrides lack connectivity and quantity of α-Ti and are therefore highly spark insensitive.

Conclusions

1. Variations in spark sensitivity in the $TiH_x/KClO_4$ pyrotechnic blends are due to structural changes in the TiH_x particles in particular variations of α-Ti quantity and distribution.

2. The phenomenon of "dancing sparks" which occurs around eutectoid ($\sim TiH_{0.65}$) compositions of TiH_x is consistent with a lack of connectivity of the α-Ti phase.

References

1. E. A. Kjeldgaard, "Development of a Spark Insensitive Actuator/Igniter," Sandia Report SAND76-0509, Albuquerque, NM, 1976.

2. W. M. Mueller, J. P. Blackledge and G. S. Libowitz, Metal Hydrides, Academic Press, NY, 1968, 336-383.

3. R. S. Carlson, Pyrotechnic Material Development Program Review Meeting, Jan. 18, 1977. R. K. Quinn, ed., SAND77-0471, Apr. 1977.

4. W. B. Leslie and R. W. Deitzel, Personal communication, Sandia Laboratories, Albuquerque, NM.
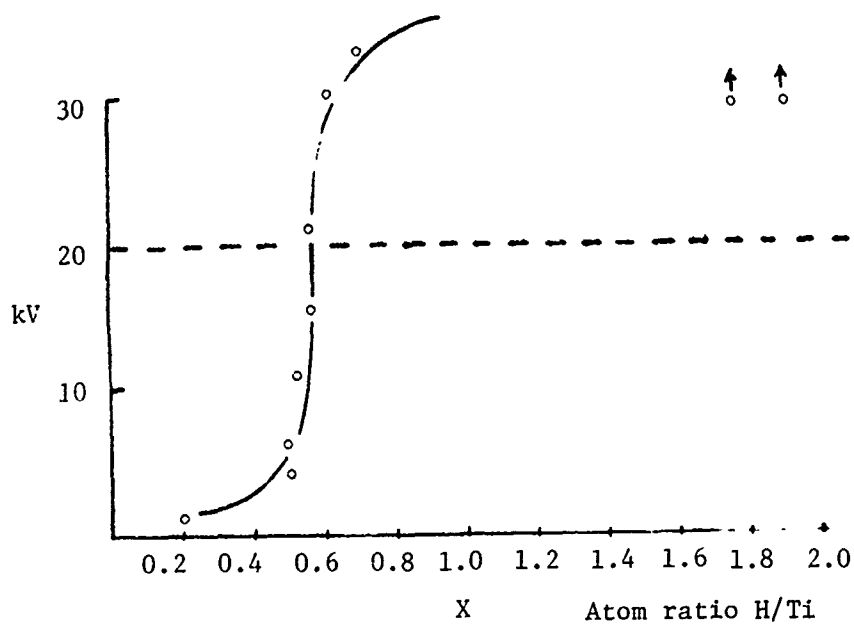
Fig. 1. Spark sensitivity threshold (10% fire criterion) of $TiH_x/KClO_4$ (33/67) bulk samples as a function of hydrogen content. (Ref. 1)
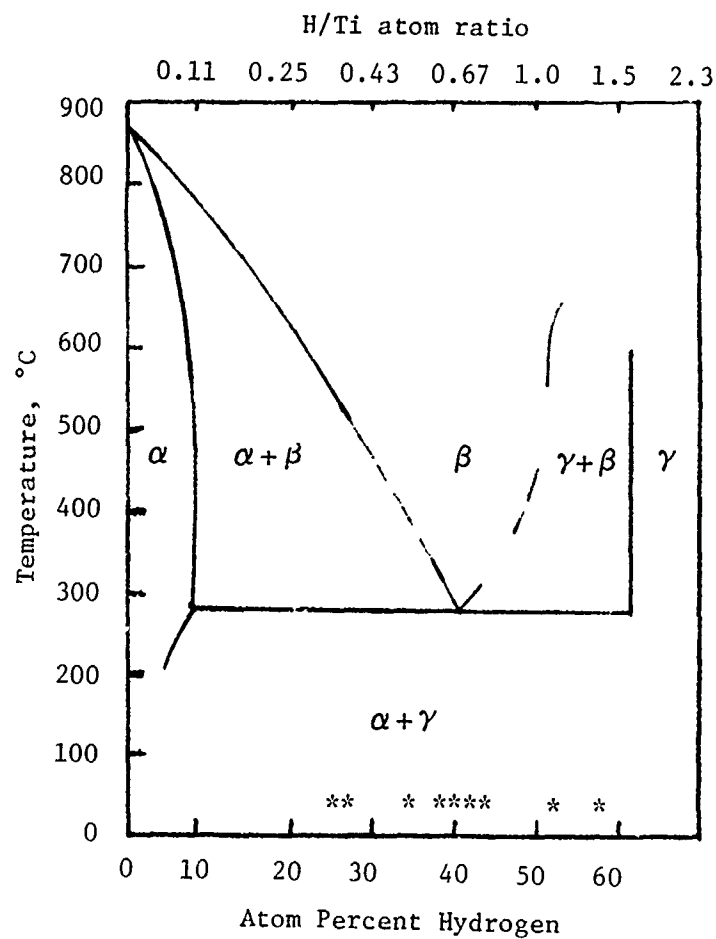
Fig. 2. The Ti-TiH_2 phase diagram. * shows stoichometry of samples examined in this study.
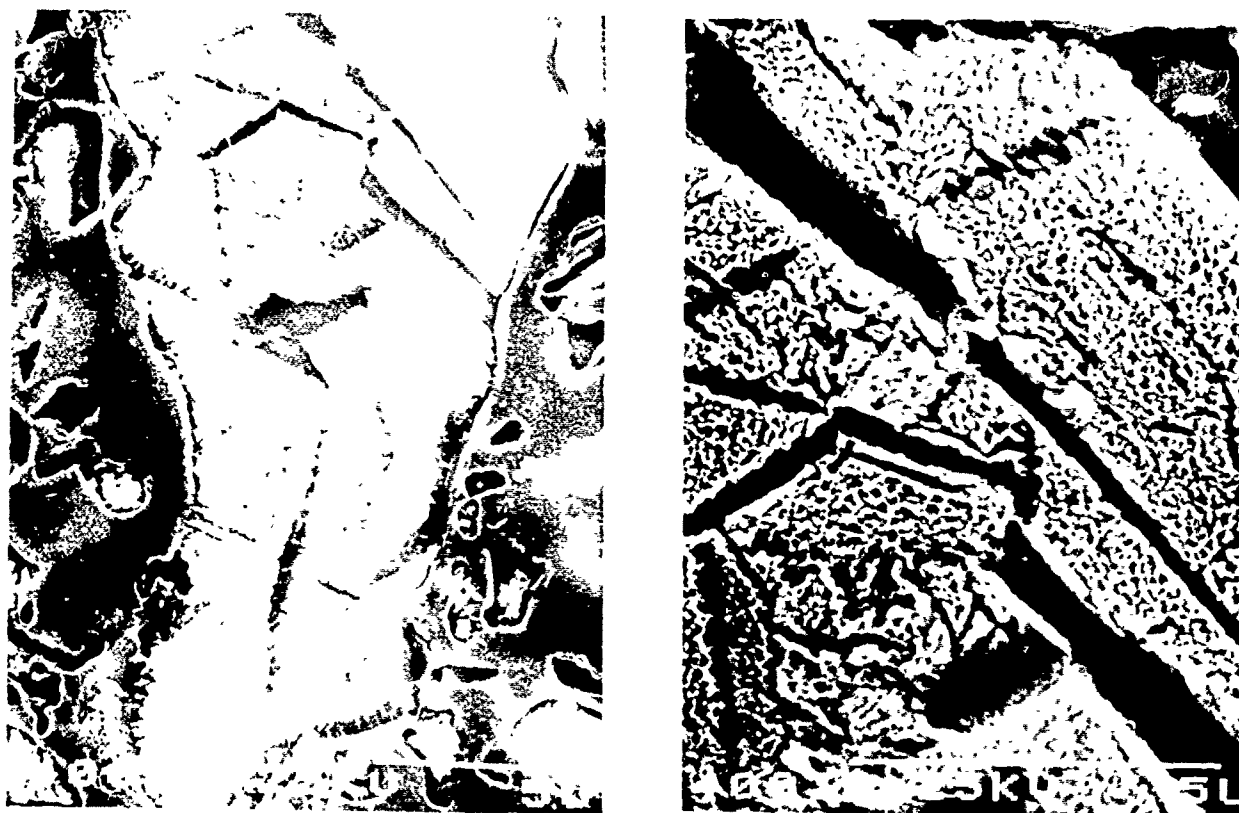
Fig. 3. TiH$_{0.33}$

Figs. 3-5. The structure of the hypoeutectoid samples
all demonstrating the wide etched regions
of α Ti surrounding fine lamellar regions
of the eutectoid.

Fig. 4. TiH$_{0.38}$
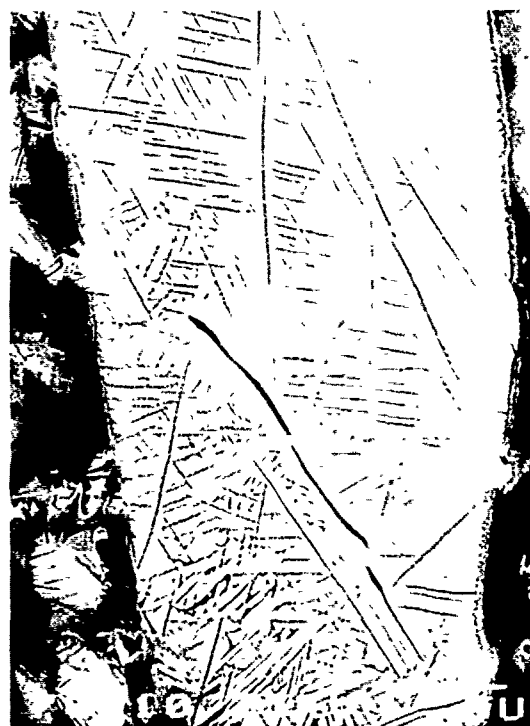
Fig. 5. TiH$_{0.54}$
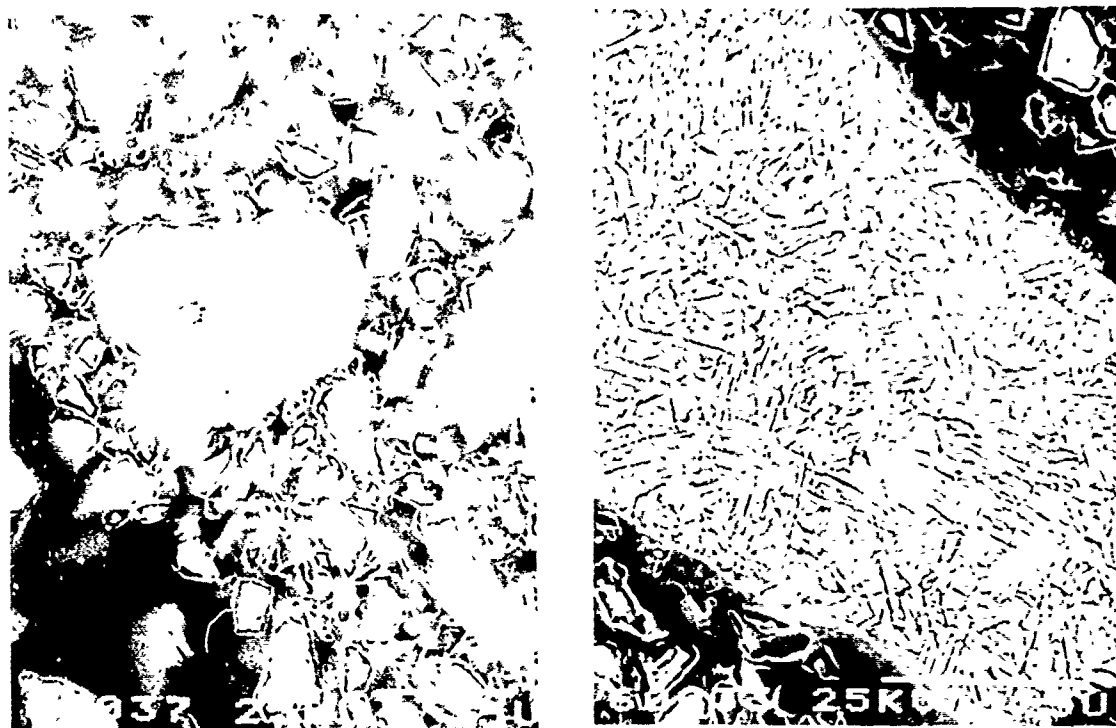
Fig. 6. $TiH_{0.63}$

Figs. 6-8. The structure of the TiH_x particles in the vicinity of the eutectoid. All samples demonstrate the fine lamellar structure present in this region.

Fig. 7. $TiH_{0.65}$

Fig. 8. $TiH_{0.68}$

235
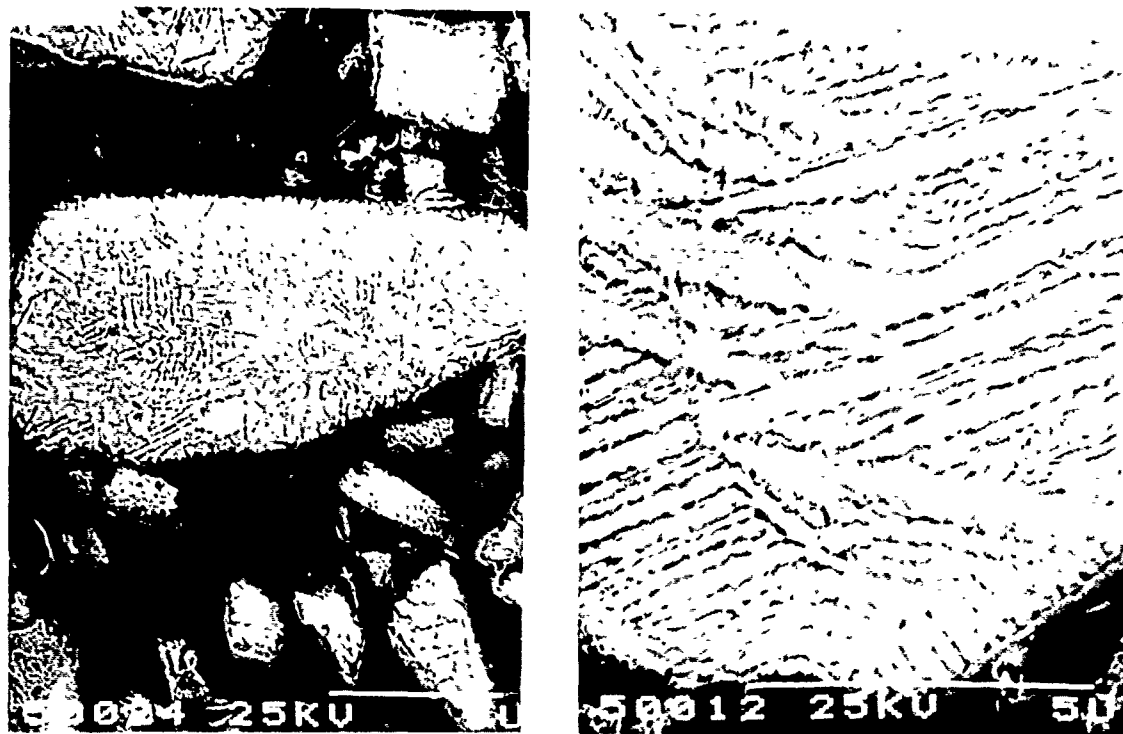
Fig. 9. Till$_{0.75}$

Figs. 9-11. The structures of the hypereutectoid samples. All samples show regions of no etching, areas of lamellar structure and regions of spheroidal etching (possibly the etching out of eutectoid lamellar areas).

Fig. 10. $\overline{\text{Ti}}H_{1.10}$

Fig. 11. $\text{TiH}_{1.32}$

237

SAND 78-0275

Through-Bulkhead-Initiator Development[*]

by

Albert A. Heckes

Initiating and Pyrotechnic Components Division

Sandia Laboratories

Albuquerque, New Mexico

For Presentation at

the

Sixth International Pyrotechnic Seminar

July 17-21, 1978

Estes Park, Colorado

University of Denver

Denver Research Institute

University Park, Colorado 80210

SAND 78-0275

Through-Bulkhead-Initiator Development

ABSTRACT

A reliable pyrotechnic to pyrotechnic Through-Bulkhead-Initiator (TBI) has been developed. The initiator is based on the device described in a feasibility report by E. A. Kjeldgaard, et. al., at the Fourth Pyrotechnic Seminar, July, 1974, Steamboat Springs, Colorado.

Significant design problems which were solved in the development of the TBI were:

1. Reliable ignition of the Pd/Al donor charge across a gap through the use of the intermetallic pyrotechnic Ti/B and an expulsion charge of $TiH_x/KClO_4$.

2. Control of the temperature of the donor charge by limiting the percentage of Al in a Pd/Al or Pd/Al Stainless Steel mixture to a range of 4 to 6.3 weight percent.

3. Control of slumping of the donor charge by the addition of up to 30 weight percent SS particles to the Pd/Al reactive mixture. This provided reliable heat transfer because thermal contact was maintained.

4. Improvement of the temperature-time profile by
    changing the L/D ratio from 2.0 to 1.0, elimina-
    tion of insulators and doubling the mass of the
    donor charge to about 6 grams.

Experimental and theoretical results will be presented
to illustrate the initiator development.

Through-Bulkhead-Initiator Development

I. Introduction

This paper describes the completed version of the
Through-Bulkhead-Initiator (TBI). A significant amount of
development work has been done to improve the functional
reliability since the first reports which were issued in
1974. The feasibility of the TBI was first reported by
its inventors, E. A. Kjeldgaard and D. J. Gould at the
Eighth Symposium of Explosives and Pyrotechnics[1]. A com-
bined analytical and experimental thermal analysis of the
system was presented by E. A. Kjeldgaard, D. W. Larson,
and D. J. Gould at the Fourth International Pyrotechnic
Seminar[2].

The requirements which were placed on the TBI during
development are summarized as follows:

1. Ignition through a stainless steel bulkhead of
    sufficient thickness to contain a constant pres-
    sure of several thousand psi.

2. Maintenance of bulkhead integrity after firing
    and under short-term conditions of high tempera-
    ture and pressure.

3. Ignition of a material with high thermal conduc-
    tivity and a high ignition temperature.

The requirements were met by utilizing the principle of thin-wall, small diameter closed end tubing in a nipple configuration which allows ignition through a thick bulkhead.

The items employed in the TBI (See Figure 1) are the initiator, the donor charge, the bulkhead (or nipple), and the acceptor charge. The initiator is a hot bridge-wire ignitor which serves to initiate the donor charge reaction. The donor charge is a low-gassing pyrotechnic based on the intermetallic reaction between Pd and Al, which is commonly called the Pyrofuze* reaction. It is the heat source for initiation through the bulkhead. The nipple is of stainless steel for high temperature strength properties. The acceptor charge which is contained in the nipple accepts the donor charge output and initiates the bulk charge. Any number of pyrotechnic materials may be used as the acceptor charge. Palladium/aluminum (Pd/Al) was used in the development work because it is a difficult to ignite pyrotechnic due to a high (600+°C) ignition temperature and a high thermal conductivity.

The problems encountered during development were primarily ones of reliability and not of the basic concept. As is often the case, the interfaces between the various

_____

*Pyrofuze is a trade-mark of the Sigmund Cohn Corp., Mt. Vernon, NY.
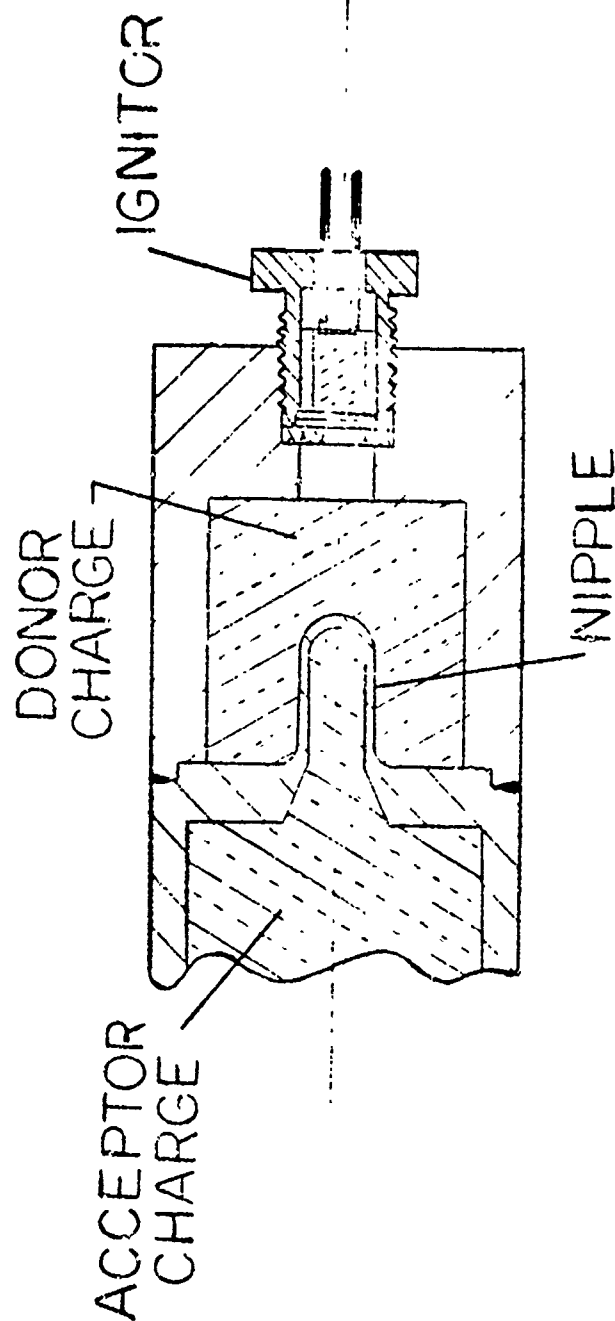
Figure 1.   Cross-Sectional Schematic of the Through-
Bulkhead-Initiator using Welded Construction
and a Pre-Pressed Donor Charge.

components in the assembly required special attention. The initiator-donor interface and the donor-nipple interface presented special challenges and are discussed further. A minor problem also developed with ignition transfer at the acceptor-main charge interface. It was quickly learned that the cause of the ignition transfer failure was a large density discontinuity at that point. It was corrected by changing the loading and pressing procedures.

II. Discussion

Initiator Development

Experimental apparatus used for the initiator development experiments is shown in Figure 2. It features ignition across a gap, a provision for the flow of titanium/boron (Ti/2B) pyrotechnic initiating material past the closure disc and an expulsion/ignition charge of $TiH_{.65}/KClO_4$. The final initiator design (not shown here) differed only in that it had a ceramic charge holder sleeve to provide pin-to-case electrostatic spark discharge (ESD) resistance, a Kapton or Mylar disc between the Ti/2B charge and the closure disc also for ESD resistance, and a welded 0.076 mm (0.003 in.) closure disc to provide a hermetic seal.

The gap width employed in the design is about 6.3 mm (0.25 in) and is not a critical dimension. Gap test
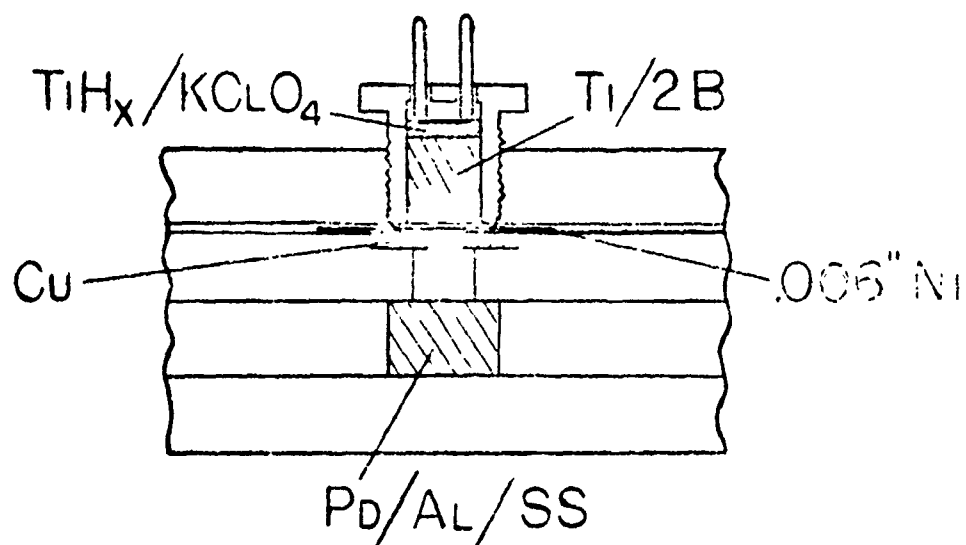
IGNITION APPARATUS

Figure 2.   Schematic of Ignition Apparatus used to
            Determine the Quantity of $TiH_x/KClO_4$
            Required to Burst Closure Disc.

experimentation showed that when a small 15 to 20 mg quantity of Ti/2B was ignited from a bridgewire so that the contained gases propel the reacting Ti/2B down a tube, in the manner of a bullet down a gun barrel, that ignition occurs regularly across a 200 mm (8 in.) gap.

An ignition problem developed when the initiator was butted up tight against the donor charge. A large force was required to set-back the donor charge and concurrently rupture the closure disc. The ignition problem was solved by using the gap data and a washer with a 4.5 mm (0.176 in.) center hole as a cutting die to shear out a section of the closure disc. The sheared disc had one-half as much area as the fire hole (ID = 6.3 mm (0.25 in.)) so that a portion of the Ti/2B could flow past the disc and contact the donor charge surface.

The washer was made of copper so it could also perform the second function of providing an igniter sealing surface. This seal has been shown[3] capable of providing leak rates $< 10^{-8}$ cc He @ STP per sec. and 1 atmosphere of pressure differential and of standing off short term pressures of 200 M Pascal (30,000 psi).

A 10 mg $TiH_{.65}/KClO_4$ first pressing charge is used against the bridgewire. It acts as the bursting charge as well as the initiating charge. The Ti/2B pyrotechnic does not form enough gas at low temperature ($-54°C$ ($-65°F$))

starting conditions to reliably burst the closure disc.
Although improved pressure performance may be achieved by
adding hydrogen to the Ti/2B in the form of TiH_x or TiH_2
(because all commercial Ti contains some hydrogen) it is
also known that pure TiH_2 will not react in a self-sustaining
manner with B despite favorable thermodynamics.[4] The reason
for selecting $TiH_x/KClO_4$ is that it is a Sandia qualified
material that is compatible with Ti/2B.

The quantity of Ti/2B used in the ignitor is enough
to fill the cavity at loading pressures near 15,000 psi.
This gives a loading of approximately 70 mg. Experiments
to determine the minimum required quantity of this pyro-
technic have not been performed because the gap experi-
ments indicate that many times the minimum quantity are
probably employed.

<center>Donor Charge Development</center>

A cross section of the donor-nipple interface is shown
in Figure 3. The temperature conditions within the TBI a
short time after ignition are indicated, where T_h is the
bulk temperature of the donor, T_o is the nipple wall
outside temperature, T_i is the nipple wall inside tem-
perature and T_c is the temperature of the cold acceptor
material. The thickness of the bulkhead is given by
$\Delta x = x_2 - x_1$.

<center>247</center>
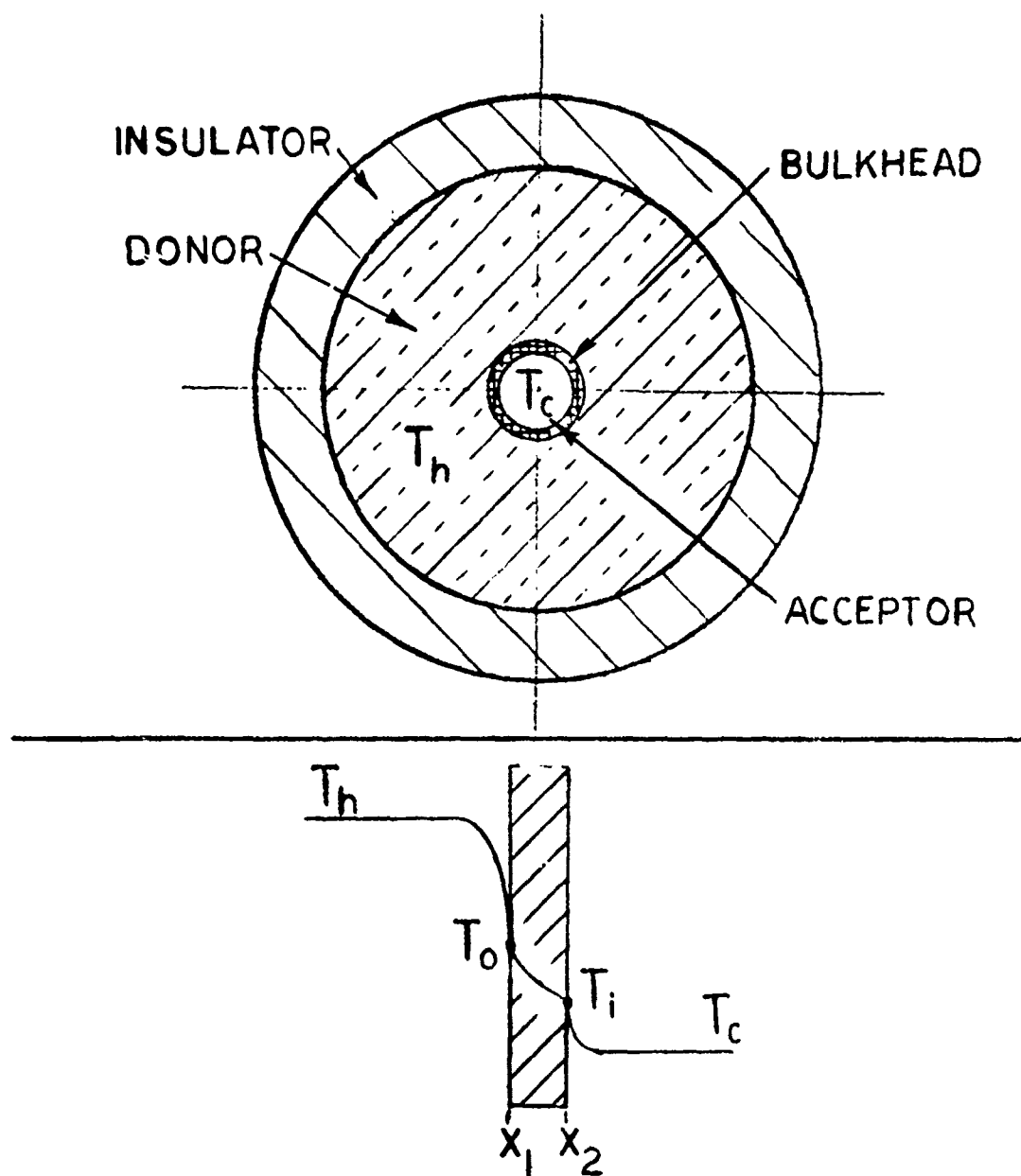
At film: $\qquad q = h A \, \triangle T_1$

Thru bulkhead: $\qquad q = k A_m \dfrac{\triangle T_2}{\triangle x}$

Figure 3.   Through-Bulkhead-Initiator Cross-Sectional View
and Temperature Profile Near the Bulkhead Nipple.

248

The major resistances to heat transfer are represented by steep temperature gradients in the temperature versus distance diagram shown in the bottom half of Figure 3. They occur at the donor-nipple interface, through the nipple and again at the nipple acceptor interface. The resistances at the powder to metal surfaces are commonly termed film resistances because despite relatively good mechanical contact of the pressed powder against the metal surface a good thermal contact is not achieved and large temperature drops are observed in very small changes in distance as the metal surface is approached from the powder side.

The heat transfer equations that apply are:

Eq. 1 $\qquad q = h_1 A_1\ \Delta T_1 \qquad$ for the donor charge

Eq. 2 $\qquad q = k\ A_m\ \dfrac{\Delta T_2}{\Delta x} \qquad$ for the nipple

Eq. 3 $\qquad q = h_2 A_2\ \Delta T_3 \qquad$ for the acceptor charge

where

$\qquad q$ is the rate of heat transfer (all q's are equal for steady state heat transfer),

$\qquad h_1$ and h_2 are film coefficients of heat transfer,

$\qquad k$ is the thermal conductivity of the nipple,

$\qquad A_1$, A_m and A_2 are outer surface areas, mean heat transfer area and inner surface areas respectively,

Δx is the nipple thickness,

ΔT_1, ΔT_2, and ΔT_3 are the temperature differences,
$T_h - T_o$, $T_o - T_1$, and $T_1 - T_c$ respectively.

To be able to maximize the rate of heat transfer, one may increase the overall ΔT (or $T_h - T_c$), improve h_1 and h_2 the film transfer coefficients, improve k the thermal conductivity, increase A the area for heat transfer or decrease Δx the nipple thickness. A limit exists on the maximum ΔT that may be tolerated, however. It is imposed by the fact that T_o may be raised to the melting temperature of the nipple to cause material loss or by the fact that the final equilibrium temperature of the whole assembly is sufficiently high that the strength properties of the nipple are reduced so that failure results. The nipple is made of stainless steel for its high temperature strength properties and because it is cheap to fabricate. This gives a poor thermal conductivity but one that can be tolerated. Extended surfaces would improve the surface area for heat transfer, which lead to the present nipple configuration instead of the flat bulkhead. Difficulty in machining would be encountered to make more elaborate shapes. The nipple thickness has been minimized so that it is about 1 mm (0.020 in.) thick. This leaves the film coefficients, h_1 and h_2 as the items which can produce

the greatest payoff in terms of heat transfer if they can be improved or at least be made repeatable from one experiment to the next.

Some ignition transfer failures were observed. To study the problem a reusable TBI test fixture was prepared as shown in Figure 4. The parts slipped together with the use of o-rings. An external clamp held the parts together during firing. A thermocouple was brazed with high temperature silver solder into the nipple so that temperature versus time traces could be made.

Post-mortem examination of the TBI hardware indicated that when the 94/6 weight percent Pd/Al donor charge reacted it partially melted. Gases given off during reaction sometimes physically moved the donor away from the nipple or alternatively the shrinkage which occurred upon melting of the donor charge caused the donor to be pulled from the nipple. Either of these phenomena (called slumping) would cause thermal contact to be lost and effectively produce low or near zero film heat transfer coefficients.

A set of matrix experiments were prepared in an attempt to eliminate the slumping phenomena. The results of these experiments led to the qualitative graph show in Figure 5 where a ternary diagram is illustrated in two dimensions. In the matrix experiment binary mixtures of Pd/Al were prepared. These mixtures were substoichiometric with respect
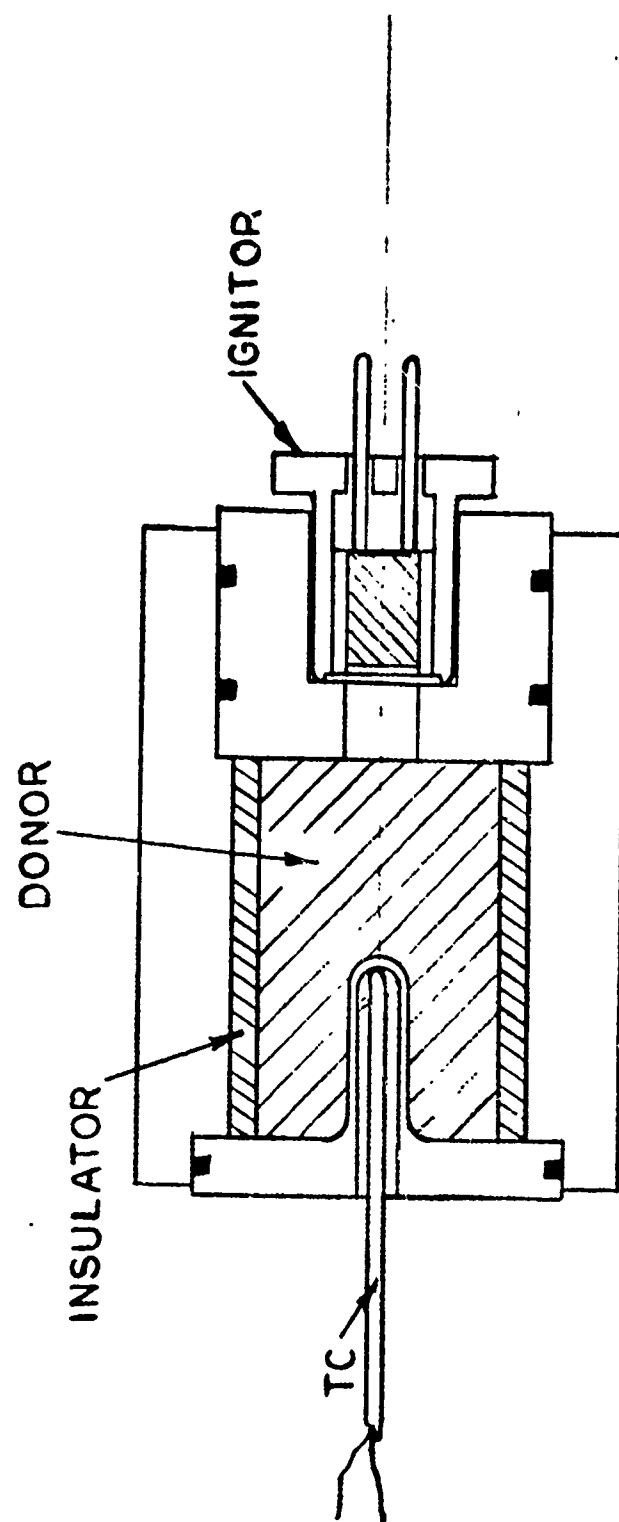
TBI TEST FIXTURE

Figure 4.   Reusable Through-Bulkhead-Initiator Test
             Fixture with Insulating Sleeve and Thermocouple.
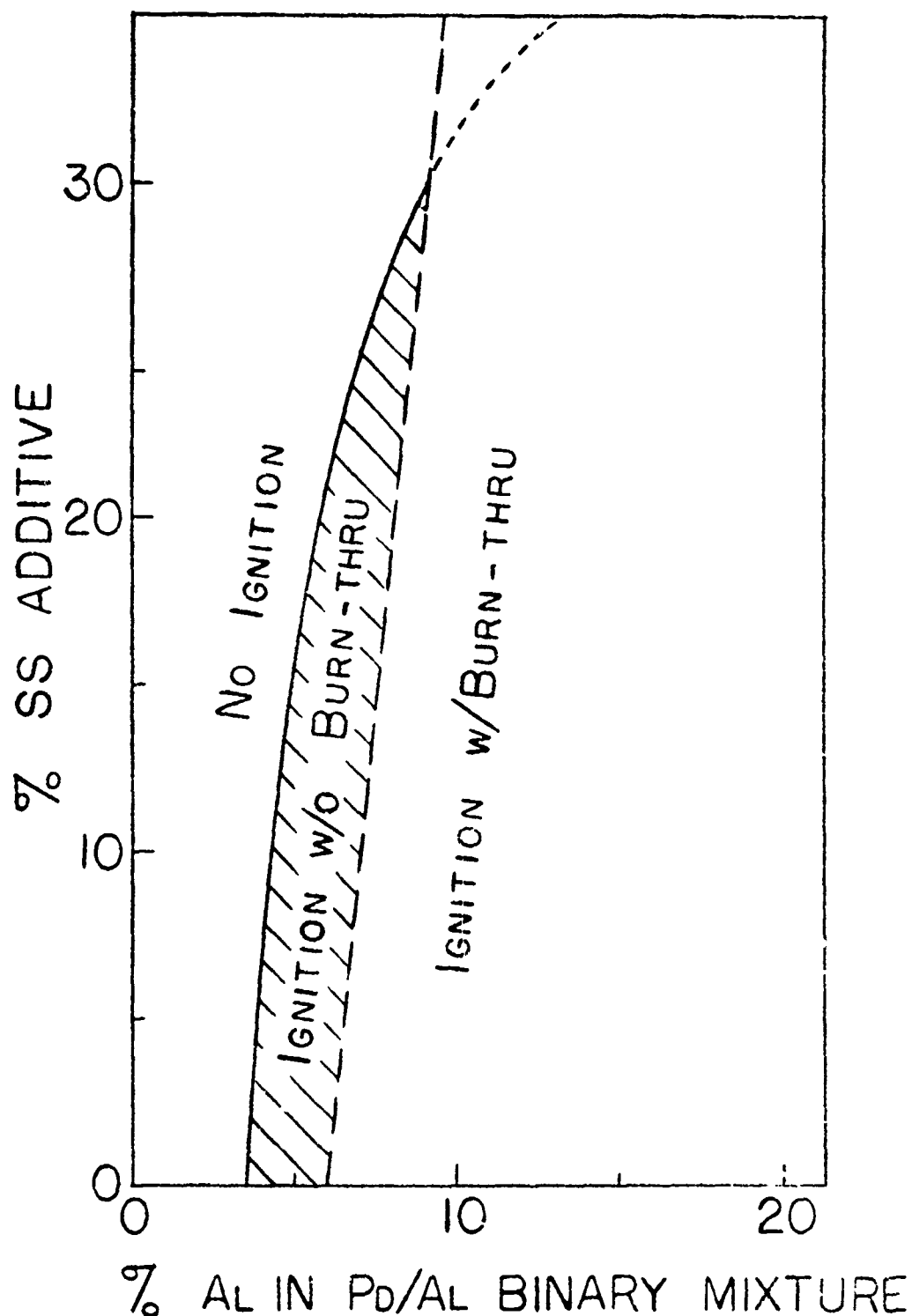
Figure 5. Graphical Representation of the Results of a Matrix Experiment to Eliminate Slumping of the Donor Charge and thereby Improve Heat Transfer. Stainless Steel Powder was added to Pd/Al to form the Pd/Al/SS Ternary System.

253

to Al so that an increase in the Al content increases the heat of reaction per unit mass of the mixture in a directly proportional manner. Given quantities of stainless steel particles were added to the binary mixtures so that the final ternary mix contained a known quantity of stainless steel (up to 30% as shown in the graph).

The graph shows that below 3.5% Al the binary mixture fails to ignite. Above 6% Al the binary mixture tends to burn through the nipple. With the addition of stainless steel relatively larger portions of Al are required for ignition and for burn-through until at 91/9 Pd/Al plus 30% SS (63.7% Pd/6.3% Al/30% SS), a practical limit for each was reached.

The experimentation also showed that a straight line could be drawn connecting the 96/4 Pd/Al point of the binary mixture with the 91/9 Pd/Al plus 30% SS point and this would define mixtures which would show no significant slumping during firing even when forces were applied during the reaction which were equivalent to gravitational fields of 200 g's or greater. Use of these mixtures caused generation of consistent temperature-time profiles, which had a variability of approximately 20°C from run to run, examples of which are shown in Figure 6.

The mixture most heavily loaded with SS particles shows a slower rise time and gave thermal arrest points
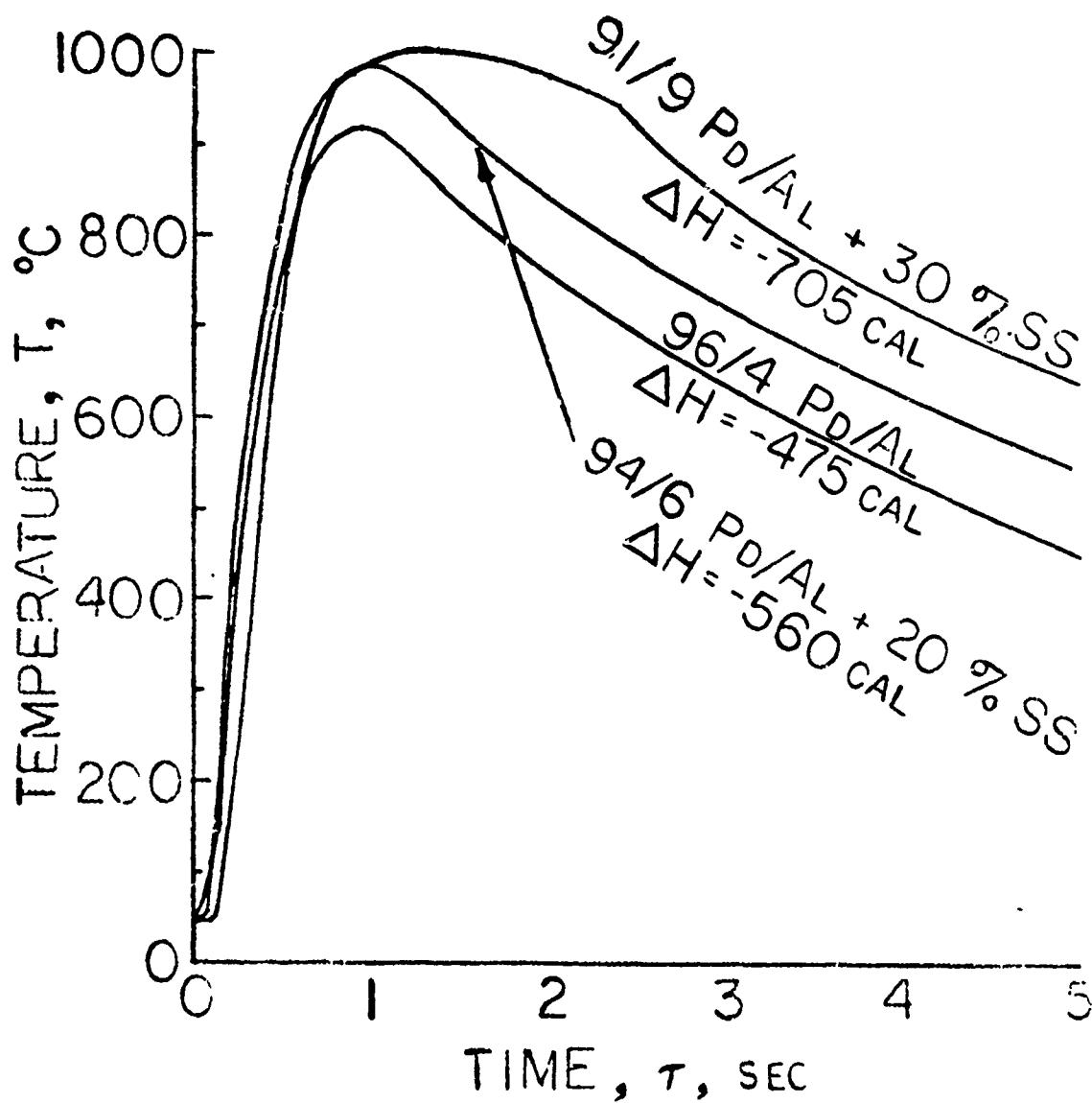
Figure 6. Typical Temperature versus Time Traces
from Experiments using Non-Slumping
Donor Charges.

near 980°C. The thermal arrests are caused by melting
and freezing of the high temperature brazing alloy used
to fasten the thermocouple in the nipple. The slower rise
time is probably caused by changes in the thermal conduc-
tivity of the donor charge and/or in its linear burning rate.
The graph shows that the quantity of energy input may be
varied to change the maximum temperature of the acceptor
charge and that the length of time at a given temperature
varies accordingly. This may have applications other than
ignition, i.e., heating or brazing, because the acceptor
appears to ignite on the temperature rise when the auto-
ignition temperature (600+°C for Pd/Al) is reached. A
high temperature soak is not required. A fast temperature
rise through the autoignition temperature is required for
reliable ignition, however. The TBI is relatively insen-
sitive to ambient temperature fluctuations because the
acceptor normally reaches temperatures several hundred
degrees above the Pd/Al autoignition temperature.

Figure 7 shows schematically how the completed device
might appear. Experimentation showed that surrounding the
donor charge with insulators had less effect on the tem-
perature rise, therefore the ignition time, than increas-
ing the mass of the donor by placing pyrotechnic in the
insulator cavity. A noticeable effect was also observed
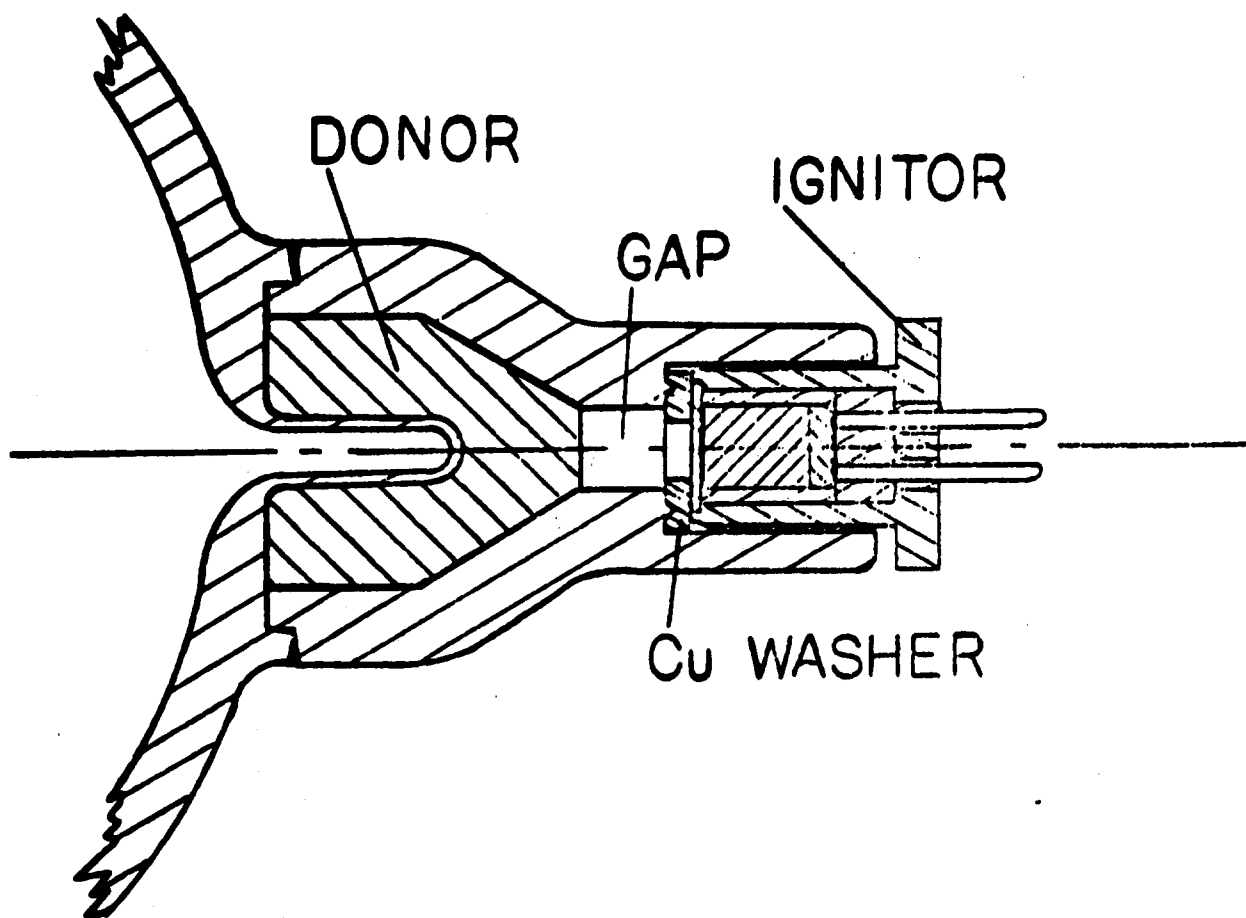
TBI PROPOSAL

Figure 7. Cross-Sectional Schematic of a Through-Bulkhead-Initiator using a Pressed-In-Place Donor Charge.

by changing the donor geometry from a L/D of about 2 to an L/D near 1 so that more mass was placed in the annular space around the nipple. The mass of the donor was 5.7 g and its density averaged 5.0 g/cc. The nipple lengths were 6.3 mm (0.25 in.) and 3.96 mm (0.156 in.) OD with a 2.95 mm (0.116 in.) ID. The donor charge length and diameters were approximately 12 mm (0.47 in.) each for a right circular cylinder. The corners of the donor charge may be removed to assist with pressing-in-place. A pre-pressed pellet may also be employed but special techniques which have been developed must be used during welding of the assembly to prevent accidental ignition of the pyro-technic.

III. Summary

The results of the experimental development are sum-marized as follows:

1. Recommended initiator loading is 10 mg of $TiH_x/KClO_4$ and 70 mg of Ti/2B to burst a 0.076 mm (0.003 in.) thick closure disc.

2. Slumping or flow of donor is controlled by stainless steel as an inert additive.

3. Temperature of donor is controlled by the composition of the mixture with respect to percentage Al.

4. Non-slumping donor pellets give consistent temperature-time curves.

5. Non-slumping donor pellets are not orientation sensitive.

6. Temperature-time profile is improved by elimination of insulator and replacing with additional donor materials.

7. Temperature-time profile is improved by low L/D ratios for a given nipple length.

8. Either pressed-in-place or prepressed donor charges may be used. Both have advantages and disadvantages.

9. Operational environments of up to 200 g's are presently feasible. Higher g forces are possible with additional development.

REFERENCES

1. E. A. Kjeldgaard and D. J. Gould, "Thermal Ignition of Pyrotechnics Through a Bulkhead", SLA-74-5094, Eighth Symposium of Explosives and Pyrotechnics, Feb. 5-7, 1974, Los Angeles, California.

2. E. A. Kjeldgaard, D. W. Larson, and D. J. Gould, "Thru Bulkhead Ignition of Pyrotechnics: An Analytical and Experimental Investigation", SLA-74-5165, Fourth International Pyrotechnic Seminar, July 22-26, 1974, Steamboat Springs, Colorado.

3. B. R. Steele, Private Communication.

4. H. S. Schuldt, Private Communication.

A METHOD FOR THE DETERMINATION OF THERMAL CONDUCTIVITY OF PROPELLANT MATERIALS BY DIFFERENTIAL SCANNING CALORIMETRY

W. W. Hillstrom

USA ARRADCOM, Ballistic Research Laboratory
Aberdeen Proving Ground, MD 21005

ABSTRACT

Benzoic acid, polymethylmethacrylate, polytetrafluoroethylene, and X-14 (a high energy, double-base propellant) were heated through decomposition and their thermal analysis curves compared. X-14 undergoes a pyrolytic decomposition beginning at $413°K$ and peaking at $573°K$. The thermal conductivities of small samples of propellant and polymer were calculated from measurements of their rate of heat flow into a heat sink in a modified Differential Scanning Colorimeter. This method will permit thermal conductivity measurements in small samples of sensitive materials, thus reducing hazards in their handling, and giving the first measurement on some very sensitive materials.

I. INTRODUCTION

The thermal conductivity of materials are commonly determined experimentally by heating relatively large samples for hours in methods such as the Guarded Hot Plate Test (ASTM C177). The large sample size and long heating periods give hazardous test conditions if the samples are explosives, propellants, or pyrotechnics. However, thermal characteristics such as the thermal conductivity of such materials are critically needed in order to model their ignition and combustion.

Thermal analysis presents an opportunity to determine thermal characteristics of explosives and propellants using very small samples of material[1]. The object of this work was to measure the heat flow rate through polymeric and propellant samples using a Thermal Analyzer with a Differential Scanning Colorimeter (DSC) and from this to calculate their thermal conductivities. In addition, the exothermicity or endothermicity of the materials were also to be measured by Differential Thermal Analysis (DTA). Their occurrence in energetic materials could indicate condensed phase reactions such as thermal decomposition or chemical rearrangements which precede ignition and/or contribute to their sensitivity.

In DTA the sample and reference are heated in a furnace at some preset linear heating rate. The furnace temperature and the difference in temperature between the sample and reference materials are displayed on the Thermal Analyzer. If the sample temperature increases faster than the reference temperature, an exothermic change is occuring and heat is given off during the process. If the sample temperature increases slower, an endothermic change is occuring and heat is absorbed in the process. The DSC is somewhat similar to the DTA except that the sample and reference are heated through a constantan disc which not only supports them, but also serves as one element of the temperature measuring thermoelectric junctions. Since the mode of heat transfer is reproducible for a given atmosphere and the thermocouple is not in the sample, the ordinate value of a thermogram at any given temperature is directly proportional to the differential heat flow between the sample and reference materials. This allows quantitative measurement of thermal occurrences.

An equation may be derived[2] from the Fourier equation of heat flux to calculate thermal conductivity from heat flow in a DSC.

---

[1] P. D. Garn, "Thermoanalytical Methods of Investigation," Academic Press, New York, 1965.

[2] F. N. Larsen and C. L. Long, 26th Pittsburgh Conference on "Analytical Chemistry and Applied Spectroscopy," Cleveland, Ohio, 1975.

$$k_T = \frac{E_T \ (S)(L)(\Delta y)(T_1 - T_2)}{A \ (T_1 - T_3)} \tag{1}$$

where

k_T = Thermal conductivity at test temperature (10^{-4}cal/cm sec °C),

E_T = Calibration coefficient of the DSC (mcal/sec °C),

S = Slope of heat flow versus temperature curve at test temp.,

L = Thickness of sample (cm),

A = Area of sample (cm),

Δy = Y-axis sensitivity (°C/in),

T_1 = Temperature at base of sample at test temperature,

T_2 = Temperature at base of sample at start of run, and

T_3 = Temperature of heat sink at top of sample.

Il. EXPERIMENTAL APPARATUS AND MATERIALS

The DuPont 900 Thermal Analyzer was used with DTA and DSC cells. The DTA were done with 4mm deep powder samples in 2mm diameter sample tubes. DSC measurements for calibration of the heat flux were done with a solid sapphire disc directly on the constantan platform without a reference.

For thermal conductivity measurements the DSC cell was used as shown in Figure 1. An insulator with 28mm diameter and 20mm height was placed over the constantan platform with an opening directly over the sample. The insulator was constructed from a machinable, ceramic-like material, Plastonium C-D, supplied by Insulation Systems, Inc., Santa Ana, California. The heat sink (25mm diameter and 20mm height) and an inset rod connecting it with the top of the sample were constructed from 99.9% purity, hard temper, deoxidized copper (Federal Specification QQC-503). A very sensitive thermistor was in contact with the top of the connecting copper rod.

The cylindrical samples were in general 5mm diameter and 4mm length, but each sample was measured accurately for calculation of the thermal conductivity. Polytetrafluoroethylene (Teflon) and polymethylmethacrylate (Plexiglass) were obtained locally. The specific gravities of the materials were measured to characterize them. The polymethylmethacrylate was 1.17g/cm^3. The polytetrafluoroethylene was 2.16 g/cm^3. Both correspond to literature values. The X-14 propellant was obtained by J. R. Ward of the Ballistic Research Laboratory from the Naval
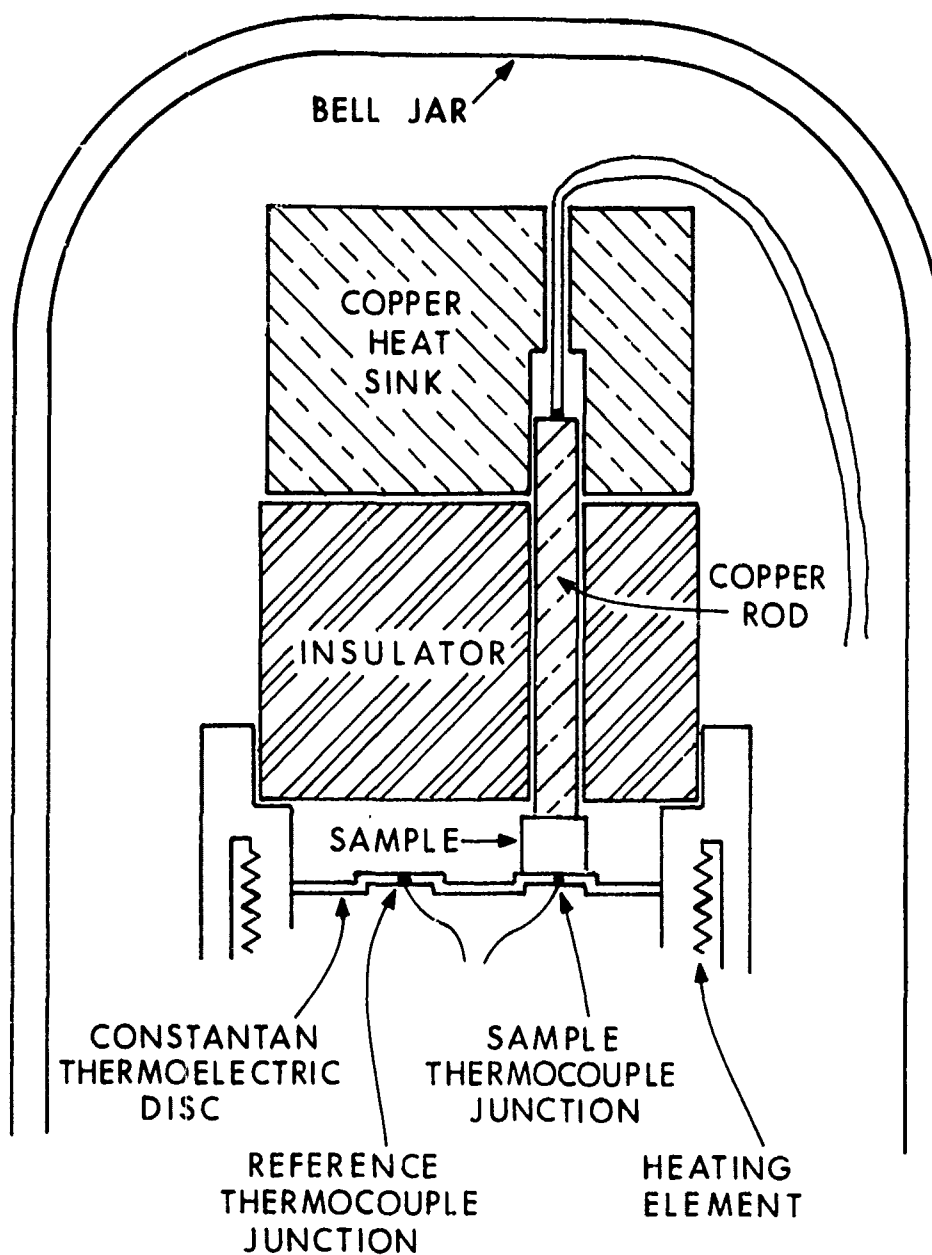
Figure 1. Differential Scanning Calorimeter Modified
for Thermal Conductivity Measurements

Ordnance Laboratory, White Oak, MD. X-14 is a high energy, double-base propellant.

III. DIFFERENTIAL THERMAL ANALYSIS

Samples were heated in both air and nitrogen atmospheres. The x-axis temperature scale of the Thermal Analyzer was calibrated by measuring the melting point of a pure sample of benzoic acid in the DTA. The x-axis zero shift was adjusted accordingly. A sample of a readily available propellant material, ammonium nitrate, was heated in the DTA for comparison with literature results. Its thermogram is shown in Figure 2. Three endotherms occur be   200°C indicating changes in structure and an endotherm at 170°C indicates melting. The jagged exotherm beginning at approximately 210°C indicates strong exothermic decomposition. This is essentially in agreement with literature results[3].

The thermogram of X-14 in nitrogen is relatively simple as shown in Figure 3. The strong exothermic decomposition begins at approximately 140°C with the highest of the multiple peaks at 198°C. No exotherms or endotherms were detected prior to the strong exothermic decomposition peaks. The temperature returned to baseline at approximately 250°C. A thermogram of X-14 heated in air as shown in Figure 4 has an additional exothermic peak at 339°C. This peak represents oxidation of the decomposition products in air.

IV. CALIBRATION OF THE DIFFERENTIAL SCANNING CALORIMETER

The DSC heat flow was calibrated by calculating the calibration coefficient E_T in a specific heat determination on a pure sapphire (Al_2O_3) sample provided with the DSC cell accessory kit. In this method the temperature lag between sample and reference systems was measured in "blank" and "sample" runs. The ΔT_{blank} and ΔT_{sample} were calculated at the temperatures of interest from the endothermic and exothermic temperature lags (absolute differential temperatures) on the thermogram multiplied by the analyzer Y-axis sensitivity. The known value[4] of the specific heat of Al_2O_3 was then substituted in the following equation to derive E_T in mcal per °C - min. at temperature T.

$$E_T = \frac{(C_p)_T \, M_a}{(\Delta T_{blank} + \Delta T_{sample})} \tag{2}$$

[3]E. I. DuPont deNemours & Co. (Inc.) Instruction Manual, 900 Thermal Analyzer and Modules, Wilmington, Del., 1968.

[4]D. C. Ginnings and G. T. Furukawa, J. Am. Chem. Soc. 75 522 (1953).
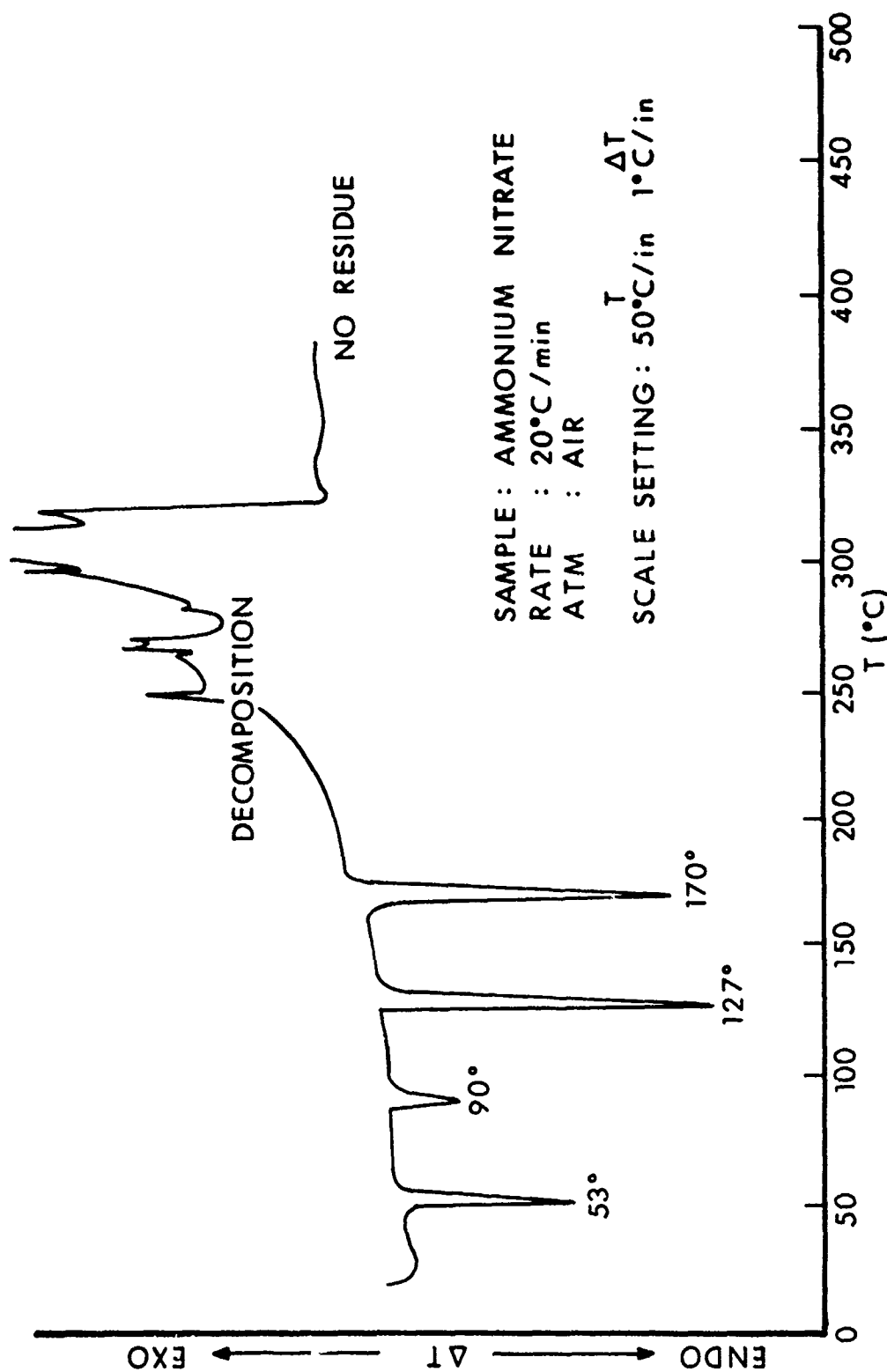
Figure 2. DTA Thermogram of Ammonium Nitrate in Air

NO RESIDUE

SAMPLE : AMMONIUM NITRATE
RATE : 20°C/min
ATM : AIR

SCALE SETTING : 50°C/in   1°C/in

$\dfrac{\Delta T}{T}$

DECOMPOSITION

170°

127°

90°

53°

T (°C)

EXO ← ΔT → ENDO

SOME BLACK RESIDUE

140°C

SAMPLE: X-14
RATE : 20° C/min
ATM : N₂ AT 0.2 LPM

SCALE SETTING : 50°C/in 1°C/in

T (°C)

EXO ← ΔT → ENDO
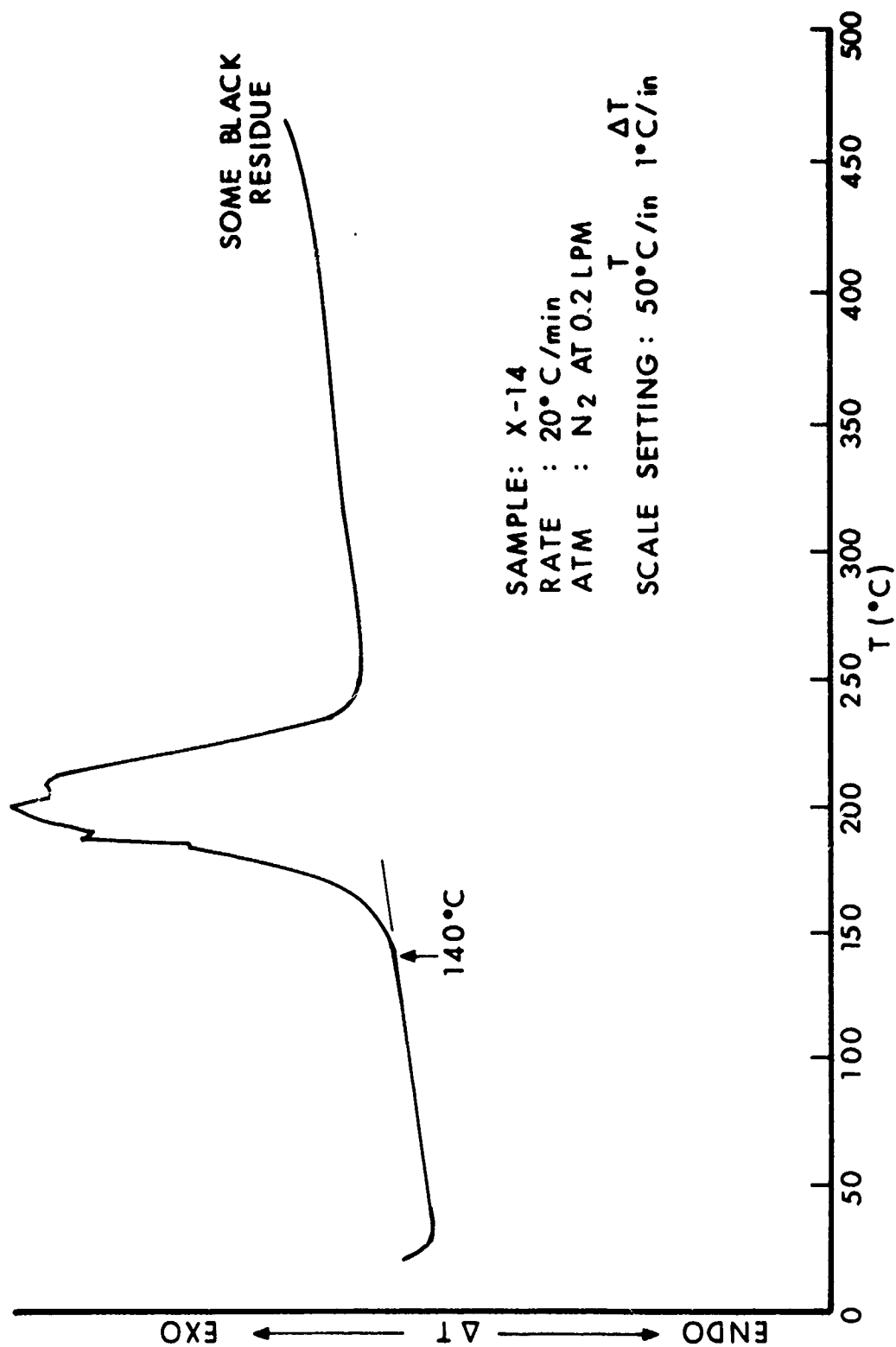
Figure 3. DTA Thermogram of X-14 in Nitrogen

266
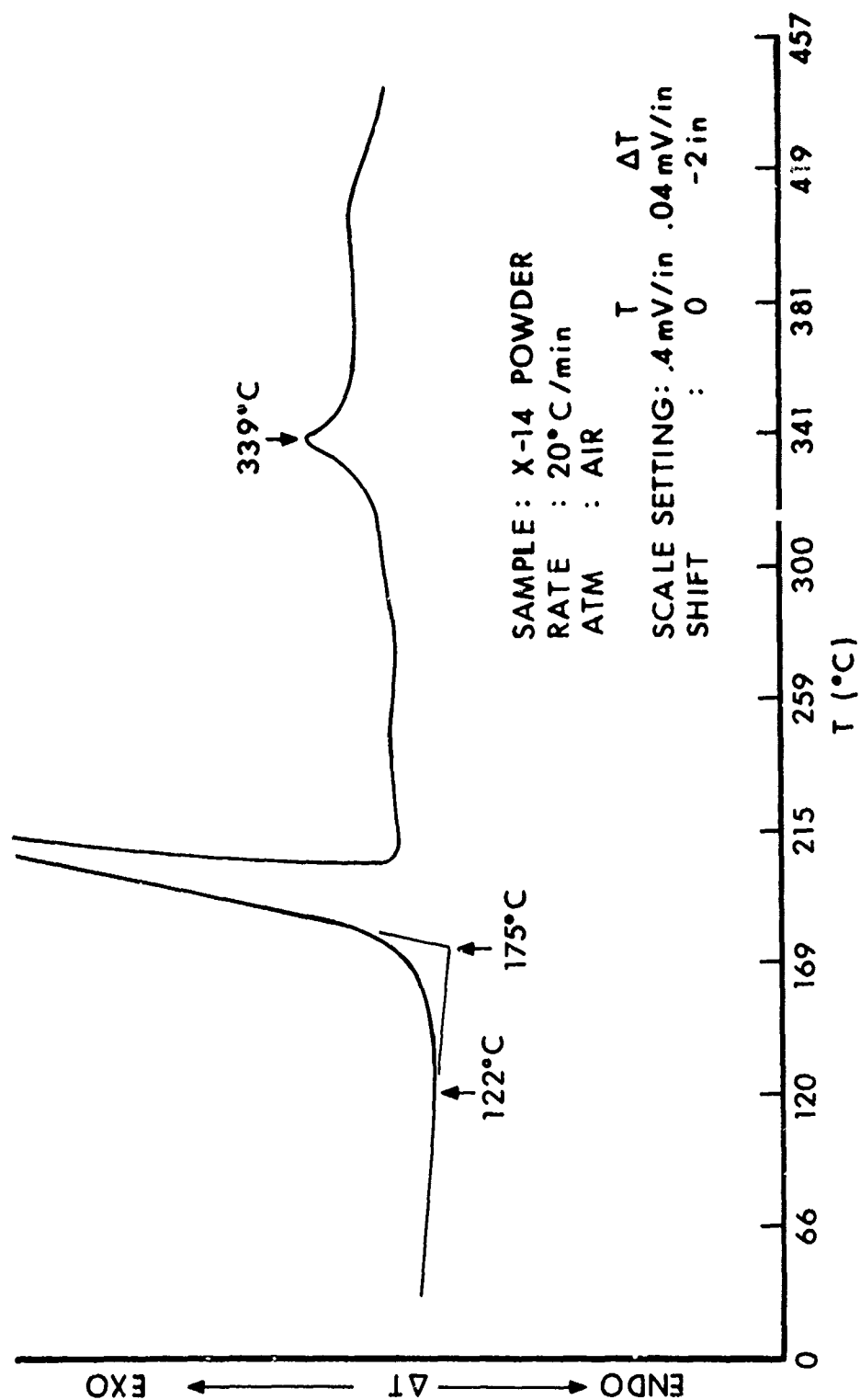
Figure 4. DTA Thermogram of X-14 in Air

SAMPLE : X-14 POWDER
RATE : 20°C/min
ATM : AIR

SCALE SETTING: .4mV/in   T
               .04 mV/in ΔT
SHIFT :   0   -2in

339°C

175°C

122°C

EXO ← ΔT → ENDO

T (°C)

0   66   120   169   215   259   300   341   381   419   457

267

where

$$(C_p)_T = \text{Specific heat at temperature } T(\frac{m\ cal}{mg - {}^{\circ}C}),$$

$$\Delta T_{blank} = \text{Absolute differential temperature without a sample } ({}^{\circ}C),$$

$$\Delta T_{sample} = \text{Absolute differential temperature with a sample } ({}^{\circ}C),$$

$$M = \text{sample mass (mg), and}$$

$$a = \text{Heating rate, } {}^{\circ}C/min.$$

A typical calibration run is shown in Figure 5. The values of E calculated in this example were 191 m cal/°C - min at 60°C and 210 m cal/°C - min at 100°C. These were averaged with two other runs to give E_{60} = 189 m cal/°C - min and E_{100} = 206 m cal/°C - min. These calibration coefficients are converted to m cal/°C - sec for use in Equation 1.

V. THERMAL CONDUCTIVITY CALCULATIONS

The following procedure was followed to determine thermal conductivities of the polymers, polymethylmethacrylate and polytetrafluoroethylene, and the propellant X-14. The sample was placed on the sample platform of the modified DSC as shown in Figure 1. A thermally conductive grease such as silicone stopcock lubricant was applied to upper and lower surfaces of the sample to insure smooth heat transfer into and through the sample. The copper heat sink, copper rod, insulator, and glass bell jar were assembled.

The sample, heat sink, and DSC cell were allowed to equilibrate as indicated by temperature constancy. The DSC cell was then heated over the temperature range of interest (eg., ambient to 100°C) at a heating rate of 10°C/min. The heat sink temperatures were recorded at the temperatures of interest. The resulting curve indicates the heat flow into the sample and to the coupled heat sink. A typical curve is shown in Figure 6 for polymethylmethacrylate. The slope of the heat flow versus temperature curve was calculated at the temperatures of interest. The thermal conductivity, K, was calculated using Equation 1 at 60 and 100°C as shown in Table I.

The thermal conductivities were averaged for each material to give Table II.

The thermal conductivities for the polymers compare favorably with literature values. Thus, Lucks et al[5] measured a thermal conductivity

---

[5] C. F. Lucks, G. F. Bing, J. Matolich, H. W. Deem, H. B. Thompson, USAF TR 6145 (1952), AD95239.
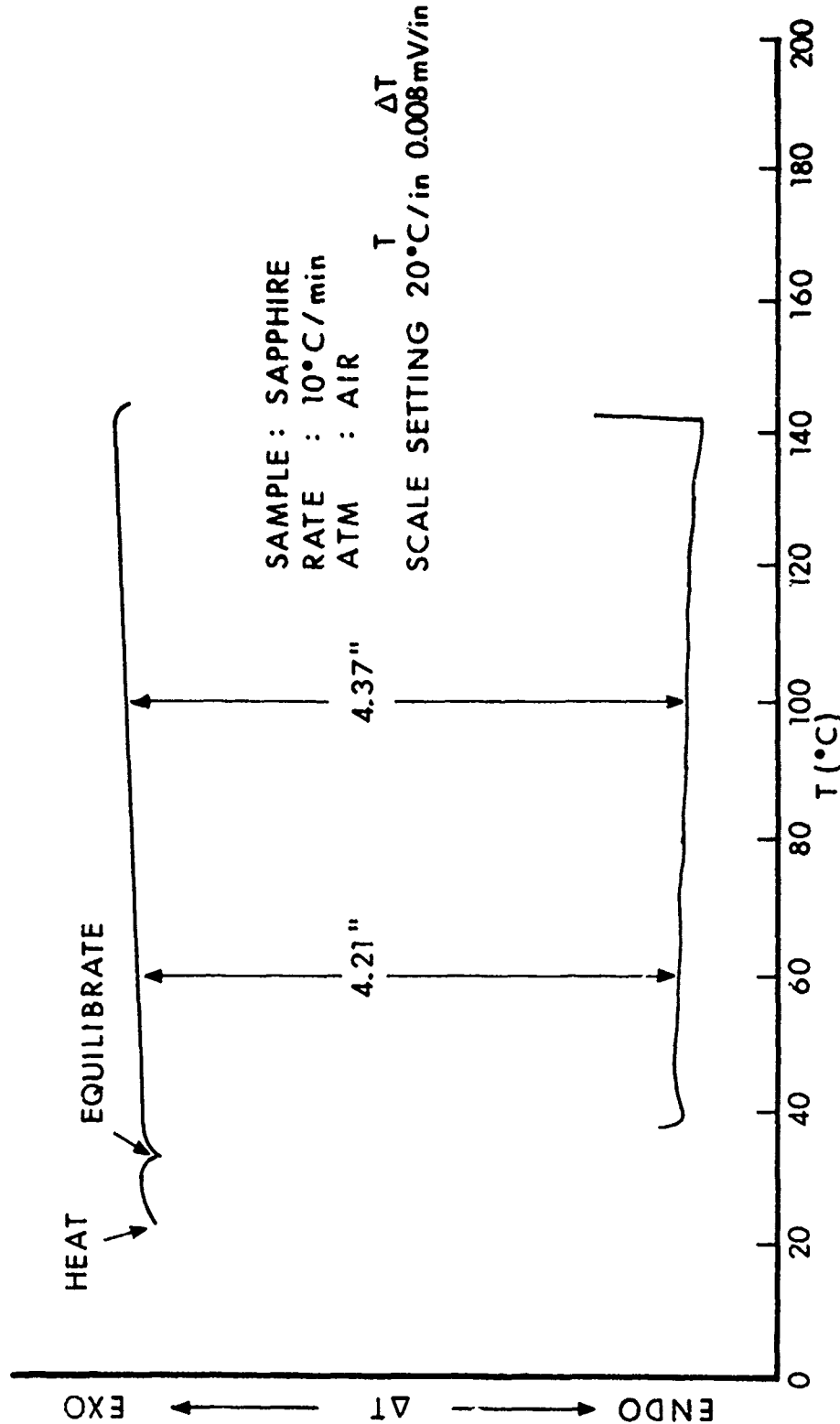
Figure 5. Specific Heat Determination of Sapphire

SAMPLE : SAPPHIRE
RATE : 10°C/min
ATM : AIR
SCALE SETTING 20°C/in 0.008mV/in

T   ΔT

4.37"

4.21"

EQUILIBRATE

HEAT

T (°C)

EXO ← ΔT → ENDO

SAMPLE : PLEXIGLASS
RATE : 10°C/min
ATM : AIR

SCALE SETTING : 20°C/in .04mV/in

23.89°C 55°5' 1.4326 SLOPE

57°45' 1.5849 SLOPE

29.03°C 51°45' 1.2685 SLOPE

50°45' 1.2239 SLOPE

33.12°C

23.01°C
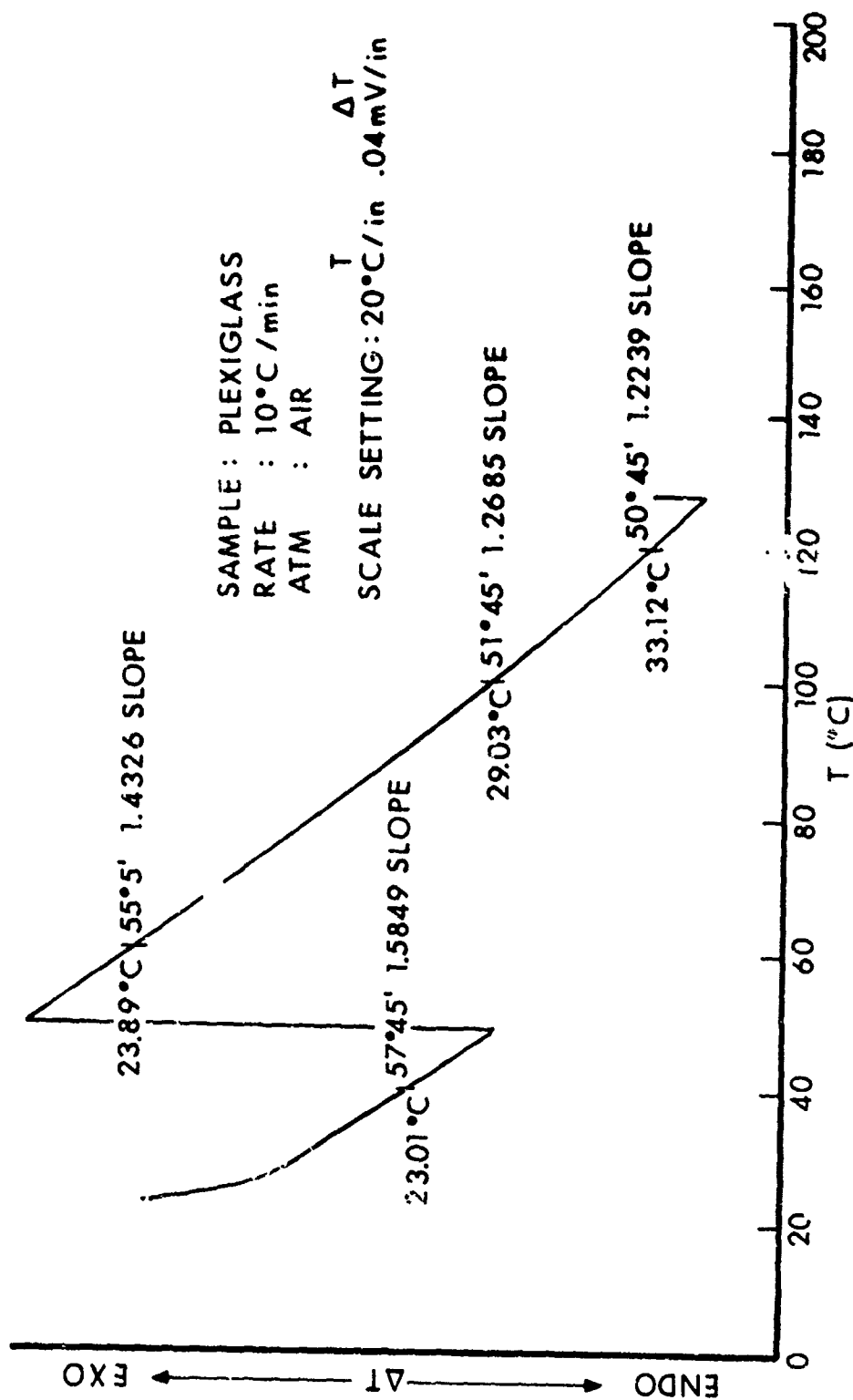
Figu e 6. Thermal Conductivity Determination on Polymethylmethacrylate

270

Table I. Thermal Conductivity Characteristics

Run No.	Sample Material*	Sample Diameter cm	Sample Length cm	Slope at 60°C	Top Temp. at 60°C	K_{60}**	Slope at 100°C	Top Temp. at 100°C	K_{100}**
1	PMM	0.465	0.447	1.130	24.0	6.00	0.971	29.0	5.64
2	PMM	0.465	0.447	1.269	24.0	6.74	1.130	29.5	6.61
3	PMM	0.465	0.447	1.171	24.0	6.38	1.140	29.0	6.70
4	PMM	0.463	0.389	1.376	24.35	6.50	1.228	29.20	6.29
5	PMM	0.463	0.389	1.433	23.89	6.68	1.269	29.03	6.49
6	PTE	0.463	0.452	1.842	24.0	9.89	1.483	30.0	8.83
7	PTE	0.463	0.452	1.901	25.0	10.78	1.585	30.5	9.63
8	PTE	0.465	0.455	1.817	24.5	9.69	1.611	30.0	9.53
9	PTE	0.465	0.452	1.949	24.42	10.7	1.664	29.74	9.99
10	PTE	0.465	0.452	1.881	23.81	10.2	1.670	29.22	9.95
11	PTE	0.462	0.451	1.861	23.10	10.11	1.580	27.95	9.35
12	X-14	0.4.?	0.391	1.532	23.0	7.57	1.339	28.5	6.84
13	X-14	0.457	0.386	1.798	24.5	8.25	1.497	30.0	7.56
14	X-14	0.462	0.389	2.050	25.0	9.48	1.648	30.0	8.33
15	X-14	0.452	0.386	1.732	23.33	8.51	1.428	28.57	7.66
16	v-14	0.457	0.386	1.901	24.70	9.04	1.555	30.37	8.16

*PMM = Polymethylmethacrylate and PTE = Polytetrafluoroethylene.

**K_T in cal/cm - sec °C x 10^{-4}.

271

of 3.75×10^{-4} g cal/sec - cm - °C (1.57×10^{-3} W/cm - °K) for poly-methylmethacrylate at 59°C (332.2°K) in a longitudinal heat flow method.

Table II. Thermal Conductivity

Sample Material	K_{60} in cal/cm - sec °C x 10^{-4}	K_{100} in cal/cm - sec °C x 10^{-4}
Polymethylmethacrylate	6.46	6.35
X-14	8.57	7.71
Polytetrafluoroethylene	10.23	9.55

Krischner and Esdorn[6] measured a thermal conductivity of 4.59×10^{-4} g cal/sec - cm - °C (1.92×10^{-3} W/cm - °K) for the same material at 25°C (298°K) using a transient heat flow method. Larsen and Long[1] measured a thermal conductivity of 4.3×10^{-4} cal/cm - sec - °C for polytetrafluoroethylene with no temperature give. Schultz and Wong[7] measured a thermal conductivity of 9.58×10^{-4} g cal/cm - sec °C (4.01×10^{-3} W/cm - °K) for the same material at 166°C (439.3°K).

The measured trend of decreasing thermal conductivity with increasing temperature seen in Table II is unusual and may be due to the increasing specific heat of the materials with temperature which is not accounted for in Equation 1.

VI.   CONCLUSION

The Differential Scanning Calorimeter method gives thermal conductivity determinations comparable with literature results using small sample sizes and short heating periods which are readily applicable to energetic materials such as explosives and propellants.

---

[6]O. Krischner and H. Esdorn, VDI Forschungshelf 450 Suppl. to Forsch. Gebiete Ingenieurw., B. (21) 28-39 (1955) in Thermal Conductivity of Non-Metallic Solids, Ed. by Y. S. Touloukian, 1970, IFI/Plenum.

[7]A. W. Schultz and A. K. Wong, ASTIA WALTR 397/10, (1958) AD154351 in Thermal Conductivity of Non-Metallic Solids, Ed. by Y. S. Touloukian, 1970, IFI/Plenum.

SHIELDING OF FACILITIES
FOR WORK WITH
PYROTECHNIC AND EXPLOSIVE MATERIAL

David J. Katsanis

Richard Thresher

CHEMICAL SYSTEMS LABORATORY

US ARMY ARMAMENT
RESEARCH AND DEVELOPMENT COMMAND

ABERDEEN PROVING GROUND, MARYLAND

SUPPRESSIVE SHIELDING — APPLICATIONS TO
PYROTECHNIC AND PROPELLANT OPERATIONS

INTRODUCTION

Viewgraph 1 - Title

Suppressive shields are a relatively new concept for providing protection to the area surrounding hazardous work with pyrotechnic or explosive material. At present, these operations are either limited to small quantities, widely dispersed, or segregated by barricades. Suppressive shields provide an alternative in the form of a vented steel enclosure.

Viewgraph 2 - Suppressive Shield Schematic

This schematic illustrates the concept of a suppressive shield. The enclosure usually consists of a structural steel framework with built-up panels of steel angles, I-beams, perforated plate, or louvered panels. The space between panel components allows gaseous products of combustion to pass through while suppressing flame and, in case of a detonation, reducing blast overpressure to a safe level. There is no direct path through the panel for fragments to pass through. All fragmentation effects are confined within the enclosure.

The shields can be of any size. They can be small transportable laboratory shields or large structures in a building similar to concrete barricades that are most often used.

Viewgraph 3 - Typical Concrete Cubicles

Typical reinforced concrete barricades are shown here. The barricades are designed as cubicles with three walls to withstand direct blast pressure and to prevent propagation of a detonation from one area to the next.

Reinforced concrete barricades do not prevent hazardous run-up reactions where a fire can start in one cubicle and, through pyrotechnic dust in the air or accumulated dust on equipment, spread from one cubicle to another until the entire facility is in flames.

In the event a detonation occurs, the concrete cubicles do not prevent wide dispersal of damaging primary and secondary fragments, nor do they prevent blast overpressure leakage beyond the open edges. The blast overpressure from the open edges of the cubicle can spread over the outside of the building wall and sometimes is large enough to make the walls collapse. A special reinforced building design can prevent this, but adds considerably to building costs.

Since suppressive shields are full enclosures, they perform in a different way from these cubicles.

Viewgraph 4 - Suppressive Shield Characteristics

Suppressive shields will:

- Confine all fragments from a detonation.

- Attenuate blast pressure to a safe level in all directions.

- Reduce fireball diameter sufficiently to prevent spreading of the fire beyond the local area.

Another particularly attractive feature of suppressive shields is that they are modular in design for quick erection and modification to provide maximum protection and flexibility.

<u>Viewgraph 5 - General Configuration of Suppressive Shield Groups</u>

Several general classes of shield designs have been conceived.

As shown here, some have cylindrical or spherical configuration while others are rectangular frame and panel designs.

Generally the configuration is governed by the dominant hazard, i.e., blast, fragment or flame. If blast pressures or fragmentation are the factors which are most important in design of the structure, the shield will usually have a cylindrical or spherical shape. The rectangular frame and panel structures are typically used where the dominant hazard is flame.

I will be discussing the Group 3 shield which is cylindrical and Group 5 which is the rectangular frame and panel shield design. These shields are both roughly similar in overall size, but completely different in design and use.

The Group 3 shield is about 10 ft high and 11 ft in diameter. It is designed to withstand the high structural loads associated with the blast overpressure effects of a detonation. The Group 5 shield is a 10 ft cube and designed primarily for flame suppression.

In my presentation today, I will first quickly summarize safety approved shield characteristics in general. Then I will present the design details of the Group 3 and Group 5 shields with a short motion picture film of Group 5 tests. I will conclude with a summary of the shielding technology program and current status of suppressive shielding.

SAFETY APPROVED SHIELDS

Viewgraph 6 - Safety Approved Suppressive Shields

To insure that Department of Defense safety offices approve site plans which incorporate suppressive shields, we have designed, fabricated, and proof tested several designs as listed here.

The characteristics of the shields approved by the Department of Defense Explosives Safety Board are summarized in the viewgraph. They include sizes and charge weights typical to munitions manufacturing, but they can be scaled up or down in size or charge weight to meet special laboratory requirements.

As this table indicates, suppressive shields are approved for use in hazardous operations involving explosive charge weights up to the equivalent of 37 pounds 50/50 pentolite for Group 3 and 30 pounds of illuminant mix for Group 5.

Approved shield sizes range from the 2 foot diameter spherical steel shell of Group 6 to the 11¼ foot diameter cylindrical Group 3 shield.

The operator safe distance shown is the distance from the exterior wall that an operator can be located and not be injured by blast over-pressure or flame venting from the shield when detonation or deflagation occur within the shield.

DISCUSSION OF GROUP 3 AND GROUP 5 SHIELD DESIGNS

Viewgraph 7, Group 3 Shield

This is the Group 3 test fixture. It has three major components:

- Cylindrical steel cage.

- Reinforced concrete roof.

- Reinforced concrete foundation.

The concrete roof is shown here being mounted on to the cage. The roof is a laced reinforced concrete slab about 13 feet in diameter — designed and fabricated using established procedures published in TM5-1300 entitled, "Structures to Resist the Effects of Accidental Explosions", also known as NAVFAC P-397 by the Navy and AFM 88-22 by the Air Force.

The foundation design is identical to the floor.

The suppressive shield part of the structure is the cylindrical cage which consists of a double row of interlocked I-Beams with supporting rings and liners.

Viewgraph 8 - I-Beam Configuration

This shows the interlocking I-Beam structure of the wall. The Group 3 shield is approved for use with explosives up to 37 pounds of 50/50 pentolite or the equivalent.

Viewgraph 9 - Group 5 Panels on Ground

One of the features that makes suppressive shields attractive for plant use is their modular design which is illustrated here. These panels for the Group 5 shield are laid out by the foundation ready for assembly.

Each panel is about 10 feet long and 5 feet wide. When erected they form a cube 10 feet long on each side.

Viewgraph 10 - Category 5 Panel Section

The panels themselves are composite structures. Each has a double row of interlocking structural steel angle beams arranged as shown in the viewgraph. There are three perforated plates, one on the outside and two on the inside. Wire screening was added between the panel layers for additional flame suppression, but it proved ineffective. Tests demonstrated that there was sufficient exposed metal surface to suppress flames effectively without the addition of the metal screens.

Viewgraph 11

Here, the panels are being moved into place. The modular characteristic simplifies the alteration of facilities to meet changing requirements.

Viewgraph 12 - Group 5 Shield

This is the Group 5 shield ready for test. This shield has been approved for use with 1.84 pounds of C-4 or 30 pounds of illuminant mix.

The Group 5 shield is especially designed for flame suppression. The structure is not as heavy as those intended to withstand the comparatively large transient blast overpressures of a detonation. The design has a large surface area and volume of steel to absorb heat and suppress flames. The venting of gaseous products of combustion precludes significant pressure and burning rate increase inside the shield.

To determine limits on flame suppression capability of this shield, thermal suppression studies have been conducted beyond those required for the safety approval proof tests mentioned previously.

Viewgraph 13 - Suppressive Shield Group 5 Testing

The tests are summarized on this viewgraph.

Single base, multiperforated, M10 gun propellant in bulk was used in the propellant tests. The illuminant material is a 50:50 mix of sodium nitrate, and powdered magnesium. The safety approval tests were conducted with 30 pounds of the illuminant mix. To be complete, the proof test charge of 2.5 pounds is shown. That charge weight stressed the shield structure to its limit and was not increased

Viewgraph 14 - Sensor Location for Group 5 Suppressive Shield Tests

Instrumentation layout for the tests is shown here (see table below: Instrumentation for Group 5 Suppressive Shield Tests). Burning time was measured using photocells in the shield wall. Thermal couples in the bulk pyrotechnic were used to obtain an indication when the material was completely burned. Static overpressure was measured on large charges to estimate confinement effects. Radiant heat flux outside the shield was measured with Keithley 860 flux meters. Blast pressure was recorded inside and outside the shield when explosive material was detonated in the shield. High speed motion picture coverage was included on all shots. Video display of each test in the instrument building was also recorded.

Viewgraph 15 - Free Field Illuminant Test Configuration

For comparison, free field temperatures and pressures were measured using instrument configuration shown here. Thermocouples were on a line in one direction spaced at 5 foot intervals and pressure was measured in a direction perpendicular to the thermocouple line. Black and white, and color film coverage was also included.

INSTRUMENTATION FOR GROUP 5 S/S TESTS

Measurement Number	Parameter	Transducer	Amplifier	Installed Time Constant	Recorder
00	Timing	N/A	N/A	—	Sangamo 4700
01	Burning time	Photocell Monsanto	Transdata	1 msec	Sangamo 4700
02	Burning time	MT-2	NEFF109-6	1 msec	Sangamo 4700
03	Burn rate	Fe-Constantan	NEFF109-6	100 msec	Sangamo 4700
04	Burn rate	Thermocouple	NEFF109-6	100 msec	Sangamo 4700
05	Burn rate	Breakwire	N/A	1 msec	Sangamo 4700
06	Static press	MB151-DBZ-177 in tube	NEFF109-6	10 msec	Sangamo 4700
07					Sangamo 4700
08		PCB101A02 in			Sangamo 4700
09	Static press	Baffle mount	NEFF109-6	10 msec	Sangamo 4700
10	Blast press (face-on)	ST-2 in Wall mount	PCB401A13	200 msec	Sangamo 4700
11	Heat flux	Keithley 860	N/A	1 sec	Sangamo 4700
12					
13					
14	Heat flux	Keithley 860	N/A	1 sec	Sangamo 4700
41	Blast press	ST-7H in			
42	"	Aerodynamic	PCB401A11	200 msec	Biomation 610B
43	"	Probe			
44	"				

Viewgraph 16 - Test Set Up

This is a photograph of a typical test set up. The open shield door was closed during test. .

Viewgraph 17 - Heat Flux as a Function of Time

Heat flux data transients five feet from outside of the shield (about 10 feet from the charge) are shown with dashed lines. The solid lines are from heat flux measurements about 10 feet from charges burned in the open. This is the same total distance from the charge for the shield tests. Comparison between open air and shielded heat flux shows 85% reduction in peak radiant flux for a shielded 50 pound charge.

Preliminary propellant tests burning a maximum charge weight of 590 pounds of M-10 single base multiperforated propellant in bulk with 0.0185 inch web resulted in no pressure rise in the shield. High radiant heat flux outside the shield wall indicated a need for improved thermal suppression. This work is not finished. The viewgraph lists some areas where more study is needed.

Viewgraph 18 - Research Needed

An exhaustive search of the literature to identify hazards and improved thermal suppression techniques has revealed a need for more research in this area.

Methods do exist for estimating free field radiant flux, fireball diameter, and burning time for unconfined pyrotechnic material, but there is, at present, no method to compute attenuated thermal effects when a suppressive shield is used. Predictive models are needed.

<u>Viewgraph 18</u> (cont)

Investigation of nonuniform venting has been initiated, but that work is not complete. Much work is required to develop the basic technology necessary to design optimal shields for flame suppression.

As a result of extensive investigation of blast and fragment effects the technology for those hazards is well understood. Predictive techniques for suppressive shield performance in attenuating blast and fragment hazards have been developed. The next few viewgraphs just briefly indicate the scope and results of that investigation.

<u>TECHNOLOGY SUMMARY</u>

<u>Viewgraph 19 - Applied Technology Participants</u>

The suppressive shield designs that we have been discussing are based on a major four-year effort by organizations listed here.

The roles they played are indicated on the viewgraph.

The lead organization for suppressive shield technology development was Edgewood Arsenal, now called Chemical Systems Laboratory. Recent Army reorganization has reassigned responsibility for suppressive shielding to Large Caliber Weapon Systems Laboratory, ARRADCOM, at Dover, NJ.

<u>Viewgraph 20 - Technology Flow Chart</u>

Technology development has proceeded along the lines illustrated in this flow chart.

Hazards identified are classified as blast, fragment and fireball. Description of each of these hazards is essential to design of a shield. Each of these hazards poses a special problem to the designer and requires consideration not only in terms of its own features, but also in terms of combined effects of all hazards acting together.

<u>Viewgraph 20</u> (cont)

The next step is to develop procedures to predict suppression of blast, fragment and flame hazards. The nature of the suppression governs the magnitude of the loads imposed on the structure. A safe, economical shield must be designed to withstand loads imposed. Suppression and design trade-offs are made to obtain the best shield which satisfies hazard suppression requirements to provide a save environment at minimal cost.

On blast environment, a predictive capability for characteristics of free air blasts is available in the literature. In the technology program techniques were developed for defining internal transient and quasi-static blast overpressures, pressure loads on the shield and attenuated pressure external to the shield.

The second major element to be considered in the design of a suppressive shield is the fragment threat. As we initiated our technology studies we found much was known about primary fragment hazards but little was known about secondary fragment hazards. Primary fragments are those from material in direct contact with detonating composition. Secondary fragments are from surrounding equipment, not in direct contact with the composition that detonates.

It was necessary to establish a methodology to predict secondary fragment hazards and fragment suppression characteristics of the composite structural steel walls of a suppressive shield.

Viewgraph 21 - Suppressive Shield Technology Summary

As a result of the Suppressive Shielding Program, engineering methodology is available for modifying or scaling approved designs to meet specific munitions plant requirements. Where approved designs do not exist to meet certain requirements there is an engineering methodology for design and proof test of new shields.

This methodology is presented in an engineering design handbook for suppressive shields, published by the US Army Corps of Engineers, Huntsville Division, Huntsville, Alabama.

Viewgraph 22 - Suppressive Shield Engineering Design Handbook

This viewgraph is a list of the chapter titles in the handbook. The information contained in each chapter is also shown.

Methods for modifying suppressive shields to meet specific production line requirements are given in Chapter II - Safety Approved Shields.

If a new shield must be designed, Information in Chapters III, IV and V are used.

Chapter VI - Structural details, has recommended designs for personnel doors, conveyor doors, as well as other penetration for utilities and the like.

Economic analysis methods and quality assurance factors are included.

With this handbook a Plant designer or engineer requiring hazardous operation protection can select, modify or design a suppressive shield for their required use. This handbook is available through DDC or National Technical Information Service and provides an alternative protective method previously not available to provide increased protection to personnel involved in hazardous operations.

Gentlemen, it has been my pleasure to brief you today. Thank you for your attention.

285

REINFORCED CONCRETE CUBICLE

FRAME FRONT WALL AND ROOF

MASONRY END AND BACK WALL
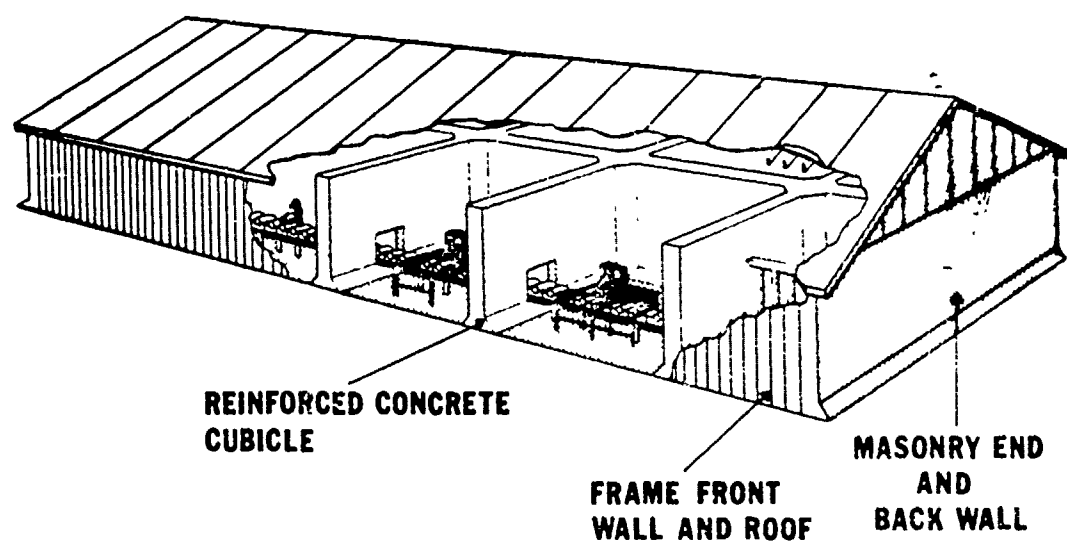
Viewgraph 3: Conventional Structure

ENVIRONMENT

REACTION

WIRE SCREENING

PERFORATED PLATES

NESTED ANGLE IRONS
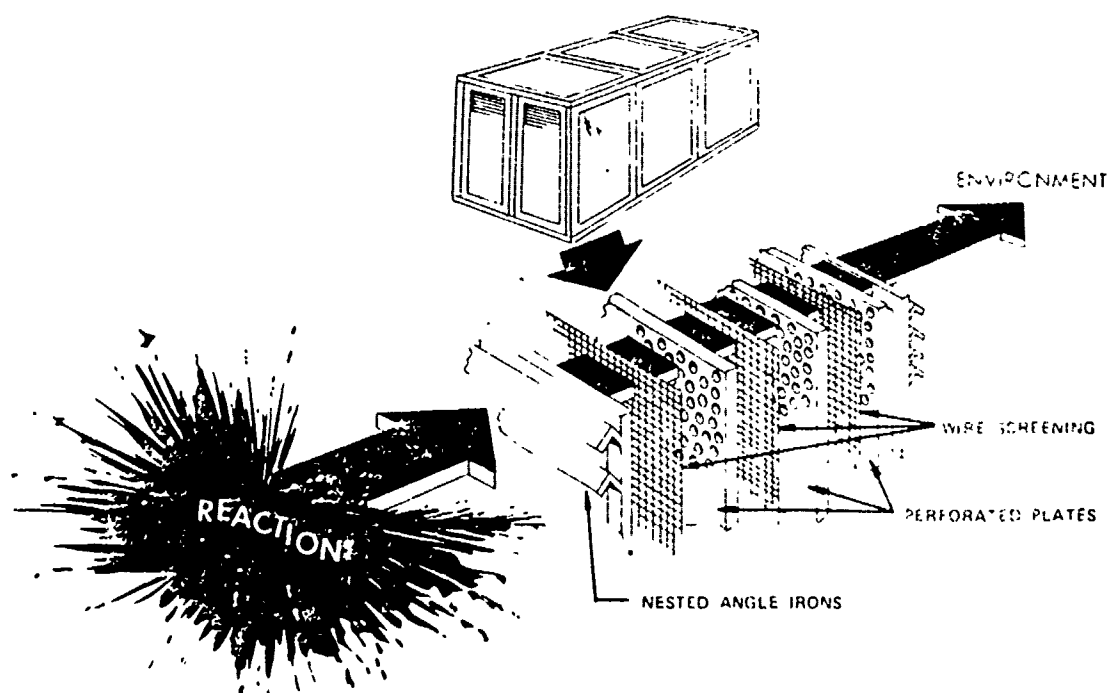
Viewgraph 2: Rectangular Suppressive Shield Venting

SUPPRESSIVE SHIELDING ENCLOSURE

- **FRAGMENT CONTAINMENT**
- **BLAST SUPPRESSION**
- **FLAME ATTENUATION**

GENERAL CONFIGURATION OF SUPPRESSIVE SHIELD GROUPS
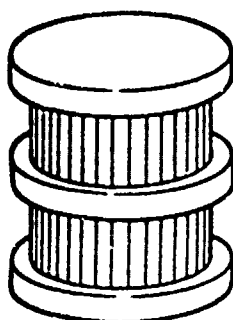
GROUPS 1, 2 AND 3
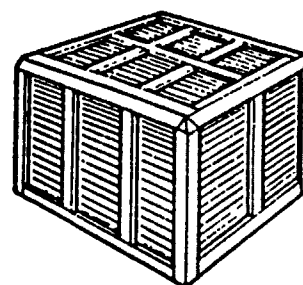
GROUP 4
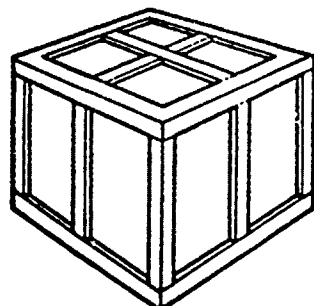
GROUP 6
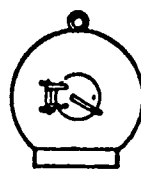
GROUP 5

GROUP 81MM

SHIELD GROUP DEFINITIONS

Shield Group	Hazard Parameter		Representative Applications	Level of Protection*
	Blast	Fragmentation		
	psi			
1	500	Severe	Porcupine Melter (2000 lbs) plus 2 pour units 250 lbs each	Reduce blast pressure at intraline distance by 50%
2	500	Severe	HE bulk (750 lbs) Minute Melter	Reduce blast pressure at intraline distance by 50%
3	500	Moderate	HE bulk (37 lbs) Detonators, fuzes	Category I hazard** at 6.2 feet from shield
4	200	Severe	HE bulk (9 lbs) Processing rounds	Category I hazard** at 19 feet from shield
5	50	Light	30 lbs illuminant Igniter slurry mixing HE processing (1.84 lbs)	Category I hazard** at 3.7 feet from shield
6	2000	Moderate	Laboratory, handling, and transportation	Category I hazard** at 1 foot from shield
7	200	Moderate	Flame/fireball attenuation	Category I hazard** at 5 feet from shield

*All shield groups contain all fragments.
**Mil Std-882, 15 Jul 69 (2.3 psi level)..

Safety-Approved Suppressive Shields

Shield type	Material limit	Operator safe distance	Size
		ft	ft
Group 3	37 lb of pentolite	6.2	11.25 diameter × 10 height
Group 4	9 lb of pentolite	19	9.2 × 13.1 × 9.3 height
Group 5	1.84 lb of C-4	3.7	10.4 × 10.4 × 8.5 height
	30 lb of illuminant mix	2	
Group 6	13.6 oz of pentolite	1	2 diameter
81 mm	Two 81 mm rounds 2.8 lb of C-4	3	14 × 18.7 × 12.4 height

VIEWGRAPH 6
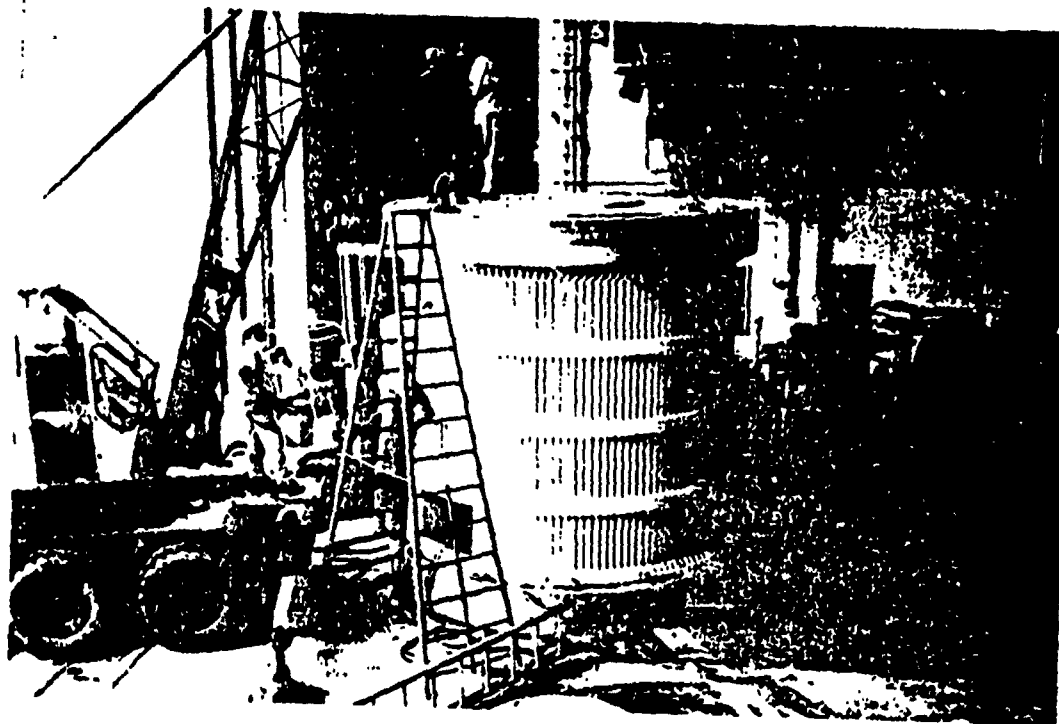
Viewgraph 7: Group 3 Suppressive Shield
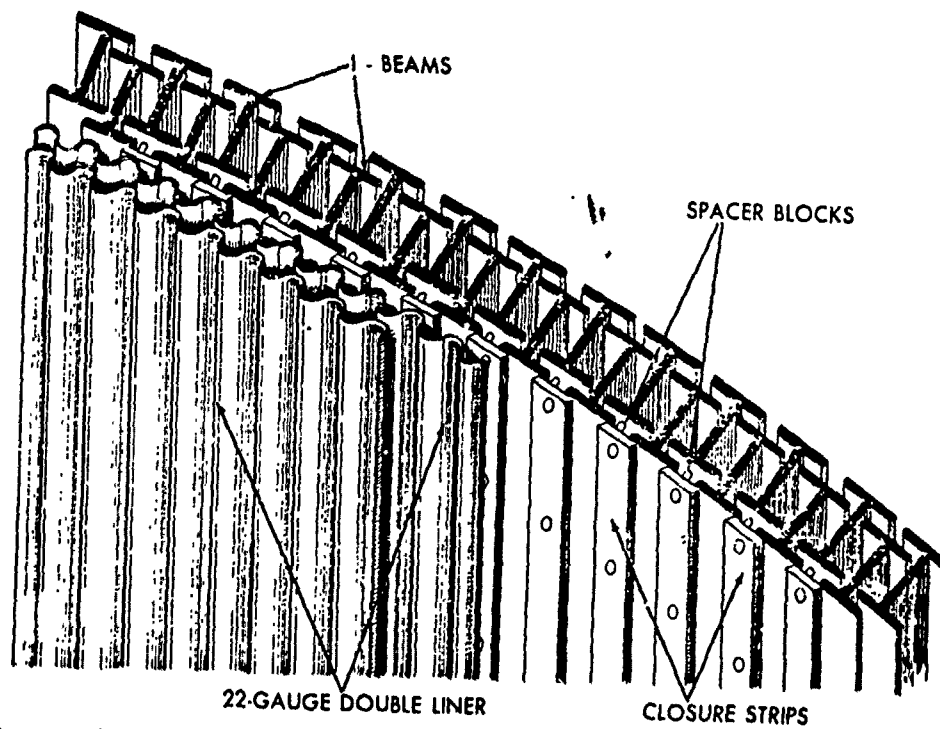
Viewgraph 8: I-Beam Configuration Showing Addition of Closure Strips and Double Liner to Group 3 Shield

Viewgraph 9

3-1/2 x 3-1/2 x 1/4 ANGLE

16 GA. PERFORATED PLATE (3)

15 ANGLES SPACED AS SHOWN

2 x 2 x 1/8 16 ANGLES EQUALLY SPACED

SCREEN 16 x 16 MESH (4 PLACES)

3-1/2'
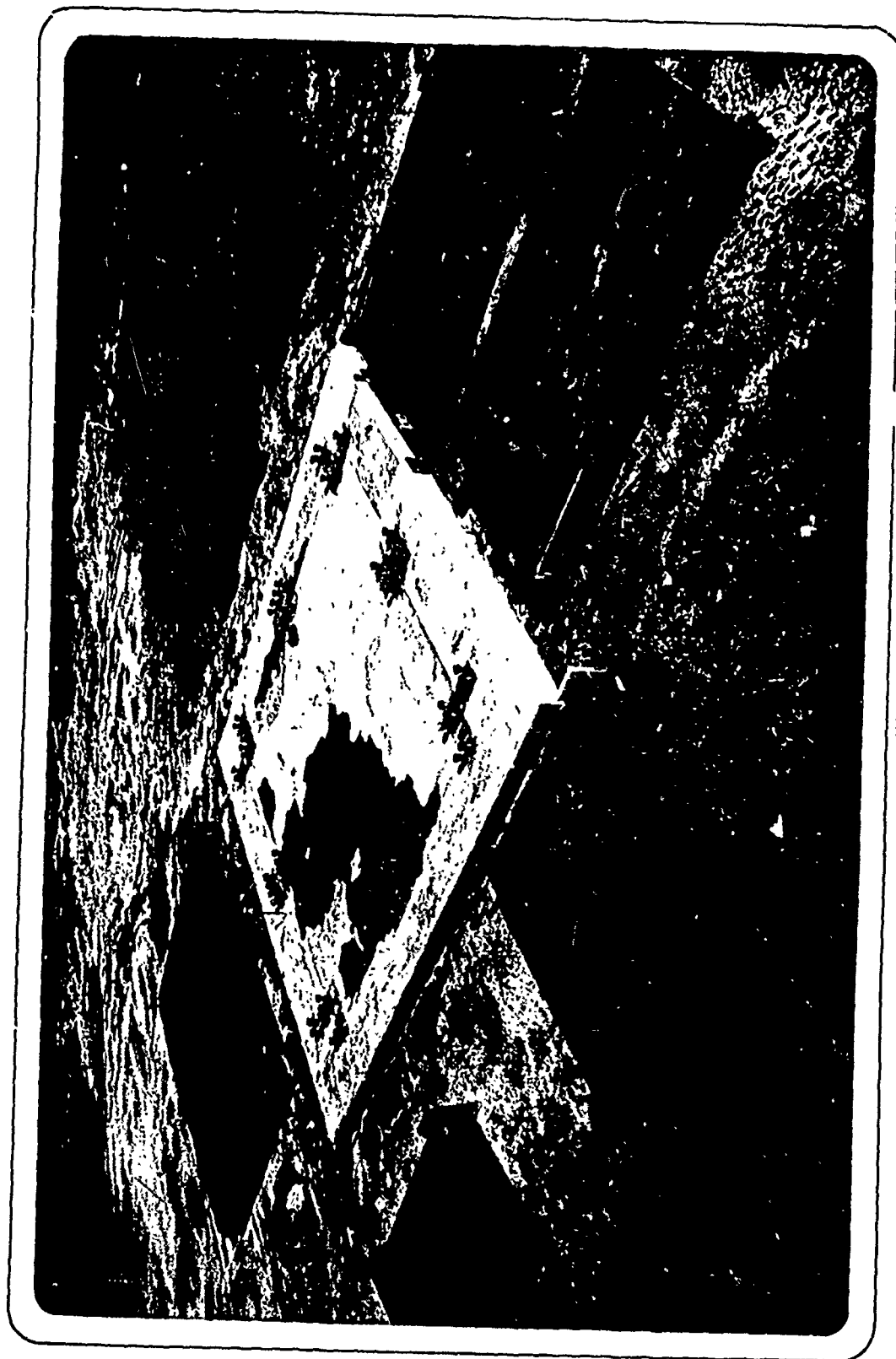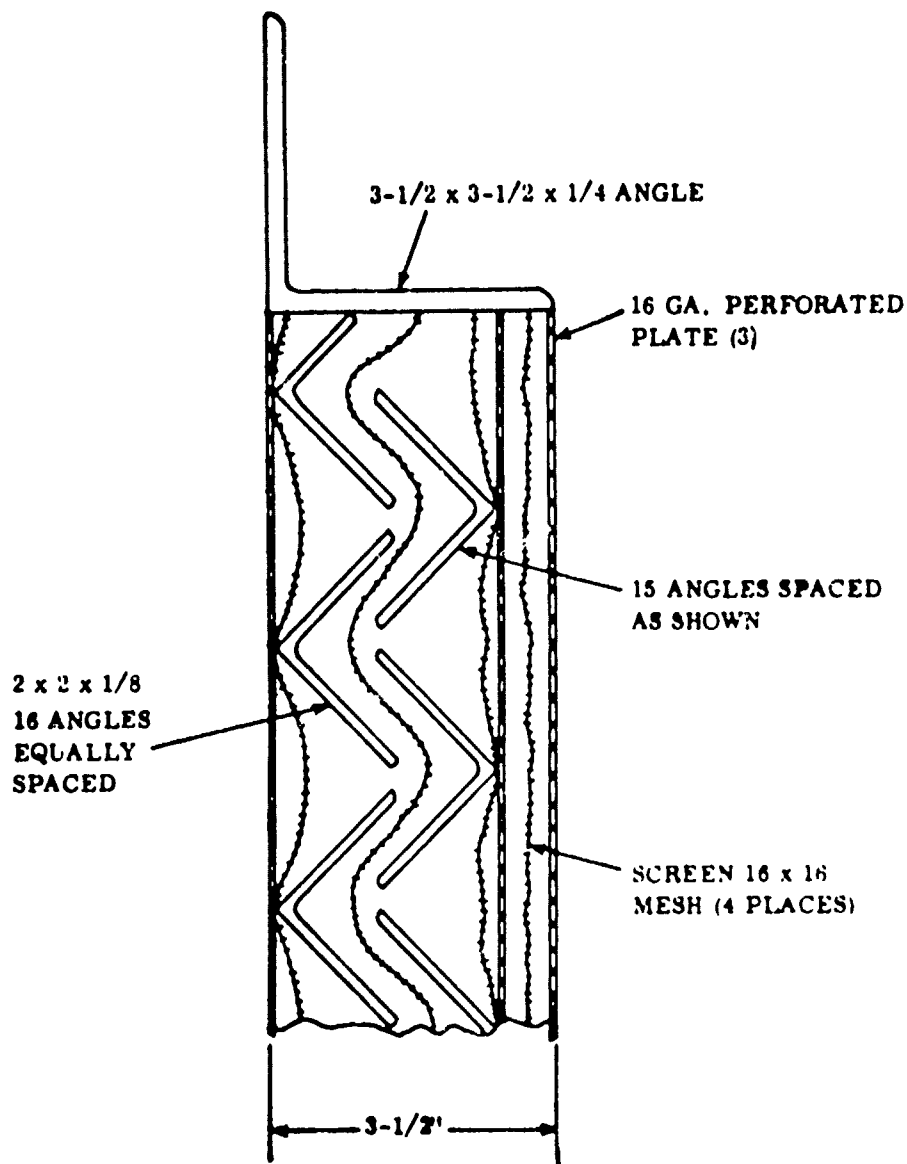
Figure 18. Category 5 Panel Section

Viewgraph 70

291
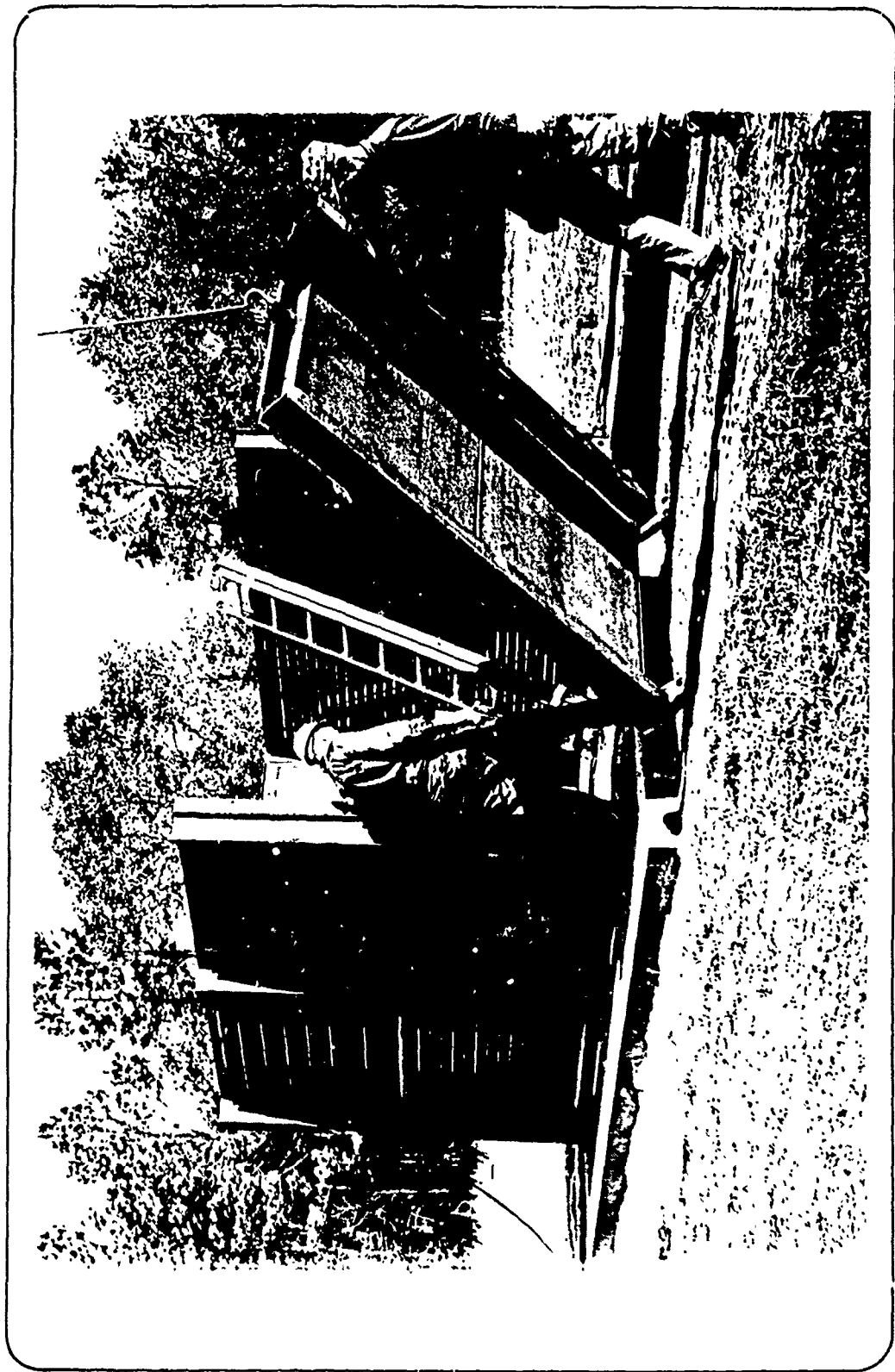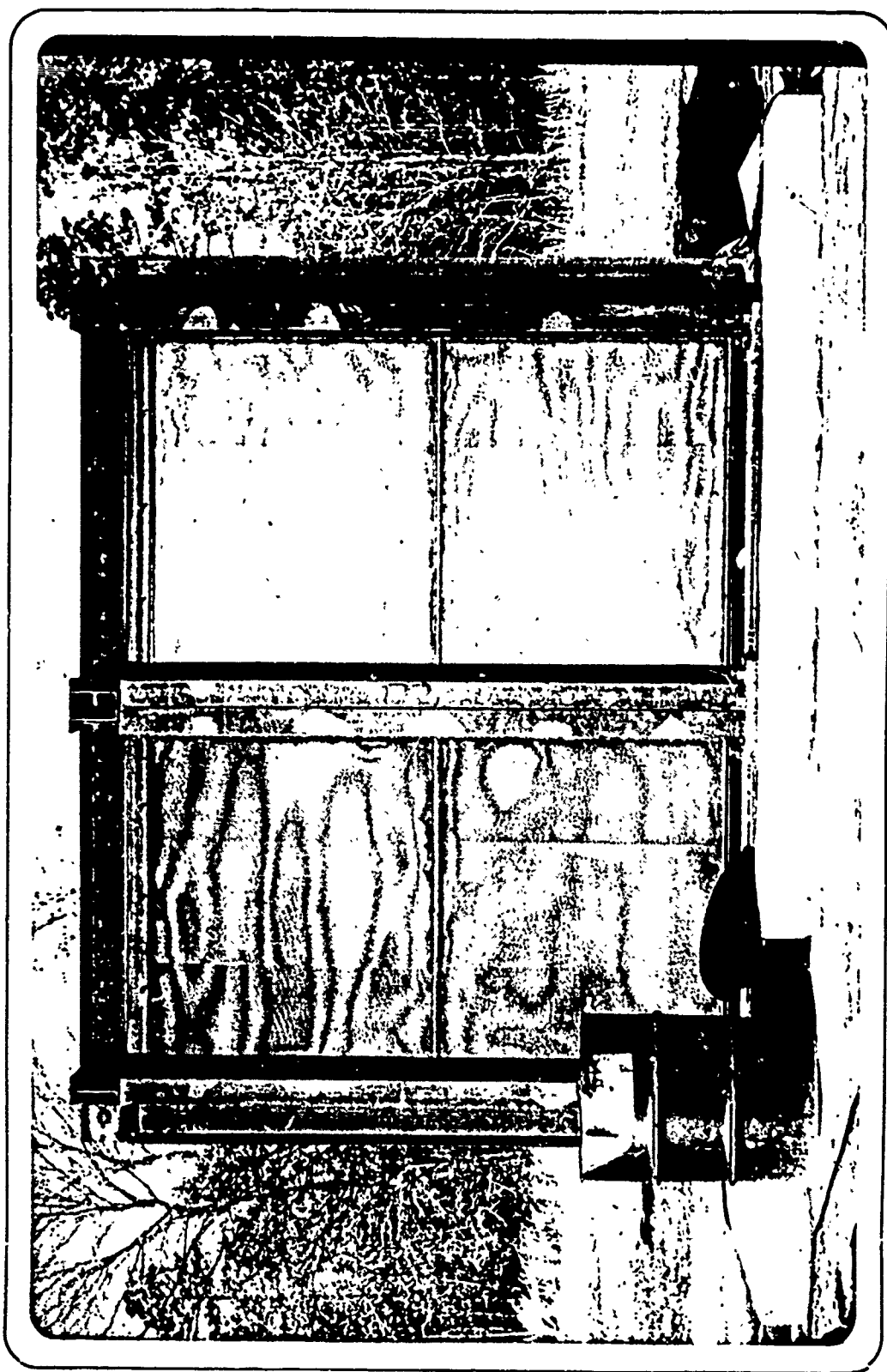
Viewgraph 11

Viewgraph 12

SUPPRESSIVE SHIELD
GROUP 5 TESTING

270 kg (590 lb) PROPELLANT

22.7 kg (50 lb) ILLUMINANT MATERIAL

1.1 kg (2.5 lb) EXPLOSIVE MATERIAL

MAY 78

Viewgraph 13

SENSOR LOCATIONS FOR GROUP 5 S/S TESTS

SENSOR KEY

◆— PHOTOCELL
▲— THERMOCOUPLE
↓— BREAKWIRE
◆— STATIC PRESS — STRAIN GAGE
●— STATIC PRESS — PCB IN BAFFLE
■— BLAST PRESS — ST-2
▮— HEAT FLUX METERS
↓— BLAST PRESS — ST-7H IN PROBE

Viewgraph 14

295
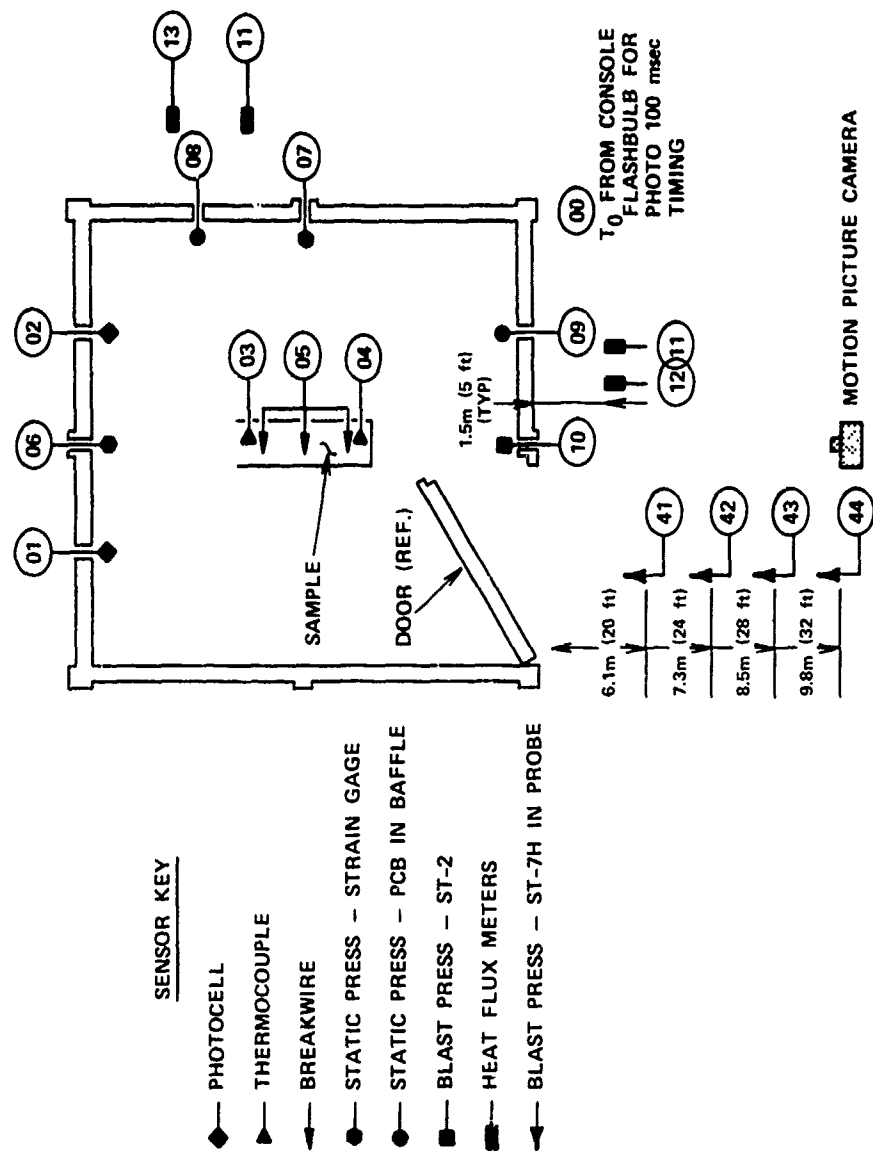
FREE FIELD ILLUMINANT TEST CONFIGURATION
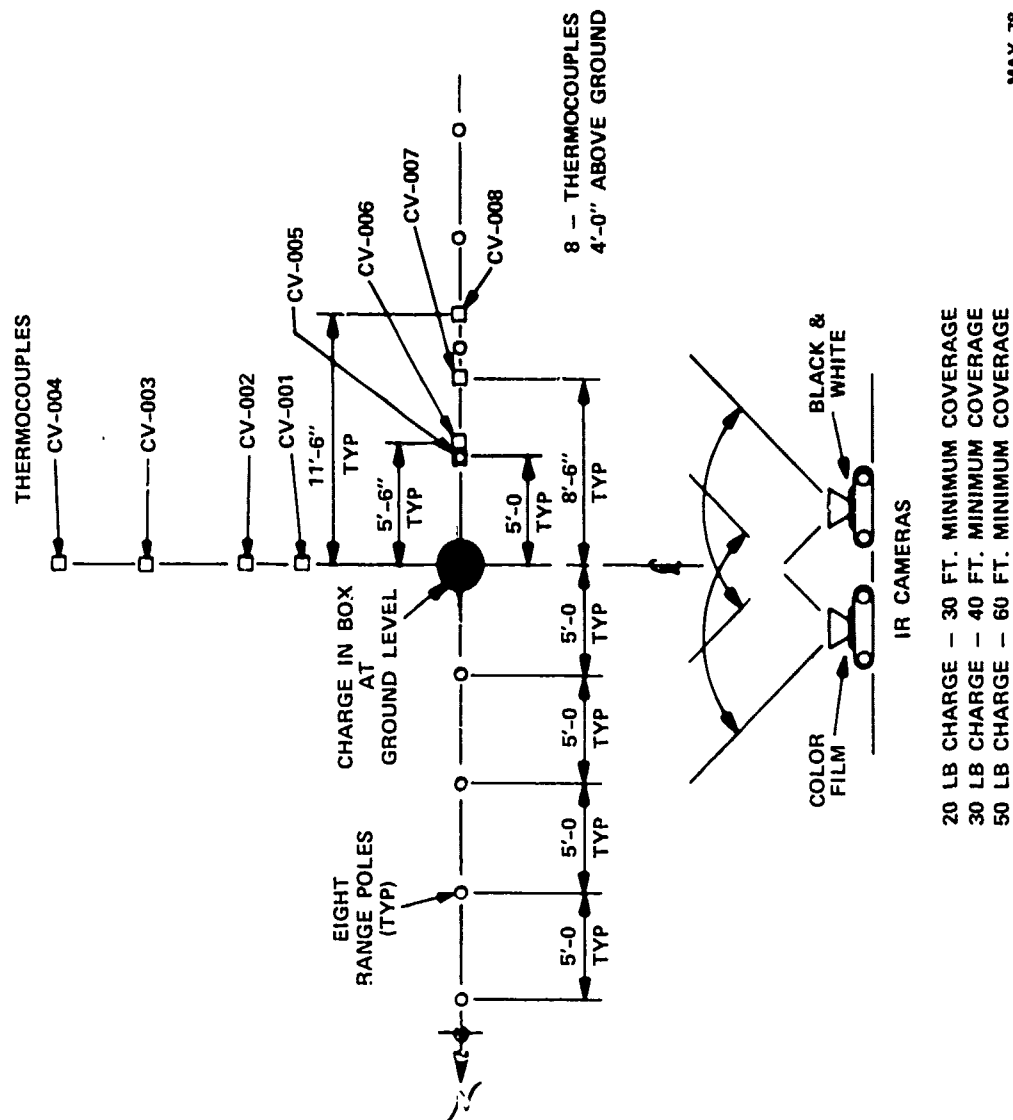
Viewgraph 15
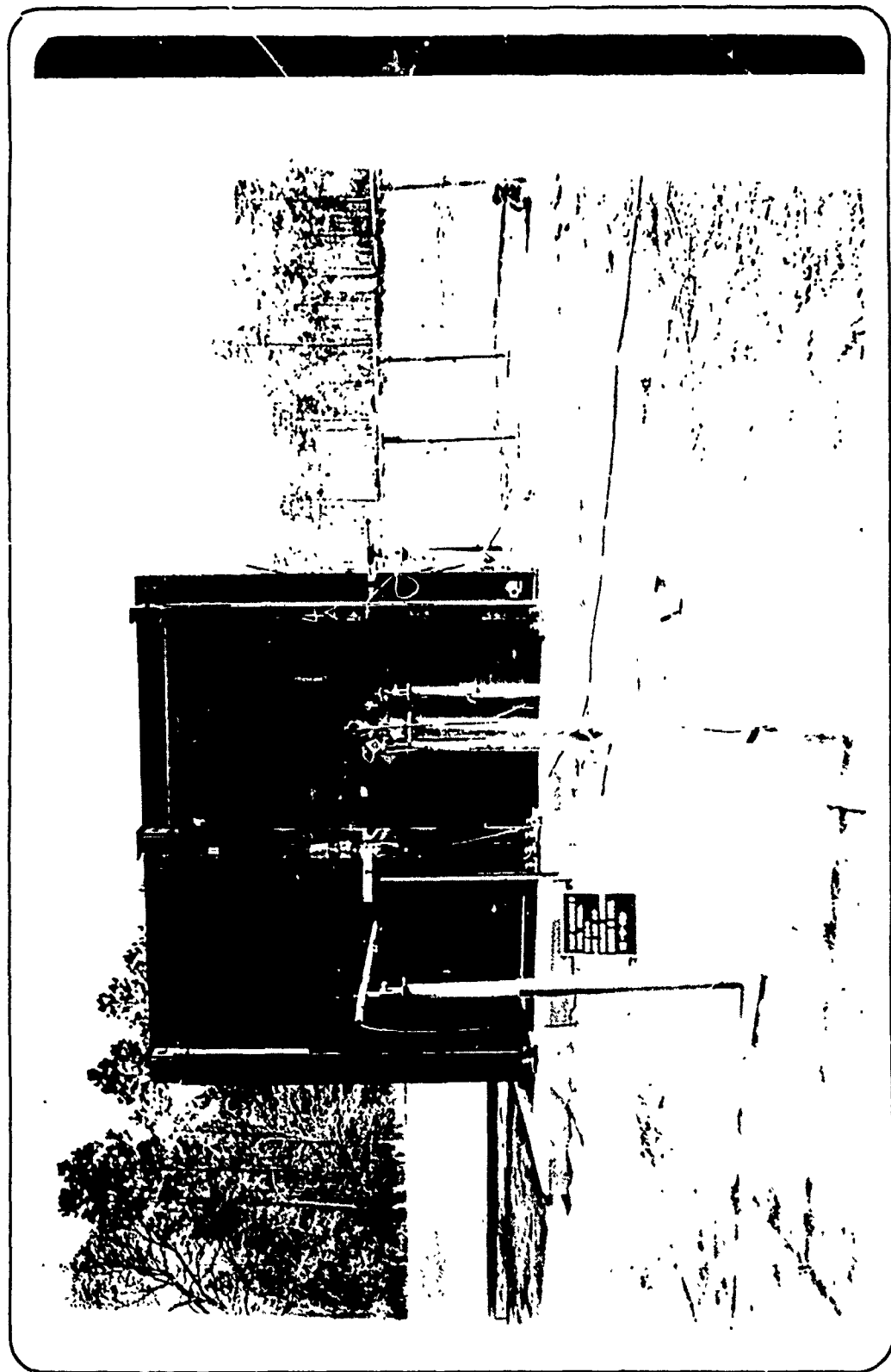
Viewgraph 16

HEAT FLUX AS A FUNCTION OF TIME

Viewgraph 17

298
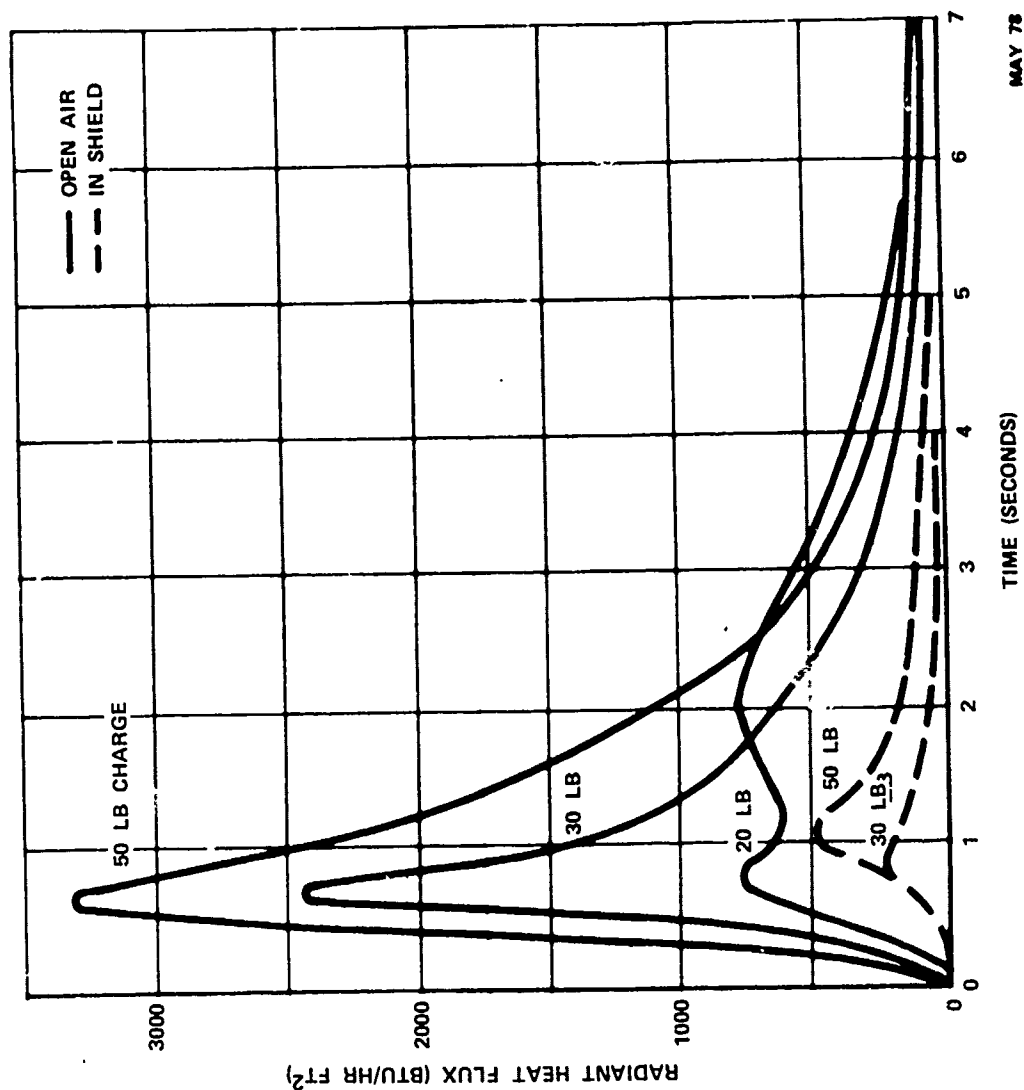
RESEARCH NEEDED

HAZARD DEFINITION

IMPROVED THERMAL SUPPRESSION TECHNIQUES

SUPPRESSED FIREBALL CHARACTERISTICS

    DIAMETER

    BURNING TIME

    RADIANT FLUX

EFFECT OF NON-UNIFORM VENTING

Viewgraph 18

299

Ballistic Research Laboratories (BRL)

1. Major contributor

2. Develop technology in areas of:

   Blast

   Fragmentation

   Thermal

   Structural

NASA National Space Technology Laboratories (NASA-NSTL)

1. Test/fabrication support

2. Obtain applied data from group shields

Naval Surface Weapons Center (NSWC)
(Formerly Naval Ordnance Laboratory (NOL))

1. Technical support in:

   Blast codes

   Structural analysis

Southwest Research Institute (SWRI)
(Contractor)

1. Consultant services

2. Data analysis

3. Model/scaling law development

VIEWGRAPH 19: Applied Technology Participants

TECHNOLOGY FLOW CHART

```
SCENARIO DEFINITION → HAZARD DEFINITION ─┬→ FIREBALL
                                         ├→ FRAGMENT → HAZARD SUPPRESSION ─┬→ FIREBALL SUPPRESSION
                                         └→ BLAST                         ├→ FRAGMENT CONTAINMENT
                                                                          └→ BLAST ATTENUATION → STRUCTURAL LOADING AND RESPONSE → DESIGN SELECTION
```
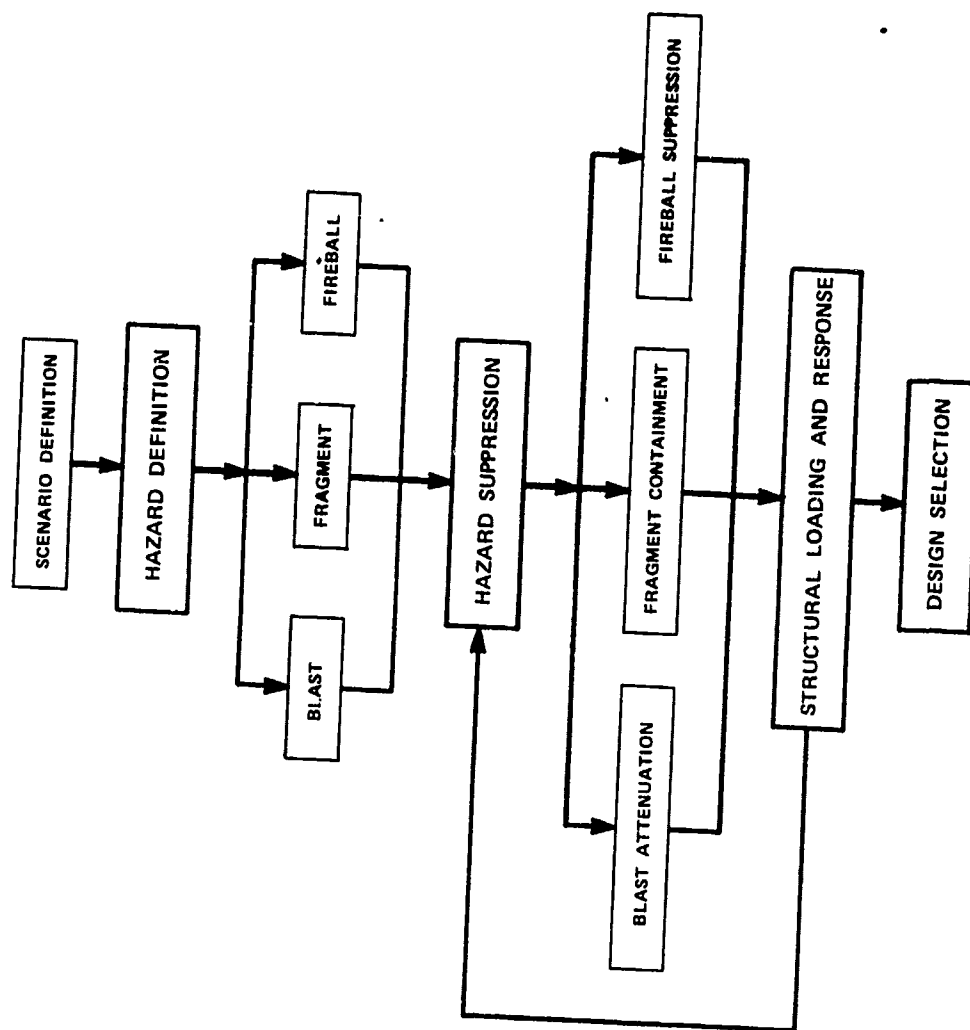
MAY 78

Viewgraph 20

301

SUPPRESSIVE SHIELD

TECHNOLOGY SUMMARY

- NO TECHNOLOGY BARRIERS
- PREDICTIVE CAPABILITY AVAILABLE
- SCALING LAWS APPEAR VALID FOR SMALL EXPLOSIVE CHARGES

Viewgraph 21

302

SUPPRESSIVE SHIELDING ENGINEERING DESIGN HANDBOOK

CHAPTER I,   INTRODUCTION

                              — HISTORY OF THE PROJECT
                              — USE OF HANDBOOK

CHAPTER II,   SAFETY APPROVED SUPPRESSIVE SHIELDS

CHAPTER III,   EXPLOSIVE ENVIRONMENTS

                              — DESCRIPTION AND USE OF APPROVED SHIELDS

                              — METHODS FOR COMPUTATION OF HAZARDS AND
                                  SUPPRESSION

CHAPTER IV,   SUPPRESSIVE SHIELD STRUCTURAL BEHAVIOR

                              — MATERIAL PROPERTIES AND ACCEPTABLE RESPONSE

CHAPTER V,   STRUCTURAL DESIGN AND ANALYSIS

                              — METHODS FOR DYNAMIC STRESS ANALYSIS
                              — DESIGN PROCEDURES

CHAPTER VI,   STRUCTURAL DETAILS

                              — DOORS, PENETRATIONS, LINERS

CHAPTER VII,   ECONOMIC ANALYSIS

                              — METHODS

CHAPTER VIII,   ASSURING STRUCTURAL QUALITY

                              — QUALITY ASSURANCE

APPENDIX

                              — ENGINEERING DRAWINGS OF SAFETY APPROVED
                                  SUPPRESSIVE SHIELDS
                              — ENGINEERING DESIGN CHARTS
                              — SAMPLE ECONOMIC ANALYSIS

Detonating Cord Failure in the F-111
Aircraft Crew Module Escape System

by

E. Eugene Kilmer

Naval Surface Weapons Center
White Oak Laboratory
Silver Spring, Maryland 20910

Abstract: A study was made to determine the cause of
detonation failures which occurred during the
tests of pilot egress systems used in the F-111
aircraft. The problem was associated with flexi-
ble linear shaped charges (FLSC) containing
DIPAM explosive. These "detonating cords" are
used in panels for the self-righting and floata-
tion bag covers. The FLSC tests had been
conducted on panels removed from aircraft after
a 48-month service life changeout. The FLSC
failures that occurred were either non-initiation
of the cord or failure to detonate the complete
cord length.

Cord detonation velocities were measured on
lengths of FLSC's from the F-111 panels. DIPAM
explosive was removed from sections of FLSC and
subjected to chemical analyses. The detonation
velocities measured indicate that the cord
explosive has been compacted to an extremely high
density.

Introduction

The Air Force is currently funding a program with
General Dynamics (GD), Fort Worth, to conduct environmental
tests on explosive components removed from F-111 aircraft.
These components are removed from various fuselage panels
after the 48-month service life changeout. The problem
under investigation at GD pertains to the self-righting
bag covers or panels and the flotation bag cover located
on the crew module. These panels contain assemblies of
flexible linear shaped charge (FLSC) loaded with 10 grains/
ft of the explosive dipicramide (DIPAM) and end boosters
loaded with hexanitrostilbene (HNS). The results of General
Dynamics' testing[1] indicate a problem with detonating cords

not being initiated by the HNS end booster[2] and with propagation-failure along the explosive cord column after initiation. This last condition resulted in a severance of the panel surface for several inches until the detonation stopped in the cord. These types of failures are tabulated in Table 1. General Dynamics had requested the Naval Surface Weapons Center (NAVSURFWPNCEN) investigate this problem by (1) studying these assemblies using chemical analyses on the explosive in the cords, and (2) by measuring the detonation velocity of cord samples removed from the aircraft panels. Previously "failed" hardware was also furnished by General Dynamics from their panel investigation program.

The hardware sent to the NAVSURFWPNCEN included complete panels as removed from the aircraft and sections of panels which had been tested by General Dynamics during their environmental study.

Experimental

The chemical analyses on the DIPAM, which was removed from the cords, were done first by determining the percent (%) DIPAM in the explosive using the Cary 16 Spectrophotometer[3,4]. The analyses should show if impurities exist in the DIPAM. Samples of cords were taken from complete panels and from sections of suspect panels. The explosive in the cords was found to be identical to the reference standard DIPAM. Additional samples of explosives taken from other cords that failed to initiate, gave results which indicate that the explosive is 100% pure DIPAM. A second set of chemical analyses was conducted using the Thin Layer Chromatography[5] (TLC) method. All samples selected show essentially 100% DIPAM purity. The question arose as to whether or not any moisture was present in the cords. The percentage of moisture in an explosive can be determined by the vacuum thermal stability test.[6] The results of this test show that the moisture content is at an acceptable level of 0.035% water (by weight). This presumes all the volatiles were water. Explosive component specifications normally allow 0.3% water by weight to be present in the final loaded hardware product.

Detonation velocity (VOD) measurements were made on sections of FLSC's from full panels. Included were curved portions of the FLSC's and the end booster sections (see Figures 1 and 2). A small HNS end booster was used to initiate each section of FLSC. The HNS booster size was selected so as not to overdrive the FLSC explosive. The VOD assembly consisted of the FLSC intact in the panel section with

ionization probes attached in saw slots cut into the apex
of the FLSC at various distances along the explosive column.
The distances between probes were measured, and the time
of detonation recorded on a Hewlett Packard 5275A time interval
counter. The probes were arranged over the slots in the
FLSC in a manner to select the areas of interest, such as
a curved section and/or straight section.

Photographs of sections which failed on initiation
by end boosters are shown in Figure 3. Some of the cords
failed to support detonation after propagating about two
inches from the point of initiation as shown in Figure 4.

Discussion

It can be seen from the results of the standard
NAVSURFWPNCEN Small Scale Detonation Velocity Test that
the detonation velocity of DIPAM increases with increasing
density (Figure 5). As the density increases, the sensitivity
to shock initiation decreases as shown in Figure 6. The
sensitivity values in this plot were obtained from the NOL
Small Scale Gap Test. Using the relationship between detonation
velocity and density, the data from Figure 5 implies that
the density of the DIPAM in the explosive cord is very high.
This high density, low sensitivity relationship offers an
explanation for the observed failures.

In reviewing the results of detonation velocity
measurements made on FLSC from panels manufactured over
several years, it would appear that between April 1968 and
August 1970, some increase in the detonation velocity occurred
in the product (Table 2). Results from these detonation
velocity measurements indicate problems were beginning to
appear earlier than 1971. The initiation schemes used for
these measurements are shown in Figure 7. The primary
initiating unit was a shielded mild detonating cord (SMDC)
as shown in Figure 7A. Because initiation was not achieved
each time, a larger, more powerful unit, (#6 Blasting cap)
was used as in Figure 7B. Even the blasting cap, in some
instances, was not sufficiently brisant to initiate some
of the FLSC. It was observed in the group of tests under
ID 2291 (Panel prior to 1971 - Table 2), that on one occasion,
the SMDC line would not initiate the FLSC. The failed FLSC
was refit with a blasting cap and retested. The FLSC did
function the full length of the panel segment. The remaining
sections of panel, ID 2291 and 2290, were initiated as in
Figure 7A and performed a cutting operation. A record of
their detonation velocities is shown in Table 2.

The detonation velocities of samples ID 2291, are higher than the heavily confined test units of the Small Scale Detonation Velocity values reported in Figure 5. It is estimated from the curve plotted for a comparable column diameter of DIPAM (0"062) that the density of the DIPAM explosive in the FLSC is approaching crystal density. This implies that high explosives are very difficult to initiate as they approach crystal density. According to Gordon[8], "detonation depends on composition, density, charge diameter and particle size, as well as other less important factors." The limits of detonation to continue propagation can be determined as a function of diameter and density. Due to the limited testing of this work it cannot be determined unequivically whether the high density explosive shifts the system into a marginal or critical density/diameter failure mode. In the case with the blasting cap, it is considered to be possible that the explosive cord was over-driven. The detonation velocity recorded may have been in error due to fading of the detonation wave. This thought seems to be substantiated by the test results shown in Table 3 on sample ID 2329 where the detonation failed after the last ionization probe. Since the measurement of the VOD was made only between two points there was no way to determine the rate of fading. However, the failure in the cord was at a point about two inches from the blasting cap and about one-half inch past the last ionization probe. The NAVSURFWPNCEN findings confirm the cord failures experienced by General Dynamics during the "changeout" and after thermal environmental preconditioning. Results in both Tables 2 and 3 showed that failures occurred in both the preconditioned and non-preconditioned units. This would lead us to believe that preconditioning probably has no effect on the observed failures.

Conclusions

1. The results of chemical analyses of the DIPAM explosive indicate the material had no impurities and was assayed at 100%.

2. The results of the vacuum thermal stability tests indicate the moisture content of the DIPAM removed from the cords was at an acceptable level of 0.035% water (by weight).

3. The thermal environmental preconditioning probably does not affect the performance of the cords.

4. The random failures of the cords to initiate by "over-boostering" with a blasting cap indicates a problem of critical diameter/critical density failure. This is also supported by the findings of a short run-distance prior to detonation failure.

Recommendation

The failure to propagate in a steady state detonation in explosive materials is a recurring problem. A program should be devised to test experimentally the minimum thickness or cross section in the DIPAM FLSC which will support detonation at various explosive densities. From the results of these tests a critical diameter/critical density curve could be generated to ensure a proper performance envelope for this detonating cord.

References

1. Monroe, K. W., "Surveillance and Temperature Aging Program for the F-111 Crew Module Explcsive Devices, Severance Systems - Failure Investigation," Contract SMALC FO4606-74-D-0063, FGT-RK-4324 VI INDEXED, 28 April 1975.

2. Kilmer, E. E. "Heat-Resistant Explosives for Space Applications", _Journal_ of _Spacecraft_ and _Rockets_ Vol. 5, No. 10, 1968, p. 1219.

3. Glover, D. and Kayser, E., "Quantitative Spectrophotometer Analysis of Polynitroaromatic Compounds by Reacting with Ethylenediamine," _Analytical_ _Chemistry_, Vol. 40, 2055, 1968.

4. Wheeler, O. and Kaplan, L., _Organic_ _Electronic_ _Spectral_ _Data_, Interscience Publications, New York, 1956.

5. Stahl, Egon, ed., _Thin_ _Layer_ _Chromotography_, Spring Verlag, New York, 1969.

6. Rosen, A. H. and Simmons, H. T., "Improved Apparatus and Techniques for the Measurement of the Vacuum Stability of Explosives at Elevated Temperatures," NAVORD Report 6629, 12 March 1959.

7. Kilmer, E. E., "Development of a High Temperature Resistant Mild Detonating Fuse," NOLTR 63-258, 1 April 1964.

8. Gordon, W. E., "Detonation Limits in Condensed Explosives," in _Fourth_ _Symposium_ _(International)_ _on_ _Detonation_, 12 October 1965, p. 179-197.

TABLE 1
GENERAL DYNAMICS TEST DATA
SUMMARY OF FAILURES

CK04327–9 AND –10 PANELS
FLOTATION–INSTALLED UNDERSIDE OF AIRCRAFT
10 GRAIN/FOOT FLSC

NUMBER OF		NO. OF FAILURES TO:		PANEL* PRECONDITION TEMPERATURE
PANELS	TESTS	INITIATE AT BOOSTER INTERFACE	PROPAGATE AFTER INITIATION	
10	20	3	1	+200°F
22	44	9	0	–65°F
12	24	1	4	–65°F

*PANELS PRECONDITIONED FOR ONE HOUR AT TEMPERATURE

TABLE 2

DETONATION VELOCITY DATA OBTAINED FROM PANEL INVESTIGATION (AFTER CHANGEOUT)

MANUFACTURING			NSWC IDENT	DETONATION VELOCITY (M/S)			
PANELS MFG PRIOR TO 1971							
LOT	MFG DATE	S/N					
8	4/68	213	ID 2290	7236	7431	7368	7460 (7339)
29	8/70	662	ID 2291	7509 (7260)	FAIL SMDC	7468 NO. 6 BLASTING CAP INIT	7606 (7661)
PANELS FROM 1971 TIME PERIOD							
35	8/71	775	ID 2288	7584	7421 (7461)*	7418 7462	7239 (7143)
39	11/71	875	ID 2289	7151	7470 7465	7260 (7232)	7493 (7362)

*PARENTHESES AROUND DETONATION VELOCITY NUMBERS INDICATES VELOCITY IN ROUNDED CORNERS OF PANELS AS OPPOSED TO THE OTHER VALUES REPORTED ON STRAIGHT SECTIONS

TABLE 3

DETONATION VELOCITY DATA OBTAINED FROM PANEL INVESTIGATION
(AFTER CHANGEOUT + THERMAL ENVIRONMENT)

LOT	MFG DATE	S/N	THERMAL ENVIRONMENT TEMP	NSWC SAMPLE IDENT DETONATION VELOCITY (M/S)
35	8/71	783	200°F	ID 2329 7243*
38	11/71	834	−65°F	ID 2334 FAILURE TO INIT NO. 6 BLASTING CAP
42	7/72	943	200°F	ID 2331 FAILURE TO INIT NO. 6 BLASTING CAP FAILURE TO INIT NO. 6 BLASTING CAP
41	7/72	915	−65°F	ID 2330 7400 7229 ID 2328 7056 7154

*PROPAGATION FAILURE AFTER A 2 INCH RUN
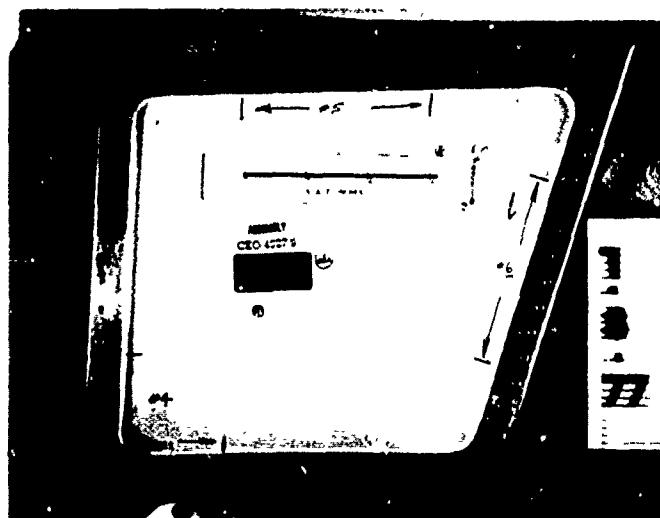
AS REC'D - IDENTIFIED FOR SECTIONING

DIPAM
FLSC
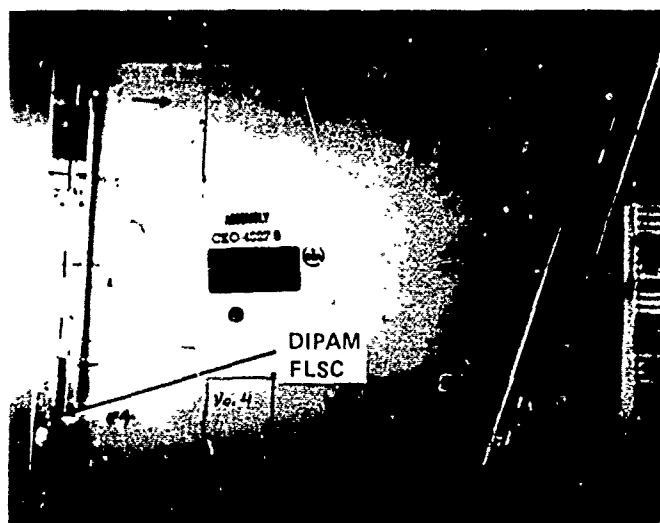
TAPE REMOVED FOR DETONATION VELOCITY PROBES

FIGURE 1 F-111 CKO 4327 PANELS
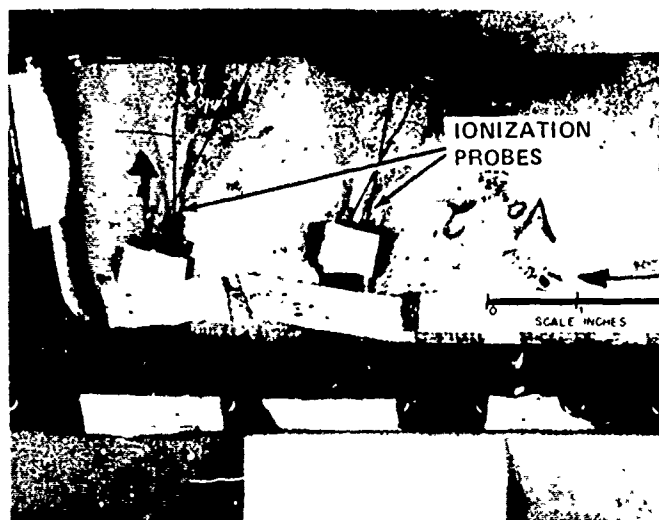
FIGURE 2 SECTIONS REMOVED FOR DETONATION VELOCITY MEASUREMENT

FLSC
REMAINING
(FAILURE)
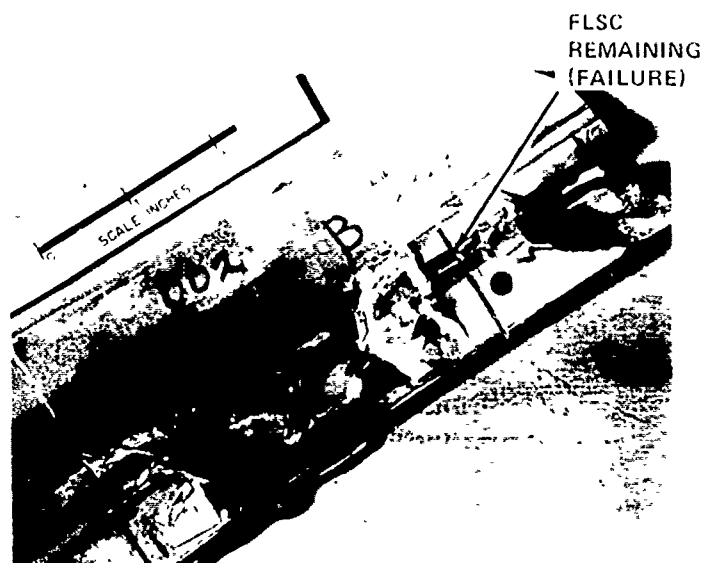
FLSC
FAILURES

FIGURE 3 FAILURES TO INITIATE AT END BOOSTER
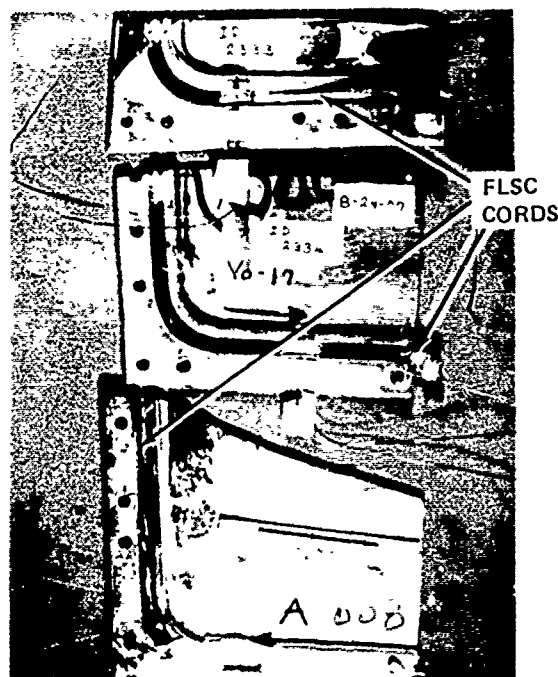
FIGURE 4 FAILURES "IN–LINE" TO SUPPORT DETONATION
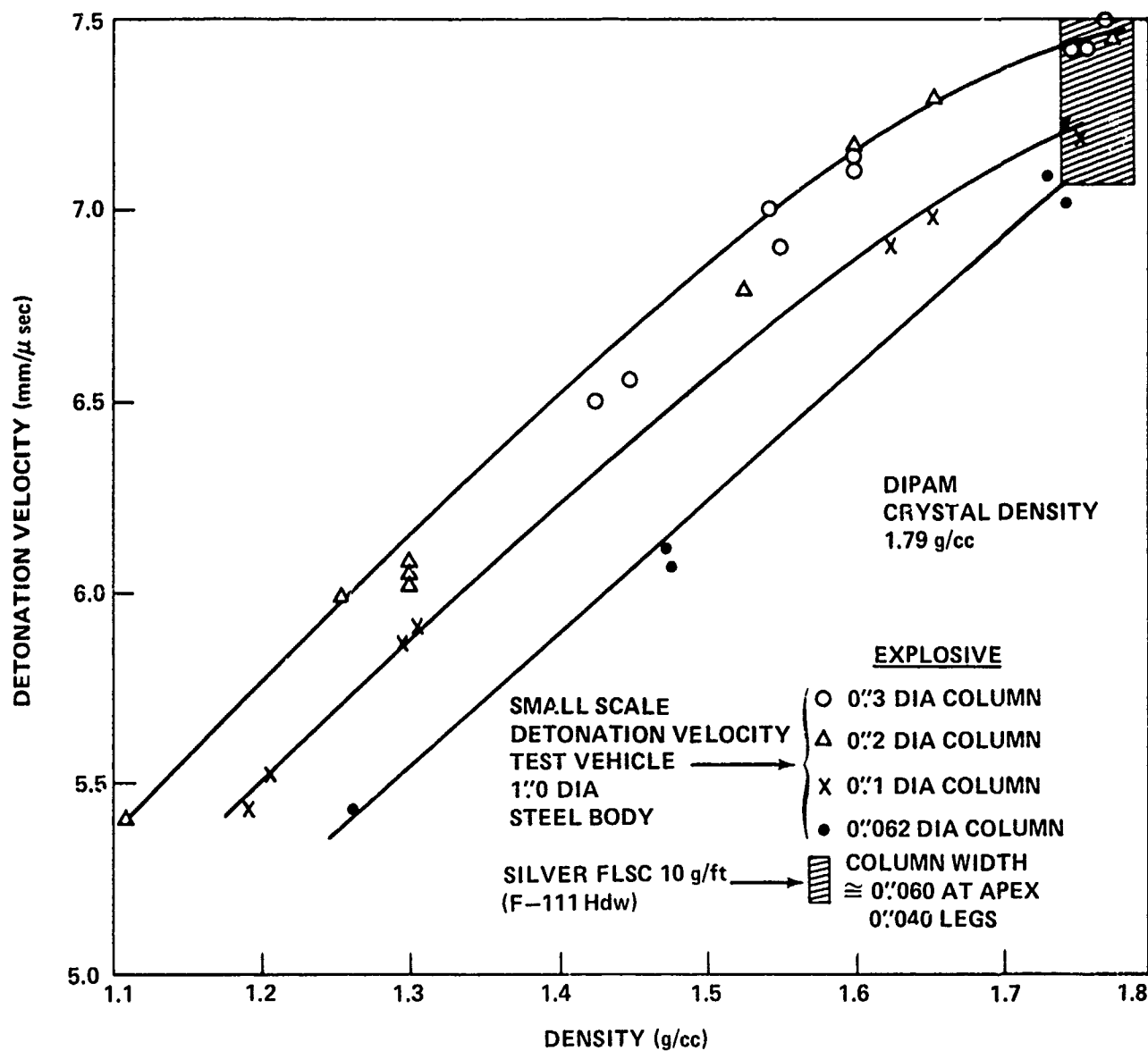
FIGURE 5 THE DETONATION VELOCITY OF A DIPAM SILVER FLSC COMPARED TO
THE SMALL SCALE DETONATION VELOCITY OF DIPAM AS A FUNCTION
OF DENSITY AND COLUMN DIAMETER
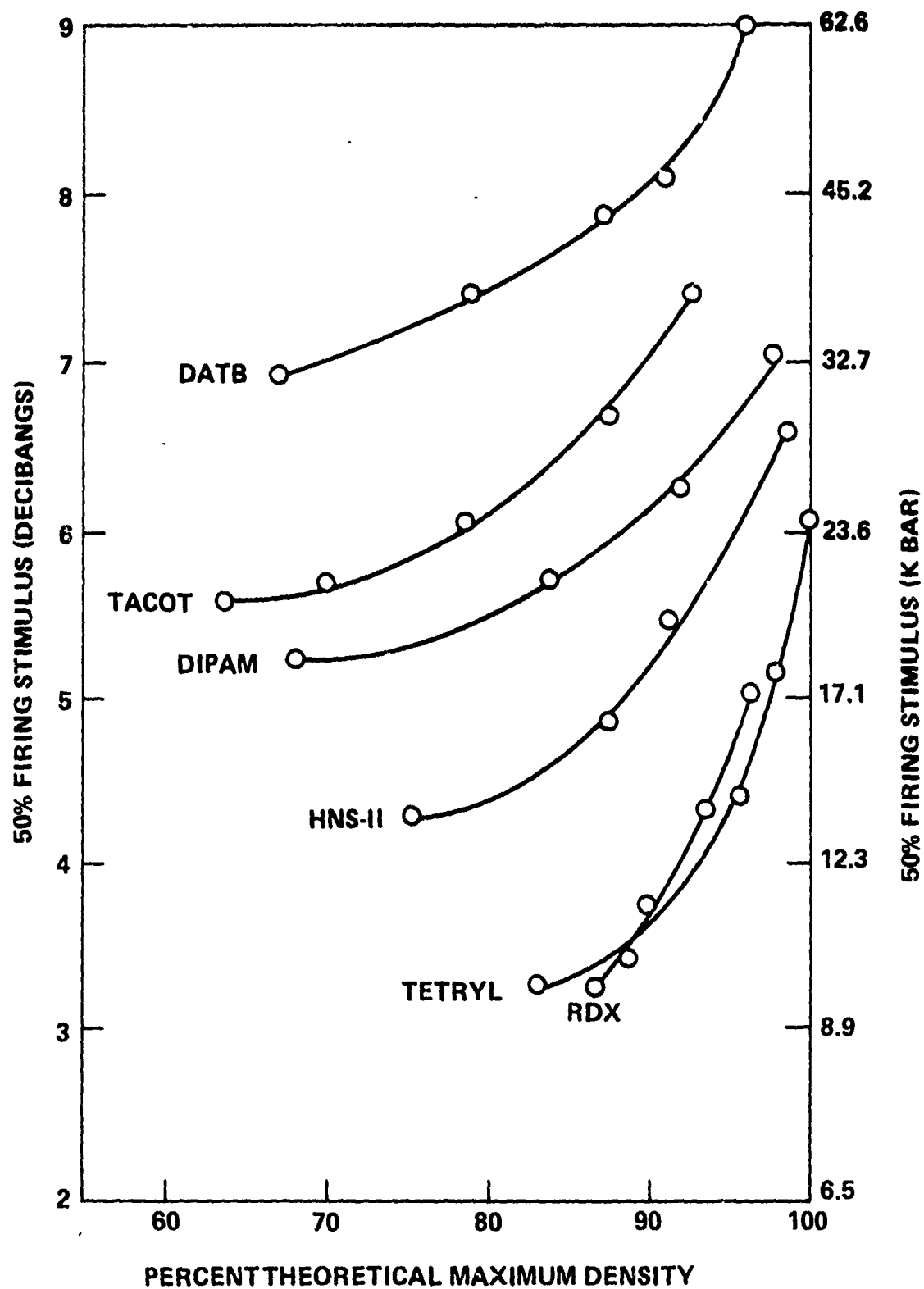
FIGURE 6 SMALL SCALE GAP TEST SENSITIVITY OF DIPAM AND SEVERAL OTHER EXPLOSIVES

318

SEGMENT OF F–111
ALUMINUM PANEL

IONIZATION PROBES
FOR VOD MEASUREMENT

DIPAM FLSC SILVER
(STRAIGHT OR CURVED
SECTION)

PLASTIC
ADAPTER

HNS – BOOSTER TIP
(1 GRAIN HNS–1)

SMDC
LINE

A

HNS – BOOSTER TIP
(1 GRAIN HNS–1)

NO. 6 BLASTING CAP
(4.9 GRAINS PETN)

B
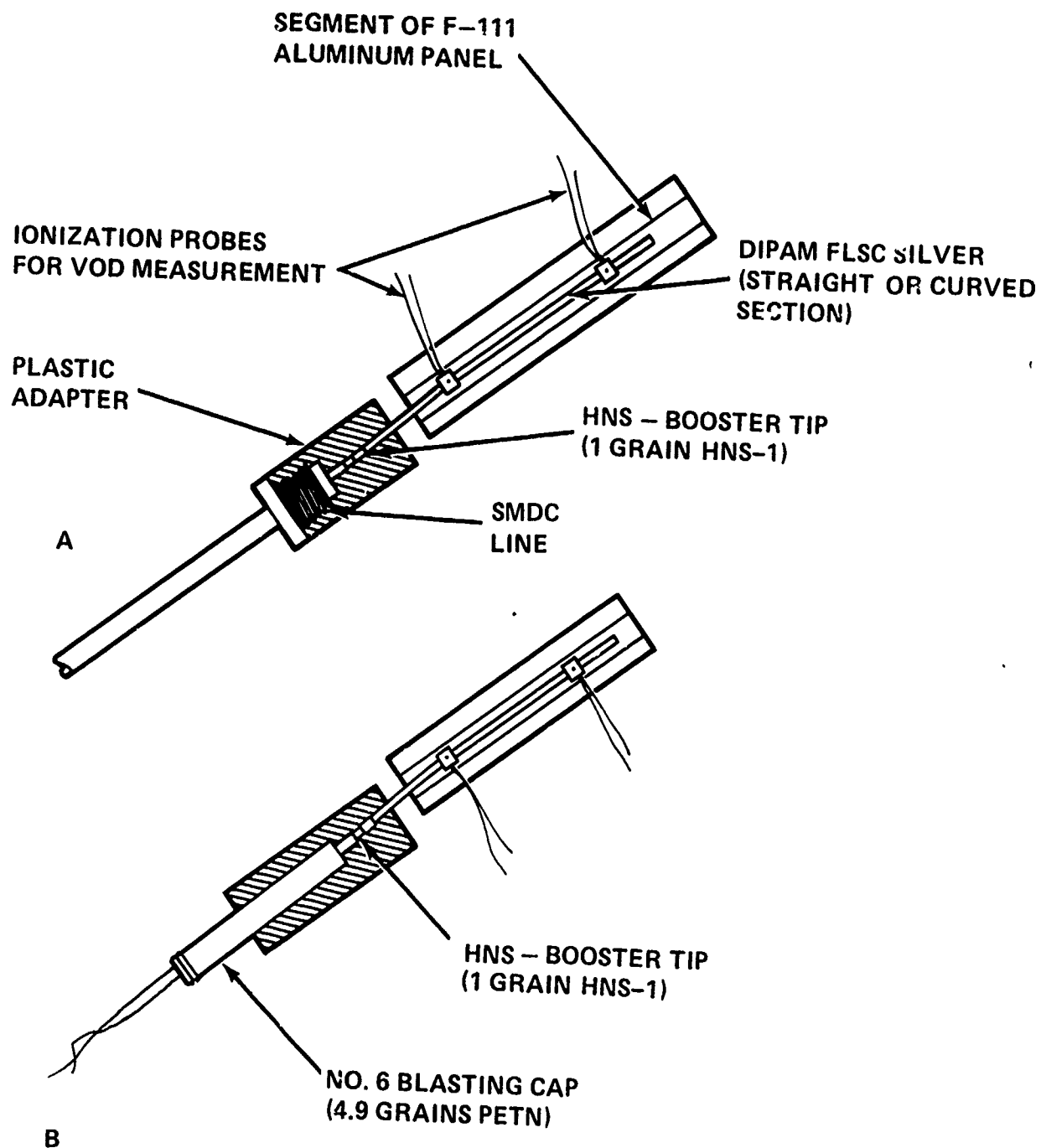
FIGURE 7 TYPICAL TEST SET–UP FOR INITIATION OF DIPAM FLSC

319

PORTABLE TRANSPORTERS FOR EXPLOSIVE PYROTECHNIC COMPOSITIONS

by

D. M. Koger
U. S. Army ARRADCOM
NASA-NSTL
NSTL Station, MS 39529

ABSTRACT

Various methods of suppressing and attenuating the effects of explosive and deflagrating pyrotechnic materials were investigated. The objective of the investigations was the design of lightweight, portable transport cases for use in safely carrying small quantities of explosive materials. Two cases were designed, tested and fabricated. One transporter was for use by the U. S. Army 2nd Infantry Old Guard in carrying 150-grain black powder cartridges; the other for 5-gram samples of a titanium/potassium chlorate composition. Suppression/attenuation materials successfully tested were vermiculite and woven stainless steel wire mesh.

I. INTRODUCTION

The objective of the investigations was the design of lightweight, portable transport cases for use in safely carrying small quantities of explosive materials. Various methods of suppressing and attenuating the effects of explosive and deflagrating pyrotechnic materials were investigated. Two transport cases were designed, tested and fabricated. One transporter was for use by the U. S. Army 2nd Infantry Old Guard in carrying 150-grain black powder cartridges; the other for 5-gram samples of a titanium/potassium chlorate composition. Suppression/attenuation materials successfully tested were vermiculite and woven stainless steel wire mesh. Details concerning the investigations, testing programs, and design criteria for the two transporters are discussed in the following paragraphs.

II. BLACK POWDER TRANSPORTER

A. Background.

The Brown Bess is a muzzle-loaded musket dating from Revolutionary times. It is displayed and fired during demonstrations and ceremonies by the "Commander-In-Chief Guards" of the 2nd United States Infantry (The Old Guard). Fort Meyer, Virginia. Its operation requires black powder cartridges. A cartridge is made of standard bond paper rolled into a 1.3-cm (0.50-in) diameter cylinder 11.4 cm (4.50 in) long, the cartridge wall being four ply. One end is crimped and fastened with cellophane tape. The cartridge is loaded with 9.72 g (150 gr) of FFFg black powder (Index 13-17). The top of the cartridge is crimped by rolling the paper three times toward the longitudinal center of the cylinder and fastening it with cellophane tape.

Sixty Brown Bess cartridges are placed in a container as shown in figure 1 for transportation. The 60-round cartridge container was designed and developed for the specific purpose of rendering the cartridges "incapable of functioning en masse as a result of the functioning of any single cartridge in the container or as a result of exposure to external flame." [Ref. 49CFR 173.100 b (3)]. The container was additionally required to prohibit a massive fire hazard.
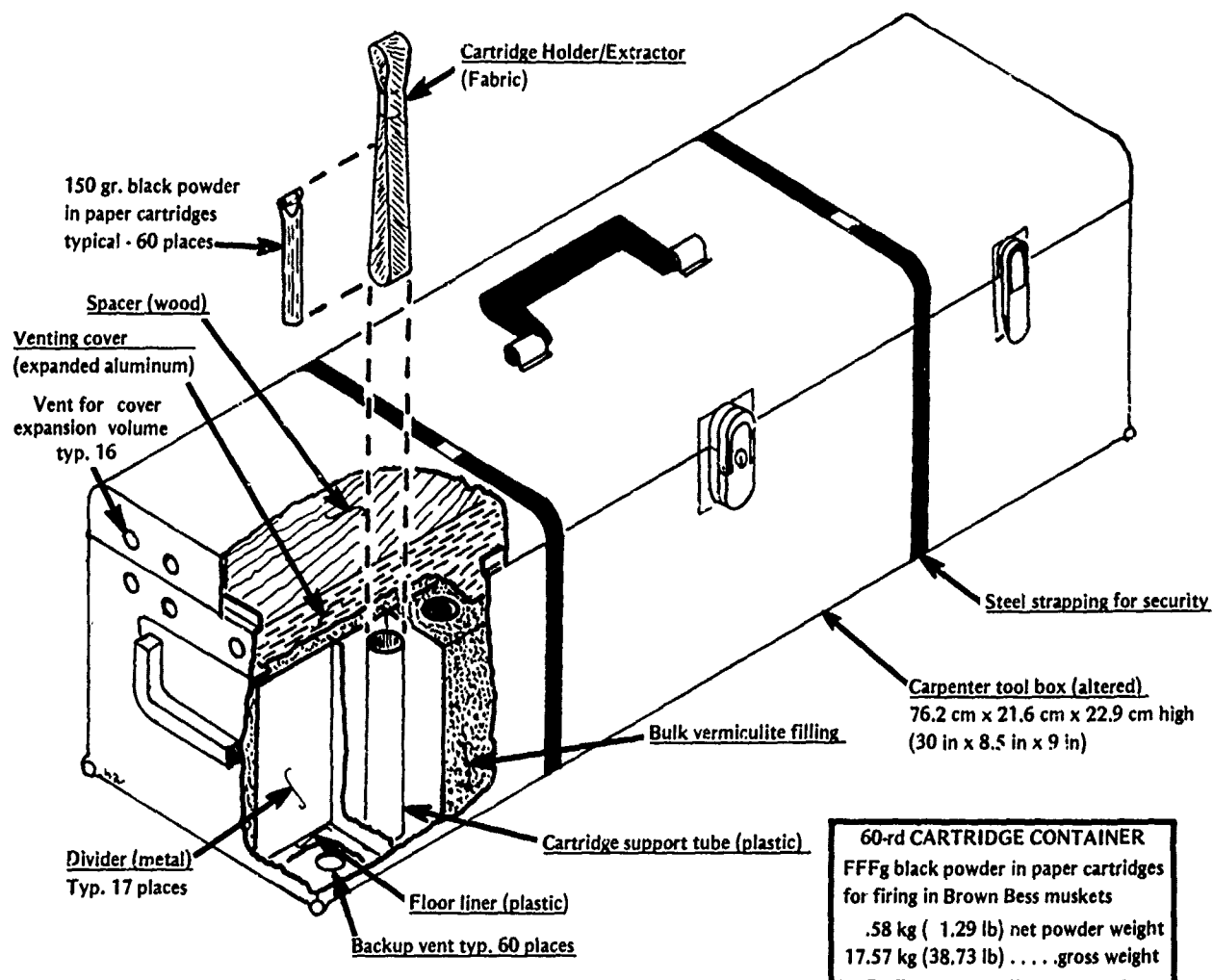
Figure 1. Black Powder Cartridge Container with 60-Round (150 Grains/Round) Capacity.

Figure labels:
- Cartridge Holder/Extractor (Fabric)
- 150 gr. black powder in paper cartridges typical - 60 places
- Spacer (wood)
- Venting cover (expanded aluminum)
- Vent for cover expansion volume typ. 16
- Divider (metal) Typ. 17 places
- Floor liner (plastic)
- Backup vent typ. 60 places
- Cartridge support tube (plastic)
- Bulk vermiculite filling
- Carpenter tool box (altered) 76.2 cm x 21.6 cm x 22.9 cm high (30 in x 8.5 in x 9 in)
- Steel strapping for security

60-rd CARTRIDGE CONTAINER
FFFg black powder in paper cartridges
for firing in Brown Bess muskets
.58 kg (1.29 lb) net powder weight
17.57 kg (38.73 lb) . . . . .gross weight

B. End Item Munition Tests.

Detonation Test "A" was conducted with the Brown Bess cartridges packaged in the 60-round container. A centrally located cartridge was primed with an electric match-head igniter.

The test was conducted five times to demonstrate:

- No propagation between donor and acceptor rounds
- No significant airblast
- No container rupture or fragment dispersion.

Ordinarily, Detonation Test "B" is required when Detonation Test "A" results in propagation between items or container rupture. In the particular case of the Brown Bess cartridge, satisfactory completion of the Detonation Test "A" series precludes conducting the "B" Test.

External Heat Test "C" is intended to simulate a condition wherein packaged end items are completely enveloped in a severe fire. The container was placed in the center of a crib 1.2 m (48 in.) square x 1.1 m (43 in.) high. The interior of the crib was filled with scrap lumber and soaked with (55 gal) of diesel fuel. The fire was ignited on opposite sides of the crib base by two electrical match-head igniters to which 10 grams of UTC 3001 propellant was attached.

External Heat Test "C" was conducted to demonstrate:

- No explosive mass reaction of the cartridges and attendant airblast
- No container rupture or fragment dispersion.

C. Results

1. Detonation Test "A".

The 60-round container of Brown Bess cartridges was subjected to the End Item Detonation Test

321

"A" five times. In each test there was no propagation to another cartridge in the container, significant airblast, container rupture or fragment dispersion. The only outward indications of donor functioning were an audible report and a puff of smoke.

2. Detonation Test "B"

Not required.

3. External Heat Test "C".

The 60-round container of Brown Bess cartridges was subjected to an intense wood and diesel fuel fire, as described in paragraph B, lasting approximately 1 hour. There was no explosive mass reaction of the cartridges, container rupture or fragment dispersion. The first observed round function was at 12.9 min. after ignition and the last at 55.0 min. The mean time to function for all rounds was 33.8 min. with a standard deviation of 9.5 min. (These data compare very favorably with a previous experimental 24-round container which functioned its rounds between 10.8 min. and 19.0 min. with a mean time to function at 14.9, 2.9 min.)

D. Weight.

The weight of the prototype 60-round cartridge container was as follows:

Empty box	14.7 kg	(32.5 lb.)
Vermiculite	2.2	(4.8)
Tare Weight =	16.9	(36.3)
Cartridges	0.7	(1.5)
Gross Weight	16.6 kg	(38.7 lb)

(This weight of 0.29 kg (.65 lb.) per round compares favorably with the experimental 24-round container that weighed 10.0 kg (22.1 lb.) or 0.42 kg (0.92 lb.) per round.

E. Conclusions

The results of these tests on the Brown Bess cartridges in the 60-round container indicate that:

- No propagation occurred within the container when a single round was functioned.
- There was no significant airblast during any of the tests.
- There was no container rupture or fragment dispersion during any of the tests.
- There was no mass reaction of the cartridges during any of the tests.
- The External Heat Test "C" pyre with the loaded 60-round container is no more hazardous to its

surroundings than it would be without the container.

III. MOUND LABORATORY TRANSPORT CONTAINER

A. Background

The Department of Energy Mound Laboratory, operated by the Monsanto Research Corporation at Miamisburg, Ohio, is currently blending a 1:2 mixture of titanium and potassium perchlorate in 100-gram quantities. The mixture is then transferred remotely to a screening apparatus where the material is separated into 5-gram quantities and placed in a 2.2-cm diameter by 2.85-cm Velostat container for later use. A single filled conductive plastic container is then placed into specially constructed aluminum suitcases for transport to line metering stations.

Previous studies by Monsanto Research Corporation have indicated that the aluminum transport case, which vented in the event of initiation, could be improved to enhance the safety protection afforded to personnel who must carry the pyrotechnic material to the metering station. Monsanto Research Corporation, through the Department of Energy, requested that a new design for a transport container be developed and tested.

B. Objective

The objective of this study was to design and test a pyrotechnic transport container that would meet the following specifications:

a. The transport container must weigh less than 4.5 kg (10 lb) when fully loaded.

b. The transport container must hold two 5-gram samples in equally subdivided compartments such that venting does not occur in the event of a pyrotechnic excursion.

c. The outward appearance must show no noticeable defects.

d. The materials of the container must be nonferreous, conductive and nonsparking.

e. The container must meet DoT Regulation 173.88 requirements, and no propagation between sample holders is allowed.

f. The contents inside the container cannot shift during hand transports.

g. There must be no external leakage if the contents are inadvertently spilled.

h. The container must be easily opened, easily cleanable and have a positive closure device.

C. Material

Titanium powder, MIL-T-13405B, with a particle size of less than 44 microns, and potassium perchlorate, MIL-

P-217A, were mixed in a 1:2 ratio by weight to provide the reactant charges for the proof tests. These materials were used as received from Mound Laboratory.

D. Prototype Containers

Prototype models of two types of transport containers were fabricated:

a. a self-contained pressure vessel 15.88 cm high by 23.5 cm in diameter which had an internal volume of approximately 6 liters and weighed 2.18 kilograms;

b. a solid aluminum block, 20.32 cm in diameter and 15.24 cm high, into which cavities were drilled. This fixture weighed approximately 6.35 kilograms. Sketches of the two prototype test figures are shown in figures 2a and 2b.

The self-contained pressure vessel was a modified cast aluminum pressure cooker. The pressure cooker has a built-in pressure relief at approximately 206 kilopascals (kPa) (30 psi) due to the stock neoprene seal. The burst pressure of the container is approximately 414 kPa (60 psi). This fixture directly met design specifications (a), (b), (d), (g) and (h). In addition, the pressure vessel was readily available as an off-the-shelf item with minimal cost. Exploratory tests were conducted in a 4-liter prototype model while all of the certification tests were conducted in the 6-liter model.

The second prototype fixture was machined from a 20.32-cm diameter 6061T6 solid aluminum extruded cylinder. This fixture was designed to hold five each 5-gram pyrotechnic samples in separate compartments and, as such, was designed to withstand a pressure of 2206 kPa (320 psig) without rupture. This design met specifications (c), (d), (f) and (h) of the objectives stated above, but the

extensive machining required made the cost significantly higher. In addition, the finished article weighed considerably more than the 4.5-kilogram desired weight.

During the course of the tests described herein it became apparent that the small Velostat cups that contain samples of the test material could contribute significantly to the test results of the transporters. A variety of sample holders were used during the test series and are shown in figure 3.

Container (a) is a standard 35-mm film container constructed from polyethylene. Container (b) is the Velostat holder originally supplied by Monsanto Research Corporation. Holder (c) is a disposable aluminum weighing dish; a second weighing dish was placed on top to form the lid. Holder (d), a cardboard container with metal bottom and a plastic top, was used to simulate a container with a lower height-to-diameter ratio. Holder (e) is a 1.09 x 6.35 x 1.07 cm plastic box that was used in a similar fashion, and holder (f) is the Velostat container that was specified for use as a result of the test program herein described.

E. Test Arrangement

Four different types of tests were conducted during this program, including (1) initiation of 5- to 10-gram samples in a closed pressure vessel; (2) open-air tests on the Monsanto specimen containers; (3) prototype tests and (4) certification tests.

The closed pressure vessel tests were conducted in a 4-liter modified pressure cooker. The sample material was placed inside the pressure vessel and initiated by a match-head igniter Two strain-gage type transducers were attached to the vessel to measure static pressure. Tests were performed on 5-, 10-, and 15-gram sample sizes.

Open-air tests in the original Monsanto specimen

(a) Self contained pressure vessel.

(b) Aluminum block
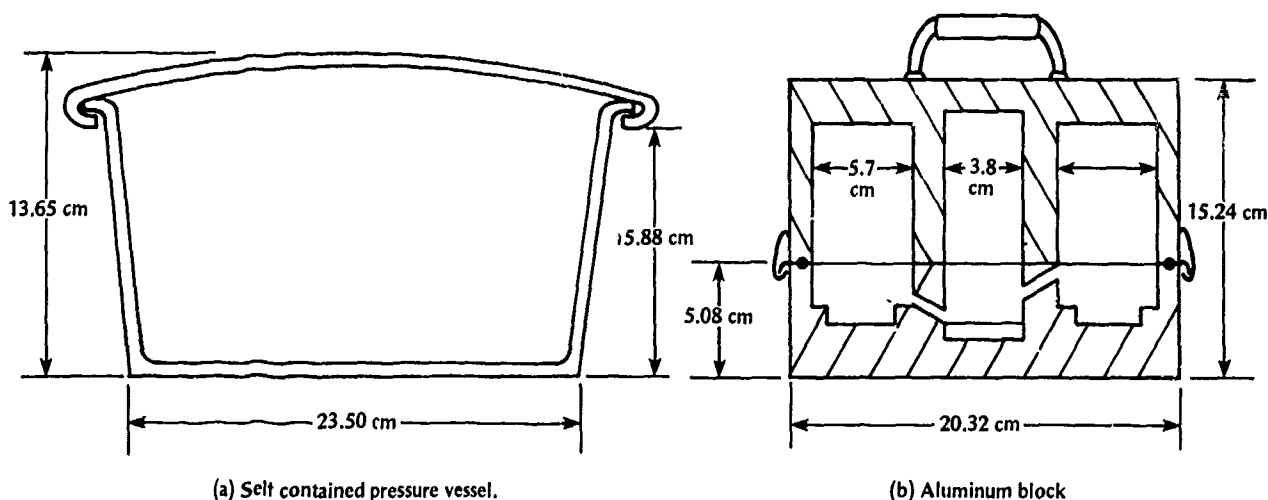
Figure 2. Prototype Transport Case.
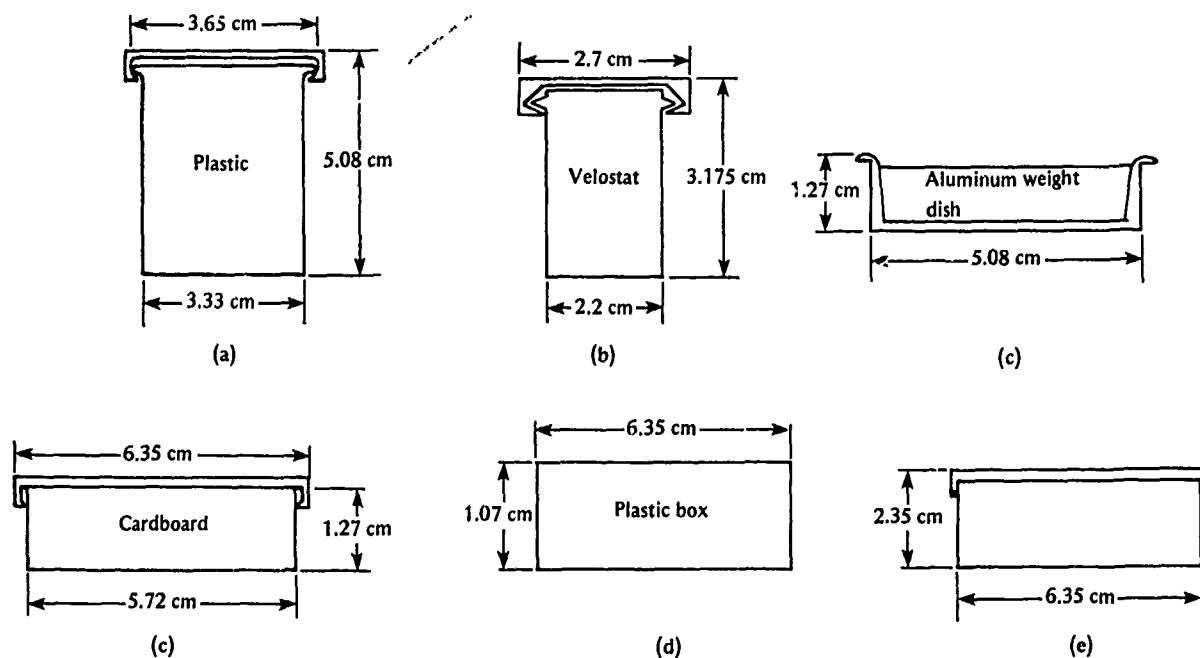
Figure 3. Various Types of Sample Holders Used in the Exploratory and Certification Tests.

container were conducted to determine detonation characteristics as a function of sample geometry. Tests were conducted on 5-, 10-, and 25-gram sample sizes. Two side-on pressure transducers were mounted at ground level on opposite sides of the test setup. Each sample was initiated by a match-head igniter.

Tests were conducted in each prototype model shown in figures 1a and 1b. Sample sizes of 5-, 10- and 15-gram quantities were placed in each container and initiated by a match-head igniter. Static pressure measurements were made using two strain-gage type transducers that were attached to the fixture.

Certification tests were conducted only on the candidate transport container. Specifically, these tests include Detonation Test "A," External Heat Test "C" and a proof test. The Detonation Test "A" is conducted on items which are packaged with more than one item in a standard container to determine if functioning of one item will cause other items in the container to function. The results of the test determine the occurrence of propagation within the container, fragmentation hazards, blast hazards and fire dispersment hazards. This test is conducted a minimum of five times or until communication to adjacent items occurs, whichever is less. For the present case, one of the two samples within the container was primed with a match-head igniter.

The External Heat Test "C" is designed to simulate a condition where containers of explosives or pyrotechnic items are completely enveloped in a hot fire. The container was placed on a crib of sufficient dimensions to hold the container 76.2 cm high. The interior of the crib was filled with combustible material; i.e., scrap lumber, etc. The crib and container to be tested were then covered with additional combustible material sufficient to sustain a hot fire. The entire mass was then saturated with approximately 50 gallons of diesel fuel and ignited in two locations by match-head igniters and 2 ounces of UTC-3001 propellant.

A single destruct test was conducted on the final design configuration. The quantity of sample material was predetermined to be sufficient to cause relief of the pressure developed within the transport container. The test was repeated using the same quantity of material but subdivided into four samples.

F. Discussion

Results of preliminary tests indicated that relatively high static pressures could be expected from initiation of the titanium and potassium perchlorate mixture in closed vessels. To reduce the pressure, vermiculite and stainless steel wool were used to dissipate the heat from the reaction. The test using vermiculite was successful in that no venting occurred, but the pressure generated from a single 5-gram sample indicated that two or more samples could not be ignited in a single transport container without venting.

Later, tests were unsuccessful with respect to suppression, and it was determined that the L/D ratio of the Monsanto sample holder was contributing to detonation rather than deflagration of the mixture. A series of open-air tests was conducted to confirm the hypothesis, and

TNT equivalencies ranging from 14% to 56% were measured. After discussion of this behavior with Mound Laboratory personnel, an alternative sample holder (figure 2c) was specified and used for certification of the final design. The specimen container was also tested in open air to determine the worst-case effects of shifting of the pyromix to one side or being stood on edge. The test results indicated that the new sample holder with an L/D ratio less than one did not cause the sample material to detonate in any configuration. Once the samples were prevented from detonating by control of the L/D ratio, the steel wool was found to be very effective in reducing the pressure within the closed vessels. A test without filler showed a pressure of 469 kPa while three other tests showed an average pressure of 50.6 kPa. The steel wool thus effects a pressure reduction of approximately 85%.

Prototype tests on the machined aluminum block (figure 1b) indicated that very high pressure could be expected within the small chambers, and that design of a simple seal or locking device would not be feasible. In tests of this concept, pressure venting was observed. When two samples were placed inside the container, propagation resulted and venting occurred. Further development of this fixture was terminated and the remainder of the prototype testing was performed in a 6-liter cast aluminum pressure vessel. All of the remaining tests were successful in that there was no venting and propagation was not observed. The use of steel wool as the filler was dismissed because it would be difficult to handle during loading and unloading operations, and could introduce contamination in the form of five pieces of metal into the pyromix during handling. The alternate heat dissipating material chosen was a wire mesh, woven from 0.014-cm diameter type-304 stainless steel wire, with a crimped edge. Rolls of this material were tested and proved to be effective for use with 15 grams of pyrotechnic material in the 6-liter vessel. The pressures observed were on the same order of magnitude for tests using the woven mesh and the steel wool.

Certification and destruct tests were conducted on the 6-liter vessel (see figures 4 and 5.) During the propagation tests no propagation or venting was observed. The proof test was conducted five times with both sample holders being ignited simultaneously during each test; no venting occurred. The destruct test was conducted with a single holder filled with 20 grams of material and ignited by a single match-head igniter. The system vented and there was extensive damage to the transport container lid which broke into three pieces. One fragment of the lid was found 77 meters from the remainder of the container. There was slight sidewall distortion in the test article. This test was repeated using four 5-gram samples, ignited simultaneously, instead of one large sample. There was no explosion nor venting. These results confirm the critical nature of the L/D ratio of the pyrotechnic material.

There was no adverse reaction when the loaded transport container was subjected to the intense heat and flame of the External Heat Test for a period of 30 minutes. No explosion resulted, and there was no evidence that any portion of the test article was ejected from the pyre.

G. Conclusions

- The original Velostat conductive plastic sample holder with an L/D ratio of approximately 1 allows 5-gram quantities of the Ti/KCLO$_4$ mixture to detonate. No detonation results from use of a Velostat sample holder with an L/D ratio of 0.33.
- Wire mesh woven from 0.014-cm diameter type-304 stainless steel wire effectively dissipates the heat generated by the reaction of the titanium and potassium perchlorate such that the pressure generated inside a 6-liter transport container is reduced to a safe, acceptable level.
- The final design of the pyrotechnic transporter passed all proof tests and meets the design criteria for in-plant transportation of two 5-gram samples of the pyrotechnic composition, with a safety factor of approximately two.
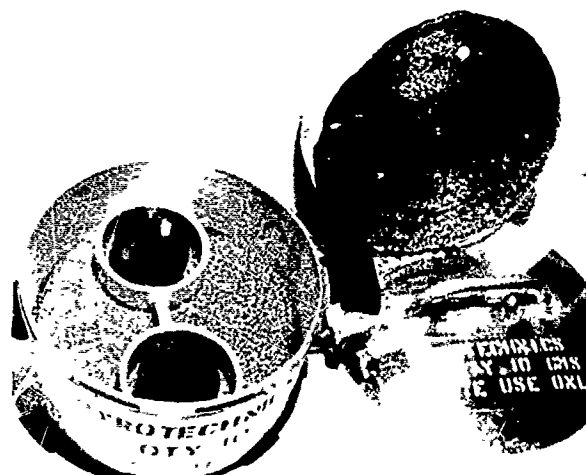
Figure 4. Pyrotechnic Sample Carrier Showing Interior with Two Sample Cups. Upper Stainless Steel Mesh Insert Is Shown Removed (Right).
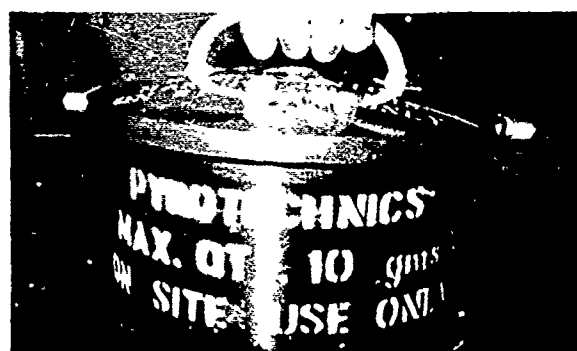
Figure 5. Pyrotechnic Sample Carrier in the "As Used" Configuration.

SAND78-0211

Load Cell Testing of $TiH_x/KClO_4$ Pyrotechnic Actuators*

Morton L. Lieberman
Sandia Laboratories
Albuquerque, New Mexico 87185

ABSTRACT

A load cell test has been utilized to characterize ignition time, function time, and pyrotechnic output of $TiH_x/KClO_4$ loaded actuators. Pyrotechnic material parameter variations include (a) fuel and oxidizer particle sizes for 33/67 $TiH_{0.65}/KClO_4$, (b) fuel/oxidizer ratio for $TiH_{0.65}/KClO_4$, and (c) fuel/oxidizer ratio for $TiH_{0.2}/KClO_4$. Generally, the ignition time increases and exhibits increased variation with increasing fuel/oxidizer ratio and particle size. The effect is more pronounced in the materials containing $TiH_{0.65}$ than those containing $TiH_{0.2}$. Pyrotechnic output, expressed as impulse per unit mass of pyrotechnic, and function time minus ignition time are constants within experimental error and are independent of the material parameter variations. The results are interpreted in terms of the chemical and physical phenomena occurring during load cell testing.

INTRODUCTION

A major effort is underway to develop pyrotechnic and explosive components which have a high degree of inherent safety. One area that has received considerable attention is the development of pyrotechnic actuators for valve applications [1]. Safety improvements in such devices are based largely on the use of spark insensitive $TiH_x/KClO_4$ pyrotechnic blends. In the present study, effects of pyrotechnic material variations on actuator performance are examined.
A variety of output tests had been established [2] prior to the development of the load cell test by Steele, Allen, and Montoya [3]. One common test of pyrotechnic output consists of firing actuators in a fixed free-volume pressure bomb and monitoring the

---

resultant pressure. This procedure may not be suitable for assessing valve performance, however, because such an application involves an increasing free volume condition. For slow burning pyrotechnics, in particular, such a test yields results which are not necessarily relevant to valve performance. At the time an output test was required, the pyrotechnic under development was $TiH_{1.9}/KClO_4$, a slow-burning material. Consequently, this procedure was regarded as unsuitable.

Other methods involve measuring the velocity of a projectile after it departs from its housing and is in free flight. These include the ballistic pendulum, photo-cell chronograph, and magnetic chronograph [2]. All have the same disadvantages relative to valve performance, namely, (a) the gas is vented prior to the measurement of velocity, (b) the resistance-after-fire cannot be measured because the gas is vented, and (c) the slow-burning pyrotechnic may not be completely burned prior to venting.

As a result of these deficiencies, Steele, Allen and Montoya [3] developed a load cell test to simulate valve conditions. Salient features include (a) variable gas free volume, from virtually zero to that of a stroked valve, (b) interference fit between housing and piston to simulate a valve and prevent venting, which permits measurement of resistance-after-fire, (c) piston mass comparable to that employed in a valve, (d) use of crush cone to simulate cutting of tubes in a valve, and (e) incorporation of a beryllium-copper disc between the piston and actuator to simulate the disc welded into the valve to permit its leak testing. The load cell test is now being used in development and as a production tester. It has been used to generate all of the actuator performance data given in this paper.

EXPERIMENTAL

The load cell test fixture is shown in Figure 1. The various components are described as follows: Part 9 is a Sunstrand Model 912 quartz load cell which is a force-sensing device. Part 6 is a transducer anvil, composed of tool steel, which is threaded into the load cell until its bottom surface reaches the top surface of the load cell. Part 5 is a brass (half hard, composition 22) crush cone which is placed on the transducer anvil. Generally, a thin un-defined layer of silicone grease is placed between these components. Part 4 is a drill bushing (American Drill Bushing Co., drill bushing P26-16) with an enlarged inner diameter in the lower portion (not shown in Figure 1) and modified such that the end surfaces are flat, smooth, and parallel. The piston (part 4, tool steel) is pressed into the bushing such that an interference fit exists over a small fraction of its length. The top of the piston is even with the top of the bushing. A beryllium-copper disc (part 8) lies on this assembly. The actuator (not shown) is screwed into part 1 to a fixed torque of 16.9 N-m (150 lb-in) which results in its leading edge causing an indentation in the beryllium-copper disc. Parts 1, 2 and 3 are assorted steel assembly fixtures.

Tests are performed in the configuration shown in Figure 1, i.e., the piston travels in a vertical, downward direction. Dimensions are given in Figure 2. In addition, it should be noted that the piston-crush cone separation is 3.56 mm and the beryllium-copper disc thickness is 0.254 mm.

Initiation time of the pyrotechnic material is determined from the bridgewire resistance by means of a Biomation waveform recorder. It corresponds to the condition of self-heating or thermal run-away. Bridgewire break time is also determined from the bridgewire resistance by the waveform recorder. Function time is defined as the period between application of the bridgewire pulse and initial response of the load cell transducer; it is determined by an independent electronic time interval counter.

All of the tests performed in this study utilized SAD-1031 actuators which were loaded flush to the top of the charge holder in two, nearly equal, powder increments at 76 MPa (11 Kpsi). The pyrotechnic materials used are described in Tables 1 and 2. A nominal fire pulse of 3.5 A was employed. The measured length of the crush cone following the test served as an independent, passive measure of pyrotechnic output.

RESULTS

The effects of three different material parameters on acutator performance have been assessed. The parameters are (a) particle size in 33/67 $TiH_{0.65}/KClO_4$, (b) fuel/oxidizer ratio in $TiH_{0.65}/KClO_4$, and (c) fuel/oxidizer ratio in $TiH_{0.2}/KClO_4$. Establishing these as independent variables, while maintaining constant charge holder volume and loading conditions, implies that the mass of pyrotechnic loaded is a dependent variable. The variation in the mass loaded as a function of pyrotechnic material is shown in Table 2. For the $TiH_{0.65}/KClO_4$ blends, the mass is maximized at a fuel/oxidizer ratio of 33/67 and for the small fuel/large oxidizer (S/L) particle size condition. For the $TiH_{0.2}/KClO_4$ blends, the mass of the 36/64 mixture is considerably greater than the others.

Consider the effect of particle size on output (Table 3). For the L/L, L/S, and S/L conditions the output, as measured by peak force, total impulse, and length of crush cone, is virtually constant. This implies that potential differences in burn rate associated with the different particle sizes do not have any apparent effect on output, as determined from the load cell tests. The same measures of output, however, indicate that the S/S condition produces a lesser yield. This is due, at least in part, to the fact that the mass of pyrotechnic loaded in the S/S case is also reduced. For purposes of comparison, it is desirable to examine the specific impulse, rather than the total impulse. Then it can be seen that the average specific impulse for the S/S condition is within 6% of the average value obtained for the other conditions. Such results imply that

the main effect of particle size over the range considered on output is simply to affect the mass of pyrotechnic material that can be loaded into the actuator under constant loading conditions.

Now consider the effect of particle size on characteristic times (Table 4). The S/S condition yields the shortest initiation (ignition), bridgewire break, and function times. The S/L and L/S conditions yield comparable times, which are slightly longer than those obtained for the S/S condition. The L/L condition yields considerably greater times. As these characteristic times increase, the scatter in the data increases (the reproducibility decreases). Note, however, that the variations of particle size have no significant effect on $t_{BB} - t_I$ or $t_F - t_I$.

The effect of fuel/oxidizer ratio of $TiH_{0.65}/KClO_4$ pyrotechnics on output is shown in Table 5. No significant variation is observed in peak force, total impulse, length of crush cone, or specific impulse. The values obtained are comparable to those obtained for 33/67 $TiH_{0.65}/KClO_4$ pyrotechnics of various particle sizes (Table 3).

Characteristic times for $TiH_{0.65}/KClO_4$ pyrotechnics of differing fuel/oxidizer ratio are given in Table 6. With increasing ratio, the initiation, bridgewire break, and function times increase. The extent of the increase in characteristic time per unit increase in fuel/oxidizer ratio is clearly non-linear, becoming more pronounced as the latter rises. Values of $t_{BB} - t_I$ appear to increase smoothly with increasing ratio, except for the unusually high value obtained in test L-202. No significant variation is observed in $t_F - t_I$. The short ignition time in test L-172 was associated with a high bridgewire resistance at the time of fire. An unexplained ignition delay was experienced in test L-185; Table 5 shows that the delay had no apparent effect on the resultant output.

The effect of fuel/oxidizer ratio of $TiH_{0.2}/KClO_4$ pyrotechnics on output is presented in Table 7. The output of the 43/57 blend, as measured by peak force, total impulse, and length of crush cone, is clearly lower than that of the other materials. Specific impulse values for the $TiH_{0.2}/KClO_4$ blends are relatively constant and comparable to those obtained for the $TiH_{0.65}/KClO_4$ pyrotechnics. The range of average specific impulse values obtained as a function of the material parameters is given by 4.41 ± 0.24 mN - s/mg.

Characteristic times of the $TiH_{0.2}/KClO_4$ materials, given in Table 8, follow the same qualitative trends exhibited by the $TiH_{0.65}/KClO_4$ pyrotechnics. Initiation, bridgewire break, and function times increase with increasing fuel/oxidizer ratio. The parameter $t_{BB} - t_I$ increases smoothly, and $t_F - t_I$ appears relatively constant. A comparison of Tables 6 and 8 shows that the materials incorporating $TiH_{0.2}$ have shorter characteristic times than those with $TiH_{0.65}$.

Chemical Considerations

The driving force exerted on the piston is the pressure produced by combustion of the pyrotechnic. Consequently, an analysis of the combustion chemistry of the various blends (Table 5) should relate to the resultant output. A simple analysis can be performed by assuming that the reaction products are only TiO_2, Ti, KCl, H_2O, O_2, and H_2. Prior [4] and current [5, 6] work imply that this yields a reasonable approximation of the thermodynamically calculated equilibrium gas compositions under relevant combustion conditions (assumed to be 2000-5000 K and 1-5 Kbars).

Tables 9 and 10 give the calculated reaction compositions for the various blends. In all cases TiO_2 is the major product of reaction. Detailed thermodynamic calculations [6] imply that at equilibrium virtually all of the TiO_2 and Ti, as well as most of the KCl are in condensed phases. This suggests that the gas pressure results primarily from H_2O, O_2, and H_2. Such a condition implies that the total number of moles of these three products (Σ Products-TiO_2-Ti-KCl) should be a measure of the gas pressure. (The total can be considered proportional to the gas pressure if non-ideality of the gas and differences in combustion temperatures are neglected.) For the blends considered, the total number of moles of these three products varies by a factor of 5.5. Recall, however, that the measured specific impulse for these blends was found to be a constant; i.e., the experimental value did not reflect any significant variation of the gas pressure.

Consider now the condition in which all of the KCl is assumed to be gaseous. Here the total number of moles of gas (Σ Products-TiO_2-Ti) varies by a factor of 2. Even in this extreme condition, the variation in the total is considerably greater than that of the specific impulse.

The major conclusion to be drawn from this section is that the simplistic chemical analysis does not satisfactorily correlate with the output data. Other parameters that can affect the pressure exerted on the piston during its displacement can be cited. These include combustion, condensation, and secondary reaction rates, combustion temperature, colloidal effects, and non-ideality of the gas. Additional work is in progress to address such factors in greater detail.

Sequence of Events

In this section, consideration is given to the total sequence of events from imposition of the bridgewire pulse to initial response of the quartz transducer. The sequence can be represented by the equation

$$t_F = t_I + t_B + t_P + t_X ,$$

where

t_F = time between bridgewire pulse and initial response of transducer,

t_I = time between bridgewire pulse and initiation,

t_B = time between initiation and complete combustion of pyrotechnic material,

t_P = time required for piston to travel piston-cone separation distance,

and

t_X = other sequential times, possibly including times required to sever closure and shearing discs.

Note that such an equation treats the events as occurring sequentially only.

Load cell tests yield values of t_F and t_I and VISAR measurements yield t_P. Values of t_B are obtained from burn rate studies. In order to calculate values of t_X, data have been used that have been generated under similar, but not identical, conditions; i.e., t_P determined for 33/67 $TiH_{0.65}/KClO_4$ and 33/67 $TiH_{0.2}/KClO_4$ in SAD-1031 actuators loaded with pyrotechnic masses of 115 mg and 107 mg, respectively, and t_F and t_I determined for the same materials in SAD-1031 actuators loaded as described in Table 2, or XMC-3004 actuators loaded with 100 mg of 33/67 $TiH_{0.2}/KClO_4$.

Evaluation of t_X has been limited to the 33/67 blends of $TiH_{0.65}/KClO_4$ and $TiH_{0.2}/KClO_4$ by the available data. For the former material, an extrapolated value of t_B is 0.01 ms [7], in agreement with other considerations [5]. A comparable, or somewhat shorter, time is expected for the latter pyrotechnic. Values of $t_F - t_I$ and t_P for the former material are 0.09 - 0.10 ms and 0.06 ms, respectively; comparable values for 33/67 $TiH_{0.2}/KClO_4$ a·· 0.09 ms and 0.05 ms, respectively. Thus, values of t_X for 33/67 blends of $TiH_{0.65}/KClO_4$ and $TiH_{0.2}/KClO_4$ are 0.02 - 0.03 ms and 0.03 ms, respectively. If comparable values of t_P and t_B are assumed for the other pyrotechnic materials considered in this study, it is found that t_X has a positive value in all cases. This implies that a period of time elapses between the conclusion of combustion and the initial motion of the piston. From the viewpoint of modeling, this condition is attractive because it means that the driving force acting on the piston can be treated simply as a gas expansion. Negative values of t_X would imply that combustion and piston motion are concurrent, rather than sequential, processes.

CONCLUSIONS

The effects of the pyrotechnic material variations on actuator performance can be summarized as follows:

1. Variations in output are primarily a reflection of variations in the mass of pyrotechnic loaded.

2. The specific impulse is virtually constant and equal to 4.41 ± 0.24 mN-s/mg.

3. Initiation time increases ahd exhibits increasing variation with increasing fuel/oxidizer ratio and particle size.

4. For constant fuel/oxidizer ratios, the $TiH_{0.65}/KClO_4$ blends exhibit greater initiation times than the $TiH_{0.2}/KClO_4$ blends.

5. The sensitivity of the initiation time to fuel/oxidizer ratio is greater in the $TiH_{0.65}/KClO_4$ blends than in the comparable ones containing $TiH_{0.2}$.

Analysis of the data imply the following:

1. A simplistic chemical treatment of combustion cannot account for the observed output measurements.

2. Combustion is complete prior to motion of the piston.

REFERENCES

1. E. A. Kjeldgaard, "Development of a Spark Insensitive Actuator/ Igniter", Proc. 5th Intl. Pyro. Seminar, July 12-16, 1976, Vail, Colorado, p. 260.

2. L. N. Tallerico, "Magnetic Chronograph Technique for Evaluating Actuators", Sandia Laboratories, Report SCL-DR-67-62, September, 1967.

3. B. R. Steele, L. C. Allen, and A. P. Montoya, Sandia Laboratories, unpublished work.

4. J. W. Reed and J. L. Ivey, "Thermodynamics of Initiation of the $TiH_x/KClO_4$ Pyrotechnic Composition", Proc. 5th Intl. Pyro, Seminar, July 12-16, 1976, Vail, Colorado, P. 443.

5. M. L. Lieberman and K. H. Haskell, Sandia Laboratories, Report in preparation.

6. M. L. Lieberman, A. B. Donaldson, and M. L. Carnicom, Sandia
    Laboratories, unpublished work.

7. A. B. Donaldson, Sandia Laboratories, personal communication of
    unpublished data.

ACKNOWLEDGEMENTS

Table 1

Characterization of Particles

Material[*]	Identification	Surface Area[+] m^2/g	Particle Size Distribution[+] 25%	50%	75%
$TiH_{0.65}$	QC 1829, QC 1787	1.0	≤ 1.5	≤ 2.5	≤ 1.0
$TiH_{0.65}$ (S)	QC 1831	1.69	0.75	0.99	1.4
$TiH_{0.65}$ (L)	QC 1831	0.85	1.4	1.8	2.8
$TiH_{0.2}$	J4705A	9-10	--	--	--
$KClO_4$	L-MD-3	0.25-0.30	3.5 ± 1	4.5 ± 1	7.0 ± 1
$KClO_4$ (S)	QC 1759	0.61	2.6	4.0	5.3
$KClO_4$ (L)	QC 1759	0.19	8.4	14.0	18.0

[*]Physical separation of material yielded small (S) and large (L) particle sizes.

[+]Surface areas and particle size distributions were obtained from BET (Kr for $KClO_4$, N_2 for other materials) and Coulter counter measurements, respectively.

Table 2

Pyrotechnic Blends Loaded in Actuators

Blend	Identification	Mass Loaded,[*] mg
30/70 $TiH_{0.65}/KClO_4$	MM-77-125	114.0 - 116.1
33/67 $TiH_{0.65}/KClO_4$	MM-77-122	118.1 - 119.2
36/64 $TiH_{0.65}/KClO_4$	MM-76-100	115.2 - 117.9
39/61 $TiH_{0.65}/KClO_4$	MM-76-102	115.2 - 117.0
42/58 $TiH_{0.65}/KClO_4$	MM-76-103	117.5 - 117.9
33/67 $TiH_{0.65}$ (L)$/KClO_4$ (L)	MM-77-113	114.3 - 117.0
33/67 $TiH_{0.65}$ (L)$/KClO_4$ (S)	MM-77-114	112.8 - 114.0
33/67 $TiH_{0.65}$ (S)$/KClO_4$ (L)	MM-77-115	119.4 - 120.3
33/67 $TiH_{0.65}$ (S)$/KClO_4$ (S)	MM-77-116	110.7 - 111.7
33/67 $TiH_{0.2}/KClO_4$	MM-76-118	101.0 - 102.3
36/64 $TiH_{0.2}/KClO_4$	MM-76-109	117.5 - 119.7
39/61 $TiH_{0.2}/KClO_4$	MM-76-108	97.8 - 102.3
43/57 $TiH_{0.2}/KClO_4$	MM-76-110	98.0 - 100.4

[*]Values for actuators used in this study only.

334

Table 3

Effect of Particle Size on Output Parameters for 33/67 $TiH_{0.65}/KClO_4$

Serial or Test No.	Fuel/Oxidizer Particle Sizes[+]	Peak Force KN	Time to Peak μs	Impulse to Peak mN-s	Pulse Width μs	Total Impulse mN-s	Specific Impulse[++] mN-s/mg	Length of Crush Cone mm
L-30*	L/L	18.48	42.6	453	51.2	542	4.74	5.33
L-31*	L/L	15.23	43.8	404	52.6	474	4.08	5.84
L-32*	L/L	19.23	35.0	368	47.8	528	4.51	5.41
					Avg.	515	4.44	
L-45	L/S	16.25	44.6	397	53.2	470	4.17	6.05
L-46	L/S	17.28	40.0	361	53.4	507	4.46	5.59
L-47	L/S	18.31	35.0	371	47.2	521	4.57	5.46
					Avg.	499	4.40	
L-60	S/L	21.38	33.2	391	45.8	567	4.71	5.28
L-61*	S/L	17.07	42.6	373	53.0	490	4.08	5.59
L-62	S/L	18.99	38.2	377	49.6	519	4.35	5.41
					Avg.	525	4.38	
L-75	S/S	16.46	38.6	330	50.8	460	4.13	5.84
L-76	S/S	15.40	38.8	337	52.2	473	4.23	5.84
L-77	S/S	15.35	41.6	349	51.8	442	3.99	5.79
					Avg.	458	4.17	

[+]Quantitative descriptions of the materials are given in Table 4.

[++]Specific impulse is defined as the total impulse divided by the mass of pyrotechnic material.

*Leaked; such data have not been disregarded because no evidence has been found to suggest that leaking has any effect on the measured values. This implies that leaking is insignificant through the period of data recording.

Table 4

Effect of Particle Size on Characteristic Times for 33/67 $TiH_{0.65}/KClO_4$

Serial or Test No.	Fuel/Oxidizer Particle Sizes[+]	Initiation Time, t_I ms	Bridgewire Break Time, t_{BB} ms	Function Time, t_F ms	$t_{BB} - t_I$ ms	$t_F - t_I$ ms
L-30	L/L	5.06	5.12	5.1505	0.06	0.09
L-31	L/L	8.02	8.07	8.1158	0.05	0.10
L-32	L/L	2.42	2.47	2.5096	0.05	0.09
L-45	L/S	1.82	1.87	1.9126	0.05	0.09
L-46	L/S	1.56	1.60	1.6398	0.04	0.08
L-47	L/S	1.80	1.84	1.8821	0.04	0.08
L-60	S/L	1.72	1.78	1.8142	0.06	0.09
L-61	S/L	1.93	1.98	2.0219	0.05	0.09
L-62	S/L	1.68	1.75	1.7768	0.07	0.10
L-75	S/S	1.36	1 41	1.4501	0.05	0.09
L-76	S/S	--	--	1.4912	--	--
L-77	S/S	1.42	1.47	1.5096	0.05	0.09

[+]Quantitative descriptions of the materials are given in Table 4.

Table 5

Effect of Composition on Output Parameters for $TiH_{0.65}/KClO_4$

Serial or Test No.	Fuel/Oxidizer Mass Ratio	Peak Force KN	Time to Peak µs	Impulse to Peak mN-s	Pulse Width µs	Total Impulse mN-s	Specific Impulse+ mN-s/mg	Length of Crush Cone mm
L-137	30/70	20.02	37.6	425	47.8	552	4.75	5.33
L-136	30/70	18.61	40.8	427	49.6	525	4.61	5.54
L-135	30/70	17.96	42.4	419	51.6	524	4.58	5.46
					Avg.	534	4.65	
L-143	33/67	19.09	41.0	429	50.6	537	4.55	5.46
L-144	33/67	16.42	45.8	419	53.8	482	4.04	5.66
L-145*	33/67	17.79	39.2	441	47.4	530	4.49	5.38**
					Avg.	516	4.36	
L-170*	36/64	16.25	44.2	412	51.6	482	4.16	5.54**
L-171	36/64	17.45	44.2	433	52.4	506	4.29	5.59
L-172	36/64	19.67	44.2	437	51.0	532	4.62	5.54
					Avg.	507	4.36	
L-185*	39/61	18.48	43.0	426	51.2	508	4.41	5.52**
L-186	39/61	15.52	45.0	395	53.6	472	4.03	5.84
L-187*	39/61	16.77	44.6	424	52.6	498	4.32	--
					Avg.	493	4.25	
L-200*	42/58	17.62	44.4	429	52.2	508	4.32	--
L-202*	42/58	18.31	42.8	397	53.8	523	4.44	--
					Avg.	516	4.38	

+Specific impulse is defined as the total impulse divided by the mass of pyrotechnic material.
*Leaked.
**Measured cone that was removed from bushing.

Table 6

Effect of Composition on Characteristic Times for $TiH_{0.65}/KClO_4$

Serial or Test No.	Fuel/Oxidizer Mass Ratio	Initiation Time, t_I ms	Bridgewire Break Time, t_{BB} ms	Function Time, t_F ms	$t_{BB} - t_I$ ms	$t_F - t_I$ ms
L-137	30/70	1.84	1.89	1.9265	0.05	0.09
L-136	30/70	1.90	1.94	1.9868	0.04	0.09
L-135	30/70	2.03	2.07	2.1121	0.04	0.08
L-143	33/67	2.55	2.60	2.6355	0.05	0.09
L-144	33/67	2.42	2.48	2.5156	0.06	0.10
L-145	33/67	2.40	2.46	2.4829	0.06	0.08
L-170	36/64	3.36	3.42	3.4557	0.06	0.10
L-171	36/64	4.34	4.40	4.4339	0.06	0.09
L-172	36/64	0.60*	0.64	0.6989	0.04	0.10
L-185	39/61	--	--	26.0687	--	--
L-186	39/61	6.59	6.66	6.6812	0.07	0.09
L-187	39/61	6.95	7.02	7.0412	0.07	0.09
L-200	42/58	10.98	11.04	11.0686	0.06	0.09
L-201	42/58	--	--	9.9437	--	--
L-202	42/58	12.91	15.85	12.9997	2.06	0.09

*Fire pulse only reached 1.287 A and bridgewire resistance at time of fire was unusually high (5.66 ohms compared to the normal value of 0.8 - 1.0 ohm).

Table 7

Effect of Composition on Output Parameters for $TiH_{0.2}/KClO_4$

Serial or Test No.	Fuel/Oxidizer Mass Ratio	Peak Force KN	Time to Peak µs	Impulse to Peak mN-s	Pulse Width µs	Total Impulse mN-s	Specific Impulse[+] mN-s/mg	Length of Crush Cone mm
L-211*	33/67	14.83	42.8	366	50.4	424	4.14	5.84
L-213*	33/67	15.05	45.0	383	52.0	439	4.35	6.10
					Avg.	432	4.25	
L-96	36/64	16.59	44.0	432	51.2	494	4.13	5.66
L-97	36/64	16.05	50.8	427	57.0	488	4.15	5.84
L-98*	36/64	22.58	19.8**	148**	47.8	510	4.26	5.63***
					Avg.	497	4.18	
L-111	39/61	15.45	46.0	407	53.6	471	4.64	5.97
L-112	39/61	15.70	45.2	394	53.4	468	4.79	5.97
L-113	39/61	14.27	46.0	396	53.4	450	4.40	6.10
					Avg.	463	4.61	
L-81*	43/57	12.15	48.4	368	54.6	407	4.06	6.29***
L-82	43/57	13.08	48.8	361	56.4	418	4.16	6.35
L-83	43/57	12.40	47.6	375	55.6	430	4.39	6.35
					Avg.	418	4.20	

+Specific impulse is defined as the total impulse divided by the mass of pyrotechnic material.

*Leaked.

**First peak on force-time curve.

*** Measured cone that was removed from bushing.

Table 8

Effect of Composition on Characteristic Times for $TiH_{0.2}/KClO_4$

Serial or Test No.	Fuel/Oxidizer Mass Ratio	Initiation Time, t_I ms	Bridgewire Break Time, t_{BB} ms	Function Time, t_F ms	$t_{BB} - t_I$ ms	$t_F - t_I$ ms
L-211	33/67	2.48	2.53	2.5668	0.05	0.09
L-212	33/67	2.18	2.29	--	0.11	--
L-213	33/67	2.19	2.24	2.2792	0.05	0.09
L-96	36/64	2.72	2.77	2.8030	0.05	0.08
L-97	36/64	2.96	3.01	3.0462	0.05	0.09
L-98	36/64	2.63	2.68	2.7221	0.05	0.09
L-111	39/61	3.26	3.33	3.3572	0.07	0.10
L-112	39/61	2.55	2.62	2.6425	0.07	0.09
L-113	39/61	5.84	5.90	5.9324	0.06	0.09
L-81	43/57	6.26	6.35	6.3681	0.09	0.11
L-82	43/57	6.86	6.94	6.959	0.08	0.10
L-83	43/57	6.07	6.16	6.1733	0.09	0.10

Table 9

Calculated Moles of Reactants and Products for 100 g $TiH_{0.65}/KClO_4$ Blends

Fuel/Oxidizer Ratio Species	30/70	33/67	36/64	39/61	42/58
Reactants					
$TiH_{0.65}$	0.618	0.680	0.742	0.803	0.865
$KClO_4$	0.505	0.483	0.462	0.440	0.418
Products					
TiO_2	0.618	0.680	0.742	0.803	0.836
Ti	0	0	0	0	0.029
KCl	0.505	0.483	0.462	0.440	0.418
H_2O	0.201	0.221	0.241	0.154	0
O_2	0.292	0.176	0.062	0	0
H_2	0	0	0	0.107	0.281
$\sum$Products	1.616	1.560	1.507	1.504	1.564
$\sum$Products-TiO_2-Ti	0.998	0.880	0.765	0.701	0.699
$\sum$Products-TiO_2-Ti-KCl	0.493	0.397	0.303	0.261	0.281

Table 10

Calculated Moles of Reactants and Products for 100 g $TiH_{0.2}/KClO_4$ Blends

Fuel/Oxidizer Ratio Species	33/67	36/64	39/61	43/57
Reactants				
$TiH_{0.2}$	0.686	0.748	0.811	0.893
$KClO_4$	0.483	0.462	0.440	0.411
Products				
TiO_2	0.686	0.748	0.811	0.822
Ti	0	0	0	0.071
KCl	0.483	0.462	0.440	0.411
H_2O	0.069	0.075	0.081	0
O_2	0.246	0.139	0.023	0
H_2	0	0	0	0.090
$\sum$Products	1.484	1.424	1.361	1.394
$\sum$Products-TiO_2-Ti	0.798	0.676	0.550	0.501
$\sum$Products-TiO_2-Ti-KCl	0.315	0.214	0.110	0.090
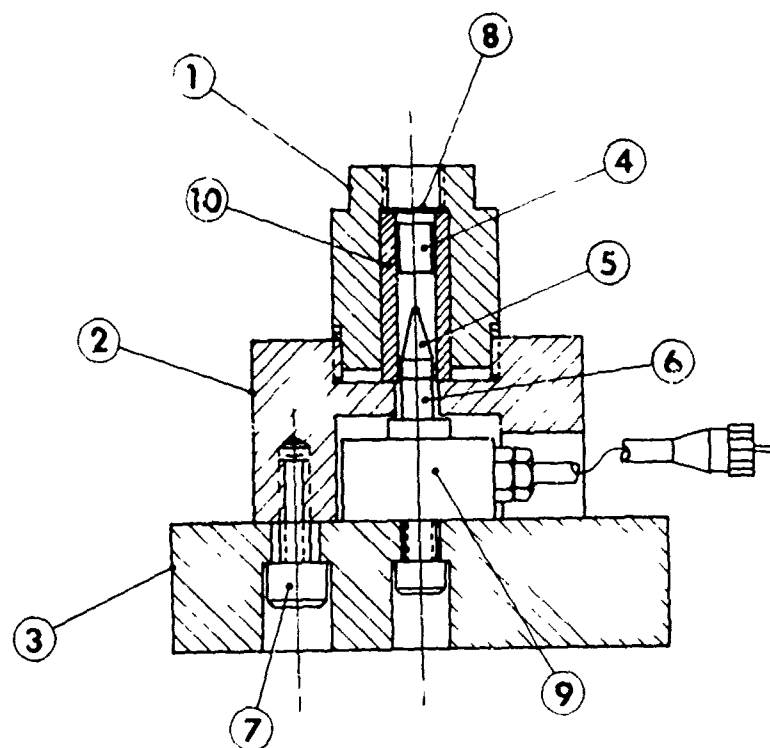
Figure 1. Schematic diagram of load cell fixture.
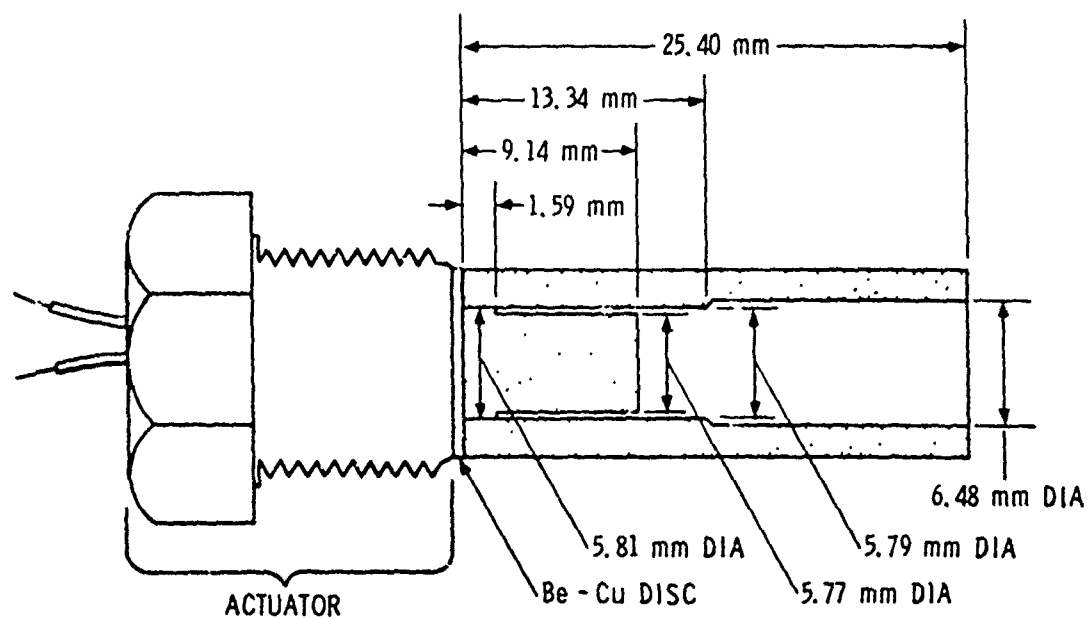
Figure 2. Schematic diagram of VISAR test fixture.

339

Pyrotechnic Output of $TiH_x/KClO_4$ Actuators
from Velocity Measurements[*]

by

M. L. Lieberman
Initiating & Pyrotechnic Components Division

and

K. H. Haskell
Applied Mathematics Division
Sandia Laboratories
Albuquerque, New Mexico

ABSTRACT

The pyrotechnic output of $TiH_x/KClO_4$ loaded actuators has been determined from analysis of piston velocity data obtained from VISAR measurements. The effects of fuel stoichiometry, fuel/oxidizer ratio, and particle size are assessed. Computer-assisted curve fitting techniques have been employed to generate pressure-volume curves for the expanding gas and to perform Gurney analyses. The former imply that pyrotechnics containing $TiH_{0.2}$ or $TiH_{0.65}$ are fast burning and are largely consumed prior to piston motion, in contrast to those containing $TiH_{1.9}$. The latter yield values of the characteristic Gurney velocities and energy conversion efficiencies. Low efficiency values (5-10%) are obtained which are consistent with chemical and gasdynamic aspects of the combustion process.

I. Introduction

During the past several years, considerable effort has been expended in the development of a spark insensitive actuator/ igniter based on $TiH_x/KClO_4$ pyrotechnic materials (1). The rapid combustion of the pyrotechnic generates a high gas pressure which serves as the driving force to propel a piston which in turn can perform a mechanical function. The mechanical output of such devices has received limited attention.

Pyrotechnic output studies that relate to valve performance are of particular interest. Ng has used a velocity interferometer system (VISAR) to assess valve performance (2 3),and has developed a computer model (4) suitable for analytical studies of valve interactions. Measurements performed on actual valve hardware are particularly relevant, but have been regarded as too costly to be performed on a routine basis.

Consequently, parametric studies commonly involve other experimental hardware. Ng has suggested two methods of measuring the pressure-volume relationship for explosives (2). Steele, Allen and Montoya have developed a load cell test that simulates valve conditions (5). Under contract to Sandia Laboratories, Systems Science and Software has obtained VISAR data using a modified version of the load cell fixture (6-8). The purposes of the present study are 1) to develop methods for the treatment and interpretation of such data, and 2) to utilize the methods in evaluating pyrotechnic output of $TiH_x/KClO_4$ loaded actuators.

341

II. Experimental

The fixture used for obtaining VISAR data is shown schematically in Figure 1. The piston was pressed into the bushing such that an interference fit existed along the circumference in the outer 1.6 mm region. A 0.34 mm beryllium-copper disc separated the piston and pyrotechnic-loaded actuator. In all cases the actuator was tightened into the firing fixture to a torque of 16.9 N-m. The constraining hardware which maintained the positions of these parts is not shown. Reflection of a laser beam from the inner flat surface of the piston provided the source of VISAR data.

Tests were performed using several types of actuators loaded with various $TiH_x/KClO_4$ pyrotechnic blends, many of which have been characterized elsewhere (9). For the series of tests in which the mass of the $TiH_{1.9}/KClO_4$ pyrotechnic was varied, the diameter of the charge holder was also varied, so that no free volume resulted. All tests were performed in a horizontal direction.

The principles and hardware of a VISAR system have been described elsewhere (3,10) and need not be repeated here. The VISAR used was operated either with an etalon delay which produced a fringe constant of 0.1740 mm/μs per fringe or with an air-lens delay which produced adjustable, lower fringe constants (6-8). It provided two velocity data channels in

quadrature and a beam intensity monitor channel (7). Data

were recorded on a series of oscilloscopes triggered in a

cascaded manner.

III. Methods of Data Treatment

A. Physics of Motion

VISAR measurements yield velocity of a projectile as a function of time. Consideration of the physics of motion permits the derivation of a variety of other parameters from such data. Recall that

$$\frac{dv}{dt} = a = \frac{F}{M} \tag{1}$$

and

$$d = \int v \, dt \ , \tag{2}$$

where a, v, and d are the acceleration, velocity, and displacement, respectively, of the projectile; t is the time of motion; and F is the net force acting on the projectile. Thus, differentiation and integration of a VISAR-generated v -t curve, yield a(t) and d(t), respectively. For a projectile of known constant mass, F(t) is also obtained.

An effective pressure P(t) can be obtained by dividing F(t) by the cross-sectional area A of the projectile. This effective pressure is identical with the driving gas pressure

only if frictional and other loss forces are negligible. Otherwise, the derived value is lower than the gas pressure. In addition, the total gas volume $V(t)$ can be evaluated from the relation

$$V(t) = V_0 + Ad(t) , \qquad (3)$$

where V_0 is the bulk volume of the pyrotechnic charge. Thus, VISAR data yield $v(t)$, $a(t)$, $d(t)$, $F(t)$, $P(t)$, and $V(t)$, as well as the interrelations between these parameters.

B. Gurney Analysis

Gurney theory, based on the application of energy and momentum balances, provides a relatively simple method for estimating the final, or maximum, velocity imparted to a metal by an explosive. The method should be applicable for estimating the final velocity imparted to a metal piston by a pyrotechnic which is consumed prior to piston motion. For the physical arrangement under consideration, Kennedy (11) has shown that

$$v_f = \sqrt{2E} \left[\frac{M}{C} + \frac{1}{3} \right]^{-\frac{1}{2}} , \qquad (4)$$

where

v_f = final metal velocity,

$\sqrt{2E}$ = Gurney velocity[*],

_____

[*] The Gurney energy E in kcal/g equals $0.120 \, (\sqrt{2E})^2$ if $\sqrt{2E}$ is in mm/μs.

M = mass of the driver metal, and

C = mass of the momentum-producing, pyrotechnic reaction products.

Thus, values of v_f can be readily predicted if the other parameters are known.

It is desirable, therefore, to determine the appropriate values of the Gurney velocity for $TiH_x/KClO_4$ pyrotechnics. For the experiments under consideration, M is the combined mass of the piston and those portions of metallic discs propelled with the piston. The final velocity values can be approximated by extrapolating the VISAR data. Selection of the appropriate values of C is less certain. When all of the reaction products are gaseous, C is identical with the mass of the explosive charge. For the pyrotechnics under consideration, however, this is not the case. To establish values of C, it has been assumed that the chemical reaction products are TiO_2, Ti, KCl, H_2, O_2, and H_2O (9). Three limiting values of C are obtained by letting it equal m_T, $m_{KCl} + m_{H_2} + m_{O_2} + m_{H_2O}$, and $m_{H_2} + m_{O_2} + m_{H_2O}$ where m_T is the total pyrotechnic mass and the other m_i parameters are the mass values of the designated chemical species.

A mechanical energy conversion efficiency (11) can be defined for the test device and evaluated from the equation

$$\text{efficiency} \equiv \frac{\text{Kinetic energy of metal}}{\text{Calorific output of pyrotechnic}} \times 100 \; ,$$

$$= \frac{\frac{1}{2} M v_f^2}{m_T \Delta H} \times 100$$

$$= \left[\left(\frac{v_f}{\sqrt{2E}} \right)^2 \cdot \frac{M}{m_T} \right] \frac{E}{H} \times 100 \; , \qquad (5)$$

where ΔH is the calorific output of the pyrotechnic per unit mass. For 33/67 $TiH_x/KClO_4$ pyrotechnics, ΔH values of 1.395, 1.517, and 1.690 kcal/g have been measured by Massis for x values of 0.20, 0.65, and 1.9, respectively (12).

C. Curve Fitting Techniques

To perform the analyses described in Sections III A. and III B., discrete v-t data of each experiment must be integrated, differentiated, and extrapolated. Integration, to obtain v-t-d data, generally presents no difficulty. The other operations, however, are rather complex and warrant some discussion.

To perform a Gurney analysis it was necessary to extrapolate discrete v-d data to a final velocity v_f attained at infinite displacement. The method used was that of constrained

least squares curve fitting, followed by extrapolation of the fitted curve. Velocity data were fit as a function of reciprocal displacement, $r = 1/d$, so that the fitted curve could be extrapolated to $r = 0$. The curve was then reconverted to a v-d curve for comparison with experimental data. This is referred to as computer plot A.

Another curve fit was performed to determine $P(t)$. Constrained least squares curve fitting was again used to fit the experimental v-t data. The P-t curve was then computed from the first derivative of the v-t curve. The coincidental P-t and v-t plot is referred to as computer plot B.

In both of the above cases a curve is fit to the data in the least squares sense using piecewise polynomials. Data are defined in an interval $[x_1, x_n]$ on the independent variable axis. Then n-1 subintervals are defined by choosing $x_2, \dots, x_{n-1}$ (the method for this choice will be discussed below). The values $x_1, \dots, x_n$ are called knots or breakpoints. Each segment of the fitted curve is represented by a polynomial defined over a given subinterval $[x_i, x_{i+1}]$.

For plot A, C^1 Hermite polynomials (13) were chosen. These C^1 piecewise cubics have continuous function and first derivative values over the entire interval $[x_1, x_n]$. This representation leads to a least squares problem where the number of equations is equal to the number of data points in

347

the experiment. The number of columns in the problem, or variables to be determined, is twice the number of breakpoints. This is due to the fact that the values of both the function and the first derivative are sought at each of the n breakpoints (13). Constraints are added (see below) to produce the least squares problem to be solved.

For plot B, piecewise cubic polynomials based on B-splines (14) were chosen. These C^2 piecewise cubic polynomials have continuous function, and first and second derivative values over the entire interval $[x_1, x_n]$. This choice was made because we were chiefly interested in a well-behaved first derivative of the fitted curve.

This representation leads to a least squares problem where, again, the number of least squares equations is equal to the number of data points in the experiment. The number of columns in the least squares problem is (N + degree - 20, where N is the number of breakpoints and the degree of the polynomials is 3. The solution defines (N + degree - 2) coefficients of the piecewise cubic polynomials. The function and derivatives of the fitted curve can then be evaluated.

The breakpoints are chosen (15) such that the total variation of the dependent variable using piecewise linear interpolation of the data is divided approximately equally

among the n-1 subintervals. Additional adjustments are made

to minimize the disparity in size of neighboring intervals.

The curve fitting is further controlled by the addition

of inequality constraints to both problems. In fitting the

data of plot A, v-r (r = 1/d) data exhibit the general char-

acteristics of being concave opening upward and decreasing

with increasing r. In particular, to achieve concave upward

behavior in the curve it is necessary and sufficient to con-

strain the second derivatives at both ends of each subinter-

val to be nonnegative. This is necessary because the piece-

wise linear second derivative function is not continuous in

C^1. This insures that the curve is open upward on the interval

$[0, x_n]$. Also, the first derivative is constrained at $r = x_n$

to be nonpositive, and the function value at $r = x_n$ to be

nonnegative. These last two constraints guarantee that the

curve is everywhere decreasing and positive on the interval

$[0, x_n]$.

The v-t data of plot A exhibit increasing v with increas-

ing t. Frequently, the curve obtained is concave opening

downward. To achieve concave downward behavior it is nec-

essary and sufficient to constrain the second derivative at

each breakpoint to be negative.* Fewer constraints are re-

quired on the second derivative of plot B than for plot A

---

*If data suggest that the v-t curve is not concave opening
 downwards over its entire range, this constraint is not applied.

because the second derivative of the C^2 B-spline polynomials is continuous over the entire interval $[x_1, x_n]$. Also, the function value at time $= x_1$ and the first derivative value at time $= x_n$ are both constrained to be nonnegative. These last two constraints guarantee that the curve is everywhere increasing and positive on the interval $[x_1, x_n]$.

In fitting plot B we also impose a constraint on the pressure curve to be concave opening upward[*]. Thus, we constrain its second derivatives to be nonnegative. However, since the pressure is proportional to dv/dt, this amounts to constraining third derivatives to be nonnegative. This constraint is applied at each breakpoint.

The FORTRAN subprogram WNNLS (Weighted Non-Negative Least Squares) has been recently developed to solve general constrained least squares problems (16). In particular, the curve fitting problems described above can be converted to a problem of this type. These problems are often rank deficient least squares problems, and WNNLS is one of the few computer codes which can find a solution in such cases.

The procedure for determining the P-V curve can now be outlined in an algorithmic fashion. As an aid to understanding the steps of the algorithm, Figure 2 shows examples of plots A and B.

---

[*] If data suggest that the v-t curve is not concave opening downwards over its entire range, this constraint is not applied.

Step 1: Convert the B-spline-based polynomial coefficients of plot B to Hermite polynomial coefficients by evaluating the curve's function and derivative at each of the breakpoints.

Step 2: From the range of d values of plot A and Equation (3), determine the minimum and maximum values of V. Within this range specify a particular number NP of equally spaced V values to be computer plotted.

Step 3: For each value of V perform Steps 4-7.

Step 4: Evaluate d from Equation (3).

Step 5: From d and plot A, determine v.

Step 6: From plot B, obtain the value of t corresponding to v.

Step 7: From plot B, determine the value of P corresponding to t.

Step 8: Plot the NP values of P versus the NP values of V.

IV. Application of Data Treatment Methods

A. Experimental Data

Figures 3-5 illustrate the qualitative features observed in VISAR data generated from $TiH_x/KClO_4$ loaded actuators. Figure 3 shows data typical of 33/67 blends of $TiH_{0.2}/KClO_4$ and $TiH_{0.65}/KClO_4$ of normal particle size (9), loaded in

351

SAD 1031 actuators. At the beginning of piston motion, an oscillatory v-t curve is obtained which is indicative of a sticking and sliding motion. The curve is concave downward over virtually its entire length. This implies that the combustion of the pyrotechnic is essentially complete prior to motion, and the driving force can be regarded simply as a gas expansion.

Figure 4 shows data obtained from 33/67 $TiH_{0.65}/KClO_4$ loaded in Type 29 actuators, rather than the SAD 1031 actuators discussed above. The data clearly shows the existence of a point of inflection at about 25 μs. Since the effective pressure is proportional to the slope of the v-t curve, this result implies that P achieves a maximum value at that point This further suggests that combustion proceeds at least to that time. The fact that a presumably identical pyrotechnic material can yield curves of the type shown in Figures 2 and 3 when loaded in different types of actuators, suggests that differences in loading parameters and/or actuator design can affect pyrotechnic output.

Figure 5 presents data obtained from 33/67 $TiH_{1.9}/KClO_4$ in Type 30 actuators. Several tests were performed for each of three values of the pyrotechnic mass. Note that the mass has a significant effect on the final velocity, but has virtually no effect on the velocity history at relatively snort

times. As in Figure 3, the data exhibit a point of inflection. Ng's measurements of time to peak pressure in a zero free volume test fixture indicate that the combustion rate for this pyrotechnic is considerably lower than those of the materials considered in the preceding paragraphs (17). Thus, the data imply that combustion of 33/67 $TiH_{1.9}/KClO_4$ proceeds during motion of the piston for 15 μs. Integration of the v-t data yields the d-t values shown in Figure 5. The slope of the d-t curve is initially very low. After 15 μs of travel, the displacement is only ~1/2 mm. This value is comparable to that obtained for the other pyrotechnic materials and is small relative to that occurring in a valve. Consequently, errors introduced by assuming complete combustion prior to first motion should be insignificant for valve applications.

The VISAR data assessed in this study were obtained by Systems Science and Software, under a series of contracts to Sandia Laboratories. Tests in which fuel stoichiometry, pyrotechnic mass, and actuator type were varied are described in Table 1. Other experiments in which pyrotechnic parameters were systematically varied, were performed with SAD 1031 actuators. The materials parameters varied were (a) fuel and oxidizer particle sizes for 33/67 $TiH_{0.65}/KClO_4$, (b) fuel/oxidizer ratio for $TiH_{0.65}/KClO_4$ and (c) fuel/oxidizer ratio for $TiH_{0.2}/KClO_4$. Three tests were performed for each of the thirteen

defined conditions (9). Consistent with load cell test
results, variations in the materials parameters had minimal
effect on pyrotechnic output (9). Use of the largest par-
ticle size combination of fuel and oxidizer yielded a v-t
curve which exhibited a point of inflection. The smallest
particle size combination showed no point of inflection.
Thus, a decreased combustion rate is apparent when the par-
ticle size of the reactants increases. Variations in fuel/
oxidizer ratio had no significant effect on output, except
for the case of the 43/57 $TiH_{0.2}/KClO_4$ blend which yielded
a final velocity ~10% lower than the other comparable materi-
als. The main factor affecting pyrotechnic output was the
mass of reactants loaded in the charge holder.

B. Gurney Values

Results of Gurney analyses for the tests described in
Table 1 are given in Table 2. For these experiments,
M/C >> 1/3 and the selection of C is reflected directly in
the value of $\sqrt{2E}$. Consequently, the Gurney velocity corres-
ponding to C = m_T can be used for estimating the final metal
velocity in other experiments, as long as M/C >> 1/3. Because
m_T is a measured parameter, its direct use as C is convenient.
From Table 2 it can be seen that the Gurney velocities are
relatively constant over wide ranges of fuel stoichiometry,

pyrotechnic mass, and actuator type. This means that one can readily predict values of v_f from Equation (4) by utilizing an average value of $\sqrt{2E}$, and the measured parameters M and C.

The average efficiencies are quite low and insensitive to variations in the independent variables. The low values mean that only a small fraction of the thermal energy produced is converted to useful work. This is consistent with thermodynamic calculations of chemical equilibrium which indicate that only a small fraction of the chemical products formed on combustion exist in the gaseous state (18).

C. Evaluation of P-t and P-V Curves

The methods discussed in Sections III B. and III C. have been utilized to evaluate the VISAR data obtained for each test. Typical v-t and P-t plots for identical tests are shown in Figures 6-8. Generally, the v-t curves are in reasonable agreement with the experimental data. Variations in the shapes of the P-t curves are seen in Figures 6-8. Usually, the plots are linear or near-linear. This is again consistent with the concept of the piston being driven by an expanding gas.

Figures 9-11 show the reproducibility of the P-V curves, obtained from test to test, for three different experimental

conditions. The reproducibility is regarded as satisfactory over much of the volume range. At low values of V, corresponding to the volume of the charge holder, P is an exceedingly sensitive function of V. As a result of the difficulty in measuring small values of V reproducibly, accurate measurements of P in the zero free volume condition are very difficult to perform reproducibly.

In contrast to this condition, high values of V can be measured with high accuracy. For this condition, however, slight changes in the slope of the v-t curve, where it is near zero, has a significant effect on the resultant value of P. Consequently, P is subject to significant error in this region. The results imply that the calculated P-V curve is subject to considerable uncertainty near either asymptote, but that it should be useful and reasonably accurate in the intermediate region.

V. Conclusions

Computer-assisted, least squares curve fitting techniques have been developed to analyze VISAR data obtained with TiH_x /$KClO_4$ loaded actuators. The effects of a variety of parameters, including fuel stoichiometry, pyrotechnic mass, fuel/ oxidizer ratio, particle size and actuator type, on pyrotechnic output have been examined. Pyrotechnic mass is the major factor

affecting the final velocity of the projectile. Particle size apparently affects combustion rate, but such effects are insignificant for projectile displacements greater than ~1/2 mm. The data imply that the assumption of complete combustion prior to first motion should be satisfactory for most valve applications.

Gurney analyses show that $\sqrt{2E}$ is relatively constant over the range of parameters considered. Consequently, an average value can be used for predicting approximate final values of the projectile velocity. Calculated efficiencies are quite low which is consistent with chemical considerations.

Calculated pressure-time curves are generally consistent with the concept of the projectile being driven by an expanding, nonreactive gas. Calculated pressure-volume curves show reasonable reproducibility, except near their asymptotic limits.

VI. Acknowledgements

357

VII. References

1. E. A. Kjeldgaard, "Development of a Spark Insensitive Actuator/Igniter," Proc. 5th Intl. Pyro. Seminar, July 12-16, 1976, Vail, CO, p. 260.

2. R. Ng, "Measurement of Pressure Output Histories of Electroexplosive Devices," Proc. 9th Symp. on Explosives and Pyro., Sept. 15-16, 1976, Franklin Institute, Philadelphia, PA.

3. R. Ng, "VISAR Measurements of Velocities in Explosive Valves," Sandia Laboratories Report SAND76-8048, Albuquerque, NM, December 1976.

4. R. Ng, "MAVIS--A Computer Program for the Modeling and Analysis of Explosive Valve Interactions," Sandia Laboratories Report SAND75-8018, Albuquerque, NM, February, 1976.

5. B. R. Steele, L. C. Allen, and A. P. Montoya, Sandia Laboratories, unpublished work.

6. R. S. Wilson and D. H. Williams, Systems, Science and Software Report SSS-R-75-2707, La Jolla, CA, August 25, 1975.

7. "VISAR Measurements of Explosive Valve Actuators," Systems, Science and Software Report SSS-R-77-3130, La Jolla, CA, January 28, 1977.

8. R. S. Wilson, Systems, Science and Software, unpublished work.

9. M. L. Lieberman, "Load Cell Testing of $TiH_x/KClO_4$ Actuators," Proc. 6th Intl. Pyro. Seminar, July 17-21, 1978, Estes Park, CO.

10. L. M. Barker and R. E. Hollenbach, "Laser Interferometer for Measuring High Velocities of Any Reflector Surface," J. Appl. Phys. 43, November 1972, p. 4669.

11. J. E. Kennedy, "Gurney Energy of Explosives: Estimation of the Velocity and Impulse Imparted to Driven Metal," Sandia Laboratories Report SC-RR-70-790, Albuquerque, NM, December 1970.

12. T. M. Massis, Sandia Laboratories, unpublished work.

13. G. Strang and G. Fix, <u>An Analysis of the Finite Element Method</u>, Prentice Hall, 1973.

14. C. de Boor, "Package for Calculating with B-Splines," SIAM J. Numer. Anal., Vol. 14, No. 3, June 1977, p. 441.

15. R. J. Hanson and J. L. Phillips, "An Adaptive Numerical Method for Solving Linear Fredholm Integral Equations of the First Kind," Numer. Math., Vol. 24, 1975, 291-307.

16. K. H. Haskell and R. J. Hanson, "An Algorithm for Linear Least Squares with Equality and Non-negativity Constraints," SAND77-0552, in preparation.

17. R. Ng, Sandia Laboratories, unpublished work.

18. M. L. Lieberman, A. B. Donaldson, and M. L. Carnicom, Sandia Laboratories, unpublished work.

TABLE 1

TEST PARAMETERS

Group	Number of Tests	Actuator	Pyrotechnic Mixture*	Pyrotechnic Average Mass, mg	Charge Holder Material
I	2	Type 30	$TiH_{1.9}/KClO_4$	67	Ceramic
II	4	Type 30	$TiH_{1.9}/KClO_4$	81	Ceramic
III	2	Type 30	$TiH_{1.9}/KClO_4$	106	Ceramic
IV	10	Type 29	$TiH_{0.65}/KClO_4$	109.4	Plastic
V	3	SAD 1031	$TiH_{0.65}/KClO_4$	115.4	Plastic
VI	3	SAD 1031	$TiH_{0.65}/KClO_4$	114.0	Ceramic
VII	3	SAD 1031	$TiH_{0.2}/KClO_4$	108.3	Ceramic

*Fuel/oxidizer ratio is 33/67 in all cases.

TABLE 2

Average Gurney Velocities and Energy Conversion Efficiencies for Various Test Parameters

Group	v_f, mm/μs	$\sqrt{2E}$,* mm/μs	$\sqrt{2E}$,** mm/μs	$\sqrt{2E}$,*** mm/μs	Efficiency %
I	.180	0.982	1.43	2.95	6.76
II[+]	.211	1.05	1.53	3.14	7.69
III	.257	1.12	1.62	3.34	8.72
IV[+]	.249	1.07	1.57	3.41	8.83
V	.225	0.937	1.38	2.99	6.83
VI	.210	0.881	1.30	2.81	6.03
VII	.198	0.853	1.26	2.79	6.14

* $C \equiv m_T$

** $C \equiv m_{KCl} + m_{H_2} + m_{O_2} + m_{H_2O}$

*** $C \equiv m_{H_2} + m_{O_2} + m_{H_2O}$

[+] Excludes one test in Group II and two tests in Group IV because VISAR data were obtained for a displacement less than 5 mm.
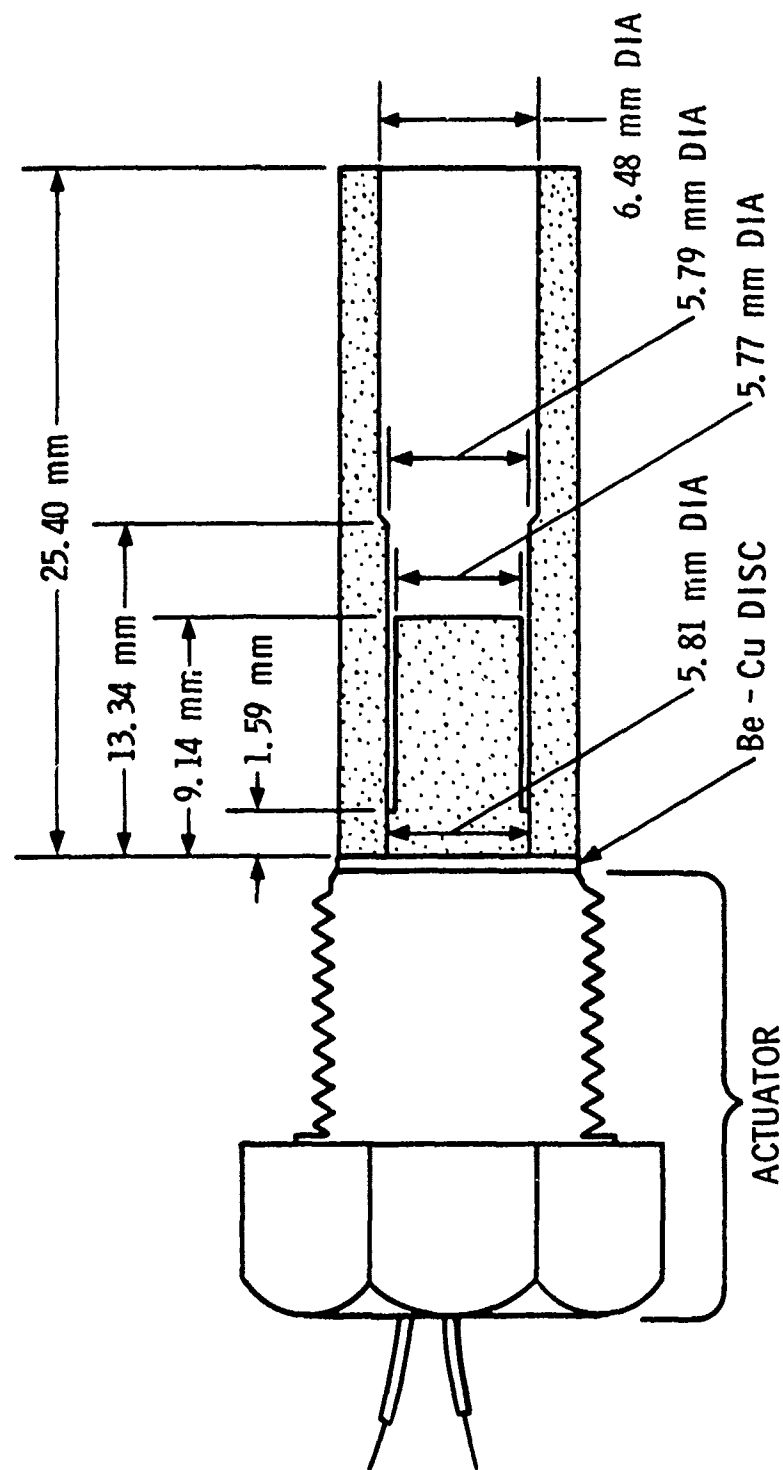
FIGURE 1. Test Fixture used for VISAR Measurements

6.48 mm DIA

5.79 mm DIA

5.77 mm DIA

5.81 mm DIA

Be – Cu DISC

25.40 mm

13.34 mm

9.14 mm

1.59 mm

ACTUATOR

PLOT A

PLOT B
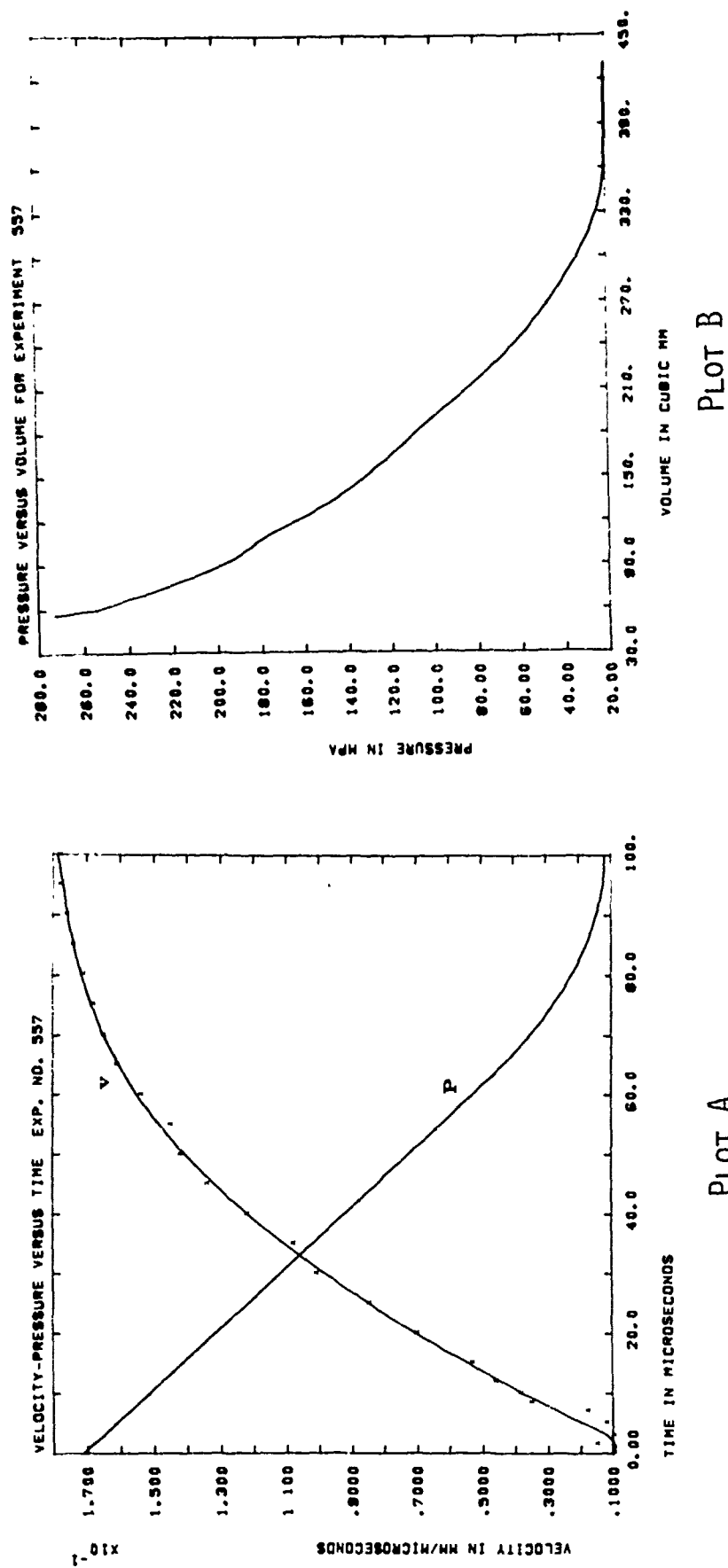
FIGURE 2. EXAMPLES OF THE COMPUTER PLOTS

363
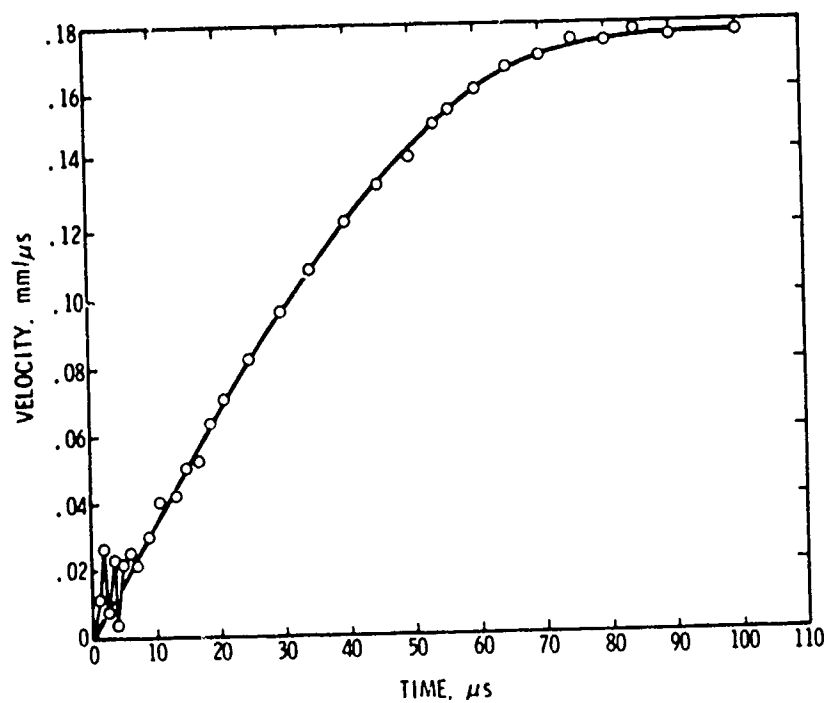
FIGURE 3. VISAR Data for SAD 1031 Actuator Number 545 Loaded with 33/67 $TiH_{0.2}/KClO_4$
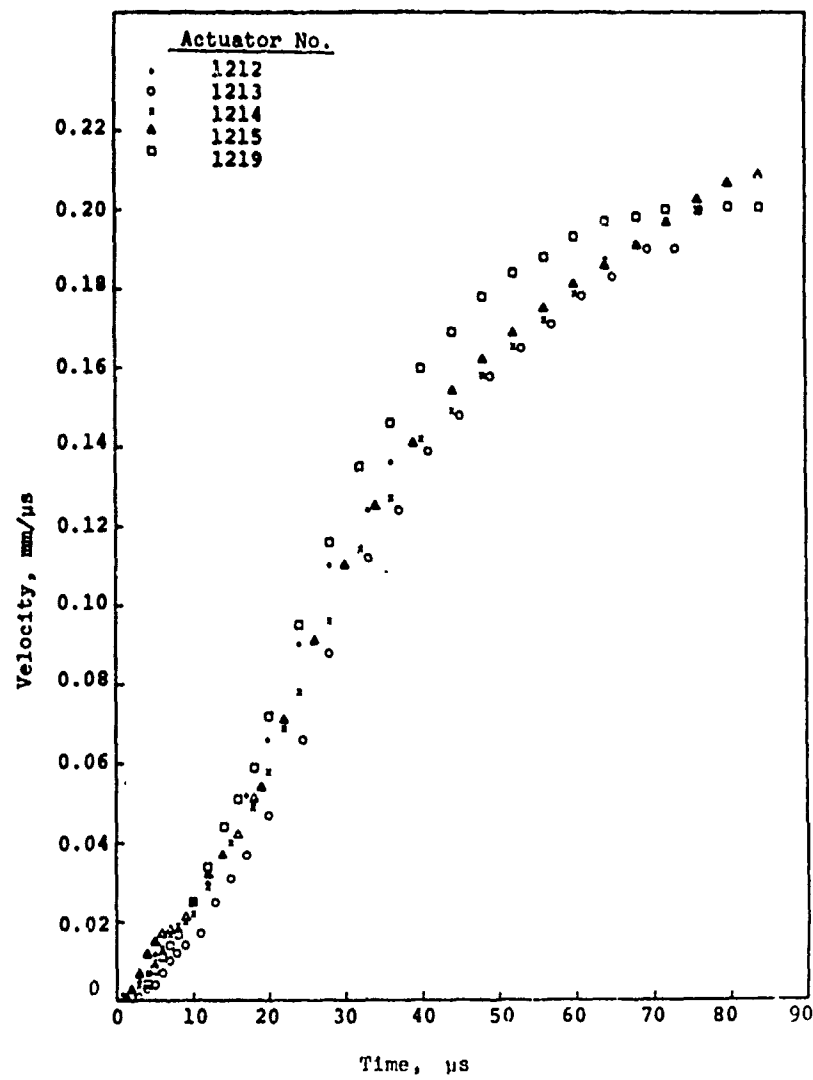
FIGURE 4. VISAR Data for Type 29 Actuators Loaded with 33/67 $TiH_{0.65}/KClO_4$
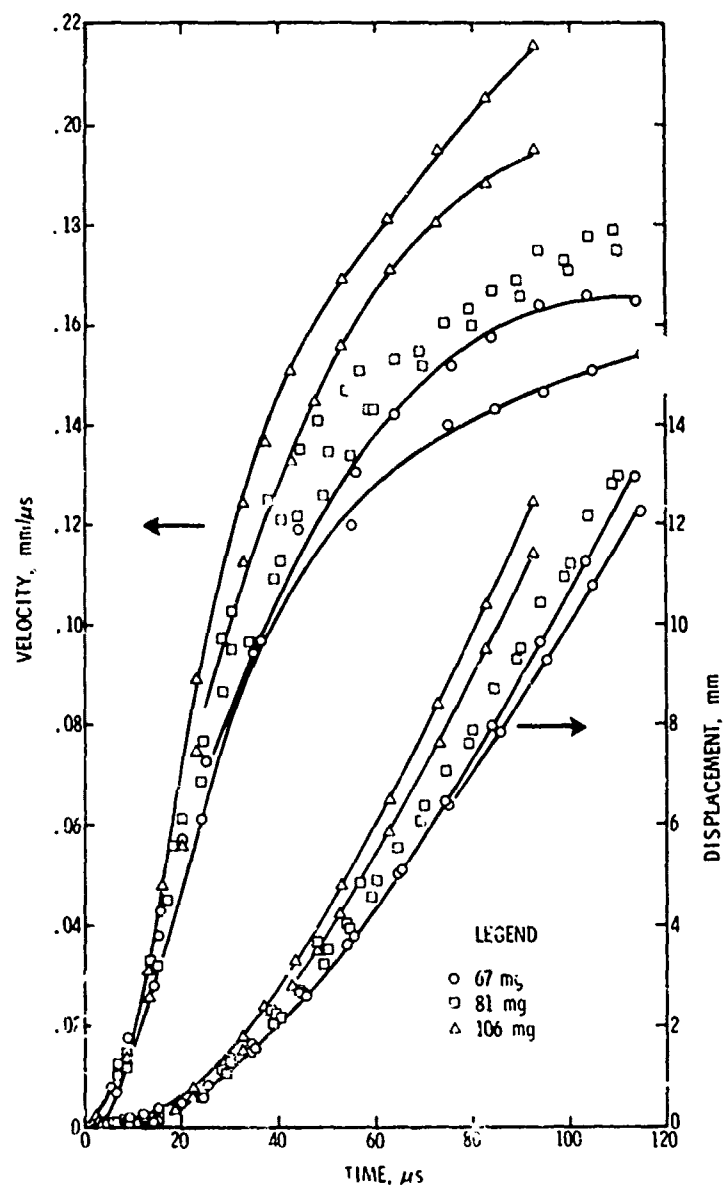
FIGURE 5. VISAR Data for Type 30 Actuators Loaded
with Different Masses of 33/67 $TiH_{1.9}/KClO_4$
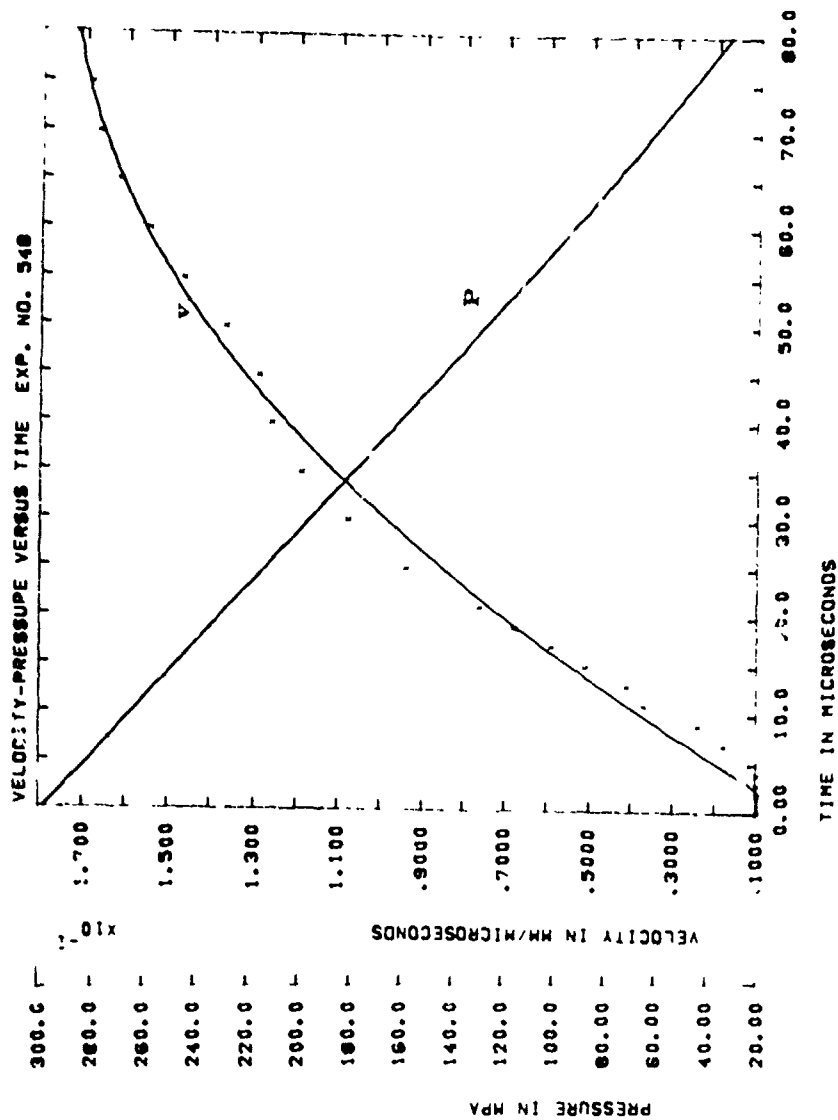
FIGURE 6. COMPUTER PLOT A FOR SAD 1031 ACTUATOR NUMBER 543 LOADED WITH 33/67 $TiH_{0.65}/KClO_4$ IN PLASTIC CHARGE HOLDER.
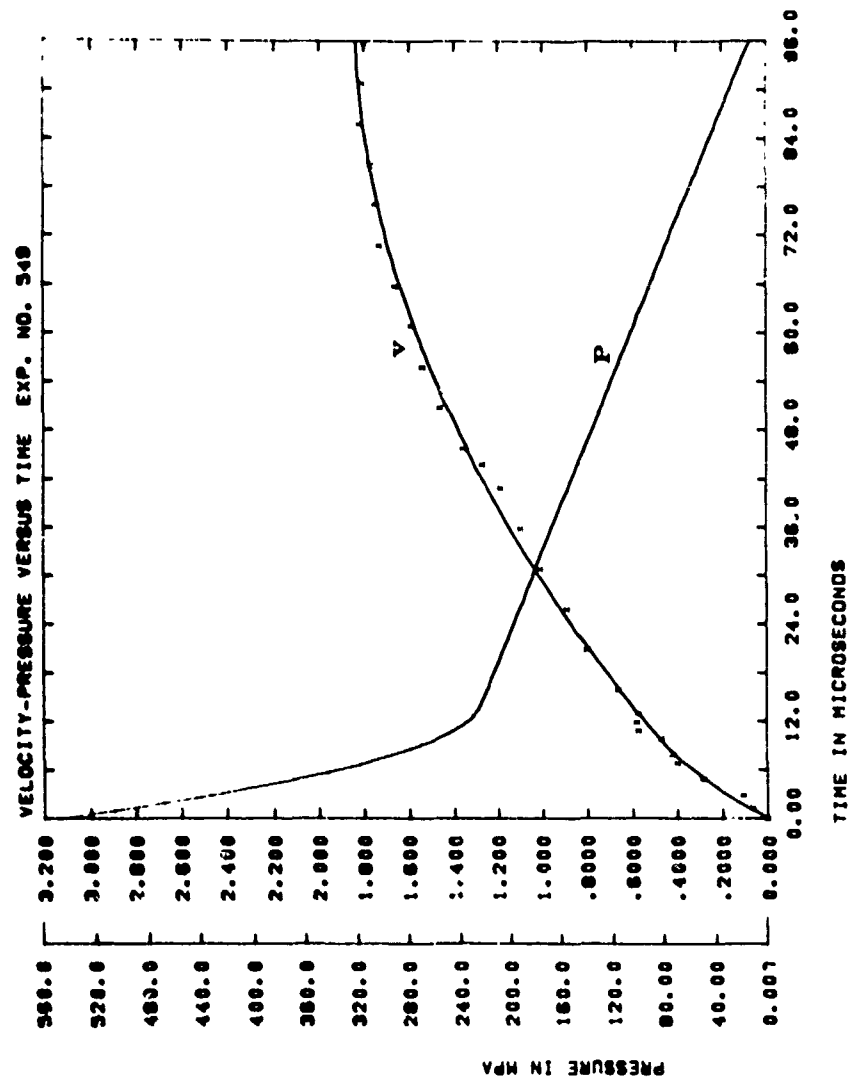
FIGURE 7. Computer Plot A for SAD 1031 Actuator Number 549 Loaded with 33/67 $TiH_{0.65}/KClO_4$ in Plastic Charge Holder.
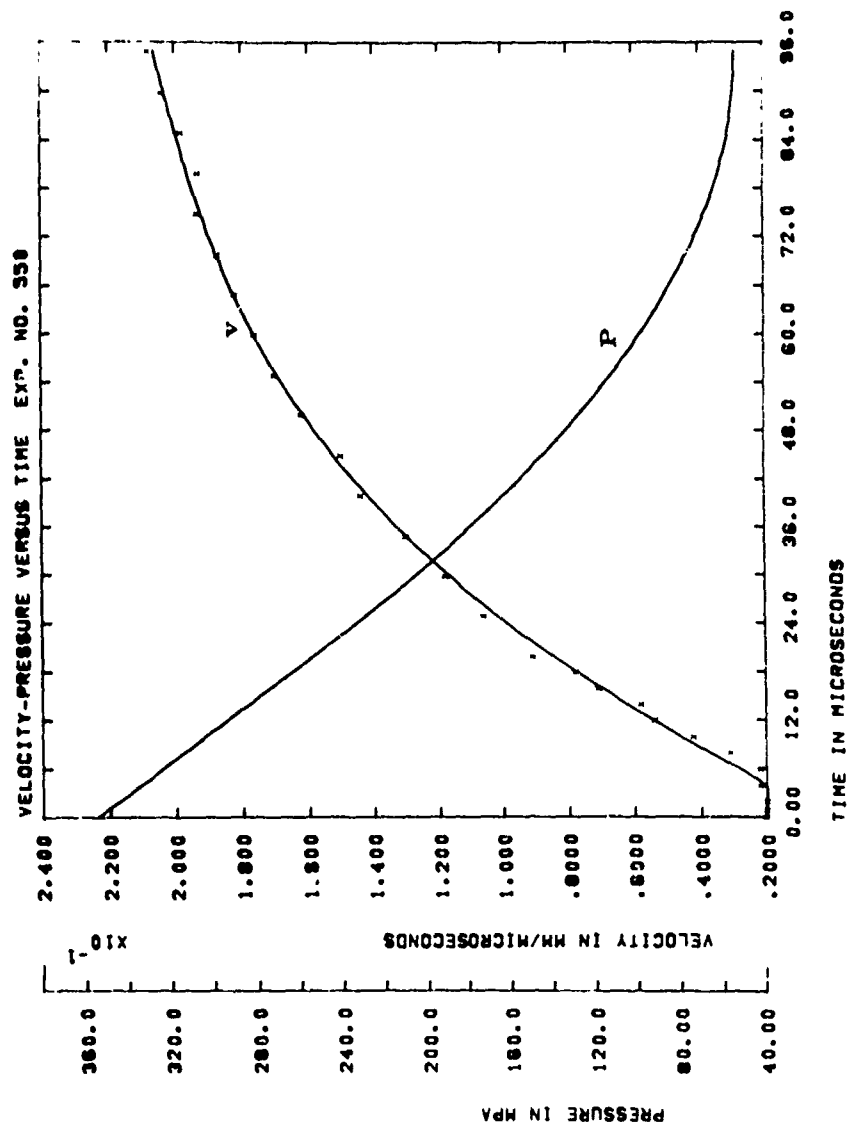
FIGURE 3. COMPUTER PLOT A FOR SAD 1031 ACTUATOR NUMBER 550 LOADED WITH 33/67 $TiH_{0.65}/KClO_4$ IN PLASTIC CHARGE HOLDER.

369
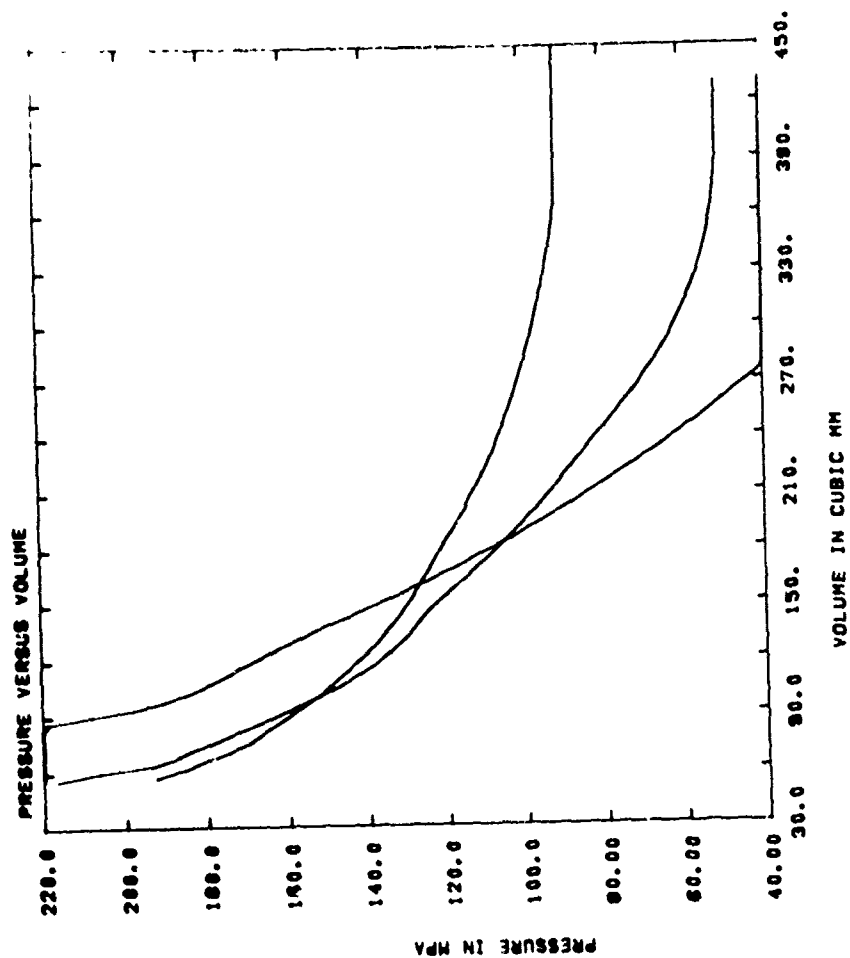
FIGURE 9. COMPUTER PLOT B FOR THREE SAD 1031 ACTUATORS LOADED WITH 33/67 $TiH_{0.65}/KClO_4$ IN CERAMIC CHARGE HOLDERS.
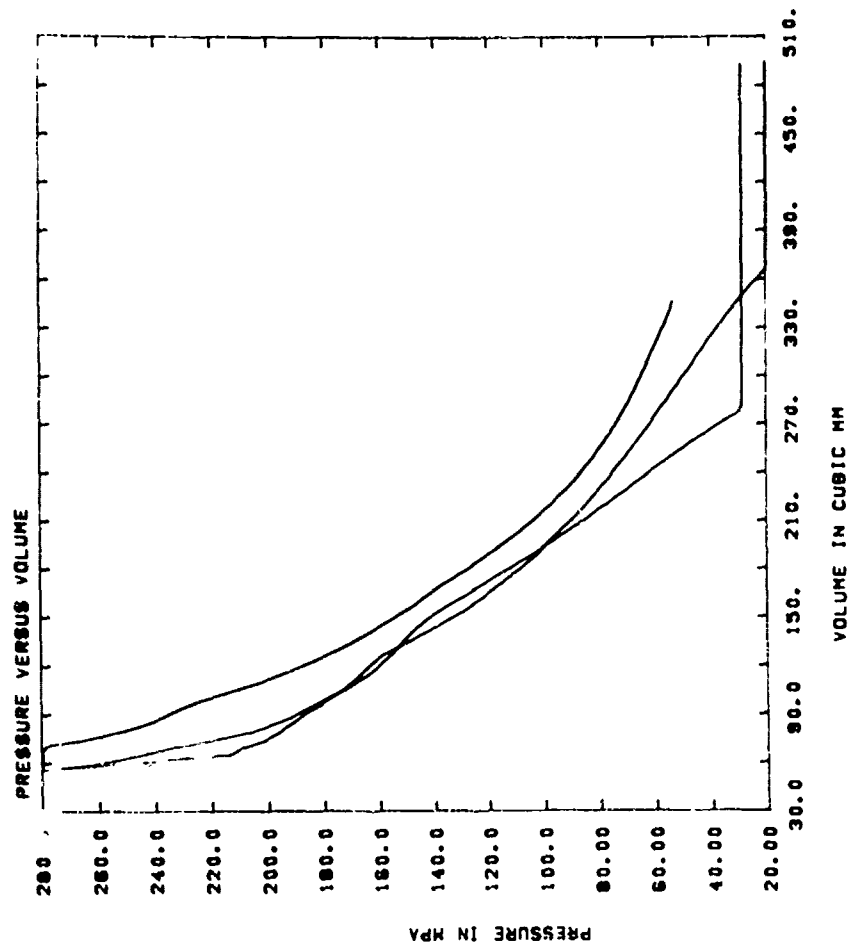
FIGURE 10. Computer Plot B for Three SAD 1031 Actuators Loaded with 33/67 $TiH_{0.65}/KClO_4$ in Plastic Charge Holders.
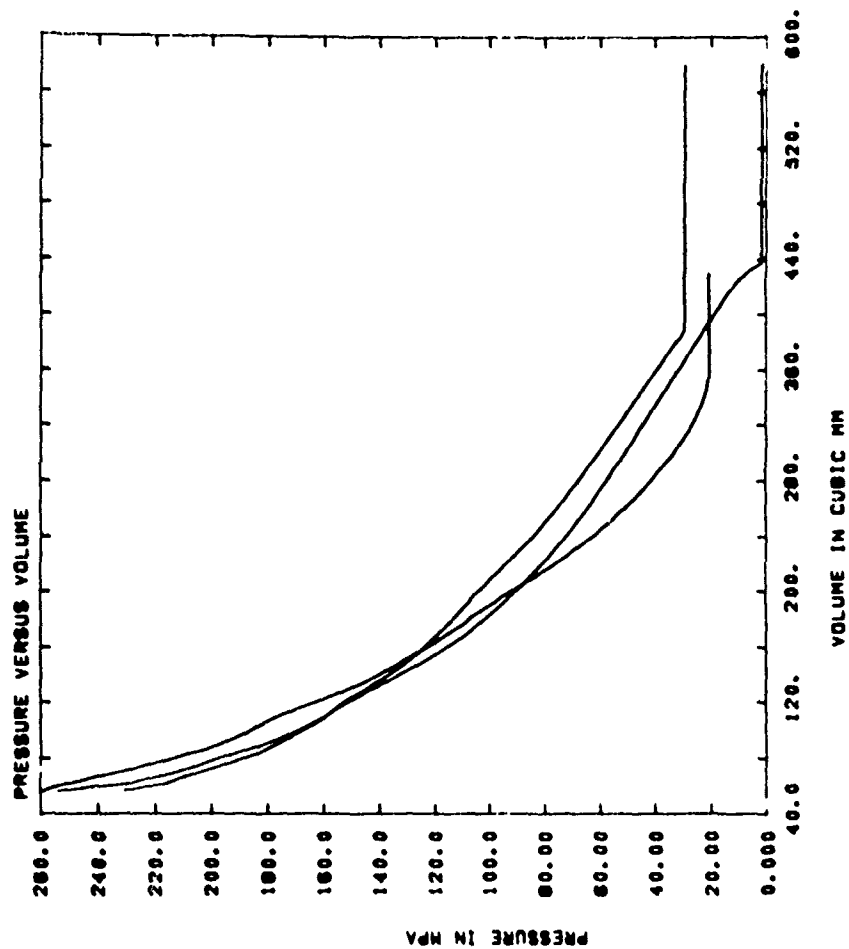
FIGURE 11. Computer Plot B for Three SAD 1031 Actuators Loaded with 33/67 $TiH_{0.2}/KClO_4$ in Ceramic Charge Holders.

ERRATA

Pyrotechnic Output of $TiH_x/KClO_4$ Actuators

from Velocity Measurements

M. L. Lieberman

K. H. Haskell

p. 8, line 16, "(N + degree - 20," should read
   "(N + degree - 2),".

p. 9, line 18, "plot A" should read "plot B".

p. 10, last line, "plots A and B." should read
   "plot B and a P versus V plot
   (defined as computer plot C)."

Figures 2, 6, 7, 8, 9, 10, and 11, "Plot A" should
   read "Plot B" and "Plot B" should
   read "Plot C".

Modelling of $TiH_x/KClO_4$ Actuator Pyrotechnic Output[*]

by

M. L. Lieberman
Initiating & Pyrotechnic Components Division

and

S. E. Benzley
Applied Mechanics Division II
Sandia Laboratories
Albuquerque, New Mexico 87185

ABSTRACT

Pyrotechnic output generated by $TiH_x/KClO_4$ loaded actuators has been modelled through an analysis of the applicable forces and utilization of relevant piston velocity (VISAR) and load cell data. The assumption of a linearly decreasing force-time relationship yields calculated piston velocity-displacement values that are in good agreement with those obtained from VISAR measurements. The resultant gas pressure-volume values are compared with those obtained experimentally and differences due to the limitations of the model are considered in terms of the physical phenomena. Modelling of load cell output testing has been performed by combining the assumed force-time relationship of the piston alone with that measured in the load cell test. Good agreement with other

---

measured parameters is obtained by limiting the decrease of force on the piston and utilizing an effective piston-crush cone separation distance somewhat greater than the experimental value. These values are shown to be consistent with the physical phenomena.

I. Introduction

The pyrotechnic output of $TiH_x/KClO_4$ loaded actuators is measured in terms of their capability to perform a mechanical function. Two output tests that have received considerable attention at Sandia Laboratories are (a) the load cell test developed by Steele, Allen, and Montoya [1] and (b) the Velocity Interferometer System for Any Reflector (VISAR) test. The two tests yield complementary information. The former yields a force-time history generated while a piston crushes a metallic cone, a condition that simulates a valve condition. The latter produces a velocity-time profile for a projectile driven by the actuator. Whereas the VISAR test generates data relevant to all motion of the piston, the load cell measurement relates only to the period of crush.

The purpose of the present study is to model the output measurements, such that one can obtain a predictive capability and a method of relating the two tests. To that end modelling has been performed based simply on the equation of motion for a rigid body.

II. Experimental

The experimental methods associated with the load cell [2] and VISAR [3] tests are described in detail elsewhere and need not be repeated here. The apparatus used for load

cell testing is shown schematically in Figure 1. Firing of the pyrotechnic shears a thin disc and propels the piston downward. When the piston compresses the crush cone, the force-time history is recorded by a quartz transducer which is separated from the cone by a connecting anvil.

VISAR testing is performed using similar hardware, major differences being (a) the propulsion of the piston in a horizontal direction and (b) the elimination of the crush cone and assorted components that stop the piston. Figure 2 shows the geometries of the various components. The laser beam of the VISAR (not shown) focuses near the flat surface of the piston through the open end of the bushing.

III. Mathematical Modelling

The mathematical modelling of both VISAR and load cell tests is accomplished by using the equation of motion for a rigid body. Figure 3 illustrates the effective forces acting on a rigid piston. The forces shown are those that may be applied on a piston in either type of output test. The equation of motion for the rigid piston of Figure 3 is

$$M\ddot{x}(t) = F_1(t) - F_2(t) - F_3(t) = F(t) \qquad (1)$$

where

M = mass of the piston,

$F_1(t)$ = driving force (i.e., pyrotechnic force) as a function of time,

$F_2(t)$ = stopping force (i.e., force applied by crush cone) as a function of time,

$F_3(t)$ = frictional force as a function of time,

$F(t)$ = net force as a function of time,

and $\ddot{x}(t)$ = acceleration of the piston as a function of time.

Equation (1) is simply reordered and integrated forward in time to provide velocity, $\dot{x}(t)$, and displacement, $x(t)$, histories, i.e.,

$$\ddot{x}(t) = \frac{F(t)}{M} \quad , \tag{2}$$

$$\dot{x}(t) = \frac{1}{M} \int_0^t F(t)\ dt + \dot{x}_0 \tag{3}$$

and

$$x(t) = \int_0^t \dot{x}(t)\ dt + x_0 \ , \tag{4}$$

where

$\dot{x}_0$ = initial velocity of the piston, and

x_0 = initial displacement of the piston.

The problem addressed in this paper involves the determination of the velocity and displacement histories for assumed or known applied loads, $F_1(t)$, $F_2(t)$, and $F_3(t)$. The major difficulty is establishing the proper values of these forces. When $F_1(t)$, $F_2(t)$, and $F_3(t)$ are complicated functions, a numerical solution to Equations (2) - (4) is warranted.

A numerical solution to the equations is implemented by assuming a linear time variation of the net force, F(t), over a small increment of time, as shown in Figure 4. Equations (2) - (4) thus define the motion of the piston as

$$t = t_I + t' \, , \tag{5}$$

$$\ddot{x}(t') = \frac{1}{M} \left[F_I + t' \, \frac{\Delta F}{\Delta t} \right] \, , \tag{6}$$

$$\dot{x}(t') = \frac{1}{M} \left[F_I t' + \frac{t'^2}{2} \, \frac{\Delta F}{\Delta t} \right] + \dot{x}_{t_I} \, , \tag{7}$$

$$x(t') = \frac{1}{M} \left[\frac{F_I t'^2}{2} + \frac{t'^3}{6} \, \frac{\Delta F}{\Delta t} \right] + \dot{x}_{t_I} t' + x_{t_I} \, , \tag{8}$$

where

t' = transformed time scale, between t_I and t_E.

F_I = net force at beginning of increment,

F_E = net force at end of increment,

$\Delta F = F_I - F_E$,

t_I = time at beginning of increment,

t_E = time at end of increment, and

$\Delta t = t_I - t_E$.

A simple computer program has been written to solve Equations (5) - (8) to provide the motion of a piston of mass M subject to forces $F_1(t)$, $F_2(t)$, and $F_3(t)$.

IV. Modelling VISAR Experiments

VISAR experiments of pyrotechnic driven pistons yield piston velocity-time data which can be graphically integrated to produce displacement values also. An example of VISAR data, obtained by Systems, Science and Software of LaJolla, California under contract to Sandia Laboratories, is given in Figure 5. It will be shown in what follows that the shape of the plotted data fits a linearly decaying function for the net force, i.e.,

$$F(t) = F_1(t) - F_3(t) = F_{MAX}(1 - t/t_A) \quad 0 < t \le t_A \quad (9)$$

where

F_{MAX} = maximum force on the piston which corresponds to the initial confined pressure generated by the pyrotechnic,

t_A = time at which the force $F(t)$ has decayed to zero, and

$F(t) = 0$ at $t \ge t_A$.

Other efforts made to obtain the derivative of the experimental data [3] are generally consistent with this functional form.

From the assumed force history given by Equation (9), the velocity and displacement histories can be expressed as

379

$$\dot{x}(t) = \frac{F_{MAX}}{M} \left(t - \frac{t^2}{2t_A} \right) \tag{10}$$

and

$$x(t) = \frac{F_{MAX}}{M} \left(\frac{t^2}{2} - \frac{t^3}{6t_A} \right) . \tag{11}$$

The parameter t_A may be determined from Figure 5 as follows:

1. Point A in Figure 5 defines the condition where $\frac{d\dot{x}}{dx}$ initially becomes zero.

2. Note that $\frac{d\dot{x}}{dx} = \frac{d\dot{x}}{dt}\frac{dt}{dx} = \frac{\ddot{x}}{\dot{x}} = 0$, which implies $\ddot{x} = \frac{F}{M} = 0$.

3. Thus, the values of displacement and velocity at the time F initially decays to zero are the values of those parameters at point A in Figure 5.

Substituting the values of $\dot{x}(t)$ and $x(t)$ at point A into Equations (10) and (11), one finds that

$$t_A = 3x_A/2\dot{x}_A \tag{12}$$

and

$$F_{MAX} = 2M\dot{x}_A/t_A = 3Mx_A/t_A^2 . \tag{13}$$

Equations (12) and (13) then provide values of t_A and F_{MAX} which can be inserted into Equations (10) and (11) to yield functional forms of $\dot{x}(t)$ and $x(t)$. The solid curve in Figure 5 is the resultant calculated curve which is in good agreement with the experimental data.

The resultant $F(t) - x(t)$ curve is shown in Figure 6. Since the abscissa and ordinate are directly proportional to pressure and volume, respectively, it can be seen that the curve resembles a P-V curve for a gas. This is in agreement with other analyses of VISAR data [3]. The only significant deviation from a typical P-V curve occurs at relatively low force values, because the model requires $F(t)$ to decrease linearly to zero, rather than achieve a limiting, non-zero value.

V. Modelling Load Cell Experiments

The numerical form of the equation of motion is also used to model the load cell tests. The assumptions and procedures incorporated are described as follows:

1. The pyrotechnic force, $F_1(t)$, is assumed to be a linearly time decaying function and is determined from VISAR experiments as described in the previous section. Recall that load cell tests terminate the travel of the piston with an impeding crush cone whereas VISAR experiments determine the piston motion in an unimpeded conditon. Consequently, the function $F_1(t)$ determined from VISAR tests only applies to the load cell test during the unimpeded travel period, i.e., $F_2(t) = 0$. From the moment of impact until the time the piston

stops, the function $F_1(t)$ must be approximated

in a manner that represents the magnitude of the

pressure of the confined gas behind the piston

(See Figure 8).

2. The frictional force, $F_3(t)$, can be postulated.

3. The stopping force, $F_2(t)$, is measured directly
   by the quartz transducer in load cell tests.

4. The piston-crush cone separation distance, δ, is
   established by the geometric definition of the
   load cell test. An effective separation, δ_{EFF},
   greater than δ, may be defined (see Figure 7) to
   account for the fact that the initial mechanics
   of crushing of the cone provides very little stop-
   ping force on the piston. This occurs because the
   small diameter at the front of the crush cone pro-
   vides an insignificant amount of material to pro-
   vide a meaningful stopping force. Experiments
   with blunted cones, discussed later, have verified
   this assumption.

Two examples of the calculations performed in modelling
load cell tests are displayed in Figure 8. Figure 8a gives
the force, velocity, and displacement histories calculated
for the experimental conditions recorded in test 685 (see
Table 1). This test used the nearly pointed crush cone nor-
mally employed in load cell tests. The piston-cone separation

distance used in the calculation was the experimental value (δ = 3.56 mm). Results of the calculation do not compare favorably with the measured length of the deformed cone (Table 1) or the observation of no piston rebound.

Figure 8b gives results obtained from a similar calculation. Here the conditions of test 685 have been assumed to differ from the experimental values. An effective piston-cone separation distance, δ_{EFF}, equal to 4.83 mm, and a 20% reduction in the total load cell impulse were assumed. The impulse minus the frictional force must equal the load cell impulse. This means the total area under the F - t curve must equal zero at the time the impact terminates. The force history, F(t), shown in Figure 8a does **not** satisfy this condition, whereas that shown in Figure 8b does. Results obtained from the latter figure compare favorably with the measured length of the deformed cone (Table 1) and the observation of no piston rebound.

Table 1 shows a comparison of calculated and experimental results for various load cell tests. Group A shows the effect of the blunting of the cone. Note that as the blunting increases, the agreement between experiment and calculation increases. This supports the contention that for nearly pointed cones, an effective piston-cone separation distance, greater than the actual separation, must be used in the calculations. Group B differs from A in that the calculations

were performed with an assumed 20% reduction in the load
cell force history. Such an assumption improves the resul-
tant agreement between experiment and calculation. Not
shown in Table 1 is the fact that the assumption reduces,
but does not eliminate, the calculated rebounding of the
piston. Group C shows the effect of utilizing an effective
piston-cone separation distance in the case of a nearly
pointed crush cone. This case effectively creates the con-
dition of a blunted cone. Good agreement between experi-
ment and calculation are obtained. This result compliments
those discussed for A. Finally, Group D presents the com-
bined conditions of an effective piston-cone separation
distance and a 20% reduction in the load cell history.
These results, plotted in Figure 8b, show good agreement
between calculated and measured cone lengths, as well as
an absence of piston rebounding.

VI. Conclusions

Modelling of pyrotechnic output, as measured by VISAR
and load cell tests, has been performed from an analysis
of the forces exerted on the driven piston. For VISAR
experiments, the assumption of a linearly decreasing force-
time relationship yields calculated results which are in
excellent agreement with experimental data. A calculated

force-displacement curve is qualitatively sirilar to the P-V curve expected for a gas; a significant deviation from the expected curve occurs at low force values, because the model requires the force, or pressure, to reach zero, rather than an asymptotic, non-zero value.

Modelling of the load cell test has been performed by combining the model of the VISAR data with the measured load cell response. Important factors included in this model are (a) the establishment of a final, non-zero pressure acting on the piston after motion has ceased, (b) the utilization of an effective piston-cone separation distance to account for the fact that little stopping force is exerted by the tip of the cone, and (c) the reduction of the load cell force history to establish conditions compatible with plastic impact. With these factors, good agreement has been obtained between experimental and calculated results.

VII. References

1. B. R. Steele, L. C. Allen, and A. P. Montoya, Sandia Laboratories, unpublished work.

2. M. L. Lieberman, "Load Cell Testing of $TiH_x/KClO_4$ Pyrotechnic Actuators," Sixth International Pyrotechnics Seminar, July 17-21, 1978, Estes Park, Colorado.

3. M. L. Lieberman and K. H. Haskell, "Pyrotechnic Output of $TiH_x/KClO_4$ Actuators from Velocity Measurements," Sixth International Pyrotechnics Seminar, July 17-21, 1978, Estes Park, Colorado.

Table 1

Comparison of Calculated and Experimental Results

Group	Test No.	Initial Cone Length,* mm	Effective* Cone Length, mm	δ or δEFF,* mm	Impulse,* mN·s	Piston Displacements mm (a)†	(b)†	Computed Final Cone Length, mm (a)†	(b)†	Measured Final Cone Length, mm	Measured Error, % (a)†	(b)†
A	655	10.80	10.80	3.56	512	6.08	6.59	8.28	7.77	5.46	51.6	42.3
	687	10.80	10.80	3.56	465	6.31	6.67	8.05	7.69	5.54	45.3	38.8
	684	10.80	10.80	3.56	513	6.30	6.85	8.06	7.51	5.38	49.8	39.6
	657	9.53	9.53	3.68	538	5.90	6.63	7.31	6.58	5.26	38.9	25.1
	605	9.53	9.53	3.68	516	6.24	6.81	6.97	6.40	--	--	--
	603	9.53	9.53	3.68	526	6.03	6.60	7.18	6.61	5.46	31.5	21.0
	602	8.26	8.26	4.95	534	6.95	7.60	6.26	5.61	5.03	24.5	11.5
	601	8.26	8.26	4.95	540	6.81	7.51	6.40	5.70	5.08	26.0	12.2
	600	8.26	8.26	4.95	540	7.22	7.81	5.99	5.40	5.21	14.9	3.6
B	685	10.80	10.80	3.56	409	7.09	7.20	7.27	7.16	5.46	33.2	31.1
	687	10.80	10.80	3.56	372	7.29	7.29	7.07	7.07	5.54	27.6	27.6
	684	10.80	10.80	3.56	410	7.31	7.41	7.05	6.95	5.38	31.0	29.2
	657	9.53	9.53	3.68	430	6.95	7.15	6.26	6.06	5.26	19.0	15.2
	605	9.53	9.53	3.68	413	7.19	7.31	6.02	5.90	--	--	--
	603	9.53	9.53	3.68	421	6.96	7.06	6.25	6.15	5.46	14.5	12.6
	602	8.26	8.26	4.95	427	7.93	8.08	5.28	5.13	5.03	5.0	2.0
	601	8.26	8.26	4.95	432	7.81	7.99	5.40	5.22	5.08	6.2	2.7
	600	8.26	8.26	4.95	432	8.13	8.28	5.08	4.93	5.21	-2.5	-5.4
C	685	10.80	9.53	4.83	--	7.76	8.28	6.60	6.08	5.46	20.8	11.3
	687	10.80	9.53	4.83	465	7.99	8.33	6.37	6.03	5.54	15.0	13.7
	684	10.80	9.53	4.83	513	7.99	8.49	6.37	5.87	5.38	18.4	7.1
D	625	10.80	9.53	4.83	409	8.86	8.86	5.50	5.50	5.46	0.07	0.07

*Experimental conditions for each of the tests are given in Group A. In Group B the impulse values have been reduced by 20%. In Group C the effective cone length has been reduced, or the effective separation increased. In Group D the conditions of Groups B and C have been combined.

**The length of 10.80 mm corresponds to the normal, nearly pointed crush cone; blunter cones were prepared by removing material from the tip.

†Two cases are treated. Case (a) defines the end of the experiment as corresponding to the completion of the load cell measurements; case (b) defines it as corresponding to the maximum displacement.
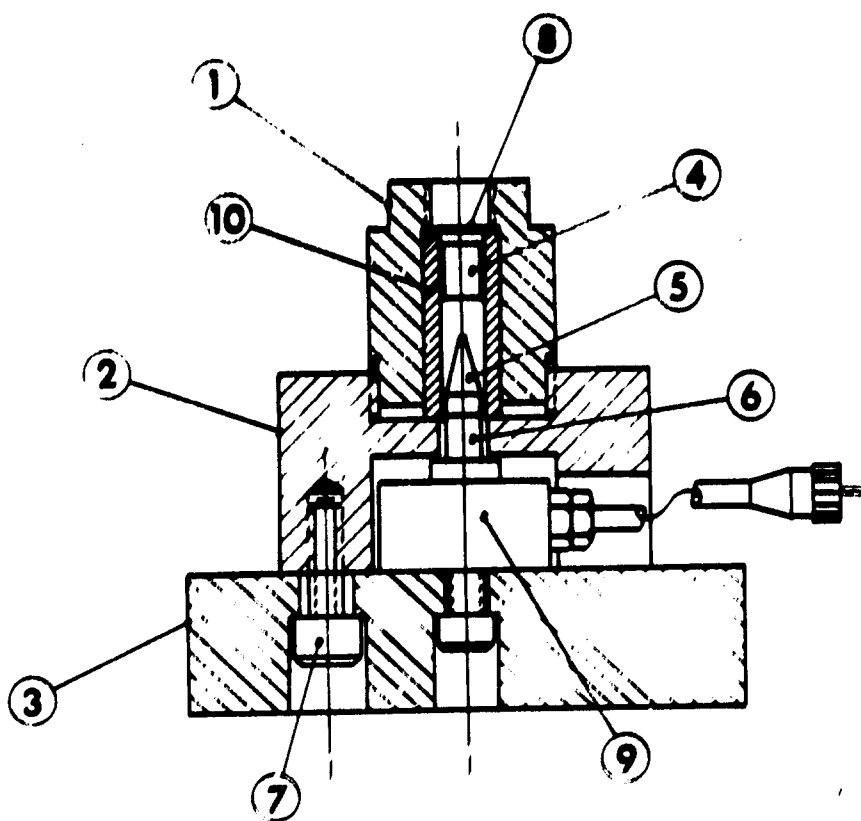
386

Figure 1. Schematic diagram of load cell fixture.
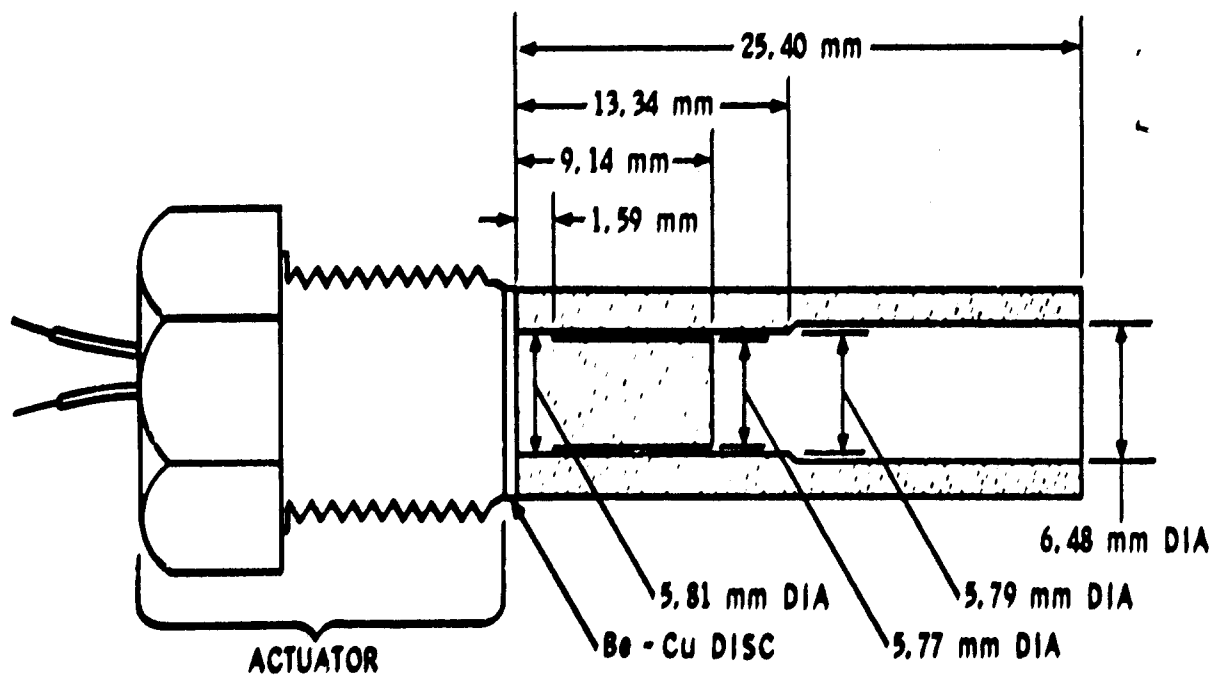
Figure 2. Schematic diagram of VISAR test fixture.
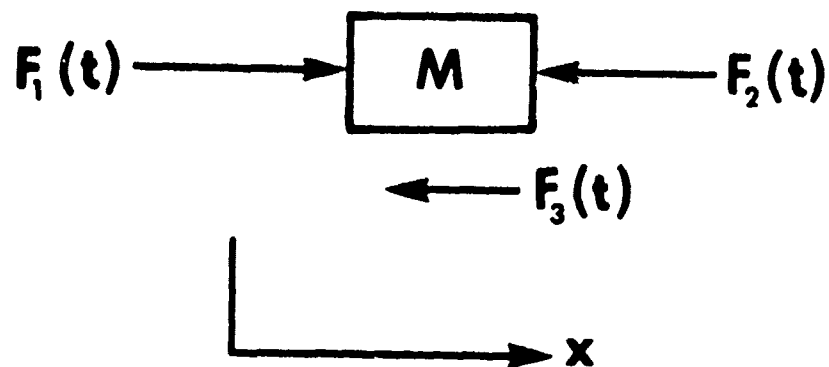
Figure 3.   Forces acting on piston and coordinate system.
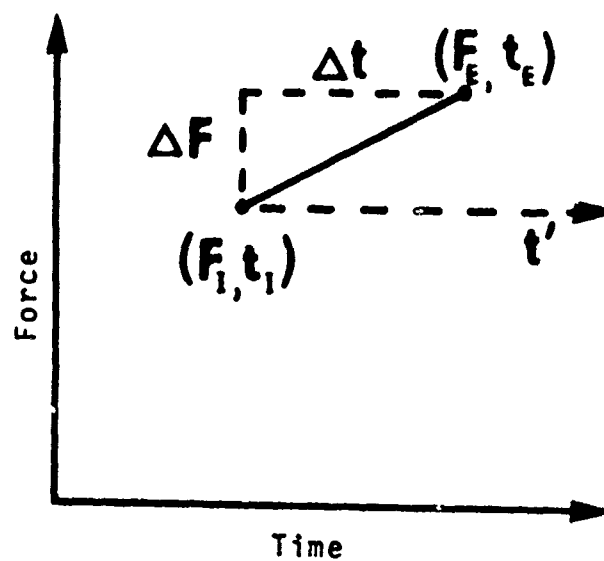
Figure 4.   Transformed time scale.
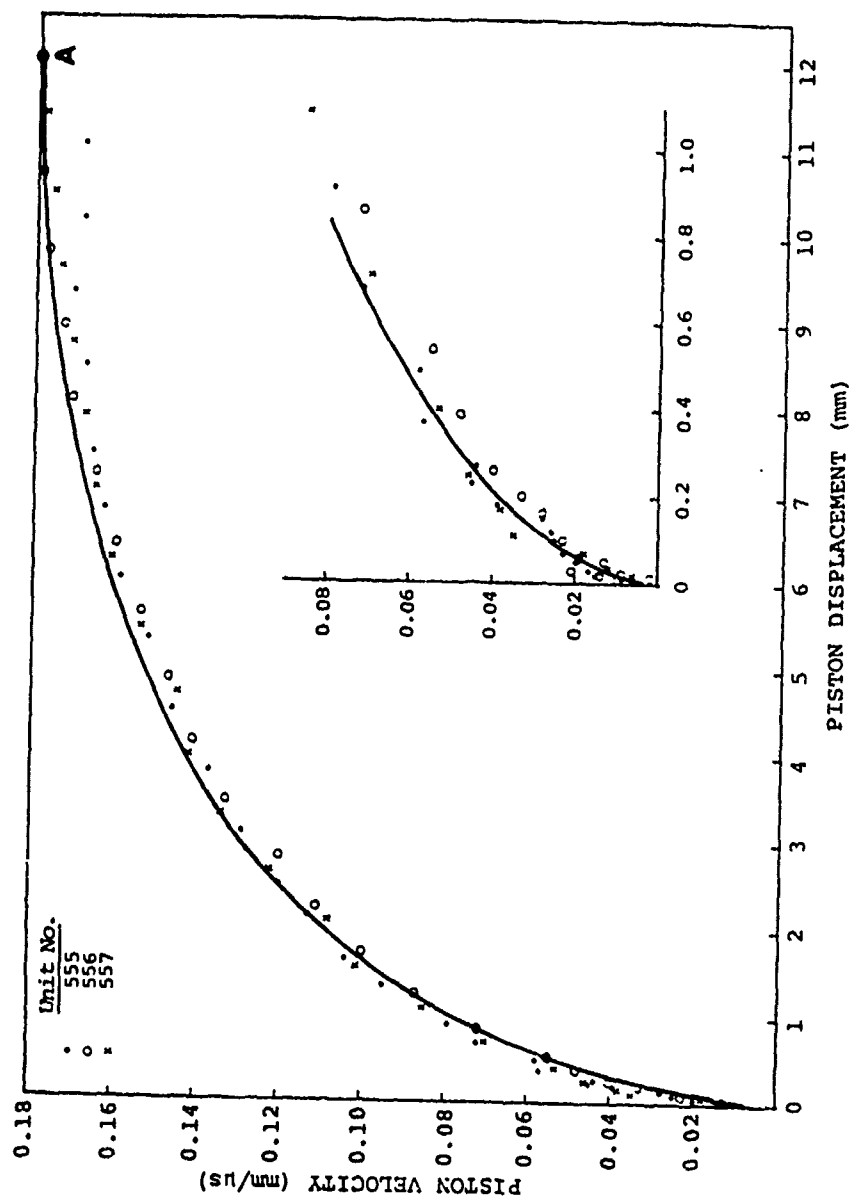
Figure 5. VISAR data for SAD-1031 actuators loaded with 100 mg 33/67 $TiH_{0.2}/KClO_4$. Solid curve represents calculated relationship.

389
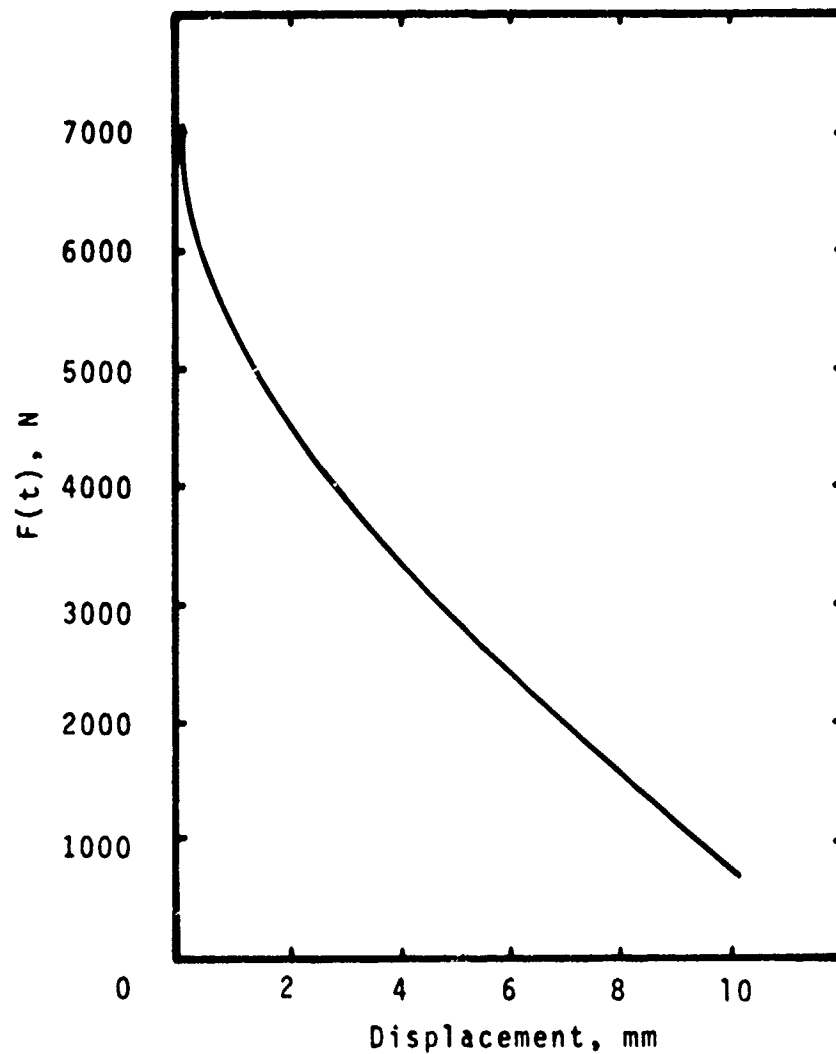
Figure 6. F(t) versus x(t) curve for VISAR test.
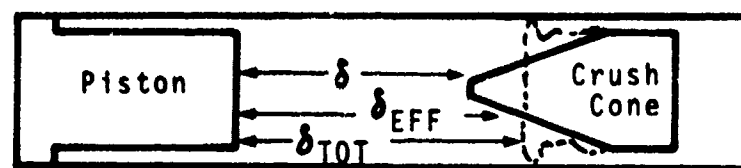
Figure 7. Comparison of piston-cone separation distances.
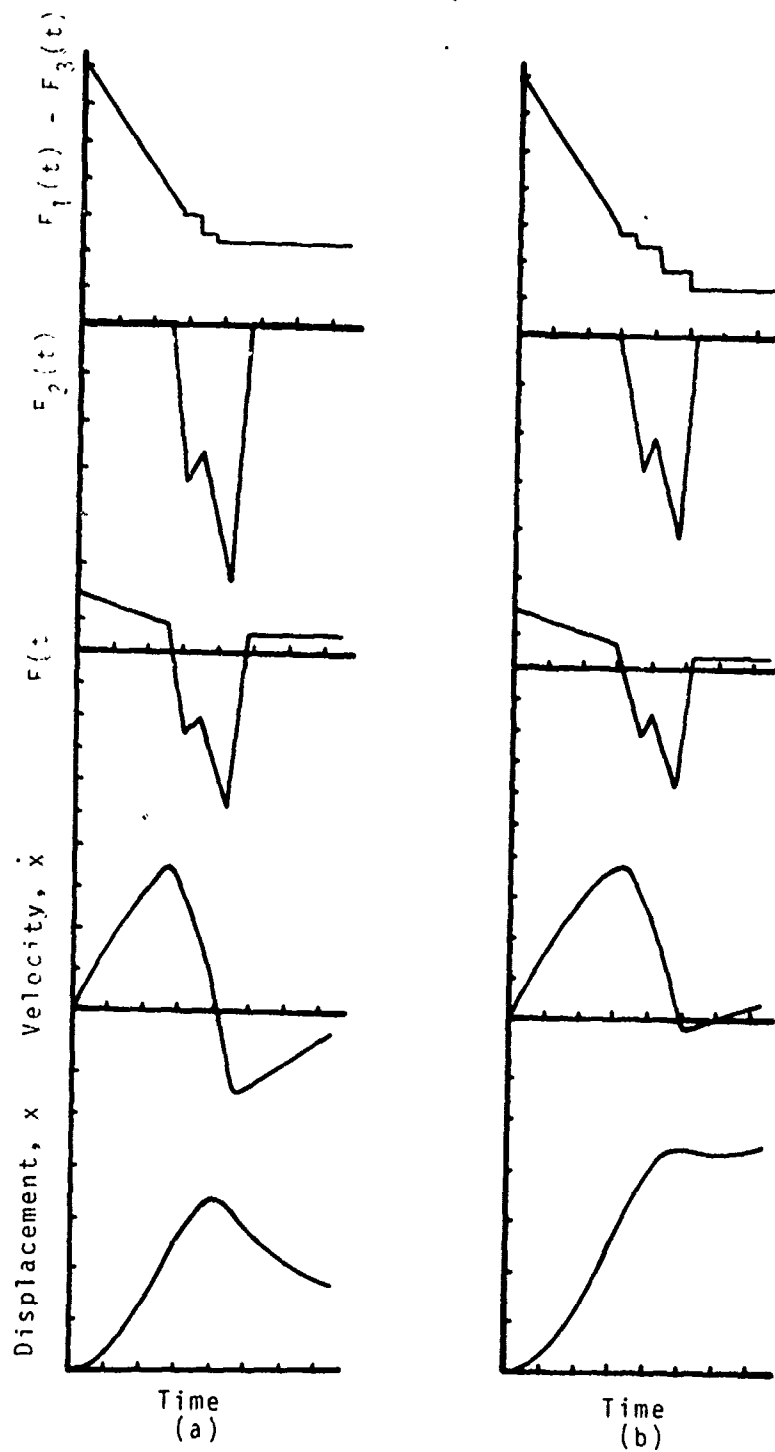
Figure 8. Force, velocity and displacement histories for two load cell test calculations.

INCIDENT/ACCIDENT SURVEY OF PYROTECHNIC COMPOSITIONS

by

F. L. McIntyre

Computer Sciences Corporation
NASA NATIONAL SPACE TECHNOLOGY LABORATORIES
NSTL Station, MS 39529

ABSTRACT

The objective of this survey was to determine the hazards and cause/effect relationships associated with pyrotechnic compositions. The results of this investigation indicated that: 1) the majority of the incidents were thermal in nature; 2) the majority of the incidents are unreported; 3) the most common stimulus cited as the source of initiation was friction; 4) there is seldom a single cause that led to the accident; 5) deficiencies, when noted, are not generally corrected; 6) while the number of incidents involving injuries or fatalities is approximately 10 percent and this number could be reduced significantly; and 7) certain types of operations are more hazardous than others.

INCIDENT/ACCIDENT SURVEY OF PYROTECHNIC COMPOSITIONS

BACKGROUND

In May 1972, a privately owned corporation, under contract to the government, was mixing a 22.7-kg (50-lb) batch of Yellow Star Mix. While the mixing operation was in progress, four women were in the same room preparing the next batch. A fifth woman, the lead technician, operated the mixer and directed the sieving/screening operation. On the day of the accident, the lead technician had complained to the production manager that the augur blade was hitting the side of the blender and that the mix seemed to be warmer than usual. The production manager shimmed the augur so that there was no metal-to-metal contact and assured her that the temperature of the mix was normal. Still, the lead technician would stop the blender every five to ten minutes and allow the mix to cool.

The blender was housed in a 6.09-m by 12.19-m (20-ft x 40-ft) corrugated tin building. The building was divided in half by a steel reinforced concrete block wall. The blender was the only piece of equipment in the mixing room. There were shelves in the room used for drying completed mixes. Each woman was sitting on a half barrel and screening the fuel and oxidizers into paper drums. The second half of the building was used as a storage area. On the day of the accident, the storage area contained approximately 5,896 kg (13,000 lb) of chemicals, 30,000 completed aircraft stars and 237,999 9-mm distress signals.

The lead technician stepped outside the door to operate the blender start/stop switch. At this point the first explosion occurred followed by a second larger explosion, one to two seconds later which totally destroyed the building. The chemicals and completed end-items began to function causing multiple fires in the surrounding area. All five women were subsequently found dead. Four of the remains were located in the mix building and the fifth was blown approximately 12-m (40 ft) away.

One explosion had occurred in the blender and the other one had occurred in the area of the sieving/screening operation. It was impossible to ascertain which explosion occurred first but investigators have hypothesized that the first explosion was the mixer and the second, larger one was the sieving/screening operation.

This is by no means a typical pyrotechnic accident but is used here to point out the gross violations of safety practices that occur. This incident prompted the author to conduct this survey.

OBJECTIVE

The objective of this survey was to identify primary hazards and cause/effect relationships associated with pyrotechnic operations.

TECHNICAL APPROACH

The initial undertaking was limited to a literature survey of incident summaries of the various reporting agencies i.e., Department of Defense Explosive Safety Board (DODESB), Army, Navy, Air Force, Department of Labor, Institute Makers of Explosives (IME) and the Department of Transportation. The difficulty of addressing such agencies and the requirement of establishing the need-to-know limits this source.

Initial research indicated that the majority of the pyrotechnic incidents are not reported because they failed to exceed a cost of 100 dollars in damage to equipment or facility and/or there were no loss-time injuries. This places such incidents in a unreportable category requiring first hand knowledge. Thus, field trips were conducted at both "Go-Go" and "Go-Co" facilities to obtain the data.

A simple form was devised to gather the information. This is shown in figure 1. This form was divided into 10 headings with each major heading sub-divided into sub-headings to facilitate expediency and avoid duplication in data collection. The specific information gathered in this investigation included:

- Type Incident - explosion, initiation-commumication-transition (multiple fire/explosion, multiple explosion, etc.), fire only and other (burn, spill, pneumatic rupture, injury, etc.).

- Severity - unreportable (those incidents with no injury or damage to equipment or facility costing less than $100), minor (first aid injury or damage in excess of $100), critical (loss-time injury or damages in excess of $1,000). Major (loss-time injury and damages in excess of $10,000) and severe (fatality or damages in excess of $100,000).

- Operation - this is the operation cited by the particular facility at the time of the accident.

- Stimulus - chemical, electrical, friction, heat, impact, pressure and static electricity. The stimulus listed was the one cited by the particular facility.

- Contributory Factors - these are the causes as determined by the investigator.

- Material - the compositions or ingredients were listed and categorized similar to Ellern* i.e., priming, illuminating, smoke, gas, sound, heat and delays.

- Mass - The quantity of material involved in the incident.

- Frequency - determined by the number of operations being performed and occurrences at various facilities performing similar functions on the same material group.

---

*Ellern, Herbert, Military and Civilian Pyrotechnics, Chemical Publishing Co., Inc., New York, N.Y. 1968.

Type Incident	Severity	Operation	Stimulus	Contributory Factors	Materials	Mass	Frequency	Date	Reference/ Remarks
X X	X X X X	X X X X	X	X X X X X	X X X X	X X X X X	X X X X	X X X	X X X X X X X X
									1380
Explosion	Minor 1 injury	Laboratory–Mixing-adding ingredients	Friction	Unsafe act (Not following SOP)	Tracer Mix Formula#	4.5kg	Batch#50 1ST inc.	4/4/72	

Figure 1. Data Collection Format.

- Date - date of the incident.

- Reference - this is a coded reference as to location and year of incident to avoid duplication.

Specifically this survey was geared to manufacturing operations; however, the final format and data amassed included: development, transportation and handling, and use.

FINDINGS

The literature survey, although useful, provided little meaningful information. These data were in the form of abstracts and summaries which were not specific enough to determine cause/effect relationships. This was because the abstracts are written anonymously to protect the perpetrator. Also, the facility submitting the initial report was not always objective. Special care was required to avoid duplication as more than one agency would list the incident and the abstracts may not necessarily agree. However, the literature survey was useful in that it was readily available and provided insight as to where to search for additional information.

Tables 1 through 4 show the type of incident, severity, stimuli and type of pyrotechnics that were cited in the incidents. Table 5 indicates the type of operation being performed versus type of incident, severity and stimuli. Table 6 lists the contributory factors in descending order that led to the incident. Table 7 shows the number of injuries and fatalities.

The most common incidents were thermal. The fact that 23 percent of the incidents were either explosion or transitioned from a fire to an explosion was significant because pyrotechnic compostions are not normally considered to be explosive.

Friction was the most often cited cause of initiation and misalignment of ram and die was the most common contributory factor. The ease at which a material will ignite due to frictional forces is not readily known. What data are available usually cannot be correlated between existing apparati used by various test groups and operating lines. However, by solving the misalignment problem, the number of incidents caused by friction could be reduced.

Intra-plant transfer, rework/demil, maintenance, assembly, disposal and pelletizing in terms of explosion versus fire were far more hazardous operations. This is also noted by the severity of these incidents during the same operation. This may be because the contributory factors cited in these operations were usually unsafe acts of the employee such as rough handling.

The reoccurrence of some of the contributory factors indicated a failure to correct the deficiency. This was particularly true in the number of misalignments and unsafe acts of employees as listed in 68 percent of all of the reported incidents. It was found that there was more than one factor that led to the incident. The misalignment of the ram and die was listed as a single cause but this is indicative of other problems such as maintenance, quality,

safety, or unsafe acts. This additional information was not available because the shift in blame could have greater legal repercussions. For whatever reason, the amount of data pertaining to the cause of the incident were either ambiguous or vague. This made it difficult in trying to establish cause/effect relationships.

Of the 577 incidents shown, only 56 reported some form of injury or fatality. This is approximately 10 percent of the total occurrences. A comparison of 1496 explosive/propellant incidents* during the same period indicates an injury/fatality rate of approximately 24 percent. The number of injury/fatality occurrences is less for pyrotechnics. Still, these numbers are capable of being reduced. A misleading factor in this table lies in the fact that some safety offices are reluctant to classify some injuries as loss-time because it would require additional investigation and additional paper work. A closer look at some of these incidents would show a greater percentage of loss-time incidents.

CONCLUSIONS

The results of this survey were preliminary and constitute approximately 10 percent of the total reportable/non-reportable incidents for the same period. The following conclusions were made:

1. The majority of the incidents were thermal or fire type incidents. This was expected because of the nature of the materials under investigation.

2. The most commonly listed source of initiation was friction for which there is the least amount of data available.

3. The most dangerous operations based upon severity and type of incident were intraplant transfer, rework/demil, maintenance, assembly, disposal and pelletizing. This was primarily due to the unsafe act of the employee.

4. The reoccurrences of contributory factors indicate a failure to correct the deficiency.

5. There is usually more than one significant contributing factor that led to the incident even though only one may be listed by the source.

6. The number of injuries or fatalities is approximately 10 percent of the total occurrences. Still, this number could be reduced.

7. Certain type injuries are not always noted correctly because of added paper work and costs.

---

*McIntyre, F. L., Edgewood Arsenal Contractor Report EM-CR-76011-EA-5711, Incident/Accident Survey (1950-1974), December 1975.

TABLE 1. SUMMARY OF TYPE INCIDENTS

Explosions	I- C- T	Fire	Other	Totals
103	27	435	12	577
18%	5%	75%	2%	100%

TABLE 2. SUMMARY OF SEVERITY OF INCIDENT/ACCIDENTS

Unreportable	Minor	Critical	Major	Severe	Totals
495	40	22	3	17	577
$495,000	$114,550	$186,000	$384,000	$4,166,000	$5,345,550
85%	10%	1.5%	2%	1.5%	100%

TABLE 3. SUMMARY OF SOURCE OF INITIATION

Chemical	Electric	Friction	Heat	Impact	Pressure	Static Elec.	Undeterm.
13	11	312	12	65	36	41	87
2%	2%	54%	2%	11%	6%	8%	15%

TABLE 4. SUMMARY OF TYPES OF PYROTECHNIC COMPOSITION

Primers	Light Producers	Smokes Signals	Gas	Noise	Heat Producers	Delays	End Items
12	21	385	35	7	59	2	56
2%	3.6%	66.8%	6%	1.3%	10.3%	0.3%	9.7%

TABLE 5. OPERATION VERSUS TYPE INCIDENT, SEVERITY, STIMULUS FOR PYROTECHNIC INCIDENT/ACCIDENT FROM 1950 TO 1976

Operation	Type Incident					Severity				Stimulus								Total Occurrence	% of Total Occurrence
	Exp	I-C-T	Fire	Other	Unreport	Minor	Critical	Major	Severe	Chemical	Electrical	Friction	Heat	Impact	Pressure	Electro Static	Unknown		
Pressing	40	7	184	0	222	4	3	0	2	1	0	159	0	5	33	2	31	231	40
Mixing	8	2	43	0	16	6	0	0	1	1	0	25	0	3	0	1	23	53	9
Reaming	2	0	43	0	44	1	0	0	1	0	0	44	0	0	1	0	3	45	8
Filling	3	0	10	0	41	1	0	0	0	0	0	20	0	5	0	15	3	43	7.5
Intra-Plant Transfer/Handling	3	6	15	0	17	3	1	0	3	1	1	2	0	17	0	0	3	21	4.2
Loading/Unloading	4	1	17	0	16	2	2	0	1	1	0	1	0	10	0	10	0	22	4
Sieving/Screening/Weighing	2	0	20	0	17	1	2	0	2	3	0	14	0	2	0	2	0	22	4
Rework/Demil	4	4	11	1	12	2	3	1	2	2	0	5	0	5	0	2	4	20	3.5
Maintenance/Cleaning/Modification	6	4	7	2	12	3	3	0	1	0	3	6	1	2	0	2	3	19	3.2
Processing*	6	0	7	2	9	3	1	0	1	3	1	1	0	2	2	0	8	15	2.5
Testing	4	0	5	5	5	3	1	0	2	0	1	0	4	3	2	0	3	14	2.4
Sealing/Crimping	3	0	11	0	14	0	0	0	0	0	0	13	0	0	0	0	1	14	2.4
Curing/Drying	1	0	10	0	11	0	0	0	0	0	0	6	1	0	0	0	1	11	1.9
Inspection/Gauging	1	0	9	1	10	1	0	0	0	0	0	8	0	1	0	2	0	11	1.9
Assembly	7	1	6	0	5	2	0	0	1	0	0	3	0	4	1	0	0	9	1.3
Packaging/Packout	1	0	6	0	4	1	1	0	1	0	0	0	1	2	0	3	1	7	1.2
Disposal	3	1	2	0	1	4	1	0	0	0	1	0	2	1	0	4	0	6	1
Pulverizing/Grinding	2	0	3	0	4	1	0	0	0	0	0	2	1	2	0	0	6	5	0.8
Storage	0	1	2	1	3	0	1	0	0	1	0	1	0	1	0	0	1	4	0.7
Pelletizing	0	0	0	0	2	1	0	0	0	0	0	2	0	0	0	0	1	3	0.5
TOTALS	103	27	435	12	495	40	22	3	17	13	11	312	12	65	36	41	87		
% TOTALS	16	5	75	2	86	7	3.5	0.5	3	2	2	54	2	11	6	8	15		

*This was used when no specific operation could be identified.

TABLE 6. SUMMARY OF CONTRIBUTORY FACTORS

Contributory Factors	Number	Percent of Totals
Misalignment	270	47
Unsafe Act of Employee	119	21
No Determination as to Cause	88	15
Improper/Poor Tools, Equipment, Design, Assembly, Facility	51	9
Weather (Temperature, Humidity, Thunderstorms/Lighting)	43	7.5
Poor/No S.O.P.	41	7.1
Excessive Pressure	37	4
Equipment Failure	27	4.7
Poor Safety/Supervision/Quality Control	19	3.3
Contamination/Corrosion	17	2.9
Chemical Imbalance	15	2.6
Insufficient Knowledge/Training	14	2.4
Excessive Quantities of Materials	11	1.9
Poor Housekeeping/Unsafe Work Area	11	1.9
Improper Safety Equipment/Protective Clothing	9	1.6
Poor Maintenance	6	1
Failure to Safe System	6	1
Excessive Heat	1	0.1

TABLE 7. SUMMARY OF INJURIES AND FATALITIES OF PYROTECHNIC INCIDENT/ACCIDENTS FROM 1970 to 1976

Type of Injury	Number of Incidents	Percent Of Total Occurrences	Number Of Injuries	Percent Of Total Occurrences
First Aid Injury Only	18	3	28	4.9
Loss Time Injury Only	20	3.5	30	5.2
Fatalities Only	9	1.6	16	2.7
Fatalities/Injuries	9	1.6	70	12.1

INVESTIGATION OF METHODS FOR DETECTION
AND CONTROL OF PYROTECHNIC
DUST FIRES AND EXPLOSIONS

G. L. McKown
U.S. Army Armament Research and Development Command
ARRADCOM Resident Operations Office
NSTL Station, MS 39529

ABSTRACT

The characteristics of reactions involving sulfur-dust dispersions and a method for control based on UV detection and suppression by high-pressure quenching agents have been investigated. A gallery was developed which could sustain a propagating dust fire/explosion of sufficient duration to allow measurements of the reaction characteristics and to permit evaluation of the detection and suppression system. It was found that sulfur-dust dispersions were subject to low-order detonations, accompanied by relatively slow-moving flame fronts. The quench system with a burst diaphragm was found to control these reactions satisfactorily, with water acting as a less efficient suppressant than a halogenated hydrocarbon.

I. BACKGROUND

The potential effect of dust fires and explosions in U.S. Army munitions plants (1-5) has recently received increased emphasis due to the introduction of new materials-handling techniques that involve automated transfer equipment and, concomitantly, much larger quantities of material. Pneumatic conveying, large-scale blenders and continuous-flow processing are being installed to replace conventional small-batch preparation of pyrotechnics and explosives. These new methods will reduce exposure of personnel to the hazards involved and, through automated control, can produce higher quality products at greatly increased output. However, the potential risk of damage to equipment and facilities must be determined, and measures for prevention of catastrophic accidents must be devised. Specifically, it is necessary to develop a system for early detection of a dust fire/explosion which simultaneously initiates some suppressive action that will minimize the hazards.

From available data on dust fires/explosions (2,6,7), it is obvious that all conditions of environment and stimuli under which these problems can occur are rarely known and difficult to simulate for repeatable laboratory studies. This project, therefore, was designed to move through a succession of steps to develop instrumentation, test methods, and experimental apparatus in which a dust fire/explosion can be initiated, propagated, measured, and suppressed with some measure of repeatability. The basic requirement was to develop a working chamber which could sustain a propagating dust fire/explosion of sufficient duration to allow measurements to be made of the reaction characteristics and to permit evaluation of the detection and suppression system.

II. EQUIPMENT AND APPARATUS

Preliminary design criteria were obtained using a micro-scale dust gallery, consisting of a glass tube extension on a standard Hartmann apparatus. This dust dispersion system was used to determine the ability of the pneumatic system to disperse and sustain a dust column of sufficient length to make the apparatus useful in developing instrumentation and design data for a larger chamber. On the basis of the information gathered in these tests, a second modification was made to the Hartmann apparatus, consisting of a steel tube chamber extension equipped with instrumentation outlets to measure the pressure wave and flame front characteristics of a sulfur dust fire/explosion (fig. 1).

Sulfur was chosen as the material to be used for the test program because it is a common fuel used in standard pyrotechnic smoke compositions, and can be expected to create dusting problems during handling. From the preliminary test data, design criteria were developed for a full scale dust gallery and the reaction time requirement was established for a suppression system.

During the design and fabrication of the larger gallery, an evaluation was made of existing commercial extinguishing systems with specifications that met the reaction time requirements and could be expected to suppress a dust fire/explosion. A combination of two commercial systems was used in this study; an ultraviolet flame sensor coupled with a pressurized deluge system. Two extinguishing agents were tested; a halogenated hydrocarbon (Halon) and water.

A schematic representation and photograph of the large test chamber, dust dispersion system and the suppression system are shown in fig. 2 and 3, respectively. The test chamber is a rectangular box, 10.36 m (34 ft) long by

0.46 m (1.5 ft) in cross section. It is closed on one end, top, bottom and back with 1.9-cm plywood which is lined on the interior with galvanized sheet metal. The top is hinged in 1.2-m sections to allow access to the dust nozzles and instrumentation sensors. Except for one plywood panel at the fire ignition end, the front is closed with a 0.64-cm thick Plexiglas sheet to facilitate observation of the reaction using high speed photography. The end through which the extinguisher nozzle protrudes is enclosed with 0.13-mm plastic sheet. The chamber is equipped with 17 combination dust holder-distribution nozzles. The nozzles protrude through the bottom of the chamber to a height of 15.2 cm and are spaced 0.61 m apart along the center line of the chamber. The nozzles are constructed of 2.54-cm schedule 40 pipe, 12.7 cm long, with an inverted cone mounted above the nozzle exit to aid in dispersal of the dust. The base of each nozzle is equipped with a plastic ring which holds a tissue paper diaphragm to retain the dust prior to dispersal. Each nozzle has a capacity of 50 g of sulfur, providing a total capacity of 850 g used in each test.

The dust distribution nozzles, except for the one located in the center of the chamber, are connected in pairs to a 10.1-cm schedule-40 steel pipe manifold, 9.75 m long. One end has a 1.27-cm valve which isolates the manifold from an auxiliary air supply bottle. Compressed air at a manifold pressure of 758 kPa (110 psi) is used for forced distribution of the sulfur dust from the holder distribution nozzles into the chamber. Control of gas flow to each pair of nozzles is accomplished by use of a 2.54-cm full-ported solenoid valve and a valve to prevent backflow of pressure from the chamber during firing. The control of the nine air distribution valves is through an electrical switching apparatus located near the chamber. Each valve can be controlled individually from this control box for checkout, and a sequencer triggers all the valves simultaneously during tests. This control system also contains a delay relay to provide a 2-second delay in valve activation after initiation of the igniter.

The test chamber is instrumented to measure the pressure wave and flame front velocity by use of pressure and optical transducers mounted on the back vertical face of the chamber. In addition, ion probes were used to measure the flame front arrival time at each location. During some tests, passive sensors (cotton balls) were installed along the gallery to indicate the limit of flame propagation.

In all tests conducted with the suppression system, a single 40-mm M43A1 red signal flare was used as the ignition source. The flare was removed from the shell casing and mounted in a trough made of 2.54-cm angle iron. The flare was installed 0.305 m from one end of the test chamber and was ignited with an electric match attached to the fuse. The flare produced a fireball approximately 0.6 m in diameter and lasted for approximately 9 seconds. Time zero (t_0) was established by ignition of the flare, and the dust dispersion system was triggered at t_0 +2 seconds. A breakwire installed across one dust nozzle indicated arrival of dust in the chamber and a breakwire across the extinguisher nozzle indicated injection of the suppressive agent into the chamber.

The extinguisher tank, a 76-l stainless steel cylinder containing the agents being evaluated, is mounted at the end of the dust gallery opposite the ignition source. The extinguisher tank deluge valve is an explosive burst diaphragm device, actuated by a signal from the UV controller. Tests were performed with the detonator in both downstream and upstream positions with respect to the burst disc.

The ultraviolet sensor and controller is in modular form and consists of electronic circuitry for processing the detector signal plus several switching relays. The detector uses a Geiger-Mueller type tube designed to detect radiation in wavelengths from 185 to 245 nm. The tube is insensitive to UV radiation from the sun (at the earth's surface) or from artificial lighting. When the detector tube senses radiation of proper wavelength, a voltage pulse is transmitted to the controller which then energizes the deluge valve detonator.
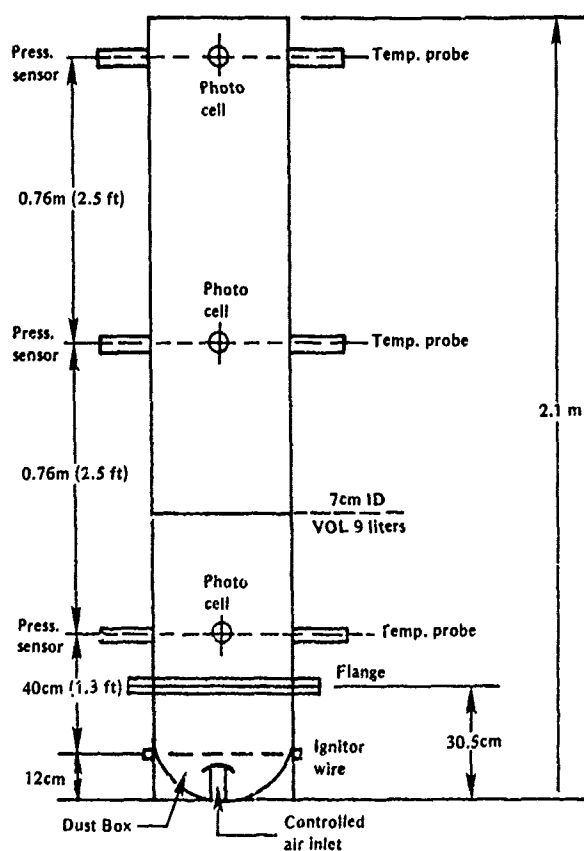
Figure 1. Extended Tube Hartmann Apparatus

10.36m

0.46m

0.46m

Air distribution manifold

Suppression system
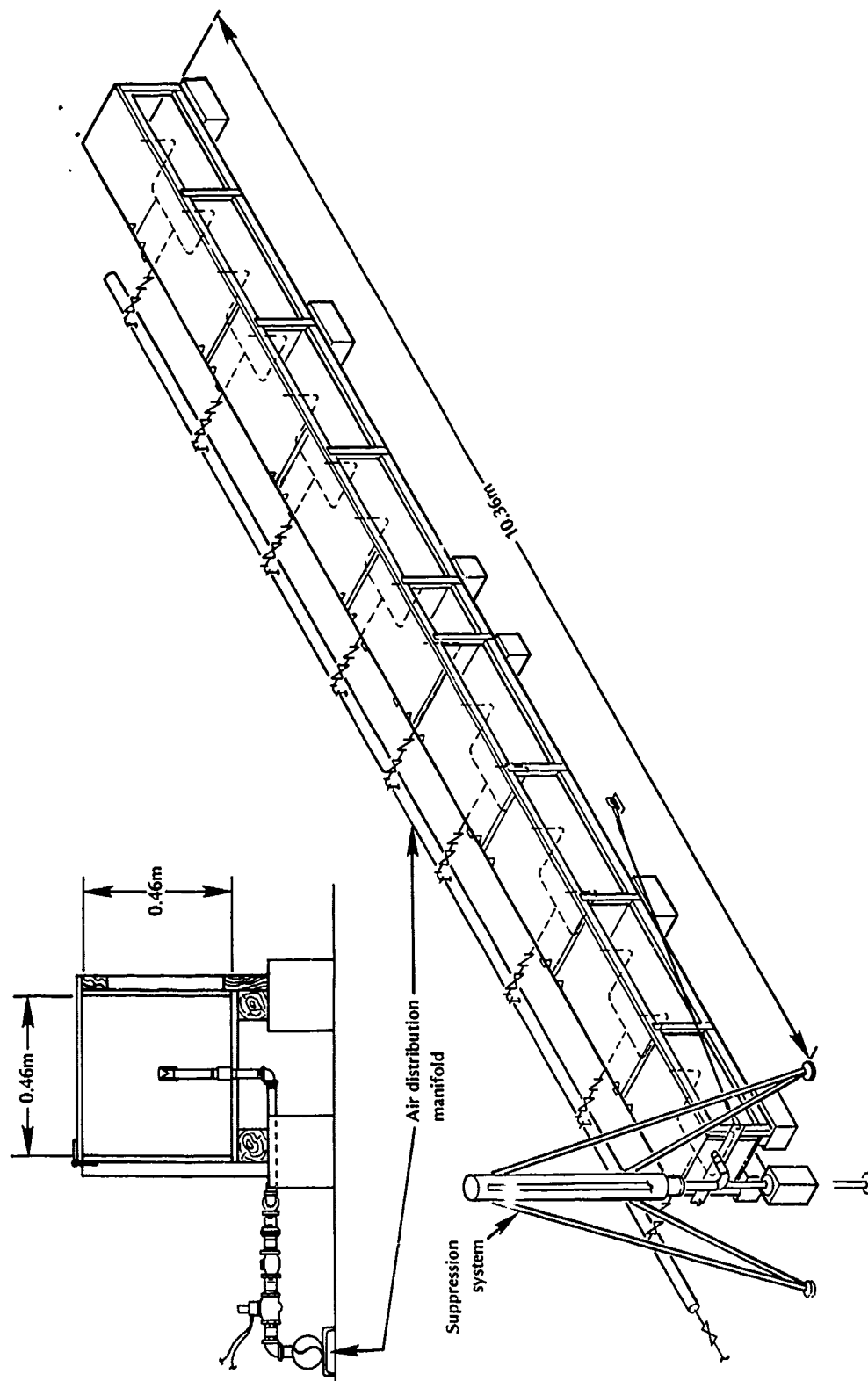
Figure 2. Plan Layout of Dust Gallery

404

Figure 3. Dust Gallery, Front View

Prior to a test, the explosive burst disc and holder were assembled and installed and the tank was loaded with extinguishing fluid (6.8 kg of Halon 131 or 57 l of water). The gallery dust nozzles were removed and paper diaphragms were installed in the base. Each nozzle was loaded with 50 g of sulfur and then reinstalled in the chamber. The M43 flare ignitor was prepared and mounted, then the gallery was closed and sealed. The gas manifold was pressurized to 758 kilopascals (kPa) (110 psi) with compressed air and the extinguisher tank was pressurized to 4140 kPa (for Halon) or 9070 kPa (for water) with nitrogen. The initiator for the burst disc valve and the flare ignitor were then connected.

The flare was ignited by the range sequencer, and two seconds later the air valves opened so that dust was injected into the chamber. Action of the UV sensor and burst disc valve then followed automatically. Visual evidence of propagation was provided by posttest inspection and by observing the motion pictures. The limit of flame advance from passive sensors, timing of ignitor, dust injection time, extinguisher injection time, pressure traces, photocell outputs and the UV sensor signal were recorded.

III. RESULTS AND DISCUSSION

A. Glass Tube Hartmann Apparatus.

Using sulfur as the sample material, good dispersion of the dust in the tube was obtained during 8 of 12 tests. Tests run with a continuous flow of air at 103-140 kPa (15-20 psi) using 0.15 g of sulfur resulted in even dust cloud distribution throughout the tube in 2-3 seconds. The average density of sulfur in the tube under these conditions was about 0.02 g/l.

B. Steel Tube Hartmann Apparatus.

Observations made using the mirror clearly showed the progress of the fireball up the tube. The dust initially produced a haze above the fireball, and was blown out the end of the tube as the fireball approached the exit. Matches placed along the tube interior failed to ignite, but after each test small molten globules of sulfur coated the tube walls. Flame propagation throughout the length of the tube resulted for charge weights of 3-6 g at an air pressure of 520-1040 kPa (75-150 psi). Improved dust distribution was noted at the higher pressures. The fireball appears as a donut-shaped bright ring on one 500 frame per second motion picture made of the propagation. Timing information as indicated by the pressure, optical and temperature sensors is given in table 1. In all cases, the top-pressure sensor either did not show a pressure trace or the signals were so erratic as to be unusable. The general form of the pressure traces showed an initial spike followed by a slow pressure rise.

TABLE 1. PRESSURE AND OPTICAL SENSOR DATA, HARTMANN APPARATUS

| Trial number | Time between sensors (ms) | | | | |
	Pressure 1-2	Optical 1-2	Optical 2-3	Temperature 1-2	Temperature 2-3
1	13.0	9.6	7.2	15.6	28.1
2	9.1	9.0	6.7	8.8	24.5
3	10.1	8.2	6.0	11.8	33.1
4	3.5*	9.4	5.1	9.0	13.3
5	1.6*	10.7	4.5	no data	19.8
6	11.8	12.4	5.1	9.1	21.8
7	2.8*	11.9	7.5	no data	19.2
8	4.3*	14.2	no data	no data	19.4
Average	11.0±1.7 *(3.0±1)	10.7±2.0	6.0±1.2	11±3	22±6

The time-of-arrival data was used to calculate average velocities of the pressure wave and flame front during propagation up the tube, results of which are given in table 2. In four of the eight tests, a pressure wave velocity

TABLE 2. REACTION PROPAGATION VELOCITIES, HARTMANN APPARATUS

Sensor position	Average velocity, m/sec		
	Pressure	Optical	Thermal
1-2	69+9 (250±70)	71±10	69±15
2-3	no data	127±20	35±8
1-3	no data	91±15	46±10

of approximately 250 m/sec was observed, compared with an average of 70 m/sec for the remaining trials. This is probably indicative of a low-order detonation in the former case, compared with a low-velocity burn during the latter runs; apparently the conditions for detonation were marginal during these tests. If the low-order pressure data is used, the correlation of velocities from all sensors at positions 1 and 2 is remarkable. On the other hand, between positions 2 and 3 the optical data shows an increasing front velocity; whereas the thermal shows a decrease. It is possible that the optical sensors triggered early due to reflections or other effects; or perhaps the thermocouples, with inherent heat capacity, may have taken longer to respond at position 3 as the fleeting flame front passed. The general indications from these experiments were that flame front propagation within the tube occurs with relatively low velocity, accompanied, or sometimes outrun, by the pressure wave.

C. Dust Gallery and Suppression System.

Visual examination of the gallery after successful test runs without the suppression system showed only small traces of unburned sulfur on the floor, with small globules of sulfur covering the walls and clouding the Plexiglas face. In tests where propagation was incomplete, a definite demarcation between clouded and clear surfaces could be observed. The cotton ball passive sensors also clearly marked the limit of flame advance. Examination of the Hulcher and high-speed motion pictures showed initiation within about 0.1 seconds after injection of the dust in the chamber. The dust as it is discharged from each nozzle forms an overlapping circular pattern which, shortly after ignition, can be observed being swept toward the chamber exit under force of the compression wave built up ahead of the flame front. The flame, clearly visible at ignition, becomes obscure due to dust and smoke buildup, and is visible only in flashes as propagation occurs. Continuous burning is visible again at the exit of the chamber.

The measurements of pressure showed an initial peak due to the compression wave from the reaction, followed by a relatively slow rise during the time that the optical sensors and ion probes indicated presence of flame. Subsequently, each pressure trace showed a sharp peak which is attributed to passage of the suppressant along the transducer array. The photocell data was extremely erratic, and, for some tests, little conclusive information could be obtained from the traces. Apparently these units responded to the initial dust injection, the movements of the dust cloud as the pressure wave passed, and the passage of the suppressant fluid in addition to the flame front. The photocell data that appeared to be consistent correlated with an average flame front velocity obtained primarily from the reaction of the UV sensor. This was corroborated by the ion probe data that was obtained during four tests.

The timing versus distance curves in figures 4 through 9 provide a display of all significant events during these
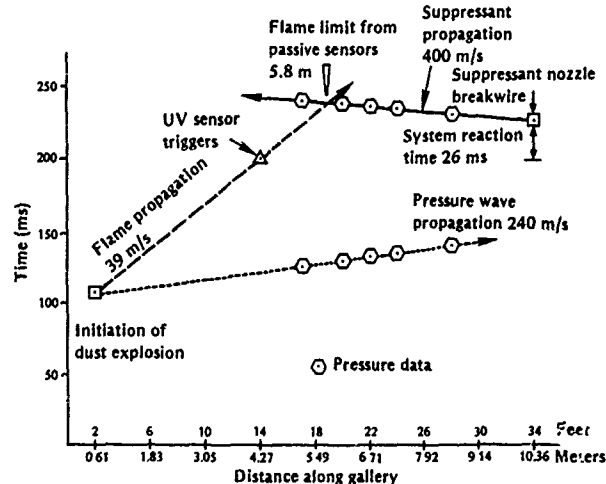
Figure 4. Test No. 40-5-01 Halon Suppressant
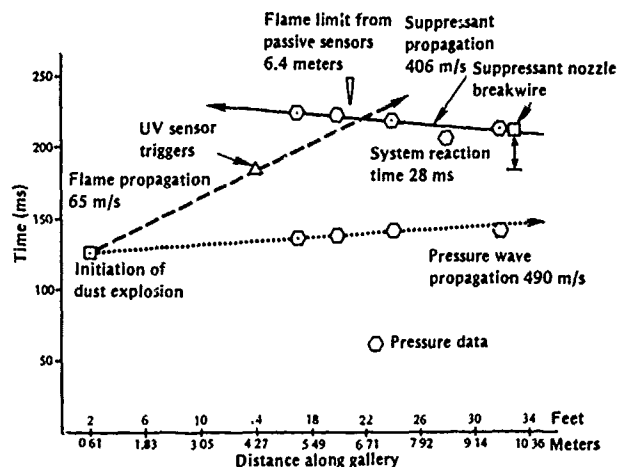
Figure 5. Test No. 41-5-01 Halon Suppressant
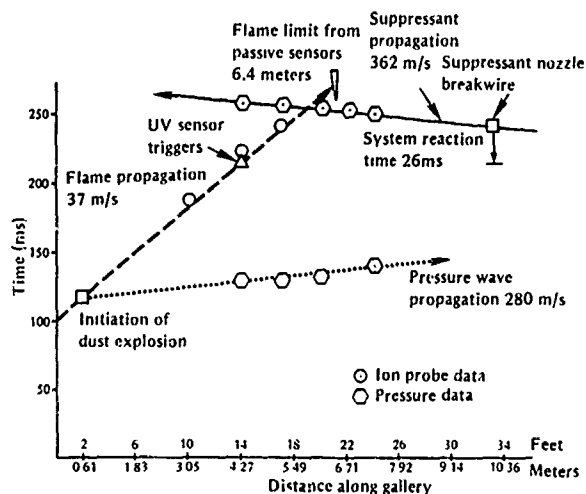
Figure 6. Test No. 47-5-01 Halon Suppressant
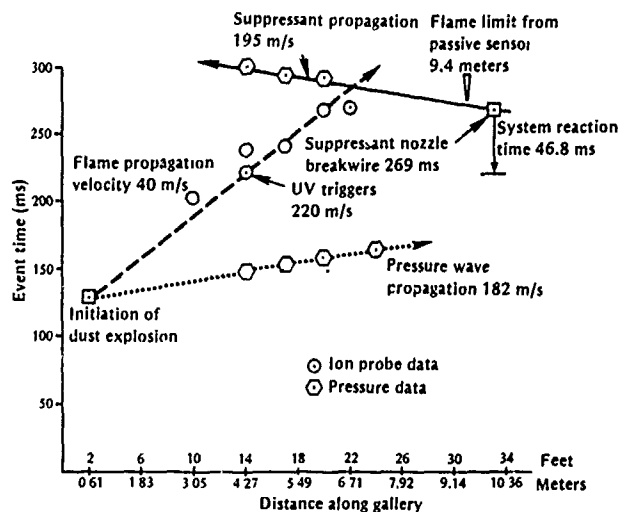
Figure 8. Test No. 49-5-01 Water Suppressant
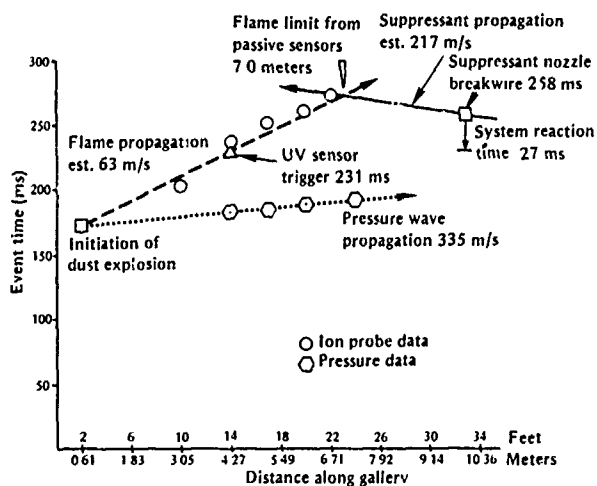
Figure 7. Test No. 48-5-01 Water Suppressant
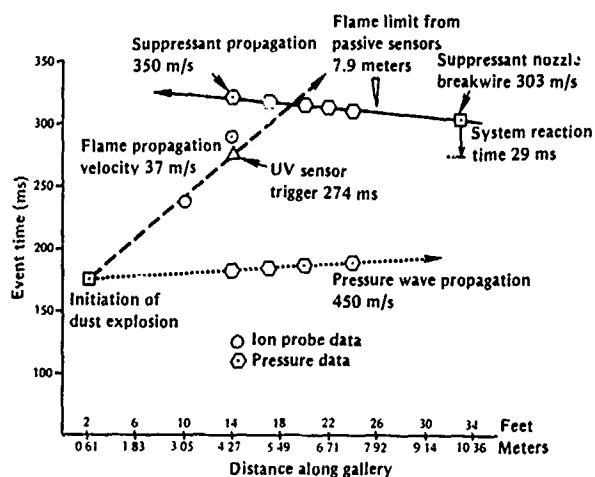
Figure 9. Test No. 49-5-02 Water Suppressant

experiments. From the point of ignition (0.61 m from the left end), a compression wave travels down the gallery at near-sound velocity. This is followed by the much slower flame front which triggers the UV sensor. After an inherent delay of about 30 milliseconds, the suppressant is released from the right end and propagates back through the gallery at, or above, sound velocity. Intersection of the flame front with the suppressant propagation curve indicates the point where the fire would be extinguished if the system were 100 percent effective. Comparison of this point with the passive sensor indicators then provides an indication of the suppression effectiveness.

A summary of the data from the dust gallery tests is given in table 3. The reaction of the ultraviolet sensor and deluge valve to the flame front was remarkably consistent. Discounting one test, the total reaction time from detection to initiation of the deluge system was 28 ±2 msec. For the Halon tests, figures 4 through 6, it is apparent that the suppression occurs with essentially no delay; the flame was extinguished within 0.5 m and within 10 msec after the suppressant arrived. For the water tests, however, the suppressive action as well as the measurement system performed less satisfactorily. The flame appeared to advance 2-3 m beyond the suppressant-flame interaction, which translates into 60-80 ms in time. In all cases the flame was extinguished prior to exiting the gallery, but the superiority of the Halon 1301 as a suppressant was clearly established. However, the additional expense and environmental problems associated with the use of halogenated hydrocarbons may offset the enhanced performance.

407

TABLE 3. SUMMARY OF FIRE SUPPRESSION TEST DATA

Test no. and fluid	Flame arrival time at UV sensor location 4.27m (ms)	Suppressant injection in chamber time from dust nozzle breakwire (ms)	System reaction time UV sensor to suppressant injection (ms)	Flame velocity ion probe parameters (m/sec)	Fire extinguish point, passive sensor location (m)	Max. flame static pressure PSIG	Leading edge pressure wave velocity (m/sec)	Comments
40-5-01 Halon	200	225	26.0		5.8	0.9	240	
41-5-01 Halon	182	210	28.0		6.4	0.8	490	
47-5-01 Halon	216.2	242.5	29.3	41	6.4	0.8	280	
48-5-01 Water	230.9	257.3	26.4	48	7.0	0.6	335	
49-5-01 Water	220.3	267.1	46.8	44	9.4	1.1	182	All the leaves on the burst disc sheared off and passed through the suppressant nozzle. Probably plugged nozzle initially
49-5-02 Water	274	303.5	29.5		7.9	1.2	450	Suppressant nozzle plugged with pieces of burst disc approximately 80 percent

IV. CONCLUSIONS

The results of this test series indicate that a UV detector/high-pressure suppression system can be highly effective in controlling the extent of damage due to flame propagation within a pyrotechnic manufacturing facility. Depending on the application, a fire can either be extinguished at the source or confined to a limited area such as the cubicle in which an operation takes place. An ultra-violet-detector/high-pressure quench system with a burst deluge valve is sufficiently fast in action to detect and extinguish a sulfur-dust deflagration within 20-100 milliseconds. Using similar systems, Halon 1301 is a better suppressant than water.

Sulfur dispersions in air are subject to low-order detonation when ignited by a hot source. A compression wave propagates outward with near-sonic velocity, followed by a flame front of much lower velocity.

V. REFERENCES

1. Nestle, W. R., G. L. McKown and R. B. Belmonte, Contractor Report ARCSL-CR-77020, Investigation of Methods for Detection and Control of Pyrotechnic Dust Fires and Explosions, June 1977.

2. McIntyre, F. L., Edgewood Arsenal Contractor Report EM-CR-76011, Incident/Accident Survey (1950 through 1974), December 1975.

3. McKown, G. L., Pyrotechnic Hazards Evaluation Program, Minutes of the Seventeenth Explosives Safety Seminar, pages 1473-1485, September 1976.

4. McIntyre, F. L., Edgewood Arsenal Contractor Report EM-CR-77008, Evaluation of Violet Smoke Initiation Under Dynamic Conditions in the Jet Airmix Blender, November 1976.

5. McIntyre, F. L., and W. R. Wilcox, Contractor Report ARCSL-CR-78004, Identification and Evaluation of Hazards Associated with Blending of Violet Smoke Mix by Double Cone Process, January 1978.

6. Nestle, W. R., Edgewood Arsenal Contractor Report EM-CR-74052, Formulation of Hazard Evaluation Indices for Pyrotechnic Processes, March 1975.

7. Tulis, A. J. and R. F. Remaly. Dispersion and Detonation of Explosive Dusts, Proceedings Fourth International Pyrotechnics Seminar, July 1974.

SELF HEATING IN CONSOLIDATED Al/Cu$_2$O THERMITES

Gary D. Miller, Jonathan H. Mohler, and Michael D. Kelly

ABSTRACT

The ignition theory of Frank-Kamenetskii, which follows from
a solution of the steady-state heat flow equation for an
isotropic chemical heat source, predicts that a measurable
temperature difference will be established between the center
and wall of a sample that is near its ignition point. We have
measured this temperature difference in a cylindrical Al/Cu$_2$O
thermite part under conditions approximating a steady-state.
The results of the measurements lead to a calculation of the
activation energy and a pseudo-zero order preexponential
factor for the thermite reaction rate constant.

SELF HEATING IN CONSOLIDATED Al/Cu$_2$O THERMITES

Gary D. Miller, Jonathan H. Mohler and Michael D. Kelly

Mound Facility*
Miamisburg, Ohio

INTRODUCTION

The Frank Kamenetskii theory of thermal ignition [1] provides a model through which the ignition temperature of an explosive or pyrotechnic material can be calculated. An interesting prediction of the model is that just below the ignition point a measurable temperature difference will be established between the center and wall of the sample because of the self-heating phenomenon. Essentially, the model predicts that for a slowly heated sample, thermal ignition will occur when a temperature is reached at which the rate of heat production from chemical exoergicity exceeds the rate of heat loss caused by thermal conduction. The basic assumptions of the model are: (1) the combustion or decomposition reaction occurs at all temperatures but is imperceptibly slow below the ignition temperature, (2) the reaction does not occur through a chain mechanism, and (3) the Arrhenius Equation is a valid description of the reaction rate constant. The physical properties required for an ignition temperature prediction are the reaction exoergicity, Q, the thermal conductivity, λ, the sample geometry and size, the activation energy, E, and the preexponential factor of the reaction rate constant, A. If it is assumed that ignition occurs before significant reaction has taken place, the concentration dependence of the reaction rate is also included in A.

Frank-Kamenetskii's theory has been described in detail elsewhere [1]. Briefly, it begins with the general heat flow equation for an isotropic chemical heat source,

$$c\rho\frac{\partial T}{\partial t} - \lambda\nabla^2 T = QAe^{-E/RT} \tag{1}$$

where: c = the mean specific heat
ρ = the density
T = the temperature
t = time
R = the gas constant
∇^2 = the Laplacian operator

411

Restriction to slow heating rates, the use of the Todes approximation [2]:

$$\frac{E}{RT} \simeq \frac{E}{RT_W} \left(1 - \frac{T - T_W}{T_W}\right), \tag{2}$$

and the introduction of two dimensionless quantities:

$$\theta = \frac{E}{RT_W^2} (T - T_W), \tag{3}$$

and $z=x/r$ lead to the temperature distribution (solution of Eq. 1) for a cylindrical sample having a length much greater than its radius:

$$\theta = \ln (8/\delta) - 2 \ln (e^{-b}z^2 + e^b), \tag{4}$$

where T_W is the temperature at the curved wall of the cylinder, θ is a reduced temperature, z is the reduced spatial coordinate, x is the real spatial coordinate, r is the cylinder radius, and δ is the dimensionless criticality parameter defined as:

$$\delta = \frac{QEAr^2 e^{-E/RT_W}}{RT_W^2} . \tag{5}$$

Finally, b is an integration constant given by $b = \cosh^{-1} \sqrt{2/\delta}$. The point of thermal ignition for a long cylinder under slow heating has been found by both numerical [3] and analytical [1] procedures to occur when $\delta = \delta_{cr} = 2.00$, at which point $T_W = T_O$, the wall ignition temperature. Substitution of $\delta = 2.00$, $z = 0$, and $T = T_c$, the center temperature at ignition, into Eq. 4 gives the center-wall temperature difference at ignition, $\Delta T_m = T_c - T_O$, as:

$$\Delta T_m = 1.38 \ RT_O^2/E . \tag{6}$$

Although the usual application of ignition theory is to use Eq. 5 and a knowledge of thermal conductivity, thermochemical properties, and kinetic parameters to predict the ignition temperature for a sample of known size and geometry, the process has been inverted here to find the kinetic parameters, E and A, in a system for which classical kinetic methods would be difficult. By measuring simultaneously the center and wall temperatures at ignition, the activation energy, E, can be found directly from Eq. 6. Once E is found, the preexponential factor, A, can be found from Eq. 5 and previously determined values for Q and λ.

The Frank-Kamenetskii theory has most frequently been applied to explosion of an unstable gas [4] or gas mixture, and as a result is usually known as thermal explosion theory. There is nothing in the mathematical treatment, however, which requires explosion. The theory only deals with processes at temperatures below the point at which heat production begins to exceed heat loss. At this point, the temperature increase becomes very rapid; in turn, heat production becomes

more rapid because of the exponential temperature dependence of chemical rate constants. The increasingly faster heat evolution boosts the system temperature still faster and the reaction is said to "run away with itself." The occurrence of an explosion depends solely upon whether the chemical reaction has gaseous products. Attempts have been made at choosing systems for study which do not explode after the ignition point to minimize damage to experimental apparatus. Collister and Pritchard, [5] for example, have studied thermal ignition for the slightly exoergic ($Q = 27.3$ kcal mol^{-1}) isomerization of methyl isocyanide.

The consolidated thermites of this study are particularly well suited to thermal ignition experiments for several reasons. First, the reaction:

$$3 \; Cu_2O_{(s)} + 2 \; Al_{(s)} \longrightarrow Al_2O_{3(s)} + 6Cu_{(s)} + 573 \; cal \; g^{-1} \quad (7)$$
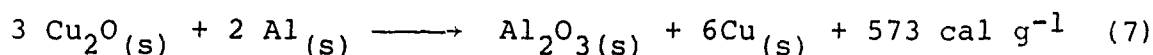
has no gaseous products to result in explosion. In addition, because the thermite mixture is consolidated to 90% of its theoretical maximum density by a hot pressing process, there is little air present to cause a large pressure increase during burning. Third, the Todes approximation used in the derivation of Eq. 4 is much better in the ignition temperature range of normal size Al/Cu_2O thermite parts (~500 °C)than at ignition temperatures of most organic explosives (~250°C). Finally, the requirements of the ignition model, that the medium be isotropic and have a definite simple geometry, are easily satisfied for consolidated thermite parts.

EXPERIMENTAL

Stoichiometric proportions of finely divided Al and Cu_2O were hot pressed into four cylindrical pellets of density, 4.71 g/cm^3. The four cylinders were aligned end to end as shown in Figure 1; the resultant cylinder had a total length of 10.19 cm and a diameter of 2.870 cm. The cylinder was inserted into a graphite sample holder (also shown in Figure 1) and end caps were screwed in place to fix the position of the thermite. Stainless-steel sheathed chromel-alumel thermocouples were inserted,to a depth of half the cylinder's length, into predrilled holes in the graphite holder and thermite sample at the cylinder wall and center. The assembled sample holder and thermocouples are shown in Figure 2. A tube furnace was placed outside the sample holder. The heating rate of the furnace was controlled by a Focal-11 program running on a PDP 11/10 computer. The computer is coupled to the thermocouples and to a relay in the furnace power line through a Digital Equipment Corporation laboratory peripheral system (LPS). Temperatures acquired by the program were compared to a linear temperature-time equation and the furnace was then turned on or off, as required, at a frequency of 1 Hz. The heating rate at the sample wall was 10°C/min from ambient temperature to 300°C, 5°C/min from 300 to 400°C and 2°C/min above 400°C. The deviation of the wall temperature from the program temperature was a maximum of ±1.5°C at temperatures above 400°C.
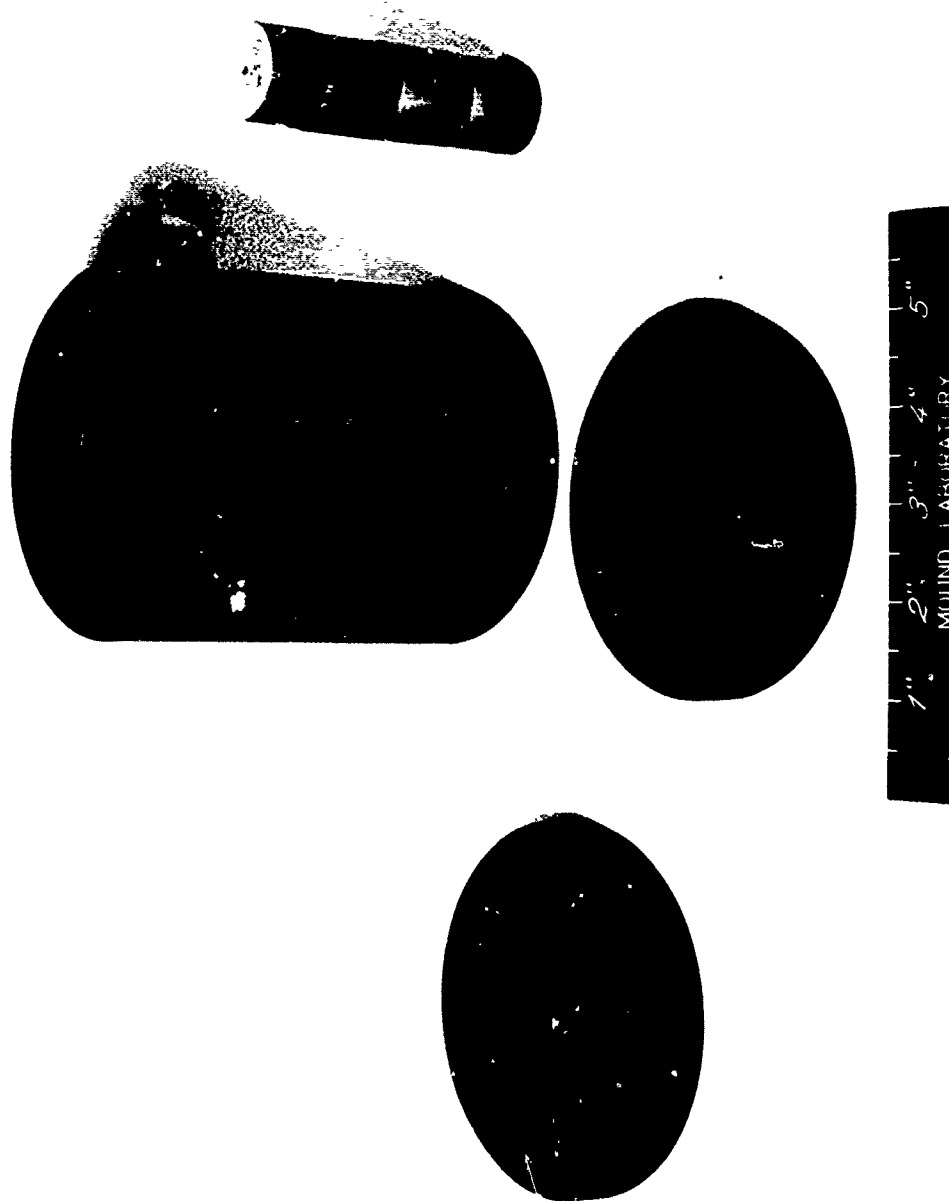
FIGURE 1 - The disassembled sample cylinders stacked end-to-end are shown with the graphite sample holder and end caps.
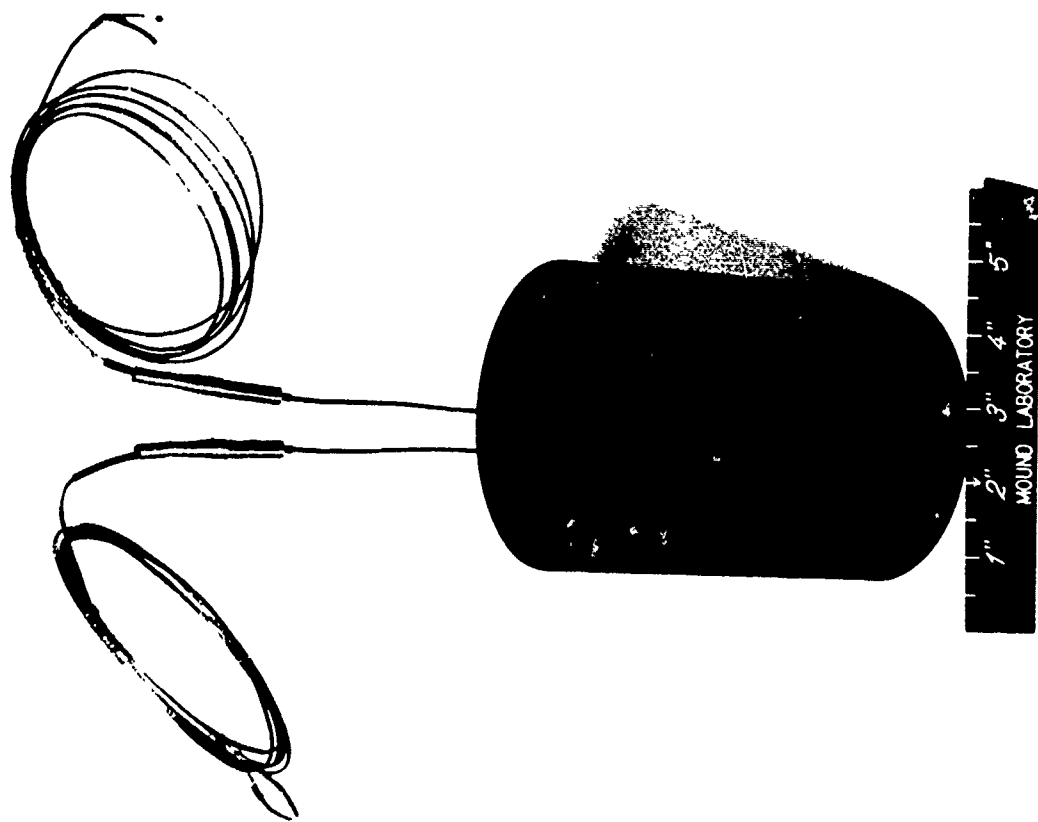
FIGURE 2 - The assembled sample holder is shown with thermocouples in-place.

RESULTS

The temperature versus time data of the experiment were read out in digital form on the computer terminal every two seconds. Samples of these data are reproduced in Figure 3. Inspection of the figure shows that significant self heating begins to occur at a wall temperature of about 470°C. The ignition point was identified by a sharp jump of the center temperature off the scale of the A/D converter in the LPS (maximum digital number corresponded to 1038°C). The wall temperature rose to only 719°C at this point, evidently because of the large heat capacity of the graphite sample holder. Inspection of the sample after burning revealed that combustion was complete. Most of the molten thermite reaction products had drained out of the sample holder through a 6.35 mm diam hole in the lower end cap.

The wall ignition temperature observed for the thermite part described above was 511.5 ± 0.5°C. At that point, the center temperature was 522.5 ± 0.5°C. From these data and Eq. 6, an activation energy of 642 ± 58 kJ/mol for the reaction of Eq. 7 was obtained.

In order to calculate the preexponential factor, A, additional measurements are required. The thermal conductivity was previously determined in our laboratory by the comparative method [6] with a Dynatech Corporation model TCFCM thermal conductivity instrument. The result obtained was λ = 6.0 ± 0.4 W/m·K at 500°C for Al/Cu_2O thermite consolidated to ρ = 4.71 g/cm^3. The heat of reaction, Q, was determined by bomb calorimetry to be 1080 ± 20 kJ/mol. The value of the pseudo-zero order preexponential factor calculated from these values and Eq. 5 is log A = 42.4 ± 3.9 when A is in $mol·m^{-3}·s^{-1}$. A summary of all relevant measurements, results, and the uncertainty in each is given in Table 1.

DISCUSSION

It is interesting to compare the observed wall ignition temperature of 511.5°C with the reported result of 545°C as measured by differential scanning calorimetry (DSC). [7] The discrepancy is easily explained by the ignition theory through Eq. 5. Though it is not immediately obvious from the form of Eq. 5, we have found through reiterative solutions by the Newton-Raphson procedure that T_0 has an inverse dependence on r. We therefore expect the very small sample used in DSC to have a higher ignition temperature than the 2.87 cm diam cylindrical sample of this experiment.

The values obtained for E and A may seem quite high when compared to those of other reactions with which chemists are familiar. One must keep in mind, however, that the thermite reaction is unusual both in its high temperature requirement for thermal ignition and in its speed once ignition has occurred. A high-activation energy is totally consistent with the high temperature required for reaction.
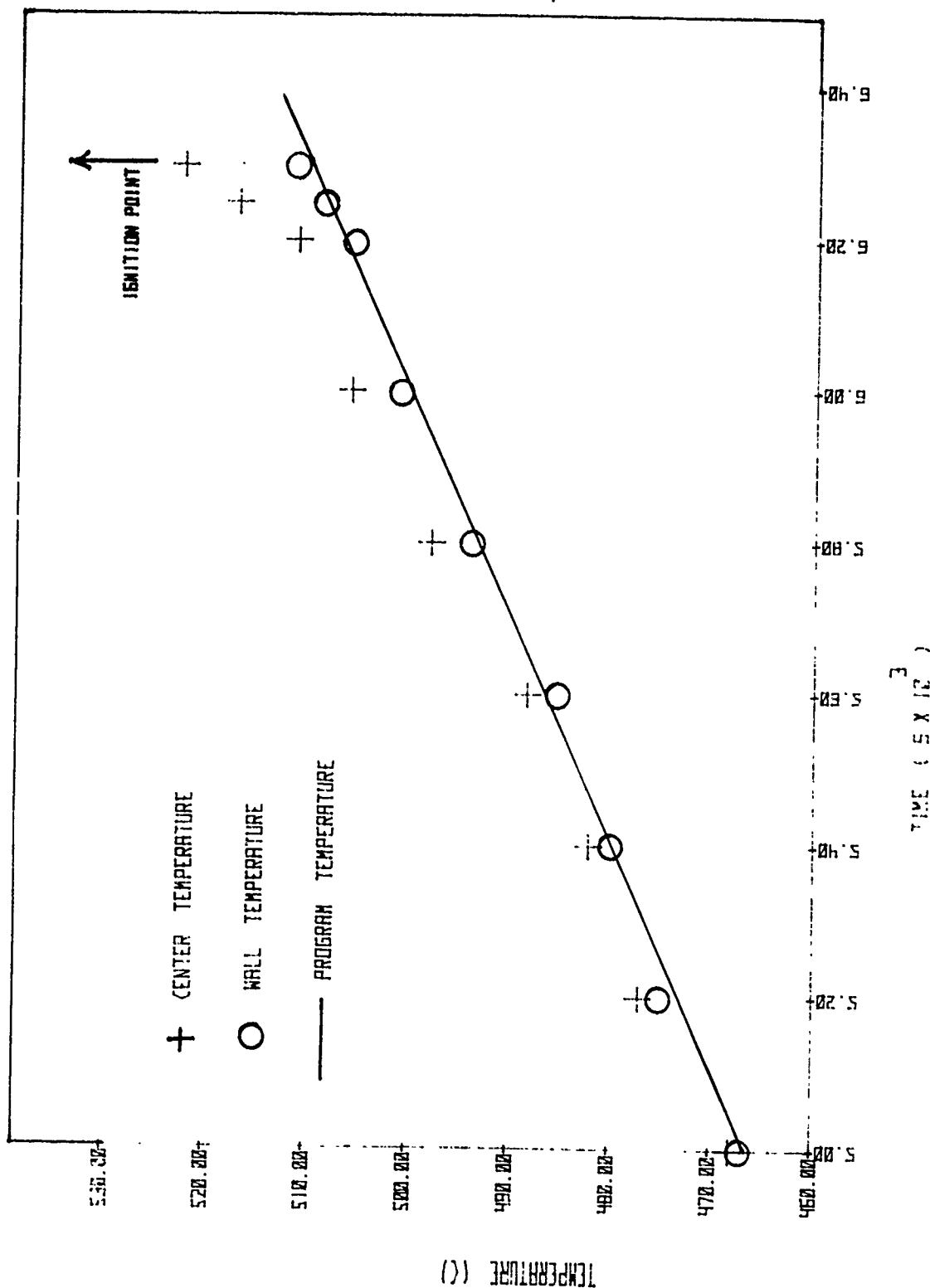
FIGURE 3 – Temperatures acquired by the FOCAL-11 program operating through the LPS are shown here. The upper set of points represents the center temperature, the lower set represents the wall temperature, and the line represents the temperature program. Because a total of over 6000 temperatures were acquired at a print out frequency of 0.5 Hz, only sample points are shown. It is clear that significant self-heating does not occur until the sample is brought within about 40°C of its ignition temperature.

417

Table 1

SUMMARY OF MEASURED QUANTITIES AND UNCERTAINTIES

Quantity	Value	Uncertainty (+%)	Method
Q (kJ/mol)	1080	2	Bomb calorimetry
λ (W/m·K)	6.0	7	Comparative
r (cm)	1.435	0.5	-----------
T_O (K)	784.5	0.06	This experiment
T_C (K)	795.5	0.06	This experiment
ΔT_m (C)	11.0	9	This experiment
E (kJ/mol)	642	9	This experiment
log A (mol/m^3·s)	42.4± 9	-	This experiment
dT/dt (°C/min)[a]	2.0	2	This experiment
ρ (g/cm^3)[a]	4.71	1	This experiment

[a]Quantities not required for determination of E and A.

Furthermore, a large value of the pseudo-zero order preexponential factor is consistent with the fast burn rate observed after initiation. The preexponential factor measured must contain a density and particle size dependence. However, additional experiments will be required to separate these factors out.

The experimental uncertainties reported for E and A compare favorably with typical uncertainties from classical kinetic methods. It should be pointed out, however, that these uncertainties are reflections of only the random error caused by least measure, resolution, and noise limitations of the technique. There may be systematic errors present that cannot be evaluated at this time. The first of these arises from the assumption that a chain mechanism is not involved in the reaction. Although a total lack of mechanistic information makes us unable to rule out a chain, it is felt that there is less liklihood of it with a solid-state reaction, which may be diffusion controlled, than with many of the gas phase reactions to which ignition theory has previously been applied. The second possible systematic error is the finite heating rate used. An improvement in experimental technique would be the determination of ignition temperatures at several slow heating rates, followed by extrapolation to the required condition, $dT/dt = 0$.

We know of no other measurements of the kinetic parameters for the Al/Cu_2O thermite reaction with which to compare our results. Such comparisons would, in any case, be difficult, for it shoud be noted that our results are specific to the Al and Cu_2O powder sizes and the density of the sample used here. The lack of other data on the kinetics of the Al/Cu_2O thermite reaction derives from three major causes. First, solid-state reactions are difficult to follow by the classical kinetic method of following concentration as a function of time. Second, the reaction occurs at an appreciable rate only at high temperatures. Finally, the reaction is so exoergic that it is impossible to carry out isothermally, as is done in most classical kinetic experiments. Therefore, we believe that this method is the best one for determination of the rate constant for the reaction of consolidated thermite. In addition, we expect that the method will be applied to ma..y other pyrotechnic systems in the future.

ACKNOWLEDGEMENTS

REFERENCES

1. D. A. Frank-Kamenetskii, Diffusion and Heat Transfer in Chemical Kinetics, Chap. VI and VII, Plenum, New York, 1969.

2. P. L. Chambre, J. Chem. Phys., 20, 1795 (1952).

3. E. J. Harris, Proc. Roy. Soc. (London), A175, 254 (1940).

4. See, for example, O.K. Rice, J. Chem. Phys., 8, 727 (1940).

5. J. L. Collister and H. O. Pritchard, Canad. Journ. Chem., 55, 3815 (1977).

6. R. P. Tye and J. R. Hurley, Proceedings of the Fifth Temperature Measurement Conference, 1967, Temperature Measurements Society, Los Angeles, pp. II-C 1-28.

7. L. W. Collins, Monsanto Research Corporation, private communication.

EFFECT OF POWDER COMPACTION VARIABLES ON THE PERFORMANCE OF A PYROTECHNIC IGNITER[*]

by
A. C. Munger-N. J. Seubert-J. R. Brinkman

Mound Facility
Miamisburg, Ohio

ABSTRACT

The compaction of the pyrotechnic powder against a bridgewire
in an igniter is very critical to performance. The density
of the compact at the bridgewire interface can be effected by
the powder characteristics, environment, surface finish and
configuration of the compact holder and the loading process.
Some of these parameters have been evaluated and the effect
determined on the bridgewire-powder interface as well as the
initiation performance.

EFFECT OF POWDER COMPACTION VARIABLES ON THE PERFORMANCE OF A PYROTECHNIC IGNITER

Alan C. Munger, Norman J. Seubert, and J. Russ Brinkman

Mound Facility*
Miamisburg, Ohio

INTRODUCTION

The premise that a uniform powder density will result from using a fixed applied pressure to load a pyrotechnic mixture into an igniter can be undermined by several physical factors. The compaction characteristics of a pyrotechnic powder are not only a function of materials but also the cavity configuration into which it is placed, the environment, and the processing conditions. All of these factors can influence the density gradient in the compact and thus, the density at the bridgewire. Since the density of the pyrotechnic around the initiating bridgewire is a critical parameter that affects the ignition of the pyrotechnic, these compaction parameters must be considered for any component design and fabrication process. This study evaluates some of these factors and the effect on performance.

Techniques were developed to estimate the density of the pyrotechnic at the bridgewire interface of an igniter. Parameters affecting the density at the bridgewire were then incorporated in the design and processing of inexpensive test components. The hot wire ignition performance of these components was determined and related to nondestructive test data and the estimated density.

DENSITY DETERMINATION

A method to estimate the density of the pyrotechnic at the bridgewire was developed. The method is a two-step process: first, measure the density of a thin compact (thin enough so that there is essentially no density gradient) as a function of applied pressure; and second, measure the pressure applied and transmitted during compaction in a configuration identical to an igniter design. The transmitted pressure data are then used to estimate the density at the bottom of the compact (relates to the density at the bridgewire in an igniter) using the pressure-density relationship established in the first step.

The system used to obtain the pressure applied and the pressure transmitted is a commercial servo-hydraulic unit (manufactured by Materials Test System, Inc.) coupled with load cells and a displacement monitor. Load and displacement data are obtained by means of an X-Y recorder; the system is shown schematically in Figure 1. A sketch of the tooling is shown in Figure 2.

The charge holder used to obtain the pressure-density relationship was a smooth steel cylinder having an inside diameter of 4.29 mm and a length of 0.50 mm. At this length-to-diameter ratio (0.12), the pressure applied and transmitted during compaction was essentially equal indicating a uniform compact density. The cylinder was tare weighed, loaded with 15 mg of pyrotechnic powder, the loaded cylinder gross weighed, and the length of the compact measured. From these data, the density was calculated; this process was repeated at various applied pressures.

A pressure-density relationship was determined in this method for a 33/67% blend of titanium subhydride ($TiH_{0.65}$) and potassium perchlorate ($KClO_4$). This pyrotechnic is a very safe static-insensitive material which exhibits good ignition performance [1]. The pressure-density relationship was determined to be as follows:

$$P = 1.351 \, \rho^{0.108}, \tag{1}$$
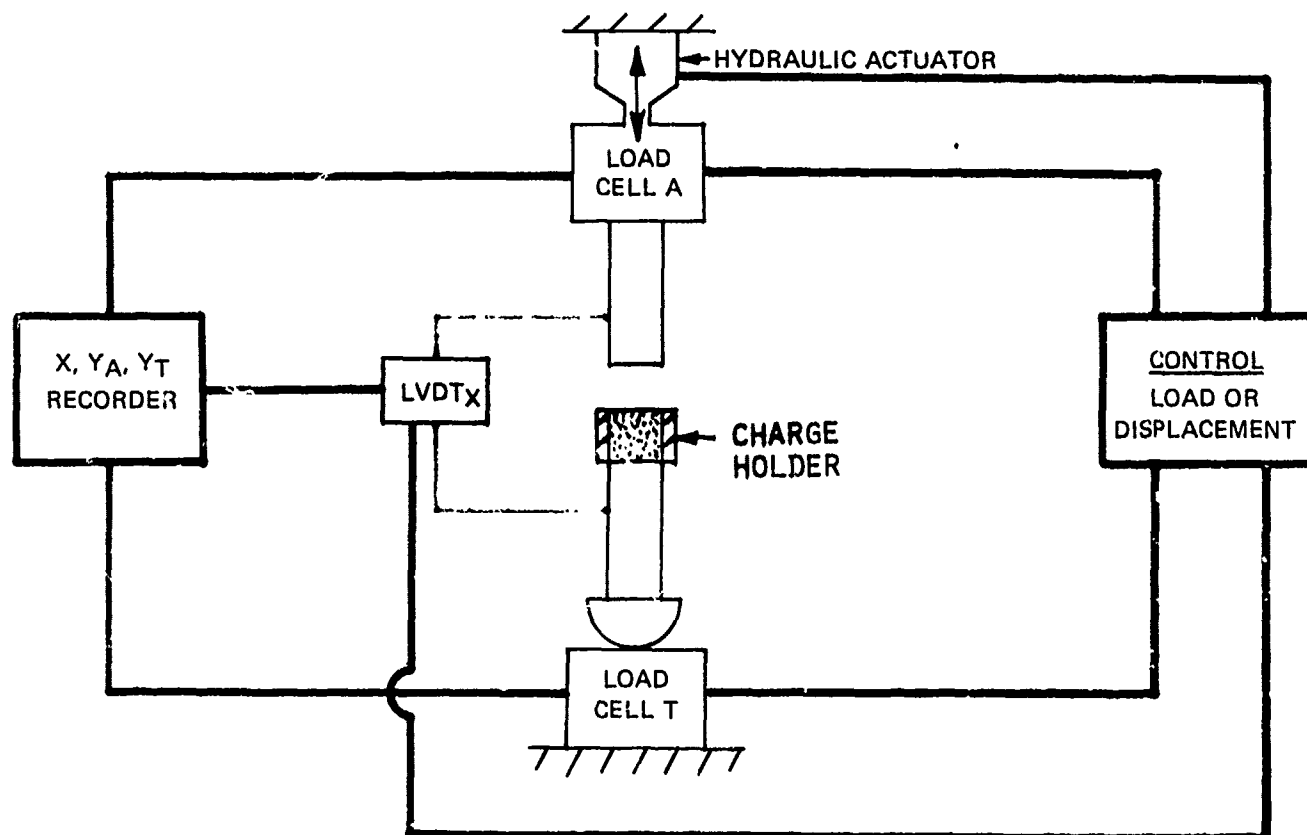
FIGURE 1 - Compaction test system.
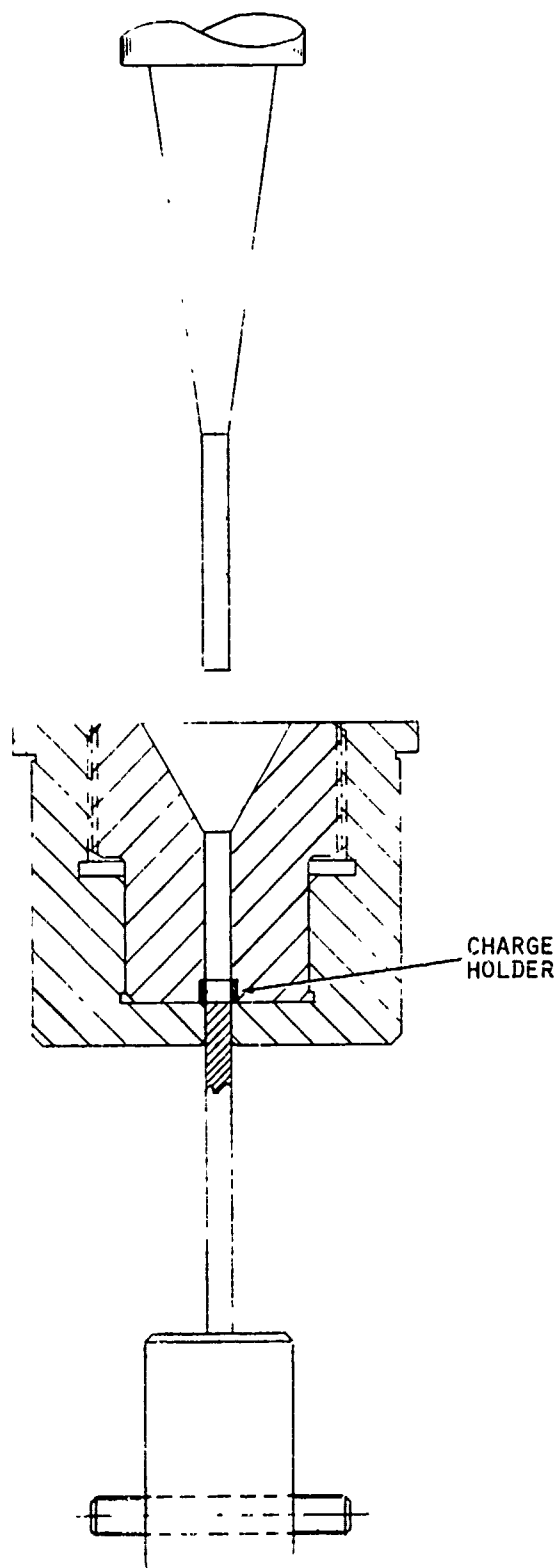
FIGURE 2 - Compaction test system tooling.

where:

P = pressure in MPa.
ρ = density in Mg/m^3.

This relationship is shown in Figure 3.

In order to estimate the density at the bridgewire of an igniter, the same test system was used. A charge holder, identical to the one in igniters, was used and subsequently tested. The cylinders had a 4.29 mm inside diameter and a length of 3.73 mm. Typical data acquired for a powder charge of 112 mg are shown in Figure 4. The force applied (F_a) and the force transmitted (F_t) are recorded as functions of displacement (compacted powder length). For these data, the pressure applied (P_a) and the pressure transmitted (P_t) can be related to the pressures during compaction of the pyrotechnic in an igniter component. The P_t can then be used to estimate the density at the bridgewire using the relationship developed in Eq. 1.

COMPACTION PARAMETERS

Three compaction parameters were evaluated: surface finish of the charge holder, powder storage humidity, and dwell time of the compaction pressure. The density of the powder at the bridgewire interface was estimated when dry pyrotechnic was compacted at 68.9 MPa into charge holders that had various surface finishes ranging from smooth (RMS <0.2 μm), to very rough (RMS >3.2 μm) and when pyrotechnic powder conditioned at 100% relative humidity for 36 hr was compacted at 68.9 MPa with smooth charge holders. These data are shown in Table 1. In addition, powder was compacted similarly at the pressure required to achieve a density of 1.89 Mg/m^3 at the bridgewire. These data are shown in Table 2.

The density at the bridgewire is 6.3% greater for the very smooth charge holder (Group A) when compared to the average charge holder (Group B). There was no difference in the average charge holder and the very routh charge holder (Group C). This is probably because the grooves in the average charge holder are larger than the particle size of the pyrotechnic. As a result, the frictional force for both the charge holders is the sliding friction of the powder against powder entrapped at the charge holder surface.

The density at the bridgewire is only 3.2% greater for the very smooth charge holders when the powder is treated at 100% relative humidity.

As shown in Table 2, 30-40% less applied pressure is required to load the very smooth charge holders and achieve the same density at the bridgewire as that obtained with 68.9 MPa in the rough charge holders.

Fig 3

Pellet Height [mm]

Fig 4

427
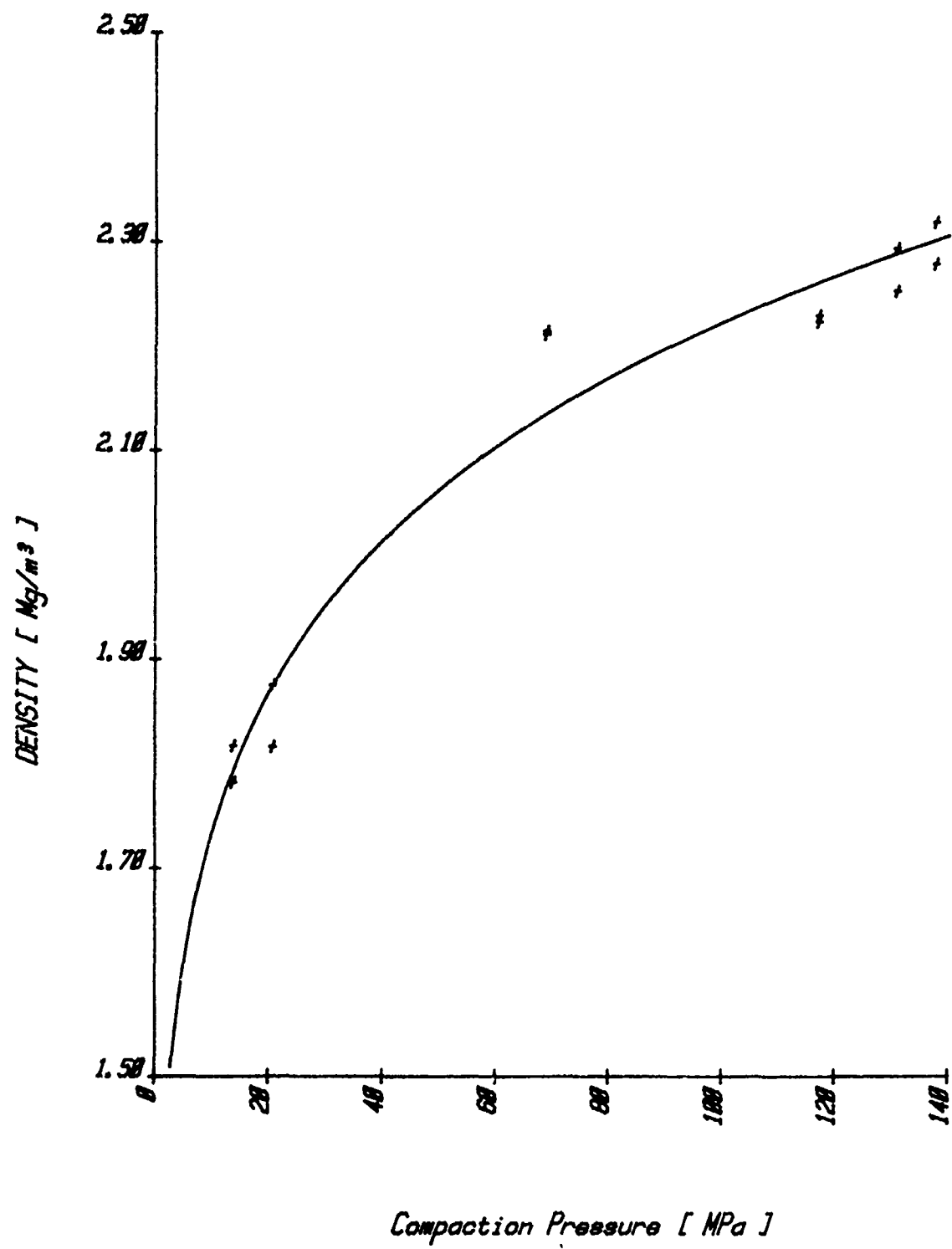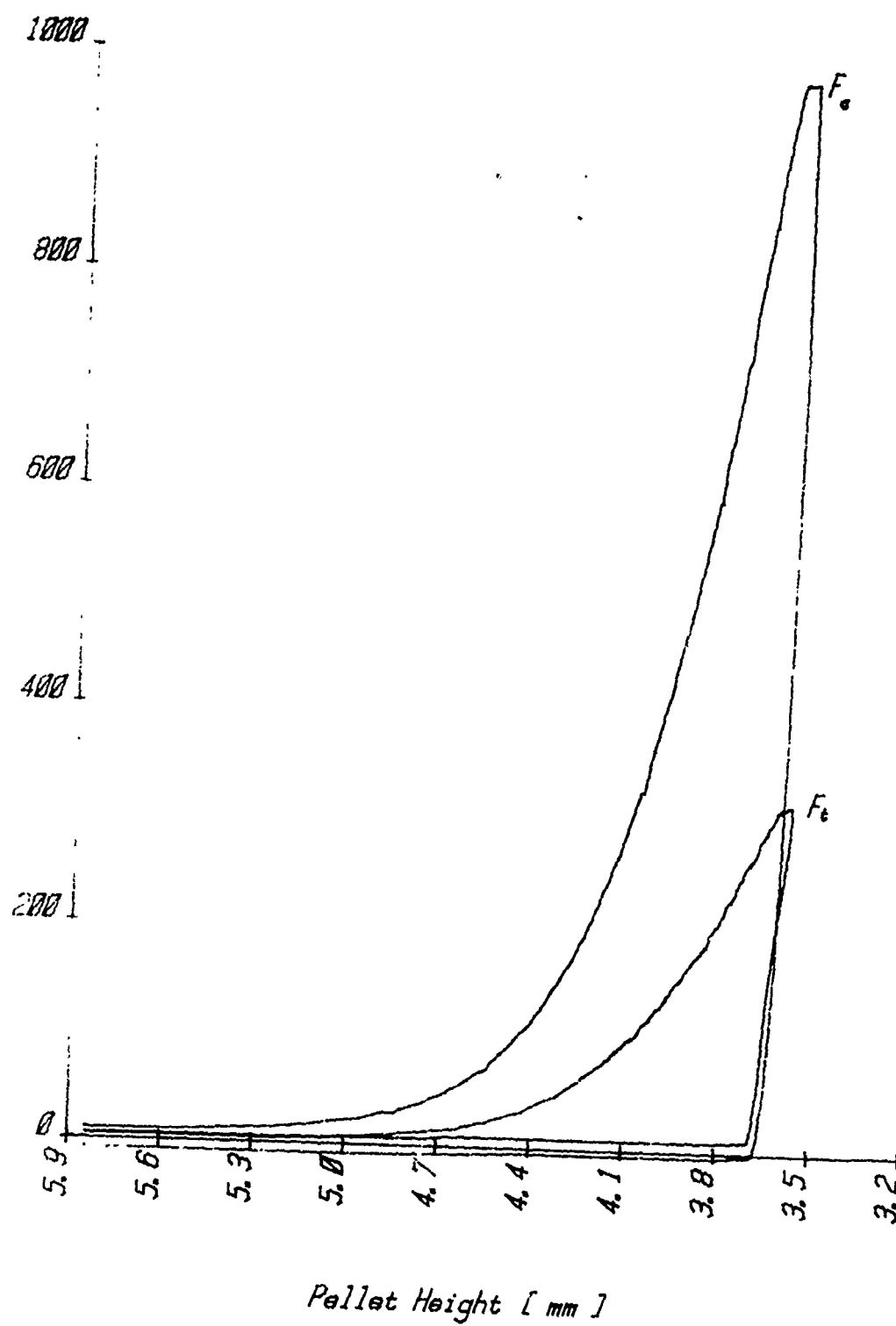
Table 1

TRANSMITTED PRESSURE AND DENSITY
WITH A CONSTANT APPLIED PRESSURE[a]

Group	Charge Holder Surface Finish (μm)	Powder Condition[b]	P_t (MPa)	P_t/P_a (%)	Average Density (Mg/m³)	Density Estimate at Bridgewire (Mg/m³)
A	<0.2	Dry	39.0	56.6	2.10	2.01
B	0.8 - 1.6	Dry	21.9	31.8	2.04	1.89
C	>3.2	Dry	21.5	31.2	2.05	1.88
D	<0.2	Wet	30.3	44.0	2.02	1.95

[a] 68.9 MPa

[b] Dry indicates powder stored in desiccator: wet indicates powder stored at 100% relative humidity for 36 ' .

Table 2

APPLIED PRESSURE REQUIRED TO ACHIEVE
CONSTANT DENSITY AT BRIDGEWIRE[a]

Group	Charge Holder Surface Finish (μm)	Powder Condition[b]	P_t (MPa)	P_t/P_a (%)	Average Density (Mg/m³)	Density Estimate at Bridgewire (Mg/m³)
E	<0.2	Dry	42.6	51.2	1.98	1.89
B	0.8 - 1.6	Dry	68.9	31.6	2.04	1.89
F	<0.2	Wet	48.1	45.3	1.94	1.88

[a] P_t - 21.8 MPa

[b] Dry indicates powder stored in desiccator; wet indicates powder stored at 100% relative humidity for 36 hr.

BRIDGEWIRE PERFORMANCE

An inexpensive test device (MAD-1031), which is shown in Figure 5, was developed that simulates igniters used in special applications. The charge holder used in the MAD-1031 was identical to that used in previous density evaluation experiments. MAD-1031 components were fabricated with smooth and rough charge holders, with dry and moisture-treated powder, and with two different compaction dwell times.

Two significant parameters were measured on these components, that is, electrothermal response (ETR) gamma* and time-to-bridge burnout (BOT)** upon application of 3.5 A. These data, along with the estimated density at the bridgewire, are shown in Table 3.

A review of the data in Table 3 reveals a significant fact. Compacting powder at a constant pressure does not necessarily result in a constant density and therefore does not result in a constant ignition time--also, the higher the density--the higher the ETR gamma. This is expected; since, at the higher density, there is a greater heat loss to the powder while the bridge temperature is rising because of the application of an ETR current pulse (500 mA for 75 msec). Similarly, there is a greater heat loss to the powder during application of the firing pulse (3.5 A) resulting in longer ignition times.

The relationship between the BOT and the density at the bridgewire is shown in Figure 6. Note that at the density of 1.88-1.89 Mg/m^3, two groups were compacted at 68.9 MPa whereas two groups were compacted at 30-40% less pressure.

The relationship between the ETR gamma and the density at the bridgewire is shown in Figure 7. Although this correlation is not as good as the ignition time--density relationship, this nondestructive technique can be used as a guide to determine or achieve the desired density at the bridgewire. Figure 8 shows the relationship between the ignition time and the ETR gamma. This relationship also indicates that ETR gamma can be used as a guide to ignition performance.

---

*The ETR test was first proposed by Rosenthal and Minichelli [2] and further developed by Strasberg [3,4]. Gamma is the most useful parameter determined in the ETR test and is related to the rate of heat loss from the bridgewire.

**For these components, the time-to-bridge burnout and the ignition time of the pyrotechnic are indistinguishable.
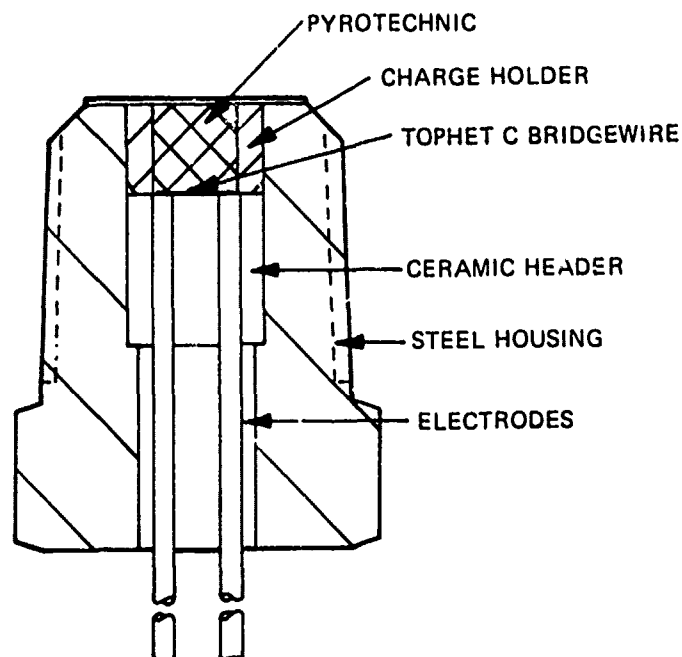
FIGURE 5 - MAD-1031 test component.

Table 3

ETR GAMMA AND TIME TO BRIDGE BURNOUT AS FUNCTION OF DENSITY AT BRIDGEWIRE

Group	Charge Holder Surface Finish (μm)	Powder Condition	P_a (MPa)	Density Estimate at Bridgewire (Mg/m^3)	Gamma (mW/°K)	BOT (msec)
A	·0.2	Dry	68.9	2.01	3.92	2.50
B	0.8 - 1.6	Dry	68.9	1.89	2.58	1.76
C	>3.2	Dry	68.9	1.88	2.97	1.79
D	<0.2	Wet	68.9	1.95	2.87	1.88
E	<0.2	Dry	42.6	1.89	2.28	1.77
F	<0.2	Wet	48.1	1.88	2.28	1.82
G[a]	<0.2	Dry	68.9	2.00	3.68	2.23

[a]Compaction pressure applied for 10 sec for Group G; compaction pressure applied for 30 sec in all other groups.

Fig 6

GAMMA [milliwatts/deg K]

DENSITY at BRIDGE [Mg/m³]
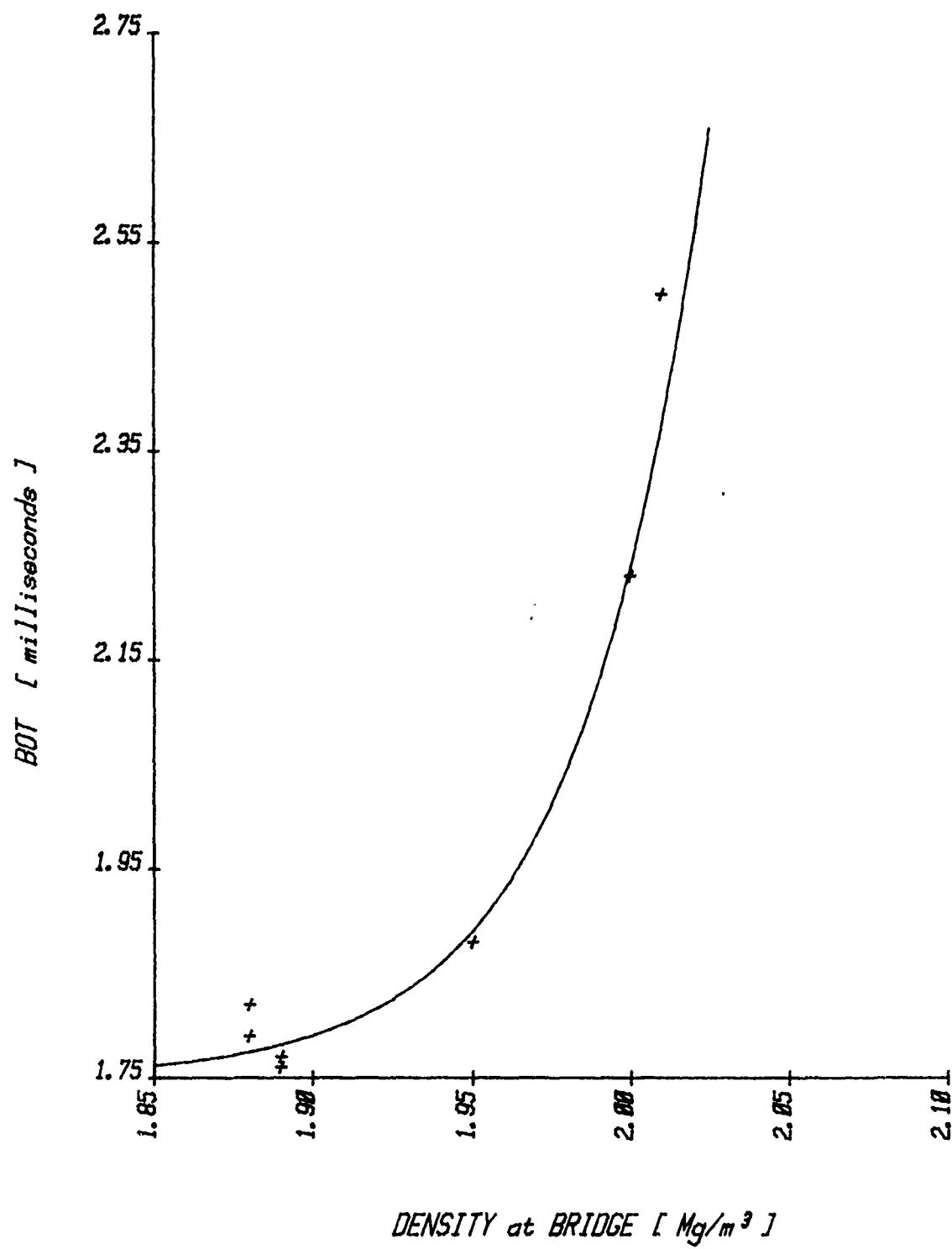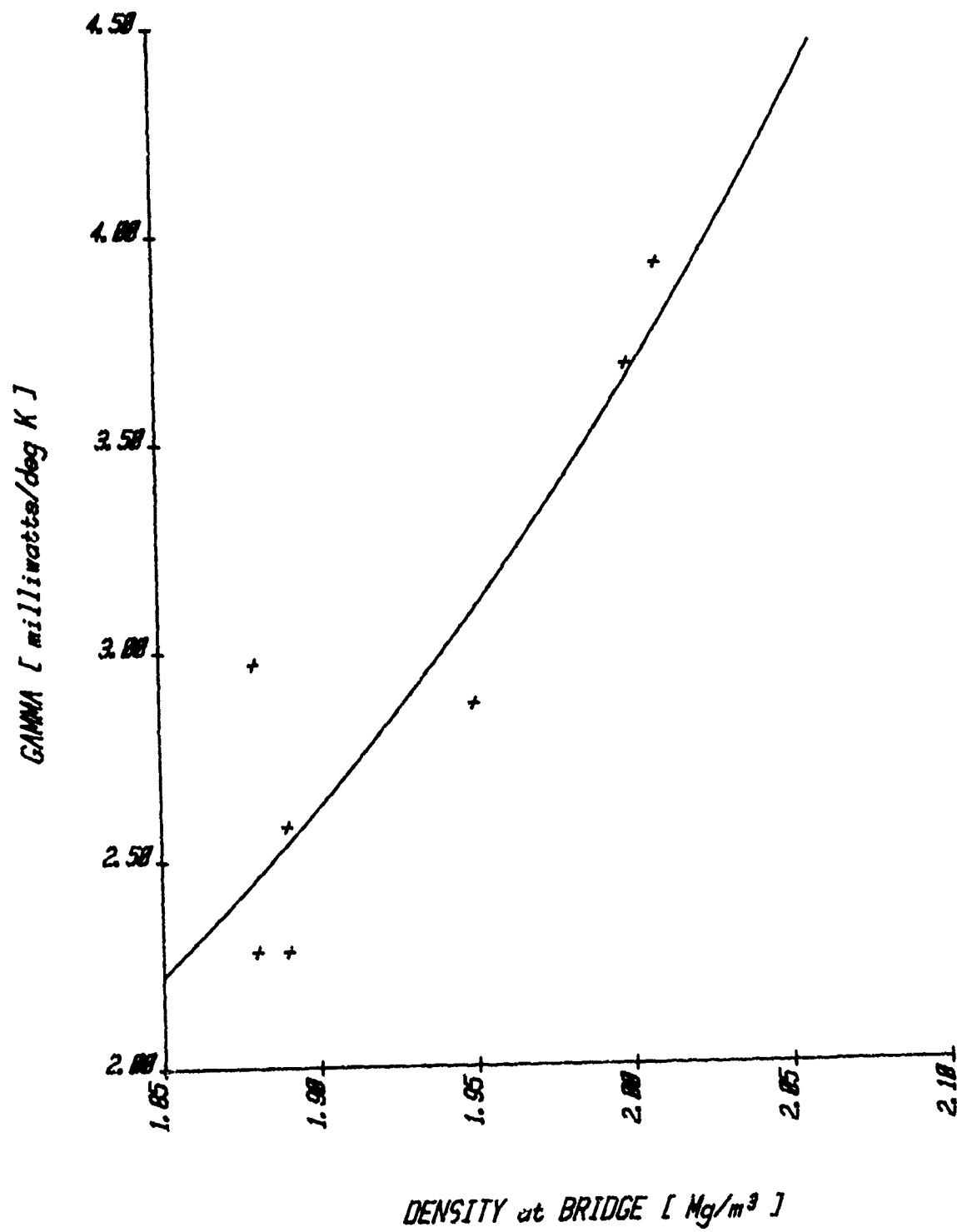
Fig 7
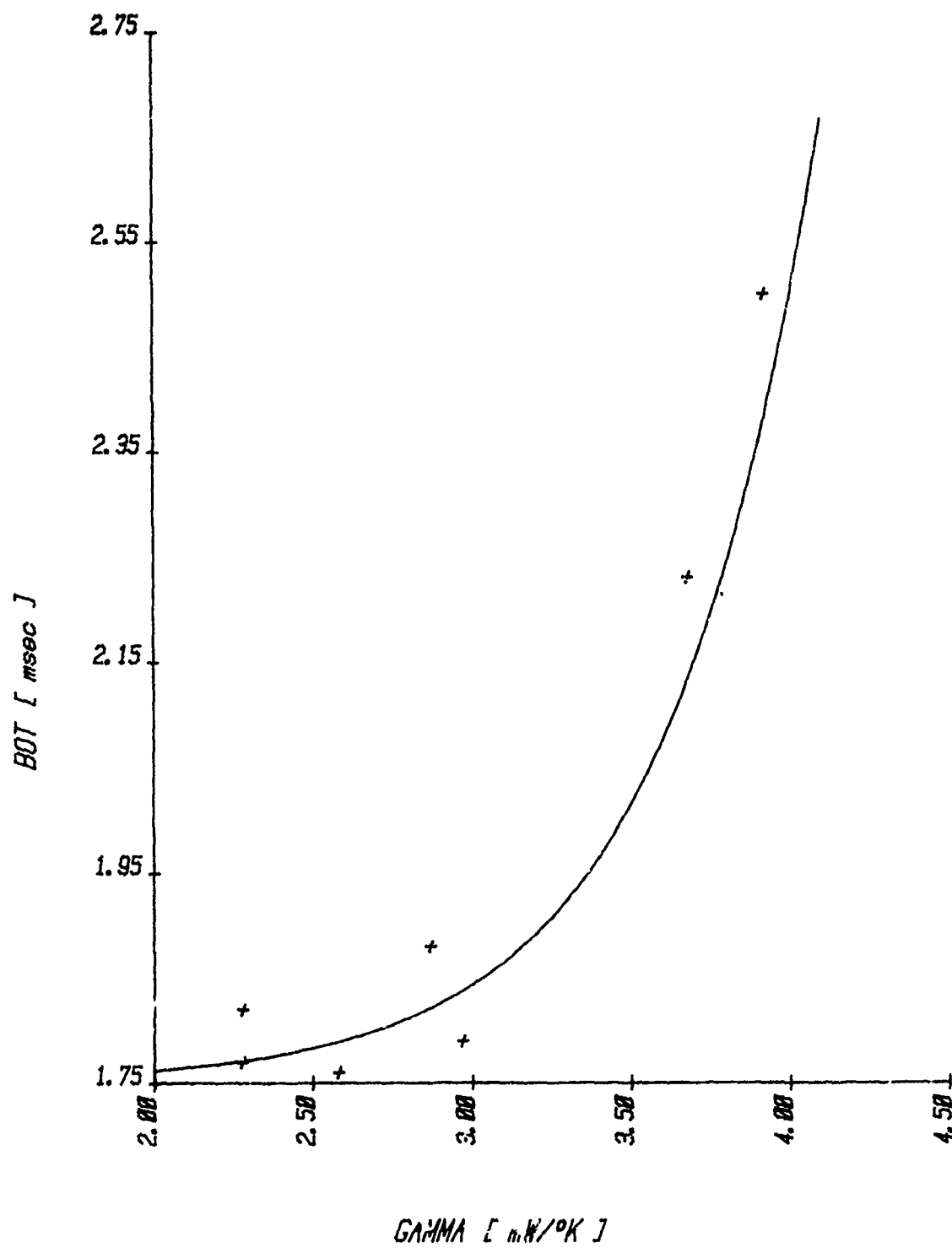
Fig 8

SUMMARY AND CONCLUSIONS

A method to estimate the density of a pyrotechnic at the bridgewire interface was developed. This technique showed that, even though a constant compaction pressure was applied, the surface finish of the charge holder, the humidity of the environment in which the pyrotechnic was stored, and the time the compaction pressure was maintained on the powder, all had an effect on the density at the bridgewire. This effect can be detected by the nondestructive ETR test.

The destructive testing showed that the ignition time is a function of the density at the bridgewire and not the average density or the compaction pressure.

Manufacture of pyrotechnic igniters is commonly performed using a constant compaction pressure to control the process. This study shows that care must be exercised in the design of the component and in the control of process parameters that can affect the density gradient in the component.

One method to eliminate some of this problem is to reduce the length-to-diameter ratio of the compact (L/D was 0.87 for this work) to a value where the density gradient is minimized. However, this would result in the need for multiple loadings to fill the charge cavity and the subsequent cost of those loadings balanced against the cost of controlling the necessary process parameters.

REFERENCES

1. E. A. Kjeldgaard, "Development of a Spark Insensitive Actuator/ Igniter," published in Proceedings of Fifth International Pyrotechnics Seminar, 1976.

2. L. A. Rosenthal and V. J. Minichelli, "Nondestructive Testing of Insensitive Electroexplosive Device by Transient Techniques," JPL Technical Report 32-1494, 1970.

3. A. C. Strasburg, "Methodology for Computation of Interface Parameters of a Hot-Wire Explosive Device from the Electrothermal Response Analog," Sandia Laboratories, Albuquerque, New Mexico, SLA-73-1034, 1973.

4. A. C. Strasburg, "A Data Acquisition System for Transient Pulse Testing," Sandia Laboratories, Albuquerque, New Mexico, SAND 75-0550, 1975.

PROBLEMS IN MANUFACTURE OF DELAY ELEMENTS BY LEAD TUBE TECHNOLOGY

BY M.V.S.N. MURTHY/S. PATTABIRAMAN/C.P. RAMASWAMY:

1.   A B S T R A C T:

1.1.   In the production of Delay Elements for use in
          Delay Detonators, there are mainly two techno-
          logies. One in which the delay composition is
          filled in die cast tubes of required lengths
          and then consolidated. In the second techno-
          logy, the delay composition is filled in a
          large diameter lead tube, which is extruded
          in stages to the desired diameter and then
          cut into the required lengths, as delay elements.
          This paper deals with some of the problems
          in the practice of the latter technology in
          delay elements manufacture.

1.2.   Preparation of delay composition, filling,
          drawing of filled tubes, calibration, cutting
          and consolidation of cut elements are the
          various processing stages dealt in this study.
          The variations obtained in each of these
          stages have been analysed statistically to
          trace the sources of variations in manufacture,
          which are responsible for the variations in
          timings of delay elements.

1.3.   A modification over the lead tube technology,
          in which the multicore delay elements are
          manufactured has also been discussed with
          reference to their advantages and applica-
          bility.

2.   CONSTRUCTION OF DELAY ELECTRIC DETONATORS:

2.1.   A delay detonator basically consists of:

                (a) a base charge of PETN or RDX or similar
                    explosives and a primary explosive charge
                    which may be either pure lead azide or
                    mixture of lead azide, lead styphnate
                    and aluminium. This explosive charge is
                    necessary to initiate a high explosive
                    charge.

                (b) the delay element to give the desired delay
                    interval and

                (c) the electro-explosive device to set-off
                    the delay element, when electric-energy
                    is supplied to it.

2.2.   There are mainly two technologies by which the
                delay elements are manufactured to be used in
                the detonators. In the first technology, the
                delay composition is individually filled and
                pressed under specified pressure in die cast
                zinc or aluminium delay elements. This tech-
                nology is supposed to give good control over
                the scatter in the delay timings. But this
                method is costlier and less in productivity.

2.3.   In the second technology, lead tubes of suffi-
                cient diameter are taken, filled with delay
                composition and then drawn through different
                dies to reduce the diameter to the required
                size, suitable for insertion into detonator
                shells. The drawn tubes are cut into elements
                after calibration and selection of required
                delay number. The cut delay elements are then
                consolidated under pressure before inserting
                them into delay filled shells.

2.4. It is the second technology that is being adopted at IDL Chemicals Limited, Hyderabad.

3. <u>BACKGROUND OF THE PROBLEM:</u>

3.1. The background of the problem is the erratic fluctuations of the delay timings obtained in the delay detonators, using delay elements manufactured as mentioned earlier. The irrational behaviour of the timings were attributed to the effects of various factors independently and collectively, so that initiation of any corrective actions in the process proved inadequate. About 25 such factors were listed, but after consideration and discussions some of these factors were deleted.

4. <u>OBJECTIVES OF THE STUDY:</u>

   i. to study the variation flow in the processing of the delay elements from raw material stage to final finished stage.

  ii. to trace the responsible factors for variations in timings at each stage of processing and rank them in order of importance on the basis of their contribution to the overall variation.

 iii. to assess the scope of interlinking variable factors in a linear regression equation and also to associate one or more factors for estimating the compound effects of them independently and collectively for the overall variations.

5. DESIGNS OF THE EXPERIMENTS:

5.1. The experiments were planned for half second delay No.5 (2.500 secs. nominal delay interval). 40 tubes were chosen at random whose length, inner and outer dia were measured. Theoretical volumes of these lead tubes were calculated from these data. Ten numbers were chosen from 40 tubes and the actual volumes were measured using water.

5.2. Five batches of half second delay composition suitable for standard delay number 5 were prepared at the same time from five cubicles. Adequate quantity of samples of composition from each cubicle were taken for quadrapling chemical analysis of percentage proportion of various ingredients and bulk density. Two identical batches were taken for study, which are identified hereafter as batch 1 and batch 2.

5.3. From 40 lead tubes selected earlier, 20 tubes were filled with batch 1 and another 20 tubes with batch 2 of delay composition. Quantity of delay composition filled in each tube was recorded. Filling of the delay composition in the lead tubes was done on the same machine, so as to avoid machine variations.

5.4. Filled tubes were then drawn and the percentage elongation of each tube was recorded.

5.5. Two sets of 20 such filled tubes having composition batches 1 and 2 were further sub divided into 2 sets of 10 tubes, for calibration and cutting operations. 4 sub sets of these tubes were processed under two different calibration methods designated hereafter as Method 'A' and Method 'B'.

5.6   In method 'A', final cutting settings suitable
           for delay number 5 on the basis of timings and
           lengths were made by selecting 4 consecutive
           elements from middle portion of a single drawn
            tube which in turn was selected randombly
           from a sub set of 10 drawn tubes. Based on
           the readings obtained from these 4 elements,
           the cut lengths were decided and the set of
           10 drawn tubes were cut into elements under
           this settings.

5.7.   In method 'B', cutting settings were made for
           each individual drawn tube for a set of 10 drawn
           tubes filled with composition batches 1 and 2
           by taking samples of 4 consecutive elements from
           the middle portion of each drawn tube.

5.8.   During cutting operations, each of the drawn
           tube was catsgorised into three zones based on
           equal distances from the holding end to free
           end which were identified at the drawing process.
           The first zone from the holding end is termed
           as beginning, the next as middle and the final
           as the end zone which had the free end. From
           each such zone, 5 consecutive cut elements were
           sampled representing five cutting blades. The
           lengths, and diameters of these elements were
            recorded.

5.9.   The cut elements were consolidated in a single
           machine at required pressure and the lengths and
           diameters of the consolidated elements were
           recorded with due identifications.

5.10.   Consolidated elements were inserted into accepted
           delay filled shells, crimped with delay fuseheads
           of an accepted batch, fired and the delay timings
           were recorded with due identifications.

5.11.   The flow chart of this design of experiment is given   Appendix-1.

6.   <u>ANALYSIS AND INTERPRETATION OF THE COLLECTED DATA</u>:

6.1.   Data collected at the intermediate stages such as volume of lead tube, ingredients ratios in half second delay composition, quantity of composition filled in the tubes, density ratio of each tube, the rate of elongation at drawing process were statistically analysed to ensure that these factors are uniform for all 40 tubes and their variabilities under different characteristics do not introduce any variability in the final performance of the delay elements.

6.2.   The factors considered for further statistical analysis to estimate the variation flow with respect to timings were:

(a) batch of composition
(b) method calibration
(c) drawn tubes
(d) zones within each drawn tube

6.3.   <u>RESULTS OF THE ANALYSIS ON THE NESTED DESIGN</u>:

6.3.1.   The results of the analysis are presented in Table-1.

T A B L E -1

ANOVA OF THE NESTED DESIGN

Sl.	Source	Degree of freedom	Sum of Squares	Mean sum of Squares	F Value
1.	Between batches	1	0.69320	0.69320	1.31764
2.	Between methods within a batch	2	1.05218	0.52609	23.66672*
3.	Between tubes within a method	36	0.80025	0.02229	0.47431
4.	Between zones within a tube	80	3.74927	0.04687	11.29296*
5.	Error	480	1.99201	0.00415	
	TOTAL:	599	8.28691		7

* Indicates significantly different when compared
  with tabulated 'F' values.

6.3.2.   It could be seen from the above table that

(a) no significant batch to batch variation
    existed.

(b) significant difference was noticed between
    methods of calibration and cutting within a
    batch.

(c) no significant difference existed between
    the tubes within a method.

(d) significant difference existed between the
    zones within a tube.

6.3.3.   The interpretation of the results indicated that
the timings did not differ significantly when
the averages of the batches were compared. The
average timings obtained from the methods within
a batch were found to be significantly different
indicating that the two methods of calibration
were not identical. When the tube averages
alone were compared among the tubes processed
under a given method of calibration, no signi-
ficant difference noticed. But when the zonal
averages were compared within a tube significant
difference existed between the different zones
viz., beginning, middle and end. This was
critical since the performance of timings
of elements need to be uniform from a drawn
tube subjected for a given delay number and
processed accordingly at each stage of manu-
facturing.

6.3.4.   In order to estimate the percentage contri-
bution of variations of these factors on the
timings, the factor "tubes" was pooled with
the zones since the former was found to be
not significant. The estimated percentage
contribution of these factors to the over-
all variation is exhibited in Table-2.

T A B L E - 2
PERCENTAGE CONTRIBUTION OF VARIATION OF DIFFERENT FACTORS
ON OVERALL VARIATIONS IN TIMINGS

S.No.	Factors	% Contribution
1.	Batch	3.72
2.	Method	21.69
3.	Zone	46.86
4.	Error	27.73
	T O T A L:	100.00

6.3.5.   From the above table, it could be inferred that
the maximum contribution of variation in the
timings was due to the different zones within
a tube as 46.86%. Next in order were the "error"
and the "method" as 27.73% and 21.69% respecti-
vely. The error term included the experimental
error, the sampling error and the variation due
to other factors which were not considered under
this experiment.

6.3.6.   It was hence necessary to investigate further
to trace out the reasons for the higher zonal
variations. It was felt that the variations
in preceeding processing operations could have
influenced for zonal variations.

6.3.7.   As of a subsidiary interest, analysis were done
on the effectiveness of the calibration methods
'A' and 'B'. It was found that method 'B' was
better than method 'A', with respect to lesser
variability in timings.

6.4.   INVESTIGATION ON THE CAUSES FOR ZONAL VARIATIONS:

6.4.1.   A thorough probing was carried out to segregate
these factors at previous processing stages which
were responsible for zonal variations. To start

442

with, the zonal-wise average timing under each
tube calibrated with methods 'A' and 'B' and
filled with compositions batches 1 and 2 were
calculated. These values are presented in chart 1
enclosed in appendix giving identifications of
zones methods of calibration and composition
batches.

6.4.2. It could be seen from chart 1 that about 24%
of the points were on the lower side of the
expected average values of 2.5 seconds. This
indicated that the determination of the conso-
lidated lengths and the timings for the delay
were not representative. About 80% of the
"end zone" averages of timings of the elements
from batch 1 under method 'A' were found to be
above the upper specification limit. About 65%
of the points were above the expected standard
average irrespective of methods of calibration
and composition batches.

6.4.3. Particulars on maximum, minimum and overall
average timings under different methods of
calibration with batch identifications are
presented in Table-3.

T A B L E - 3.

DETAILS ON THE AVERAGE TIMINGS UNDER DIFFERENT METHODS OF
CALIBRATION.

B.No.	AVERAGE TIMINGS IN SECONDS				
	Method 'A'	Method 'B'	Overall	Maximum	Minimum
1.	2.65800	2.54180	2.59990	2.86080	2.45080
2.	2.52164	2.54265	2.53215	2.69220	2.31320

6.4.4. It could be observed from Table-3 that the overall average timings in batch 1 was 2.5999 seconds against 2.53215 seconds of batch 2. The maximum and minimum averages under batch 1 were more than under batch 2. The average timings under method 'A' of batch 1 was higher than that of method 'B'. But in batch 2 method 'B' had an average of 2.54265 seconds against 2.52164 seconds under method 'A'. It is to be mentioned that the composition batches were uniform with respect to chemical ingredients. But the variation between the batches with respect to timing are not uniform irrespective of method of calibration.

6.4.5. As a continuation of the investigation, the consolidated lengths of the corresponding delay elements were analysed. Chart-2 presents the average consolidated lengths with identification of the zones, method of calibration and composition batches corresponding to the delay elements timings presented in chart-1. Chart-2 indicated that the extent of variation in the average consolidated lengths calibrated under the two different methods were non-uniform at each zone. Even the average consolidated lengths of the elements processed under method 'A', where the cut lengths were calibrated for 10 drawn tubes in totality for the drawn tubes containing composition batches 1 and 2. In this method, it was expected that the consolidated lengths should be uniform. The extent of variation was found to vary much irrespective of the zones in this method. The variation pattern of the average consolidated cut lengths under method 'B' was also found to be non-uniform though it was expected that the consolidated lengths in a drawn tube to be irrespective of the composition batches.

444

6.4.6. The average consolidated lengths of the elements processed under two different calibration methods with batch identifications were given in Table-4 along with maximum, minimum and overall averages.

T A B L E -4

DETAILS ON THE AVERAGE CONSOLIDATED LENGTHS OF ELEMENTS UNDER DIFFERENT CALIBRATION METHODS.

| B.No. | AVERAGE CONSOLIDATED LENGTHS IN MM | | | | |
	Method 'A'	Method 'B'	Overall	Maximum	Minimum
1.	18.26386	17.74334	18.00360	18.52000	17.54000
2.	17.44066	17.34933	17.40130	17.78000	17.12000

6.4.7. It could be seen from the above table that the elements from batch 1 had overall average of consolidated length as 18.0036 mm as against 17.4013 mm from batch 2, though the methods of calibration were subjected on the drawn tubes belonging to both the composition batches.

6.4.8. It could be seen that the consolidated lengths under method 'A' of composition batch 1 was more than that of batch 2, the same trend could be identified even under method 'B'.

6.4.9. Comparing charts 1 and 2, it could be observed that:
i. in batch 1, under method 'A' of calibration, the average consolidated lengths in each tube had lesser variability whereas the corresponding timings had higher variability. Under method 'B' of calibration, the average consolidated lengths varied too much but the average timings had lesser variability. Within a batch of composition which could be filled in 20 lead tubes the extent of variation in average timings were high.

445

ii. In batch 2, the extent of variation in the average timings were not much but the extent of variations in the average consolidated lengths were more irrespective of the method of calibration.

6.4.10.   Chart-3 in the Appendix exhibits the average timings under different zones irrespective of the batch, method of calibration. This chart clearly explains the phenomena of zonal variations. To sum p up:

(a) it could be observed that the existing system of calibration for any type of delay number was not representative of the entire tube which was responsible for zonal variations.

(b) the timings of the elements in any zone within a tube had direct bearing on the corresponding consolidated lengths.

(c) the extent of variations in the average consolidated lengths of the elements irrespective of the zones was high.

6.4.11.   A scatter diagram prepared between the consolidated length (X) and the corresponding timings (Y) indicated that:

(a) a trend of higher timings were found to be associated with higher consolidated lengths.

(b) about 20% of the points were seen above the upper tolerance limit for timings. About 55% of the observations were found to lie between the expected average and the upper tolerance bat limit. The rest 25% of the observations were below the expected average timings.

(c) the density of the points above the expected average value of the timing was found to exist in the range of the consolidated length more than 18.00 mm. It is quite obvious from this

chart that for the HS composition used in the
experiment the appropriate consolidated length
should have been less than 18.00 mm because
most of the points below this level of 18.00 mm
fall well under the proposed tolerance limits.

(d) the density of the elements above the upper
tolerance limit for timing may be due to the
end zone elements which were giving higher
timings.

6.4.12. A significant linear regression was found to
exist between timings and the consolidated length.

6.4.13. Correlation co-efficients were worked out for each
method of each batch and it was found that they
varied, though there was a positive correlation
between the consolidated lengths and timings for
a given batch of half second composition, con-
forming to the delay number for a given average
consolidated length. About 18.5% variations in
timings could be attributed to variations in the
consolidated lengths.

7. INVESTIGATION ON THE CAUSES FOR CONSOLIDATED
LENGTH VARIATIONS:

7.1. A critical analysis was done to investigate the
causes for the consolidated length variations.
The causes that could account for the consoli-
dated length variations are:
(i) variations in the cutlengths of the elements.
(ii) variations in the consolidation process due
to pressure pressure differences.

7.2. Examination on the variation of cut lengths of
the delay elements:

7.2.1. The average cut lengths of the elements were
estimated for all the zones in each tube. The
values had been plotted in chart-4 identifying the
method and the batch alone. The order of
plotting is in sequence of the tubes in the
particular method. In the same way, the
average consolidated lengths were plotted
correspondingly in the chart-5.

447

7.2.2.   From charts 4 and 5, it could be seen that the
          extent of variations in average consolidated lengths
          varied in accordance with the average cut
          lengths.

7.2.3.   The average cutting length, the maximum and mini-
          mum averages in each method of all batches were
          calculated and presented in Table-5.

T A B L E -5
PARTICULARS ON THE AVERAGE CUTTING LENGTHS

B.No.	AVERAGE CUT LENGTHS IN MM				
	Method 'A'	Method 'B'	Overall	Maximum	Minimum
1.	*	20.22340	20.22340	20.63000	19.72000
2.	19.46666	19.38400	19.35333	19.70000	19.04000

* Indicates not available.

7.2.4.   It could be seen from the above table that the
          average cutlength of the elements in batch 1
          was more than that of the average cutlength in
          batch 2. The average cutlength of 19.46666 mm
          of the elements under method 'A' of batch 2 was
          slightly higher than the average cutlength of
          19.38400 mm of the elements under method 'B'.

7.2.5.   A scatter diagram drawn between cutlengths and
          consolidated lengths indicated that there
          existed a significant linear relationship
          between these two. There existed a positive
          correlation between these two characteristics.
          About 20% of the variation in consolidated
          length is accountable due to variation in
          cutlengths.

7.3.   EXAMINATION OF THE PRESSURE VARIATION AT CON-
          SOLIDATION PROCESS:

7.3.1.   From the available data on the cutlength and
          consolidated lengths of the elements the rate
          of consolidation was estimated as the ratio of
          consolidated length to the cutlength. These

448

estimates could be treated as indices for the pressure exerted during the consolidation process because the pressure was set at a fixed value before the operation. Using these figures, analysis were carried out to find the existence of any pressure variation at the consolidation stage.

7.3.2. The statistical analysis on the rate of consolidation estimates were done using the analysis of variance technique. The results are presented in Table-6.

T A B L E -6.
ANOVA TABLE ON THE RATE OF CONSOLIDATION

Source	Degree of Freedom	Sum of Squares	Mean sum of Squares	F'Value
Between Tubes	29	0.01470	0.0005069	3.2472*
Within Tubes	420	0.06559	0.0001561	
T O T A L:	449	0.08029		

*Indicates 'F' calculated value of 3.2472 is more than 'F' tabulated value of 1.46 with degrees of freedom 29,420 at 95% probability level.

7.3.3. It is quite evident from the above table that between tubes variation was found significant at 95% probability level indicating the existence of pressure variation. In other words, the quantum of pressure exerted on the delay elements was not unique and uniform though during the experiment the constant pressure was aimed at. This would have been the main cause for the excess variation in the consolidated length of the elements.

8. ESTIMATION OF PROCESS CAPABILITIES AT CUTTING AND CONSOLIDATION STAGES:

8.1. Process capabilities at cutting and consolidation stages were evaluated from data available. It

was observed from the analysis that the average
cutlengths obtained were not in tune with the
set cutlengths. The extent of variations in the
cutlengths were different for different designed
lengths. The reasons could be:

(a) the variation in the cutting blades of the
    cutting machine.

(b) the variation due to improper setting of the
    machine.

(c) other factors such as adjustments of the
    cutting blades, rate of feeding, holding
    of the drawn tube etc., etc.

8.2. The process capabilities at consolidation stage
were found to be varying extensively and the
reasons that could be attributed wxere:

(a) pressure variation at the consolidation stages.

(b) the length variations in the cut elements,
    which had been discussed earlier.

9. C O N C L U S I O N S:

9.1. From the trials conducted, it was found that the
timings were not significantly different when the
average timings of the two batches of compositions
were compared. The variations in the timkingr
are affected by about 3.72% by the batches to
overall variations.

9.2. The two methods of calibration were significantly
different when the average timings of the two
methods were compared. The method variations
contributed 21.69% of the overall variations in
the timings.

9.3. The tubes within a method were not significant
indicating that the tube averages on timings
were uniform. But the zones within each tube
are significantly different. This indicated
that the average timings were not uniform within
each tube and this accounted for 46.86% of the
overall variations in the timings.

9.4.　　　The factors responsible for the zonal variations in the timings were traced to be due to the extensive variations in the consolidated lengths. It was found from the regression equation worked out between the consolidated length and timings that for an unit increase or decrease in the consolidated length, the timings were increased or decreased by about 12%. Further about 18% of variation in timings could be attributed to variations in the consolidated lengths. The relation between the consolidated length and timings were significant for any batch of composition in a given band.

9.5.　　　The average consolidated lengths were not uniform and the extent of variations were erratic in any zone of a tube which affected the process capability of the consolidation. The reasons could be:

a. Pressure variation at the consolidation stage.
b. the cutting length variations of the elements coming for consolidation.

9.6.　　　The cutting length variations were found to be extensively high for any standard cutting settings. The variations in the cutting blades of the cutting machine and improper settings were responsible for this. The improper settings arise out of lack of correct indicators on the measurements of the length, feed rate and other operational conveniences. This had affected the process capability of the cutting machine.

9.7.　　　The regression equation between the cut length and consolidated length indicated that for an unit increase or decrease in the cutting length, the consolidated length increased or decreased by about 35.66%. 20% of the variation in the consolidated length could be accounted for the variations in the cut lengths.

9.8.　　　Plant was recommended to adopt control chart techniques at intermediate processing stages and

451

other operational changes. After implementing
these suggestions, there was a marked improve-
ment in the quality of delay elements with
respect to timings. There was a drop of 20%
rejections after these corrective measures.

A variation of this technology is the multicore lead delay
element where instead of one channel of composition for
carrying the spit from the delay element to the primary
explosive, there will be a number of channels, but of a
much smaller dia like a capillary. In the process tried
at IDL, the channels were 7 in number. According to
this technology, drawn tubes are cut into further smaller
diameters. 7 such tubes are bundled, inserted into another
lead tube and drawn through different dies until the
required size is obtained which is suitable for insertion
into the filled shells. This process minimised the zonal
variations due to the extra drawing operations of inserted
tubes and randomising of primarily drawn tubes. Steps are
being initiated to minimise the variations at some of the
stages of processing by investigating through the same
statistical techniques.

KPR/13-

FLOW CHART OF NESTED DESIGN
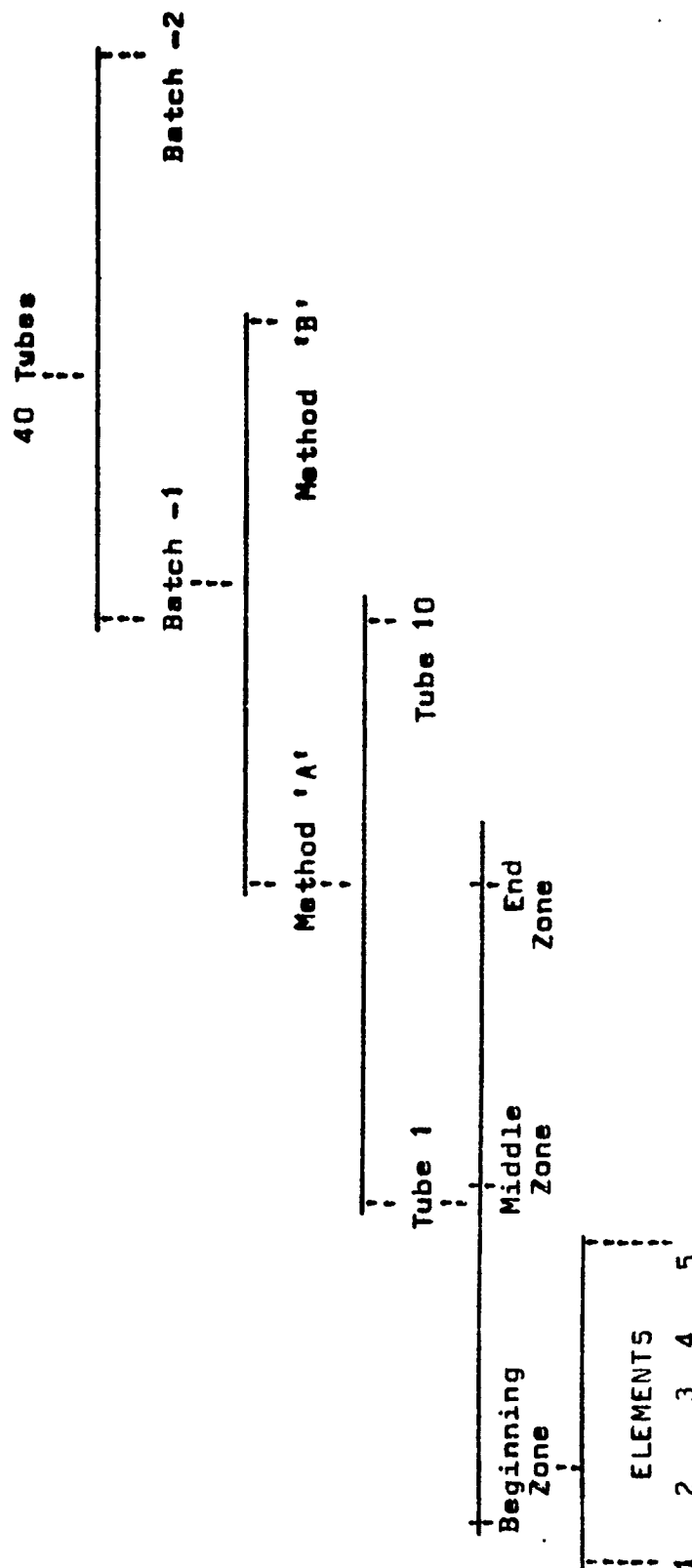
Average Timings of Delay Elements ~ Zone wise, Method wise and   CHART 1

Batch wise.

Y ↑ Timings in Msec.

X → Tubes

o   Method A

x   Method B

___   Standard Average = 2·50 msec
- - -   Specification limits Upper: 2·725 msec
                                Lower: 2·275
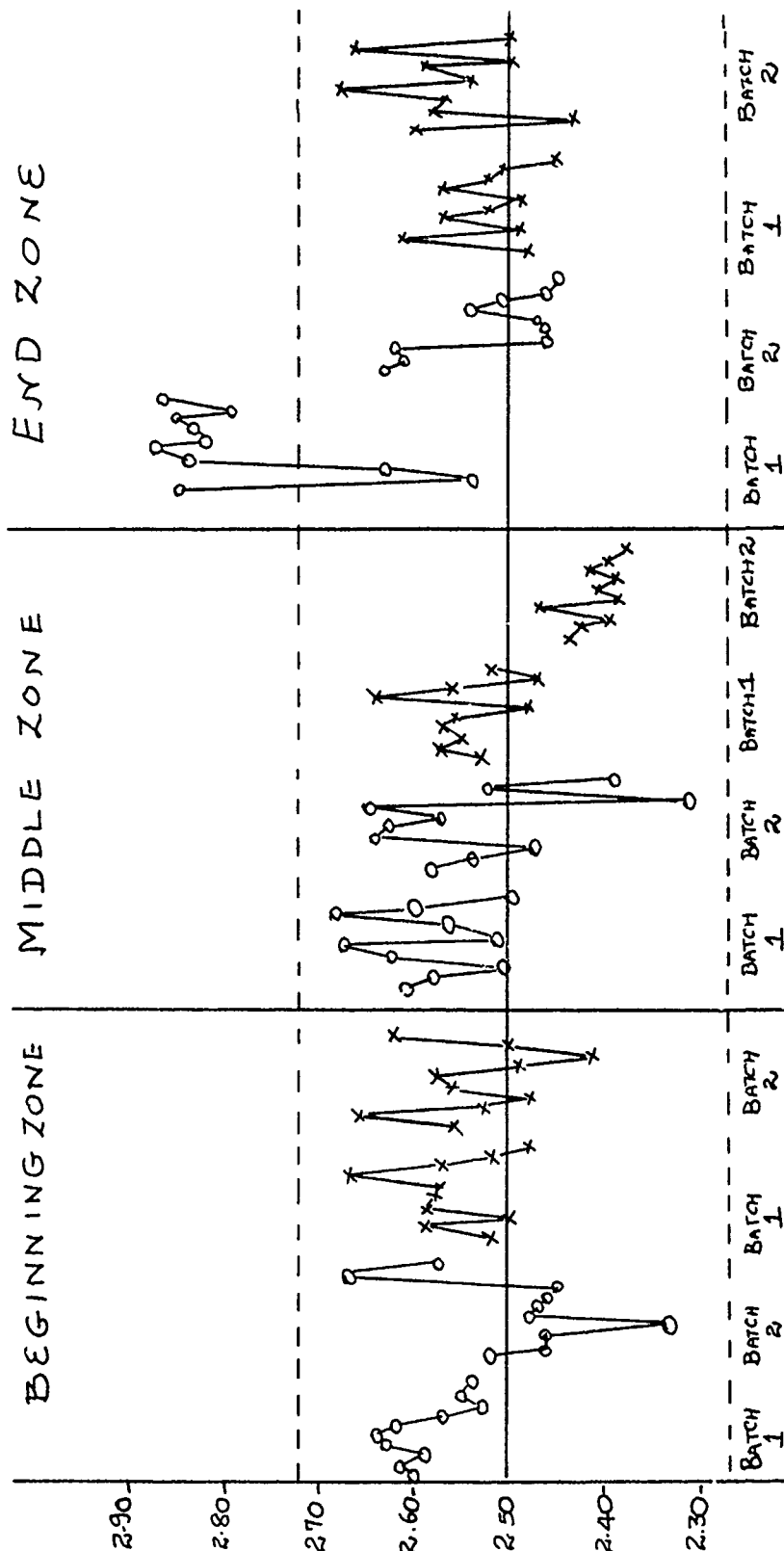
END ZONE

MIDDLE ZONE

BEGINNING ZONE

AVERAGE CONSOLIDATED LENGTHS OF DELAY ELEMENTS — ZONEWISE & METHODWISE

CHART 2

BATCHWISE

Length in mm.
x → Tube

O   METHOD A
X   METHOD B
B1   BATCH 1
B2   BATCH 2

BEGINNING ZONE

MIDDLE ZONE

END ZONE

455
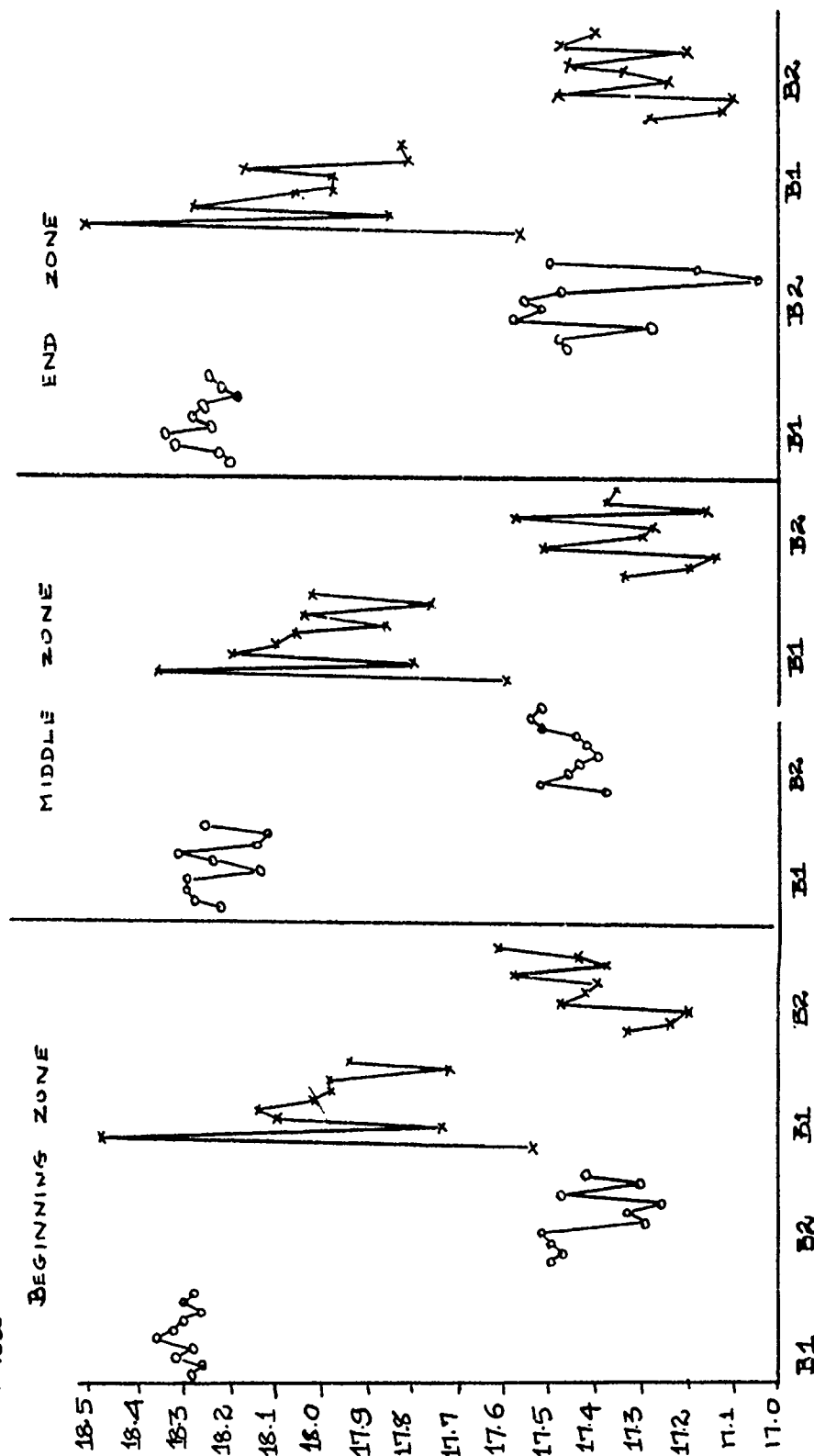
AVERAGE TIMINGS OF DELAY ELEMENTS IN DIFFERENT ZONES

↑ Timings in m sec
→ Tube

BEGINNING ZONE

MIDDLE ZONE

END ZONE

TUBES
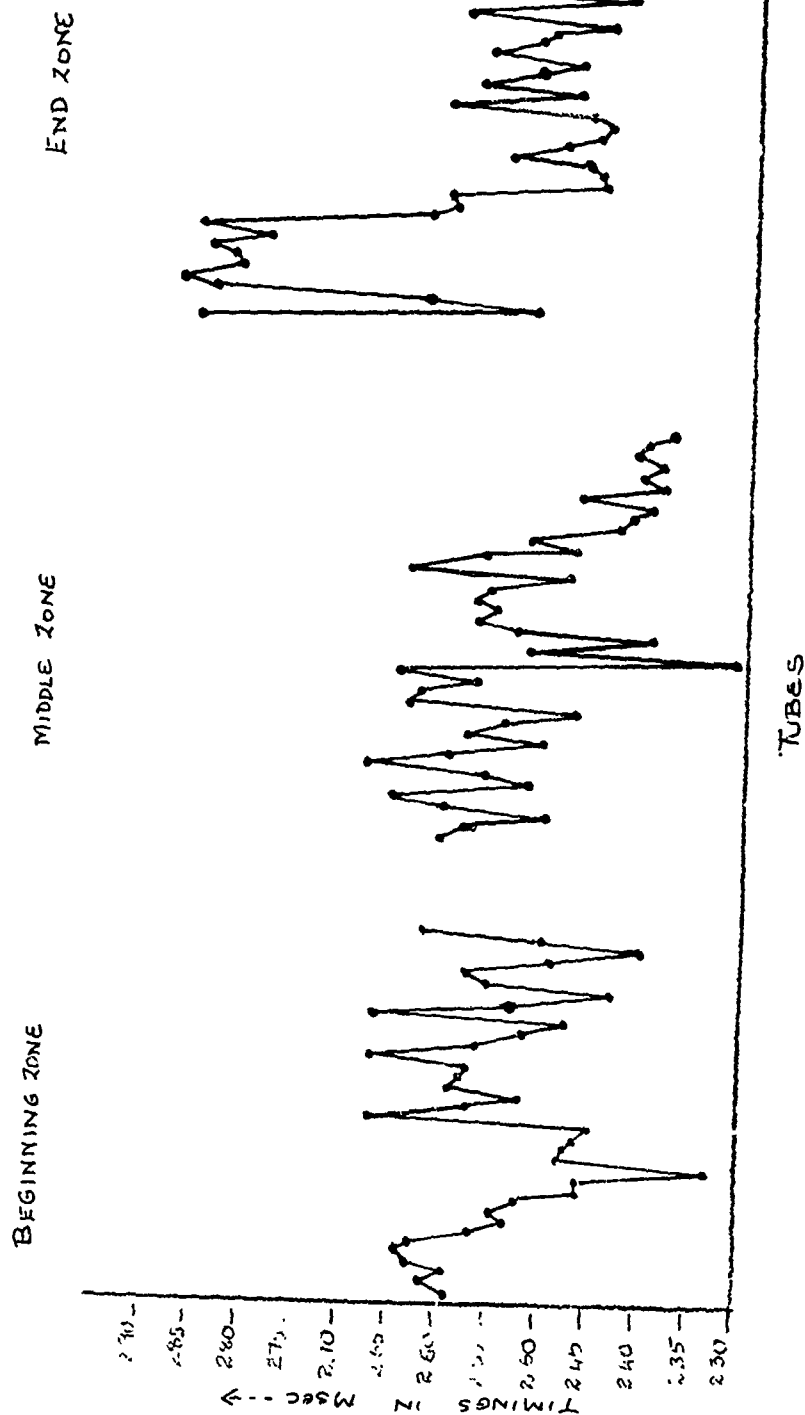
CHART 3

AVERAGE CUT LENGTHS OF DELAY ELEMENTS --- METHOD WISE & BATCHWISE

Y ↑ CUTLENGTH in mm.

x → Samples

o --- METHOD A
x --- METHOD B

CHART 4

BATCH 1   BATCH 2
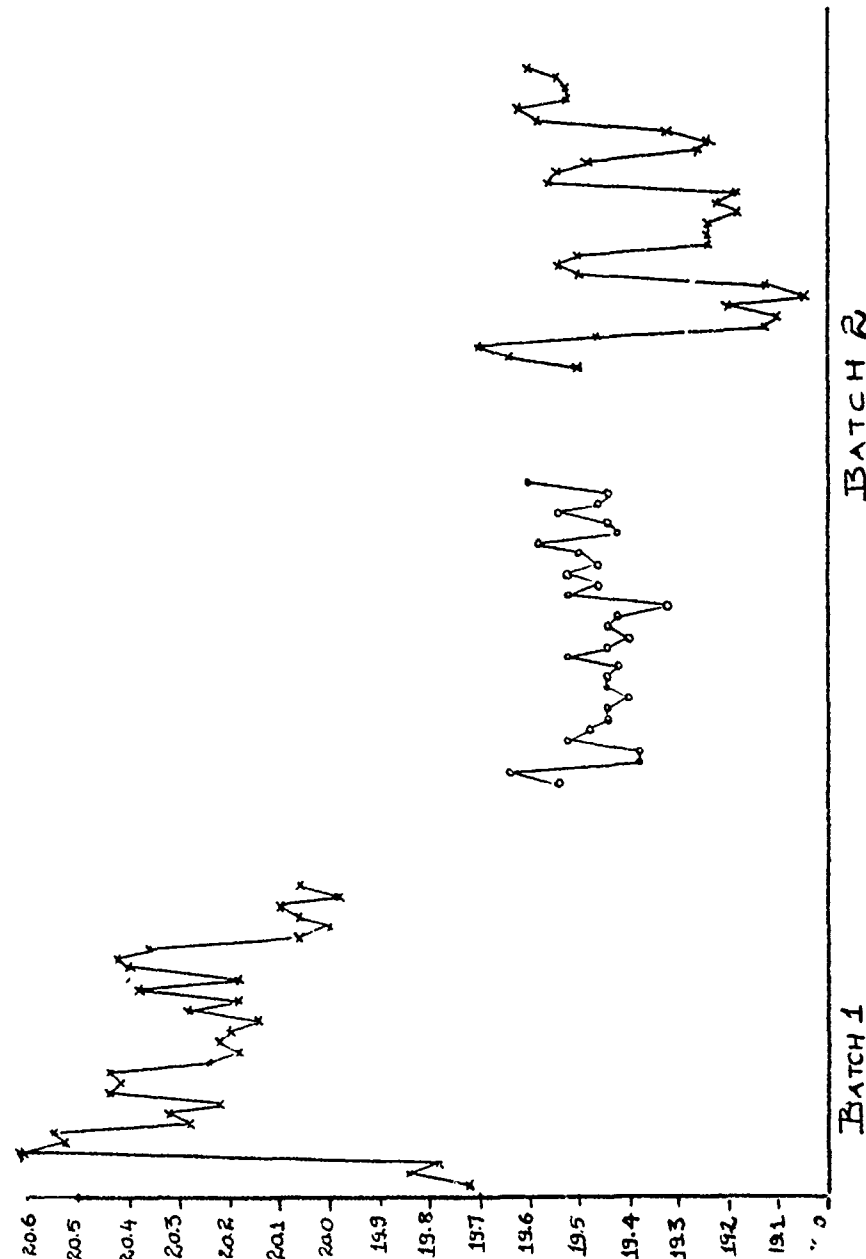
AVERAGE CONSOLIDATED LENGTHS OF DELAY ELEMENTS -- METHODWISE &
BATCHWISE

Y ↑ CONSOLIDATED LENGTHS in mm

X → SAMPLES

o ··· METHOD A
x ··· METHOD B

CHART 5

BATCH 1   BATCH 2

18.5
18.4
18.3
18.2
18.1
18.0
17.9
17.8
17.7
17.6
17.5
17.4
17.3
17.2
17.1
17.0
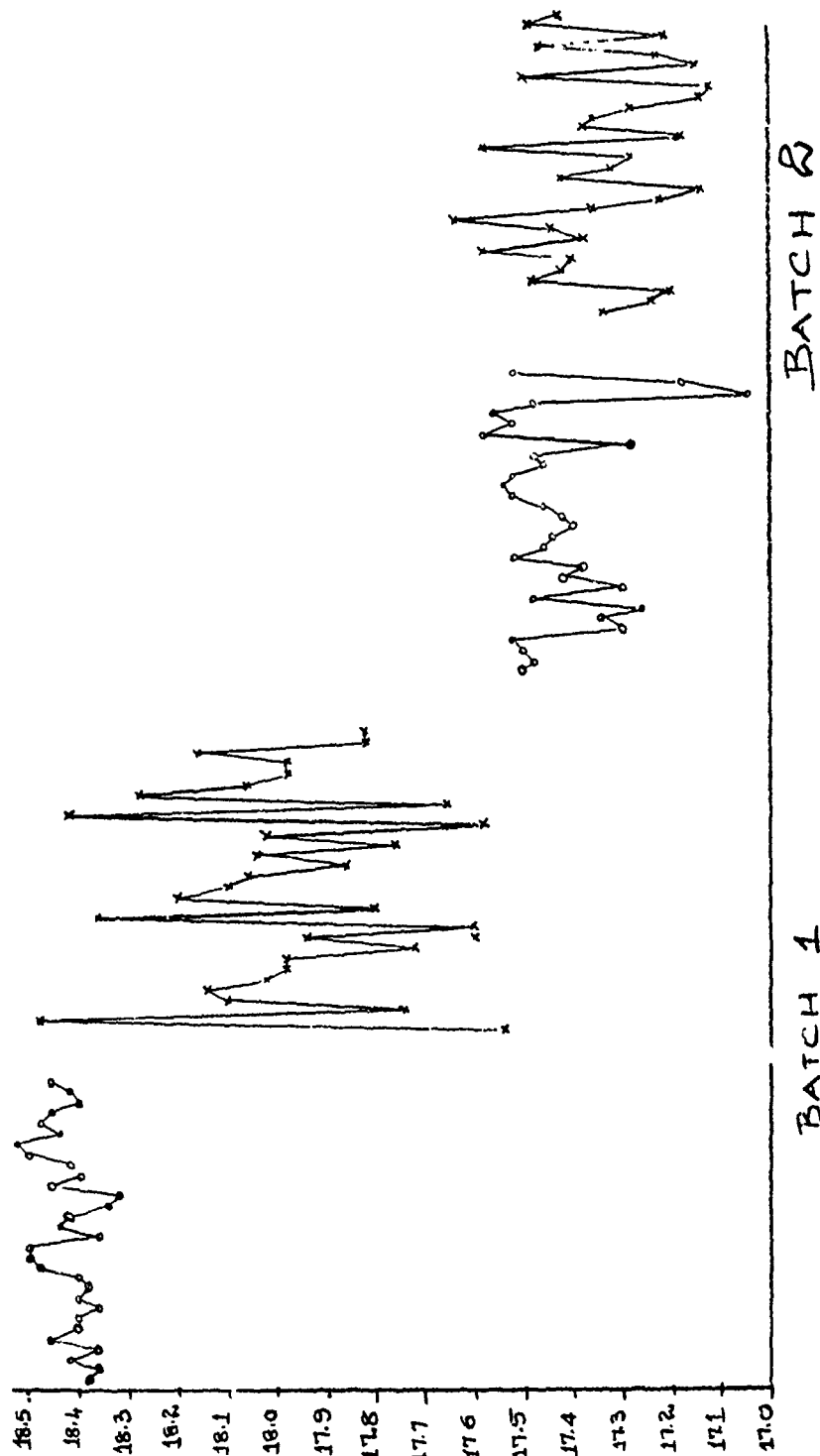
EXPERIMENTAL DETERMINATION OF THE EQUATION OF STATE
OF EXPLOSIVES AND PYROTECHNICS USED IN EXPLOSIVE ACTUATORS

Raymond Ng
Sandia Laboratories
Livermore, California 94550

ABSTRACT

An experimental explosive chamber has been designed and used for
the measurement of the pressure output history of explosives and
pyrotechnics in explosive actuators. The design incorporates a
variable volume concept, thus enabling the simulation of the pressure-
volume history of an actuator as it is used in an actual explosive
valve. A pressure transducer measures the dynamic pressure while a
Velocity Interferometer System for Any Reflector (VISAR) is used at a
sensitivity of 0.021 mm/μsec. per fringe to measure the velocity of a
moving actuator assembly. The simultaneous pressure and velocity data
are used to calculate the pressure-volume equation of state for each
explosive and pyrotechnic tested.

Introduction

Explosive actuators are used as the power source in explosively actuated valves. In this application, they are required to produce sufficient gas pressure to operate the valve. As such, it is important to know quantitatively and qualitatively the pressure output history of the different actuators. An explosive or pyrotechnic can then be tailored to meet the requirements of a certain design. This can be done, within certain constraints, by the appropriate choice of explosive mass and actuator volume. However, what is first required is knowledge of the pressure-volume equation of state of the explosive or pyrotechnic of interest.

The equation of state of an explosive is important information needed in many areas of explosive research. First, an analytical computer program[1] is being used to model the interactions present in a valve operation. The explosive equation of state is necessary for a realistic analysis to be performed. Second, variation in the pressure output within each explosive or pyrotechnic blend must be known and empirically determined. Third, equation-of-state information will be essential for the evaluation of new explosives and pyrotechnics.

This report describes a technique with which the pressure-volume relationship of an explosive is determined.

Actuator Output

As shown in Figure 1, a typical valve consists of an explosive actuator, disc, plunger, tube(s), and the housing. As the explosive burns, the resulting pressure shears a disc and exerts a force on the plunger. The plunger is propelled forward until it cuts the tube(s) and wedges itself into a tapered section of the valve housing.

It is clear from this description that the explosive is the power source for the valve. The successful functioning of valves is therefore directly dependent upon the explosive pressure. Increased knowledge of the pressure output would therefore enhance the reliability of any valve design.

BEFORE   AFTER
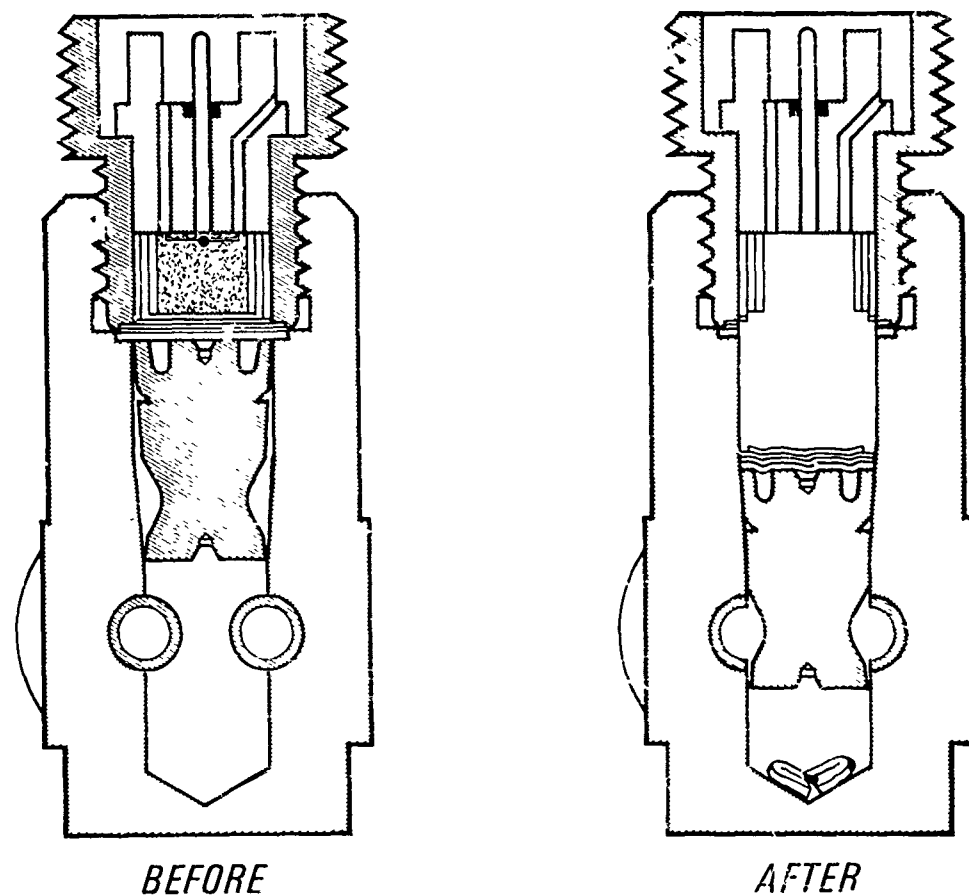
Figure 1. Explosive Valve Operational Sequence

All of the valves in present use have been designed empirically with an excess of explosive. Due to lack of information on the outputs, this was done to guarantee adequate power as well as to compensate for any variation in the output. However, there are recent efforts to understand and describe the processes and interactions involved in the operation of a valve. Furthermore, new designs are becoming such that an excess of explosive becomes more significant and the variation in output more critical. More information is demanded on the critical pressure output of the actuators.

Preliminary efforts[2] were made to derive pressure output information from available measured velocities of plungers in valves. It was shown that, while some understanding of the pressure-volume relationships can be acquired by this method, a more exact method would be to directly measure the pressure with a transducer. Such efforts were then undertaken, the resulting technique being described in the following section.

Experiment Equipment

The present design of the experimental equipment is shown in Figures 2, 3, and 4. A reusable 304 stainless steel housing is so designed as to have a threaded hole to hold a Kistler No. 607C3 pressure transducer and a smooth bore in which a slider could be press fitted.

VARIABLE
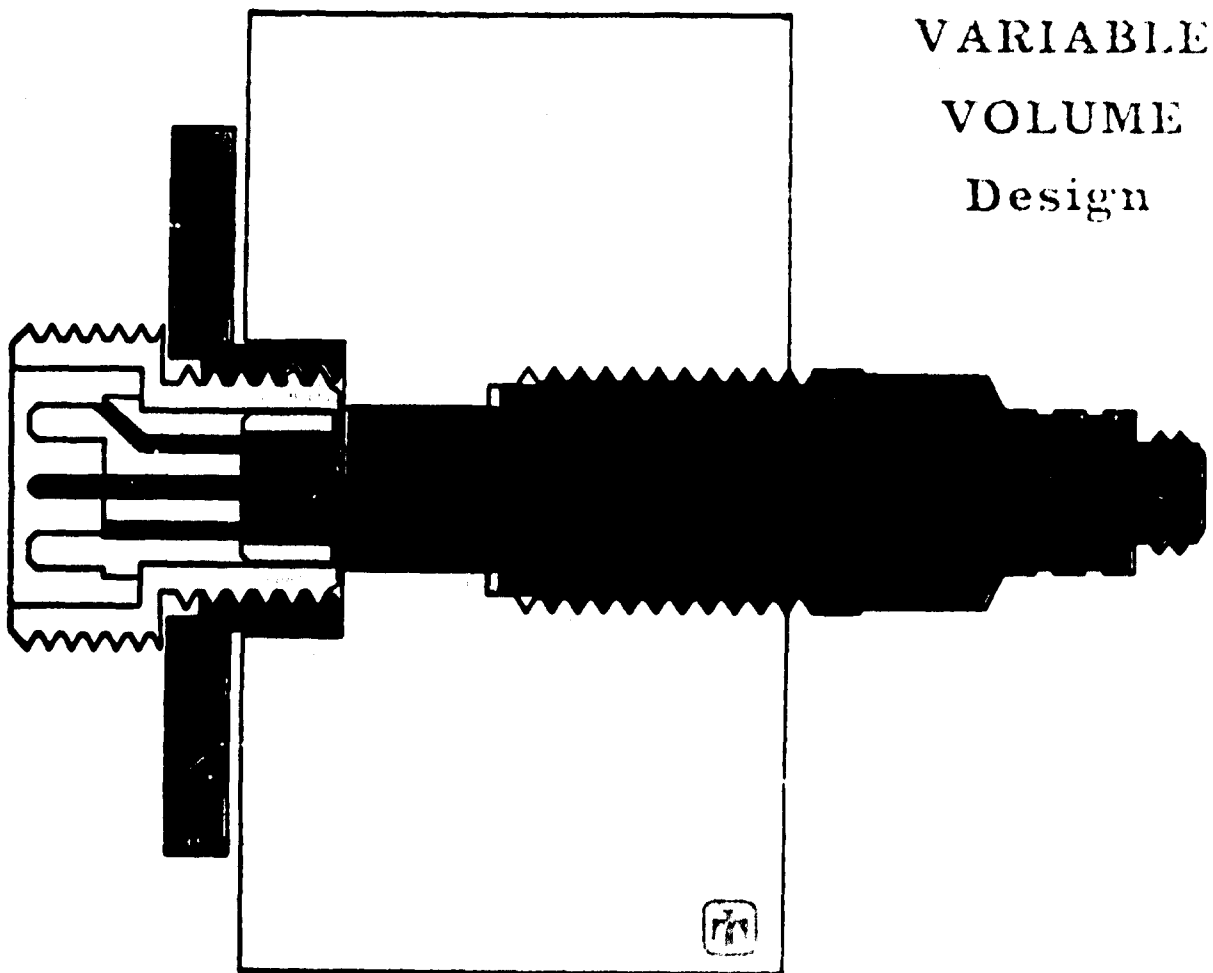
VOLUME

Design

Figure 2. Variable Volume Design

Figure 3. Variable Volume Parts
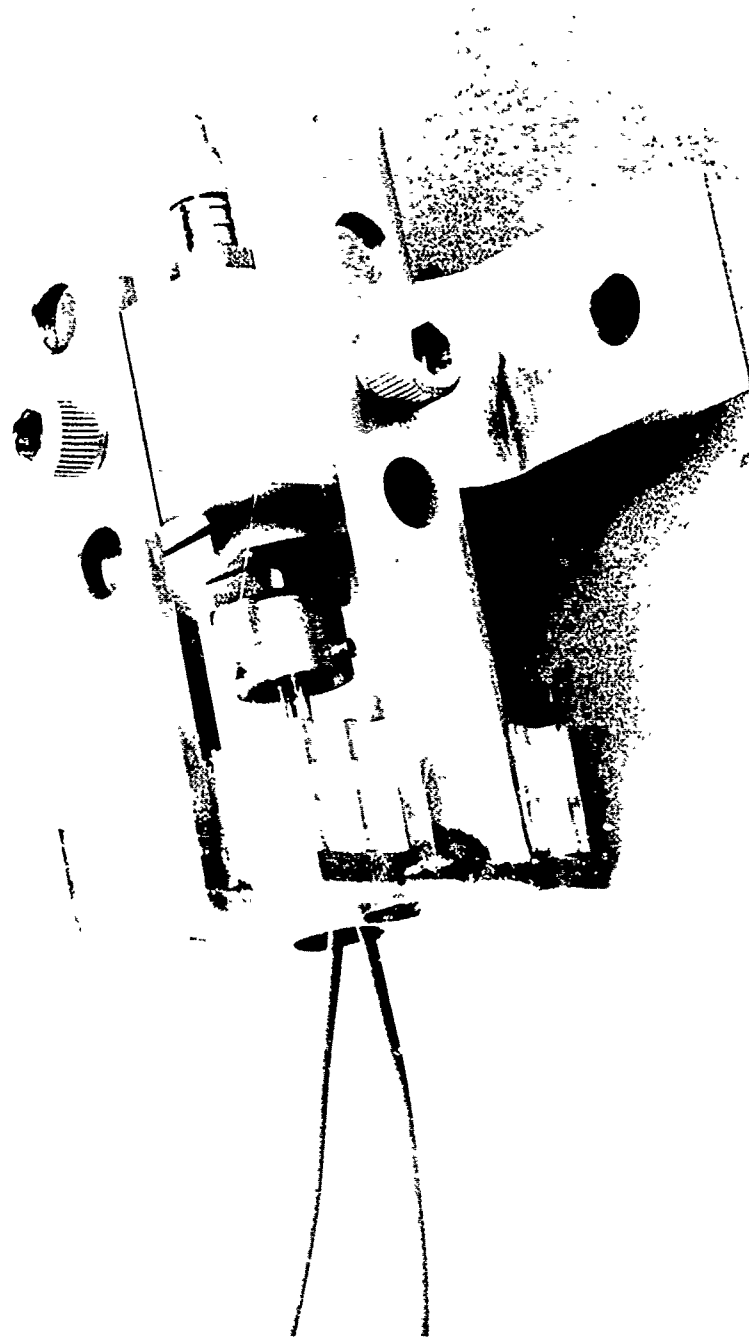
Figure 4. Assembled Test Hardware

The pressure transducer is first mounted into the housing. This transducer can record pressures up to 690 MPa (100,000 psi) and has a rise time of 1.5 μsec. Further filtering of the electronic equipment results in an effective rise time of 8 μsec., still sufficiently fast for our study.

A beryllium-copper slider is press fitted into the housing bore and the explosive actuator to be tested is placed into the slider's treaded bore. When the actuator fires, the resulting pressure will force the actuator-slider assembly out of the bore. The assembly has been sized (diameter and mass) so that the resulting volume history would be similar to that experienced in an explosive valve.

As the actuator is fired and the assembly moves out of the bore, the main feature of this design is the simultaneous determination of the pressure and volume histories. It is only through these that a resulting pressure-volume equation of state can be determined for each actuator tested.

The pressure transducer measures the pressure directly during the complete travel of the actuator-slider. A simultaneous volume history is determined by means of measuring the velocity history of the actuator-slider. The volume history is then easily calculated from the velocity data.

Velocity histories of the actuator-slider assembly are acquired by means of a Velocity Interferometer System for Any Reflector (VISAR).[3,4] This system is shown in Figures 5, 6, and 7. Figure 6 displays the interferometric optics for this system. The corresponding schematic is shown as Figure 7. This system has been used in the past to measure the velocities of plungers in the actual explosive valves.[5]

The light from a laser located on the lower level of the system's table is reflected off mirrors onto the surface of the target. This incident laser beam is then reflected diffusely from the surface, collected, and passed through a polarizer. Any surface motion causes a Doppler shift in the frequency of this reflected light. The beam is then split, with part of it going into a beam intensity monitor (a photomultiplier tube) which records the light intensity for use in normalizing the data signals. The remaining light goes into another beam splitter where it is again split into two parts. One part travels a short distance to a mirror and back again. The other portion goes to an optical delay leg composed of (in this system) two lenses and mirrors, and then rejoins the light from the first leg. (Most other laser interferometer systems use etalon rods for their delay of a two equi-distant leg system rather than the two lenses. The two lenses, as well as very long rods of etalon, result in the sensitive system needed to detect the lower-than-shock wave velocities experienced in these tests.) For these tests (and as shown in Figures 6 and 7), the lenses are positioned for a sensitivity of 0.021 mm/μsec. per fringe. The recombined beam is sent through a polarized beam
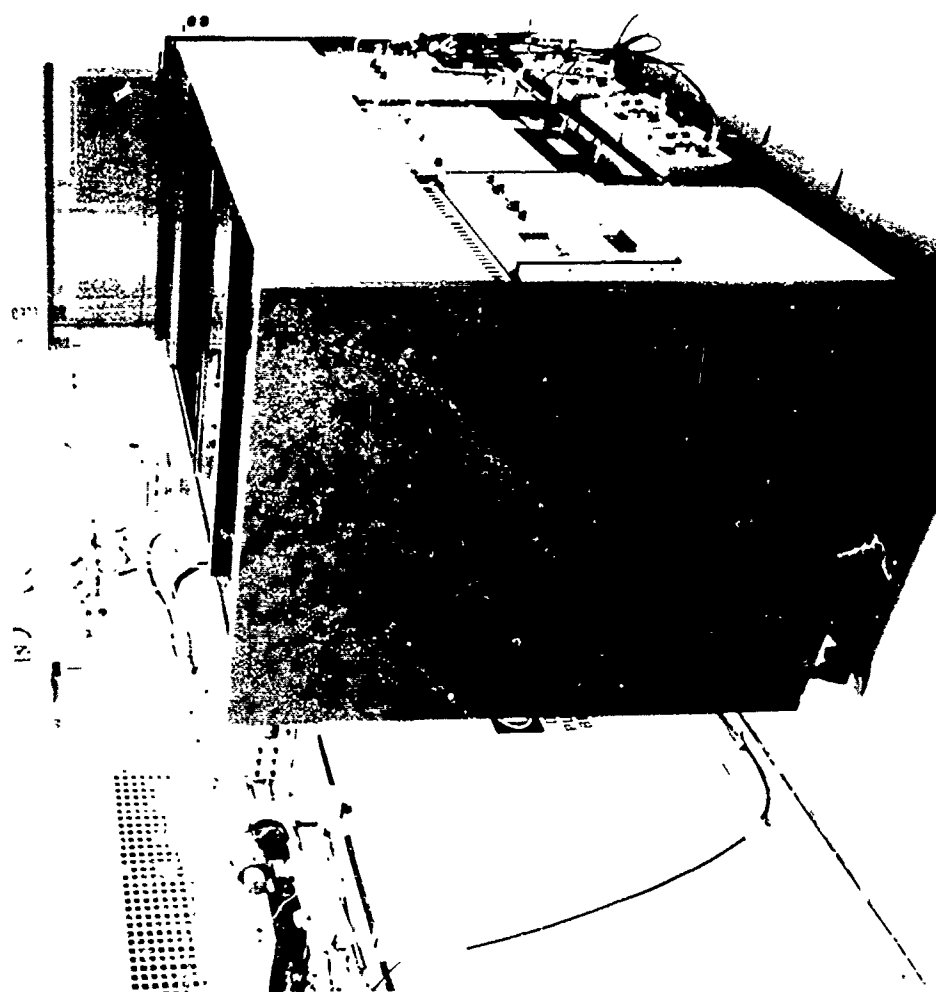
Figure 5. VISAR Table
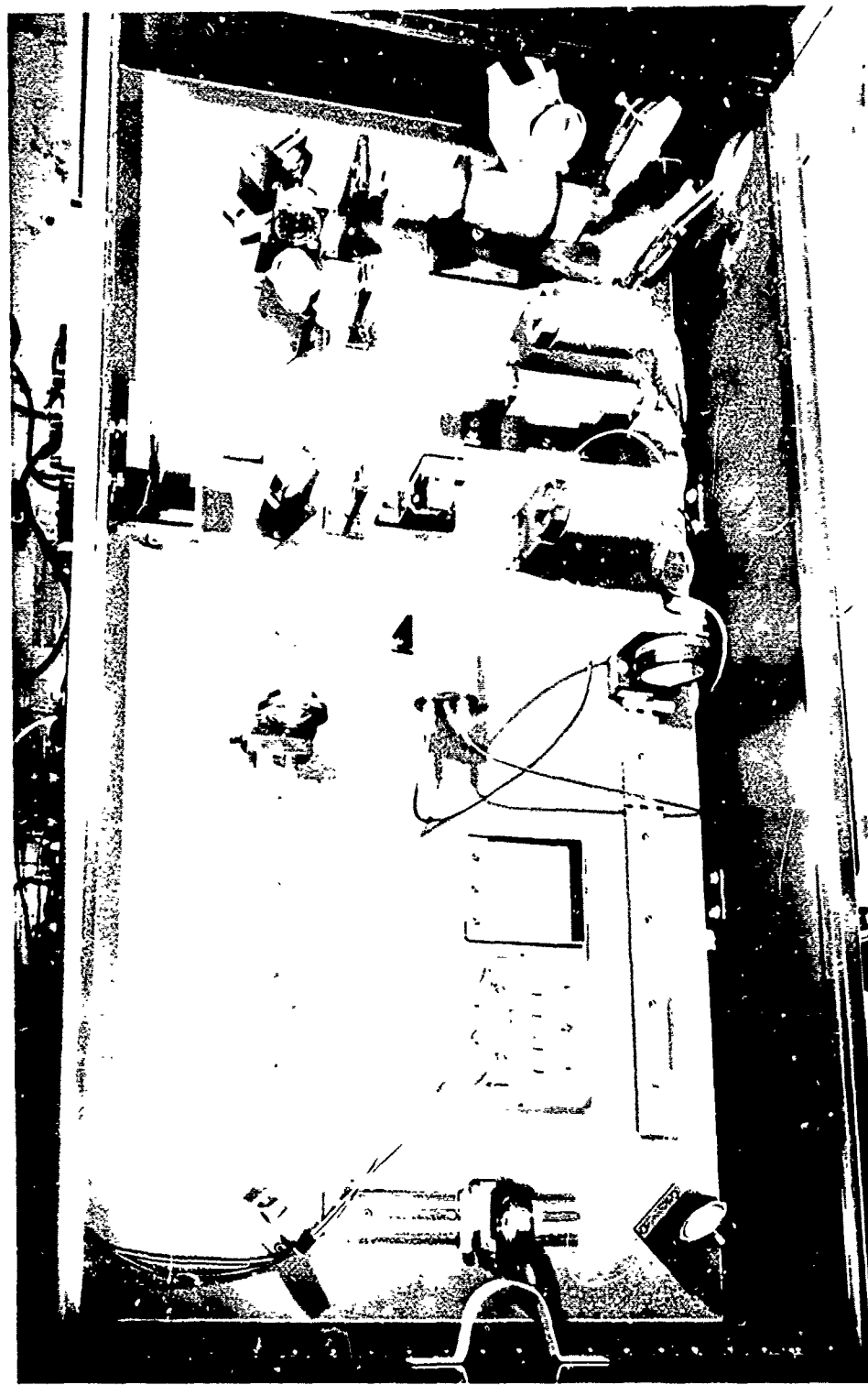
Figure 6. VISAR Optics
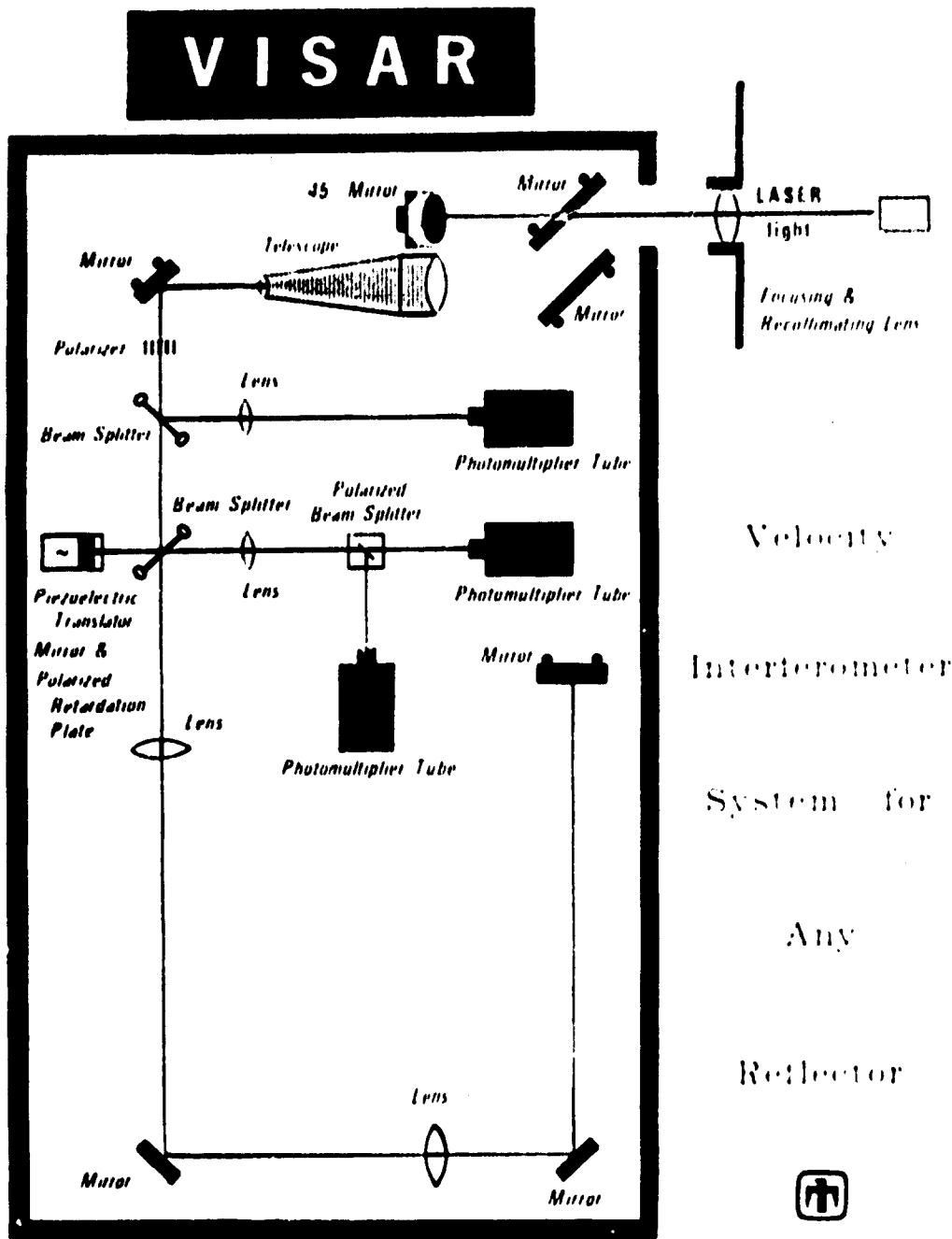
Figure 7. VISAR Schematic

splitter which splits the beam into two signals, one into each of two photomultiplier tubes which record data fringes caused by recombining the time-offset Doppler-shifted light beams. A data reduction computer program[6] converts these fringes into velocity histories.

Results

The measured data for each experiment consists of a pressure history and 3 photomultiplier data. Figure 8 displays some data from an actual experiment. Shown on the right-hand plot in Figure 8 are the pressure data and one of the fringe measurements from a data photomultiplier tube. Only 100 μsec. of the data is shown on this plot. The third curve shown on the right-hand plot is the velocity history calculated from the VISAR data. This velocity curve is then used to calculate the displacement of the actuator-slider assembly and the resulting increase in the volume containing the explosive chamber. The simultaneous pressure and volume histories are combined into the pressure-volume plot shown as the lower left-hand plot of Figure 8. The abscissa value of "specific volume" is given as the ratio of the present volume to the initial volume (the initial volume being the volume in each explosive actuator). The minimum value is therefore 1.0. For typical actuators, this system can measure the pressure for specific volumes up to 10.

The P-V Equation of State curve is a typical plot of the type of results acquired with this system. The measurement is also consistent with an actual valve history since the time required to function an actual valve is approximately 100 μsec., with a resulting specific volume of about 5. The corresponding actuator-slider location (at 100 μsec.) is also pictorially displayed at the upper left corner of Figure 8.

As designed this equipment will yield an equation of state with a single test, show the variation in output from "identical" actuators, and display the difference between different explosives. This can be demonstrated in Figure 9 by the plotting of the pressure-volume equations of state determined from 4 other tests. Two actuators containing 112 mg each of a $TiH_{.65}-KClO_4$ pyrotechnic mix are compared with another two actuators which contained 100 mg each of $Ti-KClO_4$.

Each actuator produces an equation of state curve (although not part of the pressure-volume relationship, the pressure rises are included on these plots). As can be seen, the variation between "identical" actuators is displayed, as is the more obvious difference between the different pyrotechnic mixes. The usefulness of this system is confirmed by this comparison plot.

VARIABLE VOLUME

Pressure, MPa

VISAR

(Velocity, m/s)

Time, microsec.

P–V Equation of State

Pressure, MPa

Specific Volume
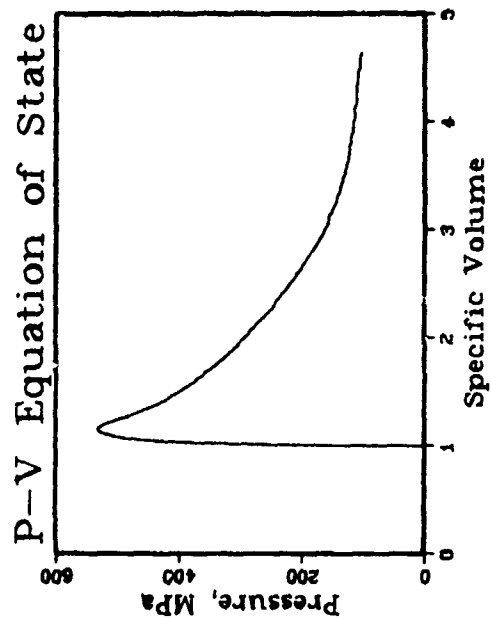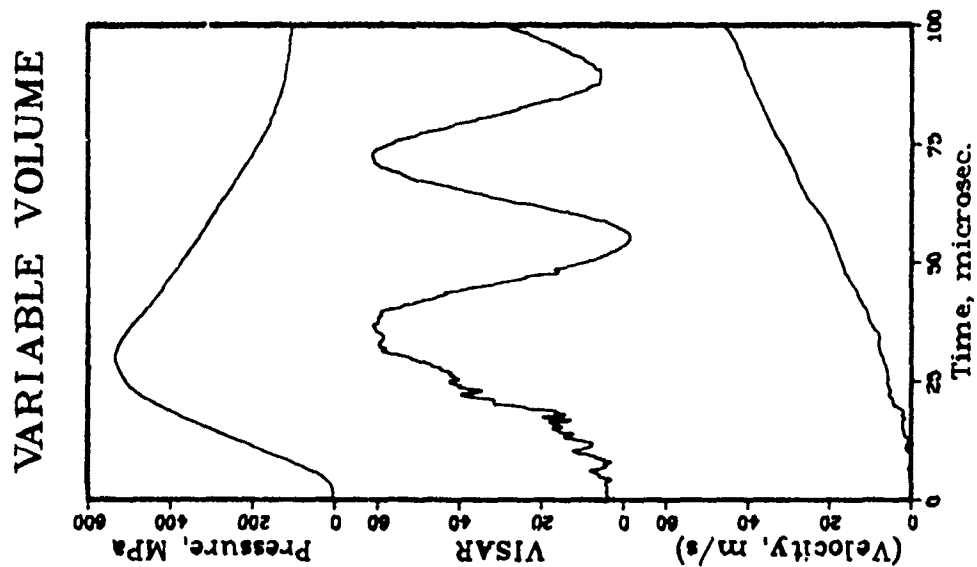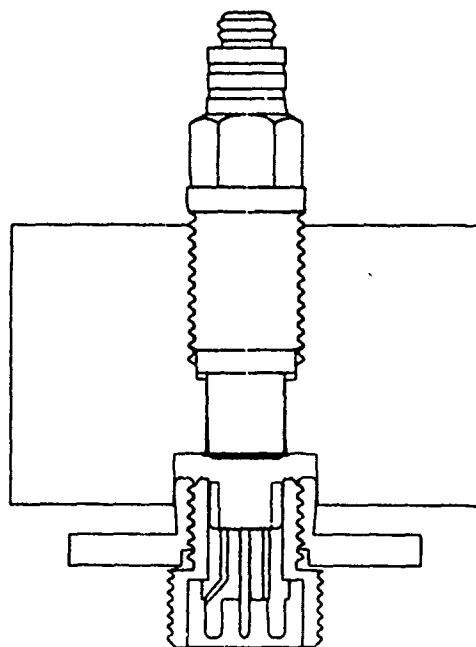
Figure 8. Experimental Result

470

P–V Equation of State
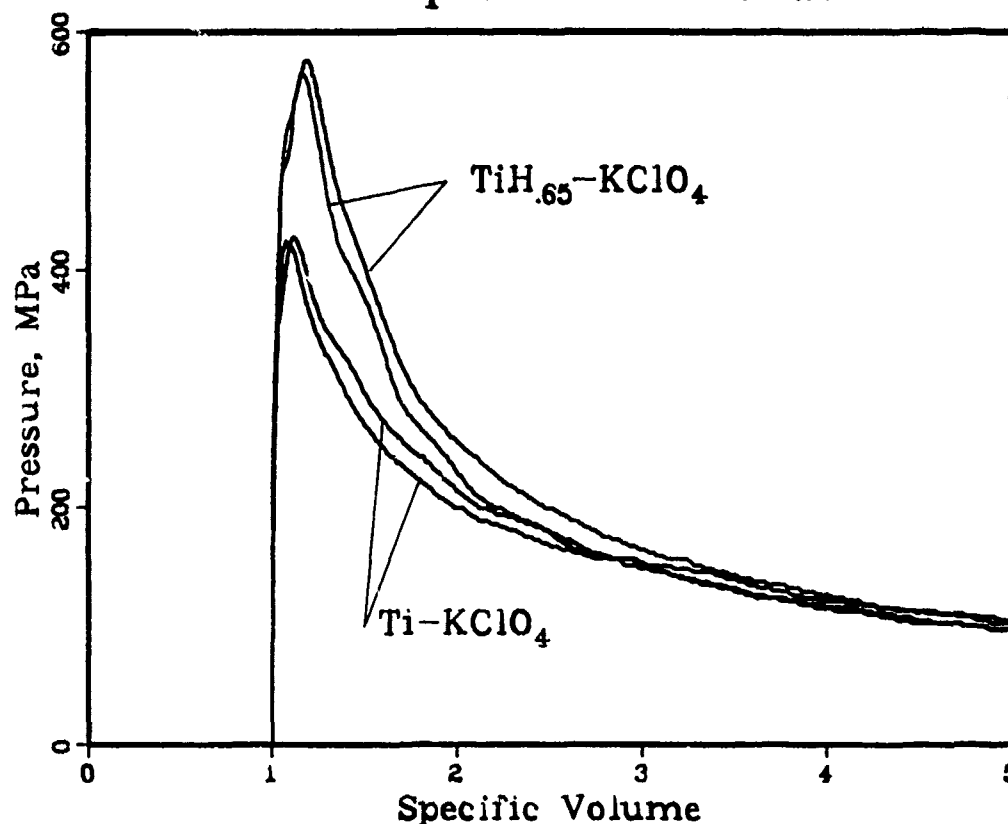
Figure 9. P—V Comparison Plot

Conclusions

A technique has been developed and used to acquire the pressure-volume equation of state of explosives and pyrotechnics used in explosive actuators. It is now possible to acquire the equation of state with a single test. Further testing on "identical" actuators can yield information on the variation present in actuator outputs. Also of major importance is the fact that differences between different explosive and pyrotechnic outputs can now be known and used for future designs.

References

1. R. Ng, _MAVIS - A Computer Program for the Modeling and Analysis of Explosive Valve Interactions_, Sandia Laboratories, Livermore, CA, SAND75-8018, February 1976.

2. R. Ng, _Measurement of Pressure Output Histories of Electroexplosive Devices_, Sandia Laboratories, Livermore, CA, SAND76-8614, October, 1976.

3. L. M. Barker and R. E. Hollenbach, "Shock-Wave Studies of PMMA, Fused Silica, and Sapphire," _J. Applied Phys., 41,_ 4208 (1970).

4. L. M. Barker and R. E. Hollenbach, "Laser Interferometer for Measuring High Velocities of Any Reflecting Surface," _J. Applied Phys., 43,_ 4669 (November 1972).

5. R. Ng, _VISAR Measurements of Velocities in Explosive Valves,_ Sandia Laboratories, Livermore, CA, SAND76-8048, December 1976.

6. E. G. Young and L. M. Barker, _VISAR Data Reduction,_ Sandia Laboratories, Albuquerque, NM, SAND75-0424, November 1975.

DREV PYROTECHNICS TEST FACILITIES AND TECHNOLOGY BASE PROGRAM

by

P. Plante

Defence Research Establishment Valcartier
P.O. Box 880 Courcelette
Québec, Canada G0A 1R0

ABSTRACT

This paper describes the pyrotechnics test facilities at the Defence Research Establishment Valcartier that are used for light intensity measurements of tracers, for aerosol studies, for ignition studies of primer-tracer compositions and for testing of smoke generators. A brief description of technology base work on castable smoke compositions, for application to coloured and screening smoke grenades, and on delay igniters is also given.

INTRODUCTION

The pyrotechnics test facilities and current related technology base programs at the Defence Research Establishment Valcartier (DREV) are described in this paper. The principal facilities are:

a. an installation for the measurement of visible light output from tracer bullets, when submitted to a rotational speed of up to 100,000 rpm;

b. a 320-m^3 aerosol test chamber for evaluating screening properties of smoke agents;

c. a high-pressure vessel for ignition studies of tracer primer compositions; and

d. a combustion chamber for testing of smoke generators.

The current R&D work in pyrotechnics at DREV also deals with the development of polymer-based castable smoke formulations for application to signalling and screening smoke grenades and with the development of delay igniters.

TEST FACILITIES

Installation for Tracer Performance Testing

Figure 1 is a pnotograph of the installation used for tracer performance evaluations. The spin apparatus is a 5.1-cm (2-in) horizontal air turbine from Barbour Stockwell Co. which can be rotated up to a maximum speed of 100,000 rpm. The 7.62-mm tracer test sample, which together with its adaptor/holder weighs about 30 g, is mounted directly on the horizontal shaft of the turbine rotor.

Figure 2 is a schematic representation of the turbine installation. The turbine speed is monitored with a control unit incorporating a speed control and a digital tachometer (B.S. Models 105E and 107B). The speed control can be operated in two modes: ungoverned, in which the operator directly controls the throttle valve and the turbine speed, or governed, in which the operating speed is initially preset, but the turbine is brought to speed under manual control. The speed of the turbine is controlled to an accuracy of $\pm$ 0.5% of the maximum attainable value.

The digital tachometer measures turbine speed by counting the electric pulses sent from a magnetic pulse transducer. The transducer is installed close to the turbine shaft which, at this location, is in the form of a six-tooth gear. In the governed mode, the measured speed is compared with a preset value and a correction signal is fed to the

throttle valve if there is a detected difference. The tachometer incorporates an independant and adjustable overspeed shut-down system which can close a solenoid valve in the air drive line, thereby protecting the turbine against overspeed damage.

The air is supplied from six air cylinders that provide a total air storage capacity of 38 m^3 at 15 MPa (2200 psig). Air passes through a regulator for depressurization to 0.5 MPa (60 psig) and is filtered before passing through the overspeed valve and the throttle valve (Valtek Mark 1). The diameters of the drive air line and the valve connections, 2.5 and 3.2 cm respectively, ensure that the pressure losses due to pipe friction are below 0.03 MPa (5 psi) for good speed control and turbine performance. The bearings of the turbine are lubricated by air laden with oil mist delivered from an oil-mist generator (Alemite No. 4977).

The spinning tracer is ignited by the flash output of a squib (CIL S-140) held in a support at a 2-cm distance from the tracer primer surface; the support falls into the horizontal position when the squib is functioned to provide a clear field of view to the burning tracer.

Figure 3 shows the instrumentation set-up for measuring the luminous flux and radiant energy output of the tracer. The radiant energy output, in watts, is measured with a radiant flux detector (Hewlett Packard Model 8334A) located at a distance of 1.2 m from the tracer. The instrument detects radiant energy in the range of 0.2 to 3 μm. The luminous flux, in foot-lamberts, which corresponds to the human-eye sensitive region of the spectrum, 0.38 to 0.78 μm, is measured with a photometer (Spectra Pritchard Photometer, Model 1980). This instrument actually measures the light reflected by a diffuse white plate (20 by 30 cm) which is located 1.5 m from the burning tracer. The instrument is 1.7 m distant from the reflector plate and its field of view, 20 minutes, is such that it only sees the reflector plate surface.

The output signals from the radiant flux meter and the photometer are digitized via an A/D converter connected to a PDP 11/10 computer, and stored on magnetic tape for later data processing. The A/D converter samples the analogue signals at a rate of 60 readings per second.

Aerosol Test Chamber

Figure 4 is a photograph of the DREV aerosol test chamber which is being used for evaluating screening agents for their screening performance over the 0.4 to 14 μm electromagnetic region. The chamber is constructed of reinforced concrete and has a total volume of 320 m^3 (11,350 ft^3). The structure at the top houses a variable speed exhaust fan for rapidly evacuating aerosol clouds after each test (Figure 5). Two fans, 198.2 m^3/min (7000 cfm), are installed at mid-chamber height opposite to each other for mixing the aerosols in the chamber to a homogeneous consistency.

Twenty-six air intakes, each 20 cm in diameter, are located on the circumference of the chamber near the base. These holes are noramlly sealed during aerosol experiments but can be used during a flare evaluation experiment for delivering a well-distributed inflow of air.

The radiant sources, which are either luminous or infrared emitters, are installed on one side of the chamber and the radiometers are located on the opposite side in a shed adjacent to the chamber; the radiant flux is transmitted to the detecting instruments through a suitable optical window. The instruments that are used for measuring radiant energy are detailed in Table I.

TABLE I

Instrumentation for Radiant Energy Measurement

Instrument	Spectral Response Range (μm)
Spectra Pritchard Photometer, Model 1980 Kollmorgan Corp.	0.35 - 0.84
Autoranging Telephotometer System Model 1C 2001 Gamma Scientific Inc.	0.30 - 0.90
Dual Pyroelectric Radiometer & Radiometer RK3440 Laser Precision Corp.	0.60 - 14
Optical Multichannel Spectral Analyser Model 1205 Princeton Research Co.	0.35 - 1.10

Two 15-cm diameter conduits that connect the chamber and the adjacent instrument laboratory are used for particle size and mass concentration sampling of the aerosol cloud. Instruments that are available for such analysis are described in Table II.

For small-scale aerosol generation and calibration purposes, a Berglund-Liu Monodisperse Aerosol Generator, Model 3050, from Thermo Systems Inc. is available. This instrument can generate monodisperse aerosols (i.e. all particles of same diameter) from liquids or soluble solid materials over a selectable particle size range of 0.5 to 50 μm.

TABLE II

Instruments for Aerosol Particle Size and Concentration Analysis

Instrument	Particle Size Range Detection (μm)	Principle of Operation
High Volume Cascade Impactor Weathermeasure Corp.	0.5 - 10	5 stages cascade impactor
1ACFM Ambient Particle Size Sampler Anderson 2000 Inc.	0.5 - 11	8 stages cascade impactor
Electrical Aerosol Size Analyzer Model 3030 Thermo Systems Inc.	0.0032 - 1	Charged particle mobility diffusion analysis
Aerosol Particle Monitor Model 220 Royco Instruments Inc.	0.5 - 5	Light scattering principle
Piezobalance Respirable Aerosol Mass Monitor, Model 3500 Thermo Systems Inc.	<3.5	Electrostatic precipitation on piezocrystal

High Pressure Vessel for Tracer Primer Ignition Study

The tracer ignition process in a 105 mm spinning tubular projectile (STUP) presents some unique problems. Figure 6 presents a schematic representation of a possible tracer configuration at the base of this STUP. When the projectile is fired in a rifled gun, the propellant gases must pass via a narrow throat in the base drive-plate to the surface of the primer composition. A study has been commenced to determine the effect of the throat design on the reliability of tracer ignition when this arrangement is suddenly exposed to hot high-pressure propellant gases over a 10-ms period in a pressure vessel.

Figure 7 shows the high-pressure vessel that has been designed for this study; it is constructed to withstand a maximum pressure of 690 MPa (100,000 psi). The exterior of the chamber is 23 cm in diameter by 37 cm in length, and the internal chamber is 7.6 cm in diameter by 13.3 cm in length for a free space of 615 cm^3.

A rupture-disc assembly is provided for the rapid depressurization of the chamber after a preselected maximum pressure has been reached. It is made of two concentric bolts between which a rupture-disc is held. The gases escape through a 1.1-cm diameter hole in the inner bolt. For this hole size, the gas-evacuation time from the chamber for a peak pressure of 414 MPa (60,000 psi) is in the order of 10 ms; this pressure is the nominal pressure developed at the base of

a 105 mm STUP projectile fired from a rifled barrel. The assembly is made of two bolts to allow for the expected erosion of the inner bolt, which may have to be replaced after each firing.

The gas pressure developed in the chamber is measured with a piezoelectric pressure-transducer (General Transducer Co. Model GT-24) and the signal is recorded with a strip chart recorder (Honeywell Visicorder 1508B).

A pressure-sealed chromel-alumel thermocouple probe (Aminco No. 45-17626) is inserted at the base of the tracer capsule to detect the end-of-burn of the charge; it is connected to a Tektronix 502 Dual Beam Oscilloscope equipped with a polaroid scope camera. As shown in Figure 7 the vessel is surrounded by a water jacket so that it can be cooled rapidly between tests.

Approximately 400 mg of tracer powder are loaded at 620 MPa (90,000 psi) into a cavity having an internal diameter of 0.5 cm and a depth of 1.2 cm; 40 mg of a primer mix are applied over the pressed tracer powder at the same pressure. The tracer body is located in a heavy steel plate which is covered with a second plate into which a 1.9 cm deep throat has been machined as shown in Figure 7. Approximately 130 g (2000 grains) of gun propellant are suspended from a rod in front of the throat opening. Ignition of the propellant is achieved via an electric squib and a black-powder priming charge.

Installation for Smoke Generator Testing

Figure 8 is a photograph of the chamber used for testing smoke generators. This installation permits the measurement of variables such as burn rate, combustion temperature, gas temperature, smoke density and rate of weight loss. It is located in a 10-m^3 room with a fan installed in the roof of the chamber to exhaust the smoke; two other fans with heating elements are located on the two opposing side walls for air intake during a test or for rapid ventilation of the room after a test (Figure 9).

The test smoke generator is installed on a weight-loss transducer (Statham UC3/UL4-50) for measuring the change in weight as a function of burn time. Combustion and gas temperatures are measured with chromel-alumel thermocouples; the "combustion" thermocouple is inserted to a 1-cm depth into the pyrotechnic composition and the "gas" thermocouple is installed at 3-cm distance from the exhaust orifice of the generator.

As shown in Figure 9, a 24 W lamp and a radiant flux detector (Hewlett Packard Model 8334A) are installed facing each other across the chimney for the evaluation of smoke density. The light is transmitted from the lamp to the detector through two 5-cm holes in the chimney. The measured smoke density is a relative density that can be used for comparing one grenade to the next; no attempts have been made to relate this measurement to an absolute optical density. A deflector is

installed at the base of the chimney for the uniform dispersion of the smoke before it passes through the light beam. The volumetric gas flow through the chimney is fixed at a constant value during a test, 28.3 m^3/min (1000 cfm).

The detector signal from the radiant flux meter is fed to a digital volt meter and then numerically printed on paper, whereas the outputs from thermocouples and the weight-loss transducer are amplified and fed to a strip chart recorder (Honeywell Visicorder, Model 1058A). The amplified signals are also fed into a minicomputer PDP 11/10 for digitizing and storage on a magnetic tape.

TECHNOLOGY BASE PROGRAM

Polymer-Based Smoke Compositions

Polymer-based castable smoke compositions, both coloured and white, are being developed at DREV for application to signalling and screening smoke grenades. The advantages associated with castable compositions, compared to conventional pressed powders, are mainly their improved mechanical properties and stability, improved safety in handling with reduced friction, lower impact and electrostatic sensitivities and greater flexibility for designing the grain configuration.

The objective of the technology base studies is to optimize smoke compositions and grain configurations for maximum smoke output and colour quality, so that subsequent design requirements for burn time and weight can be established.

Coloured Smoke Grenades

For coloured smoke grenades, formulations incorporating the following chemical constituents are being investigated:

a. an organic dye (38 - 45%);
b. an oxidizer, potassium chlorate (22 - 28%);
c. a fuel, sulfur (4 - 9%);
d. a gasifier and stabilizer, sodium bicarbonate (5 - 16%); and
e. a binder, polybutadiene R45M (18 - 20%).

The coloured smoke is produced by the vaporization of the dye using the heat generated by the oxy-reduction reaction of the oxidizer with the fuel. The expelled dye vapours then condense in the air to produce a fine particulate, coloured smoke cloud.

Figure 10 is a cutaway view of a test generator that depicts the interior grain configuration. The grain is 6 cm in diameter by 6.3 cm in length with a central chimney; it is bottom-ignited with the smoke venting upwards through the chimney. This configuration implies that

479

the unignited grain is preheated by the hot escaping smoke, so that the rate of burning is maximized. This effect leads to a possible reduction of the energetic constituents and a concurrent increase in dye content.

As shown in Figure 10, a 0.63-cm thick wafer of starter composition is placed between the primer material and the smoke grain. This wafer is similar in chemical make-up to the main composition, but has a lower dye content and, therefore, a faster burn rate. Violet, yellow, green and red formulations that give good smoke volumes and colour qualities are given in Table III.

An unexpected problem of flaming in the emitting smoke had to be resolved in the course of the development. It was found that with a single exhaust port the flaming probability was high when the grenade was burned under low wind conditions. Figure 11 shows the baffle config- urations at the base of the grenade that were successively investigated to solve the problem. Design No. 3, which forces the smoke to disperse laterally through six 0.5-cm diameter holes on the circumference of the container, was eventually chosen. This configuration eliminates the concentration of hot gases exiting from one place, as was the case for the single exhaust port design.

TABLE III

Typical Coloured Smoke Formulations

	Ingredients (% Weight)				
Colour	Dye	$KClO_3$	S	$NaHCO_3$	Binder*
Yellow	42	24	7	7	20
Violet	42	24	7	7	20
Red	42	24	9	5	20
Green	42	24	8	6	20

*R45M Polybutadiene (HTPB)

Screening Smoke Grenade

Two types of polybutadiene polymer-based formulations are being investigated for screening smoke applications in grenades. One type of mix produces zinc chloride smoke. Its principal chemicals are: hexa- chloroethane or hexachlorobenzene, zinc, zinc oxide, ammonium perchlorate, and polybutadiene R45M binder. The other type is similar to the coloured

smoke formulations in that it incorporates an organic white dye (2 - chloroanthraquinone).

At this stage of development, small-scale generators with a grain configuration similar to the one for the coloured smoke grenade, and incorporating about 30 g of smoke composition, are being used to test experimental formulations. Typical compositions being investigated are given in Table IV.

TABLE IV

Typical White Smoke Formulations

Code	Dye	$KClO_3$	S	$NaHSO_3$	Binder	C_2Cl_6	Zn	ZnO	NH_4ClO_4
Ex-9	42	24	7	7	20				
Ex-11					15	41	34		10
Ex-19					16	22		36	26

Ingredients (% Weight)

Delay Igniters

Limited development work has also been undertaken on percussion-ignited delay igniters, primarily for application to pyrotechnic devices. Commercially available delay columns, normally used in delay detonators, were incorporated into 3.5 and 15-s delay igniters and primed with caps used for 9 mm ammunition. Very reliable ignition of the delay columns was achieved even though no intermediate primer powder or fast-burning delay element was used for transferring from the primer cap to the main delay column. A boron/barium chromate powder was used at the tip of the delay column to provide the desired hot flash output.

SUMMARY

The various test facilities now operating in DREV's Pyrotechnics Group have been detailed, and current technology base studies have been described.

Figure 1 - Test Set-up for Tracer Performance Evaluation
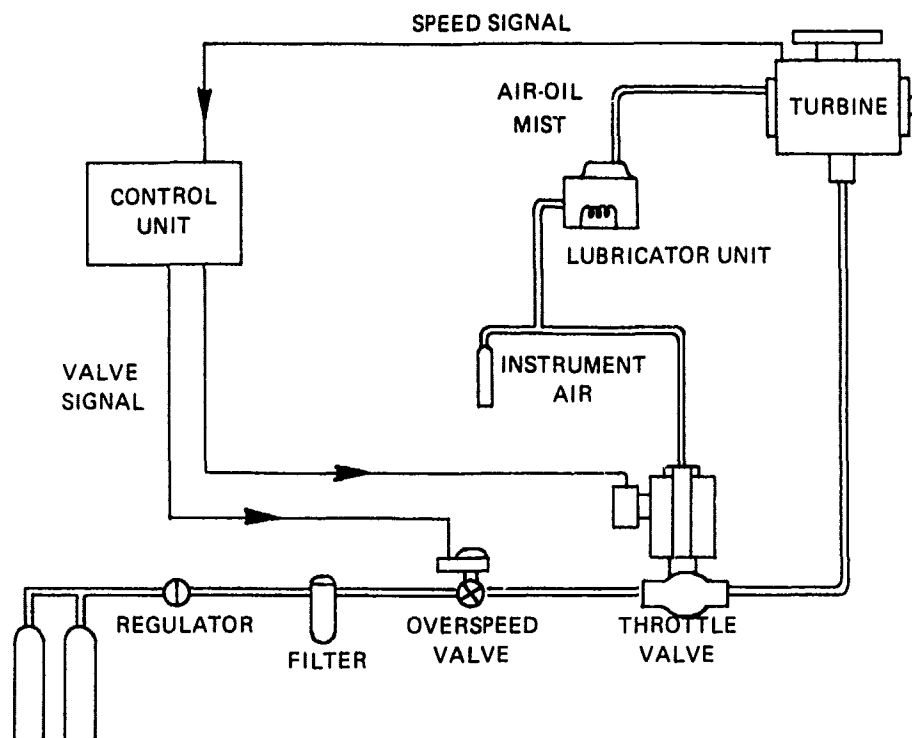
Figure 2 - Turbine Installation for Tracer Evaluation
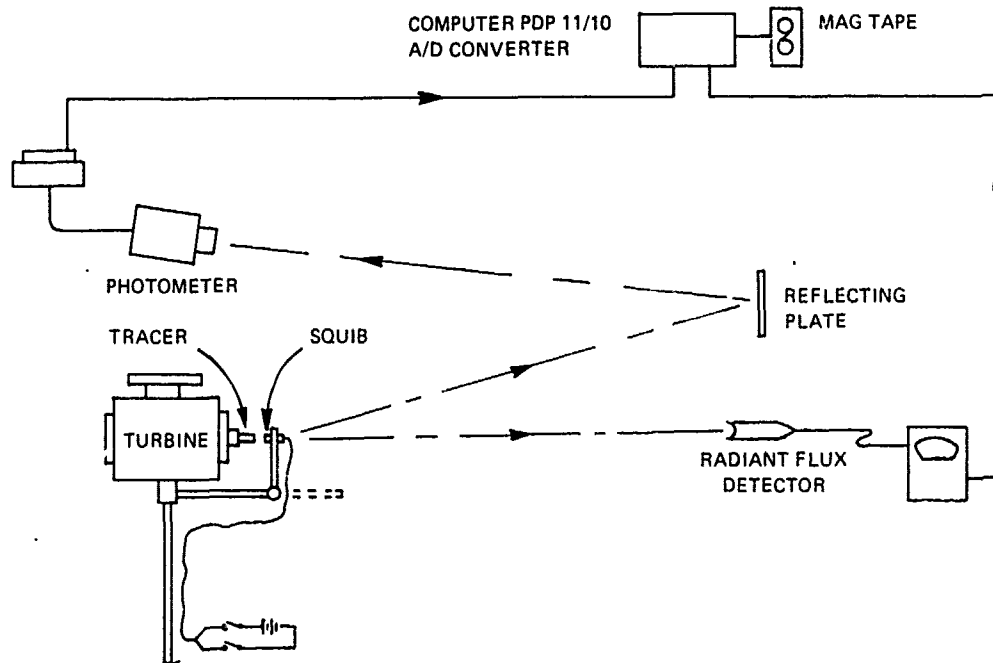
Figure 3 - Instrumentation for the Performance Evaluation of Tracers
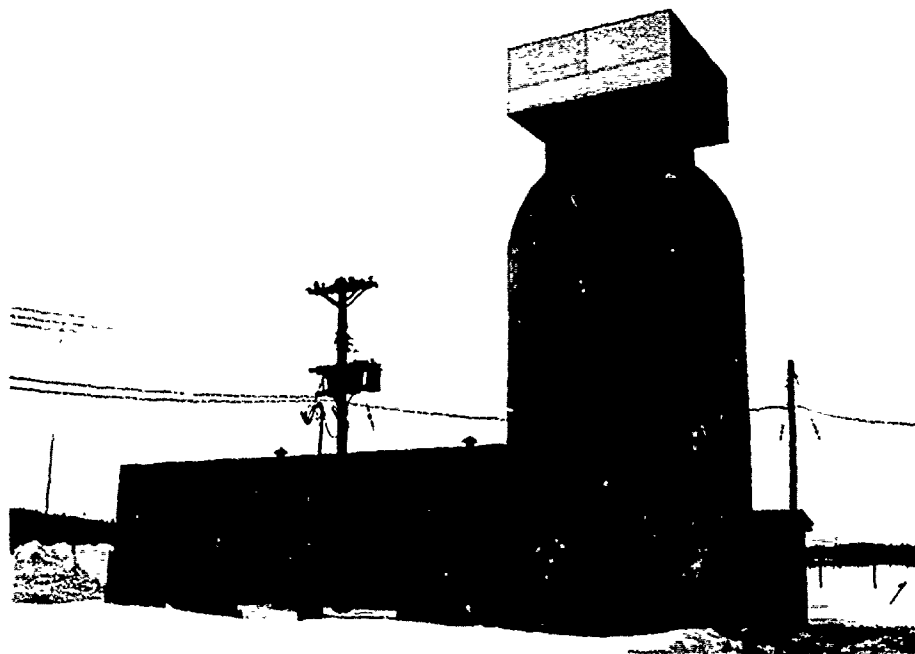
Figure 4 - DREV Aerosol Test Chamber and Instrument Laboratory
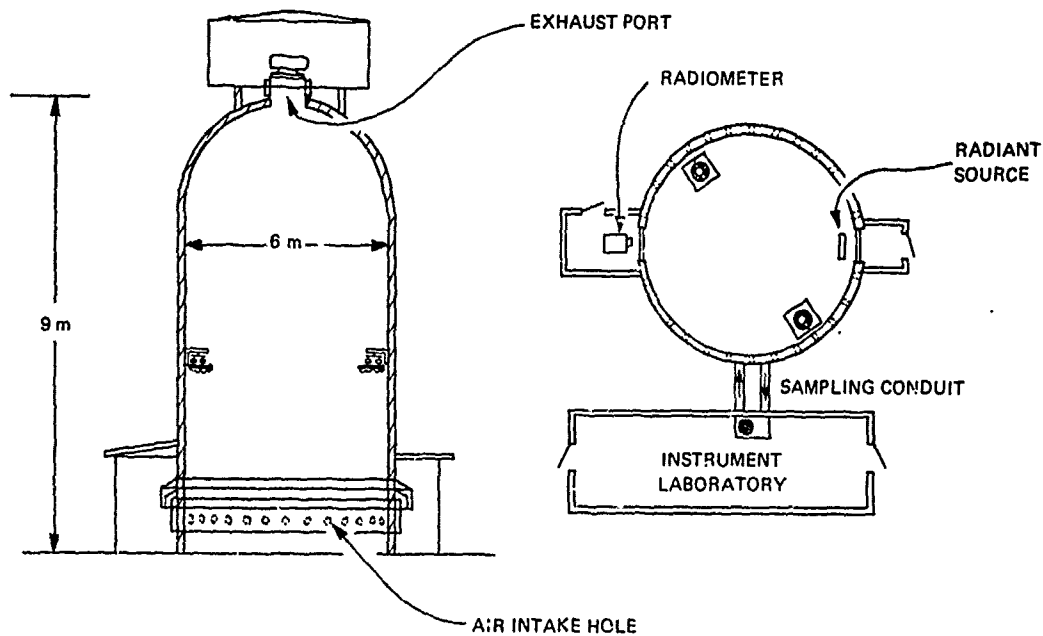
Figure 5 - Layout of Aerosol Test Chamber
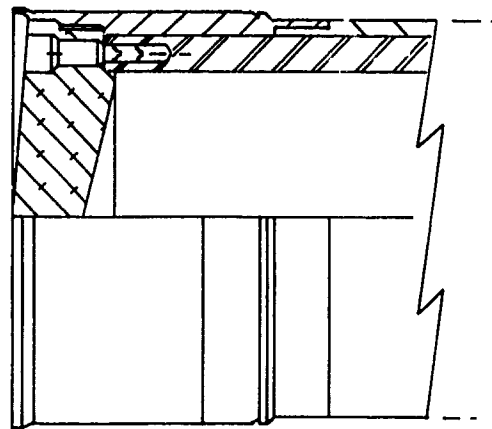
Figure 6 - Tracer Configuration for 105 mm
Spinning Tubular Projectile
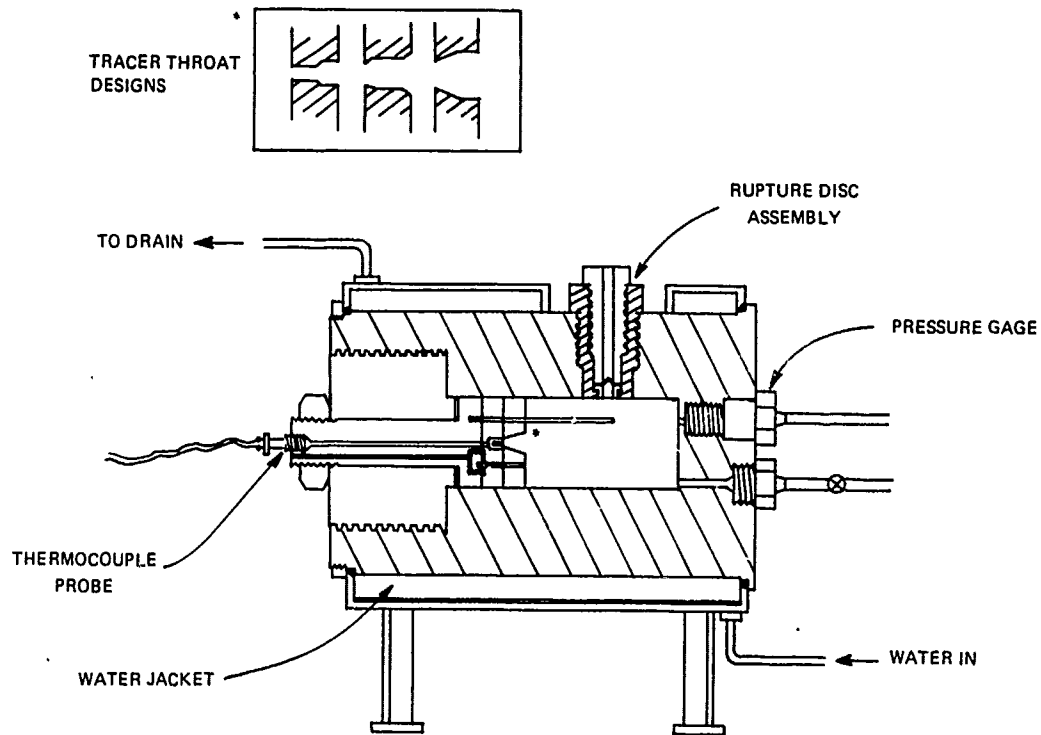
Figure 7 - Instrumented High Pressure Vessel
for Tracer Ignition Experiments
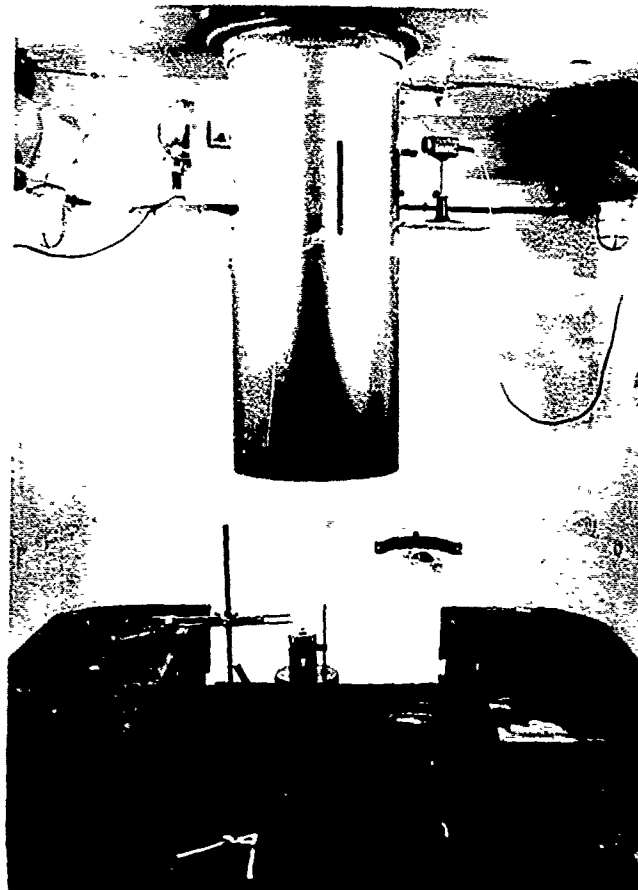
Figure 8 - Smoke Generator Test Chamber
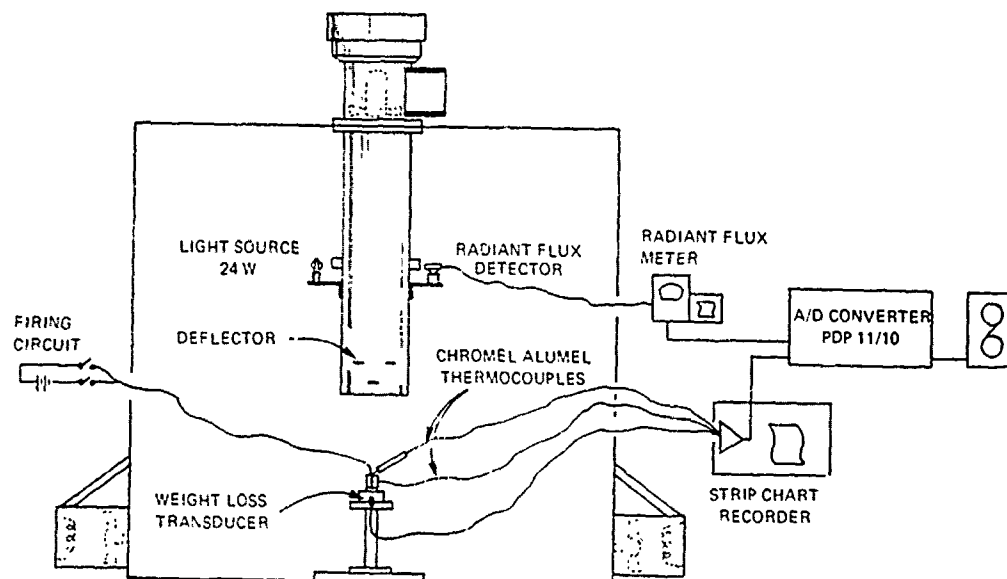
Figure 9 - Instrumentation for Smoke Generator Test Chamber
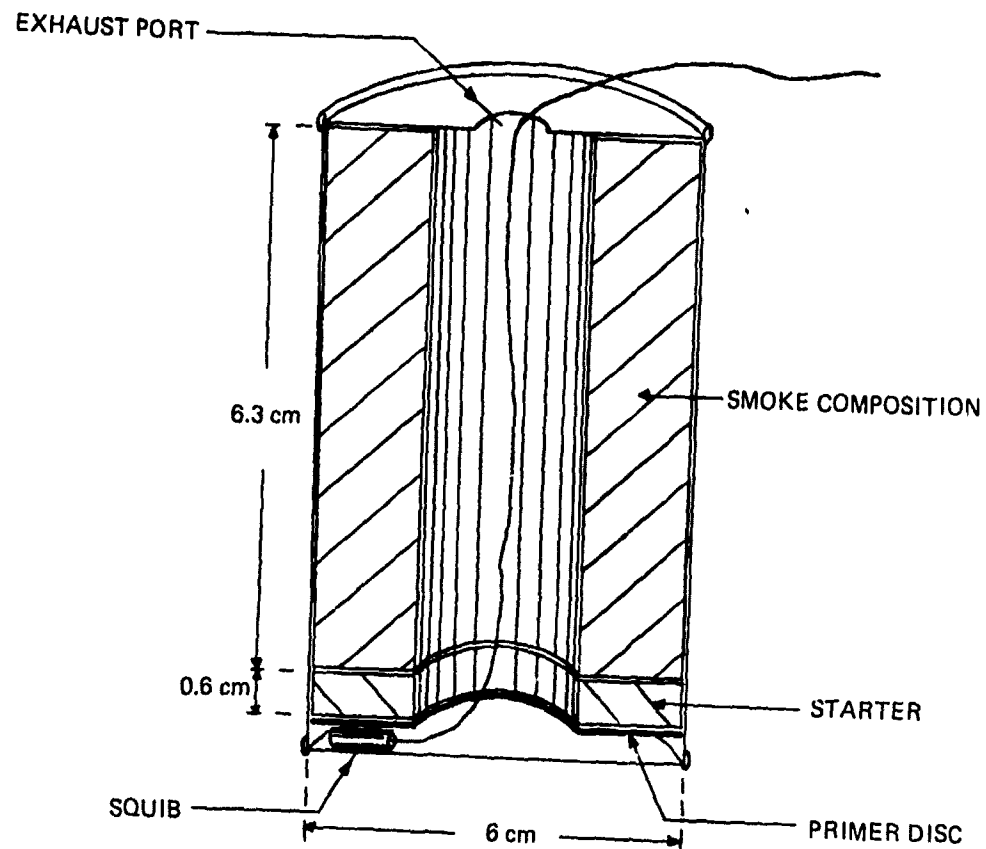
Figure 10 - Test Smoke Generator
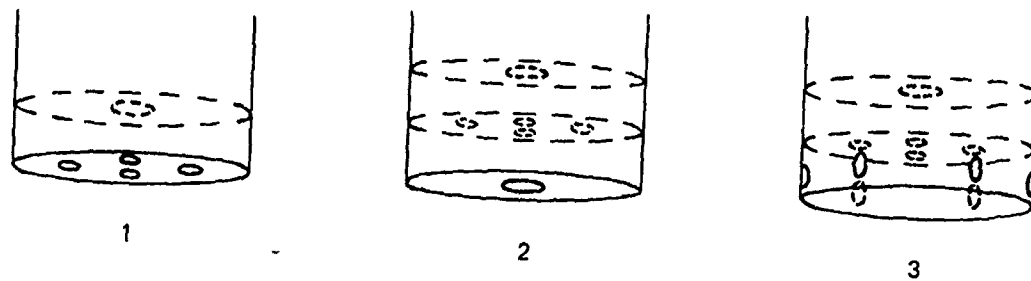
Figure 11 - Baffle Designs for Smoke Grenades

487

PASSIVATION OF THE PYROTECHNIC FUELS TITANIUM AND TITANIUM HYDRIDE IN OXIDATIVE ENVIRONMENTS[*]

By

Rod K. Quinn
Sandia Laboratories
Albuquerque, New Mexico 87115

Titanium and titanium hydride are used as fuels in pyrotechnic mixtures for explosive components. Their behavior in strongly oxidizing environments is of concern. The oxidation of these high-energy density materials has been modeled by electrochemical and thermal aging techniques. In our electrochemical experiments, the apparent thickness of the oxide was controlled by the magnitude of applied potential across the film. On previously untreated films, onset of oxidation occurred at ca. + 0.4±0.2V versus SCE; the peak potential in this faradaic process varied as a function of pretreatment and surface condition. After oxide formation, the thin film electrodes behaved as semiconducting surfaces. The electrode capacitance of the oxide film showed "ideal" semiconductor behavior. Postmortem analysis by XPS and Auger spectroscopy was used to characterize the extent of oxidation of the film surface. Observation of the dN(E)/dE and N(E) Auger spectrum indicated that the electrode surface is a mixture of TiO, Ti_2O_3, and TiO_2, as well as the respective metallic phases. This is confirmed by the predominant XPS Ti transition. The extent of oxide growth into the films was measured by Auger/depth profiling experiments and the results are comparable for the two metallic materials. The results of these experiments are compared for titanium and titanium hydride and are examined as to a model for oxide formation and growth.

The Explosive Component Department is interested in transition metal hydrides as reactive solid materials to be used in explosive components. Primarily we are interested in TiH_x as a high energy density fuel for blending with a strong oxidizing agent to form a class of explosives called pyrotechnics. As an example some of our actuators employ TiH_x + $KClO_4$ in a 33%/67% weight percent ratio. These pyrotechnic materials are usually ignited from a heated bridge-wire. Several applications of pyrotechnic materials are listed in Fig. 1. There are at least four good reasons why we are interested in pyrotechnic materials: (1) high auto-ignition temperature, (2) high resistance after fire, (3) high reliability, (4) they can be made spark insensitive.

The work to be discussed in this paper is part of an overall program at SLA and Mound to understand the chemical and physical properties that govern the performance and sensitivity of pyrotechnic materials. The major purpose for this program is to gain sufficient information to be able to design components to satisfy future system requirements.

The problem of spark sensitivity is one of utmost concern. Whereas α-Ti is sensitive to equivalent human body spark, γ-TiH_x is not. The reason(s) for this difference is uncertain. We feel at least part of the answer lies in the surface properties of these high surface area, fine particle materials. Initially we have undertaken to examine the effects of corrosion or passivation by oxidation on the physical and chemical properties of the metallic constituent. These constituent properties will probably dominate the physical and chemical properties of the pyro-technic blend, and therefore the ignition and spark sensitivity. Titanium and titanium hydrides have been examined in film, bulk and we are currently examining powders and blends. In this paper I would like to present our results on the oxidation studies of Ti and TiH_x thin films.

In Fig. 2, an outline of our experimental apparatus and techniques are shown. We perform our controlled oxidation with a 3-electrode potentiostat. The apparatus also allows charge, capacitance and surface conductance to be measured as a function of potential. The samples studied were 200-600 Å films electron-beam deposited on 450°C SiO_2 substrates. The background pressure was ~10^{-7} Torr during deposition. The AES/XPS data were taken on a Phi 548 spectrometer.

A typical linear sweep voltammogram is shown in Fig. 3 for Ti oxidation in 1N $HClO_4$. In this figure, the current flowing at the Ti or TiH_x electrode is measured as the voltage is scanned at a specific rate, e.g., 5 mV/s.

APPLICATIONS OF PYROTECHNIC MATERIALS

COMPONENTS

SPARK INSENSITIVE LOW ENERGY DETCNATORS

- DEFLAGRATION DETONATION TRANSITION (DDT) DETONATORS
- FLYING PLATE DETONATORS

SPARK INSENSITIVE INITIATING DEVICES

- ACTUATORS
- IGNITERS

LONG LIVED PROPELLENT DEVICES

- ROCKETS, THRUSTERS, ETC.

SUB-SYSTEMS

POWER SOURCES

- LIGHT OUTPUT - PHOTOVOLTIAC CELL

DISABLEMENT TECHNIQUES

- HEAT POWDERS (E.G., THERMITES)
- TORCHES (E.G., FOR TABS)

Figure 1

Some of the applications or potential
applications of pyrotechnical materials
of interest to Sandia Laboratories.

INTERFACIAL ELECTROCHEMISTRY

PAR 173 Potentiostat with auxiliary
equipment permits measurement of:

(a) Current - voltage

(b) Charge - voltage

(c) Capacitance

(d) Surface Conductance

Thin Film Electrodes:

200-600 Å Ti

deposited at 25°C to 500°C

on SiO_2 or Al_2O_3 substrates

SURFACE ANALYSIS

AES/ESCA - PHI-548 Spectrometer

Figure 2

Experimental apparatus and techniques
employed in this study.

Initially no current flows, until a potential of about 0.3 to 0.5 V (measured relative to the saturated calomel electrode (SCE)) is reached. At this point a sharp increase in current is observed with the peak occurring at potentials between 0.5 and 0.7 V versus SCE. Nearly constant current densities of 30-50 $\mu A/cm^2$ are observed at potentials between ∿0.7 and ∿2.7 V versus SCE. If the anodic potential were interrupted or reversed in direction, the faradaic current quickly decayed to zero and no currents were observed on the return scan until potentials less than -0.2 V versus SCE were reached, at which point hydrogen evolution would occur.

The exponential increase in current with applied potential above 2.7 V versus SCE is typical of exhaustive oxygen formation ($O_2\uparrow$) and is controlled by the kinetics of that reaction as well as Ti^{4+} and O^{2-} migration. We are interested in the near steady-state, field dependent oxidation of the "pre-passive" region between 0.5 and 2.7 V. To study this region we define a parameter, the oxidative onset potential-- E_{ONSET}. This is the potential one determines by extrapolation of the sharp i-E ramp at the onset of oxidation to the zero current axis. The slope of this ramp, di/dE, is also a useful parameter as it is a qualitative indicator of the height of the energy barrier to oxidation.

The shape of the oxidative curves for Ti films was independent of pH although the onset potential shifted cathodically with increasing pH. Two distinctive regions were observed--in acidic to neutral media a slope of ∿20 mV/pH unit was observed, while in basic media a slope of ∿80 mV/pH unit was found. This behavior is the subject of further study.

The dc conductance, or surface conductance for films of less than 250 Å thickness, indicates a monotonic decrease with oxide layer growth. For example, for a typical film at 2 V, a depletion of ∿2 x 10^{22} electrons from the conduction band of Ti is observed.

The capacitance versus applied potential measurements for these films indicate an oxide layer grows but the layer is semiconducting rather than insulating with an approximated carrier density of 10^{20} cm^{-3}. Linear $1/C^2$ versus potential behavior also indicates a uniform space charge layer over relatively thin (<250 Å) electrode thicknesses. The conclusion drawn is that we have an n-type or reduced titanium dioxide and not stoichiometric TiO_2.

To assist in establishing a mechanism, to quantitate the oxide formation and to examine solvent/solute effects (none were seen in the electrochemical experiments) surface analysis by Auger and x-ray photoelectron spectroscopy was employed on our thin film electrodes. In Fig. 4(a), a typical AES spectrum is shown for a Ti electrode surface. The dN(E)/dE spectrum indicates a large oxide peak relative to the Ti LMM and LMV peaks. However determination of the oxygen to titanium ratios by
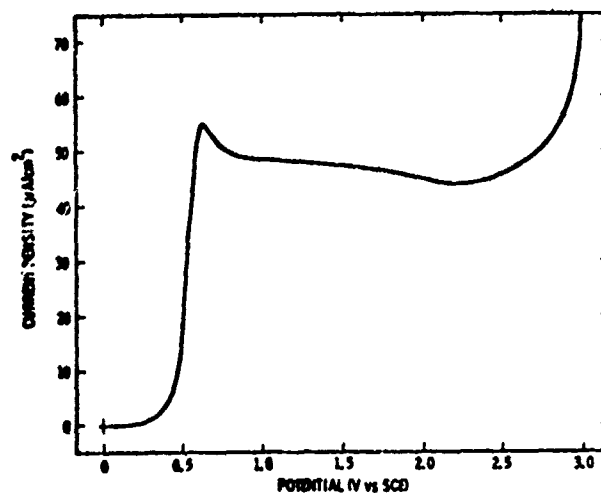
Figure 3

Typical linear sweep voltammogram for a Ti thin
film electrode in 1N HClO4, at a sweep rate of
5 mV/sec. The nearly constant current observed
between ~0.5 and 2.7 V versus SCE is indicative
of field assisted, ionic conductivity dominated,
oxide layer growth.
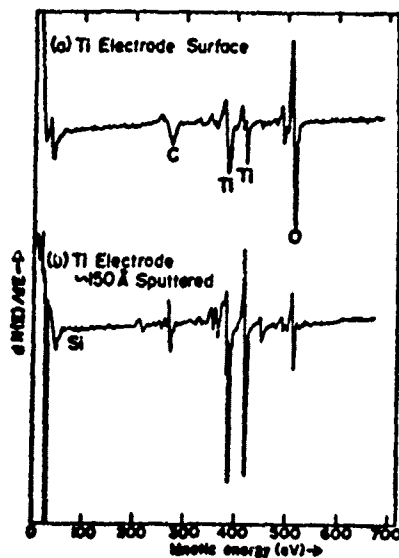
Figure 4

Auger electron spectra of (a) Ti electrode
surface and (b) the same electrode after
argon ion etching away ~150 Å.

measuring the peak heights (Ti LMM at 387 eV) and correcting for Auger sensitivities indicated a ratio of 1.6 to 1.7. The correction was made by comparison to a standard compound of known stoichiometry, namely TiO_2.[1] This sub-stoichiometric ratio, 1.6 to 1.7, was observed independent of oxidation up to ~2.0 to 2.5 V or 12 to 14 mC/cm^2 of charge. Argon-ion etching to significant sub-surface depths yields a spectrum similar to that seen in 4(b). The oxygen signal has decreased significantly but has not disappeared. Since these films were deposited on hot substrates (450°C) significant mixing of Ti and SiO_2 is expected at the interface.[2] Indeed, Si is observed at a depth of ~150 Å in this 200 Å film. Therefore, some oxygen could be contributed from this source.

The argon ion etching technique coupled to AES allowed us to profile the oxygen-titanium ratio with depth below the surface. By correction of each of the electrochemically grown profiles for the baseline blank films the amount of excess oxide produced could be quantitated. Again the oxide/titanium ratio at the surface of each electrode was invariant (1.6 to 1.7). The films appeared to have ~20 Å of native oxide and 13 mC of charge produced ~50-60 Å of oxide.

Note the change of shape of the Ti LMV peak as one proceeds from the surface into the interior. High-resolution, N(E) Auger spectra of the Ti (LMV) peak produced an interesting result. In Fig. 5, we show the dN(E)/dE and N(E) spectra of the Ti LMM and LMV peaks at a typical electrode surface. In the N(E) spectrum we have deconvoluted the LMV peak and the spectral components A, F, B are designated according to Solomon and Baun.[3] The relative proportions of these spectral components is exactly those reported by them for TiO. That is to say our surfaces are not stoichiometric TiO_2 but are principally TiO, at least to the depth of AES beam sampling, or ~15-20 Å. This same stoichiometry is observed for electrochemically treated Ti electrodes up to ~2 V or 12-13 mC/cm^2.

This substoichiometric oxide structure is substantiated by x-ray photoelectron spectroscopy (XPS or ESCA). The Ti($2p_{1/2}$, $2p_{3/2}$) XPS spectra for (a) TiO_2 standard, (b) Ti film after sputtering ~150 Å and (c) surface of Ti film electrode are shown in Fig. 6. We observe a shift in binding energy of 5.3 eV in going from metallic Ti(b) to tetravalent Ti(a). Comparison of spectrum (c) to (a) and (b) indicates that components of each of these oxidation states are present in the Ti film electrode surface. The deconvoluted Ti($2p_{1/2,3/2}$) XPS spectra for the electrode surface in 6(c) is seen in Fig. 7. The non-linear spectral background has been subtracted for presentation of the deconvoluted peaks. The deconvolution technique involves a five parameter fit[4] and yields a minimum of four oxidation states of Ti, namely Ti, TiO, Ti_2O_3 and TiO_2. These results are obtained in all our electrode surfaces even with 12-13 mC of charge. We also note no effects of the solutions on our electrodes, i.e., no solute or solvent species are seen.
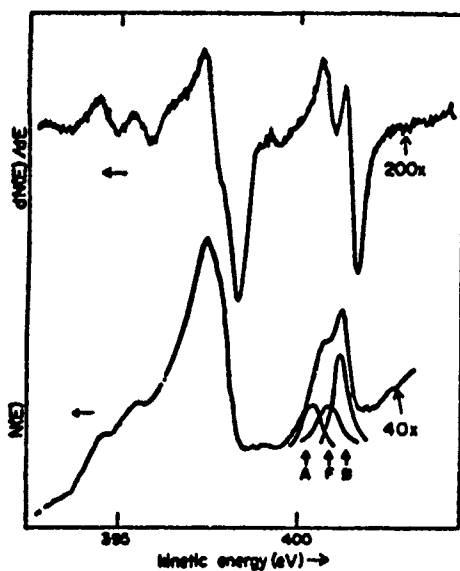
Figure 5

High resolution spectrum of the Ti (LMM) and (LMV) peaks for a Ti film electrode surface. Both N(E) and dN(E)/dE are shown as a function of Auger electron energy. The high energy band is resolved into the three components A, F, and B as defined in Ref. 3 and in the proportions they obtained for pure TiO.
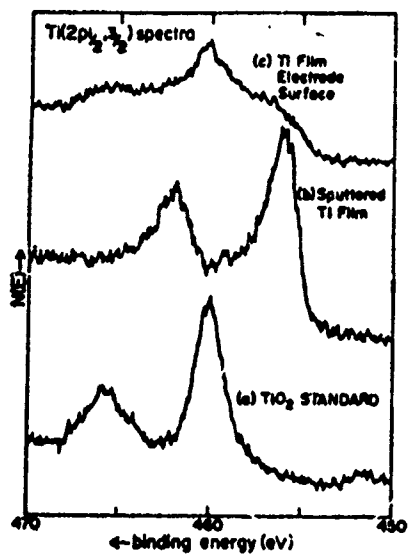
Figure 6

The Ti $(2p_{1/2,3/2})$ XPS spectra for (a) TiO_2 standard, (b) Ti film after sputtering ~150 Å and (c) the surface of a Ti film electrode.
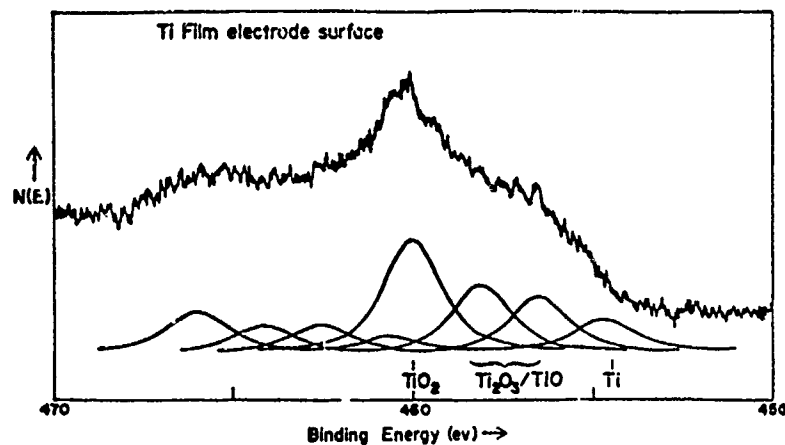
Figure 7

Deconvoluted Ti $(2p_{1/2,3/2})$ XPS spectra from Fig. 6c.
The spectral background slope has been subtracted for
presentation of deconvoluted peaks.
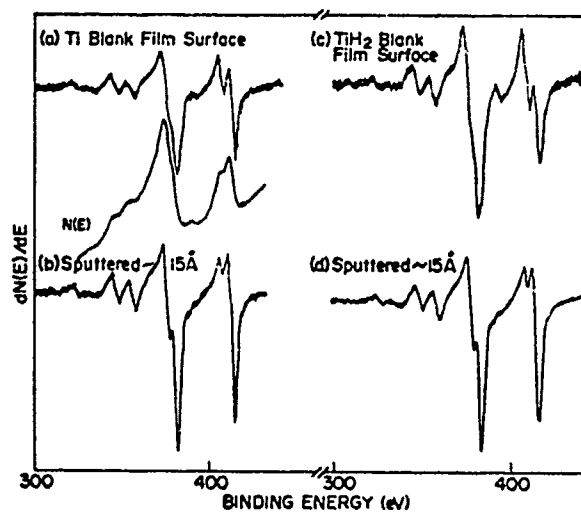
Figure 8

Auger electron spectra of (a) Ti film electrode
surface, (b) that film after sputtering approxi-
mately 15 Å, (c) TiH_2 film electrode surface and
(d) that film after sputtering approximately 15 Å.
Note the similarities in (a) and (c) as well as
(b) and (d).

495

The first 25-30 Å of the TiH_x films show analogous results to the Ti films. In Fig. 8 the LMM and LMV transitions for a Ti blank and a TiH_x blank electrode are shown. A blank is an electrode taken from the vacuum system in which it was deposited and placed in the AES/XPS system or the electrode was soaked in solvent at zero applied potential. The same results were obtained in both cases. As seen in Fig. 8, the shape of the dN(E)/dE spectra is qualitatively the same for Ti and TiH_x, although a larger contribution from the TiO_2 component is observed. Sputtering into the films ~15 Å yields identical suboxide-type spectra.

Oxygen-to-titanium ratios were computed from the intensities of the oxygen KLL transitions and the titanium LMM transition. As discussed previously, the O/Ti intensity ratio of each film was normalized to the same ratio for a TiO_2 standard material to yield a relative atomic ratio, N_0/N_{Ti}. The TiH_x film surfaces showed a slightly substoichiometric composition, with N_0/N_{Ti} = 1.8. This value includes the contribution from all surface oxygen because the oxygen Auger KLL signal does not distinguish between oxide and absorbed oxygen species. The N_0/N_{Ti} surface ratics were slightly higher than those previously observed in titanium films, N_0/N_{Ti} = 1.6-1.7. Ion sputtering of the surface lowered the N_0/N_{Ti} to ca. 0.3 within 20-30 Å of the surface, similar to the titanium films. Electrochemically oxidized surfaces showed increased N_0/N_{Ti} values at the surface (1.9-2.0), and these values remained high following ion sputtering, depending upon the extent of electrochemical oxidation.

The XPS spectra of Figure 9 were consistent with the above AES data. The TiH_x film surface gave $Ti(2p_{1/2,3/2})$ spectra (Figure 9a) which were composed chiefly of a TiO_2 component. Smaller TiO and TiH_x components were also observed which were less than 10% of the TiO_2 concentration. This type of surface spectrum is consistent with either 1) a uniform surface composition consisting of TiO_2, suboxides and titanium hydride, or 2) a TiO_2 layer of less than 10 Å thickness overlaying a gradient mixture of suboxides and titanium hydride. We consider the second option to be more likely, although we must consider the possibility that the titanium hydride may be a mixed oxy-hydride compound, e.g., TiO_yH_x. The $Ti(2p_{1/2,3/2})$ spectra of the TiH_x film which was ion-sputtered to a depth of ca. 15 Å below the surface (Figure 9b) showed spectral components from TiO_2 and suboxides which were nearly equal and were approximately 50% of the intensity of the TiH_x component. This observation would indicate a mixed TiO_y/TiH_x composition of the pre-passive surface region. The N_0/N_{Ti} ratios computed from the XPS data [$O(1s)/Ti(2p_{3/2})$ intensity ratios normalized to TiO_2 standard] showed a value of c.a. 1.6-1.7 at the film surface and c.a. 0.8 following ion sputtering to ~15 Å below the surface. The surface N_0/N_{Ti} ratio was lower than that determined by AES because the O(1s) intensity included only
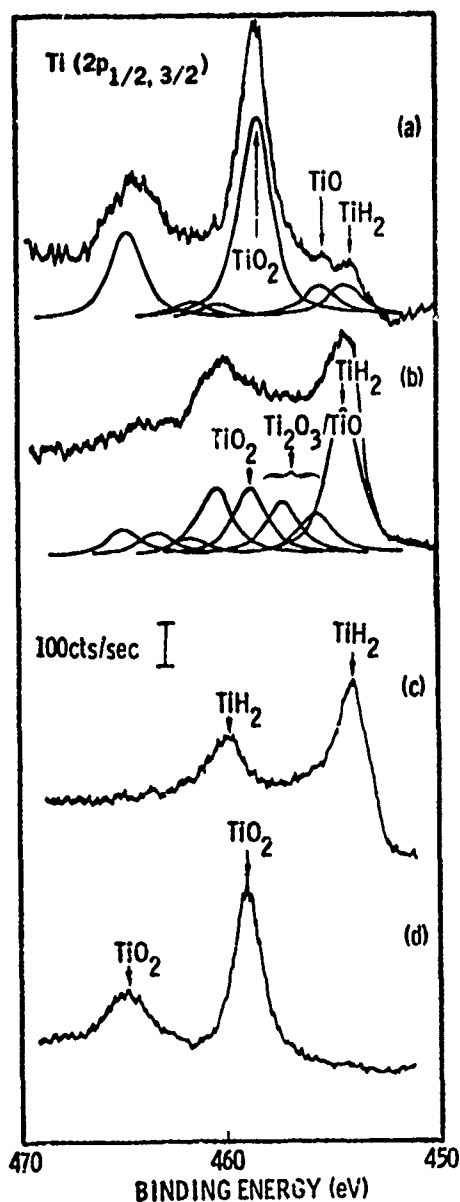
Figure 9

The $Ti(2p_{1/2,3/2})$ XPS spectra for (a) a TiH_x blank surface, (b) that film after argon ion etching away $\sim$20 Å, (c) the same film after argon ion etching $\sim$60 Å, and (d) the surface of a TiH_2 thin film electrode oxidized to 12.5 mC of charge.

oxide oxygen and not absorbed forms (OH, H_2O etc.). Ion sputtering to depths of greater than 50 Å yielded an XPS spectrum like that in Figure 9c. The $Ti(2p_{1/2,3/2})$ spectrum was comprised chiefly of the titanium hydride component and the N_O/N_{Ti} ratio decreased to c.a. 0.2. We have previously noted that the $Ti(2p_{3/2})$ binding energy for the hydrided metal is shifted to higher energies by c.a. 1.0 eV from that of the pure metal ($\Delta BE_1 \approx 76.0 \pm 0.2$ eV for TiH_x vs. 77.0 ± 0.2 eV for Ti) (1). This chemical shift is consistent with hydrogen bound in the titanium metal in a partially anionic form--although the hydrogen does not appear to be as electronegative as oxygen in the titanium oxides. The electrochemical oxidation of the hydride is certainly affected by the chemical form of hydrogen in the metal lattice and the mechanism by which it is removed during oxidation. Following electrochemical oxidation of the TiH_x film surface ($Q_T = 12$ mC/cm^2), the $Ti(2p_{1/2,3/2})$ XPS spectra reverted completely to that of TiO_2, $N_O/N_{Ti} \approx 1.9$-2.0 (Figure 9d), confirming that the oxide interface had been extended to beyond the depth to which XPS could successfully measure a TiH_x component (~ 25 Å).

Similar surface analysis and depth profiling have been performed on fine-particle (1-10 μm; 2-10 m^2/gm) powders of TiH_x. The results are analogous to the thin film data presented here. A comparison of the $Ti(2p_{1/2}, 2p_{3/2})$ XPS spectra of titanium hydride in thin film (a + b) and powder (d + e) is shown in Figure 10. Figure 10c is the spectrum for a TiO_2 single crystal standard spectrum, 10a is the TiH_x blank, and 10b is after 16 mC of oxidative charge; the latter is clearly dominated by TiO_2. The same conclusion can be drawn regarding the TiH_x powder surface (10d). Sputtering for 30 minutes removes the oxide entirely in these powder samples (10e), revealing only TiH_{x_o} structure. The native oxide thickness for the powder samples is about 20-30 Å, which is in reasonable agreement to that observed for TiH_x films and Ti metal electrodes.

As noted previously, there is no evidence of metallic titanium in the profiling and surface analysis data on the hydride samples. There is an 0.7 ± 0.1 eV positive shift, i.e., in the direction of oxidized metal (or more positive valence state). This shift would indicate a negative hydrogen site in the lattice or anionic hydrogen as seen in the electrochemical data.

The electrochemical (<2.0 V) and thermal aging behavior of TiH_x is reminiscent of the Ti electrode. With the electrochemical oxidation, a sharp onset of current occurs in the vicinity of 0.5 V versus SCE. The faradaic peak at 0.5 to 0.7 V is followed by nearly constant current densities of the 30-40 μA/cm^2 up to ~ 2 V. Charge and dc conductance versus applied potential shows the identical behavior seen for Ti film electrodes. The surface conductance indicates a depletion of conduction electrons as the oxide layer grows. The
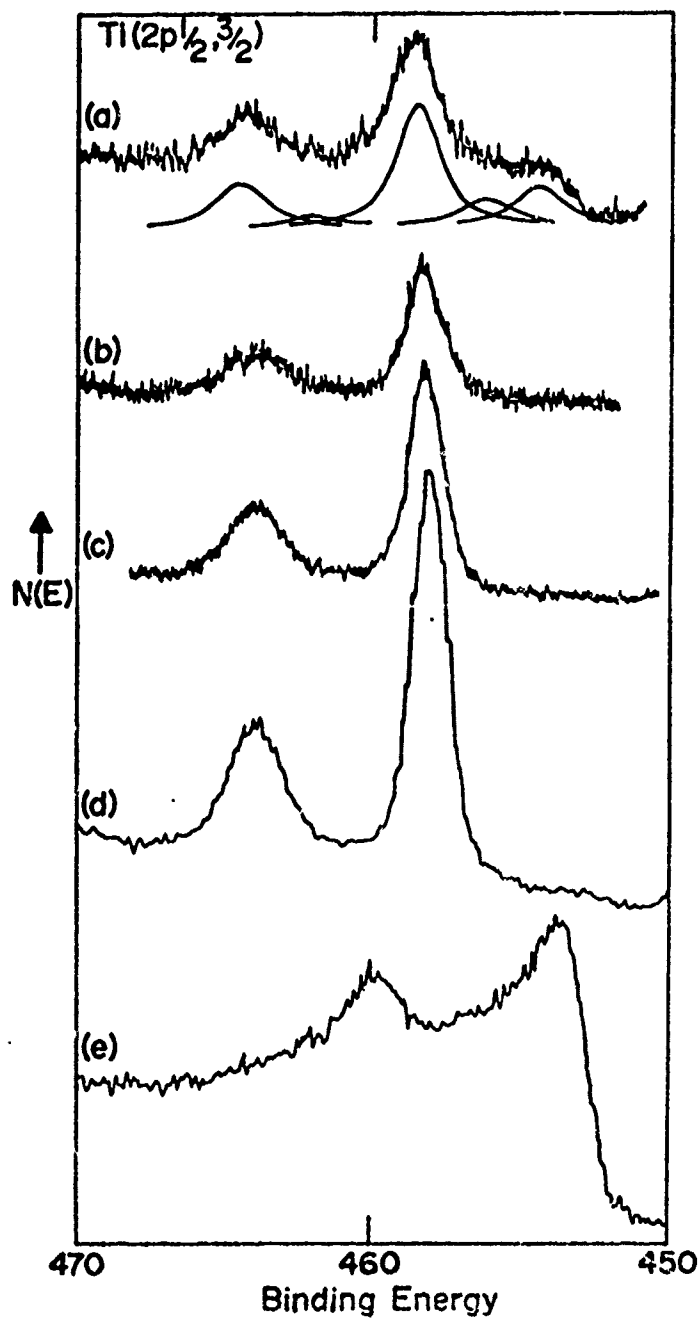
Figure 10

The Ti($2p_{1/2,3/2}$) XPS spectra for (a) a TiH_x blank surface, (b) a TiH_x thin film electrode oxidized to 12.5 mC of charge, (c) a TiO_2 standard, (d) a TiH_x powder used in pyrotechnic blends, and (e) that TiH_x powder after sputtering $\sim$1000 Å.

capacitance-voltage measurements showed the Mott-Schottky behavior typical of an n-type semiconductor once the potential is driven past the faradaic peak, i.e., ≥ 0.7 V. Again this behavior is indicative of a reduced oxide and not insulating TiO_2.

The previously reported experiments (1) and those discussed here allow a more detailed understanding of the surface region of vapor-deposited and clean bulk titanium and titanium hydrides. For example, the surface composition of the titanium films will be illustrated. We can picture the surface of the film to consist of a gradient of metal, suboxide (or TiO_2 with oxygen defects), and stoichiometric TiO_2. A graphical illustration of this picture is shown in Figure 11. The energy barrier for film oxidation is expressed chiefly across the stoichiometric TiO_2 phase (G_1), and the more conductive substoichiometric oxide phase (G_2). Following electrochemical or atmospheric oxidation, the oxide layer thickness is greatly increased, the suboxide concentration diminished, and the barrier to further oxide growth is consequently increased to G_T^1. The relative size of G_2^1 to G_1^1 has decreased due to the increase in thickness of the non-conductive oxide. Eventually, a metal/TiO_2 interface is established. Ionic transport across this interface becomes the current limiting factor and a normal corrosion/passivation mechanism is established.

Several conclusions can be drawn from the results of these studies:

i)   Electrochemical oxidation and air oxidation produce similar oxide coatings. The electrochemical process produces no extraneous results or products. There are no solvent effects on the electro-chemical or surface analytical results.

ii) The first 20-50 Å of Ti and TiH_x electrodes exposed to air or electrolyte solution are identical.

iii) The oxide on or near the surface would be mixed and not totally oxidized to TiO_2. A full range of oxides is observed from TiO to TiO_2. This observation is true for powder and bulk Ti and TiH_x, as well as films. At least eight intermediate oxides are known to exist in the region between Ti_2O_3 and TiO_2. Reduced or substoichiometric titanium oxides would be semiconducting, whereas purely stoichiometric TiO_2 would be insulating.

References

1.   N. R. Armstrong and R. K. Quinn, Surface Sci. 67, 451 (1977).

2.   D. M. Holloway and E. J. Fernandez, General Electric Co., Neutron Devices Department, St. Petersburg, FL.

3.   J. S. Solomon and W. L. Baun, Surface Sci. 51, 228 (1975).
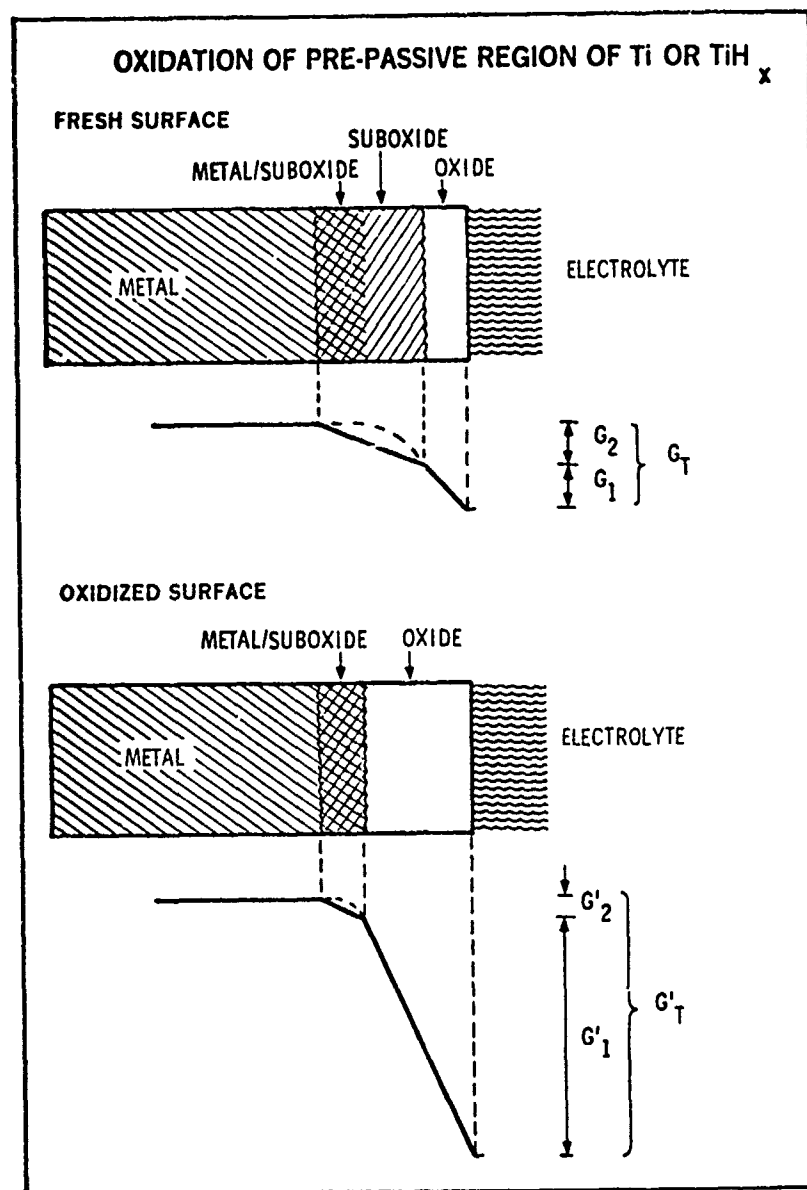
Figure 11

Proposed model for oxidation of the prepassive region in
Ti thin films. (The model also applies to TiH$_x$ samples.)
As the stoichiometric oxide thickness increases, higher
applied potentials are required to overcome the barrier
to current flow.

4.   A. W. C. Lin, N. R. Armstrong, and T. Kuwana, Anal. Chem. $\underline{49}$, 1228 (1977).

5.   P. G. Wahlbeck and P. W. Gilles, J. Am. Ceram. Soc. $\underline{49}$, 181 (1966).

CASTABLE GAS GENERANT COMPOSITIONS

by
R. Reed, Jr., B. Y. S. Lee,
R. A. Henry, and J. O. Smith
Naval Weapons Center
China Lake, California 93555

INTRODUCTION

Many gas generant propellants currently in use as power sources for missiles and as sources of gas for inflation devices have a number of serious deficiencies. Ballistic reproducibility and aging characteristics of these propellants are marginal and the production processes are tedious and costly in the case of pressed charge gas generants. Inflation devices require that non-corrosive, and in some cases, non-toxic gases be evolved at flame temperatures <1000°F and at wide ranges of flow rates. It has been difficult to attain compositions with low flame temperatures, especially if high burning rates are required.

Gas generant propellants which yield non-corrosive gases generally contain ammonium nitrate (AN), since this low cost oxidizer is unique in providing a number of advantageous properties. Compositions containing AN and suitable binders produce non-toxic gases substantially free of solids, and they generally achieve desirable ballistic properties. Gas generants containing AN are used as power sources for missiles, electrical generators, jet aircraft starters, and for a variety of other applications.

These AN-containing compositions have been manufactured by pressing or extrusion, since AN interferes with the curing of some solid rocket propellant binders. AN is hygroscopic and absorbs water if the relative humidity is above 50%. Moist AN, in view of its acidity, is incompatible with various binder curative combinations. Pressed gas generant propellants for use in tactical missiles have been processed using cellulose acetate (CA) binder, a process which does not require the polymerization of a binder. However, propellants containing this binder are troublesome to mix uniformly because of the high viscosity of the CA-plasticizer mixtures. During the difficult mixing, the AN crystals, which are relatively weak, are reduced in particle size, an effect which tends to raise the burning rates above allowable limits. Processing is also rendered difficult by the hygroscopic nature of AN. Gas generant propellants used for power sources in tactical missiles are subjected to wide temperature variations, a condition which causes the AN to undergo crystal phase transitions that produce volume changes in the AN, as shown in Table 1. As the grains are used in the field, they undergo heating and cooling and they pass through the transition temperature of

503

TABLE 1. Transition Points of AN in °C and
Volume Variations $\Delta V/V$ Occurring When
Transition Points are Crossed on Heating

°C	$\Delta V/V$
-18.0	-0.017
32.1	0.020
84.2	-0.0076
125.2	0.0135

32.1°C many times, and, as a result, they slowly expand. This effect can cause an increase in burning rate and pressure. Many compounds have been added to AN in an attempt to overcome this problem, but none have been successful, although some prevented the phase change of AN for a number of cycles before becoming ineffective.

In view of the difficulties involved in processing pressed and extruded AN-containing gas generant propellants, attempts have been made to use liquid curable binders and to process the propellants using methods commonly employed for solid rocket propellants. Dekker and Zimmerman (Ref. 1) used a styrene-methyl acrylate-containing binder to produce cast-cured compositions containing AN. Binders containing styrene tend to yield propellants with limited elongation, especially at low temperatures. The volatility of the styrene and methyl acrylate monomers causes them to be removed in processing. In this work, the monomers were condensed and returned during the mixing process, a somewhat involved procedure for manufacturing. These toxic unsaturated monomers are difficult to use in conventional solid propellant processing because they exhibit a pronounced exotherm and shrinkage on curing. Moreover, the polymerization is inhibited by a number of impurities.

A composition lending itself to processing and manufacturing by modern solid propellant techniques was devised by Vriesen (Ref. 2), who used a non-volatile liquid prepolymer, carboxyl-terminated (CT) poly-diethyleneglycol adipate cured with epoxides and aziridines, and two particle sizes of ground AN to facilitate processing. This binder is non-volatile, and has the small cure shrinkage and curing exotherm typical of modern solid propellants. Mechanical and ballistic properties of the propellants were adequate for use in tactical missile gas generators.

Low temperature (<1000°F flame temperature) gas generants present an especially difficult problem, since the usual binder oxidant combinations fail to sustain combustion when formulated with the low levels of

oxidizer required to yield flame temperatures below 1500°F. Combustion of these systems produces high residues and yields carbon monoxide, carbon dioxide, and water. These products tend to increase flame temperatures in view of their relatively high negative heats of formation.

Unusually reactive combinations of oxidizers and binders may sustain burning at sufficiently low oxidizer levels to allow sustained combustion. While non-corrosive gases are produced by using AN and nitrates, in general, this class of oxidizer tends to have a relatively low driving force to combustion and will not sustain combustion unless used at comparatively high levels. Chlorates and perchlorates, oxidizers which produce either residue or hydrogen chloride, can burn at low levels of oxidizer. Binders which are easily oxidized (such as polybutadiene and polysulfide) produce compositions capable of burning at low oxidizer levels when mixed with chlorates and perchlorates. However, these compositions produce corrosive and toxic exhausts unless suitable scavengers can be used which will react with sulfur dioxide and hydrogen chloride. Unfortunately, the use of scavengers leads to high residues and solids in the gases evolved.

Gas generant compositions used for inflation devices have not been reported which produce a solids-free gas that is non-toxic and non-corrosive at flame temperatures below 1000°F. New ingredients are required, such as high nitrogen derivatives, which can deflagrate in a process which produces nitrogen, and little or no oxides of hydrogen and carbon.

Some of the recent results of the Naval Weapons Center's work in the field of castable gas generant propellants are described in this report. This effort has addressed the problems cited above and, as a result, coated AN, AN substitutes, castable binder systems, and the effects of composition have been investigated to determine their effects on propellant performance.

DISCUSSION

This effort was directed toward the development of a technology base that would permit the formulation of castable gas generant compositions, processible by conventional solid propellant techniques, which can be tailored to achieve a wide range of properties such as flame temperature and burning rates. In order to accomplish these goals the following ingredient criteria were developed:

Binder properties
1. Hydrolytic stability
2. Non-reactive with AN and other oxidizers and deflagrating additives
3. Combustion products free of solids and corrosive gas
4. Good low temperature mechanical properties, preferably without use of plasticizer

5. Commercially available components
6. High hydrogen content to enhance gas yield and to minimize flame temperature
7. Energetic high nitrogen groups to enhance burn rate at low flame temperatures

Oxidizer properties
1. Compatibility with binders
2. Combustion products free of solids and corrosive gas
3. Particle shape and size to permit adequate processing characteristics
4. Absence of crystalline phase changes (or controllable)
5. Ballistic tailorability of burn rate, pressure exponent, and temperature coefficient
6. Commercially available or easily prepared from commercially available material
7. Non-hygroscopic (or controllable with coating)

Deflagrating additive properties
1. Rapid rate of deflagration
2. Contributes to low flame temperature
3. Combustion products free of solids and corrosive gas
4. Commercially available or easily prepared from commercially available materials

Those ingredients which were selected for this study are listed in Table 2.

TABLE 2. Ingredient Properties

Binders	ΔH_f^o, cal/g	Density, g/cm^3
Polydiethyleneglycol adipate (F17-47 Witco)	−1310	1.19
Dimer acid (Humko)	−500	1.00
Neopentylglycol azelate (NPGA Witco)	−1088	1.05
Dimer acid polyester (Emery)	−492	0.99
Tetrozole binder		
50% HHT (0.7 eq.), L-35 (0.3 eq.) 50% MET plasticizer	−390	1.136
Oxidizers		
Ammonium nitrate (AN)	−1090	1.73
Guanidine nitrate (GN)	−758	1.39
Ammonium 5-nitraminotetrazole (ANT)	+222	1.49
Guanyl azide nitrate (GAN)	+31.7	...
Deflagrating additives		
Bitetrazole	+1093	1.60
Diammonium bitetrazole	+342	...
Dihydrazinium 3,6-bis-(5-tetrazolyl) dihydrotetrazine	+647	1.653
Dinitrosopentamethylene tetramine	+269	1.51

The binders are critically important since they influence processibility, mechanical properties, and ballistic characteristics. In processing, they must allow the solids to be mixed and the slurry to be rendered free of air bubbles in a deaeration step. Several binders with a range of structure have been found to be adequate for AN propellants. A binder composed of a prepolymer having a molecular weight of 2000-3000, generally has the required rheological properties to allow mixing, but is sufficiently viscous to prevent the solids from settling prior to curing. Many prepolymers of polyesters, polyethers, and polybutadienes are found to meet these requirements. Prepolymers terminated in carboxyl (CT) or hydroxyl (HT) groups allow the formation of cured elastomers by the addition of epoxides and isocyanates as curatives. Polyesters composed of dicarboxylic acids such as adipic, azelic, and dimeric* are suitable when esterified with ethylene glycols, neopentylglycol, 1,6-hexane-diol, and similar diols. Polyesters are generally preferred over polyethers because they are able to retain plasticizers; CT polyethers are not generally available.

The composition of the binders has an effect upon the level of solids in gas, specific impulse (I_{sp}), and flame temperature. As the oxygen content of the binders (inert polymers) increases, the level of carbonaceous products in the exhaust of a propellant composition decreases. As the hydrogen content of the binder increases (oxygen content decreases), flame temperature tends to decrease; however, specific impulse increases due to the lower molecular weight of the exhaust gases, and to the more favorable heat of formation associated with binders containing fewer carbon oxygen bonds. These effects are qualitatively illustrated in Table 3. The influence of the binder on the calculated specific impulse of selected AN-containing propellants is shown in Table 4. For the power source application, a binder with a modest oxygen content, such as neopentylglcol azelate or dimer acid polyesters, may represent the best type of binder, considering this trade-off. Several binders having a range of oxygen content were found to be adequate for use with AN oxidizer in compositions having potential application as power sources.

TABLE 3. Effect of Oxygen Content of Inert Binder Upon Performance

Increasing hydrogen content of binder	I_{sp} ↑	Flame temperature ↓	Solids in exhaust ↑
Increasing oxygen content of binder	I_{sp} ↓	Flame temperature ↑	Solids in exhaust ↓

---

*Dimer acid is a mixture of 36-carbon dibasic acids composed of a variety of cyclohexenedicarboxylic acids which are formed by a Diels Alder dimerization of 18-carbon unsaturated aliphatic acids such as linoleic.

TABLE 4. Effect of Binder Upon Calculated Performance

Composition	Flame temperature chamber	Moles of gas (expanded) per 100 g of propellant	I_{sp} 1000 psi/14.68
CA/AN pressed grain	1901	4.38	187
F17-47/AN, 70% solids cast	1732	4.42	183
Dimer acid/AN 70% solids cast	1672	4.68	188
F17-47/AN, 75% solids cast	2020	4.52	189
Dimer acid/AN 75% solids	1755	4.75	192
Dimer acid/AN 80% solids	1823	4.82	195

A polyester binder, F17-47 (Table 2), was selected early in the program for 2000°F applications. This binder has adequate overall characteristics, allows formation of a clean exhaust, and contributes to the burning rate required for a specific power source application. However, its rheological properties (relatively high viscosity), when containing suspended solids, did not permit a solids loading of over 75% to be attained.

A propellant composition (70% solids) using the F17-47 binder was scaled-up to 25-gallon batches, and characterized (Table 5). Motors loaded with the propellant were temperature-cycled and fired successfully at ambient, -65, 20, and 165°F. A typical pressure-time trace is shown in Figure 1.

Polyneopentylglcol azelate, a binder containing less oxygen and more hydrogen, was used in several compositions containing AN. Mechanical properties in non-optimized compositions tended to be somewhat poorer than other binders (Table 6).

TABLE 5. Properties of Gas Generant Compositions, F17-47 Binder

Ingredients, wt%	Formulation number						
	586	589	590	593	594	595	599
Binder							
F17-47 (Witco)	25.77	26.02	26.02	26.02	26.02	26.02	21.96
ERL-0510 (Ciba Geigy)	4.16	3.91	3.91	3.91	3.91	3.91	2.97
Chromium Octoate	0.07	0.07	0.07	0.07	0.07	0.07	0.07
Oxidizer							
AN, -60/100, 0.5 MgO	68.0						
AN, -60/150, 0.5 MgO		68.00[a]	58.00	68.00[b]	63.00	48.00[c]	74.80
Guanidine nitrate, -24/60			10.00		5.00	20.00	
Additives							
Graphite	1.00	1.00	1.00	1.00	1.00	1.00	0.20
Sodium barbiturate	1.00	1.00	1.00	1.00	1.00	1.00	...
	100.00	100.00	100.00	100.00	100.00	100.00	100.00
Total solids, %	70	70	70	70	70	70	75
End of mix viscosity, KP	15	5	4	11	11	21	11
Properties							
Density, measured, g/cm^3		1.401		1.401		1.350	1.495
Burning rate, in/sec, 1000 psi	0.057	0.064	0.058	0.067	0.061	0.050	0.055
Pressure exponent, n	0.40	0.53	0.42	0.47	0.44	0.39	0.61
Mechanical properties							
σ_m, psi	...	100	...	55	39	164	136
ε_m, %	...	49	...	37	43	29	29
ε_r, %	...	60	...	39	47	31	31
E_o, psi	...	898	...	261	174	877	4407

[a] Contained 0.25% MgO coating.
[b] Contained 0.5% silane (DC 6020) coating.
[c] Contained 1.0% silane (DC 6020) coating.
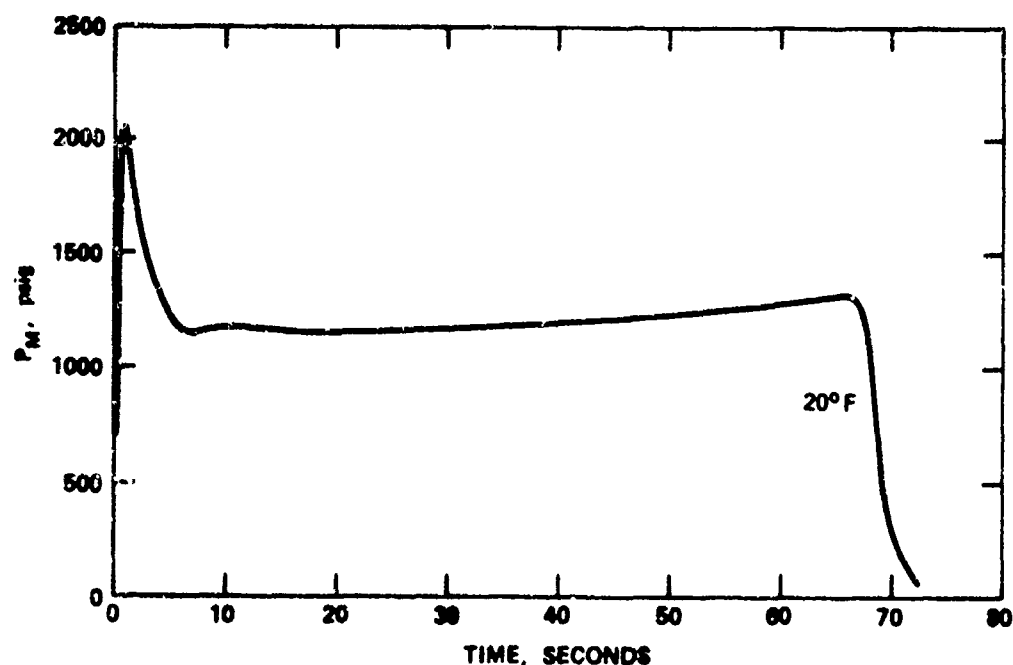
FIGURE 1. Motor Firing in Power Source Hardware
20°F, F17-47 Binder/AN (70% Solids).

TABLE 6. Properties of Gas Generant Propellants NPGA-Dimer Acid Polyesters

Ingredient, wt%	Formulation number				
	652	654	656	657	658
Binder					
Dimer acid 2178-152R (Emery)	20.94	...	13.96	...	...
Polyesters 2191-35R (Emery)	...	...	...	15.38	14.70
NPGA (Witco)	...	17.58	...	...	...
PCP-0300[a] (Union Carbide)	1.05	0.87	0.70	...	...
DDI-1410[b] (General Mills)	8.01	6.55	5.34	4.62	5.30
Triphenyl bismuth (added)	(0.05)	(0.05)	(0.05)	(0.05)	(0.05)
Oxidizer					
AN, -60/150, 0.5 MgO	68.00	73.00	78.00	78.00	73.00
Guanidine nitrate, -24/60	...	...	...	...	5.00
Additives					
Graphite	1.00	1.00	1.00	1.00	1.00
Sodium barbiturate	1.00	1.00	1.00	1.00	1.00
	100.00	100.00	100.00	100.00	100.00
Total solids, %	70	75	80	80	80
End-of-mix viscosity, KP	1.0	2.5	11.5	18.5	20
Properties					
Burning rate, in/sec, 1000 psi	...	...	0.039	0.036	0.033
Pressure exponent, n	...	...	...	0.41	0.46
σ_m, psi	81	40	103	97	98
ε_m, %	40	52	17	6	9
ε_r, %	73	107	29	12	21
E_o, psi	889	348	1750	2935	2080

[a] A polycaprolactone triol crosslinker.
[b] Dimeryl diisocyanate.

510

A binder with excellent processing properties was attained by using dimer acid cured with an epoxidized vegetable oil (Swift Epoxol 9-5). This binder was used to obtain a polymer that would be relatively insensitive to moisture or acid during processing or aging. Mechanical properties and humid aging (qualitative) were good, while burning rate was lower than compositons using F17-47 binder (see Table 7). In view of excellent processing properties, compositions containing 80% solids could be attained using this binder. At 80% solids these compositions have an I_{sp} which is 12 seconds higher than the 70% solids F17-47 containing propellant (Table 4). Five seconds of this gain is due to the higher hydrogen content and more favorable heat of formation of the binder, while the remaining 7 seconds is due to the higher solids level.

TABLE 7. Properties of Gas Generant Compositions Dimer Acid Binder

Ingredient, wt%	Formulation number				
	592	602	610	611	596
Binder					
Dimer acid (Humko)	17.91	12.34	16.76	17.76	17.91
EPOXOL 9-5 (Swift)	12.05	7.62			12.05
ERL-4289 (Ciba Geigy)			5.99	5.39	
Chromium octoate	0.04	0.04	0.07	0.07	0.04
Oxidizer					
AN, -60/150, 0.5 MgO	68.00	69.80			
AN, -60/150 1% Silane			37.2	18.9	
AN, -100, 1% Silane			24.8	44.1	
AN, -60/150 Uncoated					63.00
Guanidine nitrate -24/60		10.00	5.0	5.0	5.00
Additives					
Graphite	1.00	0.20	1.00	1.00	1.00
Sodium barbiturate	1.00		2.00	1.00	1.00
	100.00	100.00	100.00	100.00	100.00
Total solids, %	70	80	70	70	70
End of mix viscosity, KP	1	26	3	13	1
Properties					
Density, measured, g/cm^3	1.394	1.416	1.381	1.405	
Burning rate, in/sec, 1000 psia	0.036	0.043	0.035	0.036	0.032
Pressure exponent, n	0.62	0.57	0.53	0.63	0.83
σ_m, psi	...	223	125	113	128
ε_m, %	...	6	16	20	8
ε_r, %	...	11	30	31	17
E_o, psi	...	9131	1380	1050	2810

Another binder also rich in hydrogen and insensitive to water, poly 1,6-hexanediol dimerate (Emery) was also successful, and allowed AN oxidized compositions to be attained having burning rates equivalent to the dimer acid-Epoxol binder propellants. Processing properties of this binder were excellent, and an 80% solids loading was easily achieved (Table 6). Theoretical specific impulse of the 80% solids composition is similar to the dimer acid-Epoxol binder.

The polybutadiene binders are useful for propellants having low flame temperatures ($<1000°F$). They are easily oxidized and, therefore, have a tendency to burn at low oxidizer levels, a consequence of the high level of allylic hydrogen atoms (circled).

$$
\left[\begin{array}{ccc}
\text{ⓗ} & \text{H} & \text{H} \quad \text{ⓗ} \\
| & | & | \quad | \\
C - C & = & C - C \\
| & & | \\
\text{ⓗ} & & \text{ⓗ}
\end{array}\right]_n
$$
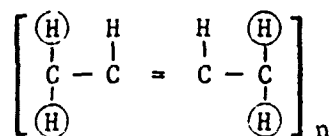
These carbon-hydrogen linkages are easily broken by oxidizing agents, reactions which have low energies of activation.

These unsaturated binders are, therefore, attractive in formulations which must have minimum flame temperatures. Carboxyl-terminated polymers are preferred, since they burn more rapidly and at lower levels of oxidizer than the corresponding hydroxyl terminated (HT) polymers. The latter are cured to form urethanes, a group with known flame inhibiting characteristics. Moreover, propellants containing HT polymers form a liquid melt phase, unlike the CT polymers. Propellants having binders which form a liquid phase in combustion tend to be extinguished more readily than those which remain solid. Unfortunately, polybutadiene binders tend to form a high residue and an exhaust with a higher content of particulates than any other binder class.

Tetrazoles should also be particularly useful as binders for gas generants with low flame temperatures since decomposition of this group yields mainly nitrogen, rather than the exothermic compounds CO, CO_2, and H_2O. The decomposition of the tetrazole moieties in the polymer backbone of the binder should facilitate combustion of low levels of oxidizer. A tetrazole diol was synthesized and used as a constituent of a polyurethane binder. The starting material, 5-(2-hydroxyethyl) tetrazole (Ref. 3 and 4), was converted to the mixed 1- and 2-(2-hydroxyethyl)-5-(2-hydroxyethyl)tetrazoles (HHT) via the following reactions:

Mixed 1- and 2-(2-Hydroxyethyl)-5-(2-Hydroxyethyl)tetrazoles
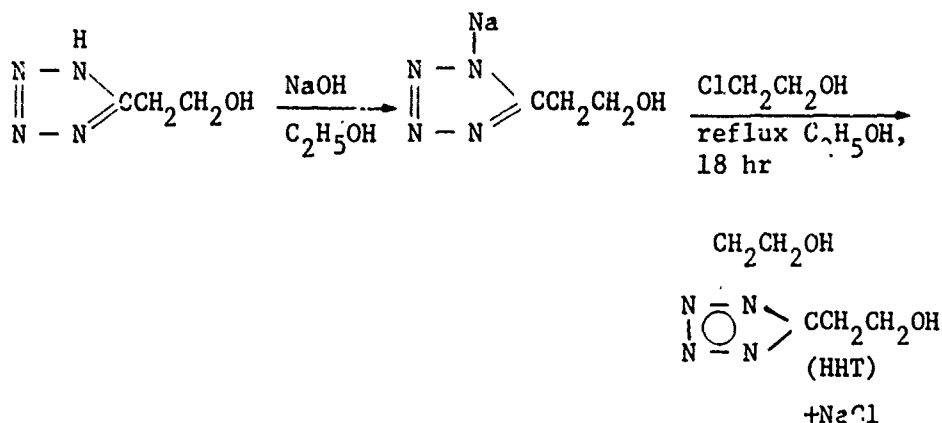
The product, HHT, was a clear, colorless, viscous liquid suitable as a binder. A polyurethane formed by reaction of HHT with a diisocyanate (methyl 2,6-diisocyanotohexaneoate, LDIM,)* produced a clear hard resin. A polyether diol (L-35)** was added to HHT and a soft flexible polymer was obtained. A tetrazole plasticizer, 1-methyl-5-(2-methoxyethyl)tetrazole (MET) (Ref. 5), was added to the binder to increase the tetrazole level. This mixture produced soft elastomeric polyurethane gum stocks suitable as a propellant binder.

Another tetrazole diol, bis-2-[1 and 2-(2-hydroxyethyl)-5-tetrazolyl] ethyl ether (HTE) was prepared by the sequence of reactions shown below. The preparation of another tetrazole (MTE) also useful as a plasticizer, is shown.
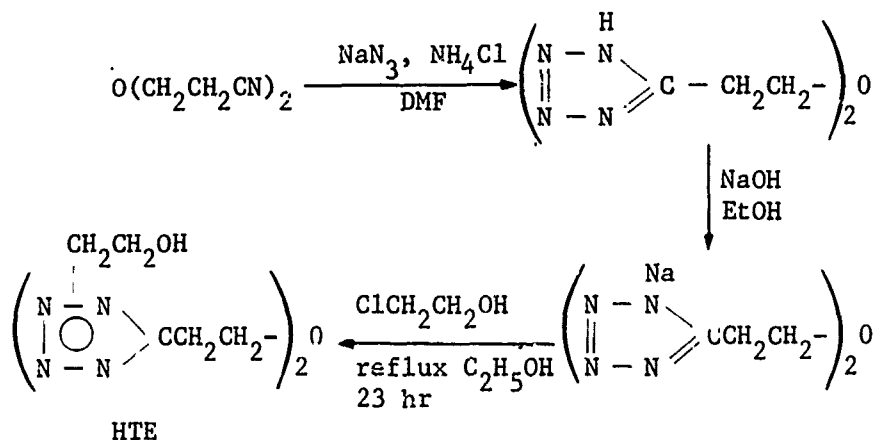
HTE

$$
\begin{array}{c|c}
\text{H}_2\text{O} & (\text{CH}_3\text{O})_2\text{SO}_2 \\
\text{35--40°C, 1 hr} & \text{NaHCO}_3,\ \text{Na}_2\text{CO}_3 \\
\text{Reflux, 5 hr} & \downarrow
\end{array}
$$

$$
\left(
\begin{array}{c}
\text{CH}_3 \\
\underset{\text{N}-\text{N}}{\overset{\text{N}-\text{N}}{\mid\bigcirc\mid}} > \text{C} - \text{CH}_2\text{CH}_2 -
\end{array}
\right)_2 \text{O}
$$

(MTE)
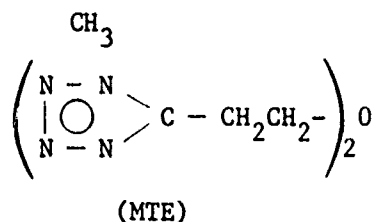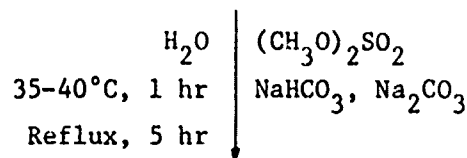
Polyurethane polymer derived from HTE and LDIM, formed readily, and while not as hard as that from the first tetrazole diol (HHT), was sufficiently firm to require the addition of the L-35 polyether diol. Gum stocks with or without plasticizer were adequate in physical properties for use as propellant binders.

Oxidizers studied included AN and guanidine nitrate (GN), compounds which were used in several binders. AN was found to retard the cure of some binder systems even when it was vigorously dried; slightly moist AN gave incomplete cures and gassing with some polyurethane binders. The AN was coated with MgO and an amine silane (fiber glass coupling agent), treatments which rendered the AN compatible with all binders examined.

Addition of MgO to AN causes an immediate evolution of ammonia as a coating of magnesium nitrate is presumably formed. Ammonium nitrate coated with 0.25-0.50% MgO was found to be compatible with the several epoxy- and isocyanate-cured binders which were used, including those which did not cure completely in the presence of uncoated AN. The details of the coating procedure are given in the Experimental section.

Amine silanes such as DC 6020 (Dow Corning), were also used to coat AN (suspended in a Freon or methylene chloride). Under these conditions, the amine silanes react rapidly with AN to produce ammonia and presumably the nitrate salt of the amine silane triol.

$$\text{H}_2\text{NCH}_2\text{CH}_2\text{NHCH}_2\text{CH}_2\text{CH}_2\text{Si(OCH}_3)_3 + \text{NH}_4\text{NO}_3 + 3/2\ \text{H}_2\text{O} \text{ (surface moisture)}$$

(DC 6020) (AN)

$$\text{NH}_3\uparrow + \left[\text{H}_2\text{NCH}_2\text{CH}_2\text{NH}_2\text{CH}_2\text{CH}_2\text{CH}_2\text{Si(OH)}_3\right]^+ \text{NO}_3^- + 3\text{CH}_3\text{OH}$$

$$\downarrow\ -3/2\ \text{H}_2\text{O}$$

$$
\text{H}_2\text{NCH}_2\text{CH}_2\text{NH}_2\text{CH}_2\text{CH}_2\text{CH}_2\overset{\displaystyle \text{O}}{\underset{\displaystyle \text{O}}{\text{Si}}} - \text{O} -
$$

(Siloxane polymer)

The silane triol rapidly loses water to form the crosslinked siloxane polymer. This treatment forms a chemically attached polymeric coating of AN, with pendant reactive amine groups which are able to react with epoxides or isocyanates used to cure the binders. A chemical linkage of the coating with the binder is established by reacting the NH_2 of the silane-coated AN, with a trifunctional epoxy such as ERL-0510*, a common curative.

Two oxidizers high in nitrogen, the ammonium salt of 5-nitramino-tetrazole (ANT)(Ref. 6) and guanyl azide nitrate (GAN)(Ref. 7), were selected as promising candidates.

ANT

GAN

Unlike AN, the high nitrogen oxidizers ANT and GAN do not appear to undergo phase changes and are not particularly hygroscopic. Both ANT and GAN have less oxidizing ability than AN, a factor which may be beneficial in reducing flame temperature. As less CO, CO_2, and H_2O

---

*Dow Corning 6020.

are produced by oxidation, the flame temperature of a propellant formulation is reduced. This effect of flame temperature reduction is somewhat offset by the positive heats of formation of these high-nitrogen compounds (Table 2).

Compositions containing these oxidizers were prepared using epoxy and polyurethane binders and they were found to produce elastomeric propellants which were capable of burning at oxidizer levels of 20-30%. Both oxidizers tend to impart a higher burning rate to compositions than does AN.

Deflagrating additives, compounds which decompose vigorously but which are not oxidizing agents, were used to sustain combustion in low flame temperature compositions which had difficulty in burning because of the low levels of oxidizer (demanded by the need for low flame temperature). Additives used included bitetrazole, bitetrazole salts, dihydrazinium-3,6-bis(5-tetrazolyl) 1,2-dihydrotetrazine, and dinitrosopentamethylene-tetramine.* Oxamide was used as a coolant in compositions.

Graphite was used as an opacifier and sodium barbiturate was added to stabilize combustion and to lower the burning rate pressure exponent, materials which are used in conventional pressed gas generator propellants.

EXPERIMENTAL

Compositions containing the ingredients discussed above were mixed and cured in conventional solid rocket propellant processing equipment. A one-pint vertical Baker Perkins mixer was used and the mixes (nominally 300 g) were made under reduced pressure so that void-free castings could be attained. In some cases, mixes of 50 g or less were made by hand. The mechanical properties and limited ballistic data were determined.

A family of gas generant compositions containing AN received the most attention in this study. Several carboxyl-epoxy and diol-diisocyanate binders were found to contribute to adequate processing, mechanical properties, and ballistics. The CT polydiethylene glycol adipate cured with the multifunctional ERL-0510 (Ciba Giegy) epoxy, and catalyzed with chromium octoate, was used in a variety of compositions; typical data are presented in Table 5. Ammonium nitrate coated with MgO and silane DC 6020 was used at various particle sizes. When an optimized particle size distribution was used, a composition containing 70% solids was processible, but 75% solids was found to be marginal in processibility. Carboxyl-terminated binders tend to be more difficult to deaerate and have poorer rheological properties than the corresponding HT prepolymers, a factor which requires higher mixing temperatures.

---

*Available from the I.E. DuPont Company as Unicel 100.

Mechanical properties of these compositions (formulations 589, 599, and 593) were generally adequate for application in existing power sources. The silane coating (1%) on the AN increased tensile strength but did not have much effect on elongation.

The burning rates were tailored by varying AN particle size, guanidine nitrate level, and solids content. Burning rate was increased by decreasing the particle size of AN (compare formulations 586 and 589). Guanidine nitrate decreased burning rate (compare 589 with 590).

Motor firings with formulation 589 were successful (even after temperature shock cycling from -65 to +165°F) and gave a burning rate of 0.064 in/sec (1000 psi) with an n of 0.55; firings at -65, 20, and 165°F were also successful. A typical pressure time trace is shown in Figure 1.

A typical cellulose acetate-AN pressed composition has a nominal burning rate of 0.055 to 0.064 in/sec with an n of 0.57. Gases from the CA propellant contained a higher solids content than those of the F17-47 propellants.

Dimer acid/AN compositions had a lower burning rate (Table 7) and a higher n than corresponding formulations containing F17-47 binder. Mechanical properties, while not optimized, tended to be poorer than those of the F17-47 propellants unless the cyclohexene oxide epoxy, ERL-4289, was used.

Dimer acid polyester/AN propellants were difficult to burn in the strand bomb unless the solids level was 80%. Burning rates tended to be somewhat lower than corresponding formulations containing dimer acid binder. Dimer acid polyester 2178-152R had a functionality approaching 2.0 and required a crosslinker such as the polycaprolactone triol (PCP-0300) while the dimer acid ester 2191-35R had a functionality of 2.3, a value which generally does not require a crosslinker. The low values of elongation attained with the latter polyester would seem to indicate that the diol crosslinker combination is preferred.

The procedure for the MgO coating of AN is as follows:

1. Ingredients: AN, technical, MIL-A-175A; MgO ("Maglite-D", Merck and Company).

2. Procedure: (a) AN is fed into Mikropulverizer fitted with 1/8-inch herringbone screens (feed rate has little effect on oxidizer particle size); (b) magnesium oxide (0.5%) is fed in during the AN addition; and (c) the AN is collected and stored with desiccant.

SUMMARY

The current status of AN gas generant propellants has been reviewed and the problem areas identified. A castable propellant would overcome important deficiencies in processing and ballistics reproducibility. A propellant of this type has been achieved using AN and epoxy and poly-urethane liquid curable elastomeric binders. A 70% solids composition containing a polydiethyleneglycol adipate binder, AN, graphite and sodium barbiturate was characterized and successfully demonstrated by hot and cold motor firings in power source hardware. Other binders were developed for use with AN at 80% solids levels which contribute to improved specific impulse and are moisture insensitive in curing and aging. Processes were devised for coating AN to eliminate its incompatibility with certain binders.

Compounds high in nitrogen were synthesized which may be useful in gas generant propellants having flame temperatures below 1000°F. Two tetrazole diols were prepared and used to formulate a tetrazole containing polyurethane binder. Tetrazole content was increased by the use of a tetrazole platicizer. Two oxidizers high in nitrogen were employed which may be able to replace AN in some gas generant propellants. Deflagrating additives containing tetrazole moieties were used to increase driving force to combustion at low oxidizer levels. These compositions are not yet fully characterized.

REFERENCES

1. A. O. Dekker and G. A. Zimmerman. "Ammonium Nitrate Propellants Based on a Polyester-Acrylate Binder," *Industrial and Engineering Chemistry*, Vol. 1, No. 1 (1962), pg. 23.

2. C. W. Vriesen. "Carboxyl-Terminated Linear Polyester Gas-Generating Compositions and Method of Preparation," U.S. Patent 3,177,101.

3. W. G. Finnegan, R. A. Henry, and S. Skolnik. "Polymers of Substituted Tetrazoles," U.S. Patent 3,004,959.

4. W. G. Finnegan, R. A. Henry, and R. Lofquist. "An Improved Synthesis of 5-Substituted Tetrazoles," *J. Amer. Chem. Soc.*, Vol. 80 (1958), Pg. 3908.

5. W. G. Finnegan and S. R. Smith. "1-Methyl-5-(2-Methoxyethyl)-Tetrazole—A Stationary Phase for Gas-Liquid Partition Chromatography," *J. Chromatography*, Vol. 5 (1961), pg. 461.

6. W. M. Ayres and R. A. Henry. "Gas Generator Composition Containing a Nitrogen Rich Compound and a Catalyst," U.S. Patent, 3,677,841.

7. von K. A. Hoffman, H. Hoch, and H. Kirnireuther. "The Effect of Nitrous Acid on Aminoguanidine and Semicarbazide," *Ann.*, Vol. 380 (1911), pg. 135.

EVALUATION OF A HOT WIRE SENSITIVE ALUMINUM/POTASSIUM

PERCHLORATE PYROTECHNIC

Charles Rittenhouse
R. D. Smith
Unidynamics/Phoenix, Inc.
Phoenix, Arizona

ABSTRACT

A hot wire sensitive pyrotechnic has been prepared using aluminum powder
and potassium perchlorate. This composition has been evaluated to determine
its thermochemical and sensitivity/stability characteristics and to establish
its properties as a bridgewire ignition material in small electroexplosive
devices (EED's). The mixture has demonstrated insensitivity to a spark dis-
charge typical of that which can be generated by a human body. However, it
ignites consistently from a hot wire, yielding high thermal output and high
resistance-after-fire (RAF).

INTRODUCTION

Many EED's contain a sensitive primary explosive such as lead styphnate on the bridgewire. Firing currents for units of this type are typically low, and all-fire reliabilities are high. However, most primary explosives are sensitive to extraneous ignition stimuli, especially electrostatic discharge (ESD). One potential source of ESD effects is the human body. For this reason, primary explosives are hazardous to handle, both in bulk powder form and when loaded into sealed units.

Devices containing a primary explosive on the bridgewire can be protected from the effects of ESD by addition of a spark ring or other mechanical means. However, a more direct solution to this problem is to use a bridgewire ignition material which is inherently insensitive to the most energetic spark discharge which the human body can generate. Under guidelines accepted by D.O.E., this effect can be simulated by the arc from a 600-pf capacitor charged to 20 kV and discharged through a 500-ohm series resistor. Development of improved hot wire sensitive ignition materials capable of withstanding arc discharges of this magnitude is a continuing objective of Unidynamics' Pyro-Explosive Department. Other properties sought in ESD-insensitive ignition materials include reliable all-fire and no-fire characteristics from small diameter bridgewires typical of those used in miniature EED's and high resistance-after-fire.

Unidynamics has recently investigated a two-component pyrotechnic which appears very promising for use as a bridgewire ignition material in certain types of EED's. This composition, which consists of a mixture of aluminum and potassium perchlorate, has been evaluated to determine its basic output parameters, handling safety, and bridgewire sensitivity characteristics in two EED's. This paper summarizes the results of these investigations.

POWDER BLENDING

The pyrotechnic evaluated by Unidynamics consisted of a mixture of aluminum and potassium perchlorate. The reaction of this material can be described by the following general equation:

$$8Al + 3KClO_4 \rightarrow 4Al_2O_3 + 3KCl$$
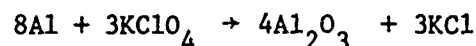
The composition was blended by screening the ingredients together, slurrying the mixture with a liquid vehicle, drying the slurry and granulating the product by screening through a coarse sieve. This technique yielded a mixture which appeared very homogenous when examined microscopically.

MATERIAL CHARACTERIZATION

Material characterization tests performed on aluminum/potassium perchlorate are described below.

Calorific Output. This test was performed using a Parr Model 1221 Oxygen Bomb Calorimeter with an adiabatic water jacket. Samples were burned under 25 atmospheres of argon. Calorific output was as follows:

Test No. 1	-	2144
Test No. 2	-	<u>2146</u>
Average	-	2145 cal/gm

Gas Evolution. This value was determined using a modified Parr Oxygen Calorimeter Bomb fitted with a pressure gauge. This fixture was designed specifically to measure the gas evolved by "gasless" pyrotechnics and has been calibrated to relate final system pressure directly to total gas volume under STP conditions. Samples were burned under one atmosphere of argon. After each test, the bomb and fittings were cooled to ambient room temperature before recording final system pressure. Gas evolution values corrected to STP conditions were as follows:

Test No. 1	-	20.0
Test No. 2	-	<u>19.3</u>
Average	-	19.7 ml/gm

Differential Thermal Analysis/Autoignition Temperature. Differential thermal analysis was performed using a DuPont 990 Thermal Analyzer with a 1200°C head. Responses obtained at heating rates of 20°C/min and 50°C/min are shown in Figure 1.

The first event is the endotherm resulting from the rhombic-cubic crystal transition of potassium perchlorate at 300°C. As the temperature is increased, very little activity is apparent at either heating rate until autoignition occurs in both samples at ≈6'/0°C. It should be noted that the autoignition exotherm of the sample heated at 20°C/min was significantly smaller than that of the sample heated at 50°C/min. This can be attributed to partial deactivation of the slow-rate sample through thermal decomposition of the potassium perchlorate and/or pre-ignition reactions between the constituents. A slow heating rate would accelerate any reactions of this type due to the longer exposure time at elevated temperature. It is also of interest to note that the slow-rate sample contained residual aluminum in the combustion products, as shown by the melting point endotherm occurring at ≈660°C. As the temperature of the combustion residue is increased, the melting point endotherm of potassium chloride can be seen in both samples at ≈770°C. This event appears to be followed almost immediately by a small exotherm in the slow-rate sample, indicating the possibility of a reaction between the molten aluminum and potassium chloride. No comparable exotherm is apparent in the trace for the high-rate sample.

Impact Sensitivity. This test was performed using a modified Bureau of Mines impact sensitivity tester with a 2-kg drop weight. Ten nominal 20-mg samples of unconfined powder were placed in a hardened steel anvil/plunger assembly and subjected to drop heights of 100 cm. None of these samples ignited or responded in any way to the impact stimulus.

Electrical Conductivity. This property was determined using unbridged four-pin deep-well headers as test vehicles. Initially, five headers were checked to determine insulation resistance between two pins in the normal bridge circuit (2.41-mm). Under an applied voltage of 500 volts DC, resistance values of 4×10^{10} ohms or greater were obtained. The five units were then loaded with nominal 100-mg powder charges consolidated at 103 MPa and confined by closure pads of compressed diatomaceous earth. Average charge density was ≈1.8 gm/cm³.

Three loaded units were tested to determine breakdown voltage across the 2.41-mm path of the normal bridge circuit. Application of 50 volts DC did not cause breakdown. However, all three units became conductive when subjected to 100 volts DC, yielding resistance values ranging from 6×10^2 to 4×10^3 ohms. One unit was then tested to determine breakdown voltage across the 3.40-mm path between two diagonally spaced pins. Again, breakdown occurred at 100 volts DC, yielding a resistance of 1.7×10^4 ohms. A final unit was tested to determine breakdown voltage in the pin-to-case mode (1.96 mm). In this unit, breakdown occurred at 50 volts DC. Resistance after breakdown was 3.5×10^3 ohms.

These tests indicate that aluminum/potassium perchlorate consolidated to a density of ≈1.8 gm/cm³ becomes electrically conductive when subjected to applied voltages of ≈25 volts DC/mm of circuit path. This characteristic may be related to the apparent resistance of the material to the effects of electrostatic discharge, as described in the next section.

RUN NO. ___ DATE ___	T-AXIS	DTA-DSC	TGA	TMA
OPERATOR ___	SCALE, mv/in __0.8__	SCALE, °C/in ___	SCALE, mg/in ___	SCALE, mils/in ___
SAMPLE:	PROG. RATE, °C/min ___	(mcal/sec)/in ___	SUPPRESSION, mg ___	MODE ___
	HEAT ___ COOL ___ ISO ___	WEIGHT, mg ___	WEIGHT, mg ___	SAMPLE SIZE ___
ATM ___	SHIFT, in __0__	REFERENCE ___	TIME CONST., sec ___	LOAD, g ___
FLOW RATE ___			dY, (mg/min)/in ___	dY, (10X), (mils/min)/in ___

Run #3 50°C/Min

Run #1 20°C/Min

FIGURE 1

DTA TRACES FOR Al/KClO₄

TEMPERATURE, °C (Pt/Pt - 13%Rh)

MEASURED VARIABLE

DUPONT Instruments

523

ELECTROSTATIC SENSITIVITY

The electrostatic sensitivity (ESD) characteristics of aluminum/potassium perchlorate were determined both in the unconfined state and with the material consolidated into unbridged two-pin test units with closure pads of compressed diatomaceous earth.

ESD testing of unconfined samples was performed using a fixture consisting of a flat aluminum plate as the lower electrode and a variable-height pointed copper rod as the upper electrode. The design of this fixture is shown in Figure 2. Each sample was spread on the base plate and the copper electrode was lowered to a position where an arc discharge could just be obtained. The sample was then subjected to the arc from a 600-pf capacitor charged to a selected voltage and then discharged through a 500-ohm series resistor. As mentioned previously, these capacitance/resistance conditions are accepted by D.O.E. as typical of those which can exist in the human body. Voltage levels from 10 kV to 25 kV were evaluated with the following results:

Charge Voltage (kV)	Number of Fires	Number of No-Fires
10	0	10
15	0	10
20	0	10
25	0	10

Although all powder samples were scattered by the arc discharge, no evidence of ignition or sparking could be detected in any test.

Electrostatic sensitivity testing of confined samples was conducted using unbridged two-pin headers assembled with stainless steel sleeves to form charge cavities. The design of the test vehicle is shown in Figure 3. Each unit was loaded with a nominal 50-mg powder charge consolidated at 103 MPa and confined by a closure pad of compressed diatomaceous earth. Average column height was 1.02 mm and average charge density was ≈ 2.1 gm/cm^3. Eight units were subjected to electrostatic discharges in the pin-to-case mode across a distance of 1.06 mm. Each unit was secured in a holding fixture and subjected to two or more discharges from a 600-pf capacitor charged to a selected voltage and discharged through a 500-ohm series resistor. Only two discharges could be applied across fresh powder columns in each unit. However, two units were subjected to a series of 10 pulses to determine the effects of repeated discharges across a previously disturbed powder column. Voltage levels from 1.5 kV to 28 kV were evaluated with the following results:

Unit No.	Charge Voltage (kV)	Number of Fires	Number of No-Fires
1a	1.5	0	1
1b	1.5	0	1
1b (retest)	10.0	0	1
2a	20.0	0	1
2b	20.0	0	1
2b (retest)	20.0	0	10
3a	25.0	0	1
3b	25.0	0	1
3b (retest)	25.0	0	10
4a	28.0	0	1
4b	28.0	0	1
5a	25.0	0	1
5b	25 0	0	1
6a	25.0	0	1
6b	25.0	0	1
7a	17.0	0	1
7b	20.0	0	1
8a	6.0	0	1
8b	8.0	0	1

These tests indicate that aluminum/potassium perchlorate, both as a loose powder and confined, is insensitive to the arc from a 600-pf capacitor charged to either 20 kV or 25 kV and discharged through a 500-ohm series resistor. The energy of the arc generated under these conditions equals or exceeds that which can be produced by a human body, based on accepted D.O.E. standards.

It can be concluded that aluminum/potassium perchlorate offers a significant degree of handling safety in the area of electrostatic sensitivity. This does not mean that the mixture is completely safe against ignition by inadvertent electrostatic discharge under all conditions. However, it does mean that the composition might not ignite in certain situations where some other bridgewire-sensitive pyrotechnics now in use would ignite.

DIELECTRIC MATERIAL

UPPER ELECTRODE (COPPER)

LOWER ELECTRODE
(ALUMINUM)

TO HIGH VOLTAGE
PULSE GENERATOR
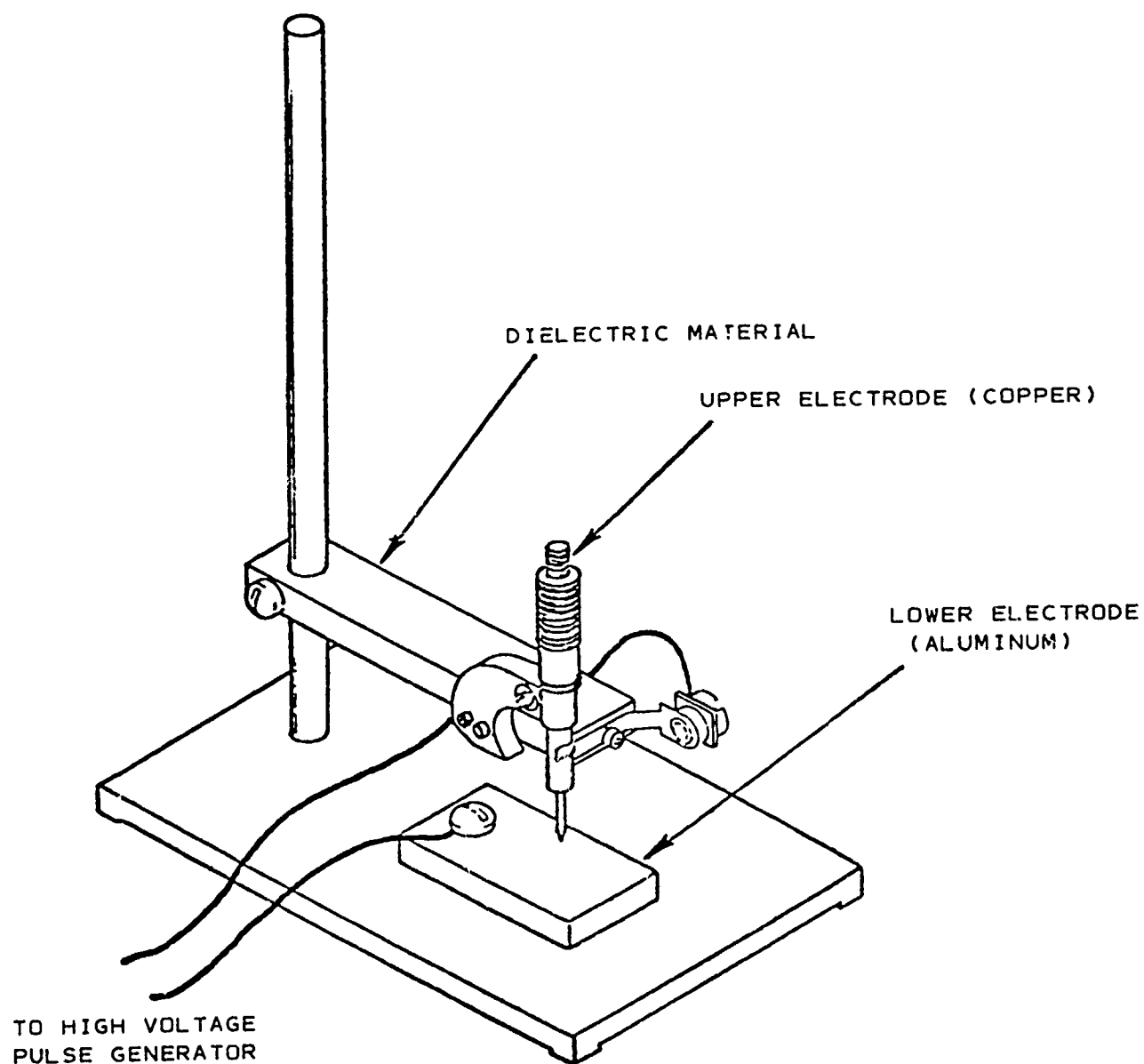
FIGURE 2
ESD TEST FIXTURE FOR POWDER SAMPLES

CLEAR PLASTIC TOP
(FOR RETAINING
STANDOFF OIL)
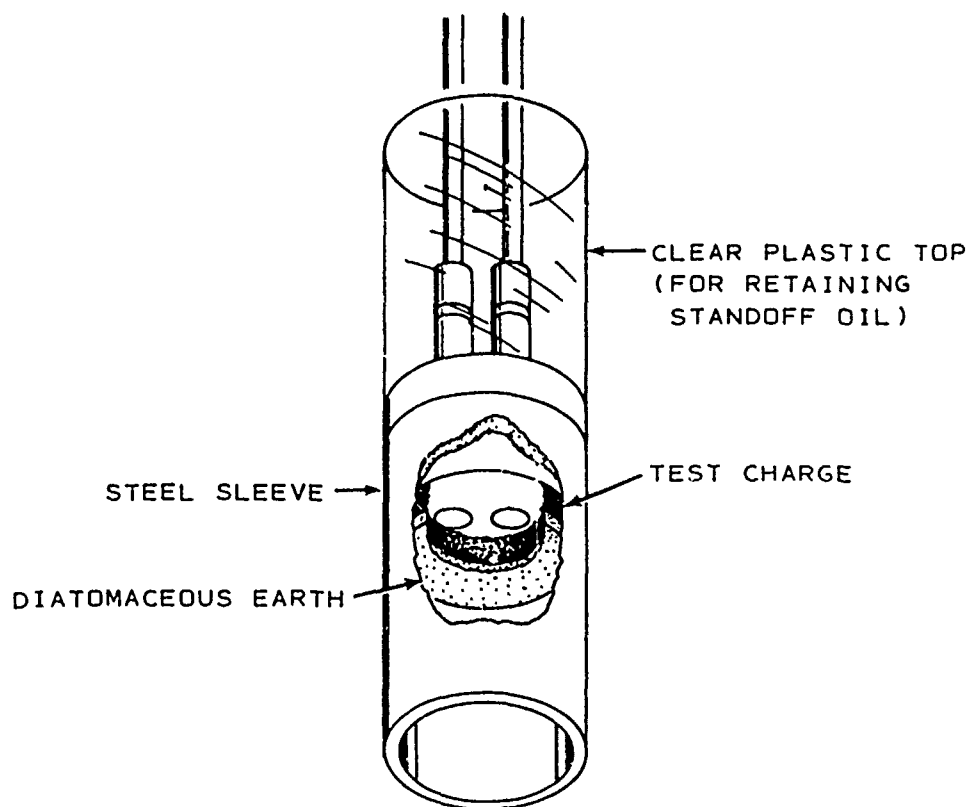
STEEL SLEEVE

TEST CHARGE

DIATOMACEOUS EARTH

FIGURE 3

ESD TEST UNIT FOR CONFINED SAMPLES

527

BRIDGEWIRE SENSITIVITY IN A MINIATURE IGNITER

Initial bridgewire sensitivity testing was conducted using the miniature igniter[1] shown in Figure 4. Units were bridged with annealed Tophet A wire which had a diameter of 30.5 microns and a nominal resistivity of 1480 ohms/meter. Initial bridge resistances were checked to determine that they all fell within the tolerance limits of 0.900 to 1.027 ohms. Using a consolidation pressure of 103 MPa, each bridged header was loaded with 10 $\pm$ 1 mg of aluminum/potassium perchlorate. A Kapton closure disk was then bonded in place with a thin layer of DC 3140 silicone sealant air-cured for 24 hours. Final bridge resistances were checked to assure that they were all within the required range of 1.0 $\pm$ 0.1 ohm. Average charge density in these units was ≈1.9 gm/cm^3. The units were divided into three groups and used to conduct the tests described below.

High Current All-Fire Bruceton Test. A group of 29 miniature igniters was used to conduct a high current all-fire Bruceton test. This test was performed at -54°C using a UN-334-E high current pulse generator, which produces a constant current pulse of 2.5 microseconds duration. The nominal energy of the pulse is controlled by varying the input voltage to the tester. Voltage and amperage levels are monitored during each test, and the energy applied to the bridgewire is computed by integrating the areas under these traces. Average voltage and current levels used in testing the miniature igniters were ≈50 volts and ≈50 amperes, respectively. Energy levels used during this test ranged from 5.10 mJ to 6.97 mJ.

When the Bruceton data were analyzed by the ASENT program, the high current mean firing energy of the 29-unit sample was found to be 5.69 mJ, with a standard deviation of 0.21 mJ. The high current all-fire energy (99.9 percent positive response at a 97.5 percent confidence level) was 6.82 mJ.

Low Current No-Fire Bruceton Test. A group of 34 miniature igniters was used to conduct a low current no-fire Bruceton test. This test was performed at 71°C using a UN-333-E low current pulse generator. Each unit was subjected to a constant current pulse of five minutes maximum duration and with a 200 microsecond maximum rise time. Current levels ranging from 1.26 amperes to 1.46 amperes were required to bracket ignition of the units.

When the Bruceton data were analyzed by the ASENT program, the low current mean firing current of the 34-unit sample was found to 1.40 amperes, with a standard deviation of 0.05 ampere. The low current no-fire current (0.1 percent positive response at 97.5 percent confidence level) was 1.15 amperes.

Low Current Resistance-After-Fire Test. A group of 20 miniature igniters was used to conduct a low current resistance-after-fire (RAF) test. This test was performed at ambient room temperature using a UN-333-E low current pulse generator. Each unit was subjected to a 3.5 ampere current at

15 volts DC and of 200 ms duration. All units ignited within ≈1 ms or less. Circuit resistance was monitored during the full 200 ms of current application. Test data were analyzed by a Computer Controlled Data System, and a resistance/time trace was obtained for each unit. A representative RAF trace is shown in Figure 5.

The resistance-after-fire of aluminum/potassium perchlorate in the miniature igniter was consistently high. In all cases, minimum resistance occurred within the first 20 ms after ignition and generally exceeded 50 ohms. Resistance rose very rapidly after 20 ms, reaching levels near or above 500 ohms in most units.

FIGURE 4

MINIATURE IGNITER

Labels on figure:
- ALUMINUM/POTASSIUM PERCHLORATE (10 MG)
- TOPHET A (30.5 μm DIA.) BRIDGE (1 OHM)
- POLYIMIDE DISK
- DC3140 SILASTIC
- KOVAR
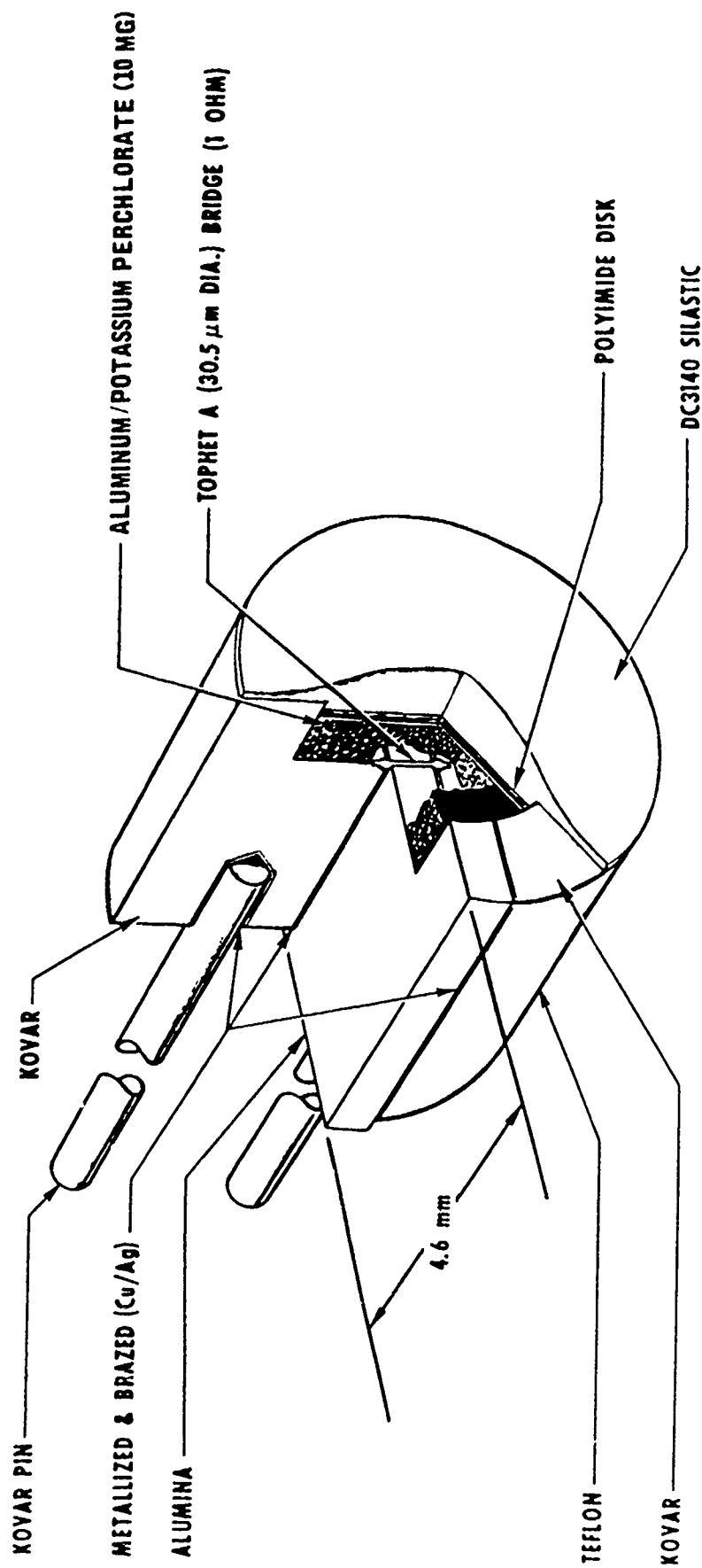- KOVAR PIN
- METALLIZED & BRAZED (Cu/Ag)
- ALUMINA
- 4.6 mm
- TEFLON
- KOVAR

DYNAMIC RESISTANCE ANALOG
POWDER SENSITIVITY TEST
SERIAL NO. 2906
MINIMUM AFTER BW BREAK = 74.01 OHMS AT   7.20 MSEC

FIGURE 5

RESISTANCE AFTER FIRE OF
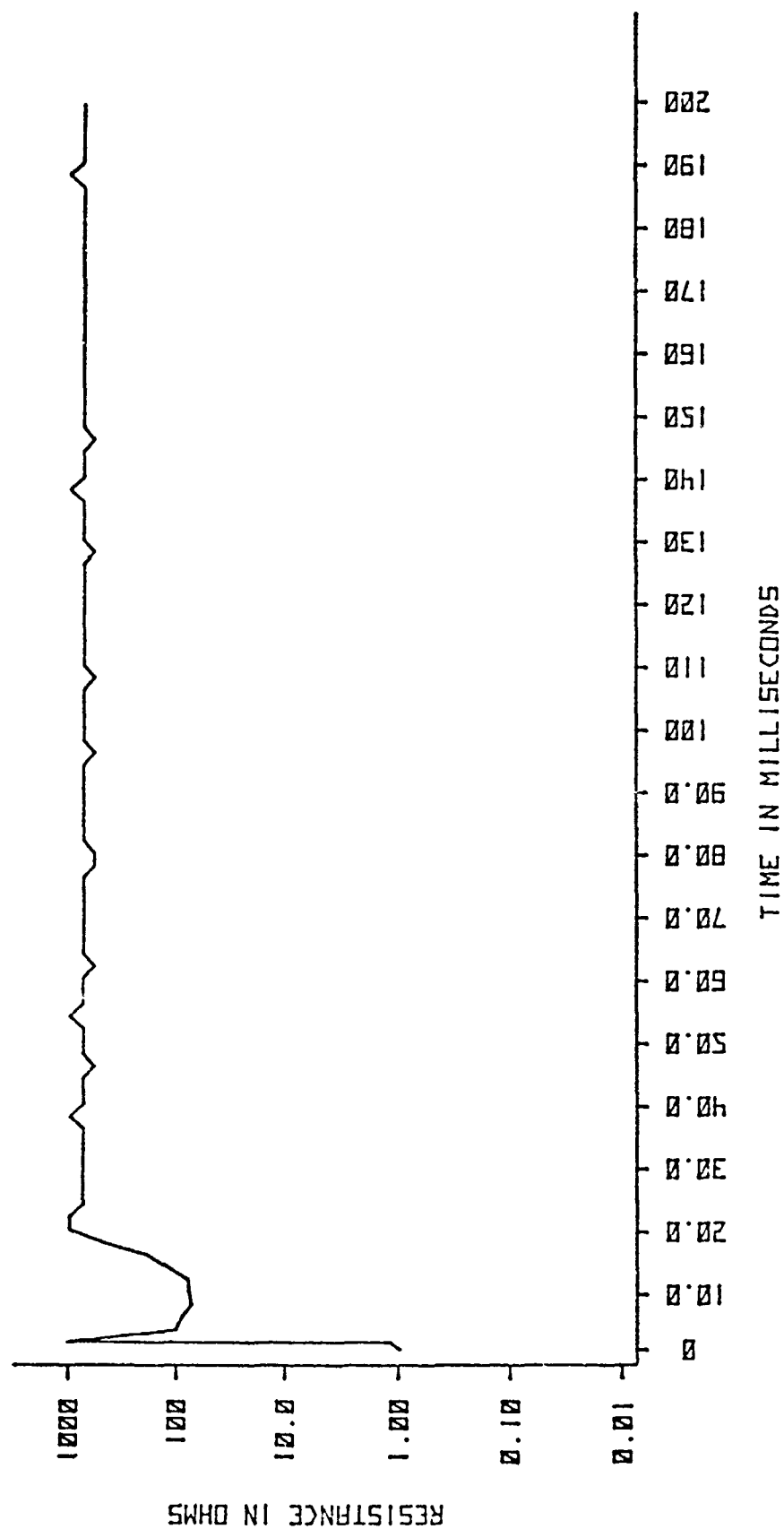Al/KClO$_4$ IN MINIATURE IGNITER

TIME IN MILLISECONDS

RESISTANCE IN OHMS

BRIDGEWIRE SENSITIVITY IN THE ACORD DETONATOR

Under contract to Lockheed Missiles and Space Company (LMSC), Unidynamics designed and developed a low voltage detonator for ACORD (Alternating Current Ordnance). This item was required to be an integral assembly capable of sustaining a 5-ampere current flow for five minutes without ignition or degradation of performance. The design of the ACORD detonator is shown in Figure 6. Major components of this unit include (1) a 304 CRES housing containing a glass-to-metal seal, (2) a ceramic charge holder to contain the bridgewire ignition material, (3) a perforated Kapton insulator disk, and (4) a 304 CRES sleeve to confine the transfer and output charges.

The header used in the ACORD detonator is bridged with Evanohm wire having a diameter of 127 microns and a nominal resistivity of 110 ohms/meter. Bridge resistance prior to loading is 0.18 ± 0.02 ohm. Using a consolidation pressure of 138 MPa, a bridgewire ignition charge consisting of 30 ± 3 mg of aluminum/potassium perchlorate is consolidated into the igniter cavity. The insulator disk and sleeve are then installed, and a transfer column of CP* is consolidated against the ignition material at a pressure of 103 MPa. This is followed by a conical output charge of HMX.

The unit is hermetically sealed by welding a 304 CRES disk over the output end. The average density of the aluminum/potassium perchlorate ignition charge in the ACORD detonator is ≈ 2.3 gm/cm^3, and the average column height is ≈ 1.5 mm. Bridge resistance of the loaded unit is ≈ 0.18 ohm.

<u>5-Ampere/5-Watt No-Fire Test Followed by All-Fire Test.</u> Tests conducted both at Unidynamics and LMSC have established that the ACORD detonator will withstand a 5-ampere/5-watt no-fire pulse without ignition or degradation of performance. In a series of tests conducted by LMSC, a 25-unit sample from the first lot was subjected to a 5-ampere/5-watt no-fire pulse of five minutes duration. None of the units ignited or underwent significant change in bridge resistance. The units were then divided into two groups and evaluated in all-fire tests, along with control units.

The first test included ten no-fired units and five control units. These units were pulsed with an input voltage of 177 volts root mean square (rms). Mean output current was ≈ 42 amperes rms. All units ignited within specified time limits.

---

*CP is a new explosive developed jointly by Unidynamics and Sandia Laboratories under the sponsorship of the United States Department of Energy (D.O.E). The material possesses many characteristics of a secondary explosive and is relatively safe to handle. However, it is capable of undergoing very rapid DDT. Chemically, CP is 5-cyano-tetrazolatopentammine cobalt (III) perchlorate.

In the second test, 15 no-fired units and 10 control units were pulsed with a 25-ampere direct current. All units ignited within specified time limits.

In a later test, 11 ACORD detonators from the second lot were subjected to a 5-ampere/5-watt no-fire pulse followed by a 25-ampere all-fire pulse. All units survived the no-fire test, then ignited from the all-fire current with an average function time of $\approx$1.5 ms.

Current-Variable Bruceton Ignition Sensitivity Test. A group of 48 ACORD detonators from the second lot was used in a current-variable Bruceton ignition sensitivity test. Current levels between 8.50 amperes and 9.75 amperes were required to bracket ignition. When the Bruceton data was analyzed by the ASENT program, the mean firing current of the 48-unit sample was found to be 9.08 amperes, with a standard deviation of 0.44 ampere. The all-fire current (99.9 percent positive response) was 11.38 amperes, and the no-fire current (0.1 percent positive response) was 6.79 amperes.

Function Time. Three groups of ACORD detonators from the second lot were used to establish the function times of virgin units tested under each of the three potential firing conditions. Mean function times at the three firing energies are summarized below and shown graphically in Figure 7.

Firing Conditions (Input Voltage/Output Amperage)	Mean Function Time (ms)
145/34	0.80
160/37	0.68
177/42	0.55

These function times are considered acceptable for the ACORD application.
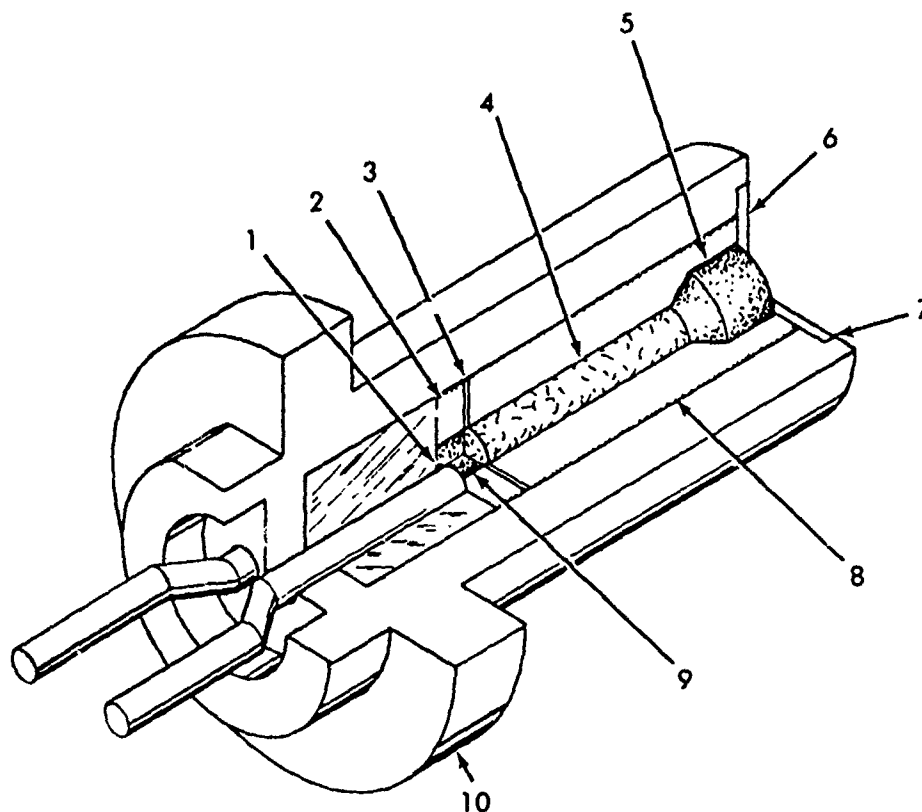
LEGEND:

1-BRIDGEWIRE   6-CLOSURE DISK
2-CHARGE HOLDER   7-WELD
3-INSULATOR DISK   8-SLEEVE
4-TRANSFER CHARGE   9-Al/KClO$_4$
5-OUTPUT CHARGE   10-HOUSING

FIGURE 6

ACORD DETONATOR ASSEMBLY
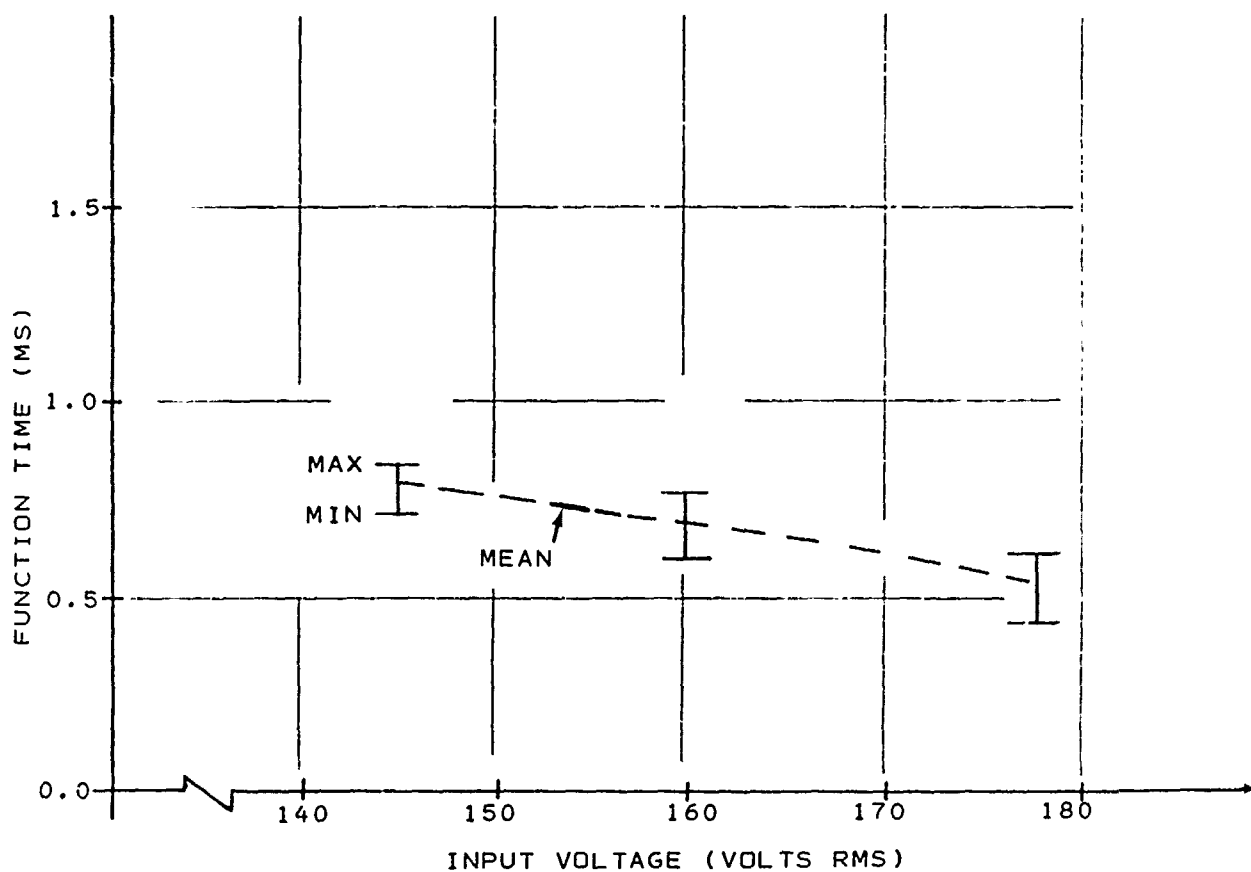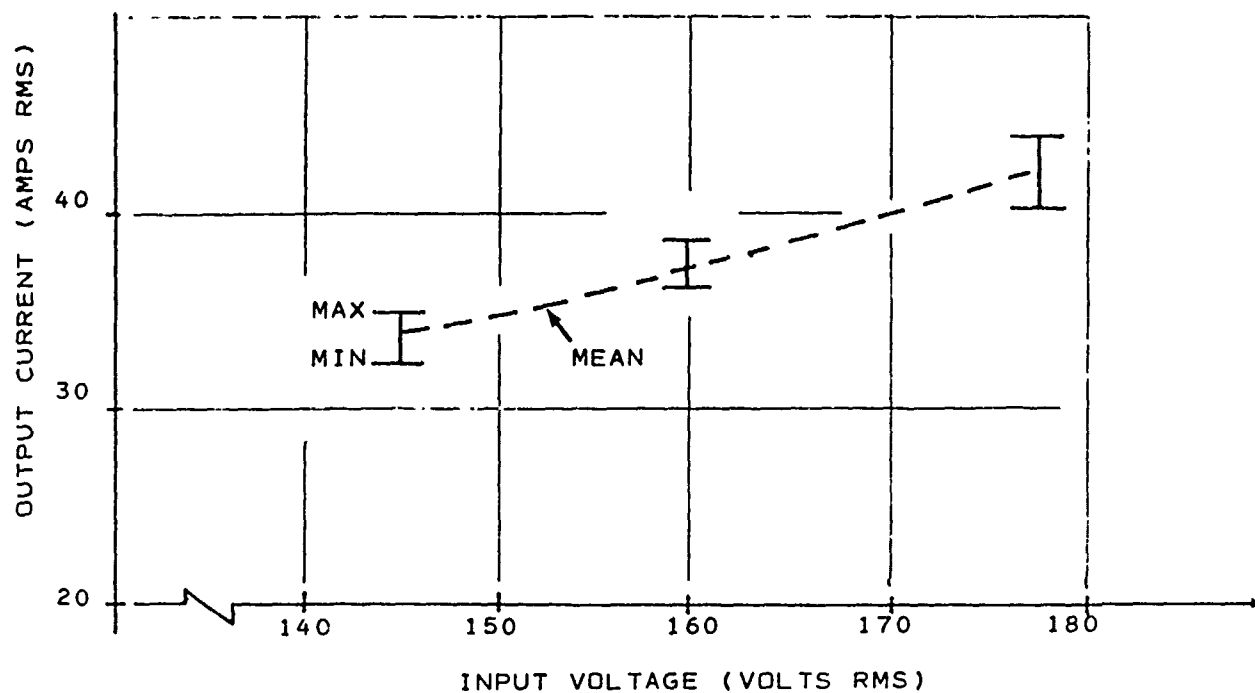
FIGURE 7

FUNCTION TIME AND OUTPUT CURRENT FOR ACORD DETONATORS

535

CONCLUSIONS

A mixture of aluminum and potassium perchlorate appears very promising for use as a bridgewire ignition material in small electroexplosive devices. This composition possesses high calorific yield and rapid burn rate. It is insensitive to normal impact and does not ignite from the arc produced by a 600-pf capacitor charged to 25 kV and discharged through a 500-ohm series resistor. The latter property makes the composition "body-safe" under D.O.E. guidelines.

In a miniature igniter containing a 30.5-micron diameter bridgewire with a resistance of 1.0 ± 0.1 ohm, aluminum/potassium perchlorate tested at $-54°C$ has a high current mean firing energy of 5.69 mJ and a high current all-fire energy of 6.82 mJ. In the same unit tested at 71°C, the material has a low current mean firing current of 1.40 amperes and a low current no-fire current of 1.15 amperes. The resistance-after-fire characteristics are consistently good.

In the ACORD detonator containing a 127-micron diameter bridgewire with a resistance of 0.18 ± 0.02 ohm, aluminum/potassium perchlorate is capable of withstanding a 5-ampere/5-watt no-fire pulse without ignition or degradation of performance. After the no-fire test, the composition will still ignite consistently from a 25-ampere all-fire current, functioning in ≈ 1.5 ms. This unit can also be functioned by applying input voltages ranging from 145 volts (≈ 34 amperes) to 177 volts (≈ 42 amperes). Mean function times drop from 0.80 ms to 0.55 ms as firing current is increased. The mean firing current of aluminum/potassium perchlorate in the ACORD detonator is 9.08 amperes. All-fire current and no-fire current are 11.38 amperes and 6.79 amperes, respectively.

REFERENCES

1. Craig, J. R. and Villa, F. J., "Miniature Igniture," U.S. Patent 3,906,858, September 23, 1975.

ACKNOWLEDGEMENTS

Environmentally Acceptable
Method for the Demilitarization
of Mk 24 and Mk 45 Aircraft
Parachute Flares

by

J. E. Short
F. E. Montgomery

The Navy currently has a large number of Aircraft Parachute Flares which are no longer usable. In addition, large amounts of production scrap are generated each year. Formerly, this material was disposed of by open burning. Open burning not only produces pollutants but also destroys potentially valuable materials.

NAVWPNSUPPCEN Crane has developed a pilot plant process to render these flares.

Figure 1 shows a cutaway of a typical aircraft parachute flare. The candle section contains approximately 17-pounds of composition.

Figure 2 shows the chemical composition of this candle.

A project of this nature is usually described using 35MM slides and viewgraphs to show the equipment and data obtained from the process. However, for our process, I plan to take a different approach. You will see a narrated 16MM color film which shows the actual pilot plant in operation. This film will enable you to actually see the automated equipment disassembling typical aircraft parachute flares.

Enclosure (1)

ENDVIEW OF MK 354 MOD O

EJECTION DIAL INDICATOR

EJECTION SETTINGS

EXPELLANT

2 SEC DELAY

STRIKER

FUZE ADAPTOR

GAS CHECK

CABLE

INSTRUCTION TAG

SAFETY CLIP

DEPLOYMENT BAG

PARACHUTE ASSEMBLY

PARACHUTE CONTAINER

OUTER CONTAINER

CANDLE TUBE

DROGUE CHUTE

CAP

RELEASE PIN

FIRING PIN

PRIMER (M42G)

IGNITER ASSEMBLY

MAGNESIUM CANDLE

EXPLOSIVE BOLT

MK 59 MOD O DETONATOR

INTERNAL DISCONNECT

EJECTION TIME DELAY FUSE

DETACHABLE FUZE ASSEMBLY
(MK 364 MOD O)

ATTACHMENT LOOP

AIRCRAFT PARACHUTE FLARE
MK 45 MOD O

Figure J

FIGURE 2

MK 45 AIRCRAFT PARACHUTE FLARE
CHEMICAL FORMULATION

61%   MAGNESIUM

35%   SODIUM NITRATE

4%   BINDER (EPOXY OR POLYESTER)

Demilitarization of the Mk 25 and
Mk 45 Aircraft Parachute Flare

Defective flares. The Navy has an inventory of about 75,000 defective Mark 24 and Mark 45 aircraft parachute flares. The Army and Air Force have thousands more. Although they constitute very little hazard, the thought of storing them forever is not attractive. And it's expensive.

This method of eliminating the problem only creates other - more serious - problems.

At the Naval Weapons Support Center, Crane a process has been developed which not only eliminates the problem, but which results in useful, profitable end-products as well. From the main part of a flare - the candle - valuable magnesium can be recovered. Among the other by-products are nylon and metal scrap. So from the present situation in which the Navy spends about $12,500 a year storing defective flares, demilitarization can produce end-products with a net profit of about $3.00 from each Mark 24 flare processed.

The demilitarization apparatus developed by the Naval Weapons Support Center, Crane has been fully tested for effectiveness and safety. It consists of a series of conveyors and machines that are remotely controlled to disassemble and reduce the flare materials.

There are three major sections to the apparatus: The flare disassembly section, the candle disassembly section, and the mixing tank section. Each section has a control area and a machine area. Except for a few safe operations that require human handling, the process is remotely controlled from behind protective shields in the control areas. The process begins in the flare disassembly area where the flare moves through a push apart fixture, separating the

parachute and smaller parts from the candle. The candle is taken
to the second section. Here saws cut the ends off, a scorer removes
the cardboard casing, and the crusher reduces the composition to
chunks. These chunks are conveyed to a mixing tank where they
interact with solvent and water. Sodium nitrate is dissolved and
drained off, leaving granulated magnesium which is screened into a
catch pan, and finally, taken to a drying oven. Now let's see the
process in actual operation.

First, each flare is readied. The protective cap, lanyard and
desiccant bag are removed from the flare, the fuze is checked to
make sure it is on safe, and the flare is vented if necessary. Then
it is taken to the first section of apparatus - the flare disas-
sembly section.

The main purpose of my section is to remove the candle assembly
from the rest of the flare. But first I have to take off the fuze.

The shield protects me from any possible accident during the hazard-
ous parts of the operation. When nothing is moving, it's safe -
like when I get the end cap and put it into a box to be sent to
scrap salvage.

Next the parachute section is pushed out.

I take the candle to a station where Bill, who usually runs the
candle disassembly section, picks it up. First he removes the
firing pin assembly.

The purpose of my part of the process is to reduce the candle compo-
sition from a solid cylinder into small chunks. I control the pro-
cess from behind a bullet-proof shield.

The two band saws cut the ends. See the water? Water coolant is
used whenever a procedure might produce heat or sparks.

All water we use is recirculated, assuring cleanliness and eliminating waste. Here's our hydraulic power unit.

Now the cardboard tube around the candle composition is scored so it can be stripped off. Although we've never had any problems at all here - I could hit this button and stop everything if I had the slighest idea that anything was going wrong. Only the supervisor is authorized to activate the system reset button. The sprinklers come on automatically, but I could start them myself also if I wanted. Now, with all the equipment off, it is safe for me to go in and remove the cardboard tube.

Now the candle composition is dropped into a water-filled tank. Here is where the composition is broken up. The crushing ram exerts tremendous pressure - producing some heat - so the actual crushing action takes place under water.

Operator #3: A conveyor brings the crushed composition from Bill's section to my area - the mixing tank section. My section is where the pay off really comes. It's in the mixing tank where the magnesium is separated from the other candle materials. I remotely fill the mixing tank with solvent before the composition is introduced. Then the composition drops into buckets in an enclosed elevating conveyor where it is lifted up to the tank. A chute directs the chunks of composition into the tank. Composition from eleven candles is processed in one batch. When I have eleven candles worth in the tank, I stop all equipment and prepare to go into the mixing room to close the top of the mixing tank.

Because of the solvent, I wear a respirator, and to be totally safe, some goggles. There is no danger to me from the candle composition since it's under the nonflammable solvent.

After closing the top of the tank I throw this door in the Y
chute so that another batch of composition can be routed off into
a second tank while the composition in the first tank is being
processed.

Now I remotely control the mixing operations. First I mix the
chunks of composition in the solvent. This dissolves the binder
holding the particles together. Then I drain out the solvent. A
bag filter catches the binder material so that the solvent can be
reused over and over. Then I fill the tank with water and mix
again, dissolving the sodium nitrate so that only magnesium is left.
The water and dissolved sodium nitrate are drained to be reused
until the sodium nitrate reaches a concentration of about eleven
percent. Now the granulated magnesium on the bottom of the tank
is dumped onto a system of vibrating screens - they screen out
any remaining chunks of composition, which will be added to the
next batch - and the magnesium is washed down onto a conveyor
which takes it to a catch pan. These catch pans are placed in a
vented drying oven. Otherwise the magnesium would retain water
for a long time.

Dry magnesium powder is the final result. A sample is always taken
to check the process. While testing is incomplete there seems lit-
tle doubt that it could be used for operational flares. Virtually
every by-product of the process can be put to use. Even the binder
material may be used for purposes such as building blocks. Some
uses are still under study. For example the sodium nitrate solution
produced by the process may be useful as fertilizer for pasture
grasses. Researchers at Purdue University are cooperating in this
evaluation.

The Naval Weapons Support Center, Crane is working on similar processes for the demilitarization of red phosphorus munitions, colored smoke munitions, photoflash cartridges and infrared emitting devices; thus creating procedures for the economical improvement of our nation's ecology.

Environmentally Acceptable
Method for the Demilitarization
of Red Phosphorus Munitions

by

J. E. Short
F. E. Montgomery

The Navy currently has a large number of Mk 25 and Mk 58 Marine Location Markers which are no longer usable. In addition, large amounts of production scrap are generated each year. Formerly, this material was disposed of by open burning. Open burning not only produces pollutants but also destroys potentially valuable materials.

NAVWPNSUPPCEN Crane has developed a pilot plant to render these flares.

Figure 1 shows a cutaway of a typical marine location marker. The candle section contains approximately 28 ounces of composition.

Figure 2 shows the chemical composition of this candle.

A project of this nature is usually described using 35MM slides and viewgraphs to show the equipment and data obtained from the process. However, for our process, I plan to take a different approach. You will see a narrated 16MM color film which shows the actual pilot plant in operation. This film will enable you to actually see the automated equipment disassembling typical marine location markers.

Enclosure (2)

MARINE LOCATION
MARKER MK 25

Figure I

OUTER TUBE

INNER TUBE

PYROTECHNIC COMPOSITION

18.54 MAX

BASE ASSEMBLY
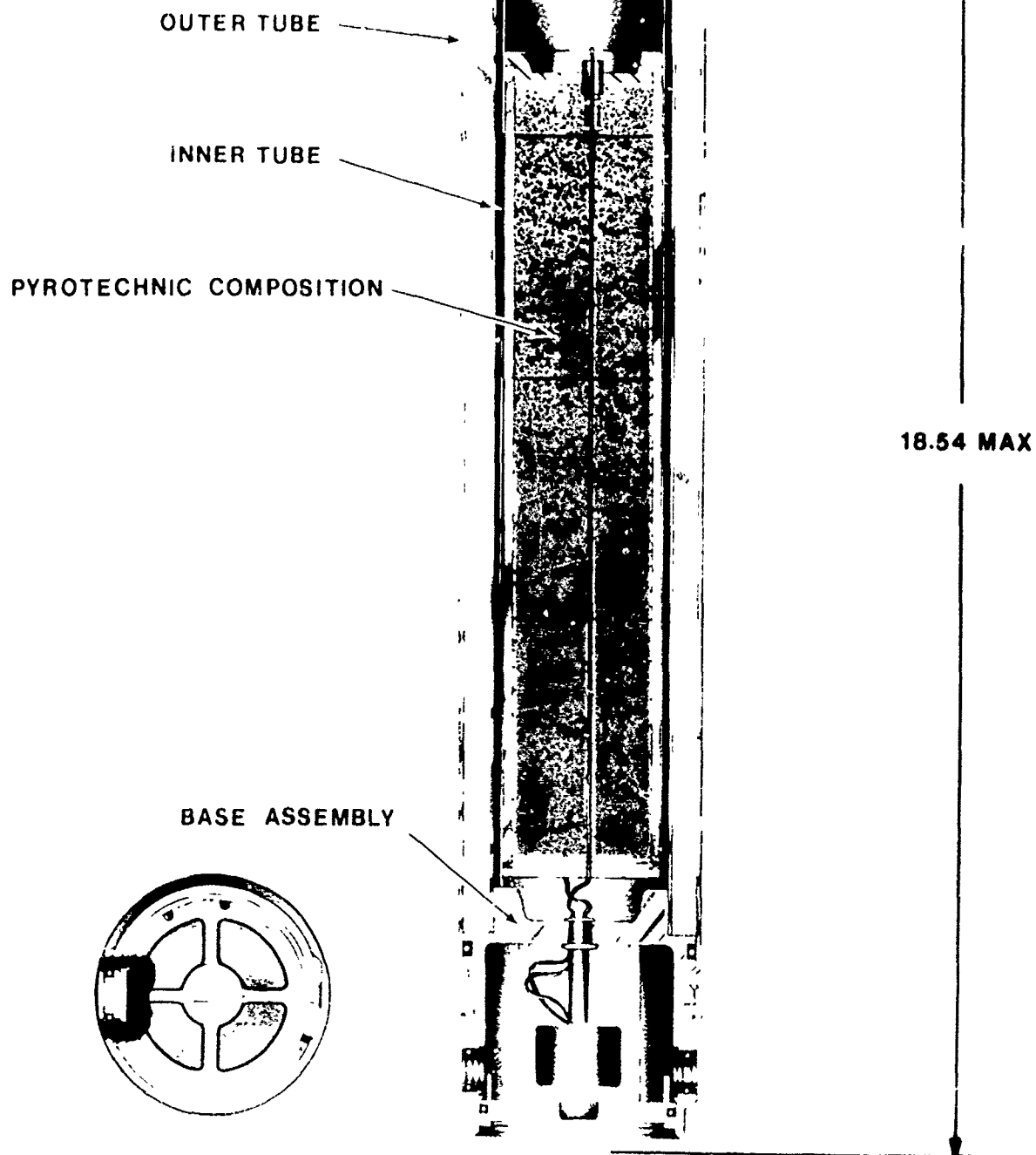
FIGURE 2

MK 25 MARINE LOCATION MARKER
CHEMICAL FORMULATION

53%   RED PHOSPHORUS

34%   MANGANESE DIOXIDE (PYROLUSITE)

7%   MAGNESIUM

3%   ZINC OXIDE

3%   LINSEED OIL

PILOT PLANT FOR RED PHOSPHORUS
RECLAMATION

MUSIC.....   CRANE logo

                                    ·Titles: PILOT PLANT FOR RED PHOSPHORUS
                                                    RECLAMATION

                                              Produced for:
                                              NWSC CRANE

                                              Under the Technical Direction
                                              of: NAVAL SEA SYSTEMS COMMAND
                                                   (SEA-033)

                                              Photographed at:
                                                BATTELLE MEMORIAL INSTITUTE
                                                Columbus, Ohio   ·
                                                        and
                                                KILGORE CORPORATION
                                                Toone, Tennessee

                                              Special Photography Courtesy
                                              of: US NAVY

                                              Edited by:
                                                AUDIO VISUAL PRODUCTION
                                                DEPARTMENT PURDUE UNIVERSITY

                Navy ship-to-ship scenes (from the Battelle film)

NARRATOR:

The red phosphorus marine

location marker...essential in many military

operations. A large number are required.

Markers must be re-stocked, so that there

will always be fresh, reliable supplies.

Outdated markers, and the inevitable

accumulation of rejects and production

scrap, a half-million pounds worth, are being

stored at NAVY installations at a cost of

several thousand dollars a year.

The material is not dangerous, but it must be disposed of in a way that is acceptable to the environment. For this reason, the Naval Weapons Support Center at Crane, Indiana, has developed a pilot plant for extracting the red phosphorus composition from marine markers, and burning the phosphorus candles in a closed environment.

Depot scenes, material being moved by fork lift, etc...

The material is disposed of effectively, and a valuable product, phosphoric acid, is recovered.

For the demilitarization of the Mk 25 Marine Location Marker, we are concerned with three primary sub-assemblies... The base assembly...the pyrotechnic composition...and the outer tube.

Drawing of the flare, pop-in titles

Now, let's look at how the pilot plant works. Virginia usually operates the marker-breakdown section. We'll ask her to show you the equipment in operation.

Virginia carries the first flare to the band saw...

Virginia: We use a band saw to cut off the inert base assembly from the marker. The controls are safely out of the way.

She inserts the flare in the saw

She walks over to the control box, pushes the buttons...

The vise automatically positions the marker...and the base unit drops harmlessly into a basket. The candle drops easily from the outer tube.

Marker is moved into place, saw cuts it off...

This pushout fixture will cut through the paper liner...	She removes the candle from the saw vise, drops inner tube out into her hand
The plastic igniter cap is saved for controlled incineration, and the ignition composition is placed in containers for reuse.	She walks over to the pushout, inserts candle, operates it, it cuts the paper
The rest of the candle will be cut into small chunks with a radial arm saw to speed up incineration. For safety purposes, I must push two buttons at the same time to start the saw.	She dumps loose material in a container She carries the candle over to the RAS, inserts it, operates the starting controls
The candle material is immersed in water, and the saw moves very slowly. These are additional safety precautions which prevent buildup of heat.	Saw moving thru the candle, water splashing...
The device automatically advances the candle between cuts, until it is reduced to small chunks.	
Water is drained off into a holding tank and saved to be used again	Virginia opens the drain valve
The candle pieces are dropped into a feeder, and I'll now move the bucket conveyor into position to receive the pieces	She opens the hopper door, pieces drop onto the feeder...
After the sawing and soaking, the paper is easily removed.	She operates the conveyor...

The vibrator-feeder drops the candle pieces into the bucket, to be transported to the incinerator charge pan	She picks out the paper scraps... Pieces drop into the bucket...
A final check is maa ㆍ see that the system is ready. These pressure and temperature gauges are monitored continuously throughout the process	She runs the conveyor, pieces drop into the charge pan Operator checks dials and gauge
NARRATOR: Here is how the incineration complex works There are four principal components	Start, animation sequence. This sequence shows the progress of the combustion gasses through the complex, keeping pace with the narration...
The first is a two-chamber incinerator, where the cut-up candles are burned, leaving a reduced quantity of inert residue.	NARRATION...
In the second chamber, the gasses undergo further combustion of residual phosphorus vapor at 800 to 1200^0 Farenheit.	
Then the gasses are cooled to less than 200^0 as they pass through a spray tower and packed column, which makes up the second component. The spray is dilute phosphoric acid, which becomes more concentrated as it scrubs the flowing gas stream, picking up phosphorus pentoxide molecules. The output of concentrated phosphoric acid can be recycled as a valuable material for agricultural fertilizer	Animation sequence, continued

The gasses then pass through a water-
cooled heat-exchanger, which reduces the
temperature further

A third component, is the mist eliminator
section, where any remaining acid droplets
are removed by filtration

Finally, the gas stream is exhausted through
a stainless steel duct. The Ammunition Pro-
curement and Supply Agency (APSA) has
specified that there must be less than one
milligram of phosphorus pentoxide per standard
cubic foot of exhaust gas. Stack gasses are
sampled continuously.

Now, we'll let Grace show you the actual
incineration complex in operation...   End of the animation
                                                         sequence

Grace: My section of the pilot plant   Grace turns on switches and
is the incineration unit. Before   opens valves on the
                                             incinerator
each operation, I heat the second
chamber to 800° Farenheit. At the   She opens move valves and
same time, I check out the entire   checks her clipboard...
incineration system instrumentation

The air pump brings the incinerator   She operates the pump...
to a slight vacuum, so that fumes will
not leak out. The vacuum condition is
maintained throughout the operation

Next I load the cut-up candles into   She loads the 1st chamber
the 1st chamber of the incinerator

Composition ignition is achieved in one to five minutes, as the burner flame contacts the charge pan, and the reaction becomes self-sustaining. Combustion takes about twenty minutes	Virginia comes out and switches on the burner
	1st chamber interior
The spray tower and packed column function continuously, cooling and scrubbing phosphorus pentoxide from the combustion gasses. The packed column is filled with a ceramic material and recycled acid spray to remove the acid fumes, leaving only a fine mist, which is removed as the gasses pass through the mist eliminator. The acid is suitable for sale, and the money the Navy receives helps pay for all of us.	Grace with her clipboard checks the system over...
NARRATOR: As the remaining gasses are pumped up the stack, they are sampled continuously for any remaining acid mist. The entire system is designed to keep the mist to an absolute minimum...below Ammunition Procurement and Supply Agency standards	Scientist at the stack gas monitor
	Scientist walks over to the cut-off valve
The efficiency of the pollution control devices on the system can be demonstrated visually	Close-up of the smoke-stack, no smoke...
This is what happens when the mist eliminator is by-passed	White smoke appears...

The smoke almost disappears when the   Smoke disappears
mist eliminator is connected back into
the system.

The end products of this incineration   Wide shot, overall view of
unit for red phosphorus disposal and   the plant
reclamation are a small amount of
chemically inert ash, suitable for
land-fill disposal or as a ceramic
glazing material, or manganese ore and
reclaimed fertilizer-grade phosphoric   Additional view of an oper-
acid, suitable for agricultural use.   ator checking over the
                                                  system...
Thus, a large stockpile of phosphorus
flare candles, rejects and scrap, can
be disposed of safely. NWSC Crane is
working on disposal methods for other
pyrotechnic systems in order to further
reduce pollution   NWSC Crane logo

PYROTECHNIC DEVICES FOR USE BY WATER-SPORT ENTHUSIASTS

AMATEUR SAILORS AND SMALL CRAFT IN COASTAL WATERS

- G. M. Simpson

Introduction

More and more people are finding real pleasure in offshore sailing and other water sports. Such activities are not without an element of danger and the sea is never to be underestimated. Every year there are tragedies when people get into unexpected difficulties and find themselves unable to cope with the situation.

Some of these tragedies might be avoided if everyone who went out on the sea in a boat carried some means of calling attention to their plight.

A distress signal does not have an easy job!

The main object of a signal is to be seen. Thus, it should be conspicuous, even at a long distance by day or by night, and it should function for as long as possible.

The signal should also be reliable. It should always perform satisfactorily whatever treatment it may have received during storage in a small boat.

It is unlikely that a signal will be needed on a calm, fine day, so the signal should work even if drenched by rain and spray or accidentally dropped into the water when ready to fire.

A distress signal is going to be used by someone in distress - who may be cold, exhausted, panic-stricken or clinging to a capsized boat. The operation of the signal should therefore be simple and absolutely foolproof to use.

Types of signals, their design and construction

Any or all of the following signals may be carried either by choice or by reason of safety legislation.

Red, white or green hand-held flares; red, one or two star signals; red, white or green rocket parachute flares; rocket fired maroons; hand-held orange smoke signals; floating orange smoke cannisters.

Traditionally, signals have been constructed in cardboard tubes rather like glorified fireworks, but such do not provide an adequate storage capability. More recently steel, aluminium and other metals have been employed and in such designs adequate sealing may be achieved. However, there are obvious disadvantages. i) The temperature reached by the tube may make it uncomfortably hot to hold. ii) There may be problems of corrosion during storage. iii) Such signals are frequently incapable of floating. iv) Use of these materials tends to make the market price higher than necessary. v) Higher weights increase packaging and transport costs.

The effective sealing of such signals frequently depends on the use of waterproofed tapes, card discs and glue and the whole operation of assembly is frequently extremely complicated and highly labour intensive, thus giving rise to high production costs which are reflected in high market prices.

By utilising components manufactured in modern light-

weight plastics such as polythene, polyvinylchloride, polypropylene etc. and by the choice of a suitable filler for the plastic e.g. talc or glass fibre may be used in polypropylene, the component can be adjusted in terms of density, tensile strength and heat insulation (or burning rate if it is desired that the component be consumed). Furthermore, these materials can be assembled into a sophisticated moisture-proof device by quick and reliable techniques such as high frequency or ultrasonic welding or by the design of snap-together components.

The elimination of metallic items can considerably enhance the storage life of the devices, as also can the use of modern resin-bonded pourable, castable or compression moulded pyrotechnic mixtures. The inherent safe-handling characteristics of many such compositions may enable filling to be accomplished automatically, thus enabling flow line production to be implemented with consequent cost savings in time and labour content.

The firing operation of many of the distress signals currently available in the U.K. leaves much to be desired. Frequently end-caps secured by adhesive tape have first to be removed, an almost impossible task for someone in the water with cold hands. It may then be necessary to remove a striker plug from the base of the flare and rub this across the face of exposed match composition at the top of the flare - to accomplish this with waves breaking over one's head is quite impracticable and the system suggests that the manufacturer has never tested his wares under realistic conditions.

In many current mechanically operated devices employing friction igniters or percussion firing (both of which have a high functional reliability if well-designed and constructed

from long-life components) the operator is required to insert a finger into a loop of string or into a pull ring designed to fit only the daintiest of digits! In a well-designed signal firing should be possible by means of a simple operation which may be accomplished with gloved hands.

Ideally, all signals should be so designed as to immediately indicate their type and mode of operation without the necessity of reading instructions in small print.

Suggested Design Criteria

The following list of desirable attributes has therefore been compiled as an outline specification for distress signals for use by amateurs in coastal waters.

1) The design of any signal should be such that failure of any component or system will cause the device to 'fail-safe'.

2) Signals must not be capable of functioning accidentally under any circumstances.

3) Packages and components of signals must be compatible with one another under moist and hot conditions.

4) Chemical or electrochemical galvanic effects must not jeopardise the safety, nor lead to degradation of the signal.

5) The packaging of signals should be designed to assist in their protection and safe-keeping but provide rapid and easy access.

6) Any signal (or pack of signals) should float if accidentally dropped overboard.

7) All signals should be so constructed that when fired, no burning material will fall which might cause injury to the operator or damage to an inflated craft.

8) Signals should be fitted with an integral means of firing, easy to operate with wet, cold or gloved hands in adverse conditions without external aid and requiring the minimum of preparation.

9) Sealing and access should not depend on the use or removal of adhesive tapes.

10) The signal should be so constructed that the operational end may be positively identified by day or night.

11) All signals should be capable of functioning after immersion under a head of water of one metre for one hour.

12) Signals for use by divers (in outer pack where applicable) should be capable of submersion to a depth of sixty metres without loss of serviceability.

13) In the 'Ready-to-fire' condition, a signal should function satisfactorily after immersion under a head of water of 10 cm. for 10 seconds.

14) All components, compositions and ingredients should be of such quality as to enable the signal to function smoothly and maintain its serviceability under average storage conditions in the marine environment for a period of at least three years.

15) The date of expiry should be marked indelibly on the signal.

16) Clear and concise directions for use in the English language, supported by illustrations, should be printed indelibly on the signal. It should be possible to read

each line of the instructions without rotating the signal

17) Hand-held orange smoke signals for daytime use should be capable of emitting dense orange smoke for a period of not less than 40 seconds.

18) Floating orange smoke signals for daytime use should be capable of emitting dense orange smoke for a period of not less than 3 minutes.

19) Hand-held flares should be of distinctive colour and should burn for a period of not less than 60 seconds with an intensity of not less than 15,000 Candela and without discomfort to the user.

20) After ignition, a flare should continue to burn after a temporary immersion under a head of water of 10 cm. for 10 seconds.

21) One and two star signals should eject stars to a height of 100 metres. The stars should continue to burn brightly for a period of 5 seconds but should be extinguished before falling to sea-level.

22) Rockets ejecting flares suspended on parachutes, maroons or radar reflective material should fire smoothly without recoil or discomfort to the user.

23) Rockets should also be capable of functioning when fired at an angle of 45 degrees to the horizontal.

24) Parachute flares should be ejected at a height of 300 – 350 metres.

25) Parachute suspended flares should burn for a period of not less than 45 seconds, fall at a rate not greater than 4.6 metres per second and extinguish at a height of not less than 46 metres above sea-level.

Development of a Small, Safe Pyrotechnic Valve Actuator[*]

by

B. R. Steele

Initiating & Pyrotechnic Components Division
Sandia Laboratories
Albuquerque, New Mexico

Abstract

Development of a Pyrotechnic Valve Actuator with several new design concepts has recently been completed. This actuator offers advantages in size, electrostatic safety, high "g" load capability, severe temperature extremes, bonfire safety, and advanced testing techniques. These advantages were obtained by the following design concepts:

Size - was enhanced by the use of a ring connector. This connector consists of a center pin and two concentric rings that are each connected to a pin which provides a dual bridgewire capability with a common ground return. Since the contacts are cylindrical, no orientation keyways are required.

Electrostatic Safety - is controlled by a shielded charge-holder, electrically connected to the center pin, with a breakdown path provided at the closure disc, outside the

powder cavity. In addition, a spark insensitive powder is used. Over 2500 units have been tested without a failure. This allows a reliability statement of .999 at 90% confidence.

Operator Safety - is enhanced by the use of $TiH_{.65}/KClO_4$ pyrotechnic powder which in itself is spark insensitive in bulk form.

High "g" Load Capability - is attained by the use of a retaining washer that holds the powder against the bridge-wire. The primary use of this actuator requires capabilities to function after loads over 10,000 g's.

Temperature Extremes - from $-40°C$ to $+71°C$ have been proven. Limited numbers have been successfully tested from $-67°C$ to $+120°C$.

Bonfire Safety - is attained by using pyrotechnic powders with auto ignition temperatures above $500°C$. Although the actuator will function at this temperature, the remainder of the system will have burned, melted or exploded by that time.

Non-Destructive Testing - is done by Electrothermal Response Test techniques. Using this test after various environments allowed us to predict failures and in dissecting units

screened by ETR, a design deficiency was found and correc-
ted. This test has also aided us in finding variations in
loading tools and loading processes.

"D" Testing - is accomplished using a load cell test fixture
that simulates the actuator function in a typical valve.
The fixture provides a volume that expands to approximately
the same final volume as the valve and the piston impacts
a force cell and provides a force vs. time curve.

Introduction

In the past, actuators have typically used primary explo-
sives (normal lead styphnate) to drive the valve plunger.
While this type of material is superior for functional charac-
teristics, it is unsatisfactory for safety reasons. It can
be ignited by very low electrostatic discharge pulses and
can grow to detonation causing shock waves and fragments.
Our goal has been to eliminate the use of primary explosives.

Our first attempt in this actuator was to use titanium/
potassium perchlorate in a 33/67 ratio. This material has
sufficient output to function valves; however the spark sen-
sitivity is similar to that of the primaries. A significant
advantage of this material over lead styphnate is that it
won't grow to detonation in small quantities.

The next material evaluated was titanium dihydride/
potassium perchlorate in a 33/67 ratio. This material is

---

extremely insensitive to initiation by sparks, has sufficient output to function valves when contained properly, but is not chemically as stable[1] as we would like. Ignition problems developed with this material and we concluded that if we could find a titanium subhydride composition that when blended with $KClO_4$ had a spark sensitivity near the charged man maximum (600 pF, 20 kV, 500 ohms) we could have a realistic trade-off. The material selected as baseline was $TiH_{0.65}/KClO_4$.

Development of the baseline powder was done in conjunction with the actuator development. Several studies have been done in support of this program and many of them will be discussed in other papers.

Actuator Design

The requirements placed on the actuator design by the system are shown in Figure 1. Those that required new ideas and techniques were: no-orientation connector, electrostatic safety with a reliability attached, high "G" load capability, temperature extremes to 150°C, and bonfire safety.

The design that resulted from these requirements is shown in Figure 2. The 3-pin, dual bridge design consists of a center pin and two concentric rings. The rings are metallized ceramic and contact is made to the pins by brazing. This results in a connector that requires no key ways or guides.

The no-orientation connector was originally designed to eliminate operator error during hook up; i.e. when more than one unit is required for a system, the cable can be made exactly the right length so it cannot be interchanged with a nearby unit. It turned out in the actual system that the most important factor for cable length was because of the high G loads and being able to to tie the cables down securely. At 10,000 G's wires are sometimes stripped from potting sleeves, insulation and solder.

Electrostatic Safety

Electrostatic safety was accomplished in two ways: 1) by using electrostatic insensitive powder, and 2) by using an electrostatic shield.

The original design utilized a titanium dihydride/potassium perchlorate mixture ($TiH_{1.9}/KClO_4$). This material is extremely insensitive to ignition by sparks such as those generated by the human body. Hot wire ignition failures in the component caused us to move away from $TiH_{1.9}$ and, based on the spark sensitivity curve shown in Figure 3 and firing data on units tested in liquid nitrogen, $TiH_{0.65}/KClO_4$ was selected as the baseline powder. Selection of this powder was a marked improvement in operator safety when compared with primaries, and titanium, zirconium and aluminum based pyrotechnics.

The marked knee in the curve and lack of historical data dictated a separate backup mechanism to meet the stringent electrostatic insensitivity requirement. Figure 4 shows the concept of the shielded charge holder. A charge holder consisting of a metal sleeve with molded epoxy on the inside and outside diameter for electrical insulation has a wire welded to it in two places. The charge holder is then bonded into the header with the welded ground wire perpendicular to the bridgewires; the wire is then welded to the center pin. After the powder is loaded into the charge holder a metal disc is welded into the metal sleeve of the charge holder. A perforated insulating disc is installed and then a metal sealing disc is welded in place. The perforated disc provides a preferential spark gap outside the powder cavity. This charge holder design was incorporated without changes to the configuration or size of the header.

We have subsequently tested in excess of 2000 units of this design by applying a 20 kV pulse from a 600 pF capacitor through 500 ohms series resistance, from shorted pins to case with no units firing. Ninety-five of these units were subjected to 10 such pulses on each unit. In addition, five groups of units were loaded with more sensitive materials such as lead styphnate, lead azide, etc. Test data of these units, shown in Figure 5, confirmed the theory that the wire size

would control the sensitivity level. Note that the units began firing in the same sequence as expected from hot wire sensitivity of the individual powders. This implies that if the wire were made larger, the unit would be even less sensitive in this mode.

High "G" Load Spin Testing

Subsequent to high "G" load spin testing, non-destructive test methods (electrothermal response testing (ETR))[2] indicated that the powder had decoupled from the bridgewire. Dissection of two units revealed that the powder had slipped in the charge holder and moved approximately 0.007 mm away from the bridgewire. Subsequent attempts to fire units revealed an approximate 50% failure rate. Previous ETR data had revealed a partial decoupling of the bridgewire-powder interface following thermal cycling. It was postulated that the powder was decoupling from the bridgewire and slipping out due to the difference in thermal expansion between the powder, charge holder and header.

Data obtained from a different component with similar materials revealed long ignition times and some failures to fire when the bridgewire was pushed down against the ceramic substrate.

Two design changes were made to compensate for these problems. The first was to raise the bridgewire above the ceramic

567

substrate. This was accomplished by grinding recesses between the pins so the bridgewire passed over the recess, thereby allowing powder to completely surround the bridgewire. This recess is 0.127 to .254 mm deep. Thermal modeling calculations indicated that a powder thickness of 0.10 mm would look like infinity to the bridgewire during all fire current pulsing, and stress calculations indicated no excess stretching of the wire would occur at 0.254 depth. This change was to compensate for very small movement or relaxation of the powder caused by thermal cycling. The recesses or cavities are depicted in Figure 4.

In order to stop the pellet from slipping in the charge holder during high "G" loads a one-way washer was incorporated. This washer is shown in Figure 2. The washer is put in place by a procedure developed utilizing a Thermal Mechanical Analyser (TMA).[3] The first increment of powder is loaded at 4000 psi; the washer is then seated and the powder is reconsolidated at 12,000 psi. The second increment is then consolidated flush with the charge holder with 8000 to 13,000 psi with a dead stop fixture.

Figure 6 shows the ETR data from units with and without the washer before and after flight testing at high "G" loads (10,000 G). Fifty percent of the first group failed while none of the group with washers failed. This chart also shows

a significant shift in gamma values upon introduction of the washer. The after thermal cycle data shown were taken following a series of three thermal cycles that were incorporated as a part of production to "stabilize" gamma prior to shipping. The data show the decoupling mentioned earlier. We have since eliminated the thermal cycles as a production process.

Output Testing

New concepts in functional "D" testing were required because of the burning characteristics of the titanium dihydride powder. In the past testing was accomplished using a closed bomb to measure pressure vs time in a known volume. More recently we have used a magnetic chronograph which propels a piston of known mass down a tube and through two magnetic coils a fixed distance apart. This results in a known mass being accelerated to a measured velocity and the resulting kinetic energy is calculated. This method yields very reproducible results with lead styphnate; however, the dihydride powder was not completely burned when the piston started free flight and extremely variable results were obtained.

In designing the load cell test fixture shown in Figure 7, we attempted to reproduce the volumes and functions anticipated in a valve. The fixture is built around a Sunstrand model 912 quartz load cell which provides a force vs time curve.

A brass cone is placed on top of the load cell to absorb the initial impact of the piston on the load cell; it also simulates the work done in cutting tubes in a valve. The piston is an interference fit (metal to metal seal) with a standard diameter drill bushing. A beryllium copper shear disc is placed on top of the piston to simulate a seal disc that is welded into the valve. Note that when the actuator is tightened into the fixture the high pressure contour seal of the actuator imbeds itself into the disc and provides essentially a zero free volume to fire into. The disc thickness of 0.25 mm was dictated by the use of titanium dihydride; however, that same thickness is utilized with the subhydride. The zero free volume allowed us to reduce the charge weight by 30 to 50 percent compared to previous designs and still maintain the same valve stroke.

When a unit is functioned, the fire pulse, piston flight time, and the force vs time curve is recorded. With the same equipment utilized for ETR testing (Biomation, HP Calculator, etc.)[4] the data shown in Figure 8 are obtained. In addition to these data we measure the crush of the cone for back up information.

Conclusions

We feel that this actuator has advanced the state of the art in several areas, and in most respects exceeds design

requirements. The piece parts and manufacturing techniques are available from non-government suppliers, including the mating connector which was not discussed. New test methodology developed on this program can detect design problems prior to failure. In addition, a new family of pyrotechnics has been developed and is ready for production.

References

1. Stability of the Pyrotechnic Mixture Titanium Hydride (TiH$_x$)/Potassium Perchlorate (KClO$_4$), T. M. Massis and P. K. Morenus. SAND75-5889

2. Transient Pulse Testing of Electroexplosive Devices, B. R. Steele and A. C. Strasburg. SAND74-5458

3. The Simulation of Powder Decoupling; Phenomena in Electroexplosive Devices by TMA, T. M. Massis, P. K. Morenus and B. R. Steele. SAND77-0258

4. Calculator-Controlled Data System for Explosive Component Testing, A. C. Strasburg. SAND76-5217

FIGURE 1.

ACTUATOR DESIGN REQUIREMENTS

- SIZE

- 90° CONNECTOR - NO ORIENTATION

- ELECTROSTATIC SAFETY (.999)

- OPERATOR SAFETY

- BONFIRE SAFETY

- TEMPERATURE EXTREMES
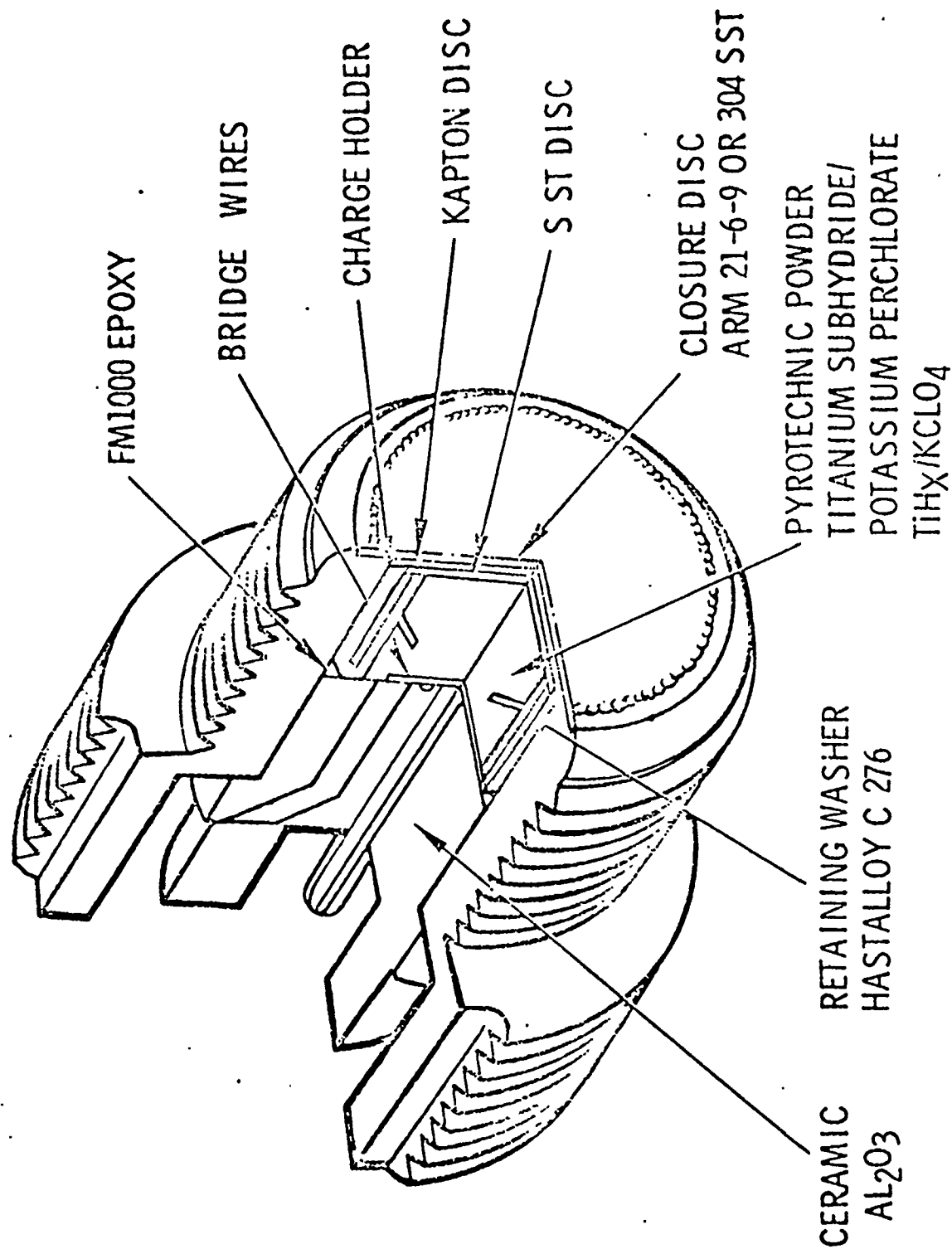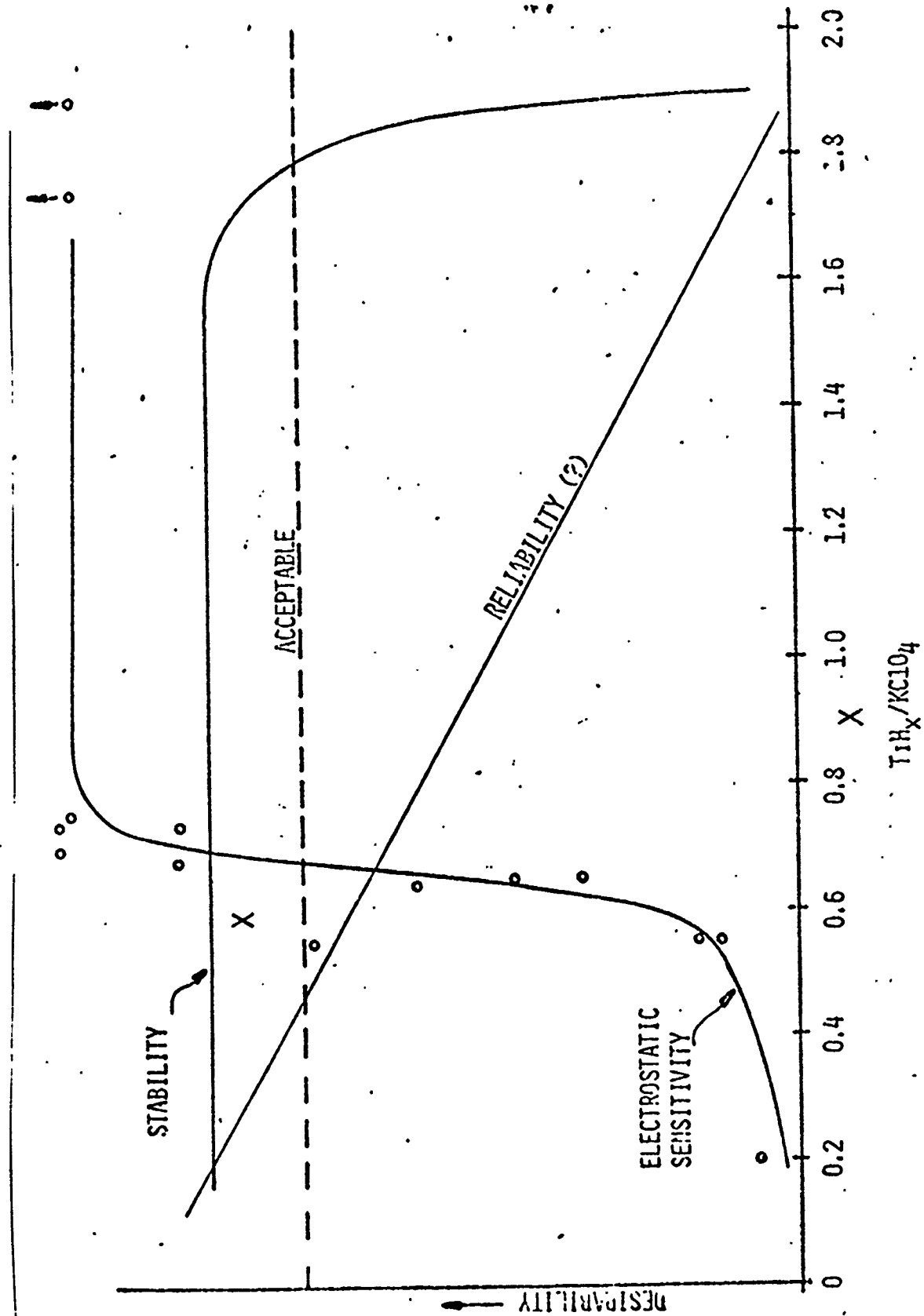
- HIGH "G" LOADS

- LONG LIFE

FM1000 EPOXY

BRIDGE WIRES

CHARGE HOLDER

KAPTON DISC

S ST DISC

CLOSURE DISC
ARM 21-6-9 OR 304 SST

PYROTECHNIC POWDER
TITANIUM SUBHYDRIDE/
POTASSIUM PERCHLORATE
$TiH_x/KClO_4$

RETAINING WASHER
HASTALLOY C 276

CERAMIC
Al_2O_3

FIGURE 2.

FIGURE 3.

CHARGE HOLDER

KAPTON DISC

S ST DISC
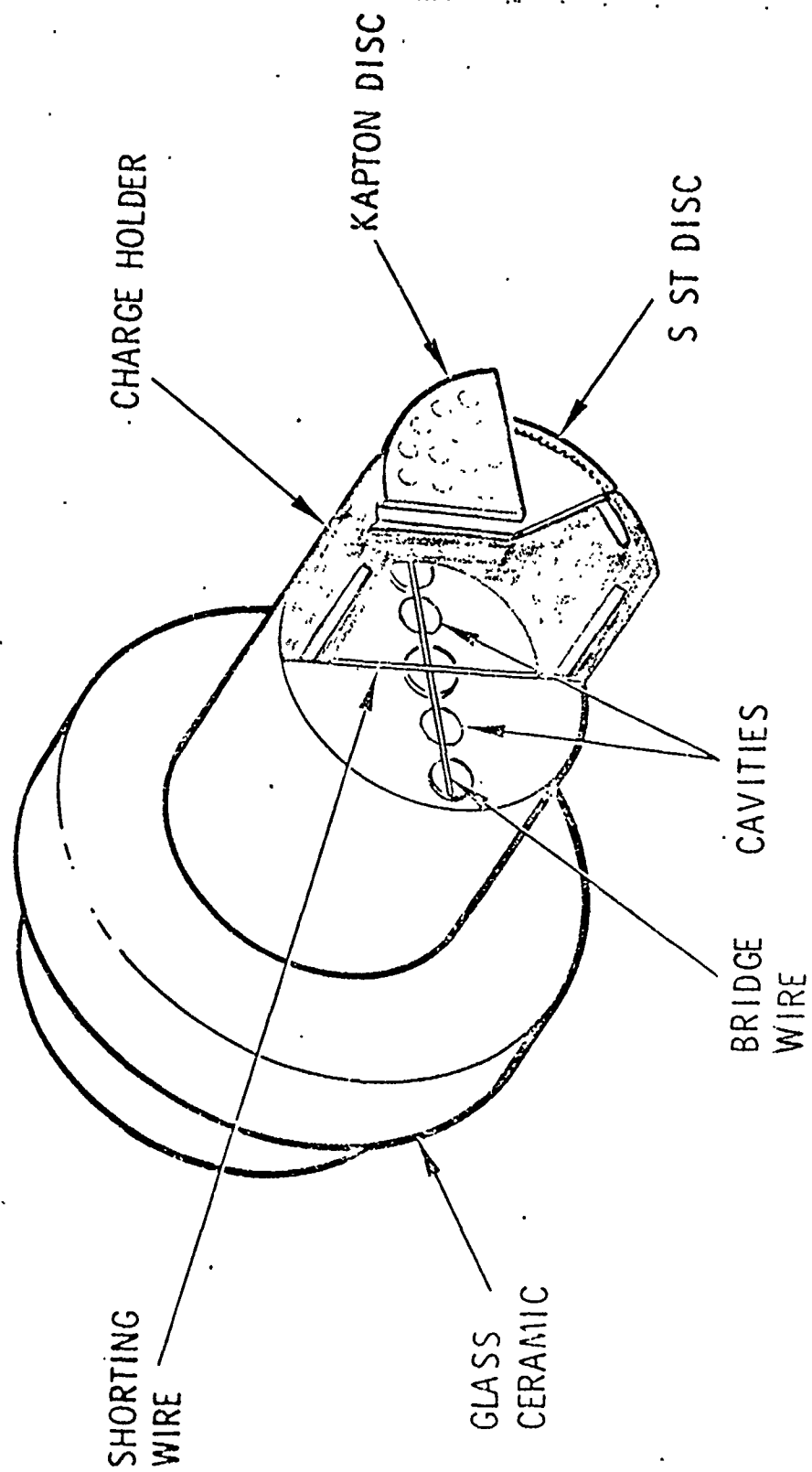
CAVITIES

BRIDGE WIRE

SHORTING WIRE

GLASS CERAMIC

FIGURE 4.

FIGURE 5.

ELECTROSTATIC DISCHARGE (ESD) IGNITION LEVELS[1]

(Material)	Minimum Ignition Levels			All-Fire Ignition Levels		
	Voltage kV	Capacitance pf	Stored Energy[2] mJ	Voltage kV	Capacitance pf	Stored Energy[2] mJ
Ti/KClO$_4$	20	4000	400	20	5000	500
CP	20	1000	100	20	2000	200
NLS	20	600	60	20	1500	150
PbN$_6$	30	600	135	20	2000 – 2500	200 – 250
TiH$_{.65}$/KClO$_4$	20	5000	500	20	5000 – 6000	500 – 600

NOTES:

(1) Determined using a UN-326-E High Voltage Pulse Generator. No series R.

(2) The total stored energy was divided by two (1/4 CV^2) to reflect equal distribution between the two ESD bridges.

POST FLIGHT TEST DATA

GAMMA - MILLIWATTS / °K

FLIGHT TEST 1.

As Manufactured
After Thermal Cycle
After Flight Test
Setback ⟶ 6 units
Spin ⟶ 6 units
Spin ⟵ 3 units
Setback ⟵ 6 units

FLIGHT TEST 2.

As Manufactured
After Thermal Cycle
After Flight Test
Setback ⟶ 6 units
Spin ⟶ 6 units
Spin ⟵ 6 units
Setback ⟵ 6 units
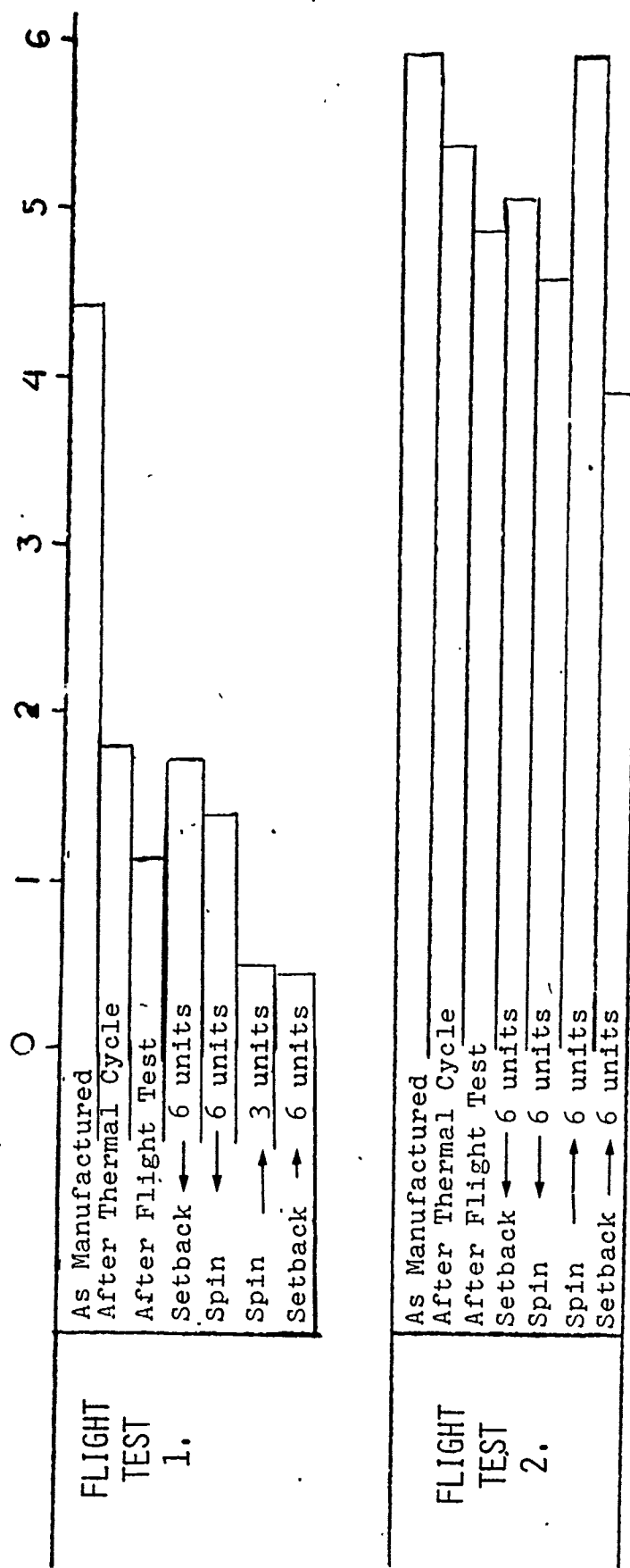
⟶ TOWARDS BRIDGEWIRE

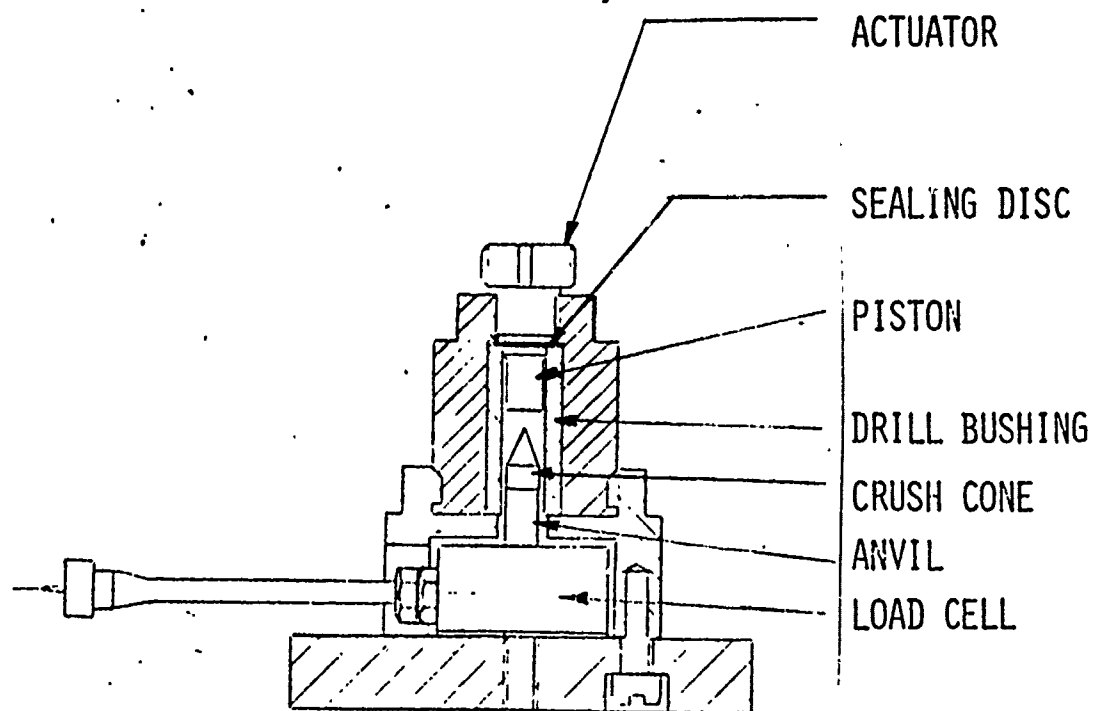⟶ AWAY FROM BRIDGEWIRE

FIGURE 6.

FIGURE 7.

FUNCTIONAL TEST DATA

```
SERIAL NO. 186
AVERAGE CURRENT      =     3.483 AMPERES
INITIATION TIME      =     1.42 MILLISECONDS
INITIATION ENERGY    =    17.96 MILLIJOULES
RES AT FIRE TIME     =     1.07 OHMS
BRIDGE BREAK TIME    =     1.48 MILLISECONDS
MINIM RESISTANCE     =    15.40 OHMS
TIME OF MIN RES      =     2.73 MILLISECONDS
PEAK FORCE           =    18.84 KILONEWTONS
TIME TO PEAK         =    47.6 MICROSECONDS
IMPULSE TO PEAK      =     450 MILLINEWTON-SECONDS
PULSE WIDTH          =    57.6 MICROSECONDS
TOTAL IMPULSE        =     573 MILLINEWTON-SECONDS
```

Typical Analog Oscillograph
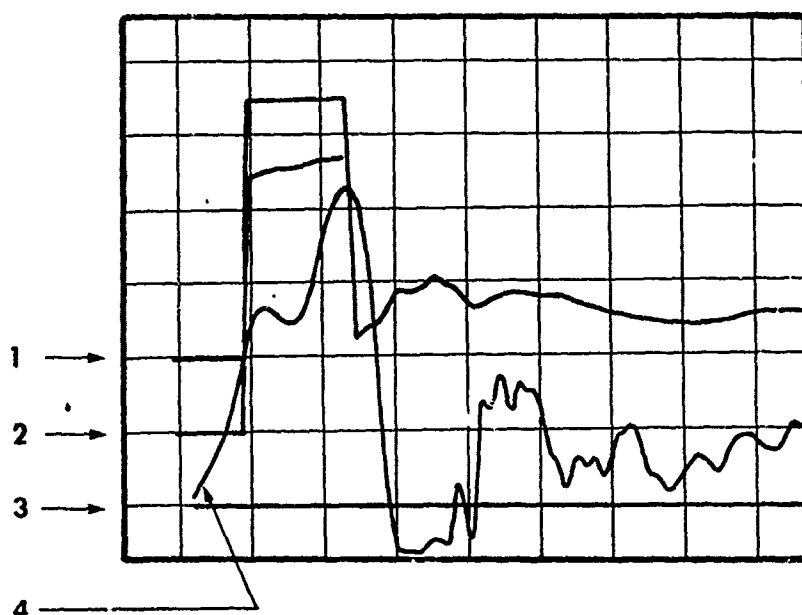
1. Fire Pulse Current; 1 Amp./Div.   1 m sec/Div.

2. Fire Pulse Voltage; 1 Volt/Div.   1 m sec/Div.

3. Load Cell Force Output; 1,000 Lbs/Div.   20 μ sec/Div.

4. Force Rise Stops counter to record time from Initial rise of fire pulse to start of rise of force. (1.486 m sec.)

FIGURE 8.

PERSHING II

REENTRY VEHICLE SEPARATION SYSTEM

by

Edward M. Storma
Martin Marietta Corporation
Orlando, Florida 32805

ABSTRACT

The Pershing II separation system was designed to separate the reentry vehicle from the missile with a high degree of reliability, minimum weight, and low cost. The separation system employs 10 grains/foot linear shaped charge fabricated with HNS-II B explosive in an aluminum sheath. This is initiated with redundant exploding bridgewire detonators. The skin is cut from the inside of the missile, immediately aft of the reentry vehicle.

1.0 INTRODUCTION

Pershing is a United States Army artillery missile with two solid propellant rocket motors. Pershing II incorporated terminal guidance into the reentry vehicle (RV). This paper will deal with the separation system that releases the PII RV.

The primary objectives for the Pershing II separation system were: 1) a high degree of reliability and safety, 2) minimum weight, and 3) low cost. Use of qualified Pershing Ia exploding bridgewire ordnance (EBW), high energy firing unit (HEFU), and high voltage firing cables was also desirable because of their proven reliability and availability in the logistics system.

2.0 PRELIMINARY STUDIES AND DEVELOPMENT TESTS

Preliminary studies early in the PII program indicated that cutting the skin to release the RV was the best selection for a separation system that would meet all of the primary objectives.

Thermal studies (Figure 1) revealed that a maximum temperature of 205°C (402°F) would be experienced by the linear shaped charge. Consequently HNS-IIB (Reference 1) was selected for the explosive charge.

Ten gr/ft HNS-IIB in aluminum sheathed linear shaped charge (ALSC) was selected from test data published by Sandia-Albuquerque (Table I and References 2 and 3) and tapered plate tests conducted at Martin Marietta, Orlando (Figures 2 and 3).

Preliminary development tests determined that initiation through the sheath of ALSC in small grain sizes is not reliable. The reason for these failures is explained by tests that were conducted on the SPRINT program using RDX (Table II). Subsequent end initiation tests verified that end initiation of 10 gr/ft HNS-IIB ALSC would be reliable.

End initiation required that the ALSC be bent inward from the skin. A special tool (Figure 4) was used to prevent distortion of the ALSC, cracking the sheath and breaking the explosive core during bending. Subsequent tests demonstrated that the ALSC would cut a 0.063 inch thick witness plate in the bent section and downstream of the bend (Figures 5 and 6).

Preliminary tests were conducted to determine the effect of the air gap between the end of the EBW detonator and the ends of the ALSC (Figure 7). The results of these tests are shown in Figure 8. These tests verified that an air gap of approximately 0.050 inch would provide an adequate safety margin for ignition. (Air gap Bruceton tests are currently being conducted and will provide data on a larger sample size and a calculated probable reliability.)
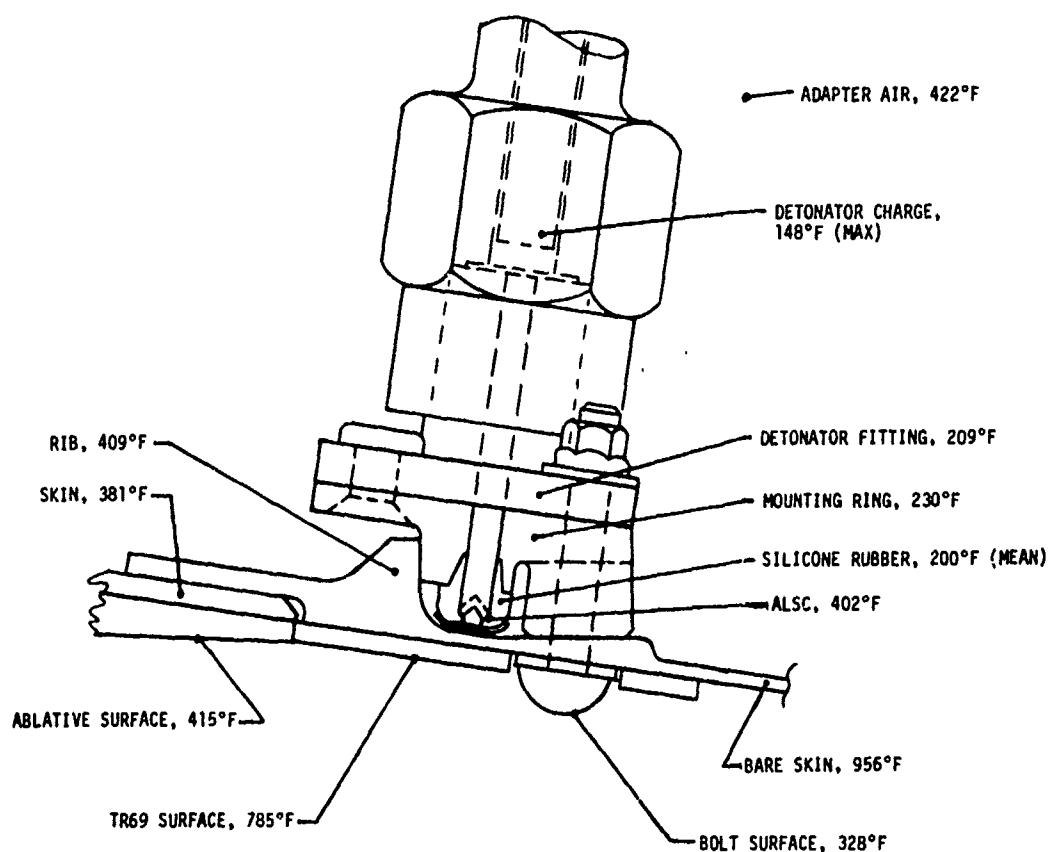
ADAPTER AIR, 422°F

DETONATOR CHARGE, 148°F (MAX)

DETONATOR FITTING, 209°F

MOUNTING RING, 230°F

SILICONE RUBBER, 200°F (MEAN)

ALSC, 402°F

BARE SKIN, 956°F

BOLT SURFACE, 328°F

RIB, 409°F

SKIN, 381°F

ABLATIVE SURFACE, 415°F

TR69 SURFACE, 785°F

Figure 1.   Separation Ring Assembly Temperatures at Burnout

TABLE I

Summary of Performance and Reliability Of
10 Grains/Foot HNS ALSC (Reference 3)

Core Weight (Grains/Foot)	Optimum Standoff To Cut Aluminum 6061-T6 (Inches)	Thickness Of 6061-T6 Aluminum Cut (Inches)	Reliability
7	0.035 - 0.055	0.072	0.99
		0.065	0.999
		0.059	0.9999
10	0.035 - 0.050	0.094	0.99
		0.089	0.999
		0.086	0.9999 (PII)
15	0.035 - 0.055	0.123	0.99
		0.117	0.999
		0.112	0.9999

HNS - Hexanitrostilbene
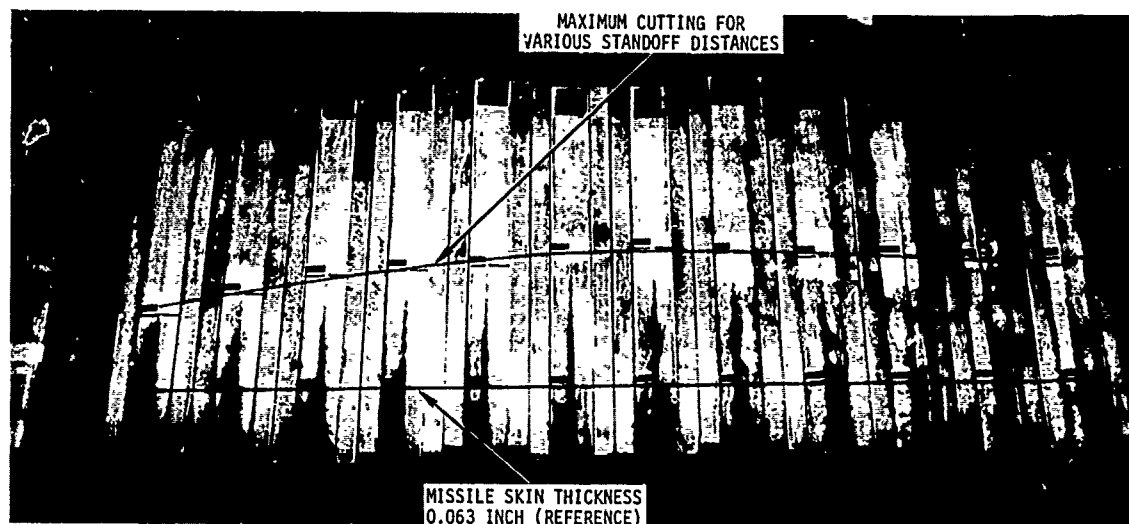ALSC - Aluminum sheathed linear shaped charge

Figure 2. Tapered Plates (2014-T6 Aluminum) Cut by
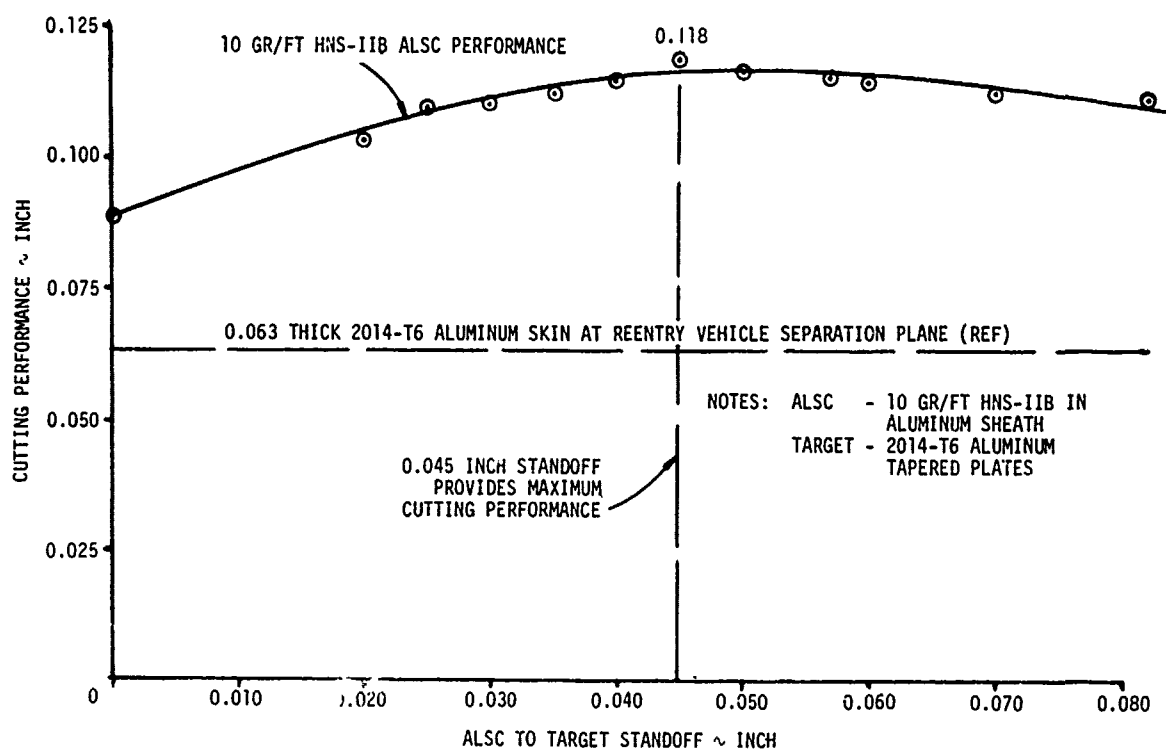10 Gr/Ft HNS-IIB Aluminum Sheathed Linear Shaped Charge

Figure 3. Linear Shaped Charge Cutting Performance
Versus Standoff

583

TABLE II

Results of Through Bulkhead Initiation Tests with RDX
to Determine Explosive Column Length Required
to Attain Nonreversible Ignition
and Constant Detonation Velocities

---

1. Density 0.9 gm/cc (EBW Bridgewire Charge)

    Bridgewire charge required 5.08 mm (0.2 inch) to attain
    constant velocity of 5620 m/s from exploding bridgewire
    stimulus

2. Density 1.55 gm/cc (TBI Doner Charge)

    Donor charge stimulus required 4.32 mm (0.17 inch) to
    attain constant velocity of 0.7800 m/s from EBW charge

3. Density 0.97 gm/cc (Through Bulkhead Initiation Charge)

    Receptor charge required 4.57 mm (0.18 inch) to attain
    constant velocity of 5640 m/s from TBI doner

4. SRI Tests of Induction Length

    1 mm (0.039 inch) is the minimum length required to attain
    nonreversible ignition in an explosive column
    Column length of 1.40 mm (0.055 inch) failed to reach steady
    state velocity
    The 50 percent ignition stimulus level was 8 kilobars

5. Column diameters tested were 4.45 mm (0.175 inch)
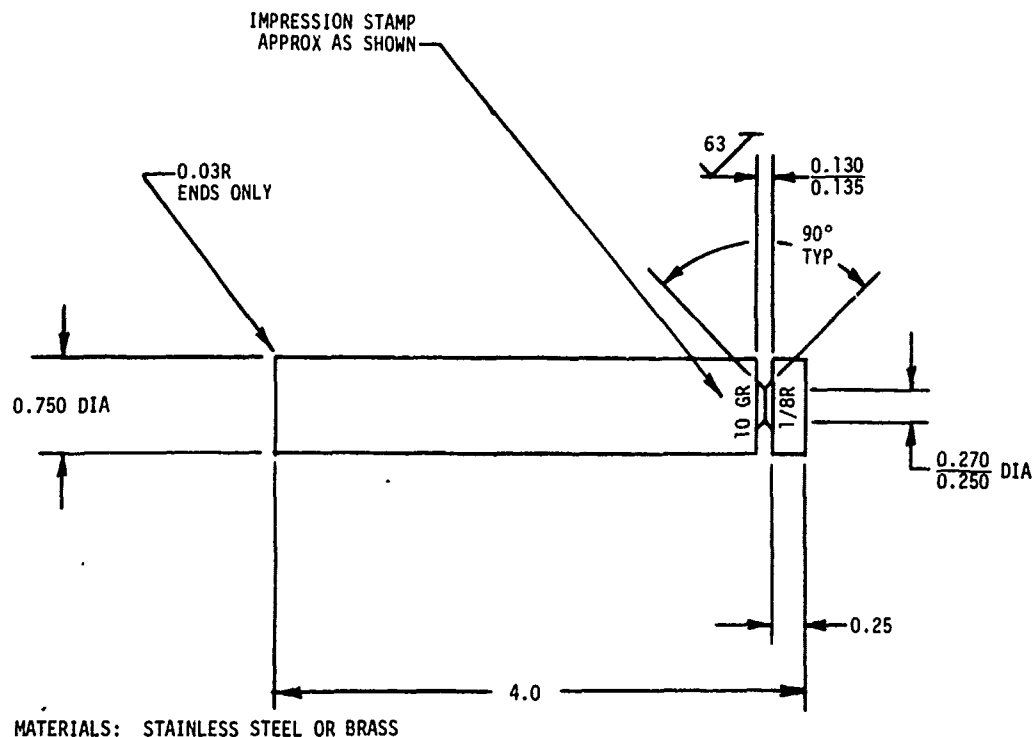

MATERIALS: STAINLESS STEEL OR BRASS

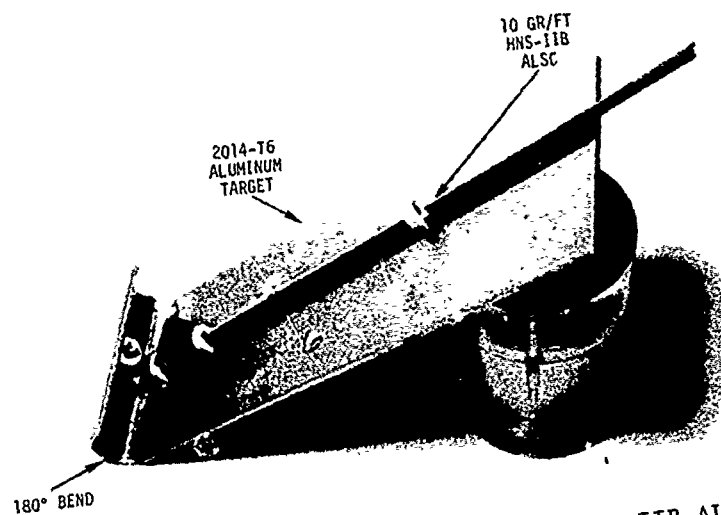Figure 4.   Ten Grains/Foot ALSC Bending Tool

Figure 5. Test Specimen with 10 Gr/Ft HNS-IIB ALSC Formed to 1/8 Inch Bend Radius
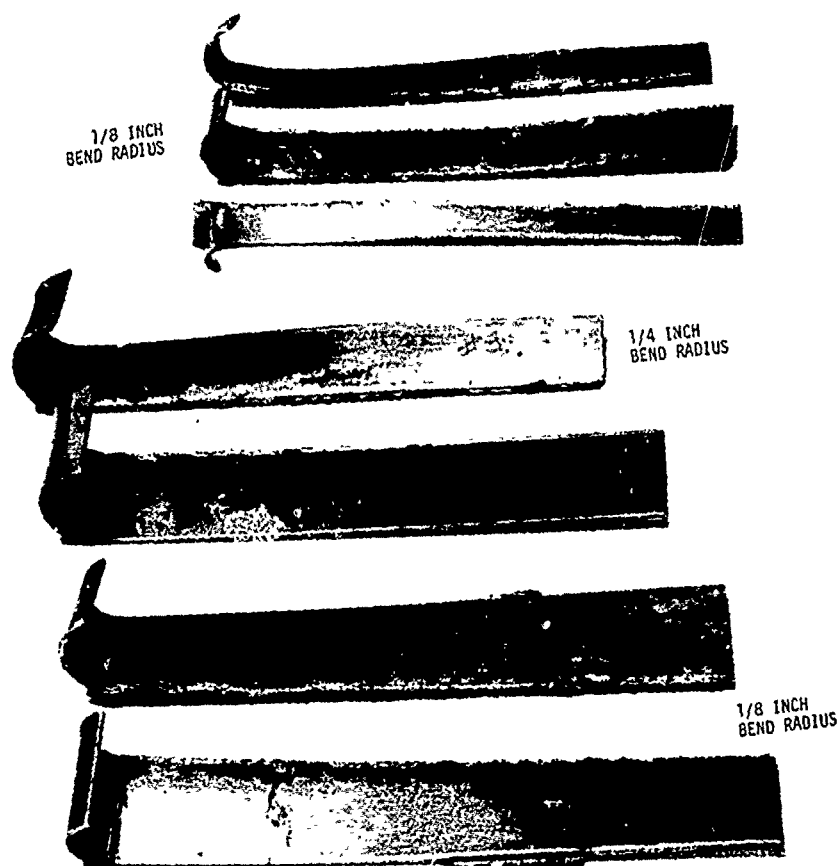

Figure 6. Performance of 10 Gr/Ft HNS-IIB ALSC When Formed to 1/8 and 1/4 Inch Bend Radius
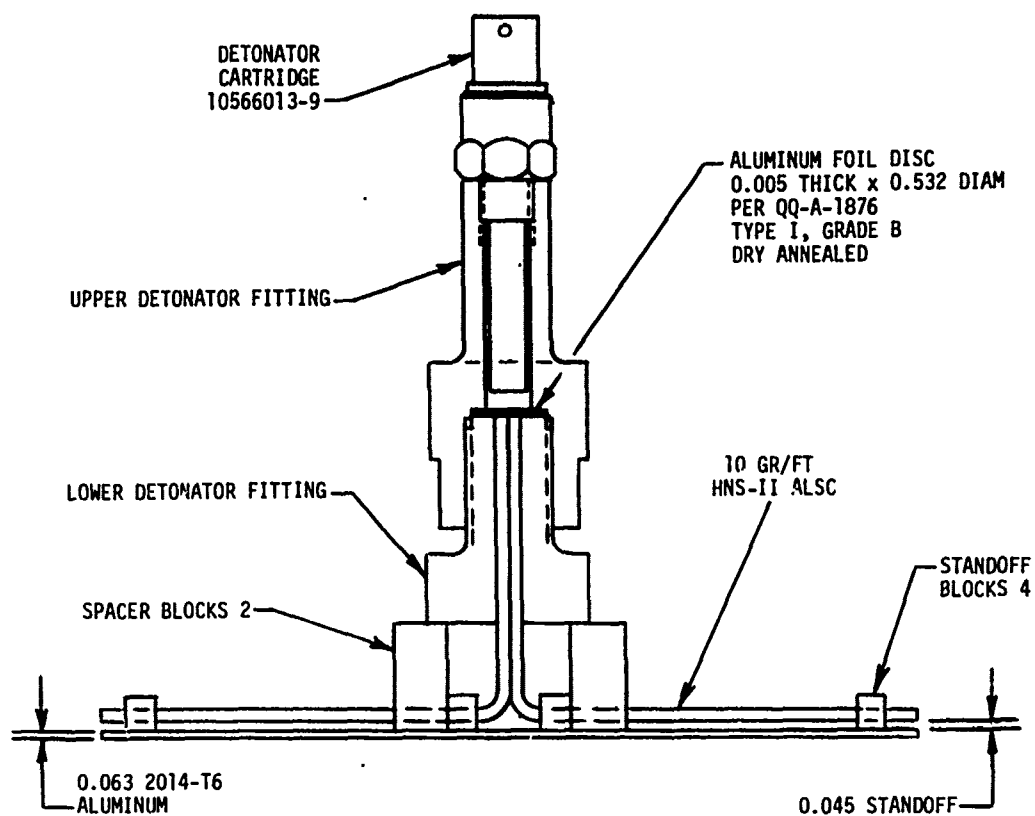
585

Figure 7. Preliminary Air Gap End Initiation Test Setup
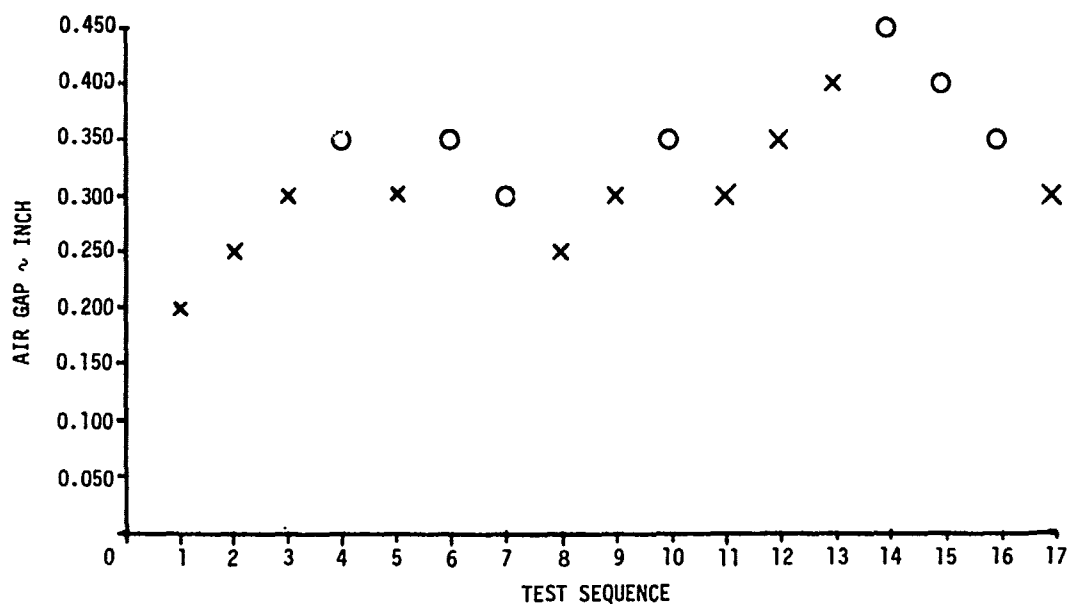
Figure 8. Preliminary Air Gap End Initiation Bruceton

3.0 DESIGN

A separation system design was generated from these studies and tests.
A cross section of the separation ring and missile skin at a detonator fit-
ting is shown in Figure 9. A view looking forward at the same location is
shown in Figure 10. The separation ring with detonators, high energy firing
cables and HEFU is shown in Figure 11.
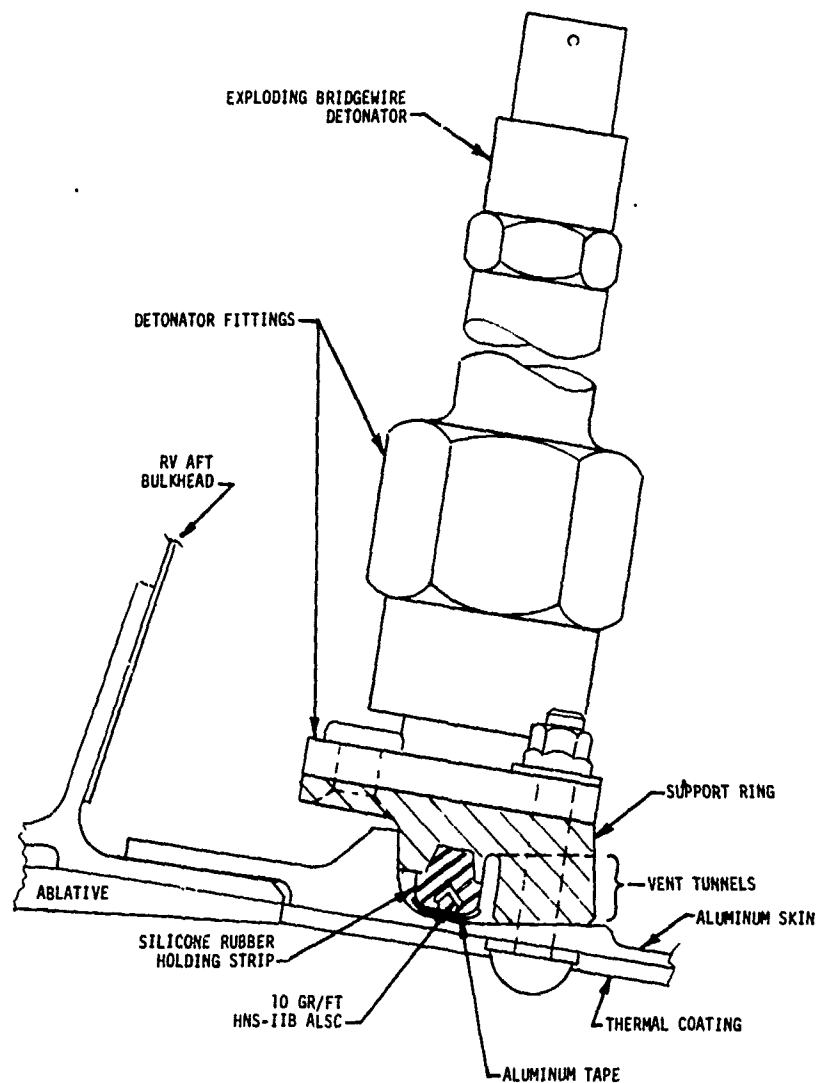
Figure 9. Section Through Separation Ring and Skin
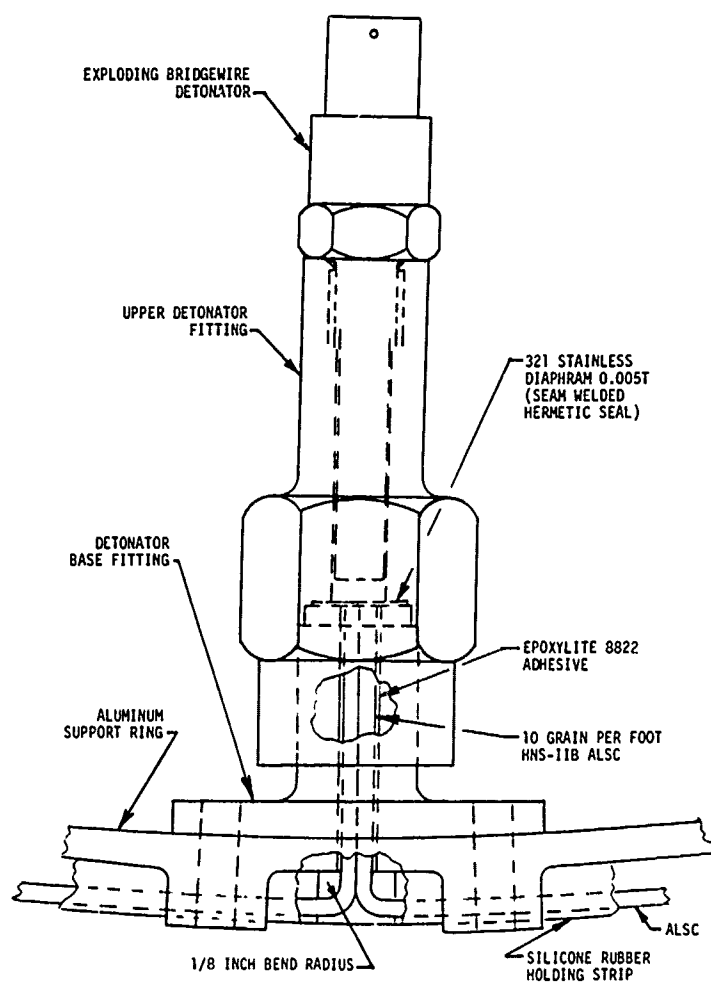
Figure 10. Detonator to ALSC Interface,
View Looking Forward

EXPLODING BRIDGEWIRE
DETONATOR

UPPER DETONATOR
FITTING

321 STAINLESS
DIAPHRAM 0.005T
(SEAM WELDED
HERMETIC SEAL)

DETONATOR
BASE FITTING

EPOXYLITE 8822
ADHESIVE

ALUMINUM
SUPPORT RING

10 GRAIN PER FOOT
HNS-IIB ALSC

1/8 INCH BEND RADIUS

SILICONE RUBBER
HOLDING STRIP

ALSC

SEPARATION RING ASSEMBLY
10 GR/FT HNS-IIB ALSC

EXPLODING BRIDGEWIRE
DETONATORS (2)

HIGH ENERGY
FIRING UNIT

HIGH VOLTAGE
FIRING CABLES

Figure 11. Pershing II Reentry Vehicle Separation System

4.0 ANALYSES

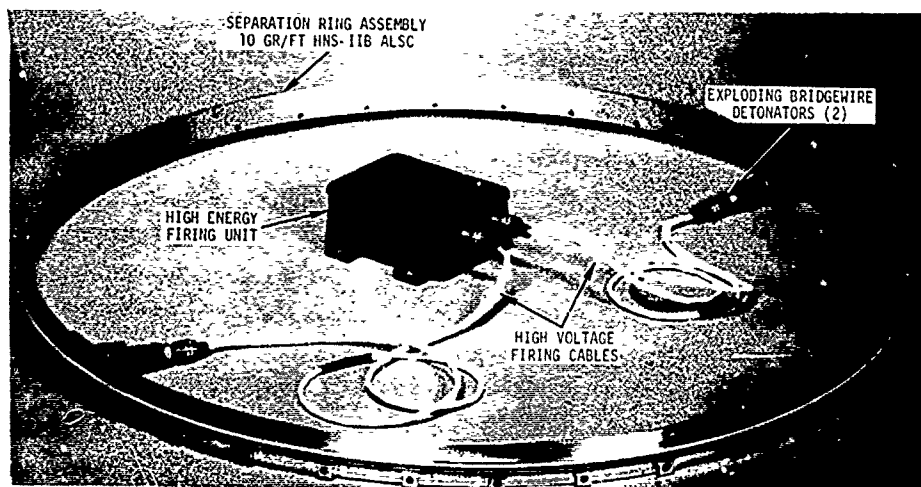A reliability math model was developed and an analysis was conducted on the separation system (Figure 12). The detonator-to-ALSC air gap is not shown but it is expected, based on preliminary test data, that this will be in the order of 0.9999 at 90°C. Consequently the total reliability should remain in the order of 0.9999 at 90 percent confidence as shown in Figure 12.

The HEFU/EBW systems on Pershing Ia have demonstrated a safety of 0.9999. The insensitivity of HNS and the protection provided by the mounting ring and skin will continue to assure a high degree of safety.

The weight of the PIa RV separation system and related structure was 35.962 pounds. In comparison, the PII system weighs 8.28 pounds. This is a savings of 27.682 pounds.
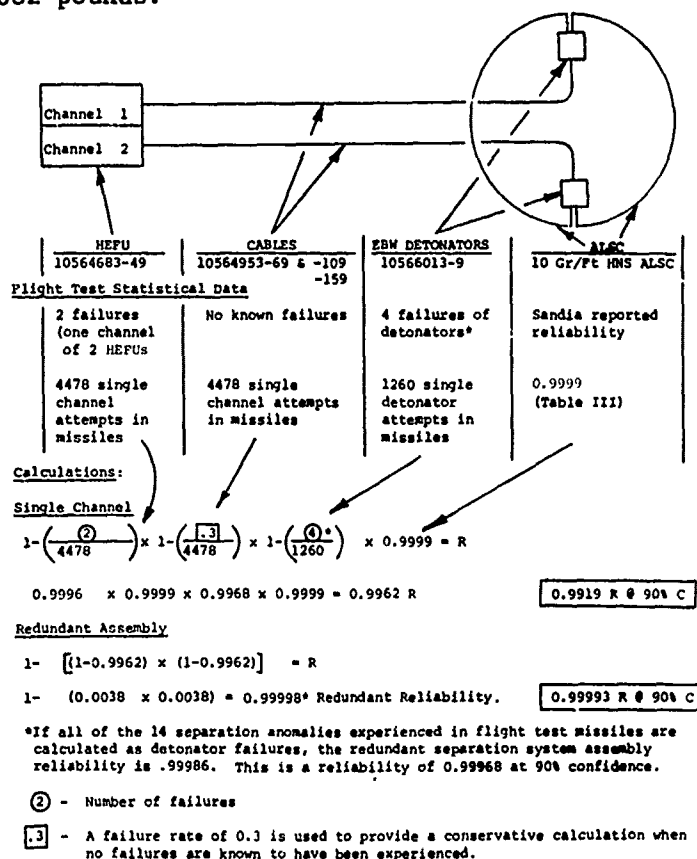

HEFU	CABLES	EBW DETONATORS	ALSC
10564683-49	10564953-69 & -109 -159	10566013-9	10 Gr/Ft HNS ALSC

Flight Test Statistical Data

| 2 failures (one channel of 2 HEFUs | No known failures | 4 failures of detonators* | Sandia reported reliability |
| 4478 single channel attempts in missiles | 4478 single channel attempts in missiles | 1260 single detonator attempts in missiles | 0.9999 (Table III) |

Calculations:

Single Channel

$$1-\left(\frac{②}{4478}\right) \times 1-\left(\frac{\boxed{.3}}{4478}\right) \times 1-\left(\frac{④*}{1260}\right) \times 0.9999 = R$$

0.9996   x 0.9999 x 0.9968 x 0.9999 = 0.9962 R | 0.9919 R @ 90% C |

Redundant Assembly

1- [(1-0.9962) x (1-0.9962)]   = R

1- (0.0038 x 0.0038) = 0.99998* Redundant Reliability. | 0.99993 R @ 90% C |

*If all of the 14 separation anomalies experienced in flight test missiles are calculated as detonator failures, the redundant separation system assembly reliability is .99986. This is a reliability of 0.99968 at 90% confidence.

② - Number of failures

.3 - A failure rate of 0.3 is used to provide a conservative calculation when no failures are known to have been experienced.

Figure 12. Reliability Math Model EBW/LSC Separation System

5.0 SEPARATION SYSTEM TESTS

Four separation tests have been conducted with the separation system Figure 11 in full scale structures. All have cut the skin and separated the RV from the second stage. The shock spectrums recorded in the structure during these tests indicated high amplitudes at high frequencies. These were not damaging to the structure and did not affect the operating equipment within the RV. A typical skin cut is shown in Figures 13 and 14.

Figure 13. Aft End of Prototype Pershing II
Reentry Vehicle Showing Skin Cut By
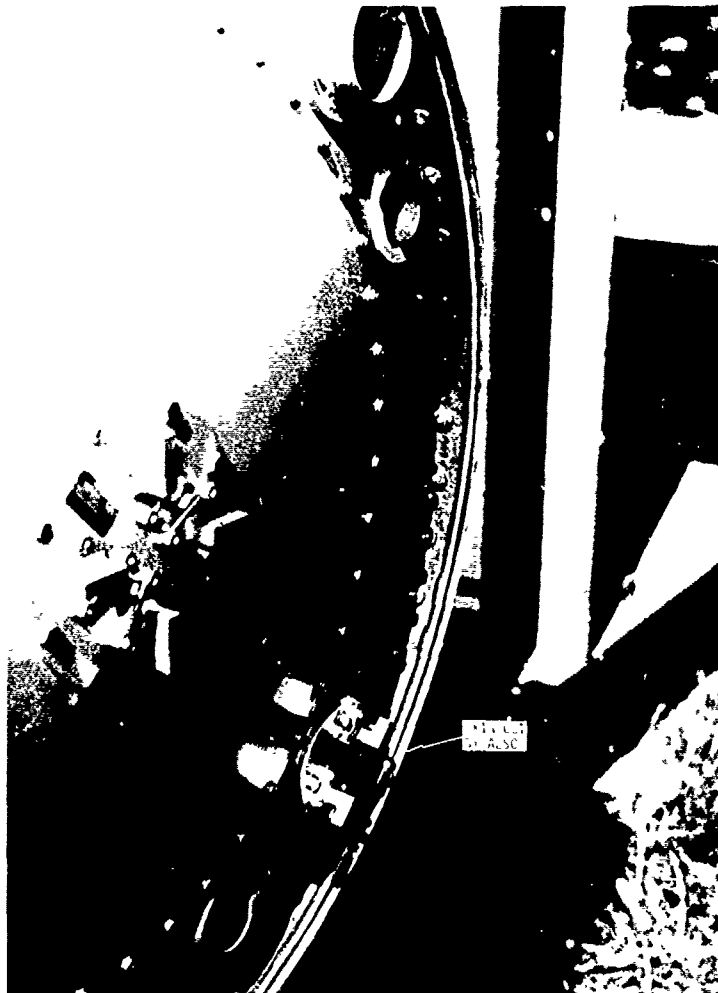10 Gr/Ft HNS-IIB ALSC (Left Side)

Figure 14. Aft End of Prototype Pershing II
Reentry Vehicle Showing Skin Cut by
10 Gr/Ft HNS-IIB ALSC (Right Side)

6.0 CONCLUSIONS

The PII separation system is a reliable, safe, lightweight assembly at a reasonable cost.

REFERENCES

1. NAVWEPS
   Naval Weapon Spec
   WS-5003F

   Hexanitrostilbene

2. Sandia Document
   SC-RR-71 0673
   May 1972

   Application of Hexanitrostilbene (HNS) in Explosive Components

3. Sandia Document
   SC-DR-71 0360
   August 1971

   Development of an Explosively Actuated Payload Separation and Panel Opening System for the High Altitude Test Vehicle

COLORED SMOKE-FLAME

J. E. TANNER and H. A. WEBSTER, III

Applied Sciences Department

Naval Weapons Support Center, Crane, Indiana

ABSTRACT

A yellow smoke-yellow flame formula has been developed. Bismuth oxide as a combustion product colors the smoke, and sodium colors the flame. The composition and its combustion products are much less toxic than lead-based formulas developed earlier, while smoke volume and quality are nearly as good.

INTRODUCTION

A large number of colored display units (smoke and/or flame) are currently in the military inventory. They are used to signal distress, identification, or warning. They are also used as markers of opposing (enemy) elements, or to indicate fuze-action and accuracy of weapons.

The basic requirement for a colored display is a highly visible, unambiguous, easily identifiable mark. Thus, at night a colored flame is generally used, and in daytime a colored smoke.

A single unit may incorporate either or both of flame and smoke. To be prepared for both day and night situations, separate smoke and flame units may be developed, or a single unit incorporating both the smoke and the flame may be devised. The advantage of the separate units is longer burn time for a given total size. The disadvantage is the necessity of stocking and handling two types of units.

Both smoke and flame may be incorporated into a single unit either in the form of separate smoke and flare compositions, or in the form of a single composition which produces both the desired smoke and the desired flame.

The advantage of separate smoke and flame compositions is that each may be optimized for the quality and quantity of its output. When the separate compositions are incorporated into a single unit there are usually problems of interference--if both are ignited simultaneously the flame may ignite the smoke. Or if the smoke is ignited first, the residual clinker may degrade the flame which follows. If smoke and flame are ignited independently out opposite ends of the unit then twice as much ignition hardware is required, and there may also be inadvertent ignition of the wrong end. In any case, spacers are required to keep the compositions apart, and the unneeded half, is in practice wasted, even if not used. Therefore if a composition could be developed which produced both a colored smoke and colored flame simultaneously many of the disadvantages now associated with day and night signaling would obviously be eliminated. Several years ago, Shaw and Reed of Thiokol Chemical Corporation, Wasatch Division, demonstrated several simultaneous smoke/flame compositions and investigated many others for the Air Force.[1] The signals developed included red flame/white smoke, red flame/red smoke and yellow flame/orange smoke. The work was quite well done and the feasibility of producing simultaneous smoke/flame compositions was demonstrated in some cases. However the direction of the program was such that few of the compositions were ever carried beyond an initial investigation.

The Thiokol yellow smoke/yellow flame combinations contained lead, and its oxides or iodides, plus an alkali perchlorate, along with a high-oxygen content polyster binder. In an effort to overcome some

of the limitations (especially toxicity) of the lead-based smoke, we have considered other heavy metal oxides and halides. Bismuth trioxide (Bi_2O_3) was selected because it has a yellow crystalline form, and the bismuth oxyiodide had been made in the pyrotechnic smoke/flames at Thiokol[1], indicating that production of the bismuth oxide should be possible.

The formulas for a yellow smoke/yellow flame based on a yellow bismuth trioxide smoke are given in Table 1. Initially, hydrated bismuth nitrate, $Bi(NO_3)_3 \cdot 5H_2O$, was used as the oxidizer, and magnesium as the fuel. These flares ignited spontaneously within minutes after pressing. Later laboratory experiments showed that a magnesium-water or magnesium-nitric acid reaction occurred which generated sufficient heat to ignite the epoxy binder and, subsequently, the remaining magnesium in the system. Consequently, all the formulas in Table 1 use bismuth subnitrate ($BiONO_3 \cdot H_2O$) as the oxidizer. Sensitivity tests (friction, impact and electrostatic) were performed on all formulas without added binder, and all were found to be relatively insensitive. A small amount of water added to each formula caused no observable reaction. There were no problems encountered in the subsequent mixing and pressing operations.

The bismuth subnitrate was used as received from the manufacturer with no drying. The magnesium was gran 18 (30/50) in all formulas except YY20 which used gran 16 (200/325). The bismuth used in YY21-YY23 was 99.5% purity and 100 mesh. The silicon used in YY24-YY26 was MIL-S-230A, Grade 1, Class B. The binder used in all formulas was a mixture of 70% DER 321 and 30% DEH 14[R], obtained from Dow Chemical Company.

After mixing, one hundred and fifty grams of composition were pressed into 4.35 cm id fishpaper tubes. The tubes had been coated with binder twenty-four hours prior to pressing. The pressing pressure was 5.7×10^7 N/m^2 (8300 psi). The overall candle length was 3.8 cm. Approximately 20 grams of fireclay were pressed on one end of the candle and 10 grams of ignition composition were pressed on the other end.

TESTING

The smoke/flame candles were tested outdoors under a variety of weather conditions. In most cases testing was done on days when the relative humidity was high; usually greater than 85%. This was done purposely to insure that the smokes produced would not lose their color due to hydrolysis of the smoke particles. Some tests were also conducted at lower humidity. Ambient temperatures during the different tests ranged from 6°C (43°F) to 35°C (95°F).

The flares were burned face-up in a static environment. A standard
yellow organic dye smoke was usually burned for a color comparison. The
data taken included burning times and a visual estimate of smoke color
and volume, and flame color and intensity. The tests were recorded
using both still and motion picture photography. No attempt was made
to quantitatively measure flame color or candlepower.

RESULTS

The results of these studies are summarized in Table 1. The burning
rate for each composition is tabulated, as are the observations on smoke
and flame color and smoke volume. Formulas YY20, YY27, and YY30, con-
taining magnesium, bismuth subnitrate, epoxy (and optionally celite),
produced good smoke color and flame color. The smoke volume of YY27
was not quite as good as the other two. YY20 burned a little too
vigorously for most uses.

The formulas YY28 and YY29 were similar in composition except for
much less magnesium, and except for the presence of a little sodium
nitrate in YY29. Both formulas yielded poor smoke color and volume.

When silicon was used as a fuel in place of magnesium, formulas
YY24, YY25, and YY26, the burning was much less vigorous. Luminous
output was estimated as less than 1000 cp. The best smoke of this
series, from YY24, had an acceptable yellow color, but not a good
volume. Smoke from the other two formulas was essentially white.

The use of metallic bismuth as a fuel resulted in formulas which
did not burn at all. In summary, YY30 produced the best smoke and
flame.

CONCLUSIONS AND RECOMMENDATIONS

A series of yellow smoke/yellow flame compositions were demonstrated
using bismuth subnitrate as the oxidizer. The yellow smokes produced
by these formulas were a much lighter yellow color and did not have the
volume produced by the lead iodide smokes. These formulas do have the
advantages of being less toxic than the lead compounds and insensitive
to humidity problems. The best yellow smoke/yellow flame was produced
by a composition containing 10% magnesium, 80% bismuth subnitrate, 5%
diatomaceous earth and 5% epoxy binder. The burning rate of this com-
position was 0.073 cm/s (0.029 in/s). Compositions were also demonstrated
which used silicon as the fuel instead of magnesium. The yellow bismuth
oxide smoke was formed but the volume was much less than the volume pro-
duced by the compositions containing magnesium.

No further experimental work is anticipated on these yellow smoke/
yellow flame compositions at this time. Any additional work on adjustment
of burning rate, volume and color of smoke, and flame intensity should be

done when specific applications and requirements are available. It is recommended that these compositions be considered for use in any new signal requiring a yellow smoke/yellow flame or in product improvement of existing signals. The advantages and cost-savings associated with the use of a single smoke/flame composition make it essential that this concept be heavily considered in any marking or signaling unit requiring a day and night capability.

ACKNOWLEDGEMENT

REFERENCE

1. G. C. Shaw and R. Reed, Jr., Smoke/Flame Pyrotechnics in Proceedings Third International Pyrotechnics Seminar held at Colorado Springs, Colorado, 21-25 August 1972. (Sponsored by Denver Research Institute, Denver, Colorado), Available DDC--AD913408L. Available DDC indicates the document may be obtained from Defense Documentation Center, Cameron Station, Alexandria, Virginia 22314.

TABLE 1. BISMUTH TRIOXIDE SMOKE/FLAME COMPOSITIONS

	YY20	YY21	YY22	YY23	YY24	YY25	YY26	YY27	YY28	YY29	YY30
Bi	--	10	30	10	--	--	--	--	--	--	--
Si	--	--	--	--	10	30	10	--	--	--	--
Mg	14	--	--	--	--	--	--	10	5	5	10
Bismuth Subnitrate	68	85	65	80	85	65	80	85	90	85	80
Sodium Nitrate	--	--	--	5	--	--	5	--	--	5	--
Celite	5	--	--	--	--	--	--	--	--	--	5
Binder	13	5	5	5	5	5	5	5	5	5	5
Burn Rate (cm/s)	.11	NB	NB	NB	.079	.111	.069	.069	.038	.042	.073
Smoke Color	Yellow/ White	--	--	--	Light Yellow	Yellow/ White	Almost White	Light Yellow	White	White	Light** Yellow
Smoke Volume	Excellent	Excellent --	--	--	Fair	Poor	Fair	Good	Poor	Poor	Excellent
Flame Color	Yellow Very Vigorous	-- Very Vigorous	--	--	Weak Yellow	Yellow	Yellow	Yellow	White Yellow	Yellow*	Yellow

* Best flame color
**Best smoke color and volume

The classification of pyrotechnic compositions and articles according to their safety hazard

by Dr. Hartwig Treumann[+]

Contents

(1) Introduction

(2) The classification for the field of production, working, processing and recovery of pyrotechnic products

(3) The classification with respect to storage

(4) The classification with respect to use and to transfer to other persons

(5) The classification with respect to transport

(6) Abstract

(1) Introduction

In the Federal Republic of Germany a number of laws and regulations control handling, commerce and transportation of pyrotechnic compositions and articles. The term "handling" as defined in the "Law on Dangerously Explodable Substances (Explosives' Law)" [1] comprises - among others - the production, working, processing, recovery, storage, use, destruction of pyrotechnic compositions and articles as well as their transportation, transfer to others and receipt within the works.

Most of these laws and regulations divide the pyrotechnic compositions and articles into groups of different safety hazards. This procedure allows to issue the necessary regulations against the specific safety hazards as well as to

---

[+] Bundesanstalt für Materialprüfung (BAM) Berlin

avoid unnecessary hindrance to manufacturers and users. The advantage gained is partly abolished by the fact that the laws and regulations use different criteria for the classification of the activities mentioned above and often prescribe different test methods for the determination of the hazard degree. Consequently, a manufacturer or importer of pyrotechnics - besides of the necessary competence - must have a considerable knowledge of the pertinent legal prescriptions and prove that knowledge during an examination.

In the following the principal classifications used will be discussed in order to aid in the reduction of barriers against the importation of pyrotechnic products into the Federal Republic of Germany. But it must be pointed out that because of the limited scope of this contribution the topic cannot be dealt with completely.

(2)   The classification for the field of production, working, processing and recovery of pyrotechnic products

This field is controlled by the "Regulations for the Prevention of Accidents 46 k. Production of Pyrotechnic Articles" issued by the accident insurance of the chemical industry (= Berufsgenossenschaft der chemischen Industrie) [2] .

This regulation divides the pyrotechnic composition into two parts: part one admitted to production, part two excluded from production.

Not allowed is the production of the following compositions:

- sulphur containing free acid or containing more than 0,1 % incombustible components

- flowers of sulphur

- spoilt or acid adhesive, for example acid artificial shellac or acid beechwood pitch

- potassium chlorate containing more than 0,15 % Bromine (calculated from content of bromate)

- powdered light-metals containing more than 0,25 % grease

- white phosphorus

- chlorates in combination with metals or antimony sulfides or potassium hexacyanoferrate(II)

- chlorates for report compositions mixed in the dry state

- chlorates in combination with ammonium salts (exception: mixtures of ammonium chloride with potassium chlorate)

The **permitted** pyrotechnic articles - according to their sensitivity against friction and ignition and their explosive effect (of the loose powders) - are divided into four hazard groups listed below. The amount of composition permitted in the manufacturing area or -buildings as well as the number of people permitted to be employed in these buildings is determined by four groups:

group 1 (most dangerous compositions):

whistle compositions, perchlorate-metal compositions, zirconium compositions, photoflash compositions if they contain zirconium or peroxides, nitrocellulose with 12 - 12,6 % N (with less than 35 % humidity per weight)

group 2 dry chlorate compositions containing more than 65 % chlorate, report compositions containing nitrate (and aluminium and sulphur)

group 3 nitrate-powdered metal compositions (exception: report compositions containing nitrate), wet chlorate compositions containing more than 65 % chlorate, dry chlorate compositions containing 35 - 65 % chlorate, black powder

<u>group 4</u> torches, wet bengals and the like containing up to
65 % chlorate, dry chlorate compositions containing
less than 35 % chlorate, wet or phlegmatized nitrate-
aluminium compositions, coloured and white smokes

The pyrotechnic articles and the intermediate stages during
their production are assigned to the corresponding composi-
tion groups.

Besides of the group number one has to specify whether the
pyrotechnic composition or article is "open", "covered" or
"packed for transport"; the "open" compositions are subdi-
vided into "loose" ones (that are powders dry or wet) and
"shaped" ones (e.g. by pressing).

The 3 terms characterizing the wrapping are defined as fol-
lows: an "<u>open</u>" composition has no wrapping at all or an in-
complete one. A "<u>covered</u>" composition is wrapped up either
completely or up to the opening for the ignition (e.g. filled
in a tube of paper or cardboard or metal). A composition
"<u>packed for transport</u>" has to be enclosed in an officially
approved kind of package.

(3)   <u>The classification with respect to storage</u>

The conditions for the storage of pyrotechnic compositions
and articles are described in the "Second Ordnance to the
Explosives' Law" [3] . This ordnance divides the pyrotechnic
compositions and articles according to their safety hazard
into four groups. But this time the decisive aspects are the
behaviour of the pyrotechnic compositions (or substances resp.)
and articles - packed for transport - during burning, defla-
gration or detonation and the resulting hazards. From the
storage group follow certain demands for safety e.g. the mi-
nimum permissible distances between the storage and the en-

dangered object.

storage group 1

These substances and articles can react in a mass explosion. The surroundings are endangered through pressure (blast waves), flames, fragments and debris. Thick-walled articles or articles with more than 60 mm diameter (= articles of large calibre) give rise to an additional hazard by heavy fragments. The **amount** of explosive material determines the severity of the damages and the extent of the damaged area.

storage group 2

Substances and articles of that group do not react in a mass explosion. Whereas at the beginning of the fire only single articles explode, the number of simultaneously exploding articles increases during its course. The pressure effect (blast waves) of the explosions is limited to the immediate surroundings; the surrounding buildings are only slightly damaged if at all. The far surroundings are endangered by light fragments and firebrands. Projected articles are able to explode upon impact and in this way propagate fire or explosion. Thick-walled articles or articles with more than 60 mm diameter (= articles of large calibre) give rise to an additional hazard by heavy fragments.

storage group 3

Substances and articles of that group do not react in a mass explosion. They burn up with great violence, producing strong heat. The fire spreads quickly. The surroundings are mainly endangered by flames, radiant heat and burning fragments. Articles can explode sporadically, single burning packages or articles may be projected. The hazard to the surroundings caused by fragments is small. In general, the

buildings in the surroundings are not endangered by pressure
effects (blast waves).

storage group 4

The substances and articles of that group do not repre-
sent a significant hazard. When they burn up single articles
may explode. The effects are mainly limited to the package.
No fragments hazardous by their size or range of flight are
produced. Burning does not cause explosion of the total con-
tent of a package.

(4) **The classification with respect to use and to transfer
to other persons**

The regulations concerning these topics are - with few ex-
ceptions - found in the "First Ordnance to the Explosives'
Law" [4] which divides the pyrotechnic compositions and ar-
ticles into 3 groups.

group 1   comprises those pyrotechnic compositions and ar-
           ticles which are not dangerously explodable. This
           group is economically unimportant; approval (see
           groups 2 and 3) is not required.

groups 2   contain the dangerously explodable compositions and
and 3   articles. To the less dangerous products of group 2
           "approval" can be granted. That is, they can be
           used if - as the "Explosives' Law" [1] demands -
           BAM (the Federal Institute of Materials' Testing)
           has examined and approved them.

group 3   To the products of group 3 approval cannot be
           granted. This group contains, to begin with, the
           compositions and articles of part 2 of paragraph 2,
           the production of which is prohibited. Next, the

following products are also included into that group

- compositions which undergo spontaneous ignition

- compositions of pyrotechnic articles and the articles themselves if storage at 50 $^\circ$C during four weeks causes alterations entailing increased hazard

pyrotechnic articles

- which when employed according to the directions of use, cannot be handled safely

- which lose their safety of handling during the normal stresses of use and commerce

- which are not sufficiently protected against inadvertent ignition

- which do not clearly show the type and point of ignition

group 2   is represented by those compositions and articles which can be approved. Approval will be granted if

- the compositions and articles when employed according to their directions of use will guarantee protection of life, health or property of employees or third parties

- the compositions and articles meet certain requirements for composition, structure and designation (see figures 2, 3, 4)

- the compositions and articles with regard to their mode of action, to usefulness and stability correspond to the respective "state of the art"

- the applicant because of his operational equipment or for any other reason is in a position to ensure that the composition and structure of the compositions and articles routinely manufactured comply with the

approved specimen.

figure 1

(4)   Use and transfer to others

group 1

|

compositions
and articles

not |
dangerously
explodable

group 2

|

compositions
and articles

|

dangerously
explodable

|

approval
possible

group 3

|

compositions
and articles

|

dangerously
explodable

|

approval
impossible

compositions   articles

articles
except
pyrotechnic
ammunition

pyrotechnic
ammunition
(incl.rocket
ammunition)

enter-
tainment

technical
use

PI PII PIII PIV PT_1 PT_2 PMI PMII

The pyrotechnic compositions within group 2 are not
further subdivided. But the pyrotechnic articles
must be divided into two types: those which are
fired from small arms (the "pyrotechnic ammunition")
and all the other ones except pyrotechnic ammunition.
As mentioned in the beginning of paragraph 4 the

606

First Ordnance of the Explosives' Law states the regulations for the articles except pyrotechnic ammunition; but the pyrotechnic ammunition - including that rocket ammunition which contains a pyrotechnic composition - is under control of the Weapons' Law [5] . According to the safety hazard the pyrotechnic ammunition is separated into the classes PMI and PMII, each with its own regulations with respect to sale.

class PMI comprises that pyrotechnical ammunition which

- does not contain report composition

- does not contain more than 10 g of pyrotechnic composition plus propellant

- which does not rise higher than 100 metres

- which upon inadvertent ignition does not produce sharp-edged fragments

- which does not undergo explosion upon fire or impact

If one of these requirements is not fulfilled, the pyrotechnic ammunition is assigned to class IMII.

The pyrotechnic compositions contained in the pyrotechnic ammunition are either admitted to production (see paragraph 2 part 1) or excluded from production (see paragraph 2 part 2)

The pyrotechnic articles controlled by the Explosives' Law are subdivided according to their purpose into those used for entertainment and those used for technical purposes.

According to their safety hazard the pyrotechnic
articles used for entertainment belong to the four
divisions <u>PI - PIV</u>, those for technical purposes to
divisions PT_1 and PT_2. This classification is ne-
cessary since the users of pyrotechnic articles
have to fulfill different requirements. In the
table below is shown which group of people is
allowed to use which group of pyrotechnic articles:

figure 2

	hazard division	requirement
PI	: toy fireworks	older than 6 years
PII	: small fireworks	older than 18 years
PIII	: medium sized fireworks	proof of basic competence
PIV	: exhibition fireworks	proof of considerable competence
PT_1	pyrotechnic articles for technical purposes	older than 18 years
PT_2		proof of specific competence

The hazard divisions lay down the permissible amounts
of composition contained in the articles as well as
the article's characteristics of structure influen-
cing its safety hazard. Because of the extremely de-
tailed regulations, only a few examples can be given.

figure 3

division	permissible amount of composition	permissible amount of report composition	
PI	3 g	nitrocellulose or phosphorus-chlorate composition	0,5 g 7,5 mg
PII	50 g	black powder chlorate composition or perchlorate composition }	10 g 10 mg
PIII	250 g		50 g

Pyrotechnic articles for entertainment exhibiting greater safety hazard than the divisions I, II, III constitute division IV.

Pyrotechnic articles for technical purposes are classified as in

figure 4

division	purpose	maximum amount of composition	maximum burning time	structure required
PT$_1$	production of white or coloured smoke	1 kg	600 s/kg	explosion must not produce heavy or sharp-edged debris
	flares and torches used as signals	0,5 kg	60 s/kg	
	sound production	10g blackpowder		
	irritants, pesticides, plant protective agents	1 kg	600 s/kg	

Pyrotechnic articles for technical purposes which are more hazardous than those of division PT$_1$, belong to division PT$_2$.

(5) The classification with respect to transport

The regulations concerning the transport of pyrotechnic compositions and articles are complex, since they vary according to the means of transportation as well as according to the range of validity. This state of affairs is illustrated by the following table:

figure 5

transport per	valid in:	
	Fed.Rep. of Germany	all countries (resp. Europe)
Rail	Anlage C zur EVO [6]	RID [7]
Road	GefahrgutVStr [8]	ADR [9]
Inland navigation	ADN (Rhein) [10]	ADN [11]
Sea	SFO [12]	IMDG [13]
Air	IATA [14]	IATA [14]

The international regulations for the transport of dangerous goods per sea or air will not be discussed here, since they are also valid for the Federal Republic of Germany. The other regulations have all a similar structure. The pyrotechnic compositions and articles in the condition and form in which they are offered for transportation are assigned to class I; that is to class Ia (explosive materials and articles), Ib (articles containing explosives) and Ic (matches, fireworks and similar products). In the field of pyrotechnic, class Ia comprises pyrotechnic compositions, class Ib pyrotechnic articles and class Ic pyrotechnic compositions as well as articles.

With respect to safety hazard one has to distinguish four groups.

group 1   Pyrotechnic compositions and articles represent <u>no</u>
          safety hazard and are not subject to transport regu-
          lations if

          - ignition by flames does not cause explosion and

          - sensitivity against impact or friction is not
            greater than that of dinitrobenzene

group 2   Pyrotechnic products are controlled by the regula-
          tions of class Ic if

          - they are designed, arranged and distributed in
            such a way that neither friction nor shock nor im-
            pact nor ignition by flame of the packed composi-
            tion or article will cause explosion of the entire
            load of the package

          - stability is not diminished by a four weeks' stor-
            age at 50 $^{\circ}$C

          - the chemical composition of some pyrotechnic com-
            positions complies with certain restrictions (e.g.
            ignition compositions must not contain chlorate)

group 3   Pyrotechnic compositions are controlled by the regu-
          lations of class Ia and pyrotechnic articles by
          those of class Ib if

          - they are capable of mass explosion

group 4   Pyrotechnic composition; and articles are so danger-
          ous that transport is prohibited.

The classes Ia, Ib and Ic contain several <u>subclasses</u> depending
on the chemical properties of the ingredients of the pyro-
technical compositions. Because of these different chemical
properties of the subclasses no uniform demarcation between
the groups 3 and 4 is possible. To each subclass applies a

specific limit beyond which group 4 is assigned.

Compositions containing chlorate, for example, will be excluded from transport if they are more sensitive against impact, friction and ignition by flame than an explosive of the following composition:

potassium chlorate	80 %
dinitrotoluene	10 %
trinitrotoluene	5 %
castor oil	4 %
wood meal	1 %

To make things worse, it must be mentioned that even the subclasses are further divided in order to provide for different types of packages, maximum amount of explosive per package and for special transport regulations.

(6) Abstract

In the Federal Republic of Germany there exist laws and regulations concerning the production, working, processing, recovery, storage, use, destruction as well as transportation of pyrotechnic compositions and articles. All these laws and regulations contain classifications of pyrotechnic compositions and articles according to their safety hazard. Since these classifications apply to different activities controlled by their own laws and regulations, a confusing abundance of schemes arises for the classification of pyrotechnic compositions and articles according to their safety hazard.

In the paper presented an attempt is made to give a survey over these classification schemes. Because of better perspicuity some classifications considering technological aspects or being of minor importance were deliberately omitted.

References

[1] Gesetz über explosionsgefährliche   SprengG
    Stoffe (Sprengstoffgesetz) vom 13.9.1976

[2] Unfallverhütungsvorschrift 46 k. Her-   UVV 46 k
    stellung pyrotechnischer Gegenstände
    1954

[3] Zweite Verordnung zum Sprengstoffgesetz   2.SprengV
    vom 23.11.1977

[4] Erste Verordnung zum Sprengstoffgesetz   1.SprengV
    vom 23.11.1977

[5] Waffengesetz vom 6.3.1976   WaffG

[6] Anlage C zur Eisenbahn-Verkehrsordnung   Anl.C zur EVO
    in der Fassung vom 1.9.1976

[7] Règlement International concernant le   RID
    transport des marchandises Dangereuses
    par chemins de fer   1977

[8] Verordnung über die Beförderung gefähr-   GefahrgutVStr
    licher Güter auf der Straße mit Anla-
    gen A und B vom 10.5.1973

[9] Accord européen relatif au transport   ADR
    international des marchandises Dange-
    euses par Route

[10] Règlement pour le transport de matières   ADN[R]
    dangereuses sur le Rhin

[11] Accord européen relatif au transport   ADN
    international des marchandises Danger-
    euses par voie de Navigation intérieure

[12] Verordnung über gefährliche Seefrachtgüter   SFO

[13] International Maritime Dangerous Goods   IMDG
      Code   1977

[14] International Air Transport Assocdation   IATA
      IATA restricted articles regulations
      1.8.1975

DETONATION OF UNCONFINED SOLID FUEL PARTICLES DISPERSED IN AIR

Allen J. Tulis

IIT Research Institute
Chicago, Illinois 60616

ABSTRACT

Detonation of unconfined solid fuel particles dispersed in air involves mechanisms both similar to and different from the detonation of liquid two-phase systems and single-phase gaseous combustible systems. The major requirement in the case of solid fuel particles is a sufficiently small particle size. The problem is that these microparticles behave differently in the convective flow field behind a shock wave than the relatively large liquid fuel droplets on the one hand and homogeneous gas phase fuel-air mixtures on the other. An experimental technique that uses hypergolic interhalogens under implosion dispersal allows a one-step fuel dispersal and subsequent initiation of detonation. The same technique can be used to obtain spatially large and extremely fast flare and photoflash outputs. With appropriate initiation coupling, detonation velocities of 1.9 mm/μsec in near-stoichiometric unconfined dispersions of aluminum particles in air have been obtained. Test results indicated that flake aluminum particles with 3 to 4 m^2/g surface area could be readily detonated, whereas the finest available atomized aluminum particles could not

INTRODUCTION

An explosive medium can generally support either a combustion
wave (deflagration) or a detonation, depending upon various condi-
tions such as confinement, composition, and initiation source. A
deflagration proceeds by means of heat transfer and diffusion, both
slow mechanisms that limit the combustion velocity to about 10 m/sec.
This is substantially slower than the velocity of sound in ambient
air, about 330 m/sec, which is the rate of pressure transmittance
in a gaseous medium. Thus, the compression wave of a deflagration
will move away from the combustion zone and continually equalize
the pressure within the system.

Almost all natural explosions are deflagrations. Those occurring
in confined spaces, such as coal mines and grain elevators, are
catastrophic. Deflagrations of most combustible air mixtures
produce peak pressures that seldom exceed 8 atm, whereas detonation
of the same mixtures can produce peak pressures in excess of 40 atm.

A detonation is a shock wave sustained by the energy of an
attached (coupled) chemical reaction. A shock wave is a compression
wave that moves through the unburned gas in a combustible mixture
at supersonic velocity, about 5 to 6 times sonic velocity. The
detonation of gas phase fuel-oxidizer systems has been extensively
studied over the years and will not be of concern in this paper
except by reference.

The purpose of this paper is to present some new concepts and
report upon some interesting experimental results in the unconfined
detonation of two-phase fuel-air mixtures. The two-phase systems
concerned involve liquid or solid fuel particles dispersed in ambient
air. Particular emphasis was placed on the detonation of uncon-
fined aluminum particles dispersed in air.

CONCEPTS

The detonation of unconfined two-phase liquid fuel in air dispersions, generally referred to as fuel-air explosions (FAE), was achieved many years ago. The overall process is a unique combination of physical and chemical mechanisms and has been postulated to occur as follows:

(1) Liquid fuel droplets form a two-phase dispersion in air, generally by explosive dissemination;

(2) A second-event explosion creates a micromist in the wake of of each drop by the aerodynamic interaction between the convective flow field behind the propagating shock wave and the rather large drops of the aerosol;

(3) A supersonic combustion wave (detonation) proceeds through the micromist of fuel in air, creating shock waves strong enough to support and propagate the incident shock wave from the second-event explosive.

The controlling mechanism is the physical breakup of the relatively large droplets into micron-sized droplets producing orders of magnitude increases in surface-to-mass ratio. It is evident that the kinetics of the combustion reaction must be fast enough to couple with the incident shock wave and the induced convective flow field of the air and micromist fuel medium. The incident shock wave not only creates the micromist of fuel in air, but also produces the very high temperature and pressure necessary for a sufficiently small induction time to elapse before the chemical reaction occurs. Induction time must not be greater than the associated droplet breakup time, lest decoupling occur and detonation fail.

The convective flow velocity induced by the shock wave is a function of the shock wave velocity. In the open air atmosphere it is about 80 percent of the shock wave velocity for weak shocks and progressively higher for stronger shocks. Table I[1] indicates this convective flow velocity for some Mach numbers (Mach $N_m = 1$ is sonic velocity) and also the associated temperatures and pressures.

Table I

CONVECTIVE FLOW PROPERTIES GENERATED BY A PROPAGATING
SHOCK FRONT IN AMBIENT AIR AT STANDARD CONDITIONS [1]

Mach No. N_m	Velocity m/sec	Pressure psia	Temperature °K
1.5	236	36	381
2.0	424	66	487
2.5	594	105	617
3.0	756	152	772
3.5	908	208	956
4.0	1061	272	1167

It has been experimentally verified that the micromist stripped from liquid drops accelerates almost instantaneously to the convective air flow velocity, whereas the droplets themselves remain relatively immobile.[2] In a gas phase detonation the shock front is only a few molecular collisions thick and occurs at the von Neumann spike pressure. Behind this shock front an ignition delay and reaction zone of a few μsec duration takes place. The end of this reaction zone is the Chapman-Jouguet plane, through which the detonation front moves at sonic velocity relative to the reacted gas. Pressure and density fall, whereas temperature increases in the reaction zone. The Chapman-Jouguet pressure is about twice the pressure of a constant volume combustion. In the subsequent expansion zone, pressure, temperature, and density all decrease; the pressure falls below that of a constant volume combustion.

The mechanism in a two-phase detonation is not the same as in a gas phase detonation. The reaction zone can be considerably extended and the reaction is not a smooth flame front. In fact, there is evidence that the reaction front is a composite of individual heterogeneous reactions of droplets with their surrounding gaseous oxidizer. Vaporization prior to reaction is not essential, although the role of vaporization and combustion is interrelated.[3,4] If the droplets were to vaporize extensively prior to reacting, the resultant fuel-vapor-in-air system would not be sufficiently mixed for

stoichiometric requirements of combustion within the time limits essential for coupling to the shock wave.

In the detonation of unconfined solid fuel particles dispersed in air, particularly metals such an aluminum, entirely different mechanistic concepts must be considered. For instance, the solid particles are preformed and will not shatter or strip into micromist particles as is requisite with liquid fuels. After the initial dissemination of a solid particle aerosol the solid particles can be considered stationary. Therefore, before detonation can proceed, the solid particles must be sufficiently small (have a large surface-to-mass ratio) and be dispersed in a satisfactory concentration in air.

The presence of the solid microparticle fuel in air suggests that any ignition should lead to detonation at a velocity controlled by the chemical reaction rate. This, of course, is not the case. Flame, heat, or spark ignitions in two-phase systems, as in nearly all gas phase systems, will result in deflagration, particularly if the system is unconfined. A transition to detonation (DDT) may occur in some instances, but is highly unlikely in unconfined two-phase systems. A nearly instantaneous detonation could be achieved only if the concentration was within the often narrow detonation limits in the presence of the high pressure and temperature conditions of a shock-induced compression, or alternative means of high-energy flux transmission. Therefore, either an explosive second-event shock wave, high-energy radiant flux, or other high-energy flux is required to reach the extremely rapid chemical energy release rates of a detonation and the formation of sufficiently strong shock waves for its propagation.

This is the major problem of unconfined detonation in solid fuel particles dispersed in air. Any supersonic combustion process will invariably lead to the formation of shock waves, which will induce a convective flow field in the air. Unlike the case of relatively large liquid droplets, which will not translate significantly, the preformed solid microparticles will translate almost instantly with the convective flow field. The coupling of the reaction zone with the convective flow field is highly critical, particularly for

initiation. A convective flow velocity greater than the associated
reaction velocity will result in decoupling and the degradation of
reaction velocity to a deflagration. Attempts to initiate detonation
in microparticle fuel dispersed in air by the detonation of high
explosive second events appears to be an overdrive leading to the
decoupling of particles from the reaction zone. The concentration
of the particles is disturbed, creating a depletion in the vicinity
of the initiation. The particles then bunch up, since the convective
flow velocity quickly degrades farther away from the initiation
zone as the spherically diverging shock wave degrades. This tendency
could be minimized by utilizing a planar initiation explosive charge.
The transition from the second-event shock wave velocity decay to
the Chapman-Jouguet velocity of a near stoichiometric gas phase
fuel-air system occurs at the point where the energy from the fuel-
air reaction becomes equal to the energy contribution from the source
shock wave.[5]

IITRI has achieved detonation in unconfined solid fuel particles
dispersed in air by matching the initiation source to the anticipated
detonation. Thus, we have departed from the traditional use of
high-explosive second events. Investigation has shown that a
hypergolic chemical initiation technique appears to be the most
promising mode of initiation becuase it dispenses with the use of
a second event altogether for a direct, one-step dispersal and
detonation.

Previous investigations [6,7] of the combustion of aluminum particles
showed that particle size and ambient oxygen concentration were
relatively unimportant variables, but that an ambient gas temperature
of about $2300^\circ K$ was the necessary condition for ignition. Presumably
this involved the melting of the protective oxide layer on the
aluminum particle with an attendant increase in surface reaction rate
leading to ignition. Oxide coating would not hinder the use of
interhalogen ignition for aluminum. Furthermore, the energy density
output of an aluminum-interhalogen reaction is about three times
as great as that of TNT.

EXPERIMENTAL

The experimental device used in our work is illustrated in Figure 1. The test procedure is described as follows:

(1) Approximately 400 g of the hypergolic interhalogen was used in its own container, a steel lecture bottle. Only liquid hypergols have been investigated so far.

(2) Dupont C-1 Detasheet was wrapped around the lecture bottle. About 400 g of explosive was used in this manner.

(3) In later tests with aluminum powder a 3 mm thick sheet of Neoprene rubber was placed between the Detasheet and the aluminum powder to minimize preignition of the aluminum.

(4) This package was positioned in the center of a cylindrical cardboard container, which was subsequently filled with five or more kg of fuel, either liquid or powder.

(5) A No 6 EBC was placed in the wooden spool previously attached to the lecture bottle at the top of the device. (Previously, a small tetryl booster pellet had been placed in the spool in direct contact with the Detasheet explosive.)

The experimental field test set-up is illustrated in Figure 2. The FAE device was placed on top of a 4 ft high platform of cement blocks. Cement blocks were also placed at 6 ft intervals as fiducial markers, or 36 ft from left to right markers. The experiments were recorded on 16 mm color film with one Bell and Howell camera at 64 f/sec and one Fastax camera at about 4000 f/sec. In several tests two Fastax cameras were used at about 4000 f/sec, but one was shuttered down from F4 to F22, so as to provide the details of the flame growth. Photographs reproduced from this later 16 mm film record of a test with aluminum and BrF_5 appear in Figure 3. The results of the tests conducted with this device appear in Table II.

Table II
IITRI ONE-STEP FUEL AIR EXPLOSION DEVICE TESTS

Test No.	Fuel	Hypergol	Result
1	diesel fuel	ClF_3	deflagration
2	water	IF_5	dispersal
3	none	IF_5	--
4	aluminum	BrF_3	partial detonation
5	aluminum	BrF_5	partial detonation
6	propylene oxide	ClF_3	partial detonation

Each teat used about 5 kg of fuel, about 400 g hypergol, and about 400 g explosive.

The explosive charge served a dual purpose: (1) it dispersed the fuel in a manner similar to central burster explosive techniques in typical FAE tests and (2) it imploded upon the steel lecture bottle containing the hypergolic interhalogen. The explosive adequately dispersed liquids but gave poor dispersal of the flake aluminum powder. For implosion dispersion of the hypergolic interhalogens the explosive fragmented the steel lecture bottle and allowed about 5 msec delay before dispersal.

Two tests with aluminum and one test with propylene oxide resulted in a partial detonation, which was evidently limited to the fuel-interhalogen reaction and its immediate environment. Air-blast wave output was felt about 500 m downrange in the observation building. In the case of the aluminum powder, which formed an insufficiently dispersed cloud, the fireball growth after the initial fuel-interhalogen detonation progressed at above sonic velocity. We concluded that these tests achieved an initiating detonation that did not propagate through the remainder (major) fuel-air cloud because of incorrect concentration. There are practically limitless possibilities of tailoring the device design and the relative amounts and types of fuel, hypergol, and explosive so that the achievement of a one-step dispersal and detonation of a two-phase fuel-air system is only a matter of expeditious development. A major problem remains, however, concerning the adequate dispersal of the flake aluminum.

In a related effort, reported elsewhere,[8] flake aluminum was dispersed into a linear fuel-air cloud about 4 m long at a near stoichiometric concentration and detonated at a velocity of about 1.9 mm/μsec. Attempts to detonate similar clouds of atomized aluminum particles of the finest size commercially available failed. It has become clear that the acheivement of detonation of aluminum particles by strong shock waves in shock tubes or small-scale laboratory confined spaces cannot be extended to the unconfined detonation of large-scale aluminum dispersions. There is a highly

complex interaction between particles in the large-scale field
tests, whereas individual or highly restricted conditions predo-
minate in the lab. Also, radiative energy transfer is substantial
in large-scale field tests and cannot be adequately assessed in
the lab.[9]

CONCLUSIONS

This work was conducted by IITRI as an internal research and
development effort. The objective was to show the feasibility
and clarify the problems inherant in the unconfined detonation
of two-phase solid fuel in air dispersions and the one-step
dispersal/detonation of a two-phase fuel-air dispersion. The
following conclusions were made as a result of this work.

(1) The energetic hypergolic reaction between fuels and interha-
    logens when explosively dispersed one into the other results
    in a detonation with an output adequate to initiate the
    detonation of the main fuel-air dispersion. A one-step fuel-
    air explosion is feasible.

(2) The detonation of an unconfined aluminum particle dispersion
    in air requires sufficiently small particles (or adequate
    surface-to-mass ratio) and proper initiation coupling. The
    detonation of such an unconfined aluminum particle in air
    dispersion has been achieved in a realistic field test.

(3) Use of the fuel-interhalogen implosion or explosion technique
    results in the very rapid (e.g., 10 msec) formation of a
    spatially large flare (e.g., 10 m in diameter). Larger flares,
    or photoflash outputs, can be just as readily achieved. The
    output durations can be extended to many seconds if desired,
    but intensity will diminish.

It is evident that much more work will be required to corroborate
these findings and to extend the results of this work to appli-
cations.

REFERENCES

1. Ranger, A.A., "Shock Wave Propagation Through a Two-Phase Medium", Astronautica Acta, Vol. 17, pp. 675-683, Pergamon Press, 1972.

2. Dabora, E.K. and Fox, G.E., "The Breakup of Liquid Droplet Columns by Shock Waves", Astronautica Acta, Vol 17, pp. 669-674, Pergamon Press, 1972.

3. Tulis, J.J. and Hersh, C.K., "Decoupling of Physical and Chemical Mechanisms in Explosive Reactions", Astronautica Acta, Vol, 17, pp. 435-444, Pergamon Press, 1972.

4. Tulis, A.J. and Erikson, T.A., "On the Explosive Sensitivity of Condensed-Phase Explosives", Recent Developments in Shock Tube Research, Stanford University Press, pp. 508-519, 1973.

5. Collins, P.M., "Detonation Initiation In Unconfined Fuel-Air Mixtures", Astronautica Acta, Vol 1, pp. 259-266, Pergamon Press, 1974.

6. Friedman, R. and Maček, A., "Combustion Studies of Single Aluminum Particles", Ninth Symp. (Intl) on Comb., pp. 703-712, Academic Press, 1963.

7. Maček, A., "Fundamentals of Combustion of Single Aluminum and Beryllium Particles", Eleventh Symp. (Intl) on Comb., pp. 203-217, the Comb. Inst., 1967.

8. Tulis, A.J., IITRI IR&D Report C-1215, December 1977, SECRET.

9. Cassel, H.M., Liebman, I., and Mock, W.K., "Radiative Transfer in Dust Flames", Sixth Symp. (Intl) on Comb., Reinhold Publishing Corporation, pp. 602-605, 1956.

Figure 1

IITRI ONE-STEP FUEL-AIR EXPLOSION DEVICE

Labels on the figure:
- Booster (tetryl)
- Detonator (No. 6 EBC)
- Holder (wood)
- Interhalogen
- Lecture Bottle (steel)
- Detasheet Explosive
- Neoprene Rubber
- Aluminum Powder
- Cardboard Container

FAE Device

Cement Block Platform
(4 ft high)

Cement Block Markers
(@ 6 ft intervals)

18'   12'   6'   0   6'   12'   18'
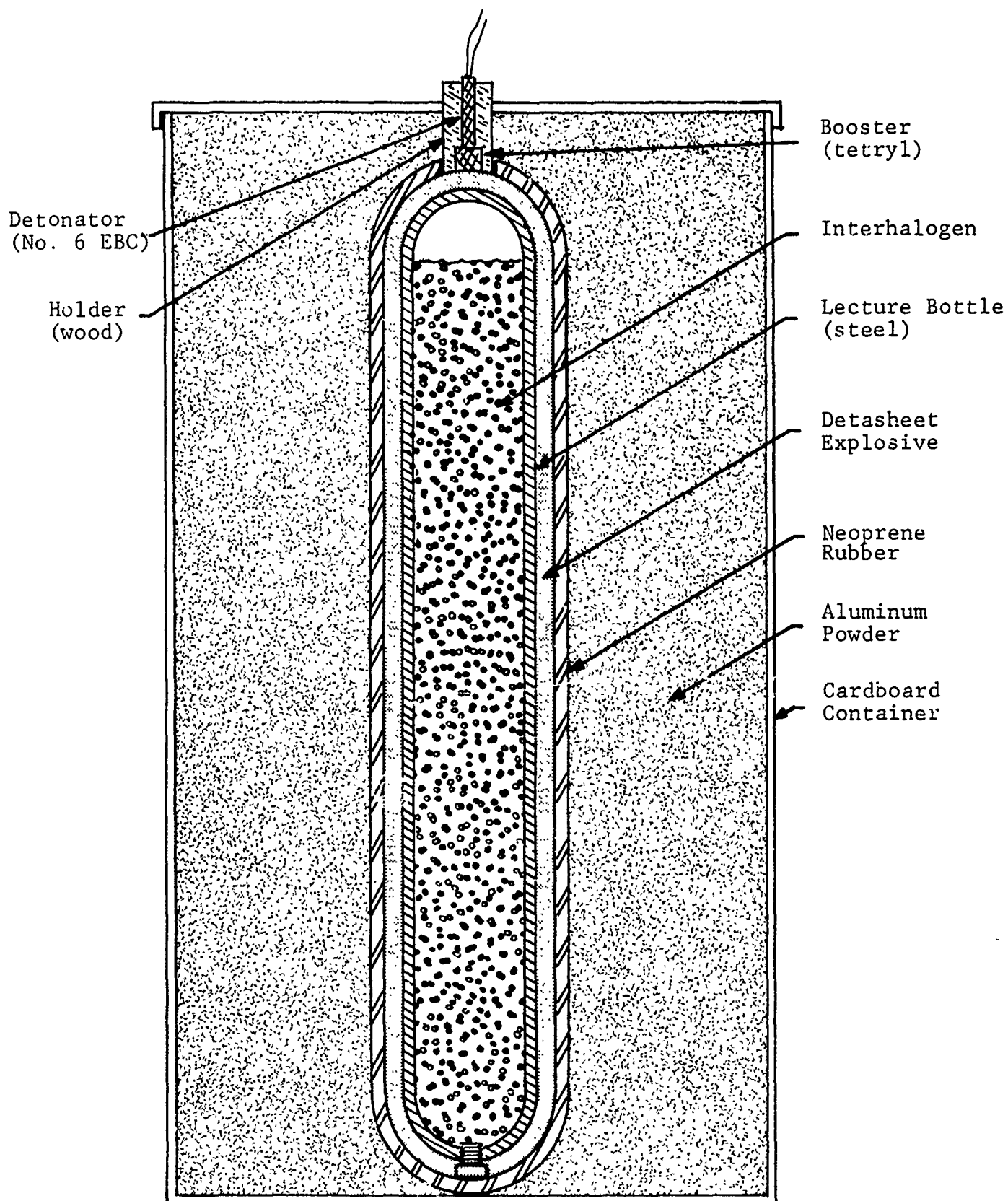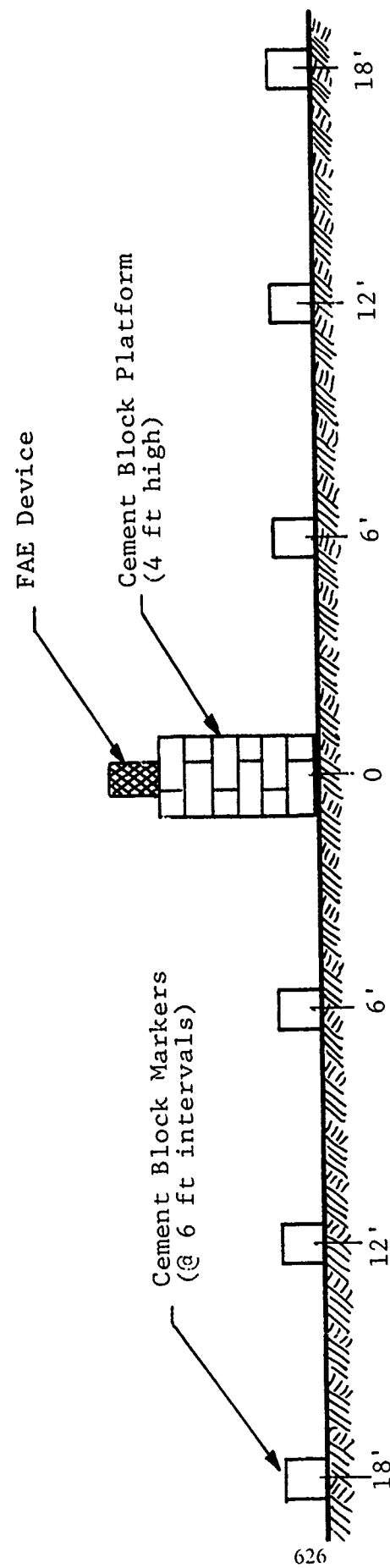
Figure 2

FIELD TEST SCHEMATIC OF IITRI ONE-STEP FAE

626

Figure 3

FASTAX FILM RECORD SEQUENCE FROM A ONE-STEP ALUMINUM FAE TEST

Figure 3 is a sequence of 60 consecutively numbered frames repro-
duced on the following pages from the 16 mm Fastax color film re-
cord of Test No. 5. The framing speed was 3800 f/sec and the lens
setting was F22; hence the appearance of nighttime for a broad
daylight test. Pertinent data for this test is as follows:

Frames	Time	Flame Diameter	Flame Velocity
	msec	m	m/sec
0	0.0	0.0	0
5	1.3	0.0	0
10	2.6	0.0	0
15	4.0	0.0	0
20	5.3	0.9	342
25	6.6	1.9	380
30	7.9	2.7	304
35	9.2	4.5	684
40	10.5	5.7	456
45	11.8	6.5	304
50	13.2	7.3	304
55	14.5	7.9	228
60	15.8	8.3	152

NOTE: The time delay to initiation due to implosion technique
       was at least 4 msec. The flame-front velocity was super-
       sonic to beyond 6 m diameter fireball growth.

627

1

2

3

4

5

6

7

8

9

10

628

11

16

12

17

13

18

14

19

15
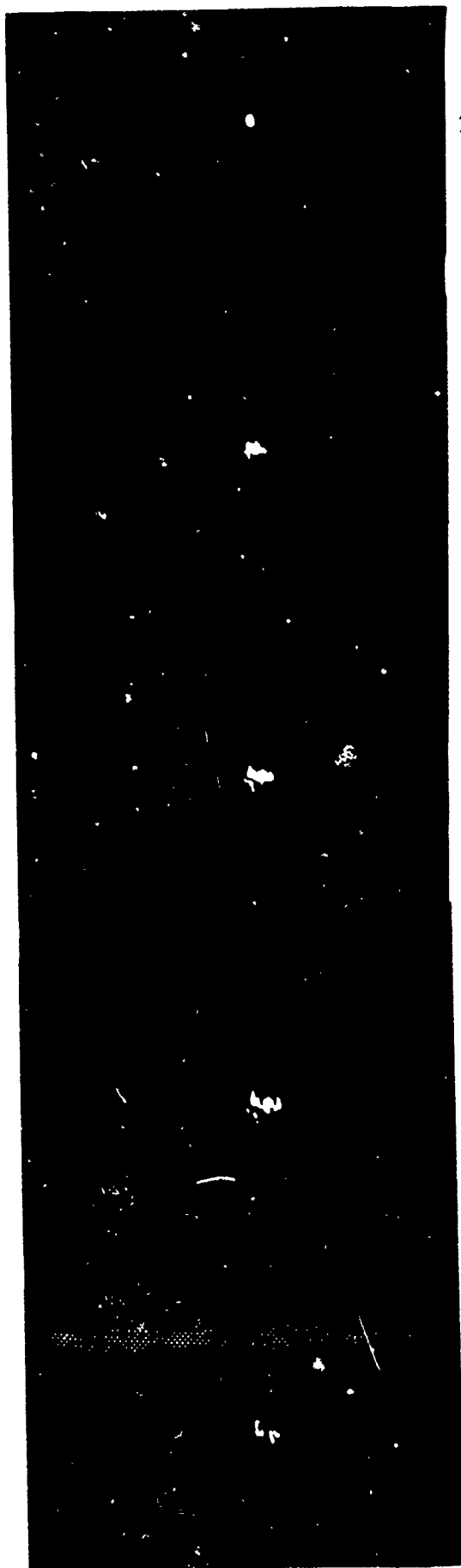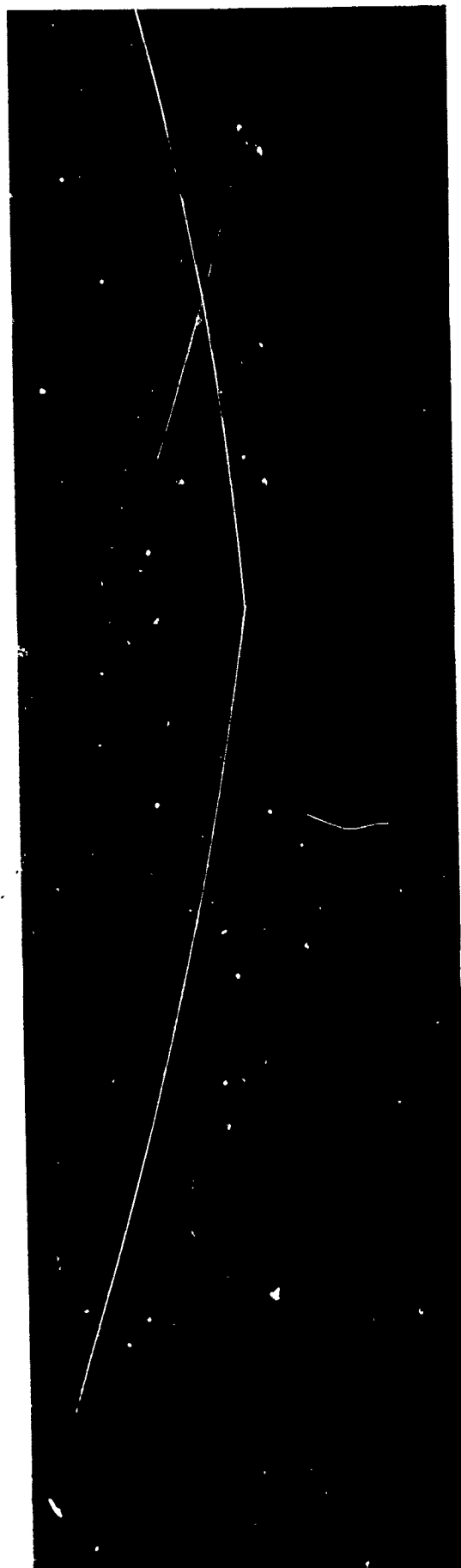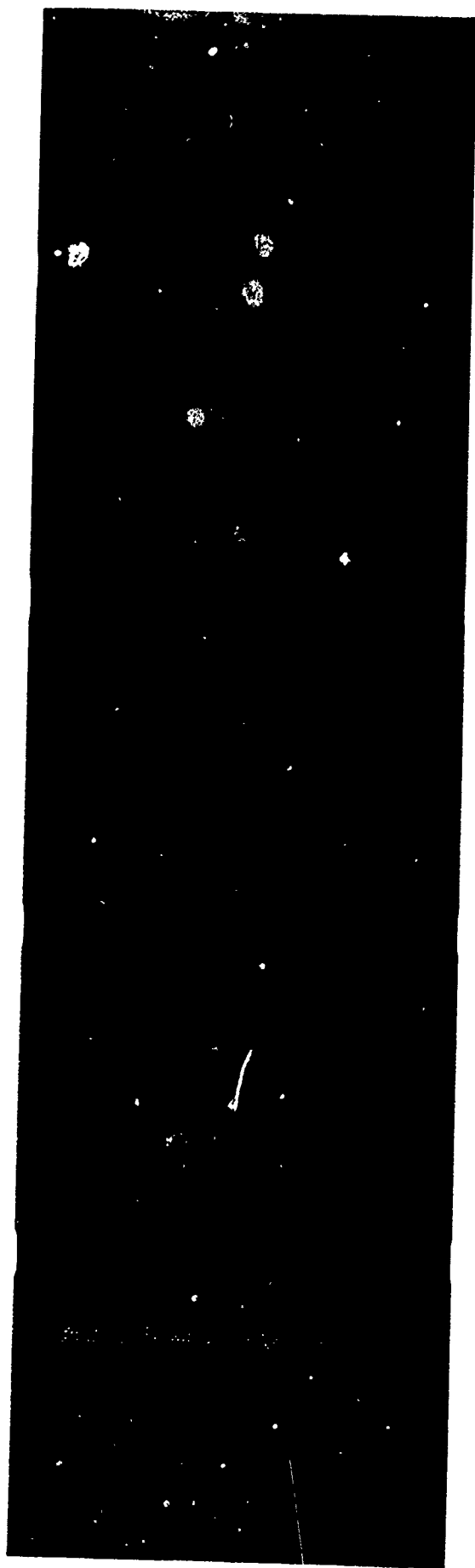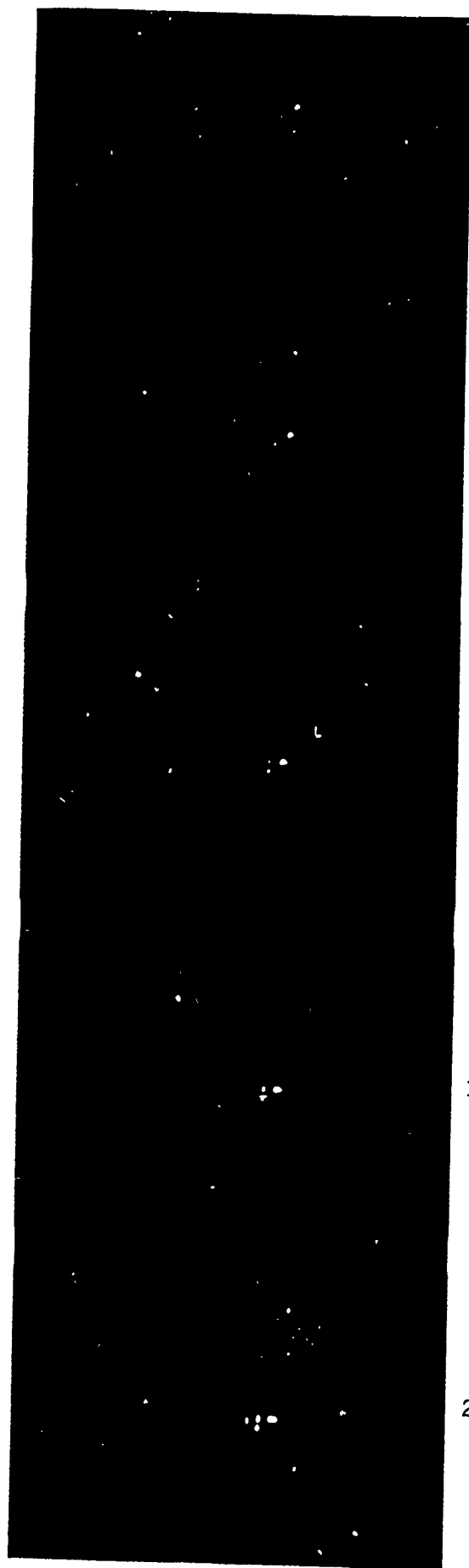
20

21

22

23

24

25

26

27

28

29

30

31

32

33

34

35

36

37

38

39

40

631
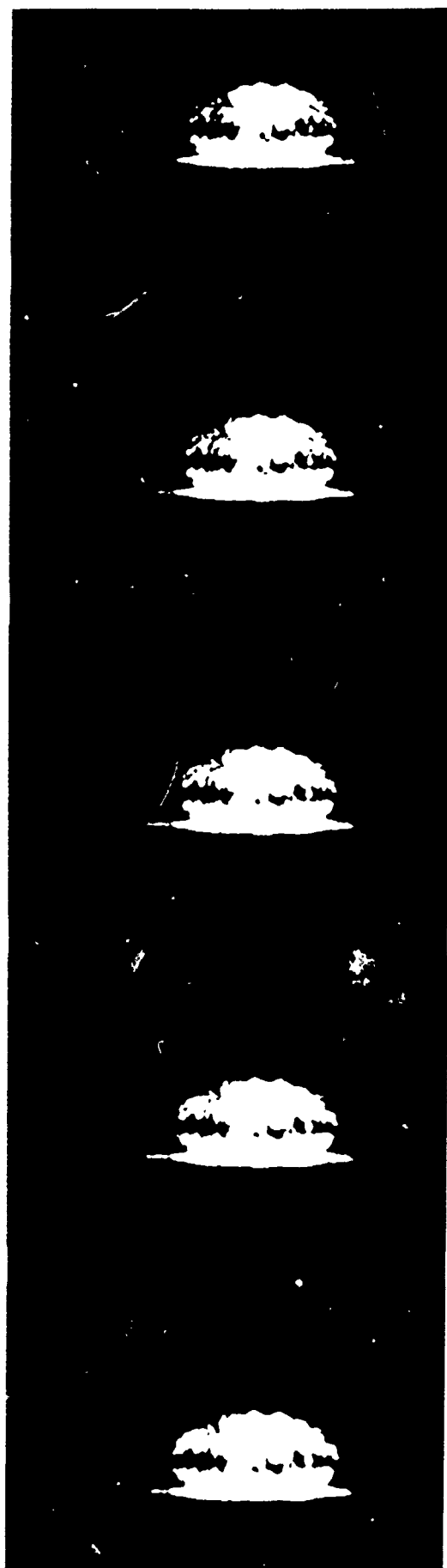
41

42

43

44

45

46

47

48

49

50

51

52

53

54

55

56

57

58

59

60

Electrical Igniter

(Hubert Usel)

1. General description

Electrical igniters are becoming more and more attractive
for weapons, as they allow simpler constructions and designs
without cumbersome mechanical firing assemblies.Reliable
electrical igniters for caseless ammunition have been
sought for many years but in the past they tended to
fouling and corrosion of the contact electrodes.

My activities in this respect date back to work performed
in 1964. Late in 1965 I made an agreement with a US company.
It aimed at developing the electrical igniter and the case-
less cartridge to salability. Due to slow progress and
technical difficulties the agreement was terminated by the
US company in 1970.

The technical difficulties lay in the fouling of the electro-
des by lead residues which led to short circuits. Therefore
the prime endeavour was to get rid of lead compounds.

In 1971 first positive results were obtained with igniter
compositions containing conductive materials which did not
leave any residues on the electrodes neither with high tem-
perature nor under high pressure. Such materials are, for
example, antimony or intermetallic compounds like silicides.
Subsequent work - always in my laboratory in my home -
resulted in a flat igniter of 5,5 mm diameter which gave
good results in connection with caseless ammunition, and
patents for this were subsequently applied for.

Slide 1 snows a cut view of a .22 caliber caseless
cartridge with said igniter.

In 1971 the simple construction of the electrical
igniter only consisted of a thin conductive layer
and a booster part of 0,3 to 0,4 mm thickness, based
on explosives. This was considerably changed in the last
three years. I wanted to obtain an increased resistance
against moisture and other environmental factors and a
shortening of ignition-time.

To understand the working mechanism of this new igniter
we also have to consider the ignition electrodes: I have
obtained very satisfactory results with two concentrical
electrodes, as shown on slide 3, together with the simp-
lified electric diagram.

On slide 4 you see the .22 caliber rifle that I used
during my development work. To date I have fired thousands
of rounds without any cleaning of the electrical parts.
The main problem of my previous efforts, namely the
fouling of the firing electrodes has thereby been proved
to be solved.

A sporting version of this rifle is currently being
developed by a European weapons manufacturer and the
cartridge for it by a big European ammunition manu-
facturer. Sport weapons licenses for USA have not yet been
issued and neither have any licenses for military uses,
even though I am in discussion with interested parties
in Europe.

2. How does this igniter work?

When a voltage is applied to the igniter across the
two electrodes, electrones pass perpendicularly through
the first layer which has a relatively high resistance
value. They then travel horizontally through the second
layer, which is relatively good conducting electrically,
toward the other electrode. By crossing the first layer
again the electrical circuit is closed and a current can
flow.

The conductive elements in the upper two layers are
special semiconductive crystals which are imbedded in
an easily flammable matrix such as nitrocellulose and
potassium picrate. Of course, both layers have a different
composition and ratio of ingredients.

With low voltages the current flow is practically nil
and causes no effect whatsoever. However, upon passing
a certain critical voltage, say 15 Volts, which depends
on the composition, the resistance in some individual
crystals collapses and a large current starts to flow
trough them. This results in local overheating and
subsequent ignition of the matrix. It then ignites the
booster part of the igniter with resulting ignition and
combustion of the propellant charge, just as in conven-
tional ammunition. The booster layer is compounded for
optimum ignition characteristics of the propellant charge
and also contains nitrocellulose as binder and picrates
for easy and reliable ignition transfer.

3. Safety aspects

The beauty of this system is its inherent safety and
reliability. It can be tested by resistance measurements
without firing the charge.
Even though ignition can be achieved with relatively low
voltages, such as 15 - 20 Volts, the igniter is
insensitive to electrostatic discharges of thousands of
Volts, such as sparks from piezoelectric devices hitting
the surface or sparks from a flintstonelighter. The reason
is the absence of the high current concentration in the
individual layer crystals which alone provide the necessary
heat to ignite the matrix.

On the other hand, even a practically worn out 22 Volt
battery will still be able to achieve ignition. This
has been proved in my laboratory with a small commercially
available battery as the one shown on slide 5.

During ignition an initial current flows during the
primary phase. It increases in strength during the
combustion in the plasma state while the igniter still
is in contact with the electrodes before the bullet starts
to move. This current can be limited by incorporation
of the resistor R shown on slide 3. This prolongs the
active life of the battery.

In extensive tests with different igniter compositions
and arrangements I have been able to reduce the total
energy consumption to currently 50 milliamperes during
5 - 10 milliseconds. This means that a small, inexpensive
battery will easily be able to fire at least 30 000 rounds
without difficulty.

Application Potential

As already mentioned, a sport rifle is currently being
developed in license in Europe for use of electrically
ignited caseless ammunition.

Since I had virtually no contact with the defence industry
the whole field of military applications is still open
to negotiations, some of which are just starting in
Europe. I think that there is tremendous potential here.

Additional fields, such as safety devices including auto-
mobile air bags, blasting caps and many others might be
of interest to more pacifically minded enterprises.

I will now be happy to answer any questions that you
may have.

----

① Electrical
Igniter

② Propellant
(caseless charge)

③ Projectile
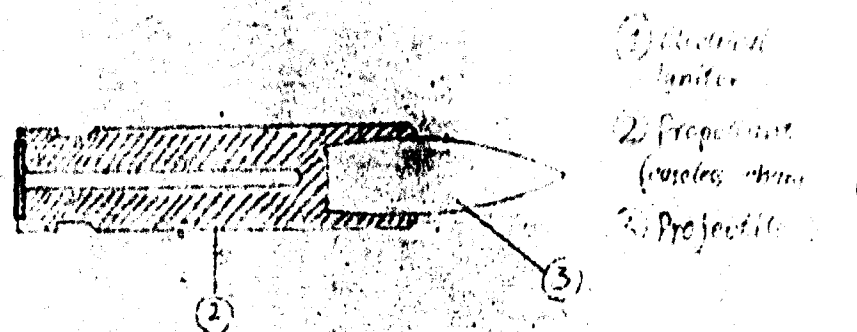
Cal .25 Caseless Cartridge with Electrical Igniter

6A

6B

7A

7B
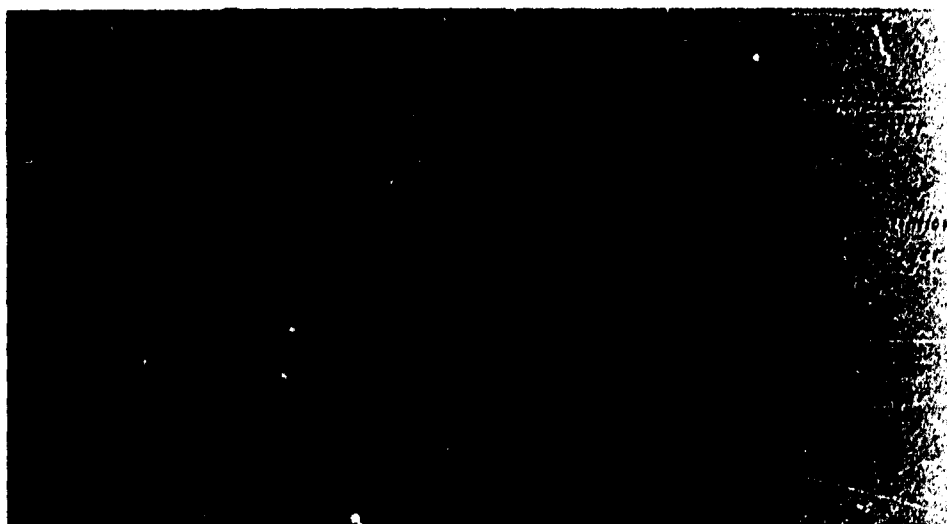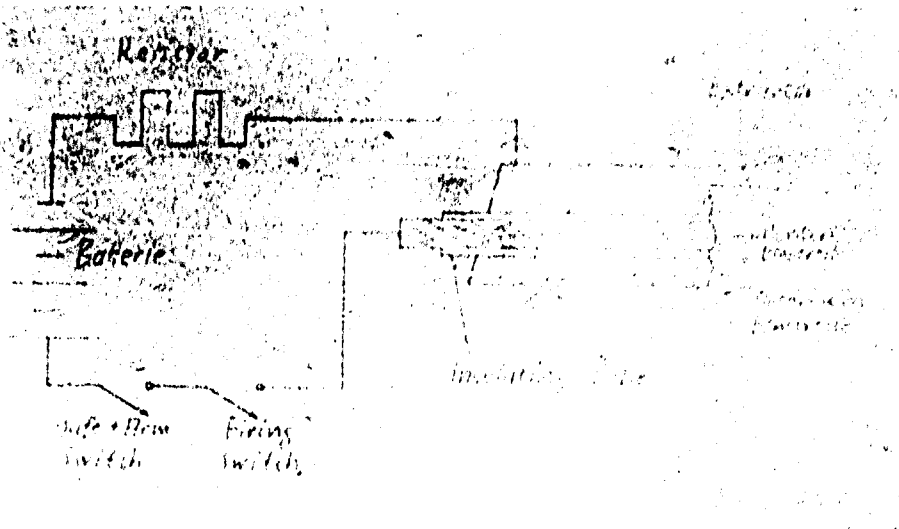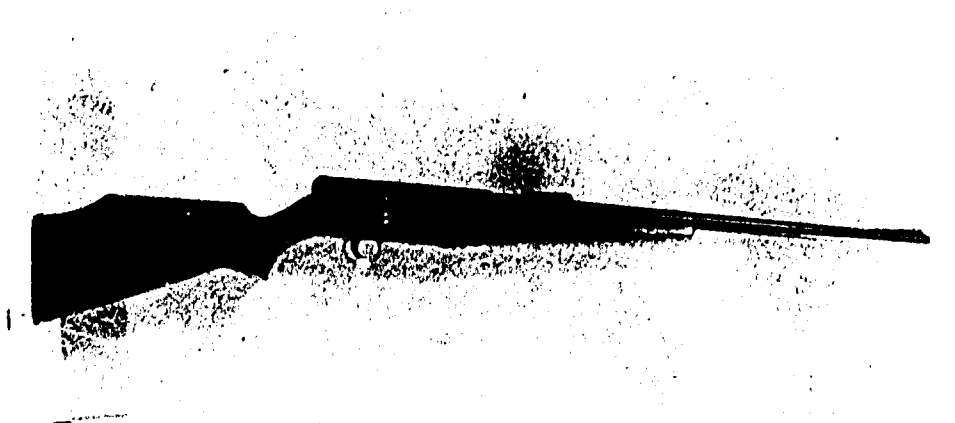
Research on plastic-bonded pyrotechnic compositions

Drs. N.H.A. van 'lam

Prins Maurits Laboratorium TNO, Technological Research

P.O. Box 45, 2280 AA Rijswijk (Neth.)

ABSTRACT

In order to overcome the disadvantages of conventional pressed powder pyrotechnic compositions, research has been done in the field of plasticbonded pyrotechnic compositions; better mechanical strength and storability were expected.

Main objectives were a smoke composition on the basis of polyvinyl-chloride and an incendiary mixture with polyurethane as a binder. The smoke composition was developed mainly for the protection of armoured vehicles against anti-tank missiles; the rapid smoke evolution is achieved by means of a progressive increase in burning surface. The incendiary composition can be used in high explosive shell to enhance the effectiveness by creating a synergetic effect: upon detonation the incendiary composition sticks to the fragments and will be ignited by the detonation products, resulting in burning fragments flying around.

INTRODUCTION

Conventional pyrotechnic compositions consist of pressed powdered mixtures of oxydizing agents, fuels and additives. These mixtures have the following disadvantages.

The porous structure of pressed powders makes them susceptible to moisture; absorbtion of water will reduce the effect of the pyrotechnic composition, resulting in failures.

The mechanical strength of pressed pyrotechnic elements is not very great. Cracks due to shock or vibration will cause irregular functioning of the pyrotechnics.

Since powders are usually compacted by pressing, by and large the outer shape of a pyrotechnic element is limited to that of a cylinder. The feasibility of programming the burning surface is poor therefore.

Handling of dry powders includes safety risks, e.g. explosions and inhalation of toxic dust.

PLASTIC BINDERS

Plastic-bonded compositions can overcome these problems, but the use of plastic binders introduces another problem; in most cases the plastic acts as a diluent, reducing the effect of the pyrotechnics as such. Plastic binders should preferably contribute to the functioning of pyrotechnic items. A good example of such a binder is described U.S. patent 3.724.382 by H.J. Zilkosky. This patent describes the

replacement of hexachloroethane, in conventional masking smoke, by polyvinylchloride (PVC); both materials are chlorine donors.
Smoke compositions on a PVC basis have some additional advantages.

The burning surface (and consequently the total burning time) can be varied over a very large range, as the smoke elements can be cast or extruded in any desired shape. This means that it is possible to create a huge cloud of smoke in a short time, or sufficient smoke during longer times.

The reaction temperature of this PVC-bonded smoke is very low compared with HC types of smoke. In the reaction zone the temperature rises till 600°C. The temperature of the plume generated from a PVC type of smoke grenade is about 240°C.
There will be less updraft of the smoke cloud compared with the hot HC smoke and consequently the covering properties will be better.
This means also a drastic reduction of the fire risk during training as the plume cannot ignite dry grass or hay.
Due to the low reaction temperature the PVC-bonded smoke composition can also be applied to evaporate tear gas or IR absorbing agents.

PREPARATION OF A PVC-BONDED SMOKE MIXTURE

PVC is plasticized preferably with a nonvolatile plasticizer such as diocthylphthalate (DOP). This plastisol is filled with zinc oxide (Zn O), ammonium perchlorate (AP) and a chlorine donor such as hexachlorobenzene (HCB). The particle size of all additives should well be controlled. Addition of surface active components may be of help in speeding up mixing time.
The pastelike substance formed in this way can be easily cast or extruded into all desired shapes of moulds.
At elevated temperatures the plasticizer migrates into the PVC, creating a solid mass.
The PVC we used forms a rigid body at 145°C; depending on the shape and mass the elements must be kept at this temperature from several seconds to one hour.
Example of smoke composition on a PVC basis.

PVC	20 %
DOP	20 %
ZnO	30 %
AP	25 %
HCB	5 %

APPLICATIONS OF PVC-BONDED SMOKE COMPOSITIONS

The rapid and well controlled smoke production provides excellent covering capabilities for tanks and armoured personnel carriers against visual as well as TV and laser guided antitank weapons. The possibility of incorporating an IR absorbing agent will extend the protective cover; this is still under investigation.

The mechanical strength of PVC-bonded smoke compositions makes it an ideal grenade filling with a very accurate burning time; conventional smoke grenades may burst due to cracks, or give irregular smoke production.

PVC-bonded smoke forms an ideal vehicle for riot controlling agents: rapid burning of caseless CS grenades.

STORABILITY OF PVC-BONDED SMOKE COMPOSITIONS

Accelerated aging tests with PVC-bonded smoke compositions and conventional HC type compositions have proved the superior qualities of the former composition. HC smoke grenades already failed after several weeks of storage in a climate cabinet, while PVC smoke grenades still functioned well after 25 weeks of storage under the same conditions.

APPLICATION OF POLYURETHANE IN THERMITE COMPOSITIONS

Another application of plastic binders is the use of polyurethane in incendiary mixtures. Conventional high explosive shells have a marginal effect on armoured vehicles. The use of an incendiary composition in combination with penetration of the armour will enhance the effect of the ammunition considerably. This can be achieved with substances such as zirconium and uranium, but also with thermite compositions.
The thermite composition will be ignited on detonation of the shell by the hot reaction products, resulting in "burning fragments".
The problems are how to stick the thermite to the shell and how to keep it in place after detonation. The unique sticking qualities of polyurethane make it the most suitable plastic binder to solve the problem.
As a coating (liner) on the inside of the shell the polyurethane-bonded incendiary mixture also constitutes a good bond between the explosive and the shell case, preventing base separation and other voids.

PREPARATION OF PU-BONDED THERMITE MIXTURE

A non-volatile isocyanate is mixed with a polyfunctional alcohol and castor oil.
Add magnesium (Mg) ferricoxide (Fe_2O_3), potassium perchlorate ($KClO_4$) and enough trichlorolethylene to keep a castable composition. After stirring vigorously the composition is poured into the desired shapes. The solvent is removed at elevated temperature ($70°C$) and under reduced pressure. The polyurethane is formed as a result of crosslinking of isocyanate, polyalcohol and castor oil. The p.u. so formed is partially decomposed at $200°C$. The result is a reactive mixture of porous structure.

Example of p.u. bonded thermite mixture

$$
\begin{array}{ll}
\text{Mg} & 28\ \% \\
\text{Fe}_2\text{O}_3 & 26\ \% \\
\text{KClO}_4 & 36\ \% \\
\text{p.u.} & 10\ \%
\end{array}
$$

The reactivity of the mixture can be varied by changing the composition or the degree of decomposition of the p.u.
The presence of ferricoxide guaranties good case bonding. Incorporation of some TNT in the p.u. binder, on the other hand, helps the bonding of the p.u. and the explosive.

DEVELOPMENT OF AN ALUMINIUM/POTASSIUM PERCHLORATE

MIXTURE FOR USE IN A AIRCRAFT BRIDGEWIRE IGNITER

By   W P Walker, AWRE, Aldermaston, England

1.   INTRODUCTION

There was a requirement for a pyrotechnic mixture for use in the exploding bridgewire igniter shown in Fig 1. The igniter was to be used for the very rapid ignition of a propellant charge. It had a 2 mil diameter platinum bridgewire connected between centre pin and case and there was a spark gap, operating at 600v, in series with the bridgewire. The time available for the project was very limited and separate tasks were alloted to members of a small team of workers.

The initial work on this project had been carried out using an SR817 (55.8% potassium perchlorate, 31.4% aluminium, 12.8% lead) filling in the igniters. This material was discarded because it gave a high proportion of failures. Diagnostic oscilloscope traces of the firing current and high speed photography of the initiation process indicated that electrical conduction through the fill was probably the major cause of the failures.

Further development work using aluminium/potassium perchlorate mixtures had indicated that a 22.5% aluminium/77.5% potassium perchlorate mixture (SR818) might be a suitable filling material. This report describes work carried out on SR818 and similar materials with a view to finding an optimum filling for an exploding bridgewire igniter.

2.   TESTS USING SR818

On the basis of the tests mentioned in the Introduction, a batch of igniters, filled with SR818, was assembled for more detailed testing. One igniter out of about 200 filled at 65% theoretical maximum density (TMD) failed to fire. The firing pulse was supplied by an equipment with a 1.0 μF capacitor charged to 2.0 kV. Fig 2 shows diagnostic oscilloscope traces of the current flowing through the bridgewires of the failed squib and a normal squib. The trace for the failed squib showed a high current peak, and current continued to flow for a short time after the first half cycle. These observations can be explained by assuming that in the failed unit a large proportion of the current passed through the pyrotechnic fill. In addition to the failed unit a small proportion of the units gave similar traces perhaps indicating that they too were near to failure.

The single failure in the 200 units tested indicated an unacceptable level of reliability. Work was therefore started to obtain more evidence on the cause of the failure and to seek ways

of improving the quality of the filling. This work will be described in the remainder of this paper. The problems of identifying the cause of a 1 in 200 failure rate and then demonstrating that a new filling gave better results were avoided by testing candidate fillings over a range of experimental parameters and choosing, on the basis of all the results, the most promising filling for the device.

3.   COMPARISON OF FIRING CURRENT LEVELS IN BRIDGED AND UNBRIDGED UNITS.

Since the EBW squib bodies were expensive, a cheaper version was made for use in the experimental programme. Fig 3 shows details of this body. The experimental device is essentially the same as the EBW squib except that it incorporates a plastic head and does not contain a protective spark gap. Trials were carried out using both types of body and no differences were found between the results.

A small number of igniters without bridgewires was filled with SR818 and subjected to the normal firing pulse. The units were filled to the 65% TMD used in the EBW igniter. Firing current voltage and bridgewire resistance waveforms are shown in Fig 4. The units fired normally and after electrical breakdown of the fill, shown on the voltage waveform, the current traces were comparable with those obtained in units with bridgewires.

The trial was repeated using standard EBW squib bodies without bridgewires. The results were compared with those given by units with bridgewires. Fig 5 shows the distribution of the peak firing currents obtained during the trials.

The results suggest that the prime source of ignition is current flowing through the pyrotechnic fill rather than through the bridgewire. To test this theory a small number of trials was carried out using standard bodies to measure the V_{50} (the voltage at which 50% of the units failed to fire) of bridged and unbridged units. For these trials a 0.1 µF firing capacitor was used to ensure that the V_{50} was above the spark gap breakdown voltage. The results were:-

V_{50}	Bridged units	=	2000v	8 tests
V_{50}	Unbridged units	=	750v	5 tests

The results certainly show that conduction through the fill is an efficient initiation mechanism. However, no information is available on the maximum no-fire level and it is possible that multiple breakdown may occur in a centre pin device in which none of the paths contains sufficient energy to cause ignition.

4.   DC BREAKDOWN TESTS ON PYROTECHNIC MIXTURES

These tests were carried out using experimental igniters. The object was to measure the DC breakdown characteristics of a range

of mixtures. While the DC values may differ from those given by
dynamic breakdown tests, nevertheless the tests were easily carried
out and gave a quick comparative assessment of the electrical
insulation properties of the various mixes.

For the first series of trials the following 22.5/77.5 w/w
mixes were tested:-

X 98/76/1   SR818 Type Aluminium sieved thro 63 μm mesh sieve

            K ClO$_4$ Coarse (thro 125 μm sieve, retained 63 μm sieve)

X 98/76/2 * SR818 Type Aluminium
           * SR818 Type K ClO$_4$

X 98/76/3   SR818 Type Aluminium

            K ClO$_4$ Fine   (thro 45 μm mesh sieve)

X 100/76   As X 98/76/2 but with 0.7% polyisobutylene coating
            on the aluminium

All were filled to a <u>nominal</u> 65% TMD and gave breakdown
voltages of 500v.

*SR818 Type aluminium contains 75-125 μm 8% max; 63-75 μm 15% max;
   63 μm remainder.

*SR818 Type perchlorate contains 60 $\pm$ 15% in the range 45-90 μm. The
remainder is smaller than 45 μm.

The next series of tests was aimed at finding the effects
of density changes on DC breakdown voltage. The mixture tested was
SR818 Batch 3 which was the material used when the squib failure
occurred. Fig 6 shows the graphical relationship between the
parameters. There was a very large change in breakdown voltage
over the density range which could occur in EBW igniters because of
variations within the allowable manufacturing tolerances.

4.   <u>ASSESSMENT OF BRIDGEWIRE PERFORMANCE</u>

These tests were aimed at estimating the proportions of
the firing current passing through the bridgewires and the pyrotechnic
fills in various situations.

Two series of tests was carried out:-

(a) experimental mixes were made of SR818 type aluminium
     and potassium perchlorate. The proportion of aluminium
     was varied between 5% and 30% (w/w). The material was
     filled to 65% TMD into experimental bodies.

(b) SR818 batch 4 was filled into EBW igniters
        The filling density was varied between 50% and
75% TMD.

648

Units were fired by the discharge from a 1 μF capacitor charged to 2.0 kV. The dynamic resistance and inductance of the circuit were 0.15 ohm. and 2.2 μH respectively.

For all firings, current and voltage waveforms were recorded and from these peak voltage (ie. voltage at bridgewire burst) and current at burst were measured. From these data peak resistances (resistance at burst) were measured.

The method for calculating the bridgewire current and current through the film is based on an experimentally found relationship between resistance at burst and burst current (Appendix A).

The results for trial (a) are summarised in Fig 7 and for trial (b) in Fig 8.

Fig 9 shows some typical oscilloscope traces used for making measurements. Some difficulty was experienced with compositions containing more than 25% aluminium since the bridge-wire burst position was not always clearly defined on the current traces.

The results indicate that with 30% aluminium almost all the current passes through the filling at 65% TMD. With 22.5 % aluminium a large proportion of the current passed through the filling even at 50% TMD.

5.   REAR VIEW HIGH SPEED PHOTOGRAPHY OF IGNITERS

High speed photography was carried out on igniters during functioning. Modified experimental bodies were used in which the bridgehead material was made from Perspex (Lucite) so that the bridgehead pyrotechnic interface could be observed during firing. An AWRE model C5 high speed framing camera was used to photograph the rounds.

The compositions tested were made from SR818 materials and the proportion of aluminium was varied between 5% and 30%. The materials were filled to 65% TMD and the rounds were fired from the standard firing circuit.

The results showed light emanating from the bridgewires using compositions with up to 20 - 25% aluminium. From this level upwards there was no evidence of bridgewire reaction but signs of electrical breakdown were observed of the filling in regions away from the bridgewire.

Examples of photographic records are given in Fig 10.

Electrical breakdown of SR818 at 65% TMD was confirmed.

6. <u>ASSESSMENT OF CANDIDATE FILLING MATERIALS FOR FILLING INTO IMPROVED EBW IGNITERS.</u>

The following criteria were set for the acceptance of a filling for use in an improved version of the EBW Igniters.

1. Consistent DC breakdown voltage levels should be exhibited over the range of filling densities likely to be found in the device. The levels should be above the 375v minimum level of SR818 Batch 3 (see Fig 6).

2. Unbridged units, when fired, should pass less current than units filled with SR818 Batch 3.

3. Bridged units, when fired, should give consistent current records with a clear indication of bridgewire burst.

4. The bulk density of the mixture should be such that the selected filling density could only be achieved by a pressing load of at least 4.8 MPa (700 psi).

The above criteria could be met by SR818 Batch 3 pressed to 60% TMD. However, this material had been used up and attempts to manufacture further batches with the same properties were unsuccessful. The new batches were unsatisfactory because of low DC breakdown voltages or density.

In view of these problems, attempts were made at AWRE to produce a mixture with the desired characteristics using readily available materials. The method of approach was (a) to use finer powders to give low bulk densities, since fine powders would have large surface areas and might be more reactive; (b) to use powders in which the constituent particles have a relatively narrow range of particle sizes.

Details of the compositions tested are given in the chart below:-

$KClO_4$ (SR818 Type)	Aluminium (SR818 Type)	Aluminium (10 μ) ex Reynolds Aluminium Co
↓	↓	↓
through 45 μ sieve	through 45 μ sieve	
Micronize ↓	↓	↓
↓		
B A	X	Y

(Average)
Particle)
Diameter)
2-3 μ)
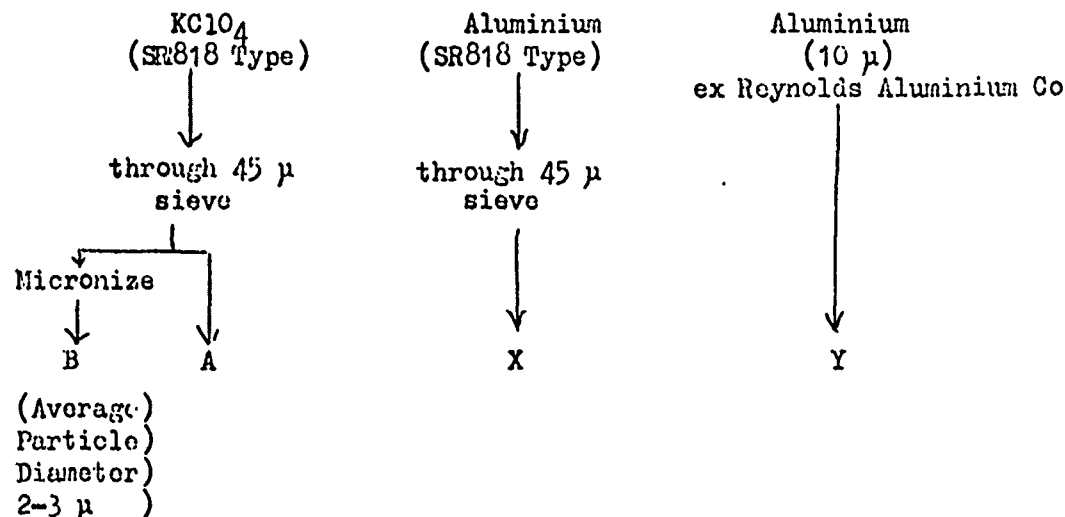
Four mixes all containing 22.5% aluminium were prepared ie AX, AY, BX and BY. The mixes were given initial electrical screening tests with the following results:-

AX   gave inconsistent results on the DC breakdown test and variable firing current records when fired in igniters.

AY   gave consistent firing current records with relatively low peaks and acceptable DC breakdown performance.

BY   gave variable firing current records.

BX   failed to fire in igniters both with and without bridgewires. On the DC breakdown test no breakdown occurred but the material ignited at 2.2 kV 6 μA and 2.7 kV, 10 μA.

Clearly mix AY was the most suitable candidate material.

6.1. Further Assessment Tests on Mix AY

The results of the DC breakdown tests are summarized graphically in Fig 11.

The pressing characteristics curve is shown in Fig 12. 14.5 MPa (2, 100 psi) is required to give 65% TMD.

Unbridged units filled with AY to 65% TMD and subjected to firing pulses gave three types of result:

(i)   some units fired giving currents comparable with bridged units.

(ii)   some units fired giving low currents ($<$10 amp).

Bridged igniters filled with AY and fired gave firing current traces which had a pronounced dip at the bridgewire burst position. The traces were reproducible and no high second peaks were found.

Rear view high speed photography in modified experimental bodies showed that ignition started at the region around the bridgewire. No firing failures occurred with igniters filled with AY to 70% TMD.

These results confirmed that AY type powder had good characteristics for use in EBW igniters. A specification was written for it and it was designated SR818A. Details of its particle size characteristics are given in Figs 13 and 14.

7. DISCUSSION

Since this work was completed over 200 igniters filled with SR818A powder have been fired successfully.

The EBW igniter filled with SR818A to 65% TMD appears to function reliably. The experimental data indicate that its reliability is due to the fact that its electrical conduction properties allow reproducible bursting of the bridgewire.

The mechanisms of initiation of aluminium/potassium perchlorate mixtures in centre electrode igniters are not well understood. It seems likely that some mixtures with good electrical conduction properties ignite in the fill. The geometry and materials of the igniter bodies are clearly of prime importance.

Although some aluminium/perchlorate compacts can be ignited by relatively low electrical energies deposited in the fill, there is evidence that this process is somewhat variable and perhaps some multiple breakdown conditions result in failure to ignite.

Where compacts are ignited by exploding bridgewires there are some parallels with EBW initiation of secondary explosives ic:-

(i)   The systems exhibit a relatively high V50. At this level failures may occur <u>although the bridgewire is fused.</u>

(ii) initiation appears to depend upon the efficient transport of energy from the bridgewire into the filling through the pores of the compact.

(EBW initiation of secondary explosives is critically dependent on the porosity, density and particle size of the explosive compact).

Failure of compacts made from very fine perchlorate and relatively coarse aluminium was interesting. It is possible that the perchlorate formed a coating around each aluminium particle (the breakdown voltages were very high). Presumably vapour from the exploding bridgewire was unable to reach the aluminium because of the perchlorate.

Many interesting problems have arisen from this work. Suggestions from experts in the field would be valued.

ACKNOWLEDGEMENTS

To Messrs R Bance, G Foan and M W Burt who made major contributions to this work.

To RARDE who supplied pyrotechnic materials and gave invaluable advice.

The following identities are used:-

R = measured total resistance of device at bridgewire burst time

I = total current flowing at bridgewire burst

V = voltage across device at bridgewire burst time

Assuming that current flows through the pyrotechnic material in paths parallel to the bridgewire

Let r_B = bridgewire resistance at bridgewire burst time

i_B = current through bridgewire at bridgewire burst time

r_S = electrical resistance of fill at bridgewire burst time

i_S = current through fill at bridgewire burst time

Also r_B^0 = resistance at burst for PETN filled rounds

i_B^0 = current at burst for PETN filled rounds

It has been shown experimentally (ref 1) that for PETN filled rounds

$$r_B^0 = \frac{K}{\sqrt{i_B^0}}$$

where K = 95 for bridgewires similar to those used in this work. Since PETN is a non-conducting fill, the current can be assumed to flow only through the bridgewire. In a conducting fill, current will flow through the wire and also through the fill, the relationship between the current flowing through the wire and its resistance is assumed to be given by:

$$r_B = \frac{K}{\sqrt{i_B}} \tag{1}$$

where K = 95, as before.

Also for the pyrotechnic filled rounds,

$$\frac{1}{R} = \frac{1}{r_B} + \frac{1}{r_S}$$

giving $$r_B = \frac{R\, r_S}{r_S - R} \tag{2}$$

Hence, from (1) and (2),

$$\frac{R\, r_S}{r_S - R} = \frac{K}{\sqrt{i_B}}$$

and since $I = i_B + i_S$ $\tag{3}$

$$\frac{R \, r_s}{r_s - R} = \frac{K}{\sqrt{I - i_s}} \qquad (4)$$

Now $\qquad V = IR = i_s \, r_s$

$$\therefore \qquad i_s = \frac{IR}{r_s}$$

Substituting in (4)

$$\frac{R \, r_s}{r_s - R} = \frac{K}{\sqrt{I - \dfrac{IR}{r_s}}}$$

which simplifies to

$$r_s = \frac{K^2 R}{K^2 - IR^2} \qquad (5)$$

Now, K is a constant and I and R are obtained from experiment, so r_s may be calculated using equation (5). The other unknowns, r_B, i_B and i_s can now be obtained using equations (2), (1) amd (3).

ref 1 · J Johnston Unpublished report
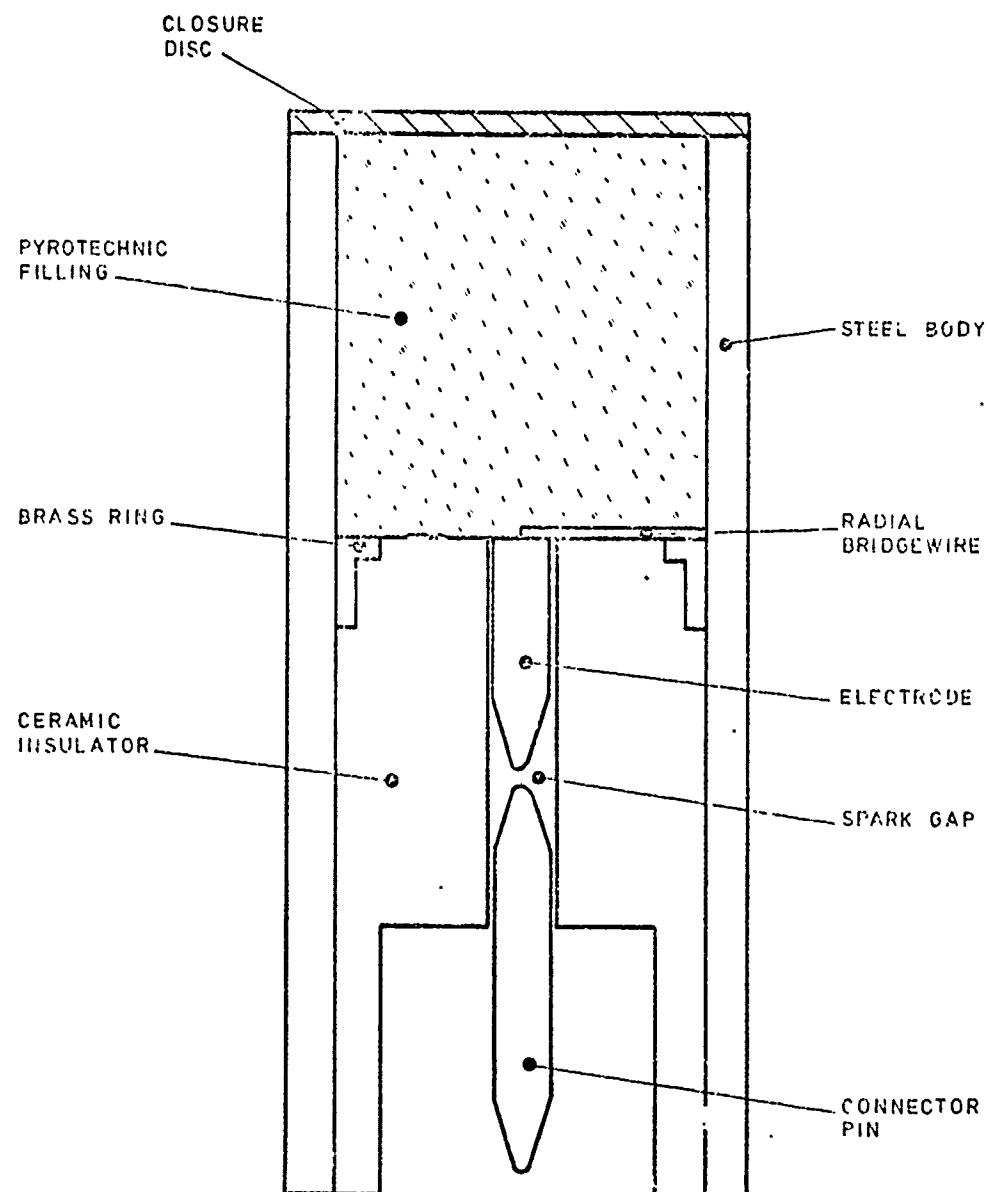
FIGURE 1 Exploding Bridgewire Igniter

The figure shows an exploding bridgewire igniter with the following labeled components: CLOSURE DISC, PYROTECHNIC FILLING, BRASS RING, CERAMIC INSULATOR, STEEL BODY, RADIAL BRIDGEWIRE, ELECTRODE, SPARK GAP, and CONNECTOR PIN.
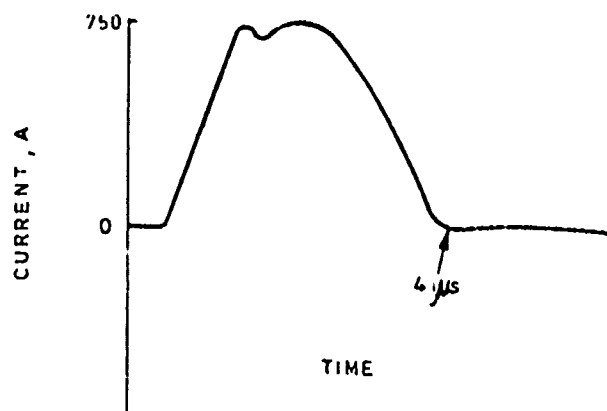
Firing Current / Time Relationship for Normal Unit
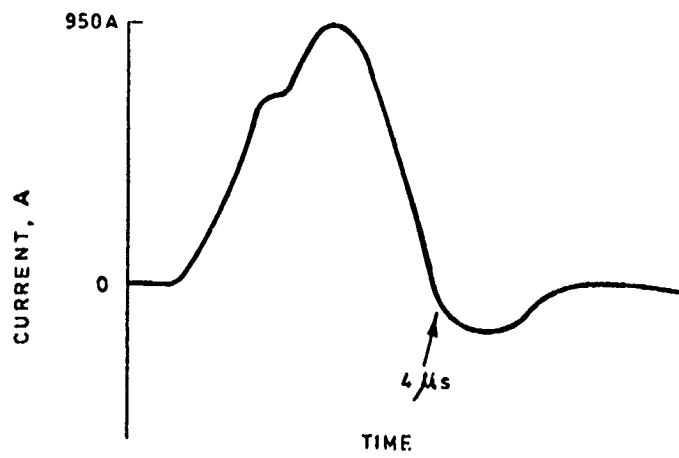
Firing Current / Time Relationship for Failed Unit

FIGURE 2.

656
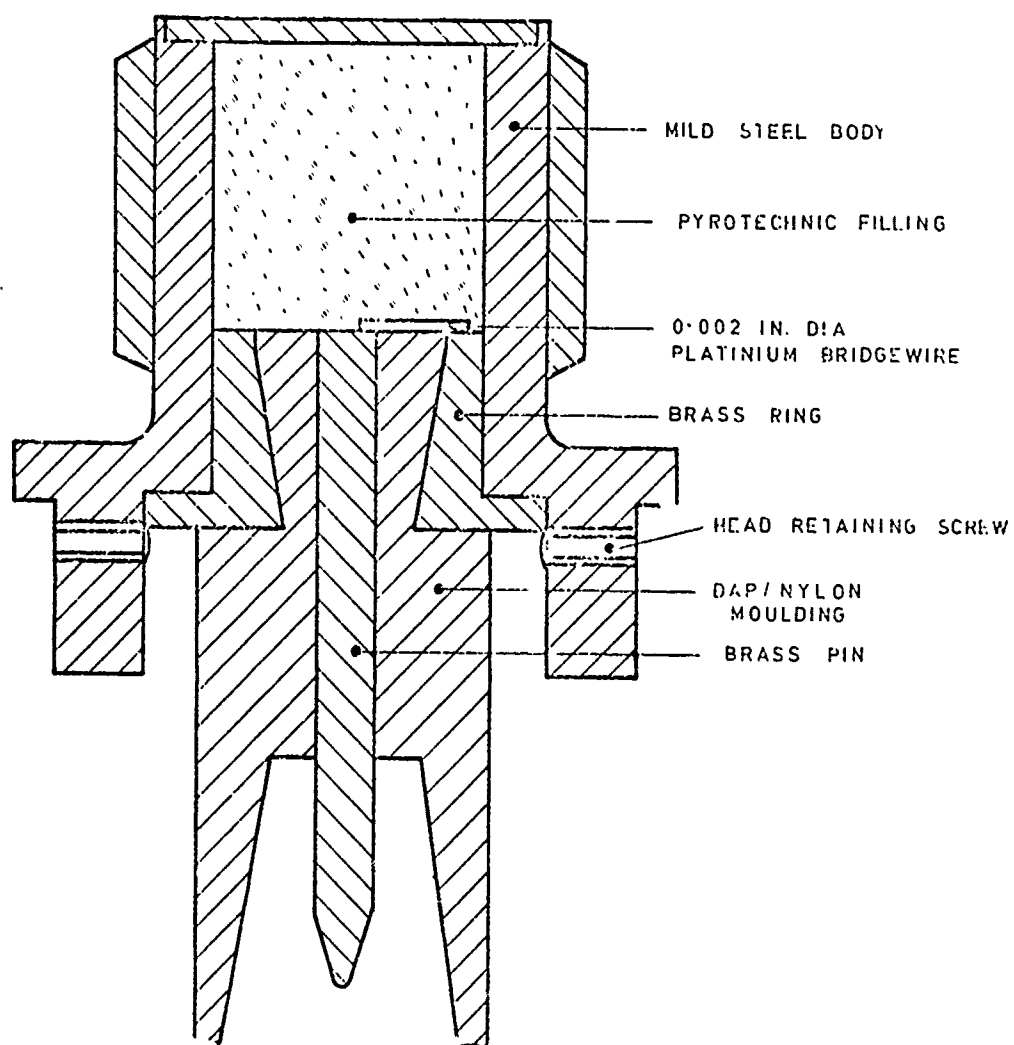
FIGURE 3. Experimental Body
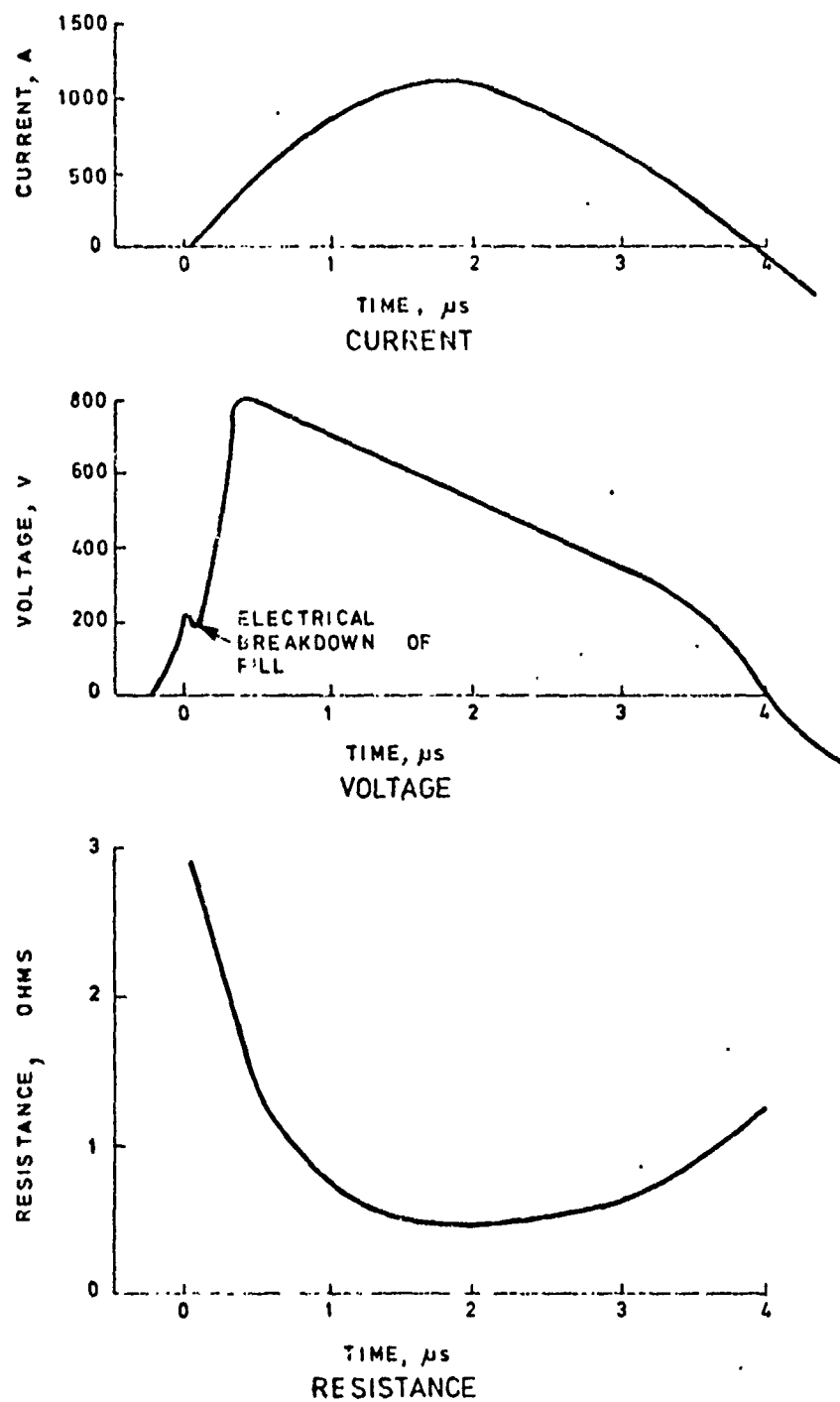
FIGURE 4 Current, Voltage and Resistance Waveforms of an Unbridged Igniter Filled with SR818
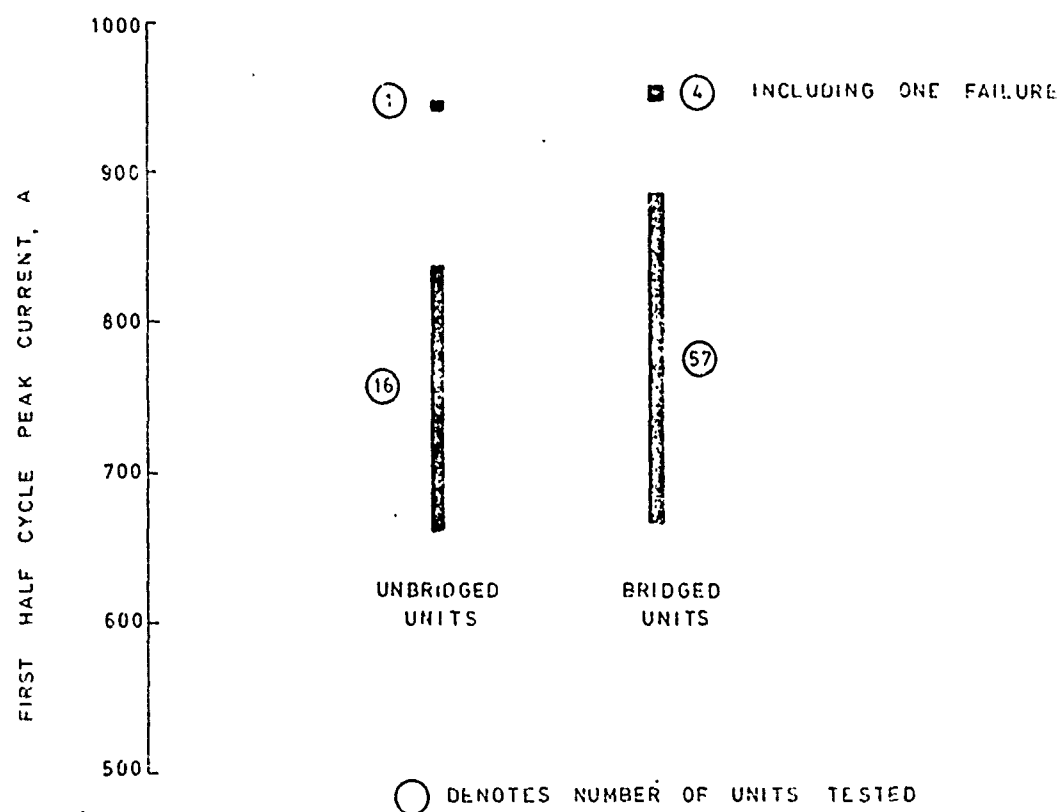
FIGURE 5 Current Levels in Bridged and Unbridged Igniters Filled with SR818 Batch 3
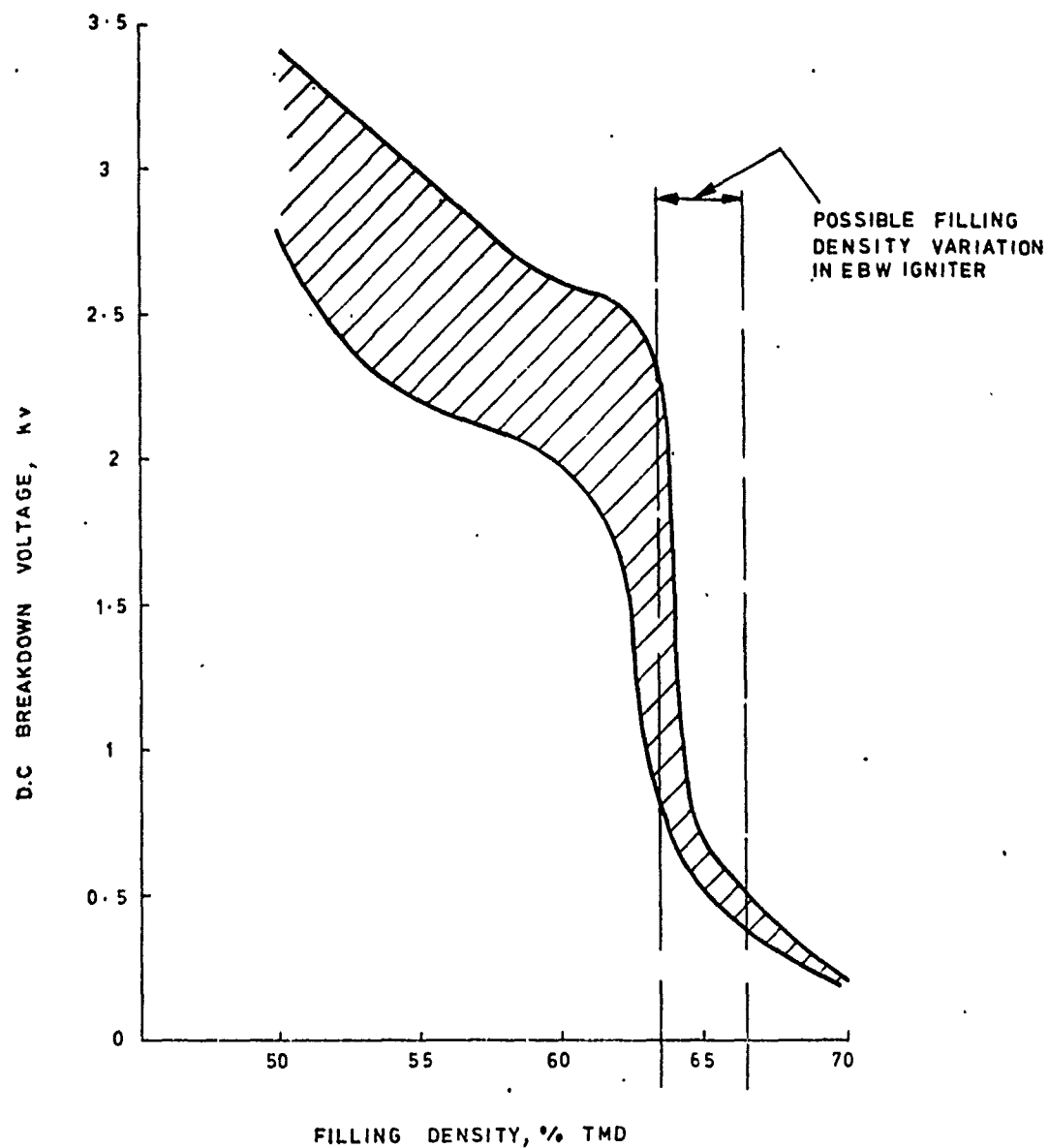
FIGURE 6 Filling Density / D.C Breakdown Voltage of Unbridged Igniters Filled with SR818 Batch 3.
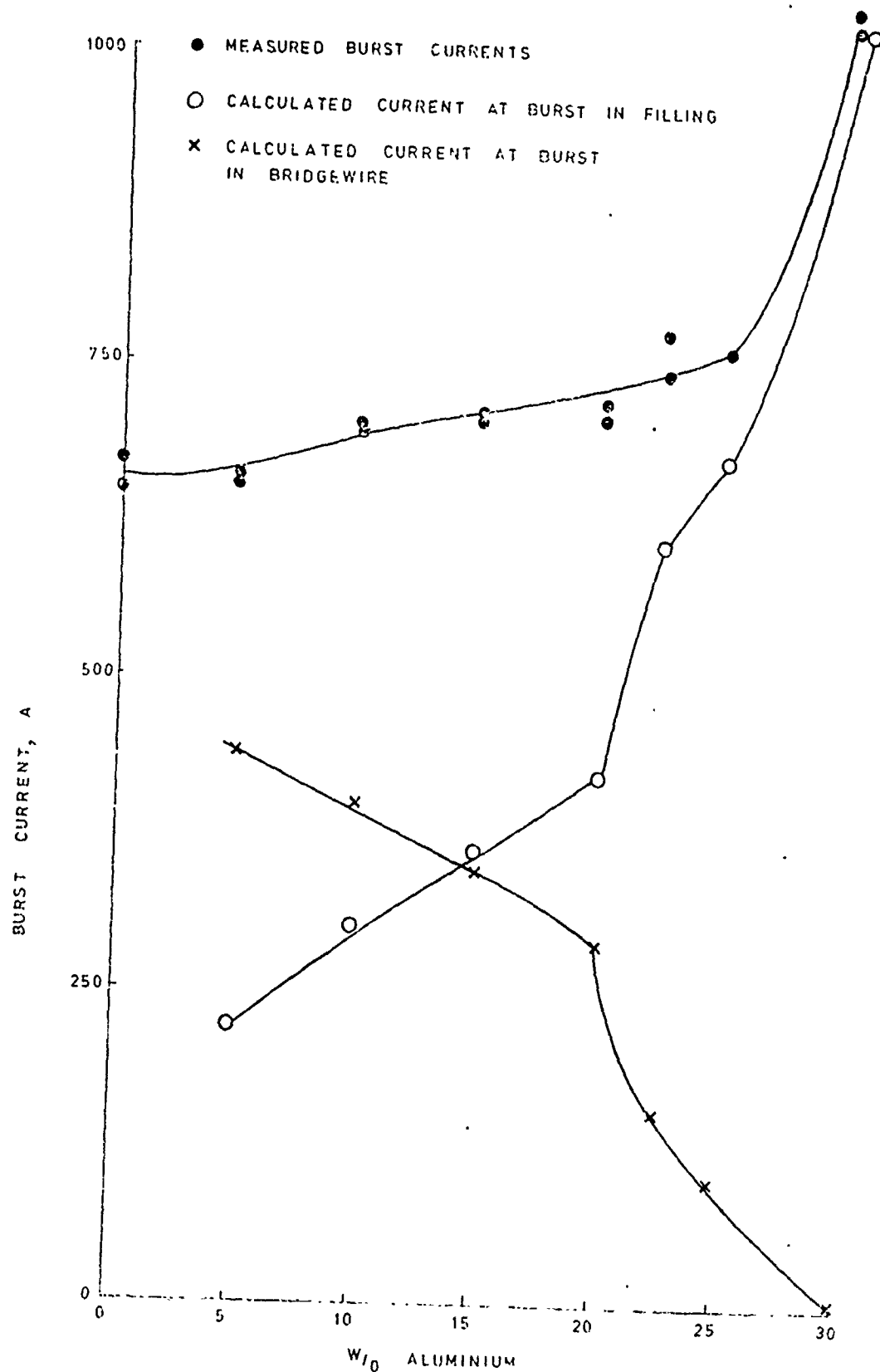
FIGURE 7 Measured Burst Currents and Calculated Current Distribution at Burst for Experimental Igniters Filled Aluminium / Potassium Perchlorate Mixes at 65% TMD

661
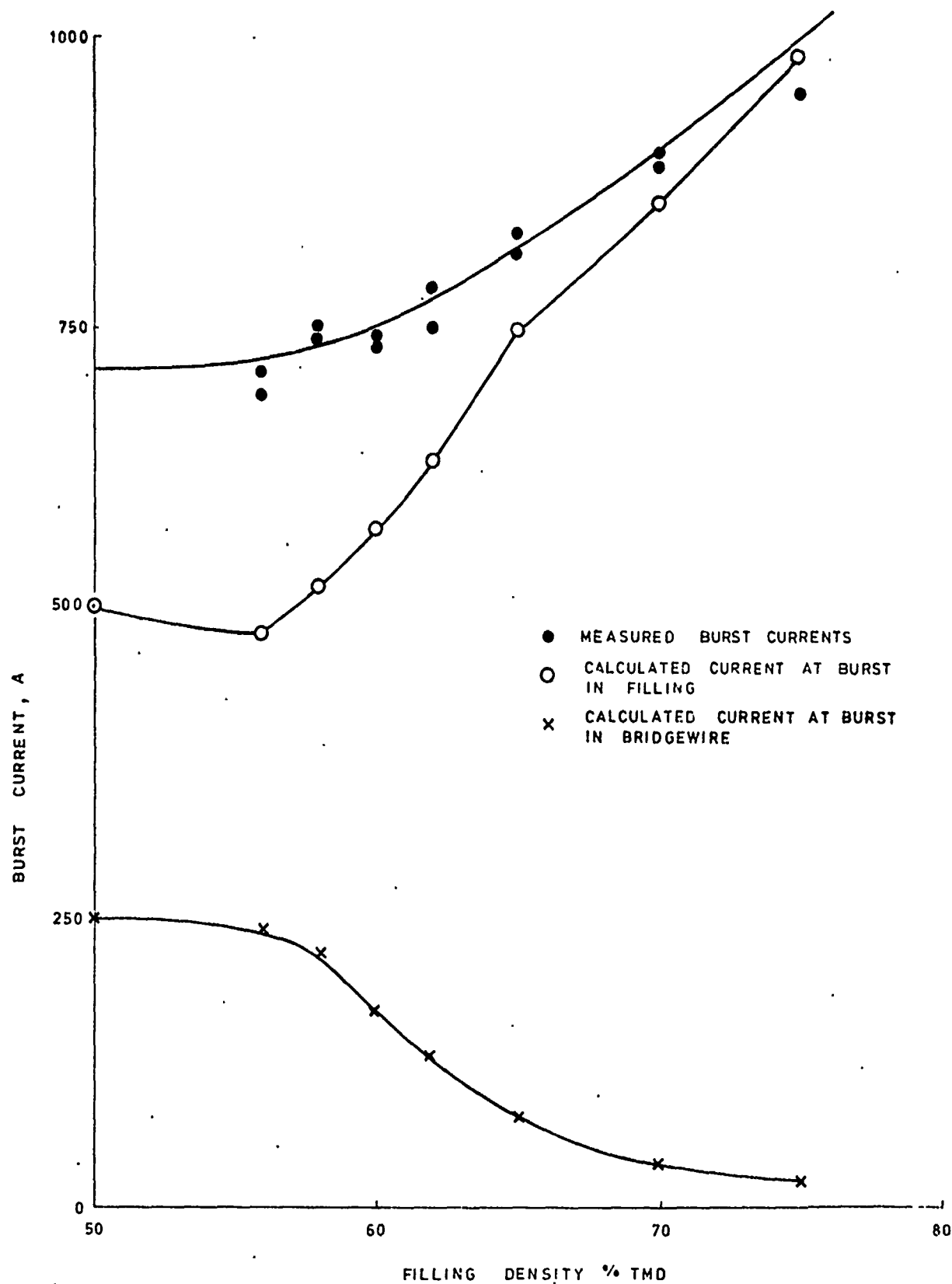
FIGURE 8. Measured Burst Currents and Calculated Current Distribution at Burst for Igniters filled SR818, Batch 4.

662
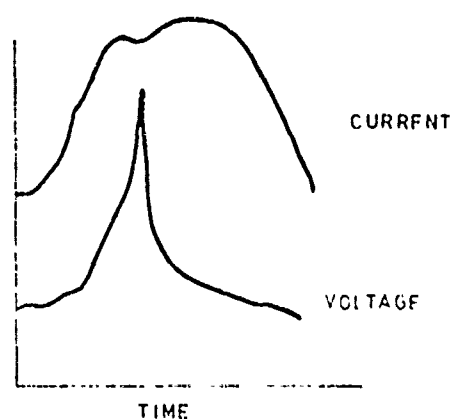
10 % ALUMINIUM 65 % TMD (EXPERMENTAL IGNITER)

25 % ALUMINIUM 65 % TMD (EXPERIMENTAL IGNITER)
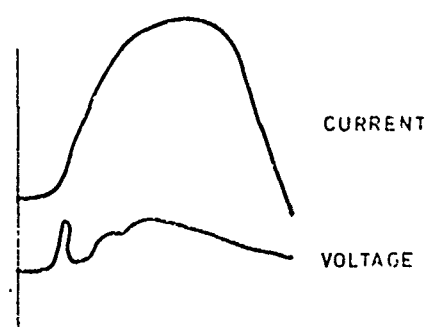
22·5 % ALUMINIUM 70 % TMD (E B W IGNITER)

FIGURE 9. Current and Voltage Waveforms
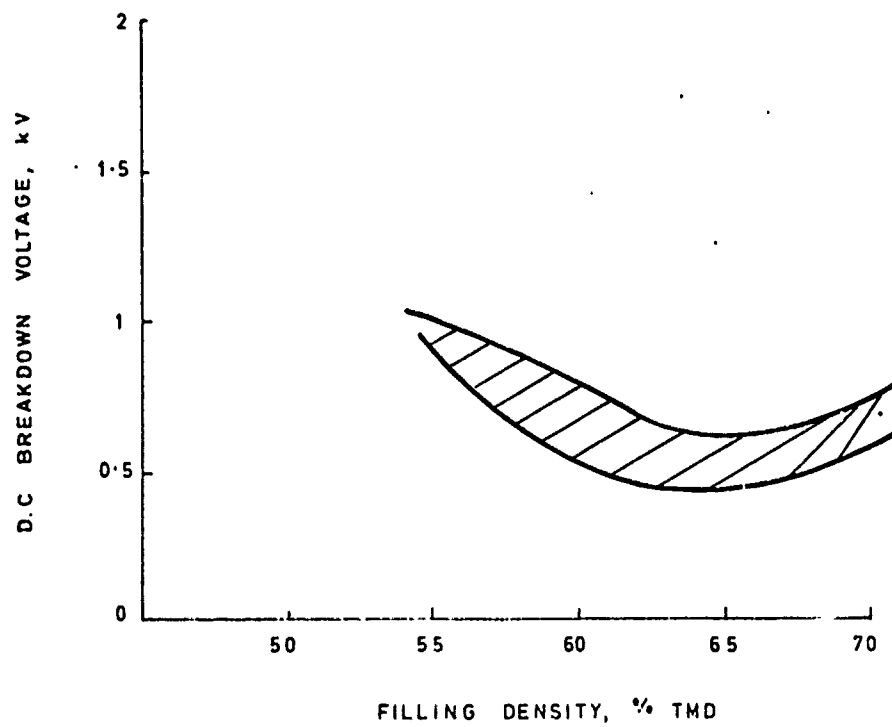
FIGURE 11 Filling Density / D.C. Breakdown Voltage of Unbridged Igniters Filled with MIXAY

664
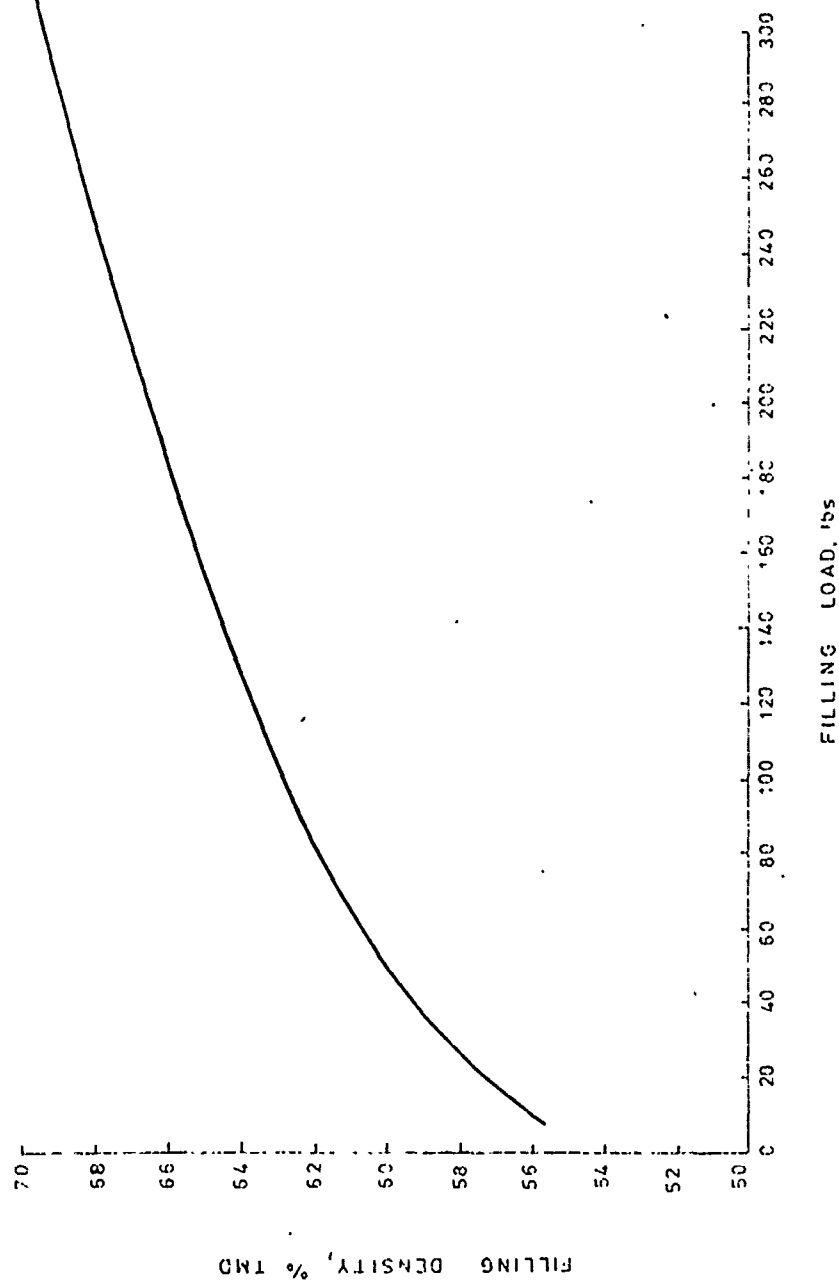
FIGURE 12 Filling Load / Filling Density for igniters Filled with MIXAY
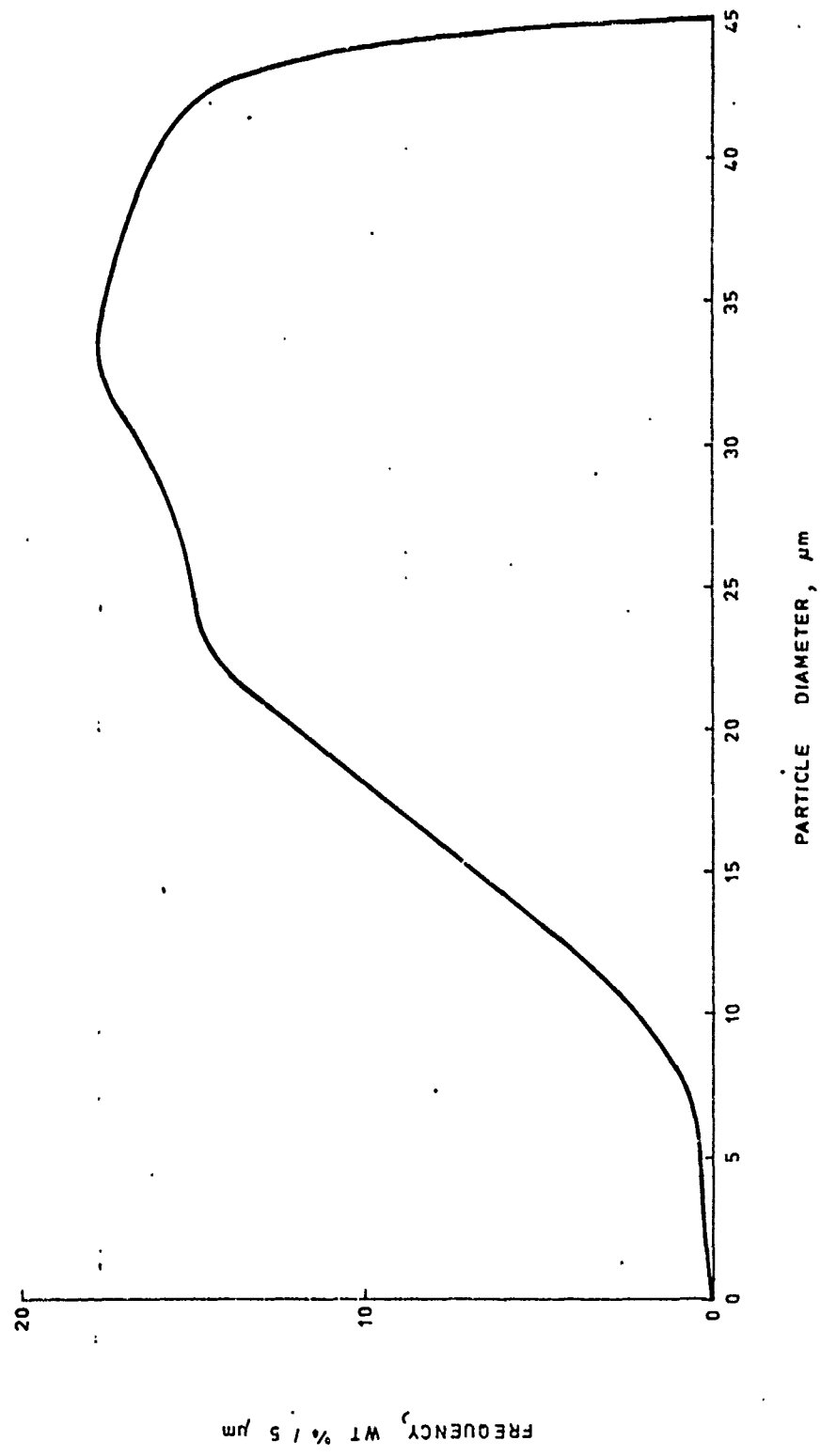
FIGURE 13. Particle Size Distribution of SR818A Potassium Perchlorate (<45 μm Mesh)
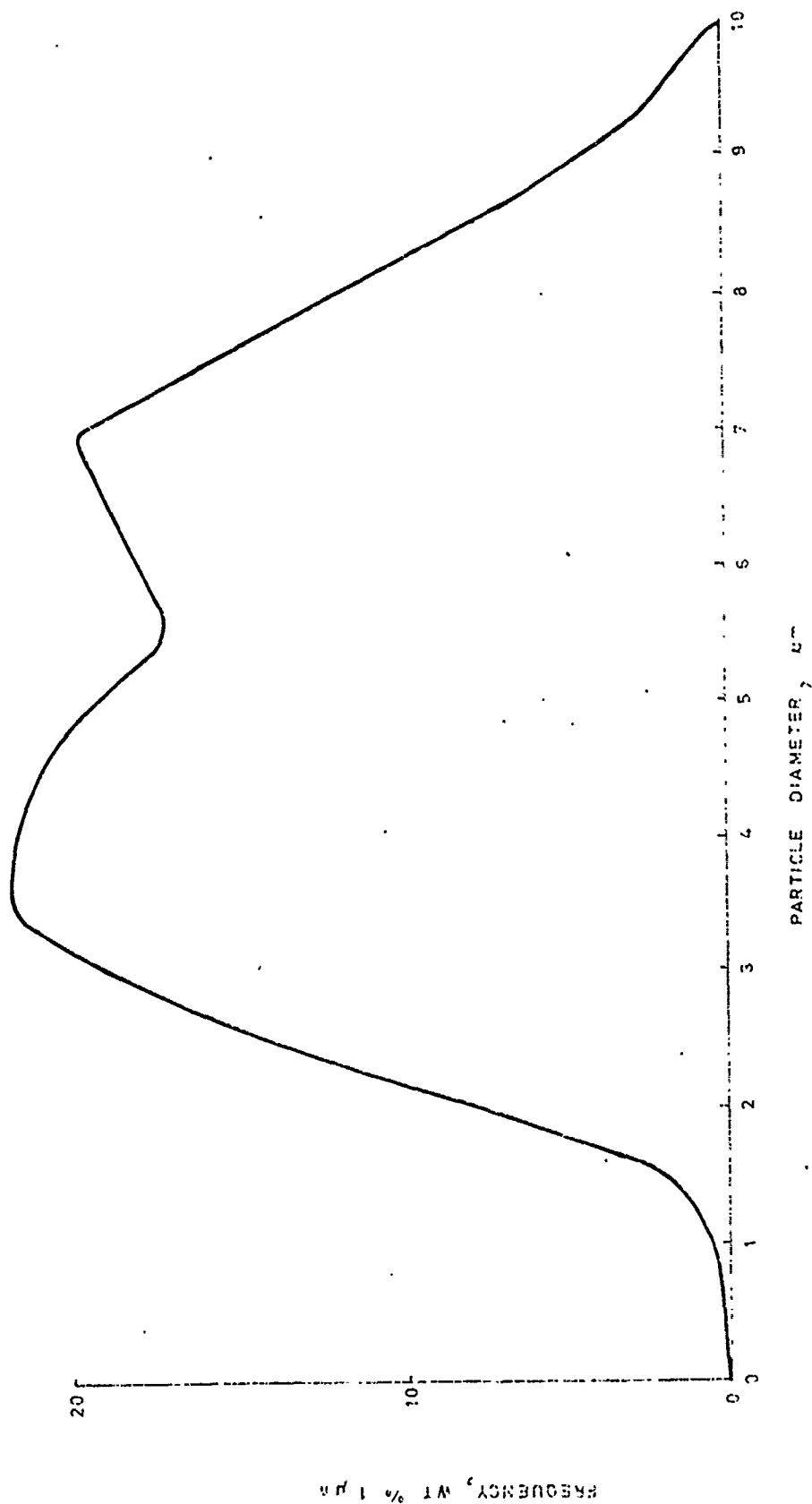
FIGURE 14. Particle Size Distribution of Reynolds Aluminium Used in SR818A

IMPROVED GREEN FLARES

H. A. WEBSTER III

Applied Sciences Department

Naval Weapons Support Center, Crane, Indiana

ABSTRACT

Formulas for improved green flares are presented. Improvements
in intensity and color are reported. Candlepower values of over
71,000 cd have been obtained with no loss in excitation purity.
Efficiencies are better than 10,000 cd-s/g. Molecular emission
from boron oxides, barium oxides and barium chlorides is observed.

INTRODUCTION

The production of a good green colored signal has long been the nemesis of the pyrotechnician. This is especially true if a good green signal is defined as one with not only good color but also a large luminous efficiency. An excellent review of green signals and their associated problems has been given by Jackson, Kaye and Taylor.[1] Green signals currently in use are composed of magnesium, potassium perchlorate, barium nitrate, some chlorine donor (e.g., polyvinyl chloride), other color additives such as copper and a binder. One standard Navy green flare has a typical output of dominant wavelength (λ_D) = 562 nm, excitation purity = 53%, luminous power (cp) = 20000 cd, a burn time of 29 seconds and a luminous efficiency of 4300 cd-s/g. In the earlier work reported by Jackson, Kaye and Taylor an improved green signal composed of Delrin ® and barium chlorate monohydrate was developed.[1] This flare had λ_D = 552 nm, excitation purity = 78%, luminous power = 320 cd, burn time = 80 seconds (calculated) and luminous efficiency = 170 cd-s/g. Thus this flare has a better color but the color can be obtained only with a large loss in luminous efficiency. In limited field tests under clear night conditions these flares were visible at slant ranges of ten miles.

In the course of some experiments on improved illuminating flares one of the compositions under consideration produced a good green flare with high intensity. This report describes preliminary investigations to provide additional information on this formula.

EXPERIMENTAL*

The formulas used in these experiments are given in Table 1. All materials were standard Mil Spec materials except the Delrin ® and barium chlorate used in CO-31. The Delrin ®** was obtained from E. I. DuPont. The barium chlorate was obtained from Ventron, Alfa Products Division. The average magnesium particle size was 375 microns. The boron particle size was approximately 1 micron. The barium nitrate, polyvinyl chloride, hexachlorobenzene and Teflon ®** particle sizes

---

* In order to specify procedures adequately, it has been necessary occasionally to identify commercial materials and equipment in this report. In no case does such identification imply recommendation, endorsement, or criticism by the Navy, nor does it imply that the material or equipment identified is necessarily the best available for the purpose.

** Delrin, Teflon-Registered Trademarks of E.I. DuPont de Nemours, Co.

were not measured but all were less than 400 microns. The binder was a mixture of Dow epoxy resin, CX 7069.7, and a polyamine, CX 3482.1, in a ratio CX 7069.7 - 80% and CX 3482.1 - 20%.

After mixing the compositions were pressed into fishpaper tubes at 5.62×10^7 N/m^2 (8000 psi). The tubes had been coated with the binder mixture twenty-four hours prior to pressing. One hundred and fifty grams of composition were used for each candle. The finished candles were 4.4 cm in diameter and 5.5 cm long.

The flares were burned face-down at a distance of 1000 cm from the radiometers and 400 cm from the spectrographs. The radiometers are fitted with filters such that the filter + detector response curves match as closely as possible the CIE color-matching functions $\bar{x}$, $\bar{y}$, and $\bar{z}$. Measurements from each detector then give the tristimulus values X, Y and Z from which the chromaticity coordinates, x and y, can be calculated. The values of dominant wavelength and purity are then determined by the standard graphical method after plotting the chromaticity coordinates on a chromaticity diagram.[2] The radiometer which gives the tristimulus value of Y is calibrated against an NBS traceable standard lamp to give the values of luminous power.

Visible spectra were taken with a Spex 1802 one meter spectrograph equipped with a 600 gr/mm grating which gives a dispersion of 16.5 A/mm in the first order. These spectra have not been reduced and were used only to qualitatively identify specific emitters.

RESULTS

The experimental results of this investigation are summarized in Table 1. Values are given for candlepower, burn time, luminous efficiency, dominant wavelength and purity for each experimental composition. The results are averages of four to six flares burned. The average experimental error in luminous efficiency is ± 7 percent. The experimental error in the value of dominant wavelength is ± 2 percent and the error in the purity is ± 5 percent.

The colors observed during the flare burns were green to greenish-white. The worst green was given by CO-26, although it was more intense than CO-22 and CO-23 both of which gave excellent greens but were not very intense. Compositions CO-12 to CO-20 all gave comparable green colors of varying intensity. These colors all appeared to be better than CO-30, the Navy standard green flare formula. The barium chlorate - Delrin formula, CO-31, would not burn. A comparison of the above data with that given in Table 1 shows good agreement between observation and instrumentation. Figure 1 shows a plot of the chromaticity coordinates for all flares.

DISCUSSION

The flares burned in these experiments fall into three basic categories: (1) those with boron, CO-12 - CO-16; (2) those with boron and a chlorine source, CO-18 - CO-23; (3) those with boron and a fluorine source, CO-26. The results indicate that the use of boron, magnesium and barium nitrate produces good green flares which have excellent efficiencies. The excitation purity of these flares is not as good as that of the flares which contain a halogen source. The replacement of 5-10% of the fuel with hexachlorobenzene tends to increase the burn time while lowering the luminous output with a resulting small loss in efficiency. The color purity does, however, improve. The replacement of fuel with polyvinyl chloride further reduces the efficiency. The replacement of oxidizer by Teflon tends to lower efficiencies while making the flare color more yellow.

The visible spectrum of a standard green flare has been analyzed previously.[1] While the spectra obtained in this study do not agree exactly with those of Jackson, et. al., they are apparently close enough to not warrant further analysis at this point. The major molecular emitters in the standard Navy green flares, CO-30, are $BaCl$ (λ = 514 nm, 517 nm, 521 nm, 524 nm and 532 nm), BaO (460-678 nm), Ba_2O_2 and $BaOH$ (480 nm, 487 nm, 502 nm, 512 nm and 550 nm), and $CuCl$ (extensive system 405-470 nm). Atomic emission from copper, barium, sodium and potassium is observed. There is also the underlying continuum due to hot solid particles such as MgO.

In the boron flares the primary emission is from the boric acid fluctuation bands system, BO_2, with maxima at 452 nm, 471 nm, 493 nm, 518 nm, 545 nm and 580 nm. These bands are overlapped by the $BaO/BaOH$ system. The increased flame temperatures of CO-12 - CO-16 when compared to the standard green, CO-30, account for the increased intensity. The increased efficiency is probably a result of the boron oxides being better emitters than the $BaCl$. The shorter dominant wavelength in the boron flares is due to reduced molecular emission in the red region of the spectrum, apparently from BaO and $BaCl$. The lower purity is due to the increased emission in the background continuum - a result of the solid particles being at a higher temperature.

When the chlorine source is added the emission is a result of $BaCl$, BaO, $BaOH$, and BO_2. The efficiency does not decrease drastically with C_6Cl_6 but does with PVC as the chlorine source. The improvement in purity when compared with CO-30 is due to added emissions in the green from BO_2 and a reduced background continuum due to the lower temperatures.

The use of Teflon® produces BaF emission at 495 nm, 499 nm and 500 nm, an as yet unidentified emission in the red, and in the flares with B the BO_2 fluctuation bands. The unexpected red emission and

the increased underlying continuum produced a flare with much higher dominant wavelength than expected. Another interesting result was the disappearance (or drastic reduction) of BaO and BaOH bands. This indicates that the BaF is forming preferentially over BaO - a not unexpected result.

To get some idea of what these increases in candlepower mean, calculations were done by the method described by Middleton[3] to determine range of visibility of a colored signal. These results are summarized in Table 2. The meteorological ranges were assumed to be 5, 10 and 20 miles. The target distances were then determied for flares of 300, 20000, and 70000 cd at illumination levels of 10^3, 10^0 and 10^{-4} ft-cds. A level of 10^3 corresponds to a clear day, 10^0 to twilight and 10^{-4} to starlight. At the lowest level of illumination on a clear starlight night a 70000 cd flare can be seen twice as far as 300 cd flare. However, under daylight conditions - not a situation where flares are now used - the 70000 cd flare should be visible at ranges of 13000 yds while the 300 cd flare is visible only for 1700 yds. This of course assumes an ideal situation where the observer knows the location of the source. Effects of atmospheric scattering and color shifts have not been considered in this calculation. Thus it is conceivable that the higher efficiency green flares could be used as day signals.

CONCLUSIONS

Green flares have been demonstrated which retain acceptable dominant wavelength and purity and produce efficiencies of 6000 - 11000 cd-s/g. The emission from these flares comes from a combination of molecular emission from BO_2, BO, BaO and BaOH. While the purity of these signals is not as good as other flares which contain chlorine sources for the formation of BaCl the dominant wavelength is shorter (as much as 100 A in the case of a comparison with a standard green flare) making the flares appear less yellow. The addition of a fluorine source causes the preferential formation of BaF instead of BaO. This could have some future application in improving the purity of green flares.
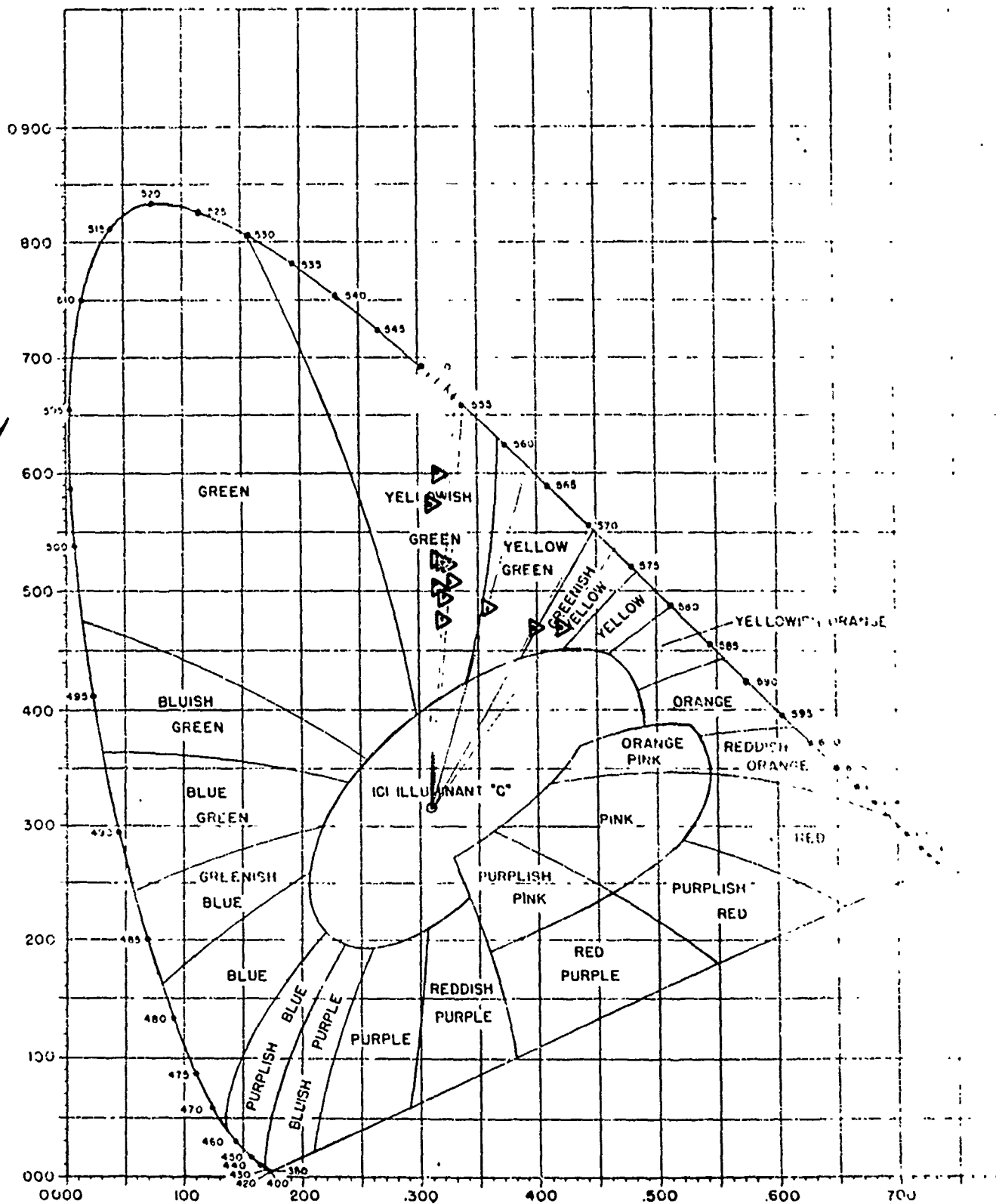
	CO-12	CO-13	CO-14	CO-15	CO-16	CO-18	CO-19	CO-20	CO-22	CO-23	CO-25	CO-30	CO-31
Mg	40	33	25	35	39	30	25	40	14	--	30	21	--
B	15	12	15	5	6	10	10	10	6	7	10	--	--
$Ba(NO_3)_2$	40	50	55	55	50	50	50	40	60	76	35	22.5	--
$KClO_4$	--	--	--	--	--	--	--	--	--	--	--	32.5	--
Cu	--	--	--	--	--	--	--	--	--	--	--	7	--
PVC	--	--	--	--	--	--	--	--	15	12	--	12	--
C_rCl_6	--	--	--	--	--	5	10	5	--	--	--	--	--
Teflon	--	--	--	--	--	--	--	--	--	--	20	--	--
BaH_2	--	--	--	--	--	--	--	--	--	--	--	--	--
Binder	5	5	5	5	5	5	5	5	5	5	5	5	--
$Ba(ClO_3)_2 \cdot H_2O$	--	--	--	--	--	--	--	--	--	--	--	--	75
Delrin	--	--	--	--	--	--	--	--	--	--	--	--	25
Candlepower (kcd)	47.8	59.9	59.5	63.4	71.7	44.6	25.7	29.0	7.9	4.0	13.7	12.2	no burn
burn time (s)	20	19	19	23	23	23	26	29	46	45	35	42	
efficiency (cd-s/g)	6373	7587	7537	9721	10994	6839	4455	5607	2423	1230	3197	3416	170*
dominant wavelength	553	554	554	552	554	555	554	554	551	552	570	562	552*
purity	58	47	47	53	52	55	60	60	70	59	63	58	78*

* From Jackson, Kaye and Taylor (reference 1)

TABLE 1   EXPERIMENTAL DATA

ILLUMINANCE LEVEL (ft-cds)

Met. Range (yds)	10^3	10^0	10^{-4}
Intensity = 300 cp			
8800	1400	7500	13500
17600	1600	11600	22000
35200	1700	16800	35000
Intensity = 20000 cp			
8800	4900	14200	21000
17600	7000	24000	36000
35200	8800	38000	61000
Intensity = 70000 cp			
8800	6500	16500	23000
17600	9500	28000	41000
35200	13000	48000	70000

TABLE 2   CALCULATED RANGES

REFERENCES

1. B. Jackson, S. M. Kaye, and F. R. Taylor, *Improved Green Signal Compositions* in *Proceedings of Second International Pyrotechnics Seminar*, held at Snowmass-at-Aspen, Colorado, 20-24 July 1970. (Sponsored by Denver Research Institute, University of Denver, Denver, Colorado), p. 83. Available National Technical Information Service, 5285 Port Royal Road, Springfield, Virginia, 22161 - AD 913407.

2. G. Wyszecki and W. S. Stiles, *Color Science: Concepts and Methods, Quantitative Data and Formulas* (John Wiley and Sons, Inc., NY, 1967).

3. W. E. K. Middleton, *Vision Through the Atmosphere* (University of Toronto Press, Canada, 1952).

ACKNOWLEDGEMENTS

ELECTRICAL RESISTIVITY OF $TiH_x/KClO_4$

Koto White, John W. Reed, Calvin M. Love,
John A. Holy and Jerome E. Glaub

Mound Facility
Miamisburg, Ohio

ABSTRACT

Various factors affecting the electrical resistivity of the pyro-
technic pressed powder $TiH_x/KClO_4$, which is sensitive to hot wire
ignition yet quite spark insensitive, were evaluated.

The electrical resistivity of the TiH_x (x = 0.19-1.9, pressing
pressure 10 - 160 kpsi) and $TiH_x/KClO_4$ (x = 0.19-1.9, pressing
pressure 10 and 20 kpsi) were correlated with their pressing
pressure, stoichiometry, and powder surface area. The resistivity
increases with x and with surface area, and it decreases non-
linearly with pressing pressure. In addition, the effect of
electrostatic discharge pulsing on resistivity was tested for
various samples of TiH_x and $TiH_x/KClO_4$ pressed pellets. For the
higher resistivity pellets ($\rho > 1$ $\Omega \cdot cm$), a decrease in resistivity
was observed. For low resistivity pellets ($\rho \leq 1$ $\Omega \cdot cm$), no change
in resistivity was observed, yet an increase in current flowing
through the pellets occurred. The effect of temperature on re-
sistivity for TiH_x pressed pellets from below liquid nitrogen tem-
perature to 500 K was also studied.

ELECTRICAL RESISTIVITY OF TiH_x AND $TiH_x/KClO_4$

Koto White, John W. Reed, Calvin M. Love,
John A. Holy and Jerome E. Glaub

Mound Facility*
Miamisburg, Ohio

I. INTRODUCTION

Objectives An understanding of electrical properties of pyrotechnic compositions is important because these properties affect ignition behavior. In hot-wire initiated actuators and ignitors, where a pyrotechnic material is in contact with a bridgewire, it is possible for the pyrotechnic material to have sufficient electrical conductivity that a parallel electrical path exists between the bridgewire posts. With the low energy delivered to this type of device, it is possible for the parallel-path condition to produce a situation where the bridgewire is insufficiently heated and a device malfunction occurs. Hence, the objective of this project is to determine and evaluate the factors that affect the electrical resistivity of the pyrotechnic material used in such devices. Since a pressed-powder mixture of titanium subhydride (TiH_x) and potassium perchlorate ($KClO_4$) is being used in certain pyrotechnic valve actuators, those two materials, individually and blended, were studied.

Four-Probe Resistivity Measurement Technique All resistivity measurements were made using the four-probe technique illustrated in Figure 1. An electrical current is carried through the two outer probes, which sets up an electric field in the sample (in the figure, the electric field lines are solid and the equipotential lines are broken), and the two inner probes measure the potential difference between point B and point C. These inner probes are made to draw no current by use of the high input impedance ($10^9 \Omega$) voltmeter in the circuit. Thus, the unwanted voltage drop (ohmic IR drop) at point B and point C caused by the contact resistance between probes and the sample is eliminated from the potential measurements. Since these contact resistances are very sensitive to the pressure with which the two surfaces are pressed together and to surface condition (such as oxidation of both surfaces), errors introduced into the conventional two-electrode technique (in which the potential measuring contact passes a current) can be quite large.

Using a four-point probe of equal spacing, the resistivity (ρ) of the sample can be calculated from measured quantities, V [potential difference between point B and point C in Figure 1, volts (V)], I [current, amperes (A)] and S [electrode spacing centimeters (cm)] as:

$$(\Omega \cdot cm) = 2\pi S \cdot \frac{V}{I} \ [1].$$

RESISTIVITY AS A FUNCTION OF PELLET CHARACTERISTICS

All resistivity measurements in this section were made using a spring-loaded, four-point probe of equal-probe spacing (S=0.025 in.) (Alessi Industries). For each sample pellet, resistivities of four different locations on each pellet side were averaged for the average pellet resistivity.

<u>TiH_x Pressed Pellets</u> In order to investigate the factors affecting the resistivity of TiH_x pressed pellets at room temperature, 10 different batches of TiH_x powder were selected from the stoichiometry group of x=1.9, 1.5, 0.65, and 0.19. Each group includes a batch with high surface area and a batch with low surface area. Each batch of material was pressed into several pellets with pressing pressures varying from 10 to 160 kpsi. The results are shown in Figure 2 as a function of pellet density with different stoichiometric groups represented.

Our findings were:

(1) When pressing, it took more force to press high surface area materials to a certain density even though they have various particle size distributions and particle sizes.

(2) When resistivities were compared within a similar stoichiometric group, a higher surface area material generally showed a higher resistivity.

(3) The difference in resistivity between batches was larger at the lower density.

(4) A resistivity versus stoichiometry relationship was seen for a group of high surface area materials, and a higher stoichiometry seem to lead to a higher resistivity. (See Figure 3)

(5) Nonhomogeneity of resistivity within a pellet was noticed and was more evident for lower density pellets.

The first four observations seem to be related to the fact that the individual TiH_x powder particles are coated with a titanium oxide

layer. As shown in a hypothetical picture of powder particles (Figure 4), overall resistivity of the sample has three components. One component is the resistivity of the titanium hydride particle core, which is in the order of $\sim 10^{-4} \Omega \cdot$cm. A second component is the resistance from the titanium oxide layer, which depends upon the thickness of the layer and the type of oxide. A third component is the contact resistance between adjacent powder particles, which is likely to depend on the pressing pressure, surface area, and particle size distribution. Since the first component is most likely much smaller than the others, the resistivity variation we observed between different batches and different pressing pressure must be caused by the second and/or third components.

$TiH_x/KClO_4$ Pressed Pellets   Several batches of $TiH_x/KClO_4$ (33/67 wt %) blends with various TiH_x stoichiometries were pressed into pellets using pressing pressures of 10 and 20 kpsi. The ratios of resistivities ($TiH_x/KClO_4$ over TiH_x) are shown in Table 1. It can be seen that the effect of blending on resistivity strongly depends on the stoichiometry of TiH_x. When blended, the increase in resistivity is as small as ~15 times for X=0.19 and as large as ~10^6 times for X=1.9. This might indicate that the surface of different stoichiometric TiH_x reacts with $KClO_4$ in a different manner while blended and develops an oxide coating of different thickness and and/or of a different type. Here again, the higher surface area TiH_x seems to yield a higher resistivity $TiH_x/KClO_4$ blend.

Table 1

RATIOS OF RESISTIVITY

Material Identification	TiHx Stoichiometry	$\rho TiHx/KClO_4/\rho TiHx$	
		10 kpsi	20 kpsi
PO2040/QC1675ET	$\chi = 0.2$	36	15
PO3074/QC1761ET	$\chi = 0.69$	2.1×10^2	61
PO3089/QC1787ET	$\chi = 0.65$	2.7×10^3	1.4×10^2
PO3060/QC1744ET	$\chi = 1.52$	1.7×10^4	7×10^3
PO3062/QC1623ET	$\chi = 1.9$	$>10^6$	1.2×10^4
PO3047/QC1709ET	$\chi = 1.9$	$>10^6$	$>10^6$
PO3084/QC1709ET	$\chi = 1.9$	$>10^6$	$>10^6$

RESISTIVITY AS A FUNCTION OF TEMPERATURE

A cryostat system which is capable of attaining from 3 to 500 K
was constructed to investigate the effect of temperature on
resistivity. The cryostat (Oxford Instrument Model CF 100) was
cooled by a controlled, continuous flow of liquid helium delivered
through a transfer tube from a 60-liter storage Dewar. A 39 Ω
internal heater on the heat exchange block and a temperature con-
troller (Oxford Instrument Model DT C2) were used along with helium
flow to maintain any desired temperature. Two thermocouples were
located inside the cryostat. One was on the heat exchange block
and was used to control the heater output; the other was very close
to the sample and used for actual temperature measurement and for
indication of thermal equilibrium. Insulation of the transfer
tube was provided by cold exhaust helium gas returning from the
cryostat and by an evacuated space in the outer jacket. The cryo-
stat was insulated by two vacuum spaces separated by a radiation
shield. The initial checkout of the system was accomplished using
a piece of titanium metal as a standard sample. The probe spacer
was fabricated from reinforced phenolic to better withstand the
thermocycle.

TiH_x Pressed Pellets Fourteen samples of TiH_x pressed pellets were
examined in this study. A thermocycle consisted of: (1) cooling to
70 K (sometimes down to 50 K), then, (2) heating to 460 K (sometimes
up to 500 K), then, (3) cooling back to the room temperature. The
heating and cooling rates were held close to 10°C/min, and the
samples were soaked at each temperature for 10 min before the measure-
ments were taken. Any residual voltage output (that is, voltage
output when no current is delivered to the sample), was probably
caused by thermal EMF's of various connections in the measuring
circuit and was subtracted from each reading. To avoid possible
crumbling around the four probe tips when being loaded in the apparatus
and during subsequent thermocycling, the pellets were pressed at high
pressures.

All resistivity data obtained as a function of temperature were
normalized by dividing by room-temperature resistivity. Therefore,
the slope of the curve is a visual indication of the temperature
coefficient of resistivity, $\alpha = 1/\rho_0 \; \partial\rho/\partial T$. This enables com-
parison of various sets of data in different resistivity ranges and
also permits visualization of percentage changes in resistivity dur-
ing each thermocycle. In doing this, the resistivity value at room
temperature before going through the thermocycle was taken to be
100%. Here, the observed change in resistivity during the thermo-
cycle is most likely because of the resistivity change of powder sur-
face coating and from the change in contact resistance between adja-
cent powder particles.

The group of $TiH_{1.9}$ samples showed large negative temperature coefficients (Figure 6-10), which indicates that the material probably has a semiconductor-like oxide coating on it. This behavior corresponds to the temperature response of Ti_2O_3 [2]. The one with higher surface area (Figure 6 and 7) showed much steeper slopes compared to the one with lower surface area (Figure 8-10). When the data are compared as a function of pressing pressure, the pellets pressed at lower pressures show slightly larger variations over identical temperature intervals. One can see that the powder contraction and expansion contribute to the negativeness in temperature coefficient. And these observations might indicate that the $TiH_{1.9}$ powder particles contract and expand noticeably with temperature, and the larger surface area enhances this effect on resistivity.

For $TiH_{0.65}$ and $TiH_{0.19}$ samples, variation in slope from variation in pressing pressure was very slight. The ones with high surface area showed a slightly negative temperature coefficient (Figures 11, 12, and 17); whereas the ones with lower surface area showed a slightly positive temperature coefficient (Figures 13-15, 18, 19) at below room temperature. Temperature responses of TiH_x, TiO and slightly off stoichiometric TiO_2 are all reported to have positive temperature coefficient. This positive temperature coefficient of oxide coating might be partially cancelled by the negative coefficient caused by particle expansion and contraction.

As for the region above 400 K, all samples examined showed a decrease in resistivity upon heating. It was also observed that once the samples were heated to above 400 K, the cooling curve did not coincide with the heating curve; and the magnitude of permanent reduction in sample resistivity upon heating depends on maximum temperature exposure. This could be because of some irreversible change in material, such as annealing or a break in the surface coating.

Some of the samples were analyzed for hydrogen content after the thermocycles; no change in hydrogen content was observed. In order to suppress the possible off-gassing of water from the samples, some experiments were conducted in a static, helium-gas atmosphere; and some experiments were performed in air above room temperature, instead of in the 10^{-5} torr vacuum. Since no significant difference in results was observed, absorbed water was probably not responsible for the resistivity changes observed under these heating conditions.

$TiH_x/KClO_4$ Pressed Pellets To date, only three $TiH_x/KClO_4$ samples have been investigated for temperature effect. Preliminary results are shown in Figures 20-22. Temperature response characteristics common to all samples are the irreversibility of the heating and cooling curves. When the sample was cooled below room temperature, the resistivity increased and even after the sample was rewarmed

the resistivity remained high (possibly because the sample was
a mixture of two materials with different expansion coefficients
which allowed the powder configuration to permanently shift upon
cooling). A very rapid increase in resistivity was observed for
above room temperature which might have been caused by a further
oxidation of the powder surface.

EFFECT OF ELECTROSTATIC DISCHARGE ON RESISTIVITY
OF TiH_x AND $TiH_x/KClO_4$ PRESSED PELLETS

All measurements in this section were made using an eight-probe
station (Alessi Industries). The probe spacing was adjusted to
S=0.02 in.

The electrostatic pulse was generated by discharging a 600 pF
capacitor through a 500 Ω resistor to simulate a human body
electrostatic discharge. The capacitor was charged at 5 kV for
all tests. The discharge path was either between four probes and
a fifth probe on the same face of the pellet or between four
probes and the entire opposite face of the pellet. Sample resis-
tivity was measured before and after being subjected to an elec-
trostatic pulse.

Test results for TiH_x pressed pellets are shown in Figure 23, and
test results for $TiH_x/KClO_4$ blend pellets are shown in Figure 24.
The data points indicate a sample examined and the arrows indicate
the magnitude of reduction in resistivity after being pulsed.
The data were plotted as a function of sample stoichiometry.

As shown in Figures 23 and 24, for both TiH_x and $TiH_x/KClO_4$, the
pellets were not affected by the electrostatic pulse when the re-
sistivity of the pellets was lower than 1 $\Omega \cdot cm$, and the pellets
with higher resistivity were all affected by the pulses. For very
high resistivity pellets, the resistivity decreased by orders of
magnitude after being pulsed. A possible explanation for this beha-
vior can be found if we review the way we pulsed the pellets.
Since we had a 500 Ω resistor in series with the pellet and the
total power (Q_O) available in the capacitor is a fixed value in
this experiment, the power actually delivered to the pellet
(Q_{pellet}) is described as:

$$Q_{pellet} = \frac{R}{R + 500} \cdot Q_O,$$

where: R is the resistance of the discharge path through the pellet.
Thus, for the pellets with approximate megaohm range resistance,
almost all the power is dissipated in the pellet; whereas for the low
resistivity pellets, only a small percentage of the total power is
dissipated in the pellet.

Overall reduction in resistivity might be caused by a breakage of
the surface oxide coating or by further introduction of defects into

the oxide structure when subjected to the pulse (defective TiO_2 is known to have a lower resistivity than that of rutile TiO_2).

For all the pellets examined, the current flowing through the outer two probes (A and D in Figure 1) increased after pulsing which may be the consequence of the probes being pushed down into the sample when subjected to pulses besides the reduction in resistivity (See the Appendix for details).

SUMMARY AND CONCLUSION

In this series of studies, we have seen the resistivity variation of TiH_x and $TiH_x/KClO_4$ pressed pellets as functions of pellet density (or pressing pressure), TiH_x stoichiometry, TiH_x powder surface area and temperature. In addition, we studied the effects of electrostatic discharge on sample resistivity.

Resistivity of titanium hydride particle cores play an insignificant role in overall pellet resistivity. The most probable explanation for the resistivity variations observed among different batches of materials and different pressing pressure is that the powder particles are coated with various thicknesses or types of oxide layers and those surface coatings break when the powders are pressed together. High surface area powders seem to have less contact area between adjacent powders when they are pressed together and they also seem to be less compactible.

Stoichiometry of TiH_x is the main factor determining the resistivity of $TiH_x/KClO_4$ blend material. High stoichiometric TiH_x seems to develop a highly resistive surface coating when blended with $KClO_4$.

When TiH_x pressed pellets were cooled below room temperature, the resistivity of the pellet went up because of powder contraction; but the resistivity of the oxide coating may go up or down depending on the type of oxide dominating. So, the overall temperature response of the samples is either cancellation or enhancement of these two effects. High surface area materials, when contracted by cooling, seem to contribute more to an increase in resistivity. For $TiH_{1.9}$, the dominating surface oxide seems to have a negative temperature coefficient. For $TiH_{0.65}$ and $TiH_{0.19}$, the dominating surface oxide has a positive temperature coefficient.

Electrostatic discharge affects the higher resistivity material more--partly because the power delivered to the sample pellet depends on the resistivity of the discharge path in the pellet from the 500 Ω resistor we have in series. The electrical discharge seems to either break the surface oxide coating or introduce further defects into the oxide structure to reduce the resistivity.

APPENDIX

The current (I) flowing through the sample can be described as:

$$I = \frac{V_O}{R+R_{contact}}$$

where

$$R = \frac{\rho}{2\pi}\left(\frac{1}{r_O} - \frac{2}{L}\right)$$

and where V_O is the voltage output of current source, $R_{contact}$ is the contact resistance between probes A, D, (Figure 1) and the sample. R is the resistance of the sample, r_O is the radius of the probe tip actually buried in the sample and L is the distance between point A and point D. R can be derived from calculating the power dissipated in the sample:

$$RI^2 = \iiint \rho \ J^2 \ d\phi \sin\theta \ d\theta \ r^2 dr.$$

Since at any point in the sample, current density, $J = I/2\pi r^2$, the above equation reduces to:

$$RI^2 = \frac{\rho \ I^2}{2\pi}\left[\frac{-1}{r}\right]_{r_O}^{\frac{L}{2}} = \frac{\rho \ I^2}{2\pi}\left(\frac{1}{r_O} - \frac{2}{L}\right)$$

Two possibilities, besides the reduction in resistivity, exist which lead to the overall decrease in current (I). One is the reduction in contact resistance $R_{contact}$; the other is the increase in the probe tip radius (r_O) actually in contact with the sample. Since the probe tip has a conical shape, r_O increases when the probe is pushed down into the sample.

REFERENCES

1. L. B. Valdes, <u>Proc. IRF</u>, Vol. 40, 1952, p. 1429, Vol. 42, 1954, p. 420.

2. J. P. Suchet, <u>Crystal Chemistry and Semiconductors in Transition Metal Binary Compounds</u>, Academic Press, N. Y., 1971.
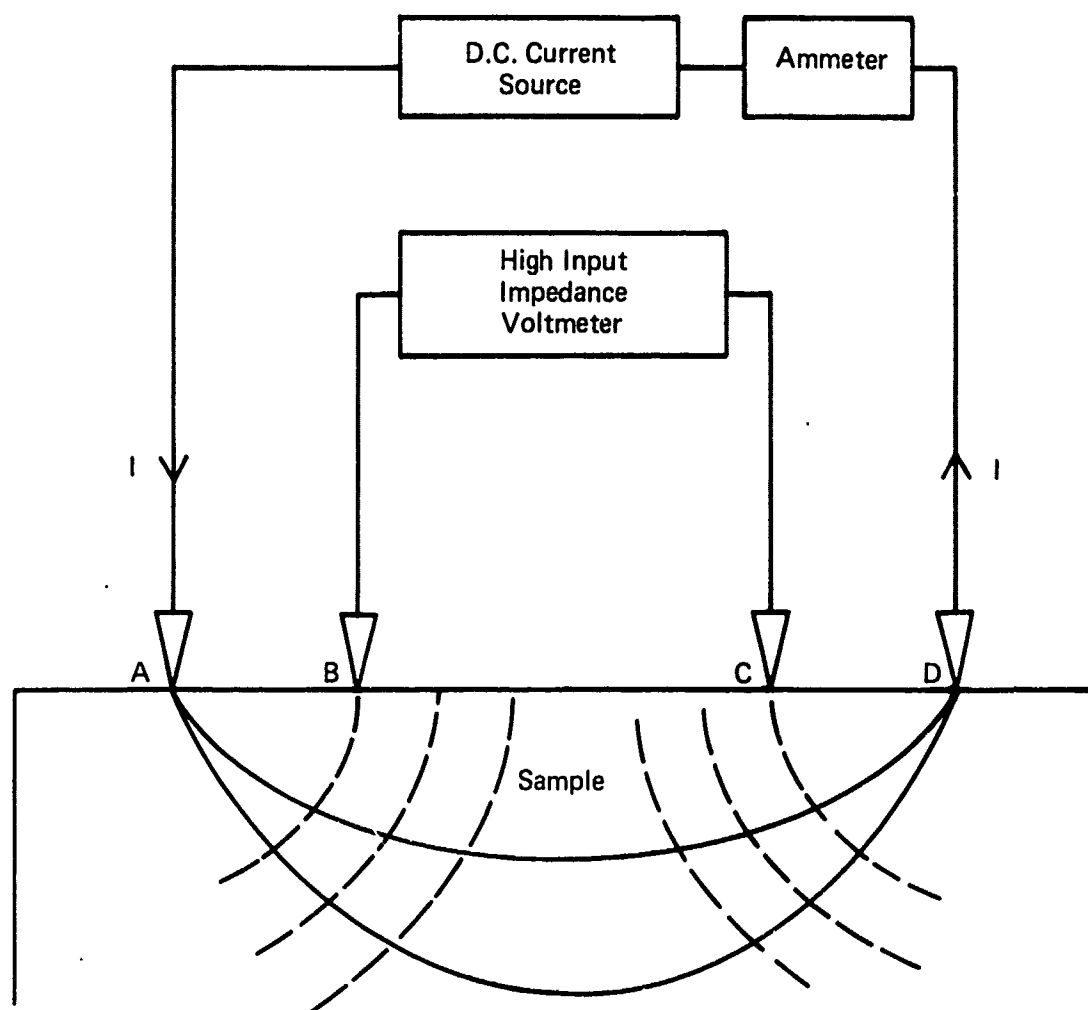
FIGURE 1 - Four-point probe.
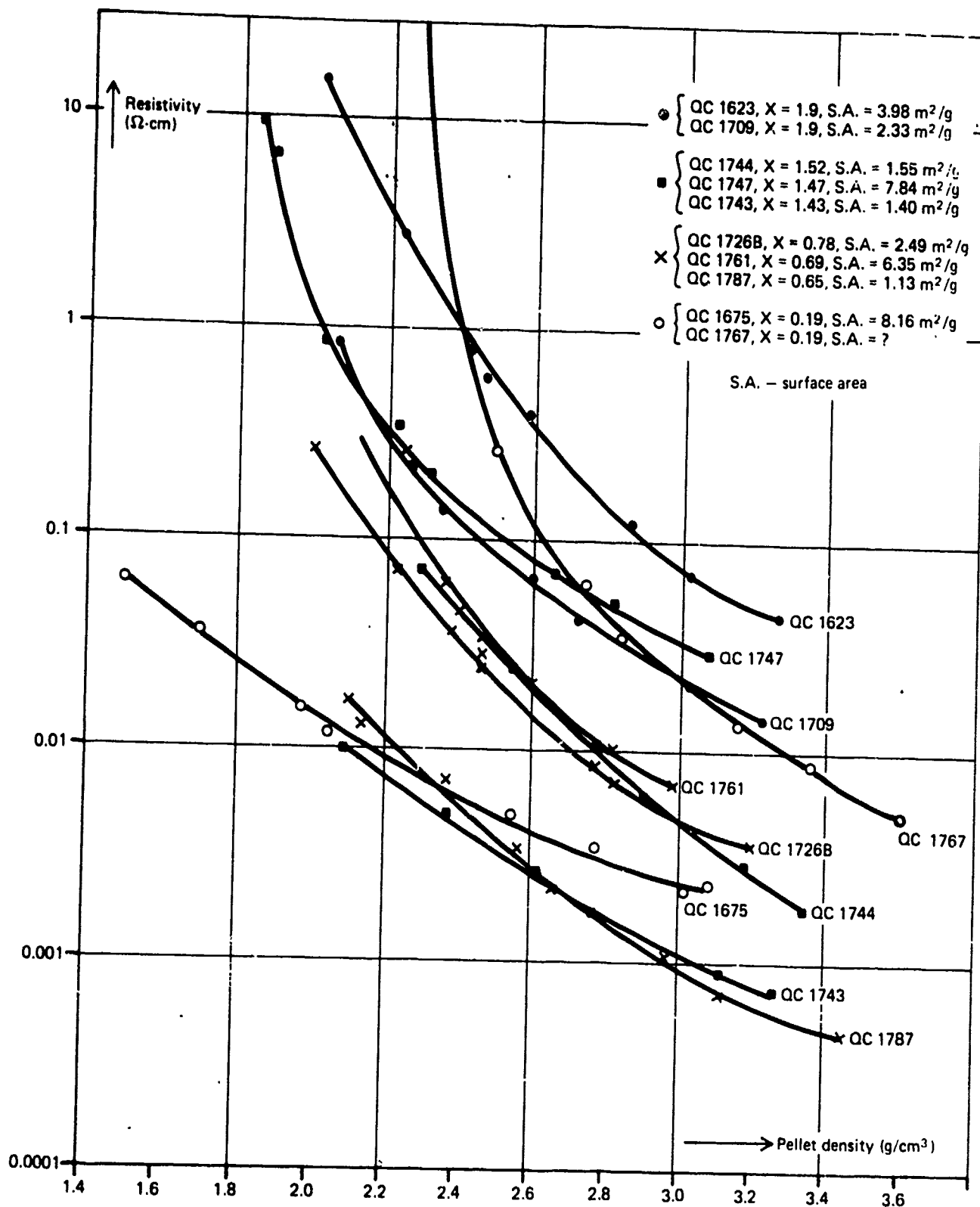
FIGURE 2 - Resistivity of TiH$_x$ pressed pellets.
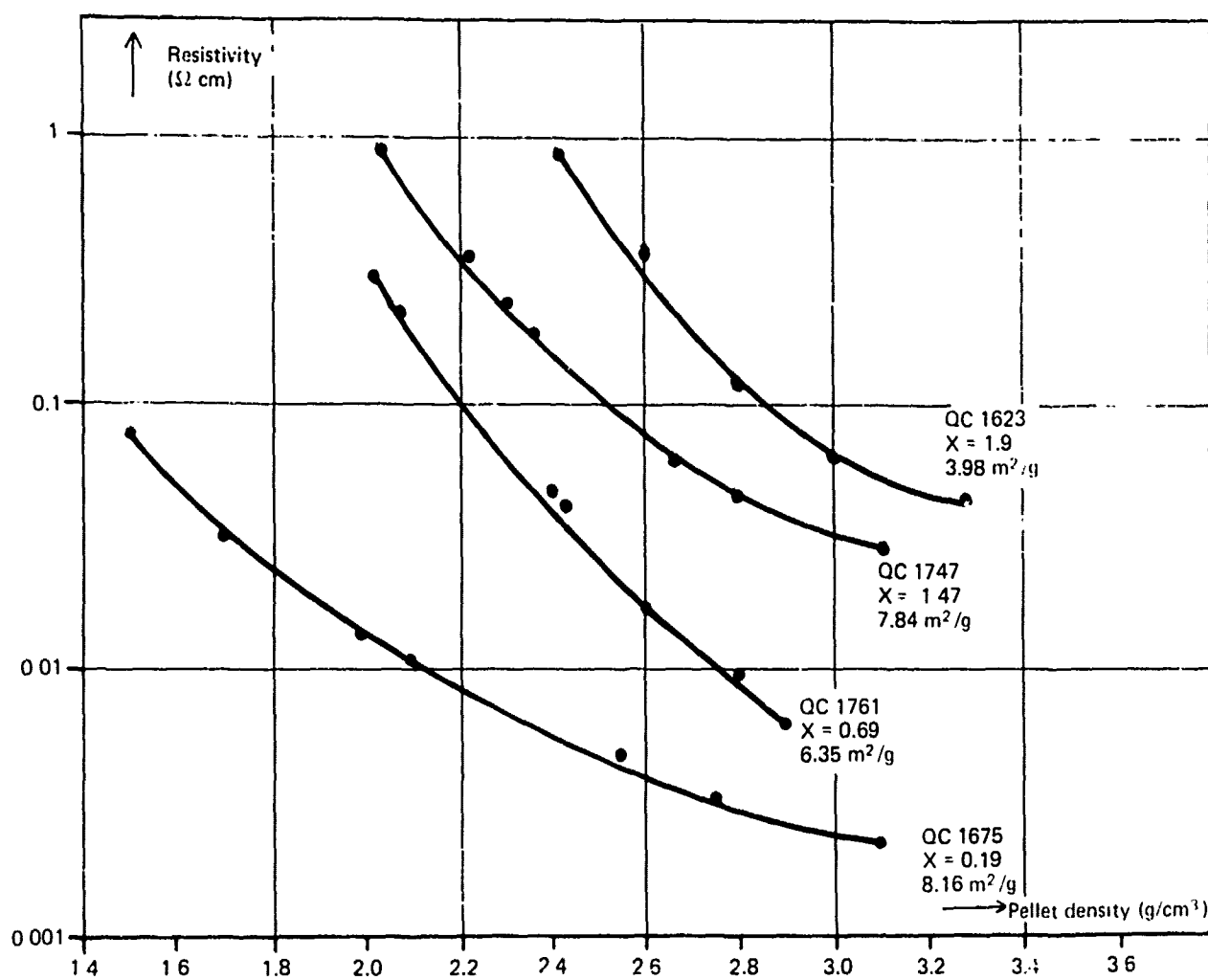
FIGURE 3 - Resistivity of high surface area TiH$_x$ pressed pellets.

$$R_{pellet} = - - - + R_{TiHx} + R_{oxide} + R_{contact} + R_{oxide} + R_{TiHx} + - - -$$

$(\rho \approx 10^{-4} \Omega \cdot cm)$

$(\rho \approx 10^{-2}$ to $10^{11} \Omega \cdot cm)$

$(\rho \gg 10^{-4} \Omega \cdot cm)$
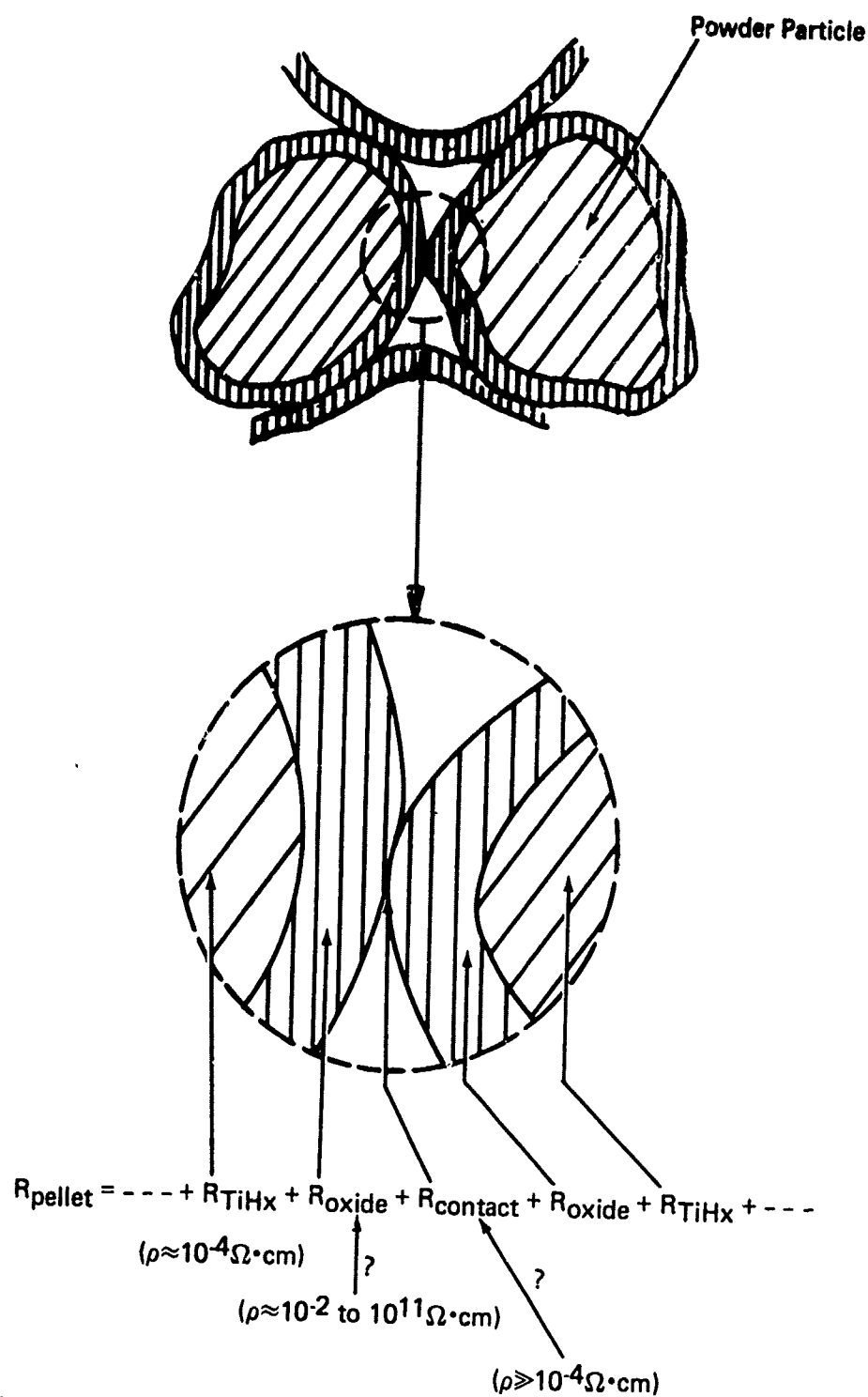
FIGURE 4 - A hypothetical picture of powder particles.
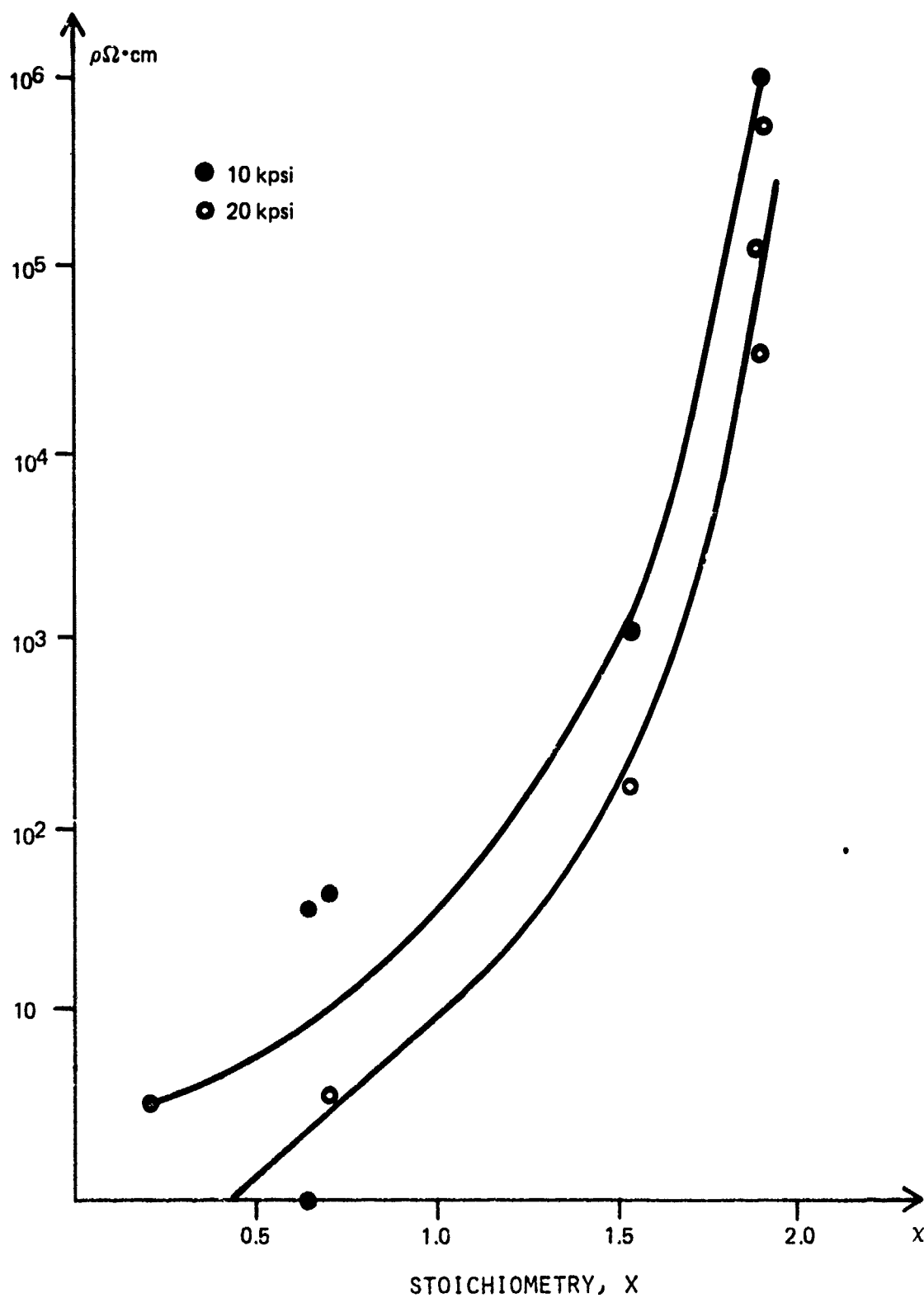
FIGURE 5 - Resistivity of $TiH_x/KClO_4$ pressed pellets.

fig. 6

fig. 8

fig. 7

fig. 9
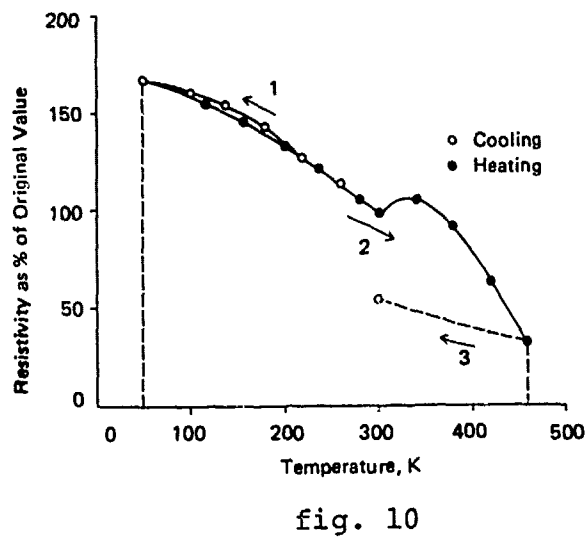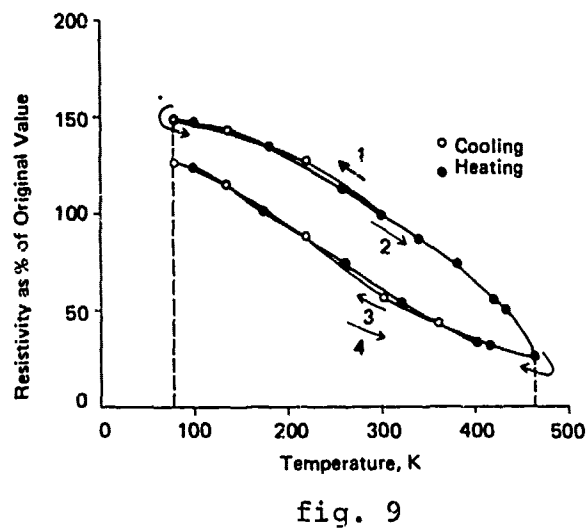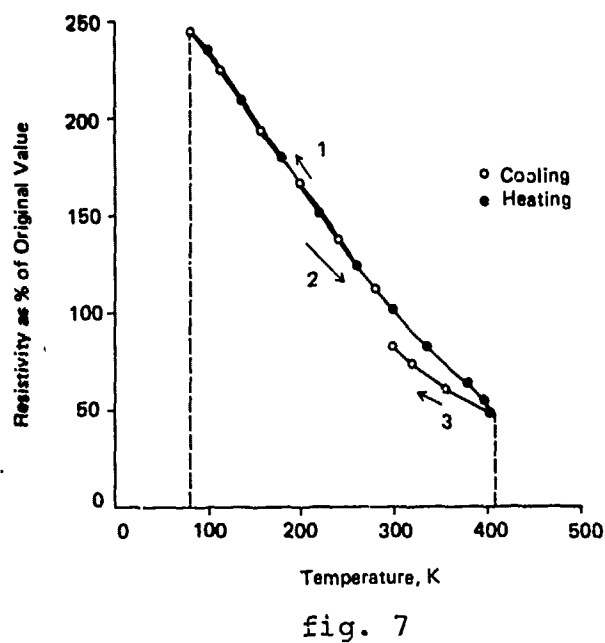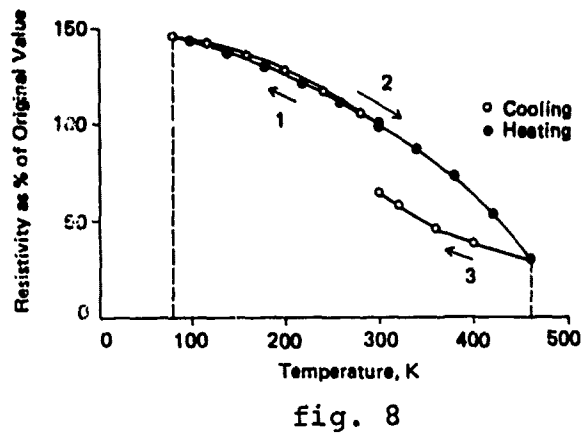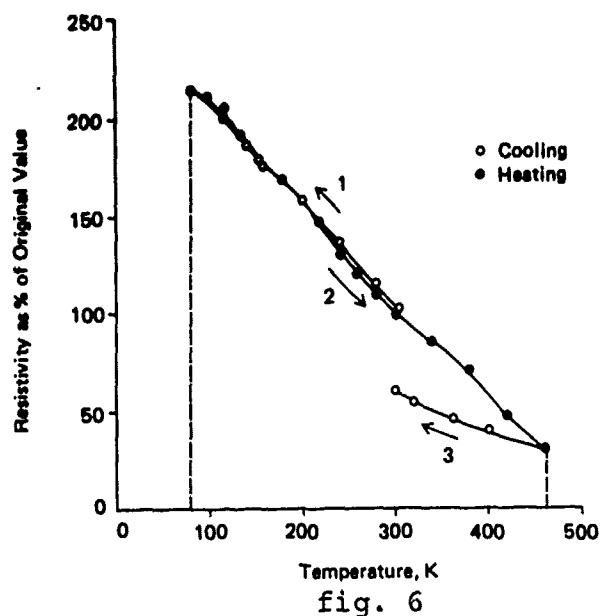
FIGURES 6-10 - Resistivity change with temperature for TiH$_{1.9}$ samples.

fig. 10
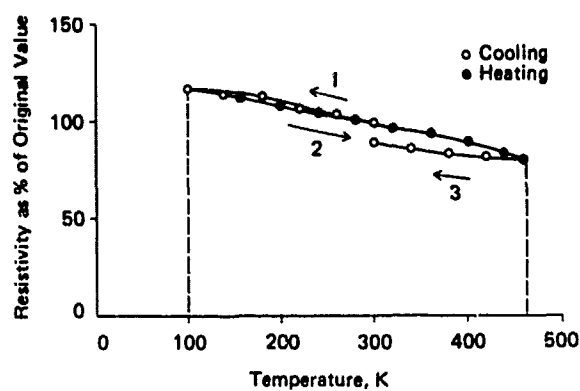
fig. 11
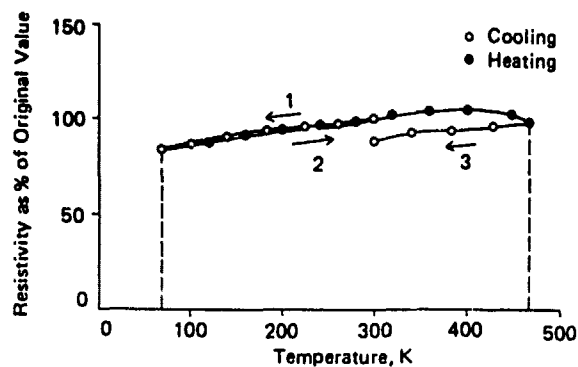
fig. 13
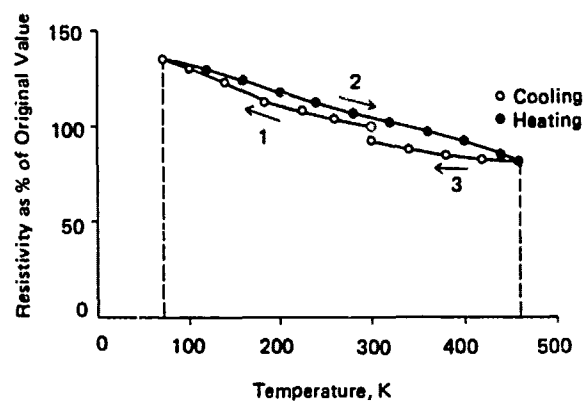
fig. 12
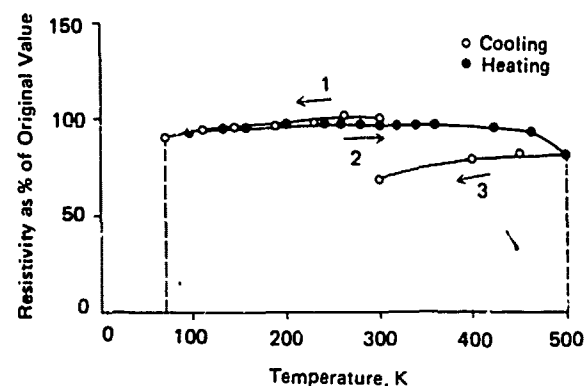
fig. 14

FIGURE 11-15 - Resistivity change with temperature' for TiH$_{0.65}$ and TiH$_{0.19}$ samples.
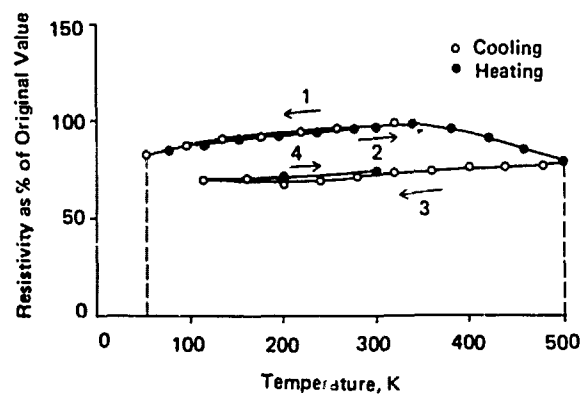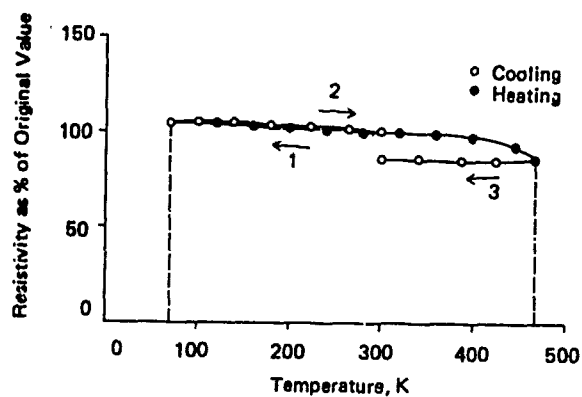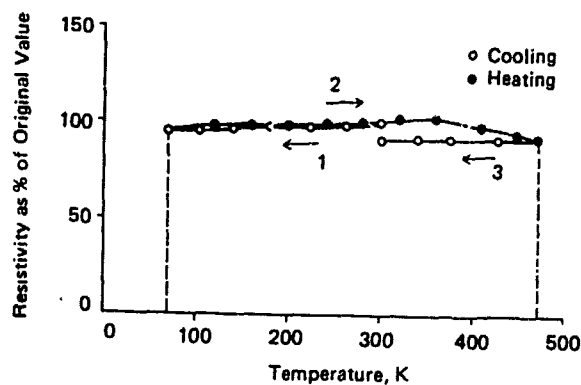

fig. 15
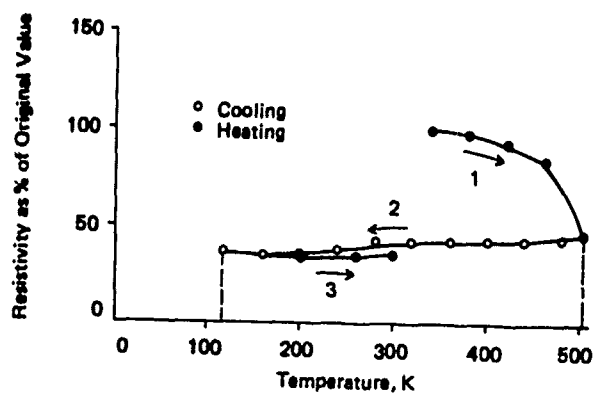
fig. 16
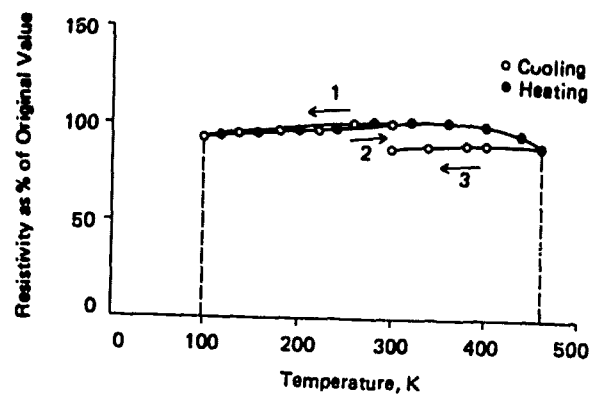
fig. 18

fig. 17

fig. 19

FIGURES 16-19 - Resistivity change with temperature for $TiH_{0.65}$ and $TiH_{0.19}$ samples.

694
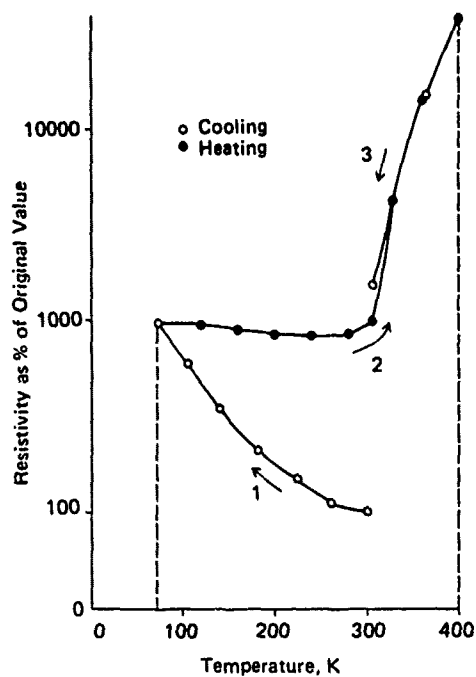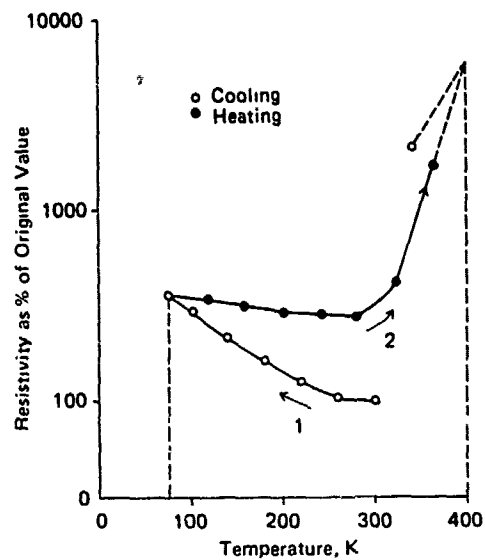
fig. 20

fig. 21

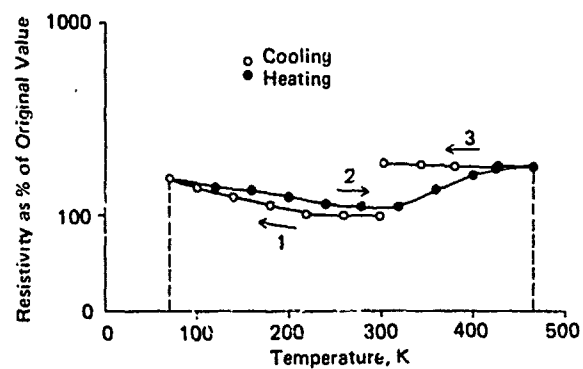
fig. 22

FIGURES 20-22 - Resistivity change with temperature for $TiH_{1.11}/KClO_4$ (fig. 22) pressed (20 kpsi) pellets.

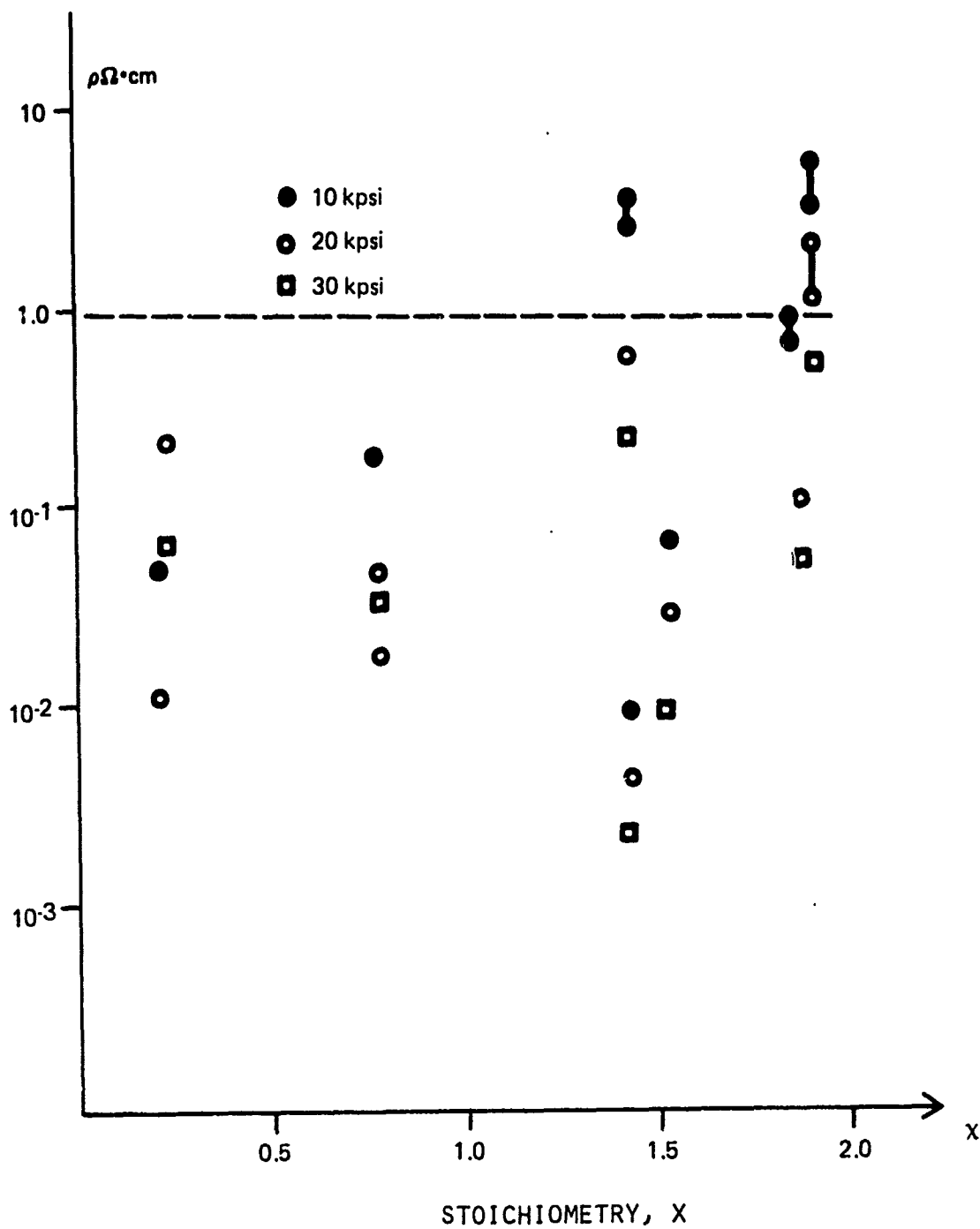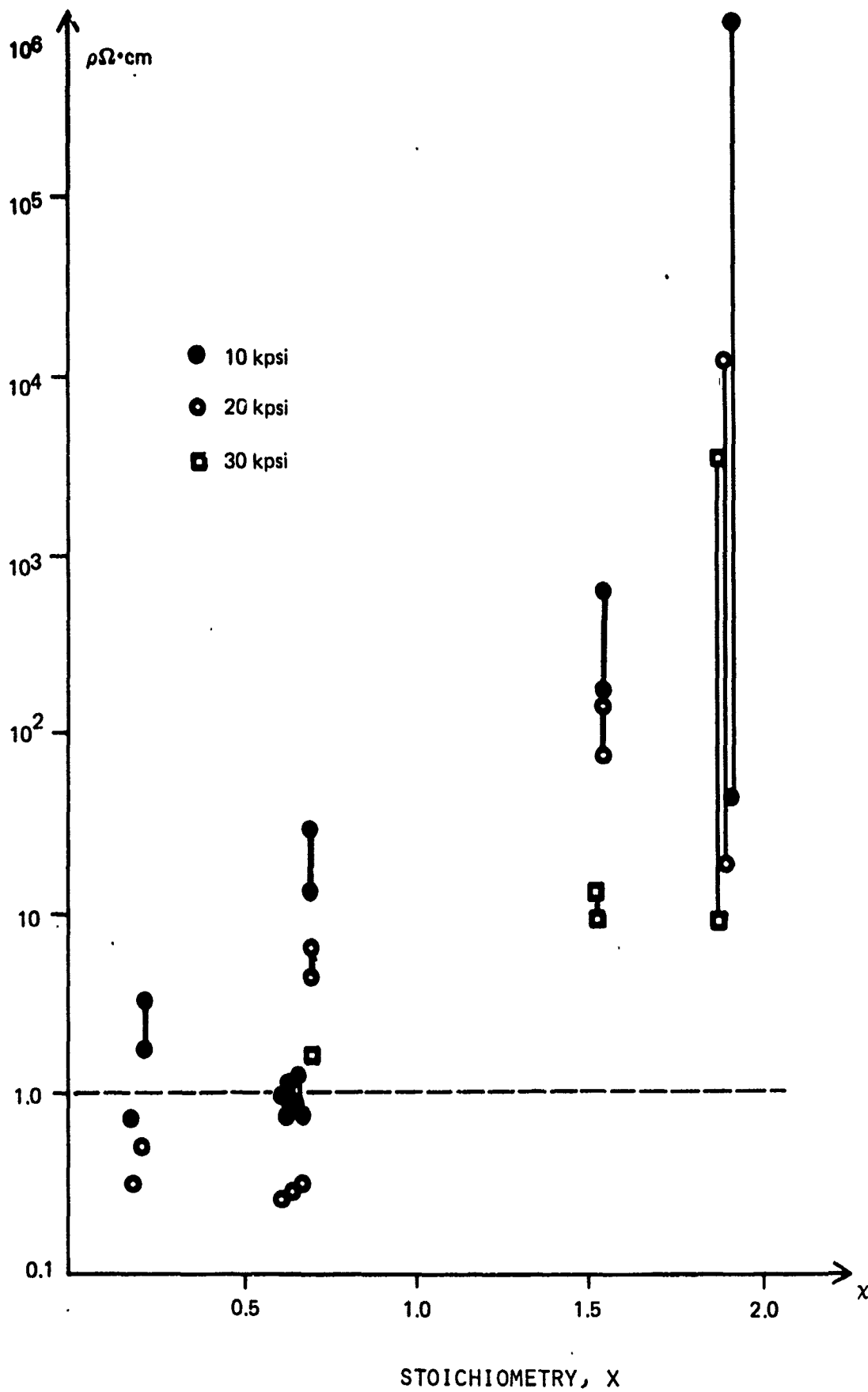FIGURE 23 - Five-kilovolt electrostatic test on TiH_x.

STOICHIOMETRY, X

FIGURE 24 - Five-kilovolt electrostatic test on $TiH_x/KClO_4$.

AN IMPROVED NAVY 5"/54 ILLUMINATING PROJECTILE

Presented by:

JOHN E. WILDRIDGE

NAVAL WEAPONS SUPPORT CENTER
APPLIED SCIENCES DEPARTMENT
CRANE, INDIANA 47522

ABSTRACT

The Navy has recently completed an improvement program for 5"/54 Illuminating Projectiles. Through utilization of a Ram Air Inflatable Decelerator (RAID) in conjunction with a cross (cruciform) parachute, functional performance has more than doubled the operational effectiveness of illuminating projectiles for search and damage assessment missions (approximately 75% of all missions). Developmental highlights are presented which relate to functional performance improvements, some examples of which are:

1. Allows fuze setting times to be reduced from 10 seconds (6500 yards downrange) to 3 seconds (2000 yards downrange).

2. Utilization of full service propellant charge throughout the range of fuze settings (the present illuminating projectile required a reduced propellant charge for fuze settings less than 10 seconds.

3. Decreased deployment distance from load ejection to full flare performance.

4. Reduce flare descent rate from 41 fps to 7 fps.

5. Increased flare performance from 2.79 million square feet for 47 seconds to 4.32 million square feet for 72 seconds (at an illuminance level of 0.2 lumens per square feet).

In conclusion, it will be shown that the operational performance of the new illuminating projectile is 2-1/2 times more cost effective than the present illuminating projectile.

AN IMPROVED NAVY 5"/54 ILLUMINATING PROJECTILE

I. BACKGROUND

The Mk 11 Illuminating Load now used in 5 Inch Projectiles represents World War II suspension system "state-of-the-art". It is a single-staged, reefed parachute with a swivel to prevent suspension line twisting during deployment (see Figure 1). The candle air burning time is 61 seconds at an intensity of 671,000 candlepower. Minimum usage range is 6,000 yards at full-service propellant charge because the projectile velocity at time of ejection must be below 1600 feet per second. After full suspension, the average candle descent rate is 41 feet per second. The area illuminated is 2.79 million square feet at a threshold illuminance level of 0.2 lumens per square foot, which is 10 times full moonlight (see Figure 2).

Acceptance and surveillance data plus fleet reports periodically indicate poor reliability and performance. Approximately 10 percent of the failures exhibit Mechanical Time Fuze (MTF) failures while 19 percent have fouled chutes or short burners. While not considered a failure, an additional 10 percent have extremely long delays to full parachute suspension. Candle burn times of all units deployed from projectiles are decreased an average of 20 seconds from those burned statically because of spin rates of up to 12,000 rpm at the time of ejection.

II. PRODUCT IMPROVEMENT

A. Introduction

During FY 69, NAVWPNSUPPCEN Crane, under the direction of the Naval Sea Systems Command, initiated a program to improve the 5"/38, Mk 50, Illuminating Projectile. This program continued at a minimum effort until an accelerated effort was initiated in early November 1972 to incorporate the Mk 18 Illuminating Load (see Figures 3 and 4) into the 5"/54, Mk 48, Illuminating Projectile.

To successfully incorporate the Mk 18 into the 5"/54 Illuminating Projectile, five major technical areas were investigated:

1. Aerodynamics performance of the payload.

2. Final decelerator performance.

3. Ballistics of the Mk 11 versus the Mk 18 Illuminating Load.

4. Collision of the base plug and payload.

5. Unknown performance characteristics of the Mk 18 Illuminating Load fired from the 5"/54 gun.

After a series of static and gun firing tests, including a TECHEVAL, the Mk 18 Illuminating Load was recommended for a release to pilot production in June 1974.

B. Mk 18 Illuminating Load Functional Performance

The Mk 18 design is a unique staged combination of supersonic and subsonic decelerators with an improved illuminating candle composition. The candle air burn time is 72 seconds at an intensity of 723,000 candlepower. Minimum usage range is 1800 yards with a full-service propellant charge at a projectile velocity, at the time of payload ejection, of 2240 feet per second. When deployed at its optimum altitude of 1050 feet, an average of 4.32 million square feet is illuminated for 72 seconds at a threshold illuminance level of 0.2 lumens per square foot (see Figure 2).

C. Mk 18 Illuminating Load Operating Sequence

This illustration presents the functional sequence of the Mk 18 Illuminating Load (see Figure 5). Sequence 1 depicts the projectile in flight. At sequence 2, the MTF functions and ignites the ejection charge. The ejection charge expels the payload from the projectile body, at 260 feet per second, and ignites two (redundant) pyrotechnic delays. Sequence 3 shows the base plug and rear ballast separation due to eccentric loading. This occurs between 5-10 milliseconds. Also, the Ram Air Inflatable Decelerator (RAID) deployment delay is initiated at this time.

When the rear ballast travels approximately six feet radially, a cap is pulled off the rear of the payload and a 12 inch RAID is deployed, as depicted in sequence 4. The RAID inflates in less than 50 milliseconds which reduces the forward velocity from 2240 to 140 feet per second and also reduces the rotational velocity from 200 to 6 rps in 1.7 seconds. This reduction of rotational velocity is necessary since excessive spin rates drastically degrade candle performance in addition to fouling the parachute.

In sequence 5, the pyrotechnic delays (1.7 seconds) initiate the ignition pellet. This pellet propels the ejection can from the candle and simultaneously ignites the candle. This then allows separation of the RAID and force transmitter, as shown by sequence 6. A pilot chute then extracts the nine foot cruciform parachute as depicted in sequence 7. The parachute and candle, when deployed, appear as shown in sequence 8.

D. **Mk 11 and Mk 18 Functional Performance**

Utilizing basic illumination theory (see Figure 6), graphs of the Mk 11 and Mk 18 performance are shown. By integrating the area under each loads' respective performance curve (see Figure 2), it can be seen that the Mk 18's performance is better than double that of the Mk 11 (311.0 million square-feet-seconds versus 131.1 million square-feet-seconds) (see Figure 7). The main reason for this is that the Mk 18, due to its much slower descent rate, allows the flare candle to operate nearer its optimum altitude. Functional performance character-istics of each load are shown in Figures 8 and 9.

E. **Mk 11 and Mk 18 Operational Cost Effectiveness**

Here are listed (see Figure 10) the costs of component parts that are consumed each time an illuminating projectile is fired. As can be seen, this amounts to 448 dollars for a Mk 11 as compared to 528 dollars for a Mk 18. Based solely on the demonstrated reliabil-ities, 0.71 for the Mk 11 and 0.87 for the Mk 18, the comparative costs to fire 10 functional rounds (see Figure 11) are:

Mk 11: 14 rounds x $448 round = $6272

Mk 18: 11 rounds x $528/round = $5808

Besides the comparative costs just to achieve 10 functional rounds, one should consider the relative effectiveness of each design to accomplish a search and damage assessment mission; the primary (75 percent) use of this round as indicated in references 1 and 2.

The relative effectiveness of an illuminating round for accomplishing the mission can be measured in terms of amount of usable illumination on the target for a given period of time; foot-candles (lumens per square foot) for so many seconds. For a flare, this can be measured by integrating the area under the area-time curve; i.e., square-feet-seconds. Values for the Mk 11 and Mk 18 are 131.1 and 311.0 million square-feet-seconds, respectively.

A typical search and damage assessment mission, references 1 and 2, required the placement of four flares around the target, such:

○Flare

○Flare   ✕Target   ○Flare

○Flare

Four flares, Mk 11's, translate into 524.4 million square-feet-seconds of illumination required. To accomplish this, the number of Mk 11's and Mk 18's required to produce 524.4 million square-feet-seconds can be determined, see Figure 12.

$$\text{No. of Mk 11's} = \frac{(524.4 \text{ million square-feet-seconds})}{(131.1 \text{ million square-feet-seconds})(0.71)} = 5.6 \text{ or } \underline{6} \text{ rounds}$$

$$\text{No. of Mk 18's} = \frac{(524.4 \text{ million square-feet-seconds})}{(311.0 \text{ million square-feet-seconds})(0.87)} = 1.94 \text{ or } \underline{2} \text{ rounds}$$

Thus, the cost to support this type of mission of 2688 dollars (6 rounds x $448/round) for the Mk 11 versus 1056 dollars (2 rounds x $528/round) for the Mk 18. Hence, it can be seen that, although the improved illuminating load is more expensive, it is 2.5 times more cost effective than the old load.
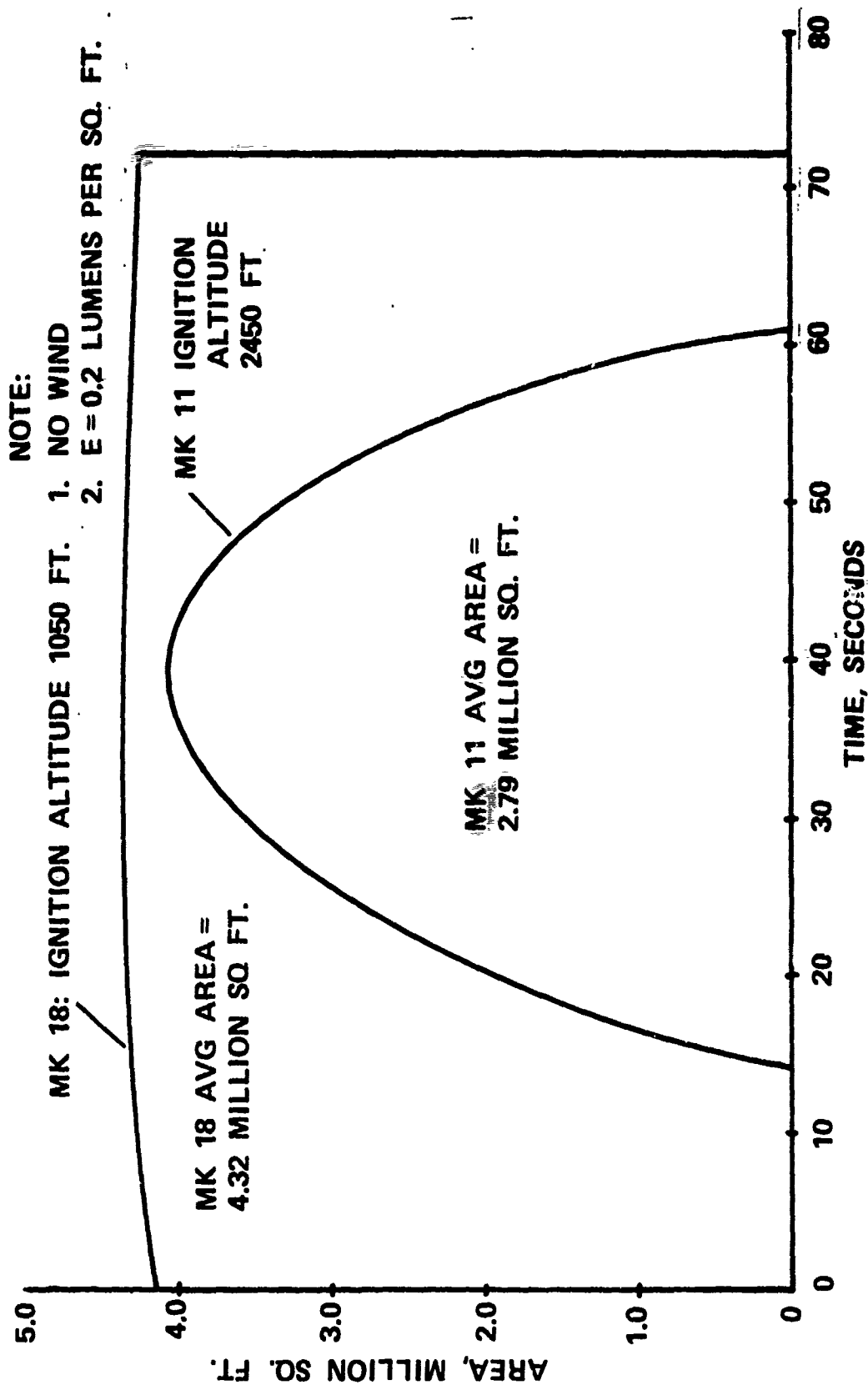
REFERENCES

1. NAD Crane Report RDTN-228; "Fleet Use of 5"/54 Illuminating Projectiles" of 22 December 1972.

2. NAD Crane Report RDTN-240; "Use of 5"/54 Illuminating Round" of 9 May 1973.

3. NWS Concord Report WQEC/CO 77-13; "Quality Evaluation of 5"/54 Illuminating Projectile Ammunition" of June 1977.

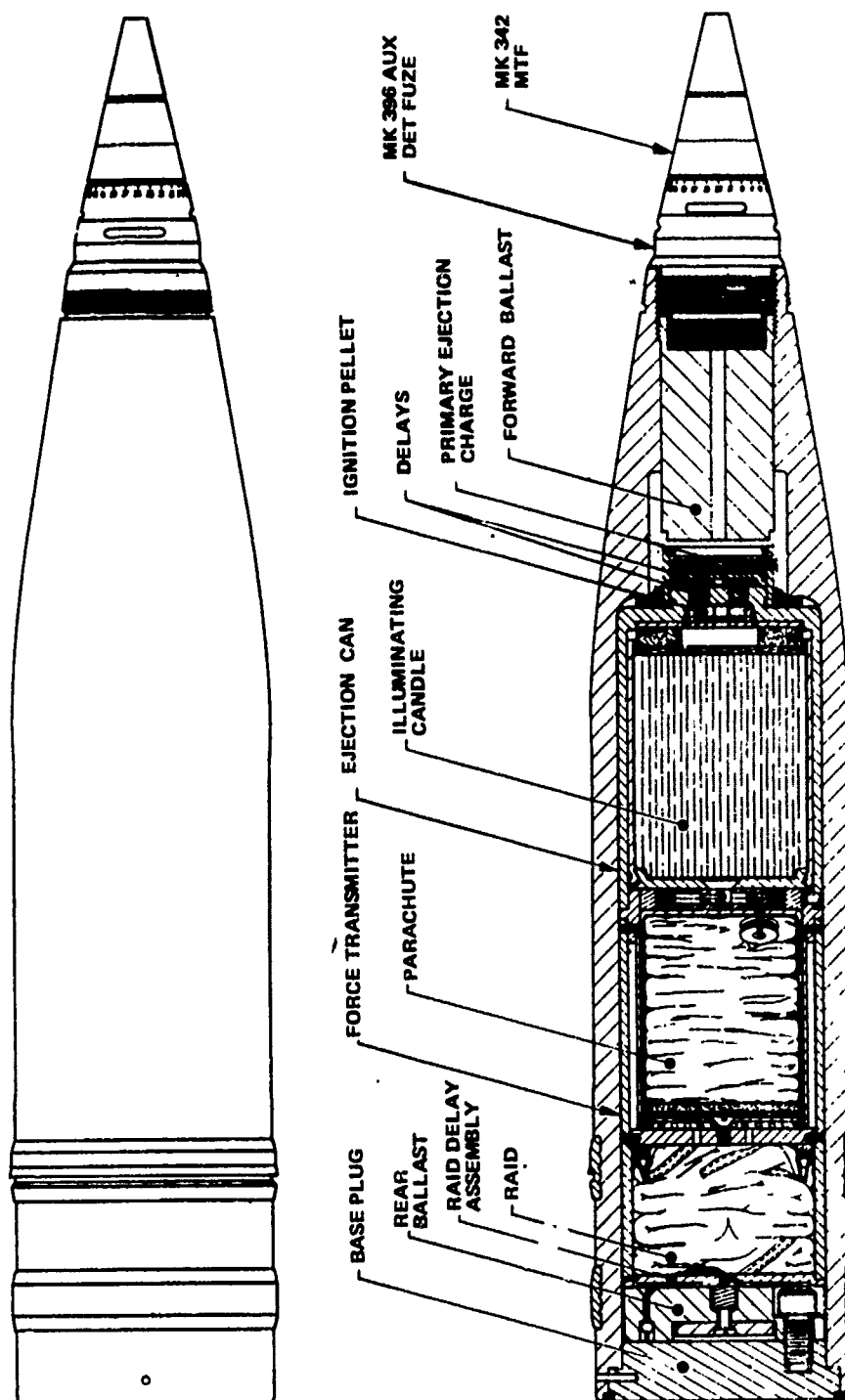4. AIAA Paper No. 73-482; "Predicting Descent Rate for Aircraft Parachute Flares", by John E. Laswell.

FIGURE 1

Mk 11 ILLUMINATING LOAD

705

AREA OF ILLUMINATION VERSUS TIME

MK 11 AND MK 18 ILLUMINATING LOADS

FIGURE 2

706

THE 5 INCH ILLUMINATING PROJECTILE
WITH MK 18 MOD 0 ILLUMINATING PROJECTILE LOAD

Labels:
- MK 396 AUX DET FUZE
- MK 342 MTF
- IGNITION PELLET
- DELAYS
- PRIMARY EJECTION CHARGE
- FORWARD BALLAST
- EJECTION CAN
- ILLUMINATING CANDLE
- FORCE TRANSMITTER
- PARACHUTE
- BASE PLUG
- REAR BALLAST
- RAID DELAY ASSEMBLY
- RAID

FIGURE 3

ILLUMINATING PROJECTILE LOAD
MK 18 MOD 0

FIGURE 4

708
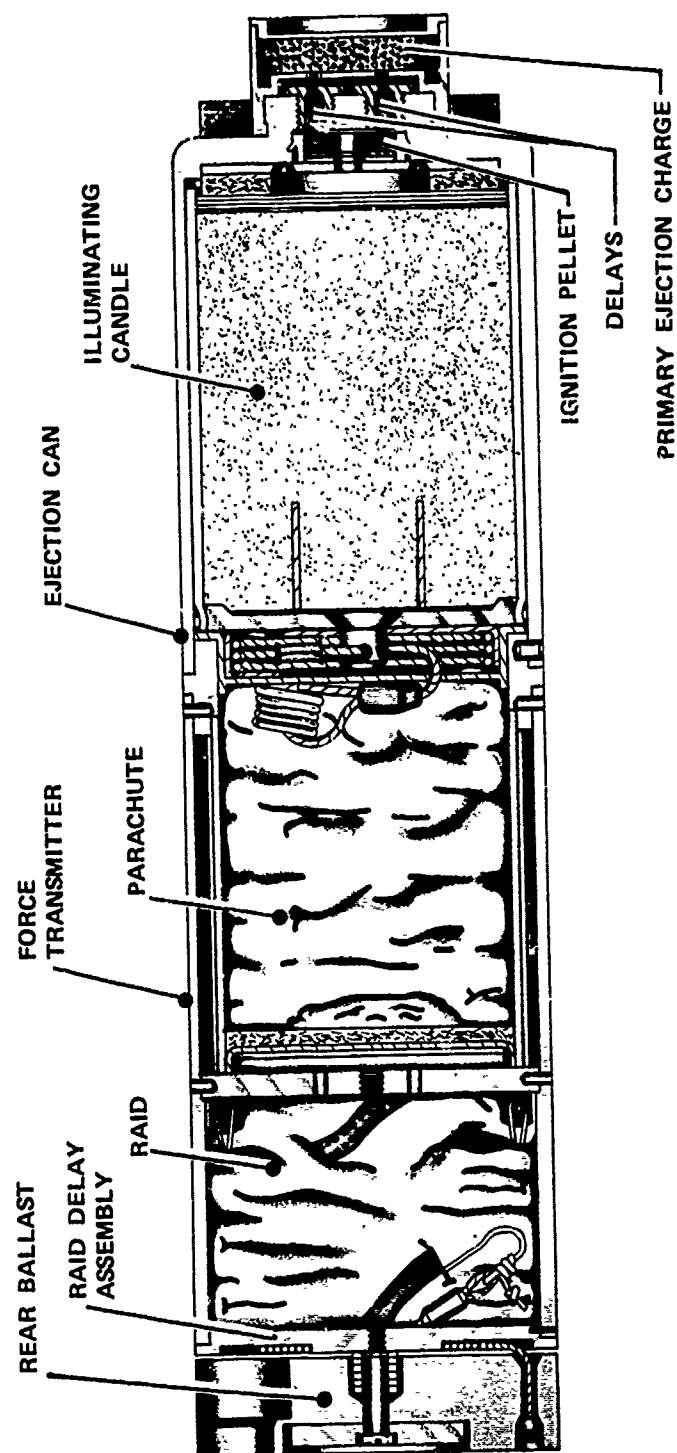
FUNCTIONAL SEQUENCE

5 INCH 54 PROJECTILE WITH MK 18 MOD 0 ILLUM. LOAD

1. MECHANICAL TIME FUZE DELAY
2. FUZE FUNCTION AND PRIMARY EJECTION (PYRO DELAY INITIATED)
3. BASE PLUG AND REAR BALLAST SPIN-OFF (RAID DEPLOYMENT DELAY INITIATED)
4. RAID DEPLOYMENT
5. SECONDARY EJECTION/CANDLE IGNITION
6. SEPARATION OF RAID AND PARACHUTE CONTAINER
7. PILOT CHUTE EXTRACTS MAIN PARACHUTE
8. PARACHUTE DEPLOYMENT

709

FIGURE 5
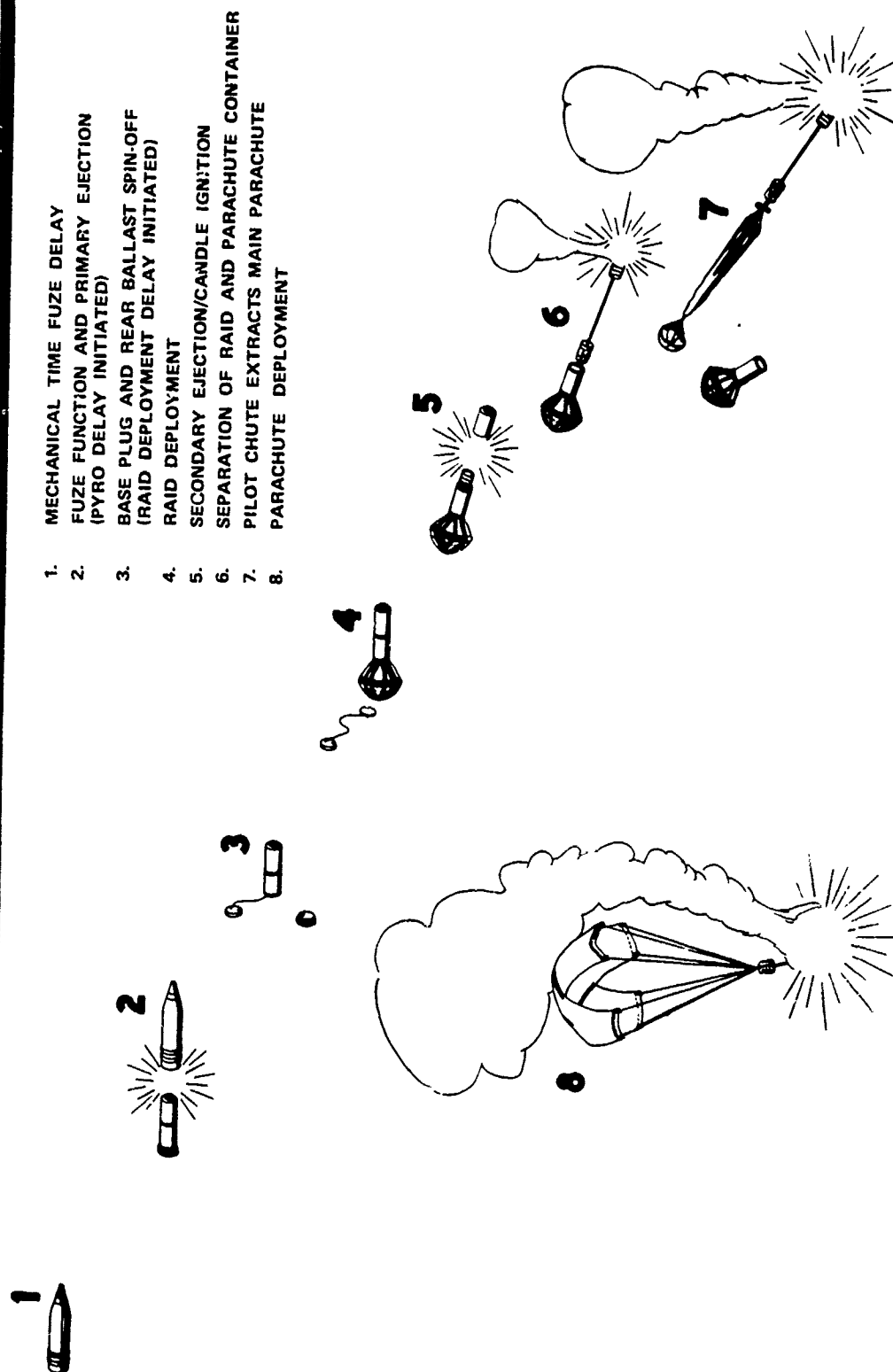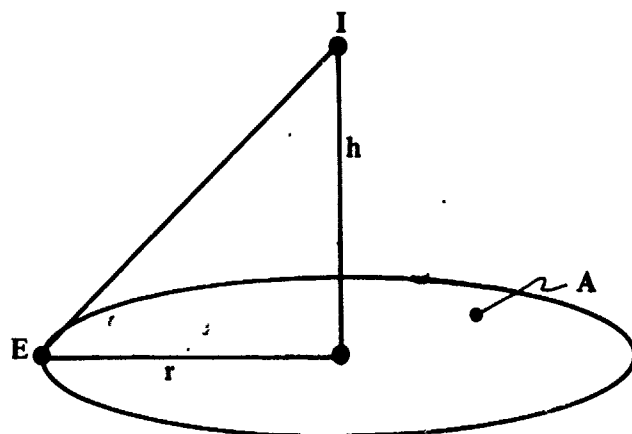
(1) $\quad E = \dfrac{I\cos\theta}{Z^2}$

(2) $\quad A = \pi r^2 = \left[\left(\dfrac{hI}{E}\right)^{2/3} - h^2\right]$

(3) $\quad h = h_{t-\Delta t} - \Delta t \left[\left(\dfrac{2W}{\rho C_d A'}\right)^{\frac{1}{2}} - V_t\right]$

(4) $\quad h_{optimum} = 0.43869\left(\dfrac{I}{E}\right)^{\frac{1}{2}}$

E	=	THRESHHOLD ILLUMINANCE LEVEL, FOOT CANDLES
I	=	FLARE INTENSITY, CANDLEPOWER
h	=	HEIGHT OF FLARE AT ANY TIME t, FEET
$h_{t-\Delta t}$	=	HEIGHT OF FLARE AT PREVIOUS ITERATION, FEET
A	=	CIRCULAR AREA ILLUMINATED TO THRESHHOLD ILLUMINANCE LEVEL (E), SQUARE FEET
r	=	RADIUS OF CIRCULAR AREA ILLUMINATED, FEET
W_w	=	WEIGHT OF FLARE SYSTEM AT ANY TIME t, POUNDS
ρ	=	DENSITY OF AIR, SLUGS PER CUBIC FEET
C_d	=	DECELERATOR DRAG COEFFICIENT
A'	=	DECELERATOR DRAG AREA, SQUARE FEET
V_t	=	FLARE SYSTEM THERMAL UPDRAFT, FEET PER SECOND
Δt	=	ITERATION TIME INTERVAL, SECONDS

FIGURE 6

AREA-TIME VERSUS
INITIAL ALTITUDE
MK 11 AND MK 18 ILLUMINATING LOADS

711

FIGURE 7
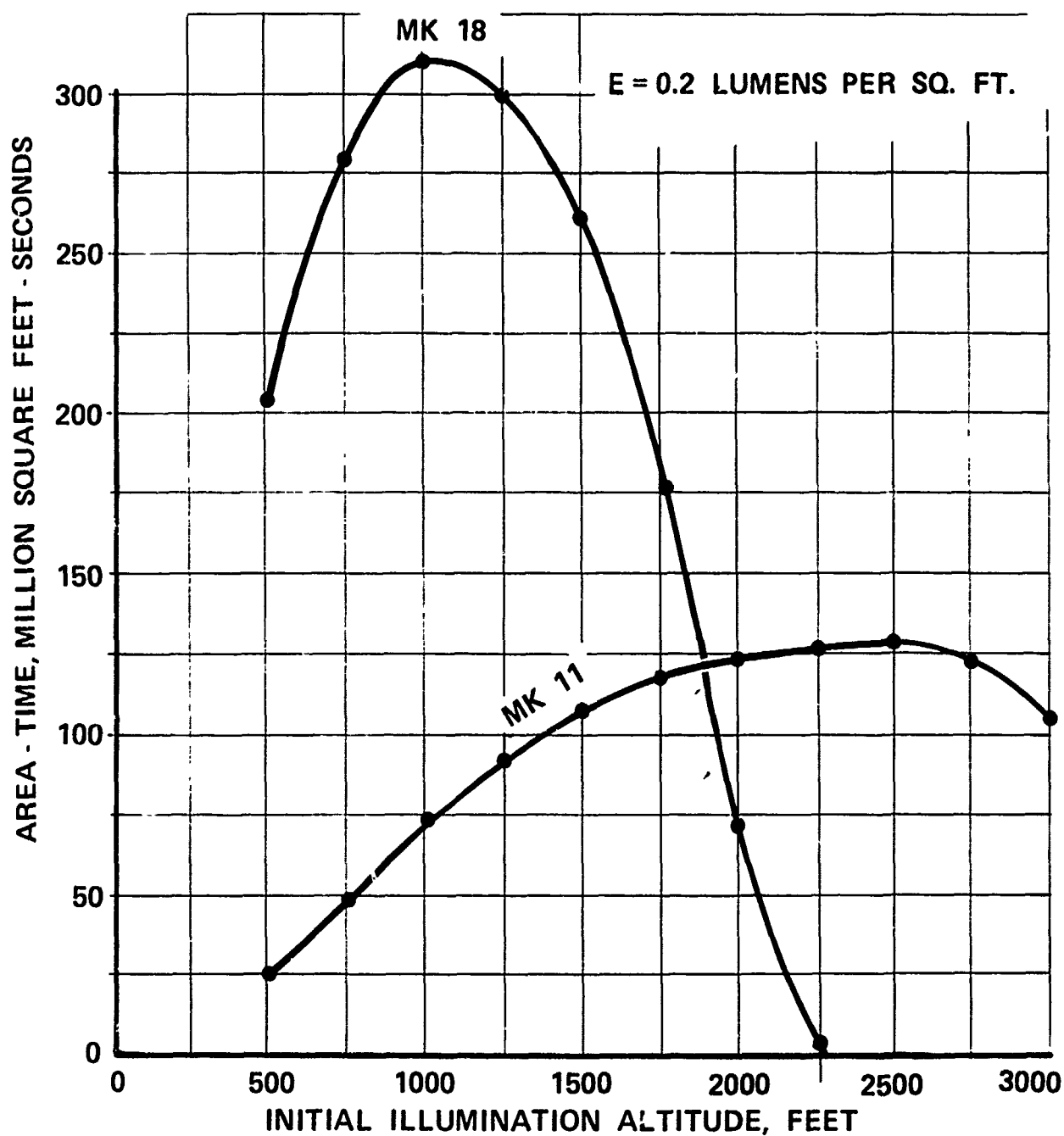
5" ILLUMINATING LOAD COMPARISON

	MK 11	MK 18
USAGE RANGE (MINIMUM/MAXIMUM - FULL SERVICE PROPELLANT CHARGE)	6000/18100 YARDS	1800/18300 YARDS
DEPLOYMENT DISTANCE AT MINIMUM USAGE RANGE	1350 FEET	1020 FEET
MAXIMUM ALLOWABLE PROJECTILE VELOCITY AT LOAD EJECTION	1600 FPS	2240 FPS
CANDLEPOWER (TUNNEL AVERAGE)	671,000	723,000
BURN TIME (AIR)	61 SEC	72 SEC
CANDLE EFFICIENCY	31,900 CP-SEC/GM	43,300 CP-SEC/GM
WEIGHT OF COMPOSITION	2.83 LBS	2.65 LBS
AVERAGE AREA ILLUMINATED (E = 0.2 LUMENS PER SQ FT)	2.79×10^6 SQ FT FOR 47 SEC	4.32×10^6 SQ FT FOR 72 SEC
PROJECTILE LOADED WEIGHT	68.2 LBS	64.0 LBS
AVERAGE DESCENT RATE	41 FPS	7 FPS
PARACHUTE	3 FT FLAT CIRCULAR	9 FT CRUCIFORM

FIGURE 8

MK 11 AND MK 18 DEMONSTRATED
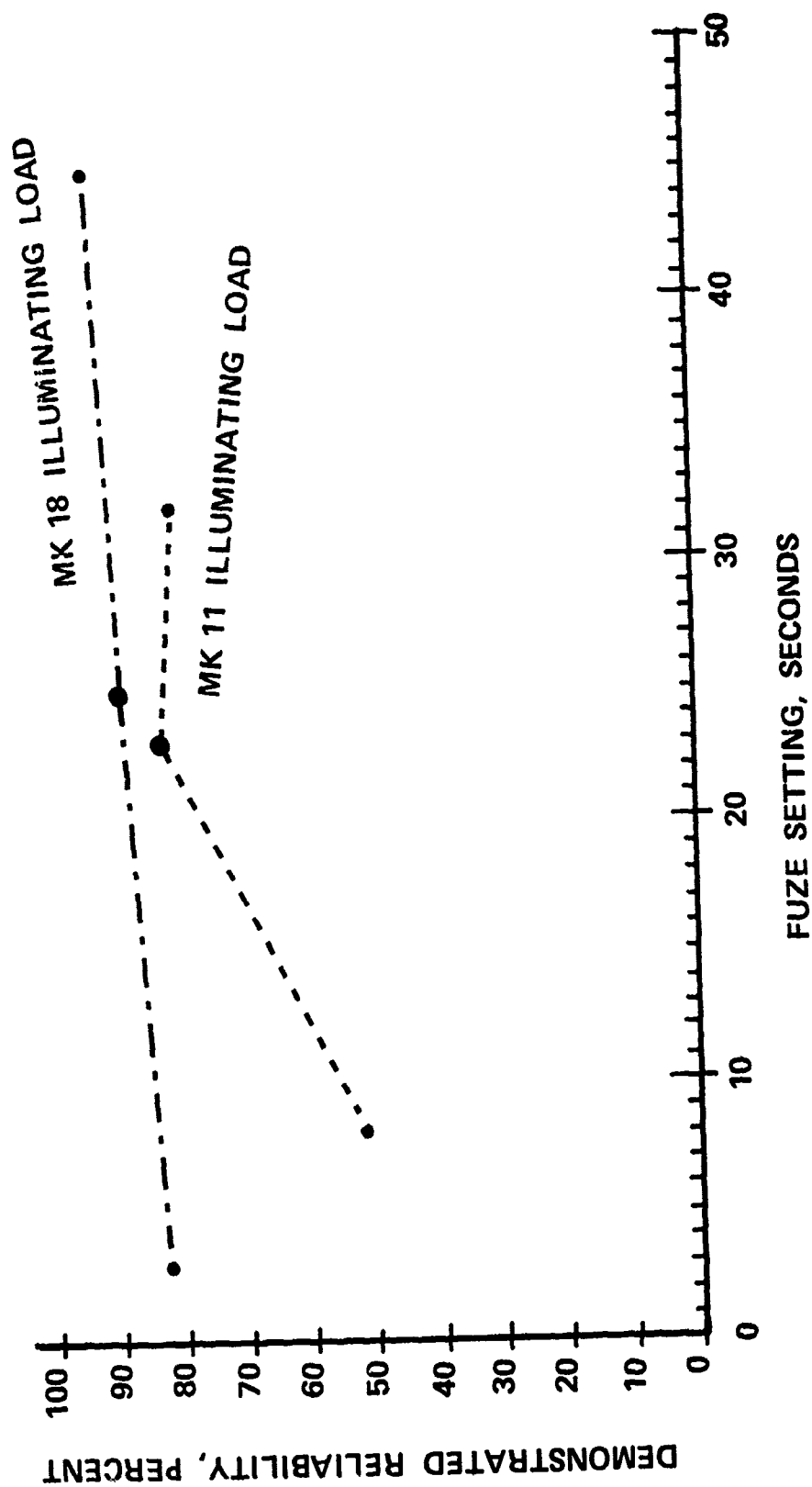## RELIABILITY VERSUS FUZE SETTING

FIGURE 9

713

ASSOCIATED COSTS OF 5"/54 ILLUMINATING PROJECTILE FIRINGS

MK 88 MOD 1 ILLUMINATING PROJECTILE

- MK 48 BODY AND BASE PLUG............$ 95
- MK 342 M T F....................... 28
- MK 396 A D F....................... 15
- MK 11 LOAD........................ 160
- MK 67 MOD 1 PROP CHARGE............ 150
                                    $ 448

MK 91 MOD O ILLUMINATING PROJECTILE

- MK 48 BODY AND BASE PLUG............$ 95
- MK 342 M T F....................... 28
- MK 396 A D F....................... 15
- MK 18 LOAD........................ 240
- MK 67 MOD 1 PROP CHARGE............ 150
                                    $ 528

714

FIGURE 10

COMPARATIVE COSTS TO FIRE
10 FUNCTIONAL ROUNDS

- MK 11:   14 ROUNDS X $ 448/ROUND = $ 6272

- MK 18:   11 ROUNDS X $ 528/ROUND = $ 5808

FIGURE 11

715

COST EFFECTIVENESS COMPARISON OF
MK 11 AND MK 18 ILLUMINATING LOADS

● FLARE

FLARE ●   X   ● FLARE
              TARGET

● FLARE

NO. OF MK 11's $= \dfrac{524.4 \text{ MILLION–SQUARE–FEET–SECONDS}}{131.1 \text{ MILLION–SQUARE–FEET–SECONDS} \times 0.71} = 5.6 \text{ OR } 6 \text{ ROUNDS}$

NO. OF MK 18's $= \dfrac{524.4 \text{ MILLION–SQUARE–FEET–SECONDS}}{311.0 \text{ MILLION–SQUARE–FEET–SECONDS} \times 0.87} = 1.94 \text{ OR } 2 \text{ ROUNDS}$

COST RATIO $= \dfrac{\$448/\text{ROUND} \times 6 \text{ ROUNDS}}{\$528/\text{ROUND} \times 2 \text{ ROUNDS}} = \dfrac{\$2688}{\$1056} = 2.55$

716

FIGURE 12